UNIVERSIDAD COMPLUTENSE DE MADRID

FACULTAD DE MEDICINA

TESIS DOCTORAL

Papel de MINDIN en la progresión tumoral y formación del nicho pre-metastásico óseo en el cáncer de próstata

MEMORIA PARA OPTAR AL GRADO DE DOCTOR

PRESENTADA POR

Luis Álvarez Carrión

DIRECTORES

Verónica Alonso Rodríguez
Juan Antonio Ardura Rodríguez

UNIVERSIDAD COMPLUTENSE DE MADRID

FACULTAD DE MEDICINA

TESIS DOCTORAL

Papel de MINDIN en la progresión tumoral y formación del nicho pre-metastásico óseo en el cáncer de próstata

MEMORIA PARA OPTAR AL GRADO DE DOCTOR

PRESENTADA POR

Luis Esteban Álvarez Carrión

Directores

Verónica Alonso Rodríguez

Juan Antonio Ardura Rodríguez

Madrid

UNIVERSIDAD COMPLUTENSE DE MADRID

FACULTAD DE MEDICINA

Programa de Doctorado en Bioquímica, Biología Molecular y Biomedicina

Departamento de Bioquímica y Biología Molecular

TESIS DOCTORAL

Papel de MINDIN en la progresión tumoral y formación del nicho pre-metastásico óseo en el cáncer de próstata

MEMORIA PARA OPTAR AL GRADO DE DOCTOR

PRESENTADA POR

Luis Esteban Álvarez Carrión

Directores

Verónica Alonso Rodríguez

Juan Antonio Ardura Rodríguez

Madrid 2020

AGRADECIMIENTOS

En una lectura de tesis, una única persona opta al grado de doctor, pero no cabe la menor duda de que una tesis no es obra de una única persona. Por ello, en estas líneas que, aunque breves, están llenas de gratitud y cariño, me gustaría mostrar mi agradecimiento a las personas que han colaborado en el desarrollo de esta tesis, tanto a nivel profesional como personal.

En primer lugar a mis directores de tesis la Dra. Verónica Alonso Rodríguez y el Dr. Juan Antonio Ardura Rodríguez por haberme dado la oportunidad de realizar esta tesis, por poder trabajar con ellos, por su gran implicación, optimismo y humildad. Gracias por la experiencia que he adquirido y por confiar en mí.

Agradecer a mi compañera Irene Gutiérrez Rojas. Gracias por haberme apoyado desde el principio del máster, pese a tener una formación casi nula, pero sobre todo haber tenido la paciencia de explicarme y enseñarme las técnicas utilizadas en el laboratorio. Gracias por estar siempre dispuesta a ayudarme, por tu implicación y apoyo para que este trabajo saliera adelante.

Agradecer también a Irene Buendía Montes su ayuda y apoyo durante la realización de esta tesis.

A mis compañeras de comidas/desayunos: Sonia, Jose, Susana, Virginia e Irenes, estos años no hubiesen sido lo mismo sin tanto humor.

Agradecer a mi tutor el Dr. Javier Fernández Ruiz, profesor del departamento de Bioquímica y Biología Molecular de la Universidad Complutense de Madrid, por su disponibilidad para resolver dudas y problemas durante este trabajo.

Finalmente agradezco a mi familia, en especial a María todo el apoyo recibido durante este tiempo.

A todos, mi más sincero agradecimiento.

ABREVIATURAS Y ACRÓNIMOS

ADN Ácido desoxirribonucleico

ADNc Ácido desoxirribonucleico complementario

ARN Ácido ribonucleico

ARNm Ácido ribonucleico mensajero

ASBMR American Society for Bone and Mineral Research

BCA Ácido bicinconínico

BSP Sialoproteína ósea

BV/TV Volumen óseo/volumen total de tejido

CaP Cáncer de próstata

cT Estadio clínico

Ct Ciclo umbral

DEPC Pirocarbonato de dietilo

DMP1 Proteína de matriz de dentina 1

EBD Dominio de unión a ezrina

EBP50 Fosfoproteina de unión a Ezrina-radixina-moesina 50

ERK 1/2 Quinasa 1/2 regulada por señal extracelular

FAK Quinasa de adhesión focal

HBP Hiperplasia benigna de próstata

HGPIN Neoplasia intraepitelial prostática de alto grado

HRP Peroxidasa de rábano

M-CSF Factor estimulante de colonias de macrófagos

MC Medio condicionado del secretoma

MMA Metil-metacrilato

MSC Células madre mesenquimales

N.Ob/Pm Número de osteoblastos/perímetro óseo

N.Oc/Pm Número de osteoclastos/perímetro óseo

NHERF Factor regulador del intercambio de Na+/H+

OCN OSTEOCALCINA

OPG OSTEOPROTEGERINA

OPN OSTEOPONTINA

PBS Tampón fosfato salino

PCR Reacción en cadena de la polimerasa

PDZ PSD-95/Discs Large/ZO-1

PIN Neoplasia intraepitelial prostática

PSA Antígeno específico prostático

PSCA Antígeno Prostático de Células Madre

qPCR Reacción en cadena de la polimerasa cuantitativa

RANK Receptor activador para el factor nuclear kB

RANKL Ligando del receptor activador para el factor nuclear kB

RUNX2 Factor de transcripción relacionado con Runt 2

SFB Suero fetal bovino

siARN ARN pequeño de interferencia

Tb.N Número trabecular

Tb.Sp Separación trabecular

Tb.Th Espesor trabecular

TBS Tris Buffer Salino

TEM Transición epitelio-mesénquima

TNM Tumor, Ganglio y Metástasis

TRAP Fosfatasa ácida resistente al tartrato

TSP TROMBOESPONDINA

TSR1 Repetición de trombospondina

VEGF Factor de crecimiento endotelial vascular

VEGFR2 Receptor del factor de crecimiento endotelial vascular 2

µl Microlitro

ÍNDICE

1. RESUMEN/SUMMARY

Papel de MINDIN en la progresión tumoral y formación del nicho pre-metastásico óseo en el cáncer de próstata

INTRODUCCIÓN

El cáncer de próstata es una de la principales patologías que afectan a la población masculina. Sin embargo, se desconocen cuáles son los factores determinantes en su desarrollo. Actualmente, el desafío en el cáncer de próstata es la identificación de marcadores tumorales específicos, fundamental para pronosticar y monitorizar los tumores de próstata con el objetivo de reducir la mortalidad y mantener una calidad de vida aceptable.

El hueso es un tejido dinámico que se remodela continuamente ante una gran variedad de estímulos. Además, es un órgano frecuentemente infiltrado por la diseminación metastásica de tumores sólidos, como el de próstata. Esta preferencia, denominada organotropismo, puede deberse a la adquisición de características osteomiméticas por parte de las células tumorales. El osteomimetismo implica que las células tumorales expresan de manera ectópica genes restringidos al tejido óseo y que las predisponen a colonizarlo.

MINDIN es un factor soluble prostático que se secreta a la matriz extracelular y está elevado en el secretoma de las células tumorales prostáticas. No obstante, el papel de MINDIN en la progresión tumoral o la formación nichos premetastásicos es desconocido.

HIPÓTESIS

La presente tesis plantea como hipótesis que los factores solubles tumorales secretados, como MINDIN, son capaces de inducir osteomimetismo en las propias células tumorales y modificar componentes celulares del tejido óseo, generando alteraciones en su actividad fisiológica. Estas modificaciones inducirían la formación

de nichos premetastásicos óseos, creando condiciones fisiopatológicas que permiten la implantación de las células tumorales en dichos nichos óseos.

OBJETIVO

Como objetivo general planteamos definir los mecanismos moleculares y celulares inducidos por MINDIN, como factor soluble secretado por el tumor primario, sobre las células del propio tumor primario y sobre el entorno óseo.

RESULTADOS

Mediante análisis proteómico del secretoma de células prostáticas (tumorales y control) y óseas se identificaron los posibles factores moduladores de la progresión tumoral. Una vez identificado MINDIN como posible factor implicado, se analizó su expresión en biopsias prostáticas humanas. Este análisis reveló que la expresión de MINDIN se encuentra aumentada en los tumores de próstata y aumenta a medida que se incrementa el grado tumoral. Además, se observó un incremento significativo de marcadores osteomiméticos, así como una disminución de la expresión de NHERF1, factor modulador óseo, en las muestras tumorales en comparación con los controles.

A continuación, se desarrolló un modelo *in vivo* de ratón de cáncer de próstata premetastático basado en implantación de células de adenocarcinoma TRAMPC1, con silenciamiento o no del gen de MINDIN. Los resultados observados en el modelo de ratón demuestran que MINDIN induce cambios osteomiméticos en las próstatas de los ratones, modificaciones en la microarquitectura ósea y un incremento de la actividad génica en el hueso.

In vitro, MINDIN induce un fenotipo osteomimético en líneas tumorales prostáticas y un incremento de la proliferación, migración y adhesión a superficies óseas. La inhibición de la quinasa ERK disminuyó los efectos protumorogénicos inducidos por MINDIN. Además, NHERF1 media en las acciones de MINDIN sobre la proliferación y capacidad migratoria de las células tumorales de cáncer de próstata.

En cultivos *in vitro* de células ósea observamos que MINDIN induce proliferación, diferenciación y activación de marcadores osteoblastogénicos y de remodelado óseo en osteoblastos. MINDIN modificó la expresión génica de marcadores óseos en osteocitos e incrementó la expresión génica del marcador de resorción ósea TRAP en osteoclastos. Además, se observó que la vía de señalización de β-CATENINA media las acciones de MINDIN en la expresión génica de los osteoblastos.

CONCLUSIÓN

Como conclusión se puede afirmar que MINDIN es un regulador del osteomimetismo y un factor promotor de la progresión tumoral del cáncer de próstata. Además, media la comunicación entre las células óseas y el tumor, creando un ambiente favorable para el alojamiento de las células tumorales en el entorno óseo antes de la diseminación metastásica.

Role of MINDIN in the induction of the bone pre-metastatic niche by prostate cancer

INTRODUCTION

Prostate cancer is one of the main pathologies that affect the male population. However, the determining factors in its development are unknown. Currently, the challenge in prostate cancer is the identification of specific tumor markers, essential to predict and monitor prostate tumors with the aim of reducing mortality and maintaining an acceptable quality of life.

Bone is a dynamic tissue that continually remodels in response of a wide variety of stimuli. In addition, it is an organ frequently infiltrated by the metastatic spread of solid tumors, such as prostate cancer. This preference, called organotropism, may be due to the acquisition of osteomimetic characteristics by tumor cells. Osteomimicry implies that tumor cells ectopically express genes restricted to bone tissue and predispose them to colonize it.

MINDIN is a soluble prostatic factor that is secreted to the extracellular matrix and is elevated in the secretome of prostate tumor cells. However, the role of MINDIN in tumor progression or pre-metastatic niche formation is unknown.

HYPOTHESIS

The present thesis hypothesizes that secreted soluble tumor factors, such as MINDIN, are capable of inducing osteomimetism in the tumor cells themselves and modifying cellular components of bone tissue, generating alterations in their physiological activity. These modifications would induce the formation of premetastatic bone niches, creating pathophysiological conditions that allow the implantation of tumor cells in said bone niches.

OBJECTIVES

As a general objective, we propose to define the molecular and cellular mechanisms induced by MINDIN, as a soluble factor secreted by the primary tumor, on the tumor cells and on the bone environment.

RESULTS

Through proteomic analysis of the secretome of prostate cells (tumoral and control) and bone cells, possible modulating factors of tumor progression were identified. Once MINDIN was identified as a possible factor involved, its expression was analyzed in human prostate biopsies. This analysis revealed that MINDIN expression is increased in prostate tumors and increases when the tumor grade increases. Furthermore, a significant increase in osteomimetic markers was observed, as well as a decrease in the expression of NHERF1, bone modulating factor, in tumor samples compared to controls.

Next, an *in vivo* mouse model of pre-metastatic prostate cancer was developed based on implantation of TRAMPC1 adenocarcinoma cells, with or without silencing of the MINDIN gene. The results observed in the mouse model demonstrate that MINDIN induces osteomimetic changes in the prostates of mice, modifications in bone microarchitecture and an increase in gene activity in bone.

In vitro, MINDIN induces an osteomimetic phenotype in prostate tumor lines and an increase in proliferation, migration and adhesion to bone surfaces. Inhibition of ERK kinase decreased the protumorogenic effects induced by MINDIN. In addition, NHERF1 mediates the actions of MINDIN on the proliferation and migratory capacity of prostate cancer tumor cells.

In *in vitro* cell culture of bone cells, we observed that MINDIN induces proliferation, differentiation and activation of osteoblastogenic markers and bone remodeling in osteoblasts. MINDIN modified the gene expression of bone markers in osteocytes and increased the gene expression of the bone resorption marker TRAP in osteoclasts.

Furthermore, the β-CATENIN signaling pathway was observed to mediate the actions of MINDIN in osteoblast gene expression.

CONCLUSION

As a conclusion, it can be stated that MINDIN is an osteomimicry regulator and a promoter of prostate cancer tumor progression. In addition, it mediates communication between bone cells and the tumor, creating a favorable environment for the accommodation of tumor cells in the bone environment before metastatic spread.

2. INTRODUCCIÓN

2.1 La próstata: Anatomía, histología y progresión tumoral

La próstata es un órgano glandular del aparato reproductor masculino que pesa alrededor de 20 gramos y mide de media 2 x 3 x 4 cm de espesor, largo y ancho, respectivamente. La función de la próstata es, junto a los testículos y la vesícula seminal, producir semen. Este líquido segregado por la próstata es alcalino y rico en espermina, calcio, sodio, potasio, zinc, colesterol, carnitina, fosfolípidos, ácido cítrico, fosfatasa ácida prostática, antígeno específico prostático (PSA) y proteasas. La acción conjunta de estos compuestos facilita y mejora la movilidad de los espermatozoides (1).

Anatómicamente, la próstata humana está formada por un único lóbulo, el cual posee una región no glandular, denominada zona fibromuscular (formada por tejido conjuntivo denso con fibras musculares), y una región glandular dividida en 3 zonas:
- zona central (ZC), la cual rodea a los conductos eyaculadores y supone el 25% del volumen prostático;
- zona de transición (ZT), la cual rodea a la uretra y supone el 5% del volumen prostático;
- y zona periférica (ZP) que supone en torno al 70% del volumen prostático (2–11) (Figura 1).

A diferencia de la humana, la próstata de los ratones no está formada por un único lóbulo, sino que está compuesta por cuatro pares de lóbulos ubicados alrededor de la uretra y que se nombran según su orientación espacial en: anterior, central, lateral y dorsal. El lóbulo o próstata anterior (PA) se encuentra unida a la vesícula seminal; en posición anterior a la uretra y caudal a la vejiga aparece el lóbulo o próstata ventral (PV), la cual puede reconocerse como una estructura rosada gelatinosa que envuelve parcialmente a la uretra. La PV está flanqueada por dos lóbulos que se encuentran a ambos lados de la uretra para dar forma al lóbulo o próstata lateral (PL). El lóbulo o próstata dorsal (PD), que tiene forma de mariposa, se encuentra bilateralmente en la base de la vesícula seminal (VS). La PL y la PD a menudo se denominan próstata dorsolateral (PDL), aunque presentan algunas diferencias en su histología (la PD posee un epitelio simple columnar con los núcleos en posición central mientras que la PL posee un epitelio simple cuboidal y columnar bajo con los núcleos en posición basal) (12–15)

(Figura 1). Según estudios anatómicos y comparaciones entre especies mediante firmas de ARNm (16,17), la próstata dorsolateral del ratón es homóloga a la zona periférica de la próstata humana y se considera que la próstata anterior del ratón es similar a la zona central de la próstata humana. La zona de transición no tiene un homólogo en el ratón (2,17).

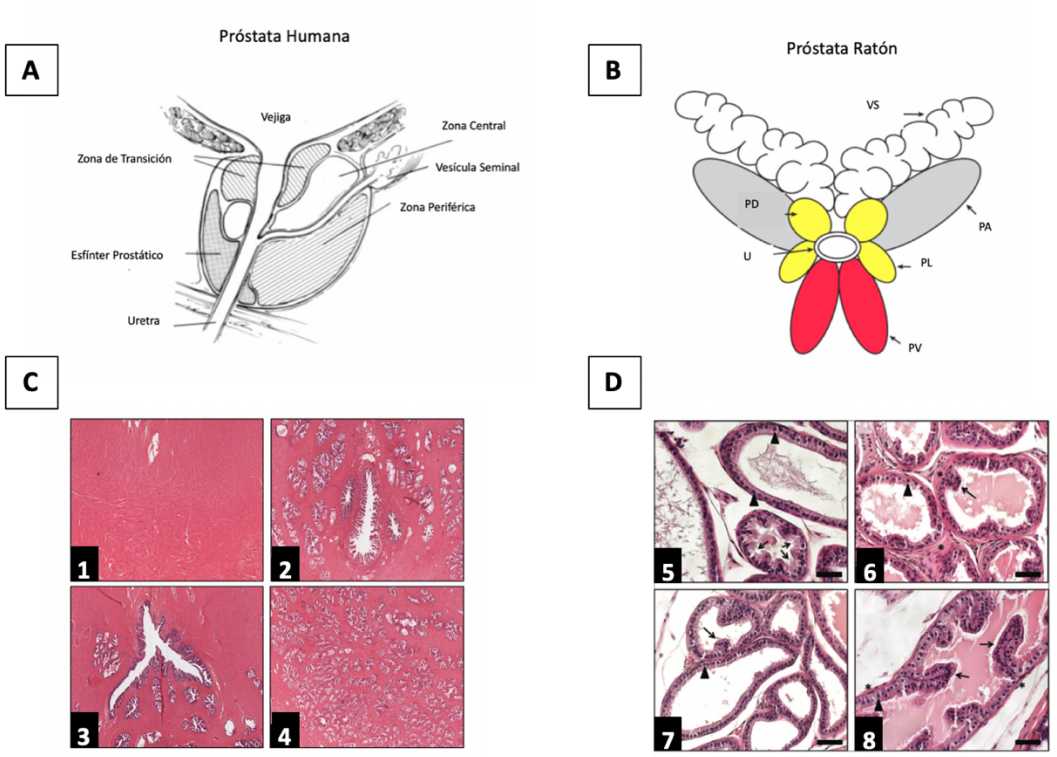

Figura 1: Comparativa anatómica e histológica entre las próstatas (A) humana y (B) de ratón. La próstata humana consta de un único lóbulo dividido en (C) una región no glandular, [1] denominada zona fibromuscular, y una región glandular dividida en 3 zonas: [2] zona central, zona de transición [3] y zona periférica [4]. Sin embargo, la próstata de ratón consta de cuatro pares de lóbulos (D): [5] próstata ventral (PV), anterior a la uretra [U]; [6] próstata dorsal (PD); [7] próstata lateral (PL) y [8] próstata anterior (PA), unida a la vesícula seminal (VS). Fuente: imágenes obtenidas a partir de: Michigan Histology and Virtual Microscopy Learning Resources (https://histology.medicine.umich.edu/resources/male-reproductive-system#v-prostate-gland), Oliveira, D.S.M. *et al.* (The mouse prostate: A basic anatomical and histological guideline), Toivanen, R. *et al.* (Prostate organogenesis: Tissue induction, hormonal regulation and cell type specification) y Peng, Y.C. *et al.* (Hedgehog signaling in prostate epithelial-mesenchymal growth regulation) (15,18,19).

Histológicamente, las próstatas humana y de ratón están compuestas por un epitelio glandular, el cual contiene tres tipos de células: células secretoras luminales, células neuroendocrinas y células basales (menos abundantes y discontinuas en la próstata de ratón y continuas en la próstata humana) (2,20,21) (Figura 2). Además, también residen otros tipos celulares como fibroblastos, células de músculo liso, células endoteliales,

células intermedias, células inmunes o fibras nerviosas. Todas estas células influyen en el comportamiento biológico de la próstata (22) (Figura 2).

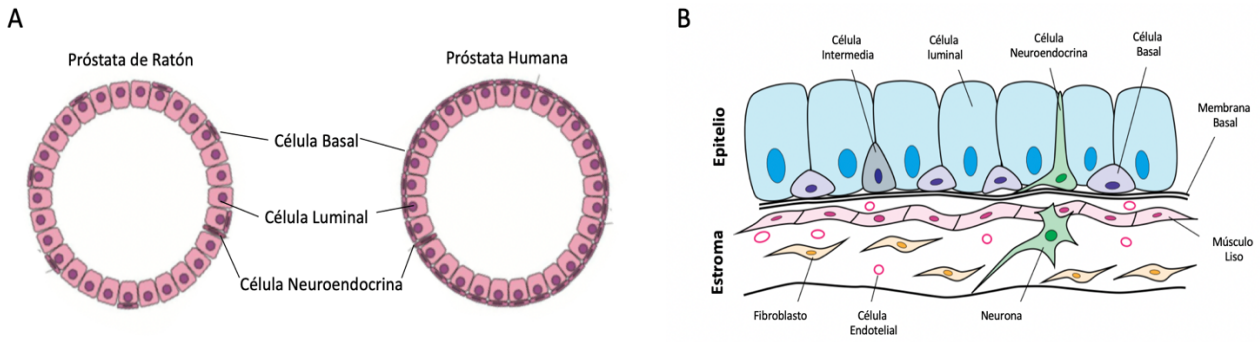

Figura 2: Diagrama de (A) la histología y (B) los diferentes tipos celulares de las próstatas humana y de ratón. Fuente: Toivanen, R. *et al.* (Prostate organogenesis: Tissue induction, hormonal regulation and cell type specification) y Valkenburg, K.C. *et al.* (Drug discovery in prostate cancer mouse models) (18,23).

El cáncer de próstata (CaP) es una de la principales patologías relacionadas con la próstata. Además, es el tipo de cáncer mas comúnmente diagnosticado en hombres, con una incidencia de aproximadamente 200.000 nuevos casos diagnosticados cada año (24). A nivel mundial, según la Agencia Internacional de Investigación en Cáncer, el CaP causó mas de 300.000 muertes durante el año 2018 (Figura 3). Debido a que la posibilidad de desarrollar CaP aumenta rápidamente a partir de los 50 años, su incidencia y prevalencia están directamente relacionadas con el envejecimiento de la población (25). Actualmente, se desconocen cuáles son los factores determinantes en el desarrollo del CaP, no obstante se han identificado algunos de ellos como son: la edad (25), el origen étnico (26), la dieta (27), consumo de tabaco y factores genéticos hereditarios (28).

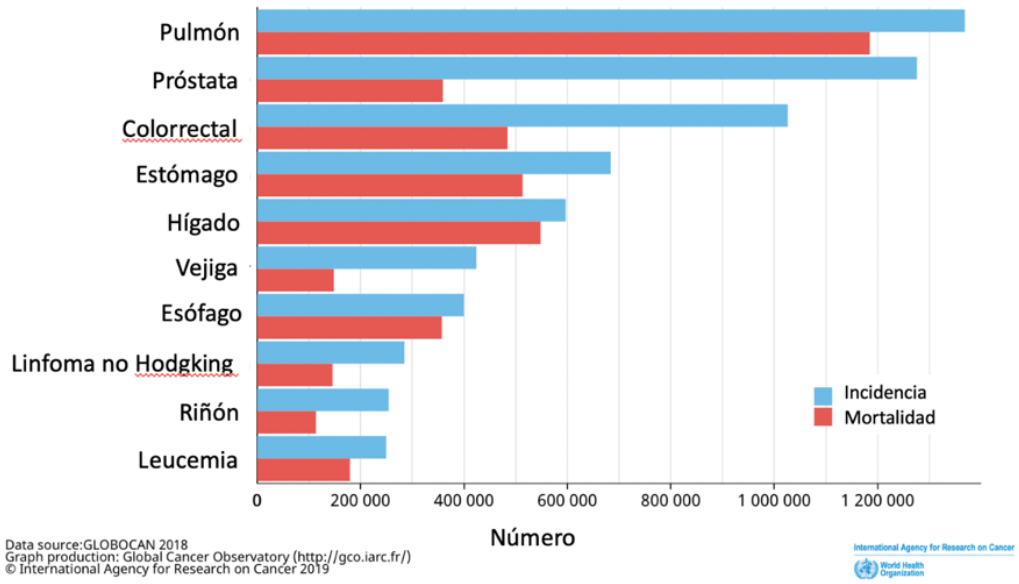

Figura 3: Gráfico de la incidencia y mortalidad a nivel mundial del cáncer de próstata. Fuente: International Agency for Research on Cancer.

Anatómicamente, según varios estudios, alrededor del 75% de los carcinomas se desarrollan en la zona periférica de la próstata, mientras que en la zona de transición se desarrolla la hiperplasia benigna de próstata (HBP). Por su parte, la zona central es la más resistente a la aparición de estas patologías, ya que en esta zona solo se desarrollan aproximadamente el 5% de las neoplasias (2,3,29,30,4–11). El cáncer de próstata puede derivar tanto de células luminales como basales. En más del 95% de los tumores de próstata, las células tumorales expresan predominantemente marcadores luminales, mientras que los derivados de células basales son raros (21). Además, las células luminales son más susceptibles a la transformación directa, mientras que las células basales parecen necesitar diferenciarse en células luminales antes de sufrir una transformación oncogénica (31).

Cabe destacar que, en el ser humano, la hiperplasia benigna de próstata no es una lesión precursora de CaP, y los pacientes con hiperplasia benigna de próstata no tienen una mayor incidencia de CaP.

Por otra parte, la neoplasia intraepitelial prostática (PIN) se caracteriza por la proliferación focal de células atípicas y parece ser el resultado de una expansión clonal

de una sola célula transformada dentro de una glándula o conducto. Aunque la mayoría de las lesiones PIN no presentan progresión tumoral, el PIN de alto grado (HGPIN) se asocia con un alto riesgo de progresión hacia el adenocarcinoma prostático (32), (Figura 4) desarrollándose en la mayoría de los casos (99%) adenocarcinomas, mientras que el 1% restante corresponderían a tumores neuroendocrinos o carcinoma de células pequeñas e incluso subtipos más raros como el carcinoma sarcomatoide (34).

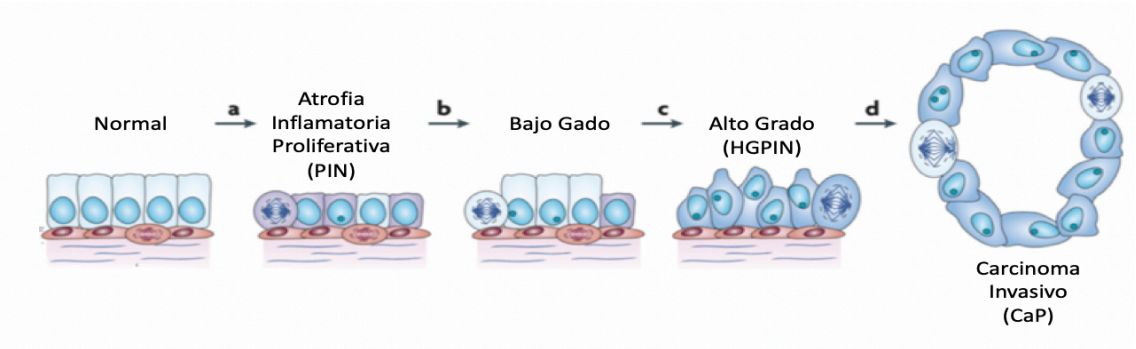

Figura 4. Modelo de la progresión inicial del cáncer de próstata. Fuente: De Marzo, A.M. *et al.* (Inflammation in prostate carcinogenesis) (33).

Por lo general, el crecimiento y desarrollo del CaP es lento y hace que muchos de los pacientes permanezcan indolentes durante 10-15 años o más, por lo que no suelen presentar sintomatología hasta los estadios más avanzados y/o metastásicos, donde ya no existe tratamiento con intención curativa. Esto apoya la necesidad de realizar una detección temprana mediante cribado de poblaciones determinadas.

Actualmente, entre otros indicadores, el diagnóstico de sospecha clínica del CaP se realiza a partir de criterios bioquímicos con el estudio del PSA, el cual se expresa y secreta por las células luminales en humanos. Sin embargo, no existe expresión del PSA en ratones, con lo que el biomarcador para la detección del CaP más empleado es el Antígeno Prostático de Células Madre (PSCA) (35,36), altamente conservado en ratones y humanos. Entre ambas especies existe un 70% de similitud en esta proteína (37). El PSCA, originalmente identificado como un antígeno promotor de tumores específico de próstata en 1998, es una glicoproteína de 123 aminoácidos unida a la membrana celular anclada al glucosilfosfatidilinositol (GPI) y regulada por andrógenos. Pertenece a la familia de antígenos de superficie Thy-1/Ly-6 (37–39). Aunque, la función biológica del

PSCA no se conoce, la familia de genes Ly-6, a la que pertenece, está involucrada en diversas funciones celulares, incluida la transducción de señales y la adhesión célula-célula (37). Aunque PSCA se expresa en algunos tejidos normales, como la vejiga, el colon, los riñones, el estómago o el intestino (40–44), su expresión es mucho mayor en los tumores de próstata. Varios estudios han demostrado que el PSCA aparece sobreexpresado en células tumorales de próstata y en las de metástasis óseas derivadas de este tipo de tumores (37,38,43,45–49). Además, el nivel de expresión de PSCA en la neoplasia intraepitelial prostática de alto grado es cuatro veces mayor que en la hiperplasia prostática benigna (50). Por todo ello, el PSCA es un antígeno tumoral asociado al cáncer de próstata y puede ser usado como biomarcador para su detección.

2.2 Diagnóstico y clasificación del Cáncer de Próstata

Por lo general, el diagnóstico de sospecha clínica del CaP se realiza a partir de criterios bioquímicos con el estudio del antígeno prostático específico (PSA), ecografías abdominales, flujometría de orina para comprobar si existen obstrucciones de la uretra causadas por un aumento del tamaño de la glándula prostática, biopsias y/o tacto rectal.

Actualmente, el desafío en el CaP es la identificación de marcadores tumorales específicos del estadio para diferenciar los tumores indolentes de neoplasias agresivas. El PSA es el marcador sérico más utilizado para diagnosticar el cáncer de próstata temprano y también para controlar el curso de la enfermedad durante y después del tratamiento. El PSA se encuentra de manera abundante en el líquido seminal, donde media su licuefacción después de la eyaculación. Sin embargo, el aumento de PSA no es específico del cáncer y puede elevarse en condiciones no malignas como HBP y prostatitis (51–53).

El sistema de clasificación de Gleason, basado en la interpretación de las características histopatológicas del CaP, es actualmente el método más empleado para clasificar las biopsias de los tumores de próstata. Se definen 5 patrones histológicos, que se nombran como patrones de Gleason 1, 2, 3, 4 y 5 (figura 5) y están basados en las variaciones que se producen sobre la arquitectura glandular en cuanto al tamaño y morfología de las

glándulas fundamentalmente (34,54). El patrón 1 corresponde a un tumor bien diferenciado y por lo tanto poco agresivo y el 5 a un tumor escasamente diferenciado y muy agresivo. Los valores comprendidos entre el 2 y el 4 se asignan a grados de diferenciación intermedia (54).

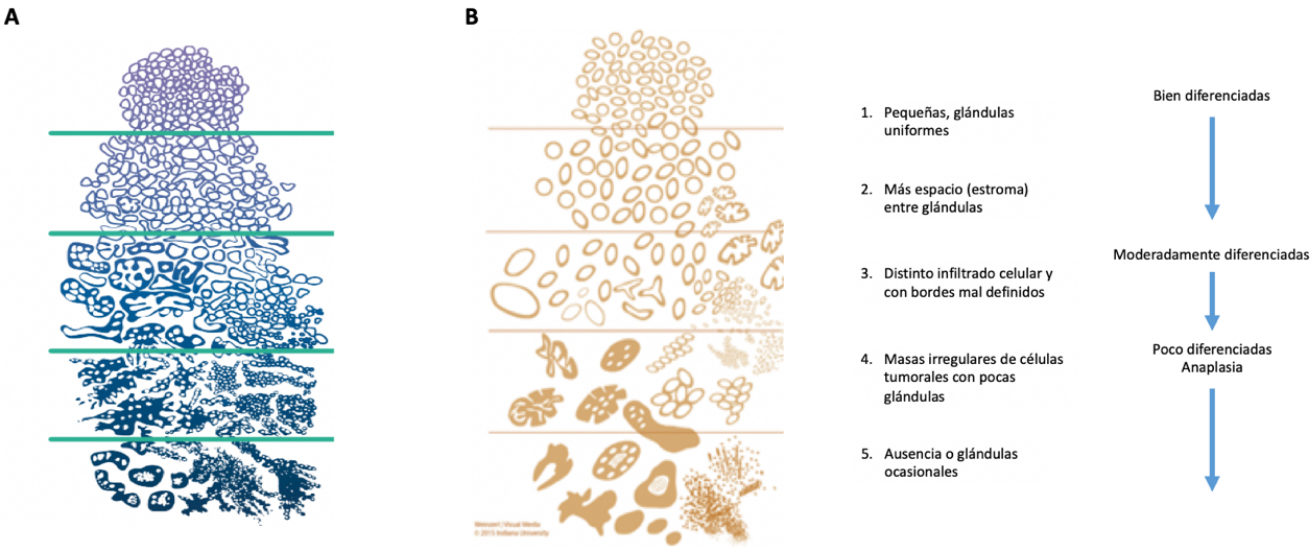

Figura 5: Diagrama histológico clásico de los grados Gleason de clasificación del cáncer de próstata y (B) diagrama de Gleason modificado. Fuentes: Gamé, X. et al. (Total and free serum prostate specific antigen levels during the first month of acute prostatitis) e International Society of Urological Pathology, Universidad de Indiana (51).

Los cinco patrones del grado Gleason se utilizan para generar una puntuación histológica, que puede variar de 2 a 10, sumando la puntuación del patrón de grado primario y el patrón de grado secundario. El patrón primario es el que predomina en el área, mientras que el patrón secundario es el segundo patrón más común (55). A continuación, se detallan los diferentes patrones Gleason:

- El patrón Gleason 1 es extremadamente raro y consiste en un nódulo muy bien circunscrito, glándulas de morfología y tamaño intermedias y uniformes. Las células tumorales no se infiltran en el tejido prostático benigno.

- El patrón de Gleason 2 se caracteriza por presentar glándulas ovales o redondeadas con bordes lisos que se disponen de forma más dispersa. El tamaño

de las glándulas es intermedio y su morfología y tamaño no son tan uniformes como en el patrón de Gleason 1. En este caso puede haber invasión, aunque mínima, de glándulas neoplásicas en la zona sana del tejido prostático.

- El patrón de Gleason 3 es el más común. El tamaño de las glándulas en general es pequeño. Además, las glándulas son irregulares, angulares y más infiltrantes.

- En el patrón de Gleason 4 las glándulas aparecen fusionadas, cribiformes e incluso pueden estar mal definidas. Las glándulas son grandes y generalmente irregulares con bordes dentados.

- El patrón de Gleason 5 se caracteriza por una pérdida casi completa del lumen glandular y por la aparición de células individuales que invaden el estroma. Puede existir necrosis asociada.

Cabe destacar que el sistema Gleason ha sufrido modificaciones significativas. En 2005 y más recientemente en 2014, la Sociedad Internacional de Patología Urológica (ISUP) ha propuesto una distribución en cinco grupos pronósticos (1-5) para su uso en paralelo al sistema de puntuación de Gleason. Este nuevo sistema refleja mejor el comportamiento biológico del CaP facilitando una guía clínica para su tratamiento y ha sido validado en estudios multi-institucionales. Este sistema se describe de la siguiente manera:

- Grado Grupo 1: se define como una puntuación de Gleason ≤6.
- Grado Grupo 2: puntuación de Gleason 3 (primario) + 4 (secundario) = 7.
- Grado Grupo 3: puntuación de Gleason 4 (primario) + 3 (secundario) = 7.
- Grado Grupo 4: puntuación de Gleason 4 (primario) + 4 (secundario) = 8.
- Grado Grupo 5: puntuación de Gleason 9/10.

Además de la clasificación por grados Gleason, también existe la clasificación según el riesgo D'Amico (56,57) (Tabla 1). Este método se basa en agrupar, en cuanto a posibilidad de recidiva bioquímica después del tratamiento, en grupos de riesgo a los

pacientes en función del estadio clínico (cT), niveles de PSA y grado Gleason de la biopsia de próstata. Una vez agrupados obtenemos tres grupos de riesgo: bajo, intermedio o alto (figura 6) como se muestra en la siguiente tabla:

Riesgo Bajo	cT1–cT2a y Gleason <7 y PSA ≤10 ng/mL
Riesgo Intermedio	cT2b o Gleason = 7 o (PSA >10 y ≤20 ng/mL)
Riesgo Alto	cT2c o PSA >20 ng/mL o Gleason >7

Tabla 1. Clasificación en grupos de riesgo según D'Amico

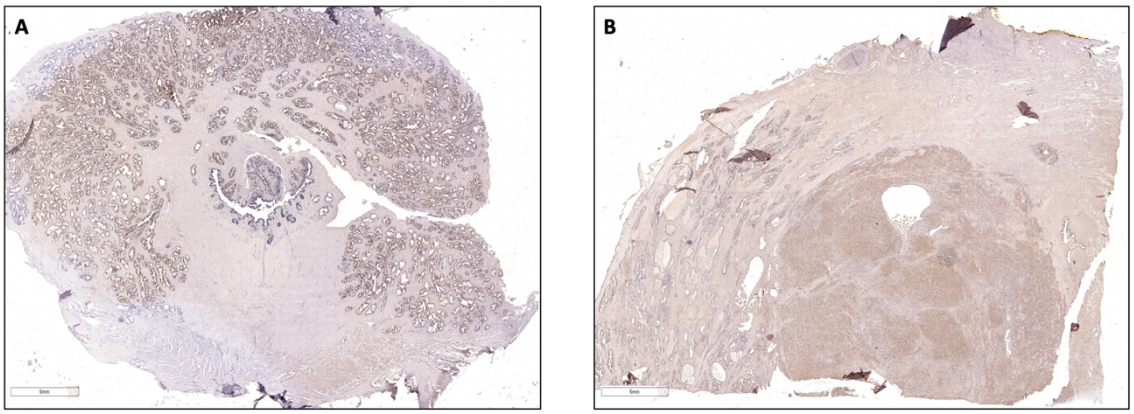

Figura 6: Imágenes histológicas de una próstata humana sana (A) y una próstata humana con un tumor prostático de alto grado (B) según la clasificación en grupos de riesgo según D´Amico. Barra de micras: 6 mm.

2.3 Microambiente óseo

El hueso es un tejido conjuntivo especializado, el cual está formado por una serie de células óseas, una matriz orgánica densa (formada por fibras de colágeno I) y con un alto componente mineral inorgánico (hidroxiapatita). El hueso es el principal componente del sistema esquelético que participa en la locomoción, protección de órganos internos y la homeostasis de calcio (58–60). Es un tejido dinámico que se remodela continuamente, en respuesta a una variedad de estímulos, para preservar su integridad y para garantizar el equilibrio homeostático. El tejido óseo proporciona un microambiente único en el cual, las células residentes como son los osteoblastos, osteocitos, osteoclastos, células hematopoyéticas, células mesenquimales y células inmunes interactúan controlando la estructura, función y remodelado del hueso (Figura 7). Este proceso engloba procesos de resorción ósea, donde los osteoclastos eliminan el

tejido óseo dañado o envejecido, y de formación de nuevo tejido óseo mediado por los osteoblastos. La gran complejidad del tejido óseo viene dada por la función que realizan de manera coordinada todos los componentes celulares que lo constituyen.

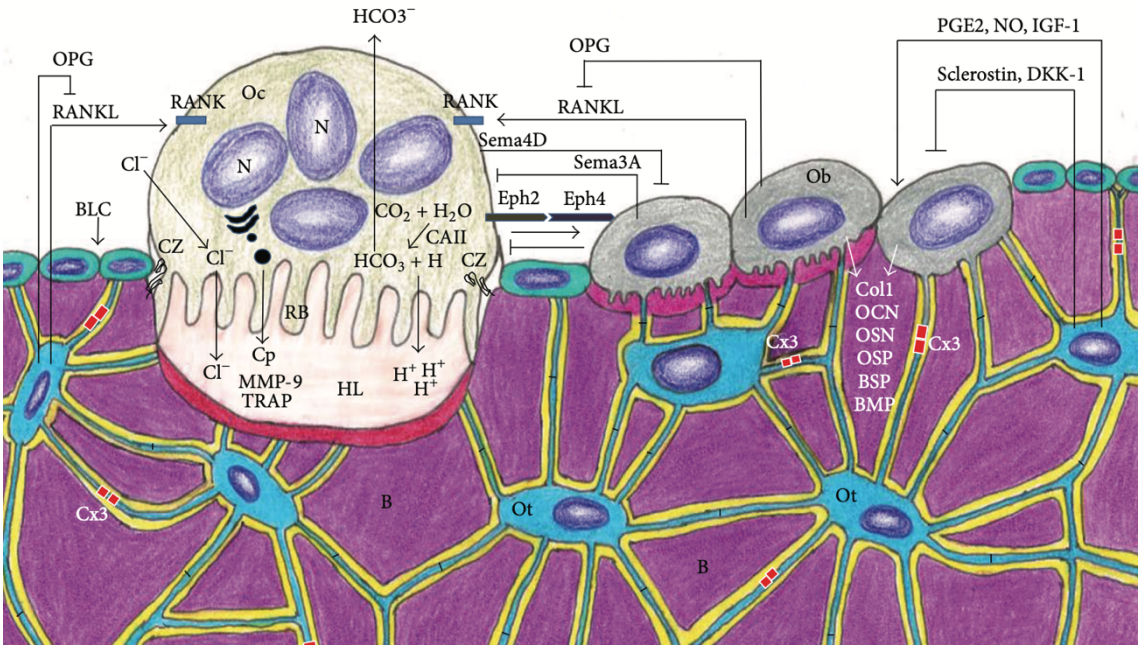

Figura 7: Diagrama de la interacción entre las células óseas. OC: Osteoclastos, cuya función es resorber hueso; BLC: Células de recubrimiento Óseo, las cuales son osteoblastos quiescentes de forma plana que cubren las superficies óseas; OT: Osteocitos, son las células más abundantes en el hueso maduro; OB: Osteoblastos, cuya función es la formación de nuevo tejido óseo. Fuente: Florencio-Silva, R. *et al.* (Biology of Bone Tissue: Structure, Function, and Factors That Influence Bone Cells) (61).

Existen dos variedades de tejido óseo:

1. Hueso trabecular o esponjoso constituido por 3 regiones (Figura 8):
    a. Región exterior o periostio: rodea al hueso y está formado por fibroblastos y células osteoprogenitoras.
    b. Región media o hueso trabecular: formado por un entramado de trabéculas o espículas constituidas por una matriz de colágeno tipo I mineralizada. En la superficie de la trabécula, denominada endostio, se asientan los osteoblastos, los osteoclastos y células de recubrimiento óseo. Embebidos en las trabéculas están los osteocitos, situados en lagunas.
    c. Región interior: es la médula ósea roja en el hueso joven (tejido hematopoyético) o la médula ósea amarilla en el hueso adulto (tejido adiposo que sustituye al tejido hematopoyético). La médula ósea roja se

comunica entre los huecos del hueso trabecular, situándose en ella el tejido hematopoyético con progenitores sanguíneos.

2. Hueso cortical o denso (Figura 8): está formado por estructuras cilíndricas denominadas osteonas. En el centro de la osteona está el canal del Havers, el cual posee vasos sanguíneos e inervaciones nerviosas. Rodeando al canal se disponen laminillas concéntricas de matriz ósea mineralizada. En las laminillas se situan los núcleos de los osteocitos, los cuales, en ambas variedades óseas, se comunican entre sí mediante prolongaciones que transcurren a través de los canalículos calcóforos y conectan por uniones nexo o comunicantes ("GAP"). Este sistema de canalículos y la laguna donde se localizan los osteocitos constituyen el sistema lacunocanalicular. Finalmente, las osteonas adyacentes se comunican entre sí mediante conductos de Volkman, los cuales conectan los canales de Havers de osteonas adyacentes.

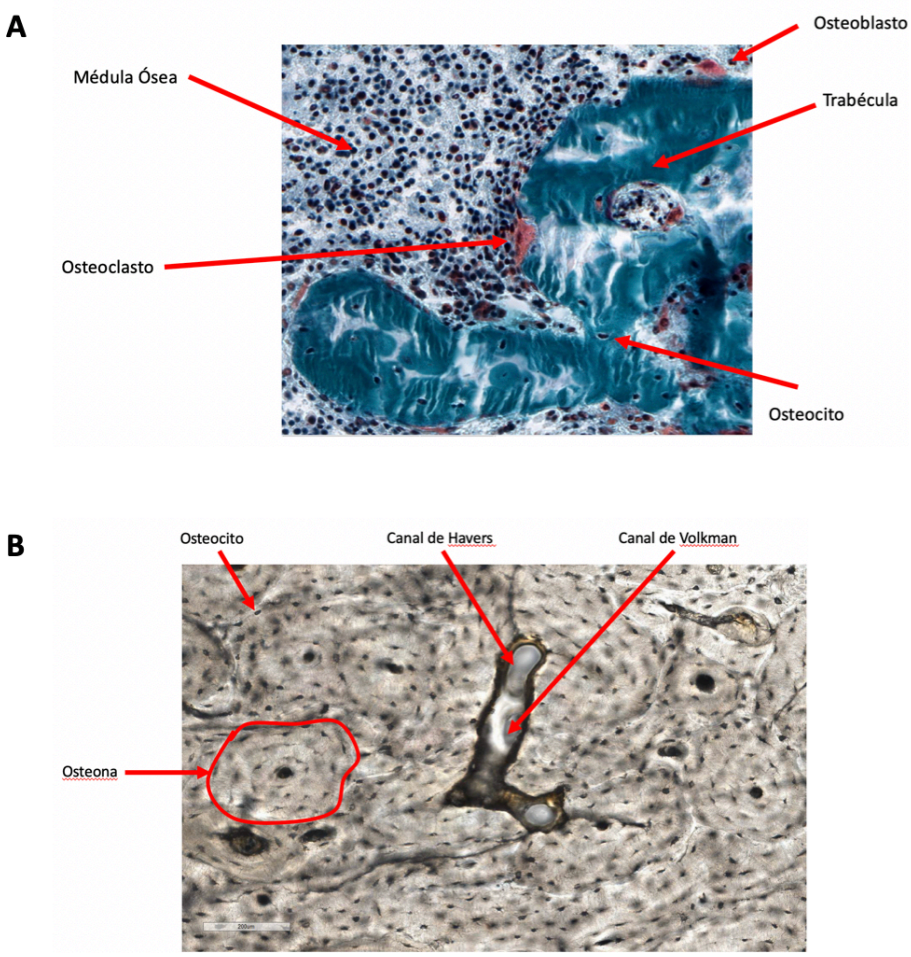

Figura 8: Variedades del tejido óseo. (A) Hueso trabecular o esponjoso teñido con Tricrómico de Goldner (100 micras) y (B) hueso cortical o denso sin teñir (100 micras).

2.4 Componente celular del tejido óseo

En el tejido óseo maduro y en desarrollo, se pueden diferenciar los siguientes tipos de células (62–64) (Figura 9):

Osteoprogenitoras: Las células osteoprogenitoras derivan de las células mesenquimales. Durante la formación del hueso las células osteoprogenitoras se dividen y diferencian hacia el linaje osteoblástico, que son células formadoras de hueso. Esto ocurre sobre todo durante el desarrollo fetal y durante la etapa de crecimiento. En el adulto aparecen sobre todo en relación con la reparación de las fracturas.

Osteoblastos: son células redondeadas o cuboidales ubicadas a lo largo de la superficie ósea. Derivan de células mesenquimales no diferenciadas que también tienen la

capacidad de diferenciarse a condrocitos, adipocitos y mioblastos (65). Comprenden del 4 al 6% del total de las células óseas residentes. Como son células polarizadas, los osteoblastos secretan el osteoide (porción orgánica sin mineralizar de la matriz ósea que se forma con anterioridad a la maduración del tejido óseo) (66). Su función principal es la formación ósea, es decir, son los encargados de la síntesis y secreción de la mayoría de las proteínas de la matriz extracelular ósea y de su mineralización. Además, los osteoblastos también influyen en la diferenciación y activación de los osteoclastos mediante la producción del ligando del receptor activador para el factor nuclear kB (RANKL) y la OSTEOPROTEGERINA (OPG) y, por lo tanto, afectan también a la resorción ósea (67,68).

La síntesis de la matriz ósea por parte de los osteoblastos se produce en dos pasos principales: la deposición de la matriz orgánica y su posterior mineralización. En el primer paso, los osteoblastos secretan principalmente COLÁGENO TIPO I (COL1), proteínas no colágenas (OSTEOCALCINA [OCN], OSTEONECTINA, SIALOPROTEÍNA ÓSEA [BSP] y OSTEOPONTINA) y proteoglicanos, que forman la matriz orgánica. Posteriormente, ocurre la mineralización de la matriz ósea, en esta fase los compuestos que contienen grupos fosfato son degradados por la FOSFATASA ALCALINA secretada por los osteoblastos, liberando iones fosfato. Finalmente, los iones fosfato y el calcio forman los cristales de hidroxiapatita (69–71).

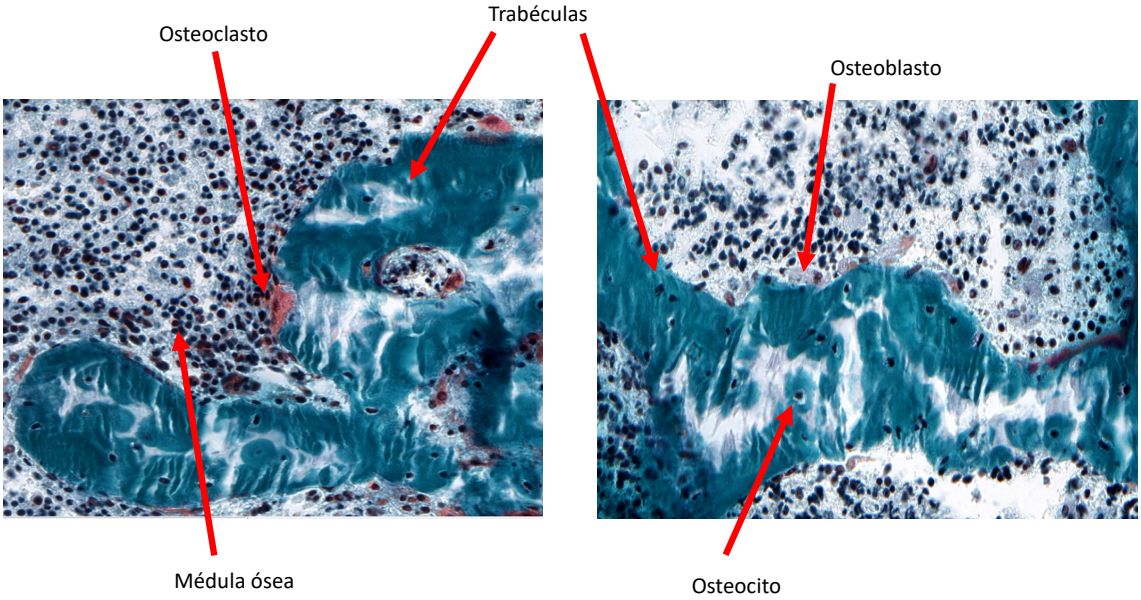

Figura 9: Componentes del tejido óseo. Secciones histológicas de tejido óseo trabecular teñidas con Tricrómico de Goldner (100 micras).

Como se ha comentado anteriormente, los osteoblastos derivan de células madre mesenquimales (MSC) comprometidas hacia el linaje osteoprogenitor. Este compromiso requiere la expresión de genes específicos siguiendo unos pasos programados oportunamente (61). Se ha demostrado que la diferenciación de los osteoblastos depende de dos reguladores transcripcionales principales: el factor de transcripción relacionado con Runt 2 (RUNX2) y OSTERIX (68,72,73), así como de la vía de WNT/β-CATENINA.

El factor de transcripción RUNX2 cumple la función de "interruptor maestro" gracias a sus propiedades únicas para mediar la activación temporal y/o la represión del crecimiento celular, a medida que los osteoblastos progresan por las distintas etapas de diferenciación (74). En la etapa inmadura, RUNX2 fomenta la osteogénesis y se ha demostrado que aumenta la expresión génica del COL1, FOSFATASA ALCALINA, SIALOPROTEÍNA ÓSEA y OSTEOCALCINA (65) (Figura 10). Sin embargo, RUNX2 no es esencial para mantener la expresión de los principales genes en los osteoblastos maduros y debe suprimirse para formar hueso maduro (75) (Figura 10). El nivel de expresión de RUNX2 es importante para el desarrollo óseo normal ya que una expresión disminuida da como resultado un desarrollo óseo incorrecto (76).

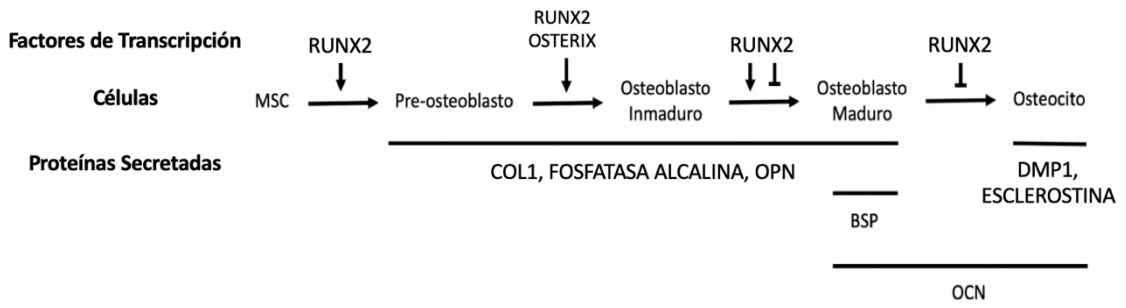

Figura 10: Diferenciación osteogénica. La diferenciación desde MSC a osteoblastos maduros está mediada por la acción de OSTERIX y RUNX2. La actividad de RUNX2 es esencial durante las primeras etapas, sin embargo, su expresión no es esencial en osteoblastos mas diferenciados y debe suprimirse para formar hueso maduro. A lo largo de la vida del osteoblasto, expresará diferentes proteínas según su estado de maduración: COL1, FOSFATASA ALCALINA, OPN, BSP, OCN. ↓:Estímulo necesario para continuar con la diferenciación osteoblástica; ⊥:Estímulo no requerido para continuar con la diferenciación osteoblástica. Finalmente, cuando el osteoblasto se diferencia a osteocito expresará, entre otras proteínas, ESCLEROSTINA, OCN y DMP1. Fuente: Liu, T.M. et al. (Transcriptional regulatory cascades in RUNX2-dependent bone development) (75,76).

Aunque RUNX2 es esencial para la diferenciación de osteoblastos, también es necesaria la participación de otros factores como OSTERIX, factor de transcripción activado por RUNX2, en este proceso (67). OSTERIX se expresa en osteoblastos (73) y condrocitos (77) y que se identificó como un regulador transcripcional para las etapas finales de la formación ósea (73) y activador de los genes de la OSTEOCALCINA y el COLÁGENO (78).

Por otro lado, una de las vías de señalización particularmente importante para la biología ósea es la vía de WNT/β-CATENINA (79,80), ya que WNT aumenta la formación ósea a través de la estimulación de la proliferación y diferenciación de osteoblastos (78,81,82). WNT es una proteína soluble que se une a los receptores de la superficie celular de la familia Frizzled, que a su vez activa a los miembros de las proteínas de la familia Disheveled. Posteriormente, el complejo de proteínas resultante estabiliza y fomenta que la β-CATENINA trasloque al núcleo y promueva múltiples efectos, como la expresión de genes específicos de osteoblastos (4,81,83). En el estado activado de la vía WNT/β-CATENINA, los osteoblastos muestran niveles nucleares de β-CATENINA elevados. Por el contrario, en estado desactivado, los osteoblastos mantienen bajos niveles nucleares de β-CATENINA (78).

Al final de su vida, los osteoblastos maduros pueden sufrir apoptosis, convertirse en células de recubrimiento óseo o embeberse en la matriz ósea y diferenciarse a osteocitos (84).

Células de recubrimiento óseo. Las células de recubrimiento óseo son osteoblastos quiescentes de forma plana que cubren las superficies óseas, donde no se produce formación ni resorción de hueso (85). Algunas de estas células muestran proyecciones de membrana que se extienden hacia los canalículos calcóforos osteocitarios. Además, se observan uniones comunicantes entre células adyacentes de recubrimiento óseo y entre estas células y los osteocitos (85,86).

Las funciones de las células de revestimiento óseo no están claras, pero se ha demostrado que estas células evitan la interacción directa entre los osteoclastos y la matriz ósea cuando no debe producirse la resorción ósea y también participan en la diferenciación de osteoclastos (87,88), por lo tanto parece que juegan un papel importante en la resorción ósea.

Osteocitos: son las células más abundantes en el hueso maduro, comprenden el 90-95% del total de las células óseas, y son las más longevas, con una vida útil de hasta 25 años (89). Los osteocitos se encuentran dentro de lagunas rodeadas de matriz ósea mineralizada, en donde muestran una morfología dendrítica (90–92). Los osteocitos producen RANKL y OPG, entre otras proteínas que son relevantes para la diferenciación osteoclástica.

Al final de un ciclo de formación ósea, una subpoblación de osteoblastos se convierte en osteocitos. El recubrimiento de un osteoblasto por matriz ósea como paso para convertirse en un osteocito se ha visto como un proceso pasivo en el que una subpoblación de osteoblastos en la superficie del hueso ralentiza su producción de matriz en relación con las células adyacentes. Estos osteoblastos son "enterrados vivos" debajo de la matriz producida por los osteoblastos vecinos (89,91,93). Los osteocitos derivan del linaje de las células mesenquimales y todas las etapas de maduración que experimentan a osteoblastos y osteocitos son parte de una diferenciación continua, por lo que diferentes autores han distinguido distintas etapas y diversas características en cada etapa (89). En la Figura 11 se resumen las fases de diferenciación desde el pre-osteoblasto hasta el osteocito.

Una vez han madurado, los osteocitos dejan de expresar varios marcadores osteoblásticos, como son OCN, BSP, COL1 y FOSFATASA ALCALINA. Por otro lado, empiezan a expresar otras proteínas como la proteína de matriz de dentina 1 (DMP1) y la ESCLEROSTINA (94–97).

Mediante el sistema lacunocanalicular, los osteocitos actúan como mecanosensores ya que su red interconectada tiene la capacidad de detectar presiones y cargas mecánicas, ayudando así a la adaptación del hueso a las fuerzas mecánicas diarias (90). De esta manera, los osteocitos parecen orquestar la remodelación ósea a través de la regulación de las actividades de osteoblastos y osteoclastos (92,98). Además, la apoptosis de los osteocitos actúa como una señal quimiotáctica para la resorción ósea (99–101), siendo los osteoclastos responsables de englobar y eliminar a los osteocitos apoptóticos durante el proceso resortivo (102–104).

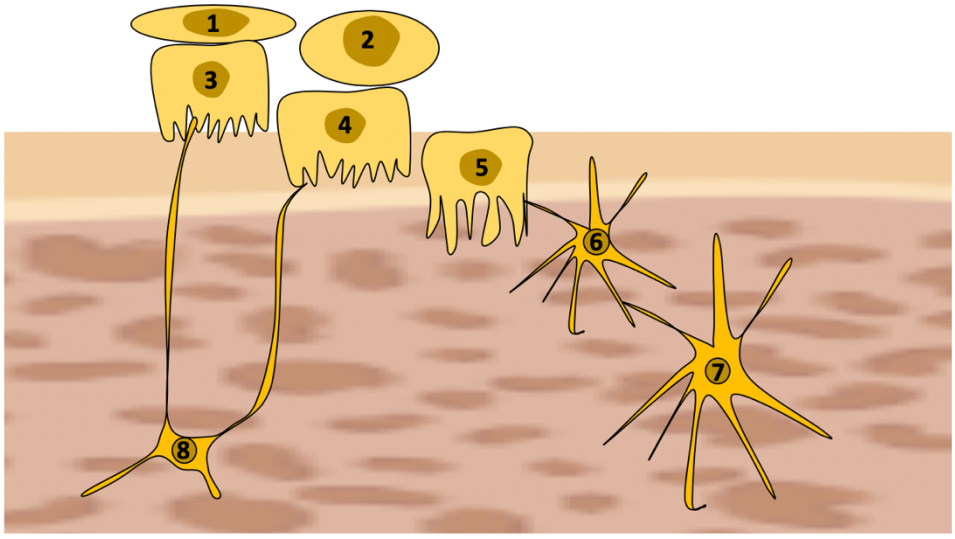

Figura 11: Diagrama que muestra la transición entre pre-osteoblastos y osteocitos. La capa de preosteoblastos (1) consiste en células en proliferación. Las uniones comunicantes están presentes entre todas las células para la comunicación directa. Durante el proceso de transformación, los orgánulos celulares disminuyen y el volumen total del cuerpo celular disminuye sustancialmente. 1) Pre-osteoblasto proliferante, 2) osteoblasto pre-osteoblástico, 3) osteoblasto, 4) osteocito osteoblástico (pre-osteocito tipo I), 5) osteoide-osteocitos (pre-osteocito tipo II), Pre-osteocito tipo III, 7) osteocitos jóvenes, 8) osteocito maduro. Fuente: modificado de Franz-Odendaal, T.A. et al. (Buried alive: How osteoblasts become osteocytes. , Developmental Dynamics) (89).

Osteoclastos: son células con varios núcleos que se originan a partir de células mononucleares del linaje de células madre hematopoyéticas (HSC) y pasan por una serie de etapas de diferenciación que dan como resultado células de resorción ósea multinucleadas que comparten citoplasma (sincitio) (61,105). Los precursores osteoclásticos llegan por los vasos sanguíneos hasta las trabéculas óseas, donde se fusionan entre sí para formar osteoclastos maduros y resorber el hueso (106). Estos precursores expresan el receptor activador para el factor nuclear kB (RANK), la fosfatasa ácida resistente al tartrato (TRAP) y la Catepsina K (105). La TRAP es una metaloenzima de la categoría de fosfatasas ácidas (67) secretada por los osteoclastos activos en la laguna de resorción, donde defosforila la proteína de la matriz ósea OSTEOPONTINA, promoviendo así el desprendimiento y la migración de los osteoclastos (107). Además, activa propiedades metastásicas en las células MDA-MB-231 de cáncer de mama (108) y se ha descrito que su expresión está incrementada en las metástasis óseas derivadas del CaP (109).

2.5 Remodelado óseo: sistema RANK/RANKL/OPG

El hueso se renueva constantemente mediante el proceso de remodelado óseo en respuesta a una gran variedad de estímulos, debiendo existir un balance entre la formación de hueso (por parte de células osteoblásticas) y su destrucción (llevada a cabo por osteoclastos) (78). El remodelado óseo es un proceso estrictamente regulado en el que un gran número de factores influyen en el desarrollo, crecimiento y reparación del hueso. Los mediadores involucrados en la osteogénesis y osteoclastogénesis incluyen: factores de transcripción, factores de crecimiento, citoquinas, metabolitos, hormonas, carga mecánica y edad (78).

Entre los factores que promueven la osteoclastogénesis se incluye el factor estimulante de colonias de macrófagos (M-CSF), secretado por las células mesenquimales osteoprogenitoras y los osteocitos (110), el cual se une a su receptor (CSF1R) presente en los precursores de osteoclastos, lo que estimula su proliferación e inhibe su apoptosis (111,112). Sin embargo, el M-CSF por sí solo no puede completar este proceso.

Otro factor clave en la maduración y activación de los osteoclastos es RANKL, secretado por los osteoblastos y principalmente por los osteocitos (76,106,113). Ambos factores (M-CSF y RANKL) promueven la activación de los factores de transcripción necesarios para la diferenciación y activación osteoclástica (110,111,114).

RANKL se une a su receptor RANK en precursores de osteoclastos induciendo la formación y activación de osteoclastos (115). RANK es un receptor transmembrana homotrimérico perteneciente a la superfamilia de receptores del factor de necrosis tumoral (TNF). Se expresa en la membrana en precursores de osteoclastos, osteoclastos maduros, células dendríticas, la glándula mamaria (116) y en algunas células tumorales derivadas de los cánceres de mama y próstata (117,118), dos tumores con alto potencial metastásico óseo (106).

La mayoría de los factores que estimulan la formación y actividad de osteoclastos inducen la expresión de RANKL por las células estromales osteoblásticas (106). RANKL es un mediador de la función y supervivencia de los osteoclastos y está regulado negativamente por un receptor señuelo, la osteoprotegerina (OPG), la cual es secretada por osteocitos y osteoblastos. OPG es miembro de la familia del receptor del factor de necrosis tumoral soluble, el cual se une a RANKL evitando su interacción con RANK y, por lo tanto, inhibe la resorción ósea (106,119–121). La expresión de OPG está regulada en los osteoblastos por una gran variedad de citoquinas, hormonas, factores de crecimiento (122) y por la vía de WNT/β-CATENINA (123).

La interacción de RANKL con su receptor, RANK, activa la señalización del factor nuclear kappa B (NF-κB) en precursores osteoclásticos y en osteoclastos diferenciados. La familia de NF-κB comprende unos factores de transcripción que regulan positivamente la diferenciación celular y la expresión de muchos genes implicados en respuestas inflamatorias (125,126). Cabe destacar que las células tumorales malignas pueden expresar RANK y RANKL, y por lo tanto, la señalización de RANKL puede regular la proliferación de células tumorales mediante un mecanismo autocrino o paracrino (117). Estudios recientes han descrito también el papel de RANKL como promotor de la migración de células tumorales e inductor de metástasis óseas (121). Respecto a esto,

varios estudios han demostrado que NF-κB promueve la supervivencia celular, la proliferación y la invasión de los tumores de próstata (127–129). Además, la expresión de RANK y su ligando por las células de cáncer de próstata promueve la transición epitelio-mesénquima y la metástasis ósea (118,130) (Figura 12).

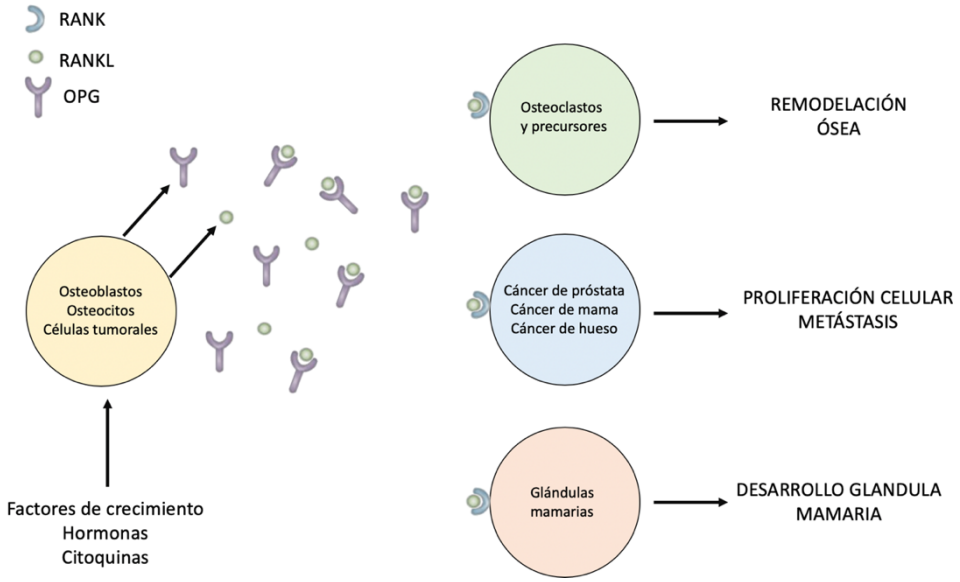

Figura 12: Diagrama del funcionamiento del sistema RANK/RANKL/OPG. Los osteoblastos, osteocitos y células tumorales producen RANKL, el cual se puede unir a su receptor RANK, presente en osteoclastos y sus precursores, células tumorales o células de epitelio de glándulas mamarias. Esta interacción incrementa el remodelado óseo del hueso, la proliferación y la capacidad metastásica de las células tumorales y el desarrollo de la glándula mamaria. OPG, secretado por osteocitos y osteoblastos, evita la interacción de RANKL con RANK, inhibiendo todos los procesos desencadenados por la unión entre RANKL y RANK. Fuente: imagen modificada a partir de Sisay, M. *et al.* (The RANK/RANKL/OPG system in tumorigenesis and metastasis of cancer stem cell: Potential targets for anticancer therapy) (131).

Aunque hay algunos datos contradictorios, en general, cuando la expresión de RANKL aumenta, la expresión de OPG disminuye o no se induce en el mismo grado que RANKL, de modo que la relación RANKL/OPG cambia a favor de la osteoclastogénesis (122,124). El número y la actividad de los osteoclastos pueden aumentar o disminuir si hay un cambio en la relación RANKL/OPG. El número de osteoclastos incrementa si hay un aumento en los niveles de RANKL, una disminución de OPG o un cambio en ambos que conduzca a una modificación en la relación RANKL/OPG a favor de RANKL (106) .

2.6 Metástasis ósea

La metástasis es la principal causa de muerte asociada al cáncer de próstata. Los ganglios linfáticos adyacentes a los tumores primarios son a menudo el primer sitio de metástasis (132), seguidos de metástasis en el hígado, los pulmones y los huesos (los cuales son frecuentemente infiltrados por la diseminación metastásica de tumores sólidos como los de próstata, mama o melanoma) (133–135). Aproximadamente el 15% de los pacientes con CaP antes de ser tratados presentan metástasis, y el 20-30% de los pacientes tratados con terapia local definitiva progresarán a metástasis (136). Paradójicamente, aunque el hueso parece una ubicación inhóspita para el establecimiento de células tumorales, donde solo unas pocas células tumorales pueden colonizar con éxito este lugar (137–140), la gran mayoría de los pacientes con metástasis derivadas del CaP padecen metástasis esqueléticas, siendo en gran medida de tipo osteoblásticas (formadoras de hueso) (141). Las metástasis óseas además pueden clasificarse como metástasis osteolíticas (presentan lesiones causadas por destrucción de hueso) o mixtas (142).

El establecimiento de metástasis óseas es una causa considerable de morbilidad y mortalidad, que a menudo resulta en dolor óseo, compresión de la médula espinal, hipercalcemia y fracturas patológicas, lo que finalmente resulta en la necesidad de cirugía (143).

Las lesiones osteoblásticas se caracterizan por la elevada formación ósea, lo que resulta en un aumento de la densidad mineral ósea (144). Suele darse en los tumores de próstata, de pulmón de células pequeñas o linfoma de Hodgkin. Los mecanismos de las metástasis osteoblásticas todavía son poco conocidos, sin embargo, pueden deberse, en parte, a que las células tumorales promueven la proliferación de osteoblastos (145). En estas metástasis se ha observado en el hueso un incremento del factor de crecimiento transformante β (TGF β), las proteínas morfogénicas óseas (BMP), así como de RUNX2, implicados en la diferenciación de osteoblastos (146). Además, varios estudios demuestran el incremento de los niveles de OPG (147).

Por su parte, las lesiones osteolíticas se caracterizan por la destrucción del hueso y suelen darse en el cáncer de mama, mieloma múltiple, carcinoma de células renales, melanoma, cáncer de pulmón de células no pequeñas, linfoma no hodgkin, cáncer de tiroides o histiocitosis de células de Langerhans. Esta destrucción ósea está mediada principalmente por osteoclastos (148,149). La aparición de una lesión osteolítica está asociada con la producción de RANKL, el cual juega un papel crítico en el desarrollo de estas lesiones por un exceso de activación osteoclastogénica (150,151).

Se ha observado que las metástasis óseas afectan al 65%–75% de los pacientes con cáncer avanzado de próstata y mama (152). Este organotropismo, es decir, que las células tumorales tengan una afinidad particular por el hueso, puede deberse a la adquisición de características osteomiméticas por parte de las células tumorales antes de colonizar el hueso. El osteomimetismo implica que las células tumorales expresen de manera ectópica genes que están restringidos al tejido óseo y que las predisponen a colonizar este tejido. Sin embargo, también es posible que estas células adquieran las características osteomiméticas después de la localización dentro del compartimento óseo. Además, el tumor de próstata y el microambiente óseo se comunican e interactúan entre sí a lo largo de la progresión de la metástasis esquelética (153). Paget desarrolló la hipótesis de "seed and soil" para explicar el tropismo de las células tumorales a un órgano específico (138), sin embargo, ahora se reconoce claramente que existe un determinante genético en el tropismo y el proceso de colonización ósea. Además, se ha demostrado la existencia de una "firma molecular" adquirida por las células tumorales dentro del tumor primario lo que les permite extenderse y colonizar el tejido óseo (154).

Las células tumorales diseminadas, que son capaces de alcanzar el hueso, se depositan en la médula ósea y entran en un estado latente en nichos específicos donde se adaptan al microambiente óseo. En la metástasis ósea se hipotetiza que las células tumorales albergan nichos específicos como el nicho endosteal, el nicho de células madre hematopoyéticas y el nicho vascular (161). Sin embargo, la proximidad de los tres nichos óseos dificulta su estudio de manera independiente en la metástasis ósea.

El nicho endosteal es una estructura especializada que bordea la superficie interna del hueso, en el cual existe una alta presencia de osteoblastos. Shiozawa y colaboradores mostraron que las células de cáncer prostáticas compiten con las células madre hematopoyéticas por ocupar este nicho. Recientemente se ha demostrado que si se incrementaba el número de nichos se producía también un incremento en el número de células tumorales que llegaban hasta él. Por el contrario, la ablación del nicho endosteal daba como resultado una disminución de células tumorales en el hueso. Estos datos sugieren la existencia de dos tipos de nichos metastásicos: el nicho pre-existente, como es el nicho endosteal, y el inducido o nicho pre-metastasico, el cual sufre modificaciones para que se puedan establecer las células tumorales (155).

Por su parte, el nicho de células madre hematopoyéticas es rico en quimioquinas como CXCL12, por lo que atrae células tumorales positivas para su receptor CXCR4. De manera similar a lo que ocurre en el nicho endosteal, las células tumorales compiten con las células hematopoyéticas para la colonización (156,157).

Finalmente, el nicho vascular también juega un papel importante en la metástasis ya que se ha demostrado que la durante la extravasación, dentro del órgano metastásico, las células tumorales permanecen estrechamente asociadas con los capilares. Estas células tumorales invasoras se extienden a lo largo de la lámina basal que rodea los capilares y proliferan, modificando la red vascular (158).

Las células tumorales diseminadas pueden volverse activas años después a medida que proliferan y alteran las funciones de las células óseas, lo que altera la remodelación ósea fisiológica y promueve la destrucción del esqueleto. A su vez, la liberación de factores de crecimiento derivados del hueso, como TGF-β, factor de crecimiento similar a la insulina 1 (IGF-1) y calcio (Ca^{2+}) del hueso, promueve el crecimiento tumoral (159,160). Debido a la liberación de estos factores se establece un "ciclo vicioso" entre el tumor y el hueso basado en la secreción de factores óseos que inducen la proliferación de la células tumorales (161). Además, se ha sugerido que la adquisición de propiedades osteomiméticas aumenta el potencial metastásico esquelético de las células de cáncer

de próstata al aumentar la migración y la localización de las células tumorales en el microambiente óseo (162–166). También se ha demostrado que, en las metástasis óseas, las células tumorales promueven la producción de RANKL por parte de las células del linaje de osteoblastos (167–170). Además, la secreción de RANKL soluble por parte de las células tumorales activa directamente los osteoclastos y está estrechamente relacionado con la supervivencia del paciente con CaP (171–173). Todos estos datos sugieren que se produce un ciclo vicioso en el que las células tumorales que expresan estos genes influyen en el entorno esquelético induciendo, a su vez, la liberación de varios factores por parte de los osteoblastos, los osteoclastos y los osteocitos, los cuales aumentan la proliferación y señalización de las células metastásicas.

2.7 Factor regulador del intercambio de Na+/H+ 1 (NHERF1) y cáncer

Los factores reguladores del intercambio de sodio (Na^+)/hidrógeno (H^+), o NHERF, son una familia de proteínas adaptadoras formada por 4 miembros (174) (Figura 13). NHERF1 (también conocido como fosfoproteina de unión a Ezrina-radixina-moesina 50 [EBP50]), y NHERF2 poseen dos dominios en tándem tipo 1 de PSD-95/Discs Large/ZO-1 (PDZ) y un dominio de unión a ezrina (EBD) en el carboxilo terminal. Los dominios PDZ muestran una identidad del 74% entre sí (174–176), y se unen con la β-CATENINA a través de su dominio PDZ2 (177). La inhibición de la expresión NHERF1 induce la translocación de la β-CATENINA al núcleo e induce la transición epitelio mesénquima en las células epiteliales (177,178).

NHERF1 y NHERF2 son los factores NHERF que presentan mayor distribución de las cuatro proteínas. Además, tienen la capacidad de homo o heterodimerizar y existe una mayor expresión de estas proteínas en tejidos que poseen un epitelio polarizado, localizándose principalmente en la zona apical de las células epiteliales humanas (174,179). NHERF1 se encuentra predominantemente en membranas apicales con borde en cepillo, aunque también está presente en las membranas basolaterales (180,181). Su función se basa en el reclutamiento de receptores y transportadores de membrana, así como proteínas de señalización citoplasmáticas y co-activadores transcripcionales regulando procesos como la proliferación celular, la supervivencia, la

apoptosis, la migración y la invasión (174,182–187). Además, se ha descubierto que NHERF1 tiene un papel importante durante la osteoblastogénesis (188).

También es capaz de reclutar al supresor tumoral PTEN para inactivar la vía de señalización PI3K/AKT en el glioblastoma multiforme (189–191), así como para proporcionar estabilización cortical a la β-CATENINA en las uniones celulares en fibroblastos embrionarios murinos (192), ambos indicativos de una función supresora de tumores. A pesar de esto, NHERF1 aparece sobreexpresado en el carcinoma hepatocelular y la sobreexpresión citoplasmática de NHERF1 también se ha relacionado con la progresión del carcinoma colorrectal (177,193).

No obstante la relación existente entre NHERF1 y el cáncer no se conoce, aunque estudios de expresión génica sugieren que la sobreexpresión de NHERF1 está asociada con características tumorales agresivas y mal pronóstico en algunos tumores (179,184,186,193–196), Zheng y colaboradores sugieren un papel supresor tumoral para NHERF1 en el cáncer cervical. Además, estudios *in vitro* han demostrado un papel inhibidor de NHERF1 en el crecimiento tumoral (183–185,192), lo que sugiere que NHERF1 funciona como un supresor tumoral.

Figura 13: Esquema de los dominios proteicos de los miembros de la familia NHERF. NHERF-1 y NHERF-2 poseen 2 dominios PDZ y un dominio EBD. NHERF-3 y NHERF-4 poseen 4 dominios PDZ y no tienen ningún dominio EBD. Fuente: imagen modificada a partir de Ardura, J.A. et al. (Regulation of G Protein-Coupled Receptor Function by Na+/H+ Exchange Regulatory Factors) (174).

En el cáncer de próstata, un estudio inmunohistoquímico en 237 casos reveló una expresión diferente de NHERF1 entre tejidos normales o tumorales. La expresión más alta de NHERF1 se detectó en el HGPIN, mientras que la más baja se detectó en el adenocarcinoma prostático y en las metástasis derivadas de este tipo de tumor (175). En contraste con este estudio, Quiang Ma y colaboradores demostraron que NHERF1 estaba involucrado en la regulación de los comportamientos malignos en las células tumorales prostáticas PC3M, lo que sugiere que este factor podría tener un papel oncogénico (197).

2.8 MINDIN

Las ESPONDINAS son un grupo de proteínas que se secretan a la matriz extracelular y pertenecen a la superfamilia de TROMBOESPONDINAS (TSP). Se encuentran en organismos eucariotas, y están evolutivamente conservadas agrupándose en diferentes familias (198):

1. Familia R-ESPONDINA
2. Familia del ÓRGANO SUBCOMISURAL (SCO-ESPONDINA)
3. Familia M-ESPONDINA
4. Familia ESPONDINA.

Al ser miembros de la familia TSP tienen estructuras modulares complejas que permiten a las ESPONDINAS participar en diversas funciones biológicas vitales. Se ha demostrado que, en el hueso, las R-ESPONDINAS activan la señalización WNT canónica (314–316), lo que activa el remodelado óseo. Entre otras funciones biológicas de las ESPONDINAS destacan la regulación del desarrollo del esqueleto, la formación de extremidades y el mantenimiento de la masa ósea adulta (R-ESPONDINA) (199,200), regulación de células madre (R-ESPONDINA) (201–203), interacción neurona-glía, diferenciación y desarrollo neuronal (SCO-ESPONDINA) (204,205), interacción con la proteína precursora β-AMILOIDE (APP) y su proteólisis controlada (F-ESPONDINA) o para iniciar respuestas inmunes innatas y adaptativas (M-ESPONDINA) (206,207).

MINDIN, también conocida como ESPONDINA-2 (SPON-2) y DIL-1, pertenece a la familia ESPONDINA. En humanos esta proteína consta de 331 aminoácidos y estructuralmente posee un péptido señal en el extremo N-terminal (residuos 1-26), un dominio de F-ESPONDINA (residuos 31-221) que media la unión a integrinas y contiene 2 secuencias conservadas denominadas dominio FS1 y dominio FS2. Por último, posee un tercer dominio que contiene repeticiones de TROMBOESPONDINA tipo 1 (TSR1) (residuos 277-331) y que se localiza en el extremo C-terminal y es capaz de unirse a lipopolisacáridos bacteriano (198,206,208,209) (Figura 14).

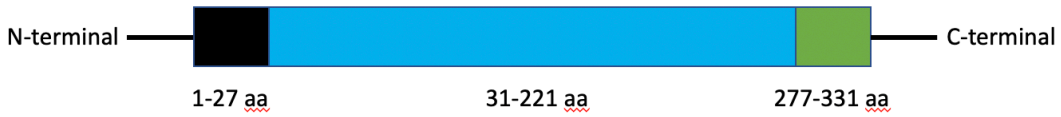

Figura 14: Diagrama de los dominios proteicos de la MINDIN. Negro: péptido señal; azul: dominios F-ESPONDINA; verde: dominio TSR (198,206,208–210).

Es una proteína muy conservada donde la proteína madura de ratón comparte el 88% y 99% de identidad de secuencia con los ortólogos humanos y de rata, respectivamente (207) (Figuras 15, 16).

MINDIN es esencial para iniciar respuestas inmunes innatas y adaptativas. Se ha demostrado que es un receptor de reconocimiento de patrones para patógenos bacterianos y funciona como una opsonina para la fagocitosis de bacterias por macrófagos (206,207). Sin embargo, los mecanismos de la fagocitosis mediada por MINDIN no están bien descritos (207,211).

Además, la interacción MINDIN-Integrina es crítica para el reclutamiento de células inflamatorias *in vivo* (212) y sirve como ligando para las integrinas leucocitarias (206). Es fundamental para la estimulación de células T y el reclutamiento de macrófagos y neutrófilos en zonas de inflamación (212,213), regula el tráfico de eosinófilos y granulocitos al espacio aéreo y desempeña un papel en el desarrollo de la alergia en las vías respiratorias (214). Actualmente se desconoce cuál es su receptor aunque se ha

demostrado que las integrinas $\alpha_M\beta_2$ y $\alpha_4\beta_1$ son ligandos de la proteína en neutrófilos (206,212).

```
CLUSTAL O(1.2.4) multiple sequence alignment

sp|Q9BUD6|SPON2_HUMAN       MENPSPAAALGKALCALLLATLGA-AGQPLGGESICSARALAKYSITFTGKWSQTAFPKQ 59
sp|Q8BMS2|SPON2_MOUSE       ME--NVSLALGRALWVFLLAMIGSTTSQPLGGESVCTARPLARYSITFIGKWSQTAFPKQ 58
                            **  . : ***:**.:*** :*: :.*******:*:** **:***** **********

sp|Q9BUD6|SPON2_HUMAN       YPLFRPPAQWSSLLGAAHSSDYSMWRKNQYVSNGLRDFAERGEAWALMKEIEAAGEALQS 119
sp|Q8BMS2|SPON2_MOUSE       YPLFRPPAQWSSLLGAAHSSDYSMWRKNEYVSNGLRDFAERGEAWALMKEIEAAGEKLQS 118
                            ****************************:************************** ***

sp|Q9BUD6|SPON2_HUMAN       VHEVFSAPAVPSGTGQTSAELEVQRRHSLVSFVVRIVPSPDWFVGVDSLDLCDGDRWREQ 179
sp|Q8BMS2|SPON2_MOUSE       VHAVFSAPAIPSGTGQTSTELEVHPRHSLVSFVVRIVPSPDWFVGIDSLDLCEGGRWKEQ 178
                            ** ******:********:****: ********************:******:*.**:**

sp|Q9BUD6|SPON2_HUMAN       AALDLYPYDAGTDSGFTFSSPNFATIPQDTVTEITSSSPSHPANSFYYPRLKALPPIARV 239
sp|Q8BMS2|SPON2_MOUSE       VVLDLYPHDAGTDSGFTFSSPNFATIPQDTVTEITASSPSHPANSFYYPRLKSLPPIAKV 238
                            ..******:*****************************:****************:******:*

sp|Q9BUD6|SPON2_HUMAN       TLVRLRQSPRAFIPPAPVLPSRDNEIVDSASVPETPLDCEVSLWSSWGLCGGHCGRLGTK 299
sp|Q8BMS2|SPON2_MOUSE       TFVRLQQSPRAFAPPSLDLASRGNEIVDSLSVPETPLDCEVSLWSSWGLCGGPCGKLGAK 298
                            *:***:****** **:  * **.****** ********************** **:**:*

sp|Q9BUD6|SPON2_HUMAN       SRTRYVRVQPANNGSPCPELEEEAECVPDNCV      331
sp|Q8BMS2|SPON2_MOUSE       SRTRYVRVQPANNGTPCPELEEEAECAPDNCV      330
                            **************:***********.*****
```

Figura 15: comparación de secuencias proteicas entre la proteína MINDIN de ratón y la humana. *posiciones que tienen un residuo único y totalmente conservado; : indica conservación entre grupos de propiedades muy similares con una puntuación mayor a 0.5 en la matriz PAM 250; . indica conservación entre grupos de propiedades débilmente similares con una puntuación menor o igual a 0.5 en la matriz PAM 250. Fuente: clustal omega.

Fuera del sistema inmune, se ha demostrado que MINDIN promueve la adhesión y el crecimiento de las neuronas embrionarias del hipocampo y es un mediador importante en la lesión isquémica cerebral y la hipertrofia cardíaca (210). Además, se ha sugerido que MINDIN puede servir como marcador para el cáncer de próstata y ovario, así como para la nefropatía diabética (215,216).

Figura 16: Dominio F-ESPONDINA de MINDIN. Fuente: estructura obtenida del NCBI.

Las investigaciones de Renate Parry sugirieron que MINDIN se expresa predominantemente en la próstata (muestras tumorales y normales), y en niveles significativamente más bajos en otros tejidos (217). Además, se ha demostrado que la expresión de MINDIN está enriquecida en líneas celulares derivadas del cáncer de próstata humana en comparación con otras líneas celulares de tumores humanos (218). Además, se ha observado que existe una elevada presencia de MINDIN en el suero de pacientes con CaP en comparación con hombres sanos e incluso la expresión de MINDIN es mayor en muestras de pacientes con metástasis ósea derivada del CaP seguido de pacientes con CaP y sin metástasis y finalmente pacientes con HBP y controles sanos (219). Sin embargo, se desconoce el papel de MINDIN en este tipo de patologías.

3. HIPÓTESIS

Los factores solubles tumorales secretados son capaces de inducir osteomimetismo en las propias células tumorales y modificar componentes celulares del tejido óseo, generando alteraciones en su actividad fisiológica. Estas modificaciones inducirían la formación de un nicho pre-metastásico óseo, creando condiciones fisiopatológicas que permiten la implantación de las células tumorales en dichos nichos óseos.

4. OBJETIVOS

Como objetivo general planteamos definir los mecanismos moleculares y celulares inducidos por el factor del secretoma tumoral MINDIN sobre el tumor primario y el microambiente óseo.

Para alcanzar este objetivo general nos planteamos los siguientes objetivos específicos:

1. Identificación de los factores solubles con capacidad pro-tumorogénica y ostegénica en el secretoma de distintas células tumorales prostáticas.
2. Evaluación clínica del osteomimetismo y del regulador tumoral NHERF1 en relación con la expresión de MINDIN en biopsias humanas de adenocarcinoma prostático.
3. Estudios preclínicos de la expresión de NHERF1 y del osteomimetismo en el tumor primario de próstata inducido en un modelo de ratón en relación con la expresión de MINDIN.
4. Evaluación de los efectos de MINDIN sobre las células tumorales prostáticas de ratón y su relación con el regulador tumoral NHERF1.
5. Estudio de los efectos de la comunicación cruzada de los secretomas de células óseas y tumorales prostáticas.
6. Determinación de los cambios moleculares y celulares que ocurren en el microambiente óseo inducidos por los factores solubles tumorales y el papel específico de MINDIN en un modelo de ratón de tumor prostático pre-metastásico.
7. Estudio de los efectos del secretoma de células tumorales prostáticas y el papel específico de MINDIN sobre las distintas estirpes celulares óseas (osteoblastos, osteocitos y pre-osteoclastos).

5. MATERIALES Y MÉTODOS

5.1 Aprobación ética

Los diferentes estudios tanto con biopsias humanas como en el modelo animal fueron evaluados y aprobados por los distintos comités de ética. El uso de muestras humanas fue aprobado por el Comité de Ética y Ensayos Clínicos (CEIC) de los Hospitales del grupo HM. El procedimiento de experimentación animal fue evaluado por el Comité de Bioética y Bienestar Animal con referencia de aprobación CEBA40.1. Su mantenimiento, cuidado y condiciones experimentales fue realizado en el Servicio de Animalario y Cirugía Experimental de la Universidad San Pablo CEU cuyo nº de registro es EX-029-UC, de acuerdo con las guías institucionales que están contempladas en las leyes y políticas nacionales e internacionales cumpliendo con las pautas ARRIVE.

5.2 Muestras humanas de tejido

Se recogieron 51 muestras de pacientes con adenocarcinoma prostático procedentes de prostatectomías radicales (laparoscópica y laparoscópica asistida por robot) de pacientes intervenidos en el Hospital Universitario HM Norte Sanchinarro (entre 2012 y 2014) diagnosticados de CaP. Los pacientes incluidos en el estudio aceptaron los términos del consentimiento informado del paciente aprobado por el Comité de Ética.

Además, procedentes del Hospital de la Princesa (Madrid), se obtuvieron muestras de 22 tejidos prostáticos sin cambios hiperplásicos subclínicos, obtenidas en el proceso de extracción multiorgánica de órganos para transplante, realizado en varones adultos sanos que fallecieron en accidentes de tráfico y que no habían padecido enfermedades endocrinas ni relacionadas con el tracto genitourinario. La extracción de la próstata se realizó tras la firma del consentimiento informado por los familiares de los fallecidos. El uso de muestras clínicas fue aprobado por el Comité de Ética y de Investigación Clínica del Grupo Hospitalario HM Hospitales y del Hospital de la Princesa (Madrid).

Todas las muestras fueron fijadas durante una semana en paraformaldehído al 4% en PBS (tampón fosfato salino) pH 7,4. Después de la fijación, de cada pieza se obtuvieron

secciones de 2 mm de espesor perpendiculares a la uretra y posteriormente fueron procesadas para la obtención de bloques con la pieza incluida en parafina.

De cada bloque que representaba un caso de CaP o control se efectuaron cortes de 3 µm de espesor con micrótomo (Reichert Jung 2030). Los cortes fueron teñidos con Hematoxilina-Eosina (H-E) para definir la estructura histológica. Las muestras fueron estudiadas según las recomendaciones del Colegio Americano de Patólogos, usando la 7ª edición de la TNM (AJCC/UICC) y clasificados por el servicio de anatomía patológica del Hospital HM Sanchinarro.

Los datos clínicos de muestras humanas se compilaron en una base de datos de muestras de adenocarcinoma siguiendo criterios anatomopatológicos, como la edad, diagnóstico, los niveles de antígeno prostático sérico (PSA), la puntuación Gleason, el riesgo D'Amico, la tinción patológica del Tumor, Ganglio y Metástasis (TNM) y la invasión perineural (ANEXO I: Detalle de los pacientes diagnosticados de cáncer de próstata).

5.3 Modelo animal

El modelo animal se realizó en ratones machos C57BL/6 de tres meses de edad (Charles River, Wilmington, MA) que permanecieron en jaulas en condiciones estándar (temperatura ambiente 20 ± 0.5ºC, humedad relativa 55 ± 5% e iluminación con un fotoperiodo de 12h/12h luz/oscuridad) y sin restricción de movimiento. Además, se mantuvieron con una dieta estándar de pellets (Dieta Global de Roedores con Proteína al 18% de Teklad, Envigo Madison, Wisconsin, EE. UU.) y agua corriente *ad libitum*. Las intervenciones quirúrgicas se realizaron en condiciones asépticas en ratones anestesiados mediante inhalación de isoflurano/inyección de xilazina (10 mg/kg) y ketamina (25 mg/kg). A los ratones se les inyectó en el lóbulo prostático dorsolateral, a través de una incisión en la línea media inferior abdominal, una solución de 50 µL de solución salina tamponada con fosfato (PBS) o una solución con 5 x 10^5 células TRAMP-C1 transfectadas con tres ARNs pequeños de interferencia (siARN) que actúan como silenciadores de la región codificante de MINDIN (s97640; s97638; s87252) (Life Technologies, Paisley, Reino Unido) o con un siARN frente a secuencias no codificantes

("scrambled" siARN) usado como control negativo de la transfección. Esto dio lugar a la existencia de tres grupos de estudio: un grupo control que no desarrolló tumor (al que sólo se le inyectó PBS); un grupo "scrambled" tumoral que desarrolló un tumor que expresaba MINDIN (a los animales de este grupo se les inyectaron células tumorales TRAMP-C1 transfectados con "scrambled" siARN); y un grupo MINDIN siARN tumoral que desarrolló un tumor que no expresaba MINDIN (grupo al que se le inyectó células tumorales TRAMP-C1 con el gen de MINDIN silenciado por siARNs).

La observación de una ampolla bien localizada dentro del lóbulo prostático inyectado fue el criterio considerado para la determinación de una inyección técnicamente aceptable. La cavidad abdominal, el músculo y la piel se cerraron con grapas quirúrgicas. Después de 1 mes, periodo de tiempo suficiente para el desarrollo de tumores primarios detectables sin presencia de metástasis (220), se sacrificaron los ratones y se extrajeron las próstatas, las cuales fueron almacenadas en Trizol para su posterior análisis mediante PCR en tiempo real. Además, se recogieron los fémures y tibias para realizar los estudios histomorfométrícos óseos y determinaciones génicas, respectivamente.

5.4 Histomorfometría ósea

5.4.1 Inclusión de las muestras en metilmetacrilato (MMA)

Se preparó una disolución de metilmetacrilato, la cual contenía metil-metacrilato (MMA) 0,8 M (Merck), dibutil-ftalato 16 mM (Sigma) y peróxido benzoico 160 mM (Sigma).

Los tubos de vidrio de fondo plano 25 X 90 mm (BI Médica–Barna Import Médica-N504/40), con una base de MMA polimerizada previamente, se llenaron con la mezcla de MMA hasta una altura de 2,5 cm y se sometieron a 32ºC (en estufa) hasta que la mezcla polimerizó y se endureció.

A continuación, se deshidrataron las muestras de fémur con etanol 96% (24 horas) y etanol 100% (24 horas). Tras este proceso, se colocaron las muestras en los tubos de

vidrio con MMA, y se almacenaron a 4ºC. Cada una de las muestras óseas impregnadas en MMA se colocaron sobre una base polimerizada en los tubos preparados previamente y se rellenaron con la mezcla de MMA.

Los tubos de vidrio se incubaron a 30ºC en la estufa, tapados herméticamente con parafilm dentro de un tubo de 50 mL. Se realizaron evaluaciones del estado de viscosidad del MMA cada 24 horas. La polimerización se produjo entre dos y siete días. Cuando el MMA polimerizó, se sacaron los tubos de la estufa y se rompió el vidrio, con lo que se liberó el bloque de MMA con la muestra en su interior.

5.4.2 Corte de las muestras

Utilizando una sierra isomet 1000 se eliminó el metilmetacrilato que quedaba por debajo de la muestra hasta llegar al plano donde se situaba la muestra. Se colocó el bloque en el portamuestras del microtomo (Leica RM 2255) y se realizaron cortes a 7µm. Las muestras cortadas se recogieron con pinzas y se colocaron sobre un portaobjetos previamente preparado con gelatina de Haupt. Después, se colocó encima un film de polietileno. Se apilaron los cortes con el film de polietileno hasta agrupar 20 o 30 portas. Se colocaron en una prensa con unos soportes de madera, entre los portaobjetos y la prensa, y se hizo presión hasta que el paquete ofreció resistencia. La prensa con el bloque de cortes se dejó en la estufa durante toda la noche a 60ºC.

5.4.3 Tinciones

Se seleccionan dos cortes por muestra: uno para tinción Von Kossa, la cual tiñe el hueso calcificado en negro y el osteoide en rosa. Usando el objetivo 4x, medimos tres parámetros con esta tinción: área medular o total, área trabecular y longitud trabecular.

El otro corte se usó para la tinción con Tricrómico de Goldner, con la cual observamos en azul (hematoxilina férrica) los núcleos celulares; en rojo/rosado (Pounceau de xilidina) los ribetes de osteoide, y en verde (verde luz) el hueso mineralizado/calcificado.

Esta tinción es la más apropiada para visualizar los osteoblastos y osteoclastos. Utilizando el objetivo de 20X medimos el número de osteoblastos y osteoclastos.

Las muestras se introdujeron en metilacetato (*Merck*) durante 15-30 minutos para eliminar el MMA. Tras esto, se hidrataron: etanol 100%, etanol 70%, etanol 50% (5 minutos en cada uno) y agua destilada (Figura 17).

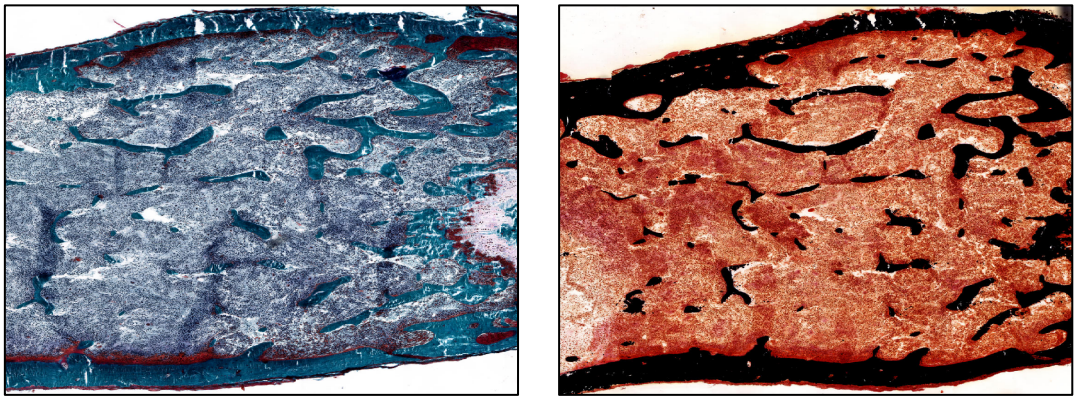

Figura 17: Muestras teñidas con Tricrómico de Goldner (Izquierda) y Von Kossa (derecha). El hueso calcificado aparece teñido de verde (tricrómico) o negro (von Kossa)

5.4.4 Análisis de las tinciones

Una vez teñidas las muestras, se analizaron en un microscopio óptico con una rejilla incorporada (Figura 18). De acuerdo a las recomendaciones de la "American Society for Bone and Mineral Research" (ASBMR), utilizamos la nomenclatura estandarizada, los símbolos y las unidades del Comité de Nomenclatura de Histomorfometría de la ASBMR (221). A partir de los valores obtenidos se calcularon los siguientes parámetros: volumen óseo/volumen total de tejido (BV/TV), espesor trabecular (Tb.Th), separación trabecular (Tb.Sp), número trabecular (Tb.N), número de osteoblastos/perímetro óseo (N.Ob/Pm) y número de osteoclastos/perímetro óseo (N.Oc/Pm).

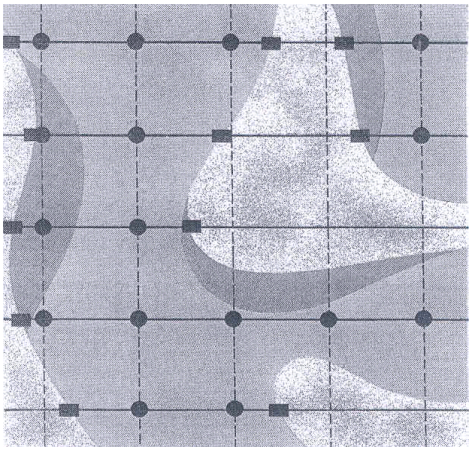

Figura 18: Rejilla acoplada al microscopio óptico

5.5 PCR en tiempo real

El ARN total de las muestras de tibia de ratón almacenadas en "RNA later" o de células fue aislado mediante un procedimiento estándar (Trizol, Life Technologies). Se usaron 200 µL de cloroformo por cada mililitro de Trizol utilizado, se agitó y se dejó reposar durante 15 minutos. A continuación, se centrifugó a 12000g durante 15 minutos a 4ºC, recuperándose la fase incolora superior e incubándose con 0.5 mL de isopropanol por cada mililitro de Trizol usado y durante 15 minutos. Tras los 15 minutos, se centrifugaron las muestras a 12000g durante 10 minutos a 4ºC y se descartó el sobrenadante por decantación. Finalmente, se realizaron lavados con 1 mL de etanol al 75% por cada mililitro de Trizol usado. Se secaron los pellet y se resuspendieron en 30 µL agua. Las muestras fueron almacenadas a -80ºC.

Posteriormente, se realizó la retrotranscripción de 2 µg de ARN con un kit de retrotranscripción de ADN complementario (ADNc) de alta capacidad (Applied Biosystems, Grand Island, NY, EE.UU.). Las muestras de ADNc se diluyeron 1:5 con agua estéril DEPC (pirocarbonato de dietilo) y se almacenaron a -40ºC.

El estudio de expresión por PCR en tiempo real se realizó en base a la emisión de fluorescencia del fluorocromo SYBR Green premix ex Taq (Takara, Otsu, Japón), utilizando un sistema ABI PRISM 7500 (Applied Biosystems). El fluorocromo SYBR Green,

específico de ADN de doble cadena, se une al ADN inmediatamente después de ser sintetizado. La fluorescencia detectada es proporcional a la cantidad de ADN formado. La reacción de PCR se llevó a cabo en placas de 384 pocillos (Durviz) en un volumen de 10 µl (1 µl de ADNc, 3,5µL de agua DEPC, 0,25 µl de cada cebador y 5 µl de SYBR) y con el siguiente programa:

Ciclos	**Temperatura**	**Tiempo**
1	95ºC	10 minutos
45	95ºC 60ºC 72ºC	15 segundos 15 segundos 15 segundos
1	95ºC 65ºC 95ºC	0 segundos 15 segundos 0 segundos
1	40ºC	30 segundos

En la tabla que aparece a continuación se detallan los genes analizados y las proteínas que codifican. Aparecen nombrados según los estándares de nomenclatura para genes y proteínas (“Guidelines for Formatting Gene and Protein Names”, BioScience writters). Durante el texto se hará siempre referencia al nombre de la proteína codificada.

Gen	**Proteína Codificada**
Acp5	TRAP
Actb	β-ACTINA
Alpl	FOSFATASA ALCALINA
Bglap	OSTEOCALCINA
Ctnnb1	β-CATENINA
Kdr	VEGFR2
Psca	PSCA

Rna18s5	18S
Runx2	RUNX2
Slc9a3r1	NHERF1
Sp7	OSTERIX
Tnfrs11a	RANK
Tnfrsf11b, Opg	OPG
Tnfsf11	RANKL
Vegfa	VEGF

Además, los cebadores ("primers") de ratón, y sus temperaturas de fusión (T_m), utilizados se resumen en la siguiente tabla:

Cebador	**Forward (5'--->3')**	**Reverse (5'--->3')**
β-ACTINA (222)	GAACCCTAAGGCCAACCGTG T_m=61.1	ACCAGAGGCATACAGGGACAG T_m=63
β-CATENINA	ATGGAGCCGGACAGAAAAGC T_m=59,8	TGGGAGGTGTCAACATCTTCTT T_m=60,9
FOSFATASA ALCALINA (222,223)	CCAGAAAGACACCTTGACTGTGG T_m=62,9	TCTTGTCCGTGTCGCTCACCAT T_m=65,2
NHERF1 (224)	TCGGGGTTGTTGGCTGGAGAC T_m=67,3	GAGCTCGCGCAAGTGGCTCT T_m=63,5
OPG (222,223)	CAGAGCGAAACACAGTTTG T_m=54,1	CACACAGGGTGACATCTATTC T_m=57,6
OSTEOCALCINA (222,223)	GCAATAAGGTAGTGAACAGACTCC T_m=59,6	CCATAGATGCGTTTGTAGGCGG T_m=62,4
OSTERIX (223,225)	CTGCCTGACTCCTTGGGACC T_m=62,9	GCCATAGTGAGCTTCTTCCTCAA T_m=61,0
PSCA (226)	TTCTCCTGCTGGCCACCTAC T_m=61,1	GCAGCTCATCCCTTCACAAT T_m=56,8
RANK (223,227)	GCAACCTCCAGTCAGCA T_m=57,0	GAAGTCACAGCCCTCAGAATC T_m=60,3
RANKL (223,228)	TGTACTTTCGAGCGCAGATG T_m=56,6	AGGCTTGTTTCATCCTCCTG T_m=56,8

RUNX2 (222,223)	CCTGAACTCTGCACCAAGTCCT T_m=63,7	TCATCTGGCTCAGATAGGAGGG T_m=62,4
TRAP (223,225)	CACGAGAGTCCTGCTTGTC T_m=57,6	AGTTGGTGTGGGCATACTTC T_m=56,7

Alternativamente, la PCR en tiempo real se realizó con sondas TaqMan MGB específicas de ratón para MINDIN (Mm00513596_m1), VEGF (Mm00437306_m1), VEGFR2 (Mm01222421_m1) y el gen ribosómico 18S (Life Technologies). La reacción de PCR se llevó a cabo en un volumen de 10 µl (1,5 µl de ADNc, 3,25 µL de agua DEPC, 0,25 µl de sonda TaqMan y 5 µl de 2X PCR master mix [Applied Biosystems]) con el siguiente programa:

Ciclos	**Temperatura**	**Tiempo**
1	50ºC	2 minutos
1	95ºC	10 minutos
40	95ºC 60ºC	15 segundos 1 minutos

El número de copias de ARNm se calculó para cada muestra utilizando el valor del ciclo umbral (Ct). Los genes del 18S o β-ACTINA (control interno, "housekeeping") se amplificaron en paralelo como genes control, permitiendo el calculó del número de pasos de amplificación requeridos para alcanzar una intensidad arbitraria Ct. La expresión relativa de los genes se definió como la expresión relativa en comparación con el control calculada como $2^{-\Delta\Delta Ct}$, donde ΔΔCt = ΔCt tratamiento - ΔCt control y ΔCt = Ct gen problema - Ct gen control (18S/ β-ACTINA). La expresión génica de muestras de animales se representó como puntos de datos individuales calculando $2^{-\Delta Ct}$, como se ha descrito previamente (229). La especificidad de cada amplicón se confirmó como la presencia de un único pico en la curva de disociación para cada reacción de qPCR.

5.6 Inmunohistoquímica y cuantificación

Los análisis inmunistoquímicos se llevaron a cabo en secciones de 3 µm de tejidos parafinados. Los cortes de tejido, una vez desparafinados e hidratados, se incubaron durante 30 minutos en oscuridad con una disolución de peróxido de hidrógeno (PanReac AppliChem) al 3% en PBS pH 7,4 con el fin de bloquear la peroxidasa endógena.

A continuación, se procedió a la realización del desenmascaramiento antigénico de las muestras mediante un tampón citrato pH 6 a una concentración de 10 mM. Las muestras se sumergieron en el tampón citrato caliente y se dejó enfriar a temperatura ambiente.

Para evitar uniones inespecíficas se realizó el bloqueo de las muestras mediante solución de bloqueo sérica (Histostain-SP Broad Spectrum HRP, Life Technologies, Frederick, MD, USA) o con una solución con 10% de suero (burro o cabra) en PBS durante 1 hora. Posteriormente, se incubaron los tejidos con el anticuerpo primario durante toda la noche a 4ºC. Los anticuerpos empleados fueron: NHERF1 1:500 (Abcam), MINDIN 1:100 (R&D Systems, Minneapolis, MN) y OSTERIX 1:100 (Abcam).

Al día siguiente, tras lavar con PBS, las muestras se incubaron durante 1 hora a temperatura ambiente con un anticuerpo secundario (anti-raton o anti-cabra, según corresponda) a una concentración 1:1000 y conjugado con HRP (Peroxidasa de rábano) (Santa Cruz Biotechnology). Tras varios lavados, se procedió al revelado mediante incubación con 3,3-diaminobenzidina (DAB, Life Technologies). Las muestras se contratiñeron con hematoxilina diluida (1:4). Finalmente, las secciones se deshidrataron en etanol y se montaron con una resina sintética (Depex, Serva, Heidelberg, Alemania). Como control negativo se utilizó el mismo procedimiento descrito en cortes de tejido salvo la incubación con el anticuerpo primario. Se obtuvieron imágenes de las inmunohistoquímicas realizadas mediante la cámara Leica DFC 425 concectada al microscopio Leica 5500B. La cuantificación de los valores de la intensidad de las tinciones se llevaron a cabo a través del programa Image J.

5.7 Análisis del secretoma mediante espectrometría de masas

El análisis proteómico se realizó con extractos proteicos (50 µg) obtenidos a partir de los medios condicionado de células TRAMP-C1, LNCAP, PC-3, células normales de próstata, osteoblastos humanos, MC3T3-E1 y MLO-Y4. Este análisis fue realizado por la unidad proteica del Centro de Biología Molecular Severo Ochoa perteneciente a ProteoRed, PRB2-ISCIII, con el apoyo de la subvención PT13/0001.

Los extractos proteicos se analizaron mediante cromatografía líquida acoplada a espectrometría de masas seguida de cromatografía líquida de fase inversa acoplada a espectrometría de masas. Todo ello se llevó a cabo en un sistema Easy-nLC II acoplado a un espectrómetro de masas híbrido Velos-Pro LTQ-Orbitrap (Thermo Scientific), como se describió previamente (230). El procesamiento de los datos de espectrometría de masas se llevó a cabo como aparece descrito anteriormente (230). La identificación de péptidos a partir de los datos brutos se llevó a cabo utilizando el algoritmo SEQUEST (Proteome Discoverer 1.3, Thermo Scientific).

5.8 Cultivos de celulares

Se cultivaron células de adenocarcinoma prostático de ratón TRAMP-C1 (ATCC: CRL-2730) en DMEM suplementado con 5% de suero fetal bovino (SFB [Life Technologies]), 5% de Nu-serum IV, 0,005 mg/ml de insulina bovina y 10 nM de deshidroisoandrosterona. Las líneas celulares humanas de carcinoma prostático LNCaP (ATCC: CRL-1740), células metastásicas andrógeno dependientes de nódulos linfáticos derivadas del cáncer de próstata humano; y PC-3 (ATCC: CRL1435), células metastásicas andrógeno independientes de hueso derivadas del cáncer de próstata humano, se cultivaron en medio RPMI, suplementados con SFB al 10%. La línea celular humana de próstata normal (ATCC: PCS-440- 010) se cultivó con el kit de crecimiento epitelial prostático: medio basal suplementado con L-glutamina 6mM, extracto P 0,4%, epinefrina 1mM, rh TGF-a 0,5 ng/mL, hemisuccinato de hidrocortisona 100 ng/mL, rh insulina 5 mg/mL y apo-transferrina 5 mg/mL. Los pre-osteoblastos de ratón MC3T3-E1 (ATCC: CRL-2593) se cultivaron en α-MEM sin ácido ascórbico mientras que los

monocitos de ratón RAW 264.7 (ATCC: TIB-71) se cultivaron en DMEM, ambos suplementados al 10% con SFB. Los osteocitos de ratón MLO-Y4 (generosamente cedidos por la Doctora Lynda Bonewald) se cultivaron en α-MEM con suero fetal de ternera al 2,5% (SFT) y SFB al 2,5% en una superficie recubierta de colágeno (solución de colágeno de piel de ternera [Sigma-Aldrich, Darmstadt, Alemania]). Todas las células se cultivaron con un 1% de penicilina (100 unidades/ml) y estreptomicina (100 µg/ml) en un incubador humidificado a 37ºC con 5% de CO_2. Los osteoblastos humanos (ATCC: CRL-11372) se cultivaron en un incubador a 34ºC con 5% de CO_2 en un mezcla 1:1 de los medios Ham´s F12 y DMEM con 2,5mM de L-Glutamina y sin rojo fenol. El medio se suplementó con 0,3 mg/ml de G418 y 10% de SFB.

En aquellos experimentos donde los cultivos celulares fueron tratados farmacológicamente con inhibidores, las células fueron pre-tratadas 1 hora antes con el inhibidor (U0126, [Calbiochem]) de la quinasa 1/2 regulada por señal extracelular (ERK 1/2) a una concentración de 5 µM cuando fue apropiado.

Las células se estimularon con 5 ng/ml del péptido recombinante de ratón MINDIN (R&D Systems, Minneapolis, MN) durante 3, 6, 24, 48 o 72 horas o bien 15 o 21 días, según el experimento correspondiente.

Los monocitos de ratón RAW 264.7 se diferenciaron a osteoclastos mediante la estimulación con 35ng/mL del péptido recombinate de ratón RANKL (Peprotech, USA) durante 6 días.

Para la obtención de los medios condicionados (MC), se cultivaron células TRAMP-C1, LNCAP, PC-3, células normales de próstata, MC3T3-E1, MLO-Y4 y osteoblastos humanos hasta alcanzar confluencia en un flask de 75 cm^2 con sus medios de cultivo correspondientes. Al día siguiente, se retiró el medio de cultivo de las células en confluencia, se lavó con PBS y se añadió medio de cultivo sin suero. Tras 24 horas, se recolectó este medio, el cual fue centrifugado a 4800g durante 10 minutos para eliminar restos celulares y de desecho. Los medios condicionados se guardaron a -40ºC para su posterior uso.

5.9 Silenciamiento celular

Las células se sembraron en placas de 6 pocillos a una concentración de 20.000 células/cm^2. Cuando las células sembradas alcanzaron a una confluencia del 70-80%, se silenciaron con una mezcla de tres siARNs (cada uno a 20 nM) contra la secuencia codificante del gen de MINDIN de ratón (s97640; s97638; s87252; Life Technologies, Paisley, Reino Unido), o con dos siARNs contra la secuencia codificante del gen de la β-CATENINA de ratón (s63418; s63419; Life Technologies, cada una a 20 nM), utilizando Lipofectamina RNAiMax (Life Technologies) durante 24 horas a 37ºC.

Para ello, se retiró el medio, se lavó con PBS y se añadieron 700 µl de medio fresco. A continuación, se prepararon los silenciadores. Para cada pocillo se preparó una mezcla con 300 µl de OptiMem al cual se le añadieron 6 µl de lipofectamina RNAiMax y 3 µl en total de silenciadores. La mezcla se vorteó y se dejó reposar 5 minutos. Tras, estos pasos se añadieron los 300 µl de la mezcla a cada pocillo según correspondía.

Se usó una secuencia "scrambled" (control siARN-A, Santa Cruz Biotechnology, Dallas, TX) como control negativo. La eficiencia del silenciamiento de MINDIN y β-CATENINA se evaluó mediante PCR en tiempo real (Figura suplementaria 1).

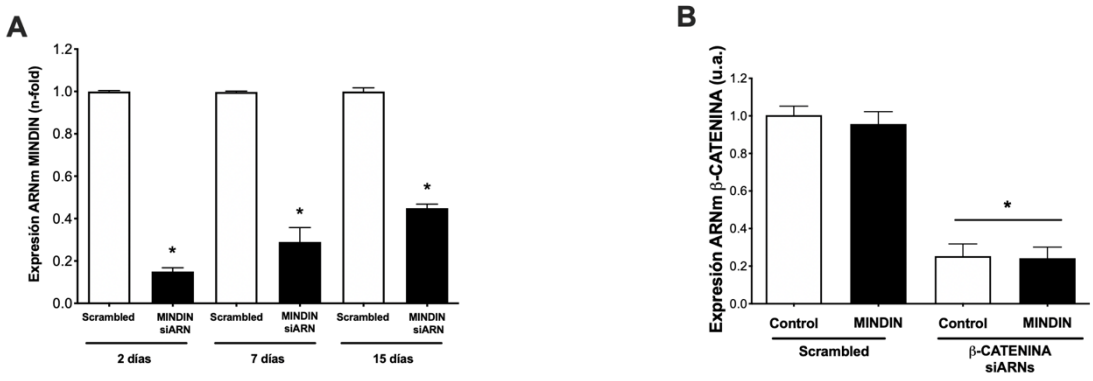

Figura suplementaria 1. Eficiencia del silenciamiento de MINDIN en células TRAMP-C1 y β-CATENINA en células MC3T3-E1. Las células TRAMP-C1 y MC3T3-E1 se silenciaron con diferentes siARNs como se describe en materiales y métodos durante 2, 7 y 15 días. Los resultados se representan como la media ± SEM de tres experimentos independientes por triplicado. *p<0,05 vs "scrambled".

5.10 Transfección transitoria

Las células TRAMP-C1 se sembraron sobre placas de 6 pocillos. Cuando las células alcanzaron una confluencia del 70-80% se procedió a realizar la transfección transitoria con 2 µg de plásmido que codifica para NHERF1 unido a proteína verde fluorescente ("Green Fluorescent Protein" (GFP)-NHERF1) (generosamente donado por Peter Friedman) usando lipofectamina 2000 (Life Technologies) durante 48 horas a 37ºC.

Para la transfección con lipofectamina 2000 se preparó una mezcla con 300 µl de OptiMem a la cual se le añadieron lipofectamina 2000 y plásmido en una proporción 3:1. La mezcla se vorteó y se dejó reposar 5 minutos. Posteriormente, se añadieron 300 µl de la mezcla a cada pocillo según correspondía y se completó con el medio correspondiente hasta 1 mL. Tras 24 horas de transfección, se estimuló con MINDIN según correspondía.

Como control negativo, se transfectaron células TRAMP-C1 con 2 µg del plásmido con vector vacío pCDNA3.1 (generosamente donado por Peter Friedman), siguiendo el mismo protocolo descrito anteriormente.

5.11 Análisis proteico mediante "Western Blot"

Las células se sembraron en placas de 6 pocillos. Cuando llegaron a confluencia fueron estimuladas con MINDIN según el experimento correspondiente. Al finalizar el tiempo de estimulación, las placas se lavaron con un tampón Tris Buffer Salino (TBS) frío sobre hielo. A continuación, se lisaron las células de cada pocillo con 150 µl de buffer RIPA (Sigma) complementado con un cóctel de inhibidores de proteasas Set I (Calbiochem) y un cóctel de inhibidores de fosfatasas Set II (Calbiochem), ambos a una concentración 1:100. Tras 20 minutos en hielo y con el buffer de lisis, se rascaron los pocillos y se guardaron las proteínas a -80ºC durante 24 horas como mínimo. Finalmente, las muestras fueron centrifugadas a 17.900g durante 18 minutos y las proteínas fueron recogidas en el sobrenadante. El contenido de proteína en los extractos celulares se

determinó mediante el ensayo de ácido bicinconínico (BCA) (Thermo Fisher Scientific, Rockford, IL), utilizando la albúmina de suero bovino como estándar.

Las proteínas celulares (30–60 µg/banda) se separaron en geles de poliacrilamida-SDS (dodecilsulfato sódico) al 5-12% en condiciones reductoras. Después de la electroforesis, las muestras se transfirieron a membranas de nitrocelulosa (Bio-Rad, Hercules, CA), se bloquearon con leche desnatada al 5% en TBS con Tween 20 al 0,1%, y se incubaron "overnight" a 4ºC con los siguientes anticuerpos primarios:

ANTICUERPO	CASA COMERCIAL	CONCENTRACIÓN
β-CATENINA (Conejo)	Abcam	1:1000
EBP50 (NHERF-1) (Conejo)	Abcam	1:1000
ERK (Conejo)	Cell signaling	1:1000
LAMINA B (Ratón)	Abcam	1:1000
GAPDH (Ratón)	Abcam	1:1000
OSTERIX (Conejo)	Abcam	1:1000
FOSFO-ERK (Conejo)	Cell signaling	1:1000
FOSFO-β-CATENINA (Conejo)	Cell Signaling	1:1000
RUNX2 (Ratón)	Abcam	1:1000
α-TUBULINA (Ratón)	Abcam	1:10000

Al día siguiente, después de 3 lavados exhaustivos, las membranas se incubaron con los siguientes anticuerpos secundarios conjugados con peroxidasa de rábano (HRP), según correspondía:

ANTICUERPO	CASA COMERCIAL	CONCENTRACIÓN
Anti-cabra (HRP)	Santa Cruz/Abcam	1:1000
Anti-ratón (HRP)	Santa Cruz/Abcam	1:5000 (Tubulina)/1:1000 (resto de anticuerpos)
Anti-conejo (HRP)	Santa Cruz/Abcam	1:1000

Tras 1 hora de incubación, se revelaron mediante quimioluminiscencia con ECL (GE Healthcare, Buckinghamshire, Reino Unido). Los valores densitométricos de las diferentes bandas, obtenidos mediante el programa Quantity One, se normalizaron con los valores de la banda del control α-tubulina o GAPDH correspondiente.

5.12 Inmunofluorescencia

Se cultivaron células pre-osteoblásticas de ratón (MC3T3-E1) en cubreobjetos. Cuando alcanzaron una confluencia del 70-80%, se estimularon con MINDIN, durante 1, 3, 6 o 24 horas. Tras la estimulación, se lavaron con PBS, se fijaron en paraformaldehído al 4% durante 15 minutos y se permeabilizaron con Triton-X-100 al 0,1% durante 5 minutos. Después de bloquear con BSA al 10% durante 1 h, se incubaron con un anticuerpo anti-β-CATENINA a una dilución 1:100 o con NHERF1 a una dilución 1:500 durante toda la noche a 4ºC. Al día siguiente, tras lavar con PBS, se incubaron con un anticuerpo secundario fluorescente Alexa fluor 568 1:500 (Life Technologies) durante 1 hora a temperatura ambiente. Se tiñeron los núcleos con DAPI durante 5 minutos. La ausencia de anticuerpo primario se utilizó como control negativo. Finalmente, se montaron en Fluorsave (Merck KGaA, Darmstadt, Alemania) y se examinaron utilizando un microscopio de epifluorescencia Leica DM-IRB.

5.13 Estudios de proliferación celular

Para los estudios de proliferación celular se sembraron 20.000 células MC3T3-E1 o TRAMP-C1 por pocillo, en placas de 24 pocillos. Al día siguiente fueron estimuladas con 5 ng/ml del péptido MINDIN según corresponda.

Tras 24 horas de estimulación, se recolectaron células de 3 pocillos de cada línea celular y de cada condición (control y estímulo con MINDIN [5 ng/mL]). Se realizaron lavados de cada pocillo con PBS y se incubaron las células con tripsina durante 5 minutos a 37ºC. Posteriormente se inactivó la tripsina con medio de cultivo completo y se recolectaron las células en un tubo junto con el lavado anteriormente mencionado. El tubo se centrifugó durante 5 minutos a 314g y se resuspendió en 1 mL de medio completo. El

número de células vivas y muertas se cuantificó mediante el método por exclusión con azul de tripán en una cámara de Neubauer (231) obteniendo la tasa de proliferación a las 24 horas tras la estimulación. El proceso de recolección de células se repitió a las 48 y 72 horas para obtener los distintos puntos de la curva de proliferación.

5.14 Ensayo de migración o herida

Las células se sembraron y cultivaron en placas de 6 pocillos hasta alcanzar confluencia. A continuación, se realizaron varias heridas por pocillos con una punta de micropipeta de 10 µL. Tras un lavado de los pocillos con PBS estéril, se sustituyó el medio completo por un medio sin SFB y se estimularon con MINDIN (5 ng/mL) o se silenciaron, según correspondiese. Se obtuvieron imágenes de las distintas heridas realzadas a las 0, 24, 72 y 48 horas usando una cámara Leica DFC 425 conectada al microscopio Leica 5500B.

El ensayo de migración se evaluó cuantificando el número de células presentes en las diferentes heridas y relativizándolo frente al área de cada herida.

Alternativamente, como control, la migración se analizó en condiciones anti-proliferativas utilizando células TRAMP-C1 incubadas con 5 µg/ml de mitomicina C (Santa Cruz Biotechnology).

5.15 Experimentos de adhesión celular

La adhesión de las células de adenocarcinoma TRAMP-C1 a superficies cubiertas con colágeno, a tejidos óseos (fémures de ratón), osteocitos MLO-Y4 o pre-osteoblastos MC3T3-E1, se evaluó mediante la cuantificación de células TRAMP-C1 marcadas con calceína-AM (Thermo Scientific) adheridas a dichas superficies. Para ello, las células TRAMP-C1 se pre-incubaron con 2 µM de calceína-AM durante 30 minutos. Posteriormente, se lavaron con PBS y se depositaron 20.000 células/cm^2 sobre las distintas condiciones durante 30 minutos. Las superficies utilizadas fueron: secciones de hueso desparafinado de las distintas condiciones del modelo animal (control, tumoral y tumoral con el gen de MINDIN silenciado), una placa de 24 pocillos pre-incubada con

colágeno, con células MLO-Y4 o MC3T3-E1 en confluencia y en presencia o no del péptido MINDIN (5 ng/mL) durante 24 h. Tras los 30 minutos de incubación las células no adheridas se eliminaron mediante dos lavados con PBS. Estas células, procedentes de ambos lavados y el medio inicial, se recogieron para su posterior contaje mediante el método por exclusión con azul tripán. Por otro lado, las células adheridas a las superficies se fijaron con paraformaldehído al 4% y se obtuvieron imágenes con un microscopio de epifluorescencia (Leica DM-IRB). El número de células marcadas con fluorescencia se contó en 10 campos diferentes por condición.

Con objeto de inhibir la quinasa de adhesión focal (FAK) y la quinasa SRC se añadió 1 µM del inhibidor Fak 14 (Merck) o 1 µM de saracatinib (Santa Cruz) durante 24 horas, respectivamente.

5.16 Ensayo de mineralización: tinción con rojo de Alizarina

Las células pre-osteoblásticas MC3T3-E1 se sembraron en placas de 6 pocillos. Una vez alcanzado el 90% de confluencia, se sustituyó el medio por un medio de diferenciación (alpha-MEM suplementado con ácido ascórbico [50 µg/mL] y β-glicerolfosfato [10mM]) suplementado con 10% de SFB y 1% de penicilina/estreptomicina. Este medio se mantuvo durante 21 días, renovándolo cada 3 días. Además, las células se estimularon con 5 ng/mL de MINDIN, según correspondiese. Como control negativo de diferenciación, se realizó el mismo procedimiento de estimulación con MINDIN pero en ausencia de medio de diferenciación.

Tras 21 días de diferenciación, se llevó a cabo la tinción con Rojo de Alizarina. En primer lugar, las células fueron lavadas con PBS y fijadas con paraformaldheído al 4% durante 10 minutos. Tras la fijación y posteriores lavados con PBS a temperatura ambiente, se tiñeron las células con Rojo de Alizarina a 40 mM (Sigma) durante 1 hora a temperatura ambiente. Finalmente, se lavó con agua destilada para quitar el exceso de colorante.

5.17 Tinción de TRAP

La tinción de TRAP se realizó en fémures de ratón mediante un Kit comercial (Kit de Fosfatasa Ácida Leucocitaria [Sigma]). En primer lugar se desparafinaron los diferentes cortes histológicos. Se fijaron los tejidos con una solución citrato/acetona durante 30 segundos a temperatura ambiente, siguiendo las instrucciones y los reactivos provistos en el kit. Tras fijar las muestras, se incubaron durante 1 hora a 37ºC en las soluciones A, negativo (constituida por acetato, Naphthol AS-BI Phosphoric Acid y una cápsula Fast Garnet GBC Salt y enrasada con agua hasta alcanzar un volumen de final 50 mL), o B, positivo (constituida por acetato, Naphthol AS-BI Phosphoric Acid, tartrato y una cápsula Fast Garnet GBC Salt y enrasada con agua hasta alcanzar un volumen de final 50 mL). Estas soluciones se calentaron a 37ºC antes de su uso siguiendo las recomendaciones del fabricante.

Tras 1 hora de incubación, se lavaron las muestras con agua destilada y se tiñeron con hematoxilina. Las imágenes de las muestras se obtuvieron utilizando la cámara Leica DFC 425 conectada al microscopio Leica 5500B.

Tras 1 hora de incubación, se lavaron las muestras con agua destilada y se tiñeron con hematoxilina. Las imágenes de las muestras se obtuvieron utilizando la cámara Leica DFC 425 conectada al microscopio Leica 5500B.

5.18 Análisis estadístico

El análisis estadístico de los resultados y los gráficos se realizaron con el programa GraphPad Prism. Todos los resultados se expresan como la media ± error estándar. Para analizar las diferencias entre las distintas condiciones se realizaron test no paramétricos ya que las muestras no siguen una distribución normal. No se puede asumir una distribución normal debido a que la muestra es demasiado pequeña, menor de 30 datos, por lo que no se puede asegurar la normalidad de los datos. Se consideró un grado de confianza del 95% y que el test era estadísticamente significativo cuando $p<0,05$. Las diferencias globales entre todas las diferentes condiciones se evaluaron mediante un

análisis de varianza no paramétrico (Kruskal-Wallis) seguido de la prueba de Dunn, para comparar las muestras una a una. También se realizaron comparaciones uno a uno mediante una prueba de U-Mann-Whitney, con la cual se analizaron las diferencias entre muestras control, scrambled o PCDNA 3.1 y muestras estimuladas con MINDIN, silenciadas con los diferentes siARNs o transfectadas con GFP-NHERF1. Además, se realizaron estudios de correlación para analizar si existe una relación entre la expresión de MINDIN y otros genes. Este análisis se realizó a través del test de correlación de Pearson, obteniéndose un coeficiente de correlación (r) y un valor de p asociado.

6. RESULTADOS

6.1 La proteína MINDIN se expresa en células tumorales prostáticas humanas y de ratón y regula la expresión de genes óseos en tumores de próstata

Con el fin de determinar si las células tumorales secretan factores que pudiesen afectar al microentorno tumoral o al futuro microambiente metastásico, analizamos y comparamos el secretoma del medio condicionado (MC) de tres líneas celulares de cáncer de próstata, LNCaP (células metastásicas de ganglios linfáticos derivadas del cáncer de próstata humano), PC-3 (células metastásicas de hueso derivadas del cáncer de próstata humano) y TRAMP-C1 (células de adenocarcinoma de próstata de ratón); con la línea celular epitelial de próstata primaria (células no tumorogénicas humanas). También analizamos el secretoma de células osteoblásticas (MC3T3-E1) y osteocíticas (MLO-Y4). Este análisis nos permitió identificar las proteínas secretadas que podrían ser utilizadas como nuevas dianas para inhibir el fenotipo osteomimético de los tumores de próstata.

Tras el análisis proteómico del secretoma, identificamos varias proteínas que fueron secretadas por las células tumorales prostáticas pero no por células epiteliales de próstata no tumorogénicas ni por células óseas (Anexo II). De la lista de proteínas identificadas, buscamos aquellas que pudieran presentar relación con el entorno óseo y que tuvieran características pro-tumorogénicas. Tras la evaluación de la función molecular de las proteínas seleccionadas del secretoma identificamos la proteína MINDIN (ESPONDINA-2 o DIL-1) como un posible candidato promotor de la tumorogenicidad del cáncer de próstata. Esta proteína, forma parte de una familia con propiedades de remodelación ósea (232) y participa en la regulación positiva de citoquinas tumorogénicas en el cáncer de próstata, como son la interleucina-6 (IL-6) y el factor de necrosis tumoral-α (TNF-α) (233). Por lo tanto, debido a su potencial tumorogénico y posible papel como modulador del entorno óseo enfocamos nuestro estudio en este factor (Figura 19A).

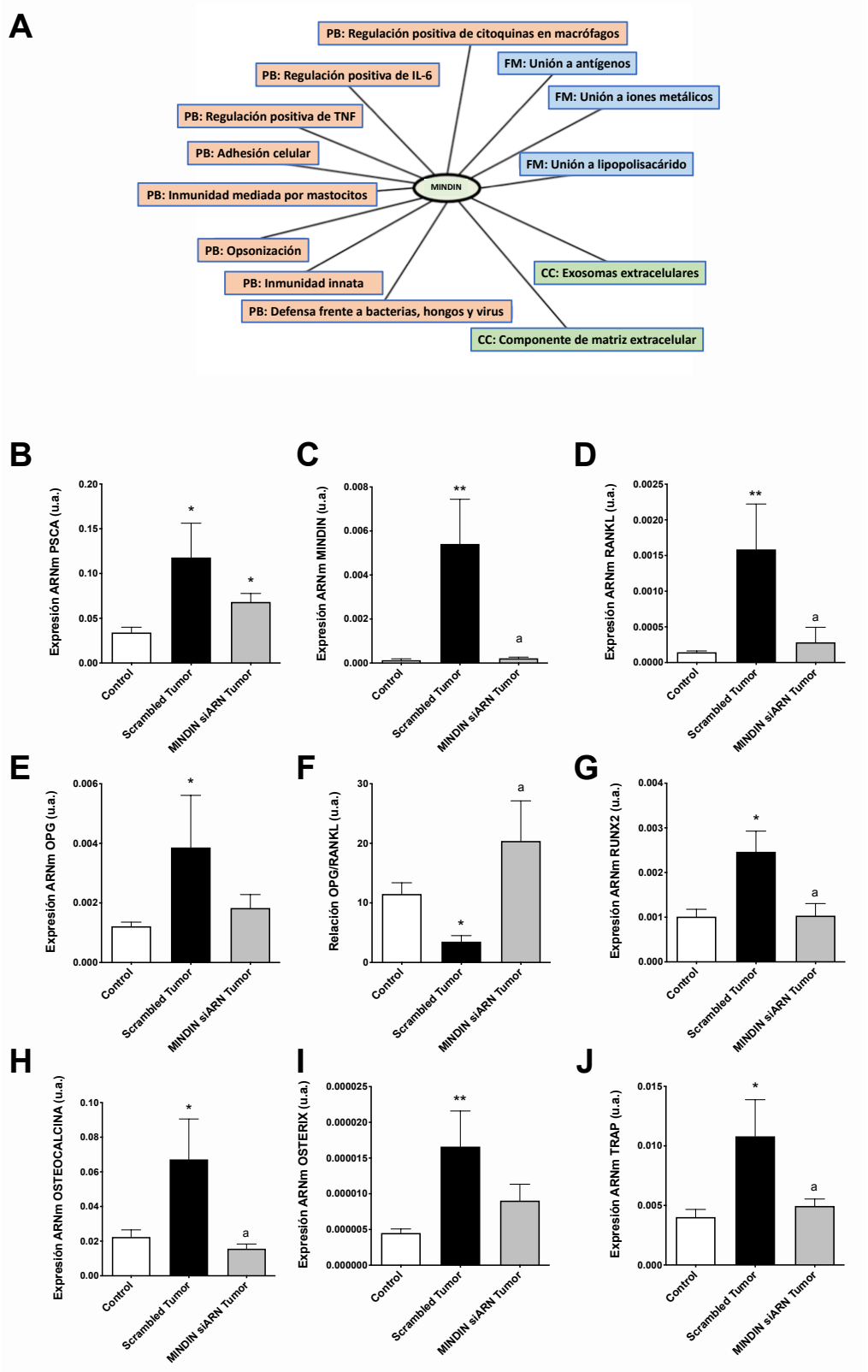

Figura 19. MINDIN aumenta la expresión de genes osteomiméticos en tumores de próstata inducidos por células TRAMP-C1. (A) Diagrama que representa los procesos biológicos (PB), funciones moleculares (FM) y componentes celulares (CC) con los que MINDIN está asociada. Diagrama generado utilizando información de bases de datos Uniprot. (B-J) Expresión de ARNm evaluado mediante PCR en tiempo real en próstatas de ratones control (sin tumor), "scrambled" tumor (con tumores inducidos por células TRAMP-C1 silenciadas con secuencias no codificantes "scrambled") y MINDIN siARN tumor (con tumores

inducidos por células TRAMP-C1 silenciadas con secuencias para MINDIN) (B) Antígeno prostático de células madre (PSCA), (C) MINDIN, (D) RANKL, (E) OPG, (F) relación OPG/RANKL, (G) RUNX2, (H) OSTEOCALCINA, (I) OSTERIX y (J) TRAP. Los resultados se representan como la media ± SEM (n = 7-10 por grupo). *p<0,05 vs control; **p<0,01 vs control; [a]p<0,05 vs "scrambled".

Con el fin de estudiar el papel de MINDIN en la inducción del osteomimetismo en el tumor primario prostático establecimos un modelo experimental *in vivo* en ratones machos C57BL/6. A los ratones se les inyectaron ortotópicamente en la próstata células TRAMP-C1, transfectadas con tres ARN silenciadores contra la región codificante de MINDIN (MINDIN siARN) o con una secuencia no codificante como control ("scrambled"). Este modelo de cáncer de próstata en ratones inmunocompetentes desarrolla tumores de próstata detectables a las cuatro semanas después de la inyección. Además, el modelo recapitula la progresión del cáncer de próstata, desde la hiperplasia hasta la neoplasia intraepitelial prostática, para potencialmente metastatizar a los ganglios linfáticos, los huesos y los pulmones (220,223).

En el modelo de cáncer de próstata inducido por TRAMP-C1, confirmamos que los tumores primarios inducidos por las células TRAMP-C1 sobreexpresaban MINDIN y el marcador tumoral PSCA en comparación con muestras de próstata control sin tumor (Figura 19 B-C). Sin embargo, los tumores con el gen de MINDIN silenciado presentaron niveles bajos de expresión de MINDIN, pero se mantuvieron elevados los niveles de PSCA (Figura 19 B-C), indicando la presencia de tumor primario a pesar del silenciamiento de MINDIN. Además, observamos, en el grupo tumoral "scrambled" (sin silenciamiento de MINDIN), un incremento de la expresión génica de marcadores osteomiméticos como RANKL, OPG, RUNX2, OSTEOCALCINA, OSTERIX y TRAP y una disminución de la relación OPG/RANKL en comparación con el grupo control (Figura 19 B-J). Por otra parte, evaluamos los efectos del silenciamiento de MINDIN en los tumores prostáticos y la implicación de las células tumorales en la adquisición de un fenotipo osteomimético. Respecto a esto, observamos que en los tumores de próstata inducidos por células TRAMP-C1 con el gen de MINDIN silenciado (Figura 19C) se produce una disminución de la expresión génica de RANKL, RUNX2, OSTEOCALCINA, OSTERIX y TRAP y un aumento de la relación OPG/RANKL (Figura 19 D-J), en comparación con los tumores inducidos por las células TRAMP-C1 transfectadas con una secuencia no codificante "scrambled".

Mediante el análisis de correlación de rangos de Spearman, observamos que el aumento de expresión de MINDIN se correlacionaba con el incremento de expresión génica de varios marcadores óseos que tienen un papel clave en la remodelación y el metabolismo óseo. En este análisis se incluye la correlación positiva significativa con RANKL, OPG, RUNX2, OSTEOCALCINA, OSTERIX y TRAP y la correlación negativa con la relación OPG/RANKL (Tabla 1).

Correlación de MINDIN con	Número de animales comparados	Coeficiente de correlación de Spearman	P valor
RANKL	36	0.41	0.018*
OPG	36	0.40	0.018*
OPG/RANKL	32	-0.51	0.003**
TRAP	30	0.47	0.017*
OSTERIX	33	0.40	0.021*
RUNX2	36	0.36	0.034*
OSTEOCALCINA	37	0.34	0.04*
FOSFATASA ALCALINA	37	-0.12	0.49

Tabla 1. Análisis de la correlación entre la expresión de MINDIN y la expresión de genes osteomiméticos en tumores de ratones C57BL/6 inducidos por células TRAMP-C1 mediante el uso del coeficiente de correlación de Spearman. *p<0,05: correlación lineal significativa de MINDIN con otro gen**.** **p<0,01: correlación lineal significativa de MINDIN con otro gen

Para corroborar estas observaciones realizadas en un modelo de ratón, analizamos mediante inmunohistoquímica biopsias de próstata humana, en la cuales observamos un aumento de expresión de MINDIN en los tumores primarios de próstata en comparación con las muestras control no tumorogénicas (Figura 20A). Datos previos han sugerido que los adenocarcinomas de próstata humana adquieren propiedades osteomiméticas que se asocian positivamente con la invasividad tumoral (162). En este sentido, analizamos cambios en los marcadores óseos asociados al aumento de inmunomarcaje de MINDIN en muestras de tumores de próstata humanos. De forma similar a lo que ocurría con MINDIN, la expresión de OSTERIX fue mayor en tumores en comparación con próstatas no tumorales (Figura 20B). Además, encontramos un

incremento significativo de la expresión génica de RANKL en los tumores de próstata y una disminución de la expresión de OPG (Figura 20 C-D).

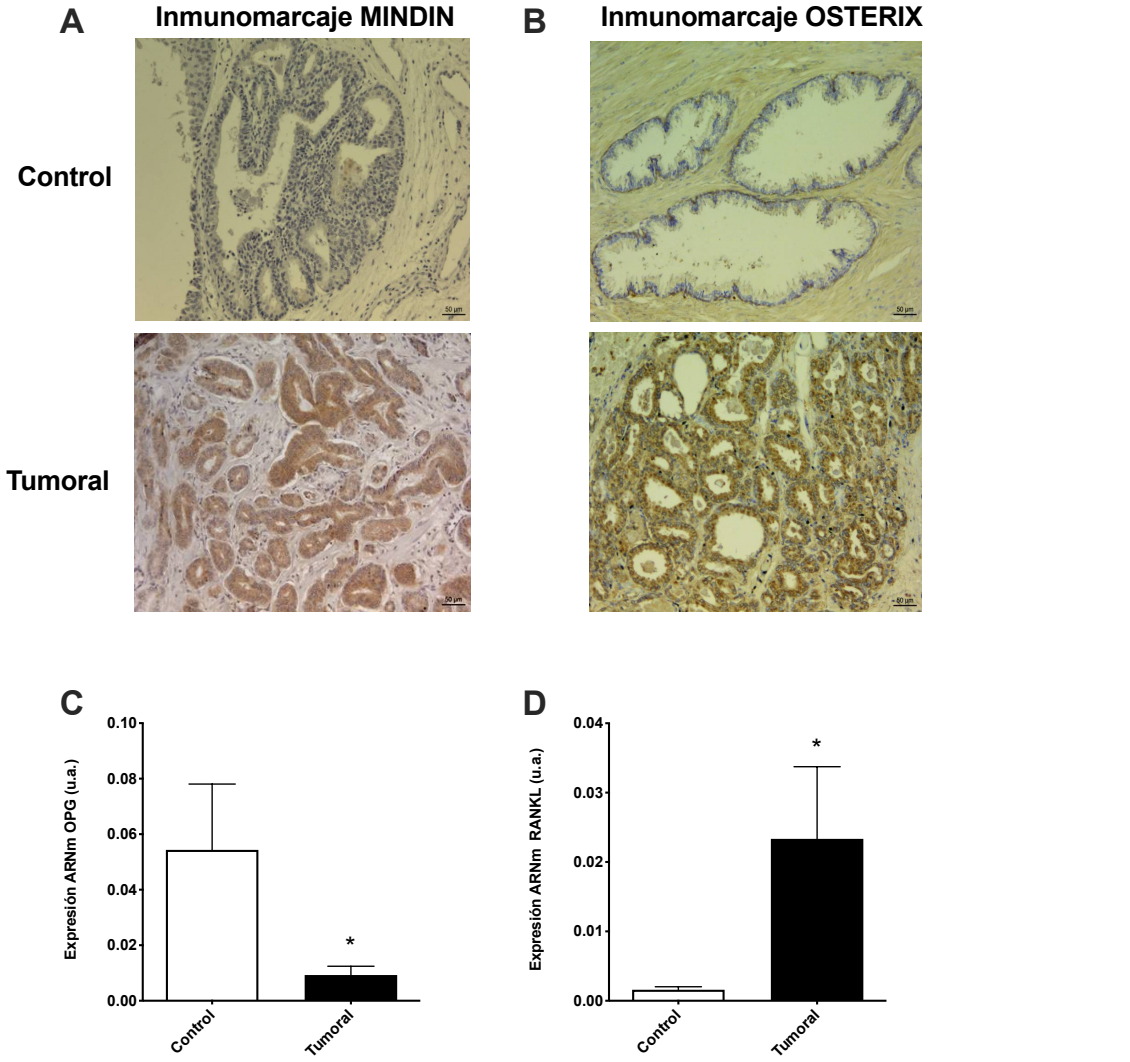

Figura 20. Aumento de la expresión de MINDIN y cambios osteomiméticos en tumores de próstata humanos. Inmunomarcaje de MINDIN (A) y OSTERIX (B) y expresión de ARNm de OPG (C) y RANKL (D). Se muestran imágenes representativas del inmunomarcaje de MINDIN y OSTERIX. Los resultados se representan como la media ± SEM. *p<0,05 vs control, **p<0,01 vs control.

Estos datos muestran que, tanto en un modelo animal como en muestras humanas, los tumores de próstata presentan niveles elevados de MINDIN asociados a la adquisición de marcadores osteomiméticos.

6.2 MINDIN y NHERF1 muestran patrones de expresión opuestos en tumores de próstata humanos y de ratón

Dada la relación observada entre la sobreexpresión de MINDIN y el aumento de expresión de marcadores relacionados con el tejido óseo, seguidamente buscamos un factor que pudiese mediar tanto los procesos tumorogénicos como los osteomoduladores observados. La proteína reguladora NHERF1 ha demostrado ser capaz de regular factores de transcripción ósea y procesos de osteoformación en osteoblastos (188). Además, se ha descrito su papel en la regulación de la progresión de diversos tumores (179,184,186,193–196). Por ello, planteamos la hipótesis de que la regulación de NHERF1 es uno de los mecanismos utilizados por MINDIN durante la progresión del tumor de próstata hacia un fenotipo metastásico óseo.

Para comprobar si existía una relación entre NHERF1 y la expresión de MINDIN en el cáncer de próstata, primero analizamos la localización y expresión de NHERF1 en muestras control y de próstata tumoral de pacientes clasificados según la edad, la invasión perineural, el riesgo D`Amico, el grado Gleason y los márgenes quirúrgicos. Respecto a esto, observamos expresión de NHERF1 en la parte apical de la membrana plasmática y en el citoplasma de células en las próstatas control, mientras que en los tumores avanzados NHERF1 se localizó prioritariamente en el citoplasma (Figura 21 B,E). Sin embargo, la localización de MINDIN se observó en la membrana plasmática, citoplasma y espacio extracelular en las células de próstatas tumorales, mientras que no se detectó expresión de MINDIN en muestras control (Figura 21 A,C).

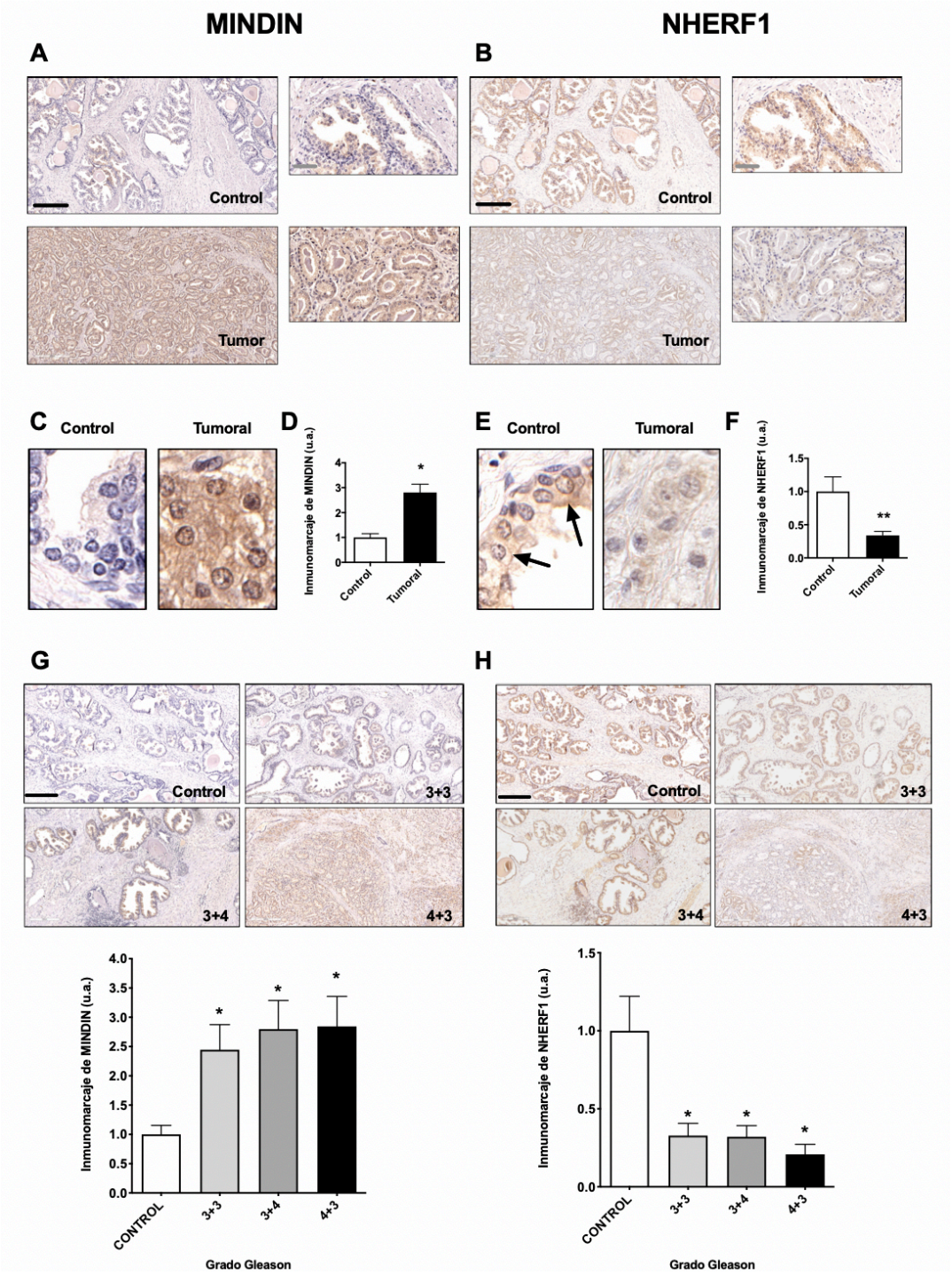

Figura 21. Los tumores de próstata humana clasificados según el grado Gleason muestran niveles elevados de MINDIN y disminución del inmunomarcaje de NHERF1. La evaluación de los niveles de inmunomarcaje de MINDIN y NHERF1 se realizó mediante inmunohistoquímica en muestras humanas de tumores de próstata y controles. Se muestran imágenes representativas, gráfico de barras e imágenes detalladas de los niveles de inmunomarcaje de MINDIN (A,C,D) y NHERF1 (B,E,F) en muestras de controles y de tumores. Se muestran imágenes representativas y evaluación de los niveles de inmunomarcaje de MINDIN (G) y NHERF1 (H) de acuerdo con la clasificación de puntuación de Gleason. Las flechas negras indican inmunomarcaje apical de NHERF1. Las barras de escala negras y grises representan 500 µm y 100 µm, respectivamente. Los resultados se representan como la media ± SEM. n = 12-18 muestras/grupo. *p<0,05 vs control; **p<0,01 vs control.

Además, observamos aumento de la expresión de MINDIN en los tumores primarios de próstata en comparación con los controles. También se produjo una disminución de la expresión de NHERF1 en los tumores primarios de próstata en comparación con los controles (Figura 21 E-F). Respecto al grado Gleason, el inmunomarcaje de MINDIN aumentó y NHERF1 disminuyó en tumores con grados Gleason 3+3, 3+4 y 4+3 (Figura 21 G-H). También observamos en la clasificación según el riesgo D`Amico que a medida que se incrementa el grado tumoral la expresión de MINDIN es mayor, por lo que observamos una mayor expresión de MINDIN en tumores de alto riesgo seguido de tumores con riesgo medio y bajo (Figura 22A). Sin embargo, y en contraposición a MINDIN, la expresión de NHERF1 disminuyó en tumores con alto riesgo, seguido de riesgos medio y bajo (Figura 22B). Cabe destacar que no encontramos diferencias en la expresión de NHERF1 y MINDIN entre pacientes agrupados en los diferentes grupos según la invasión perinerual o márgenes quirúrgicos (Figura 23).

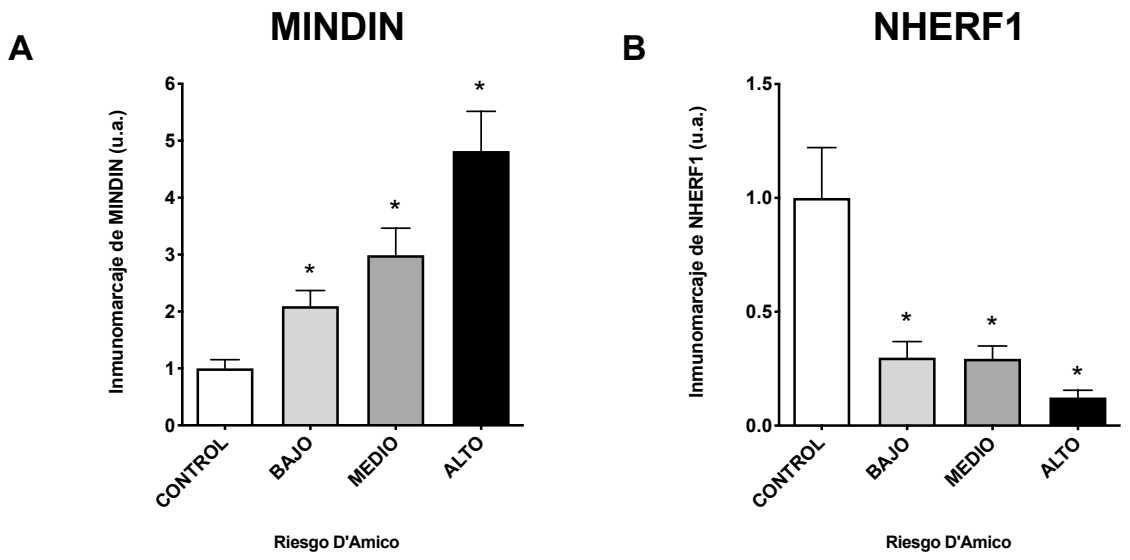

Figura 22. Los tumores de próstata humana clasificados según el riesgo D'Amico muestran niveles elevados de MINDIN y disminución del inmunomarcaje de NHERF1. La evaluación de los niveles de inmunomarcaje de MINDIN y NHERF1 se realizó mediante inmunohistoquímica en muestras humanas de tumores de próstata y controles. Los gráficos de barras representan los niveles de inmunomarcaje de (A) MINDIN y (B) NHERF1 en muestras de controles y tumores clasificadas según el riesgo D'Amico. Los resultados se representan como la media ± SEM. n = 12-18 muestras/grupo. *p<0,05 vs control.

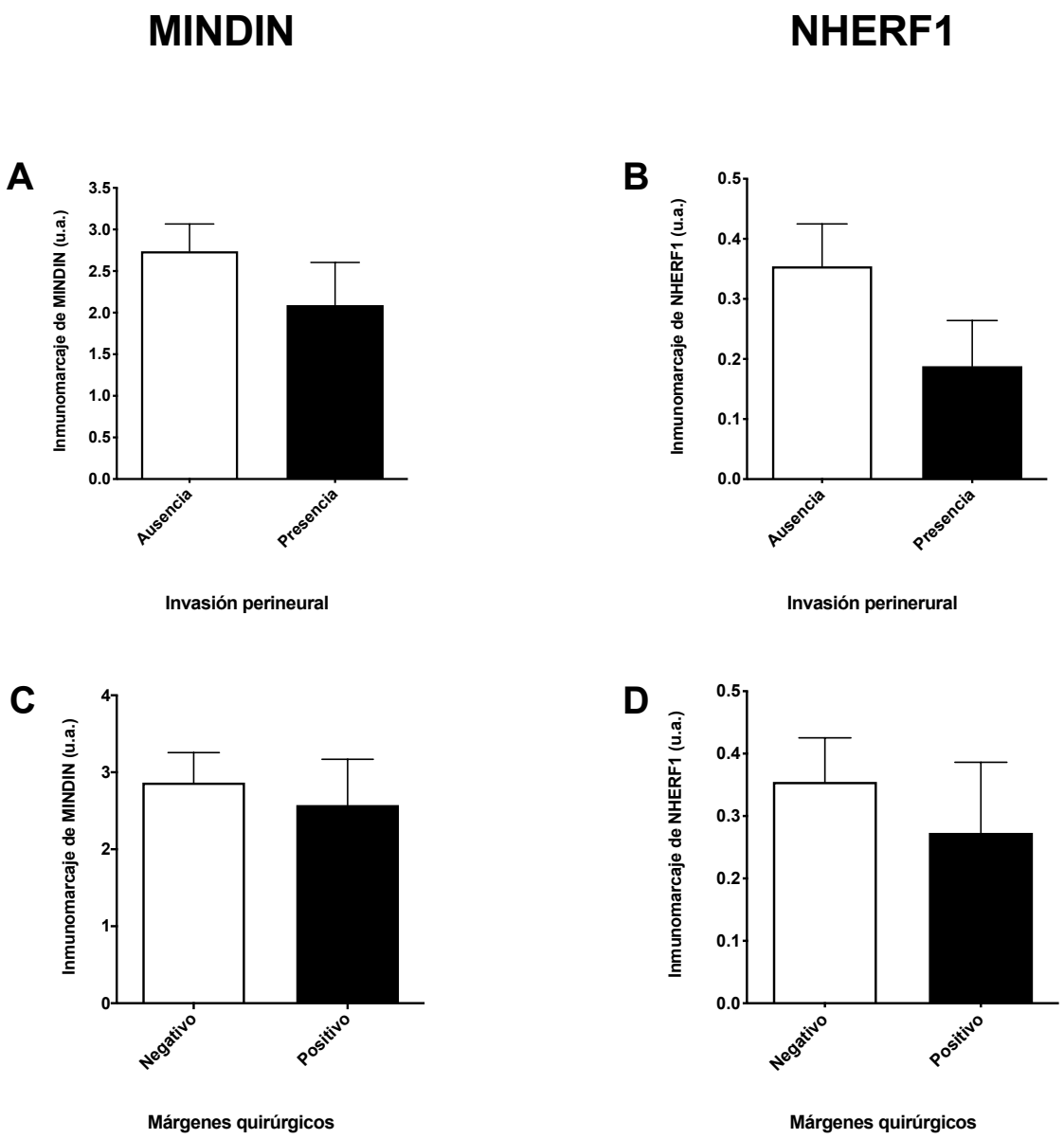

Figura 23. Evaluación de los niveles de inmunomarcaje de MINDIN y NHERF1 realizada mediante inmunohistoquímica en muestras humanas de tumores de próstata y controles. Los gráficos de barras representan los niveles de inmunomarcaje de MINDIN (A-C) y NHERF1 (B-D) en muestras de controles y tumores clasificadas según (A-B) invasión perineural y (C-D) márgenes quirúrgicos. Los resultados se representan como la media ± SEM. n = 12-18 muestras/grupo.

En el modelo de tumor en próstata de ratón observamos que la expresión génica de NHERF1 disminuyó en el grupo tumoral comparado con el grupo control (Figura 24B), al igual que ocurría en las muestras de próstata humanas. Sin embargo, cuando se silenció MINDIN en los tumores primarios, la expresión de NHERF1 aumentó significativamente en comparación con el grupo tumoral que expresaba MINDIN (Figura 24B).

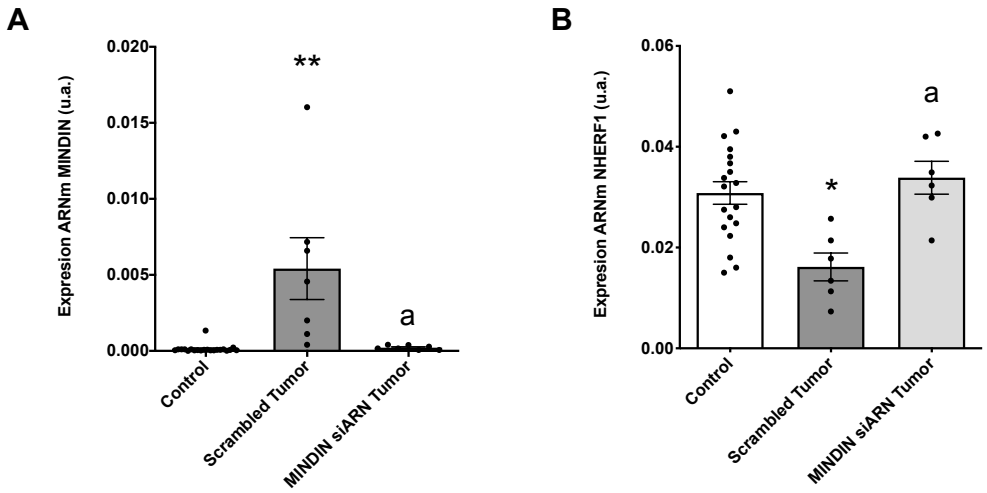

Figura 24. La expresión de NHERF1 está disminuida en los tumores que no expresan MINDIN del modelo animal de ratón. Expresión de ARNm evaluada mediante PCR en tiempo real en próstatas de ratones control (sin tumor), "scrambled" tumor (con tumores inducidos por células TRAMP-C1 silenciadas con secuencias no codificantes "scrambled") y MINDIN siARN tumor (con tumores inducidos por células TRAMP-C1 silenciadas con secuencias para MINDIN). (A) MINDIN y (B) NHERF1. Los resultados se representan como la media ± SEM. *p<0,05 vs control; **p<0,01 vs control; [a]p<0,05 vs "scrambled".

Estos resultados en su conjunto muestran que los niveles elevados de MINDIN observados en tumores de próstata humana y de ratón y asociados a la sobreexpresión de marcadores osteomiméticos, se encuentran relacionados con la disminución del inmunomarcaje de NHERF1.

6.3 MINDIN regula el osteomimetismo, la proliferación, migración y adhesión celular en células de adenocarcinoma de próstata

En base a lo observado en el modelo experimental *in vivo*, establecimos un modelo experimental *in vitro* con células tumorales prostáticas TRAMP-C1, en las que comprobamos si MINDIN afectaba a la expresión génica de marcadores osteomiméticos. Para ello, estimulamos las células TRAMP-C1 con el péptido MINDIN o silenciamos su expresión mediante la transfección con siARNs específicos.

Observamos que la estimulación con MINDIN durante 6h a una concentración de 5 ng/mL (concentración previamente detectada en suero de pacientes con cáncer de próstata) (219) incrementó la expresión génica de RANKL, RUNX2, OSTEOCALCINA, FOSFATASA ALCALINA, TRAP y MINDIN y una disminución de la relación OPG/RANKL

(Figura 25A). Tras 24 horas de estimulación con MINDIN, las células TRAMP-C1 también mostraron sobreexpresión de OSTERIX (Figura 25B). Los niveles de ARNm de RUNX2, OSTEOCALCINA, TRAP y MINDIN permanecieron sobreexpresados durante todo el periodo de estudio (Figura 25 A-B). Así mismo, tras 24 o 48 horas de estimulación con MINDIN se produjo un incremento de la expresión proteica de RUNX2 y OSTERIX, dos factores de transcripción claves en la regulación de diversas proteínas óseas (65,78) (Figura 26). Por el contrario, el silenciamiento de MINDIN desencadenó la sobreexpresión de OPG y aumentó la relación OPG/RANKL (Figura 25C).

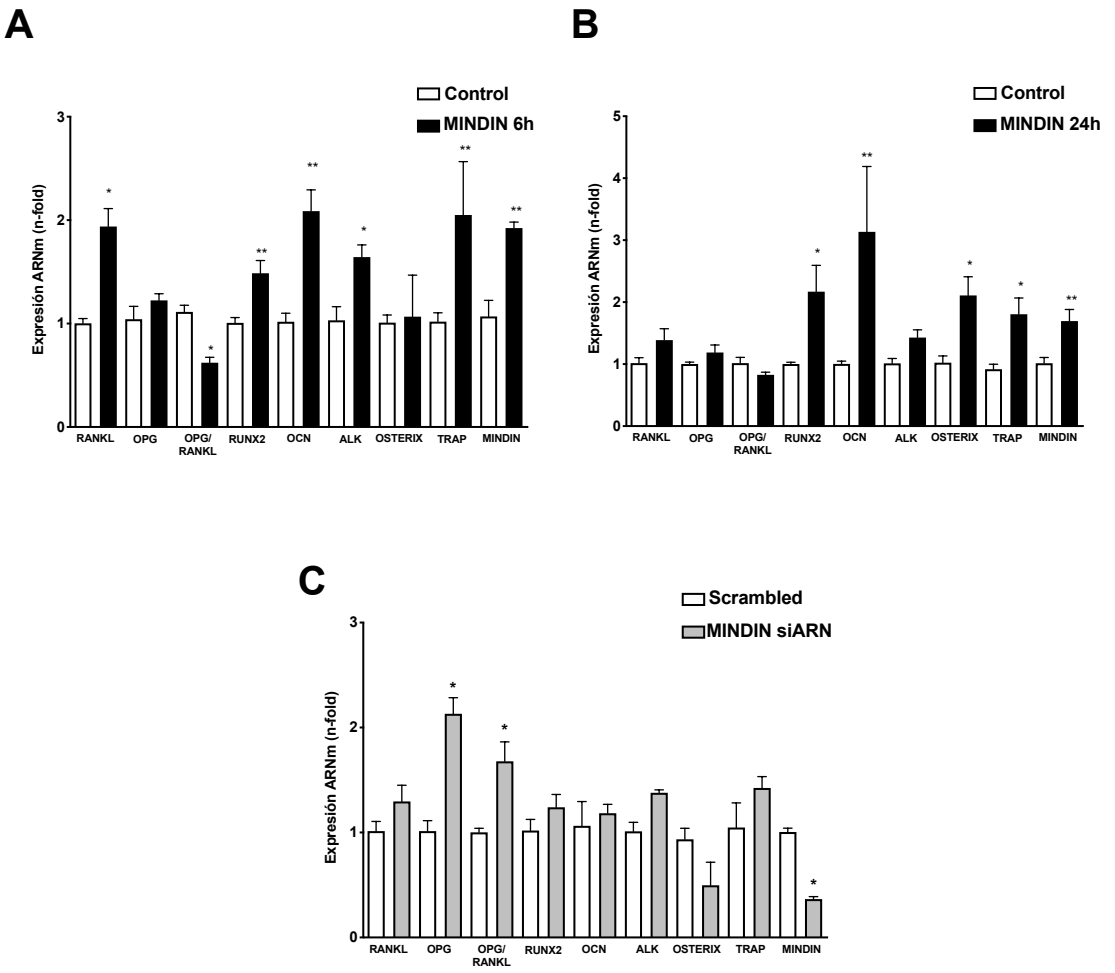

Figura 25. MINDIN induce la expresión de genes osteomiméticos en células TRAMP-C1. Expresión de ARNm en células TRAMP-C1 evaluada mediante PCR en tiempo real tras (A) 6 horas o (B) 24 horas de estimulación con MINDIN (5 ng/mL) o (C) transfectadas con tres siARNs contra MINDIN durante 48 horas en células TRAMP-C1. Los resultados se representan como la media ± SEM de tres experimentos independientes por triplicado. *p<0,05 vs control correspondiente (control o "scrambled"), **p<0,01 vs control correspondiente (control o "scrambled"). ALK: FOSFATASA ALCALINA; OCN: OSTEOCALCINA.

La expresión génica del resto de marcadores óseos no se vio alterada significativamente por el silenciamiento de MINDIN. Observamos efectos similares en las líneas tumorales LNCaP, PC-3 y células no tumorales de próstata humana (Figura 27).

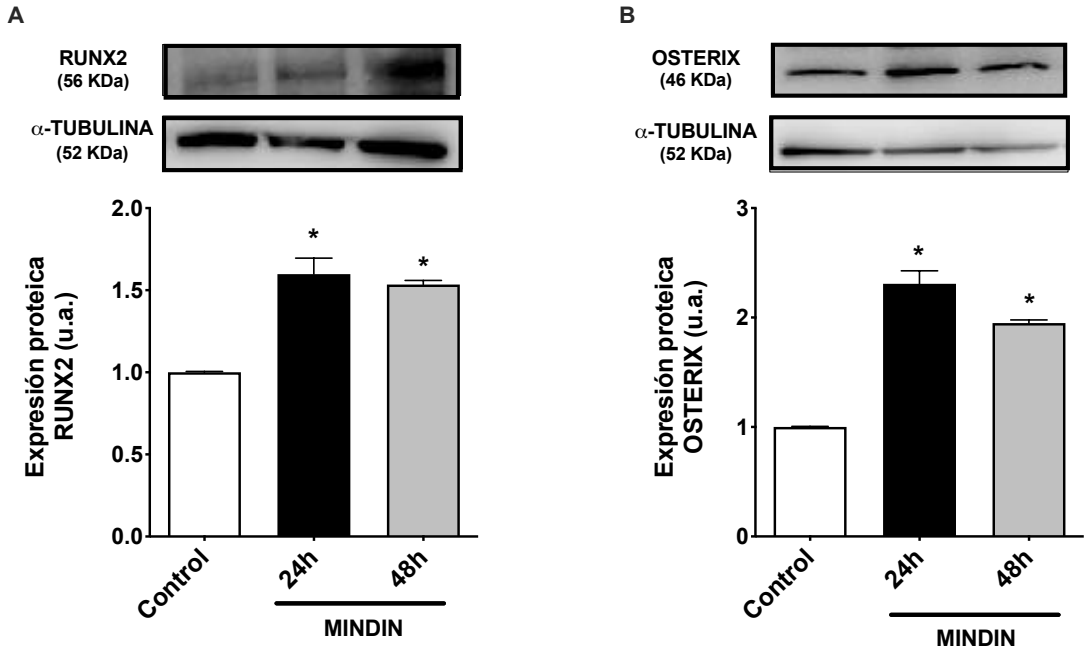

Figura 26. MINDIN aumenta la expresión proteica de RUNX2 y OSTERIX en células TRAMP-C1. La expresión proteica de (A) RUNX2 y (B) OSTERIX se evaluó mediante Western Blot después de la estimulación con MINDIN (5 ng/ml) durante 24 o 48 horas en células TRAMP-C1. Se muestran imágenes representativas de los geles. Los resultados se representan como la media ± SEM de tres experimentos independientes por triplicado *p<0,05 vs control.

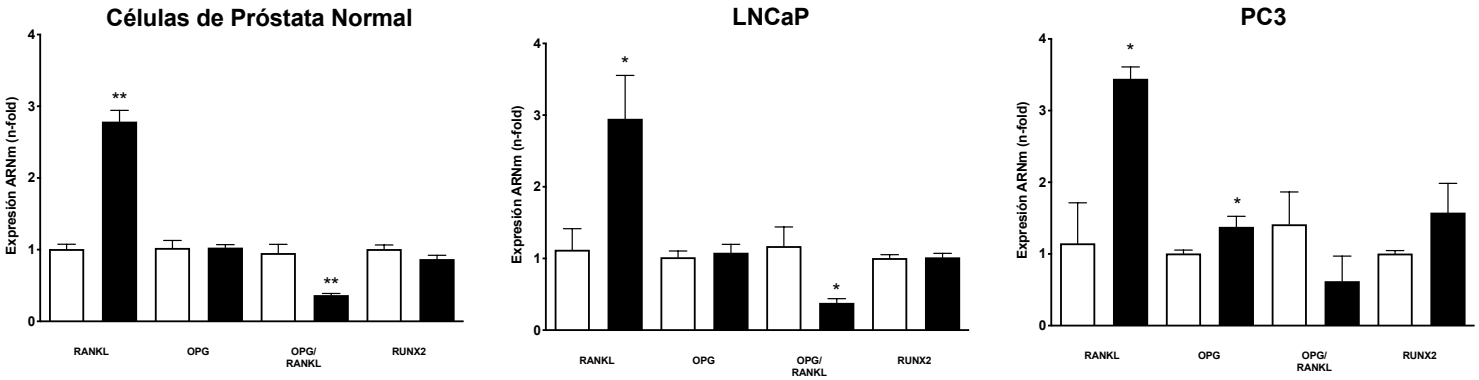

Figura 27. MINDIN regula la expresión de genes osteomiméticos en células epiteliales normales de próstata y en células tumorales humanas LNCaP y PC-3. La expresión de ARNm de RANKL, OPG y RUNX2 y la relación OPG/RANKL se evaluó mediante PCR en tiempo real después de la estimulación con MINDIN (5 ng/ml) durante 6 horas en células epiteliales normales de próstata humanas y células tumorales LNCaP y PC-3. Los resultados se representan como la media ± SEM de tres experimentos independientes por triplicado. *p <0.05 vs control, **p <0.01 vs control.

Además de causar cambios en marcadores de osteomimetismo, la estimulación con MINDIN indujo un incremento de la proliferación (Figura 28A) y la migración celular (Figura 28 B-C) en células TRAMP-C1 , así como de la adhesión de estas células tumorales a células óseas osteocíticas MLO-Y4 y osteoblásticas MC3T3-E1 (Figura 29 A-B). Por el contrario, el silenciamiento de MINDIN redujo la proliferación (Figura 28A), la migración celular (Figura 28 B-C) y la adhesión de células tumorales de próstata a cultivos celulares de osteocitos MLO-Y4 y osteoblastos MC3T3-E1 (Figura 29 A-B). El número de células TRAMP-C1 adheridas a las superficies recubiertas de osteoblastos MC3T3-E1 en condiciones control (silenciamiento con siARN "scrambled") (60.75 ± 5.9) fue significativamente mayor que a las superficies cubiertas con osteocitos MLO-Y4 (44.1 ± 2.82). Para confirmar que las acciones pro-migratorias de MINDIN eran independientes de la proliferación, se incubaron las células TRAMP-C1 con el fármaco antiproliferativo mitomicina C en un ensayo de migración. En estas condiciones, aunque se inhibió la proliferación celular, MINDIN indujo cambios significativos en el número de células observadas en la zona de herida del ensayo de migración en comparación con las células incubadas solo con mitomicina C (Figura 30). Estos datos sugieren que MINDIN promueve la migración de células tumorogénicas de próstata de manera independiente a su efecto proliferativo.

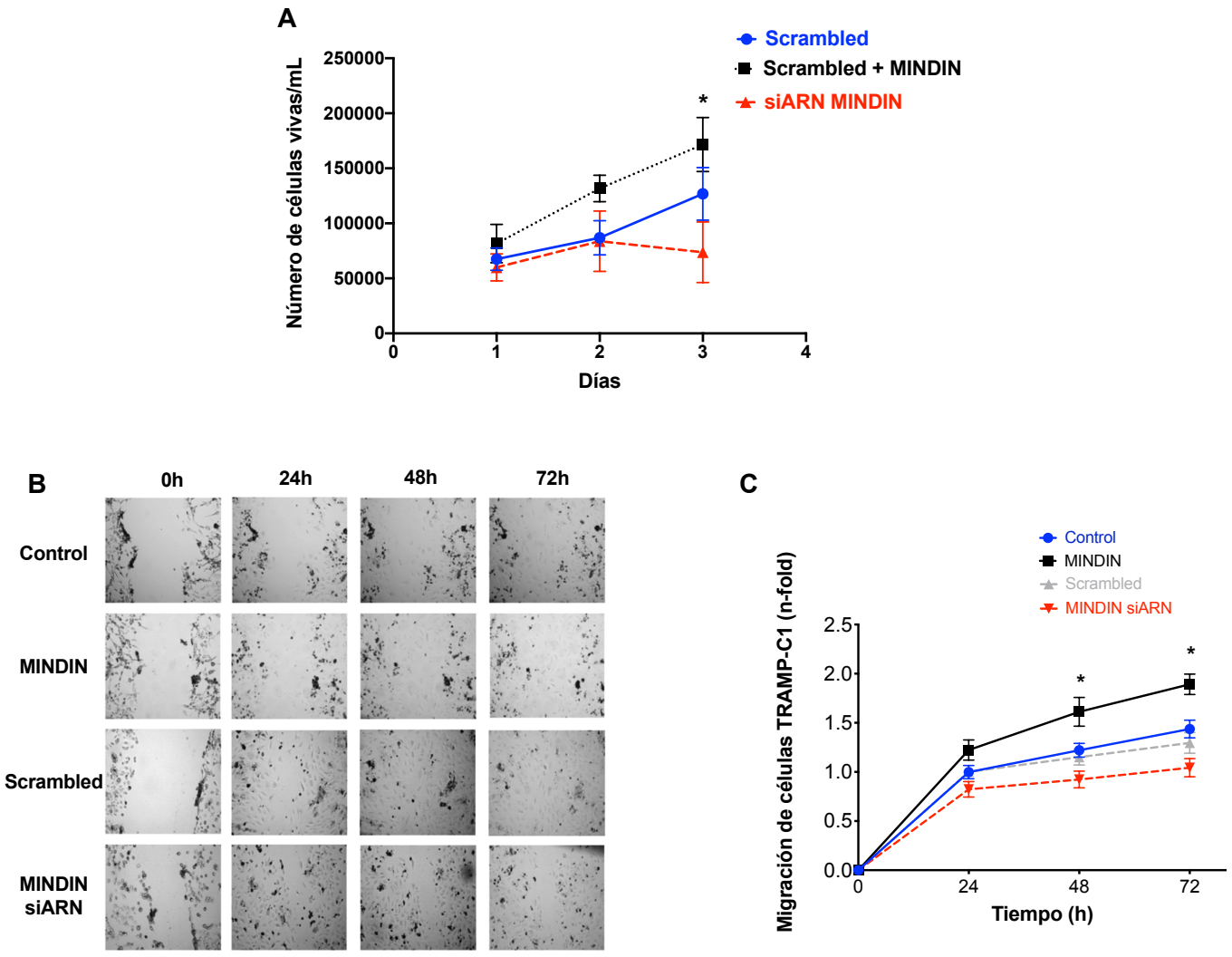

Figura 28. MINDIN promueve la proliferación y migración de células TRAMP-C1. (A) La proliferación de células TRAMP-C1 estimuladas con MINDIN (5 ng/ml) o silenciadas con siARNs contra MINDIN durante 48 horas se evaluó mediante un ensayo de proliferación con azul tripan. (B-C) La migración de células TRAMP-C1 estimuladas con MINDIN (5 ng/ml) o silenciadas con siARNs contra MINDIN durante 48 horas se evaluó mediante un ensayo herida en condiciones de 0% de suero. Los resultados se representan como la media ± SEM de tres experimentos por triplicado. *p<0,05 vs control correspondiente (control o "Scrambled"). Se muestran imágenes representativas de los experimentos de migración.

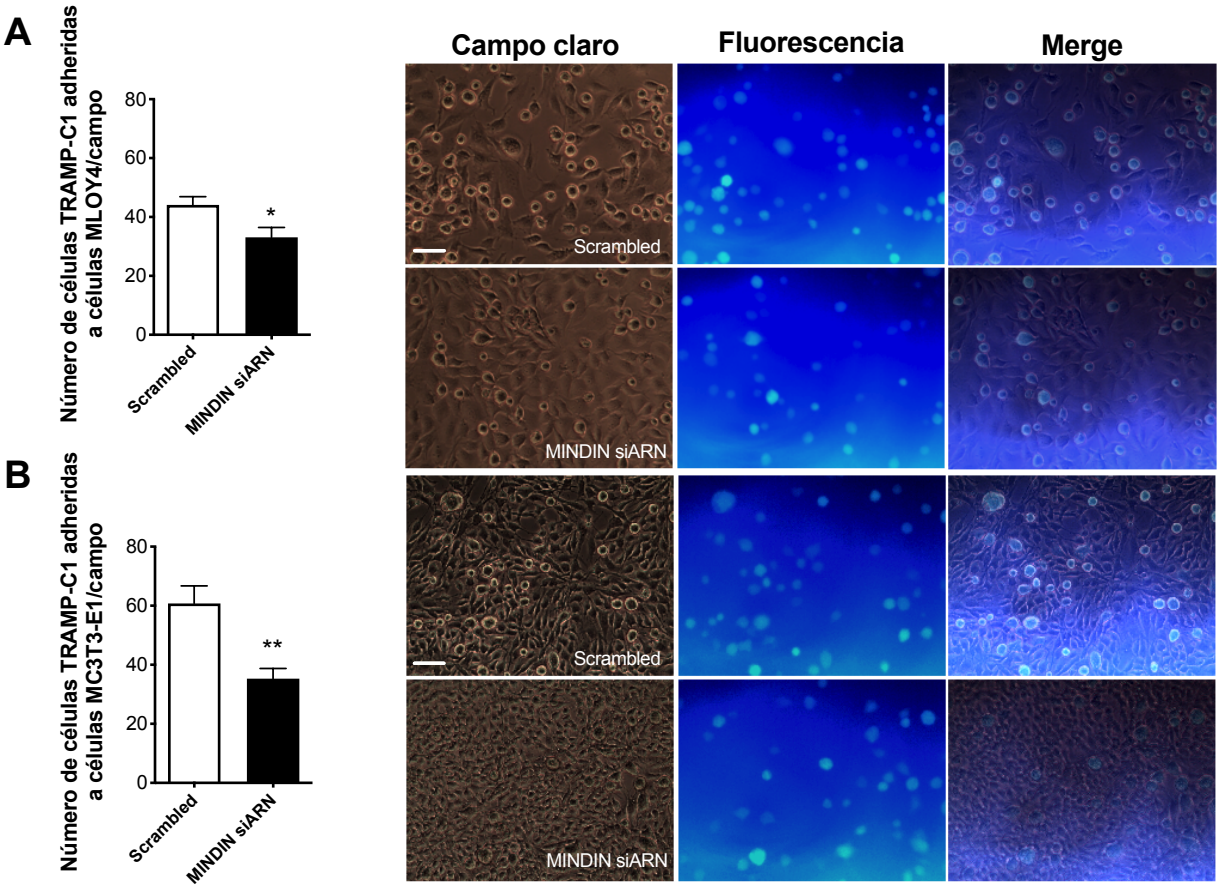

Figura 29. MINDIN promueve la adhesión de células TRAMP-C1 a células óseas. Se muestra el número de células TRAMP-C1 (silenciadas o no con siARNs contra MINDIN durante 48 horas) adheridas y marcadas con calceína-AM por campo a superficies cubiertas de (A) MLO-Y4 o (B) MC3T3-E1. La barra denota 50 µm. Se muestran imágenes representativas de tres experimentos por triplicado. Los resultados se representan como la media ± SEM de tres experimentos por triplicado. *p<0,05 vs "scrambled"; **p<0,01 vs "scrambled".

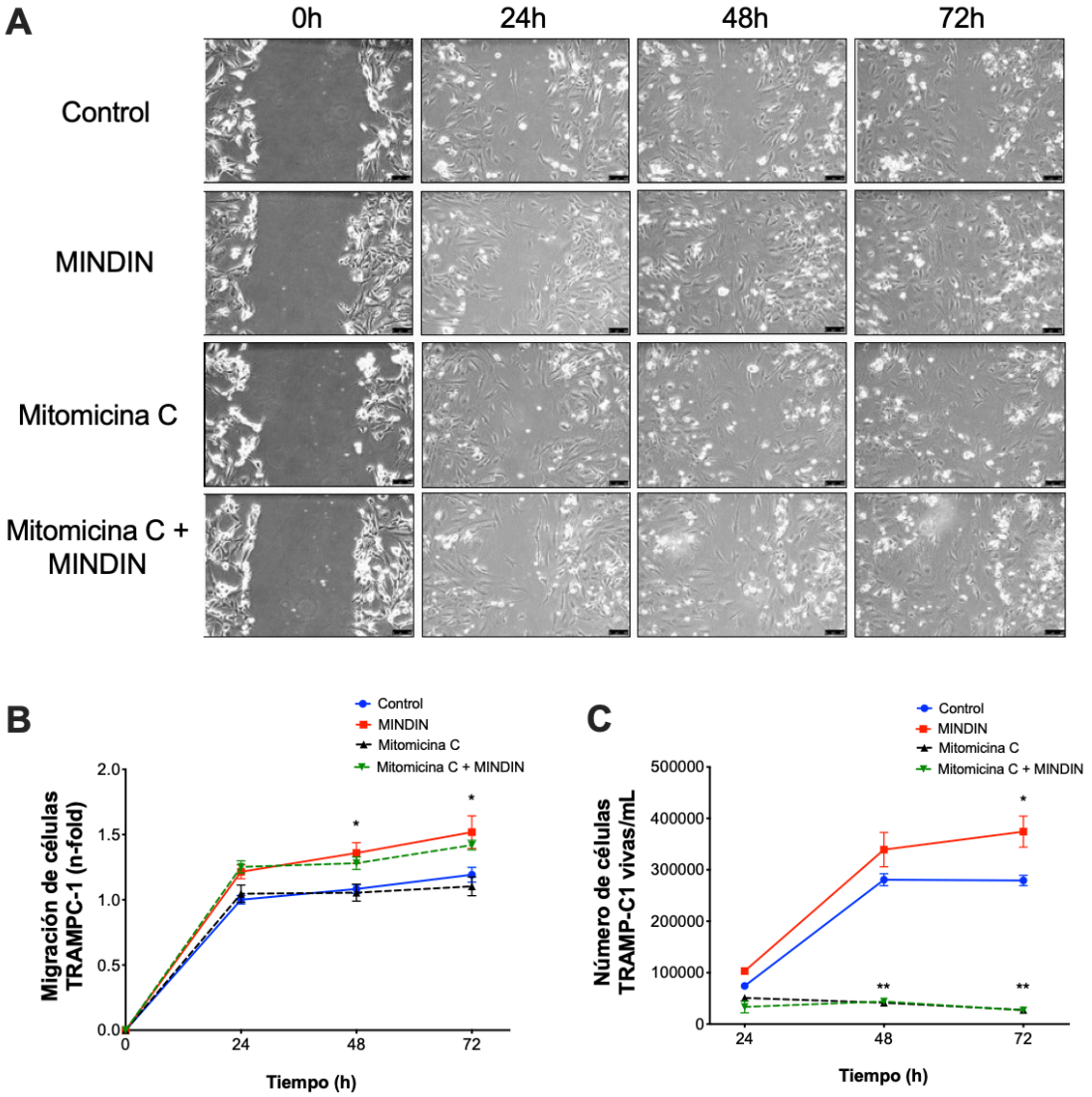

Figura 30. MINDIN promueve la migración de células TRAMP-C1 sin modificar su proliferación. (A-B) La migración de células TRAMP-C1 estimuladas con MINDIN (5 ng/ml) y/o incubadas con 5 µg/ml de mitomicina C, se evaluó mediante un ensayo herida en condiciones de 0% de suero. (C) La proliferación de las células TRAMP-C1 se evaluó mediante un ensayo de exclusión con azul tripan. Se muestran imágenes representativas (A) de tres experimentos por triplicado. Los resultados se representan como la media ± SEM de tres experimentos por triplicado. *p <0.05 vs control; **p <0.01 vs control.

6.4 MINDIN reduce la expresión de NHERF1 y desencadena su movilización hacia el citoplasma en las células tumorales de próstata, afectando a la migración y proliferación de estas células

Nuestro siguiente objetivo fue evaluar si la expresión de NHERF1 es modulada por MINDIN y si NHERF1 podría mediar los efectos proliferativos, promigratorios y adhesivos de MINDIN en las células tumorales de próstata. Para ello, estimulamos las células TRAMP-C1 con el péptido MINDIN durante 6 o 24 horas o inhibimos la expresión de

MINDIN usando siARNs. Los datos obtenidos mostraron una disminución de la expresión del gen de NHERF1 en células TRAMP-C1 tras la estimulación con MINDIN en comparación con las células control no estimuladas. De manera similar, la expresión proteica de NHERF1 disminuyó 24 horas después de la estimulación con MINDIN en estas células. Por el contrario, el silenciamiento de MINDIN indujo la sobreexpresión del gen NHERF1 en células de adenocarcinoma prostático TRAMP-C1 (Figura 31A). Se observaron efectos similares en las células LNCaP (Figura 31B). MINDIN no sólo disminuyó la expresión de NHERF1, sino que también indujo la relocalización de esta proteína desde regiones cercanas a la membrana plasmática de las células TRAMP-C1 hacia el citoplasma de estas células (Figura 31C). Estas observaciones sugieren que niveles elevados de MINDIN, como los observados en tumores de próstata, ocasionan alteraciones en la funcionalidad de NHERF1 mediante la disminución de su expresión y fomentando el traslado de esta proteína desde la zona de membrana plasmática al citoplasma de células de adenocarcinoma de próstata.

A continuación, evaluamos las acciones de NHERF1 en los procesos celulares pro-tumorogénicos mencionados previamente y que son activados por MINDIN en las células tumorales de próstata. Para ello, se sobreexpresó NHERF1 mediante un vector de expresión plasmídico marcado con GFP para contrarrestar la disminución en la expresión de este factor ocasionada por MINDIN. La eficacia de la sobreexpresión de NHERF1 por el vector plasmídico se confirmó mediante comprobación de la expresión génica y proteica de NHERF1 (Figura 32 A-B).

Respecto al osteomimetismo, la estimulación durante 24 horas con el péptido MINDIN indujo un incremento de la expresión génica de TRAP, RUNX2 y OSTEOCALCINA (Figura 32 D-F) respecto a células control (transfectadas con el vector vacío PCDNA 3.1). Sin embargo, la sobreexpresión de NHERF1 no revirtió las características osteomiméticas inducidas por MINDIN (Figura 32 D-F). Por el contrario, la sobreexpresión de NHERF1 aumentó los niveles basales de la expresión del gen RANKL, disminuyendo la relación OPG/RANKL en comparación con las células que no sobreexpresaban NHERF1 (Figura 32 H-I).

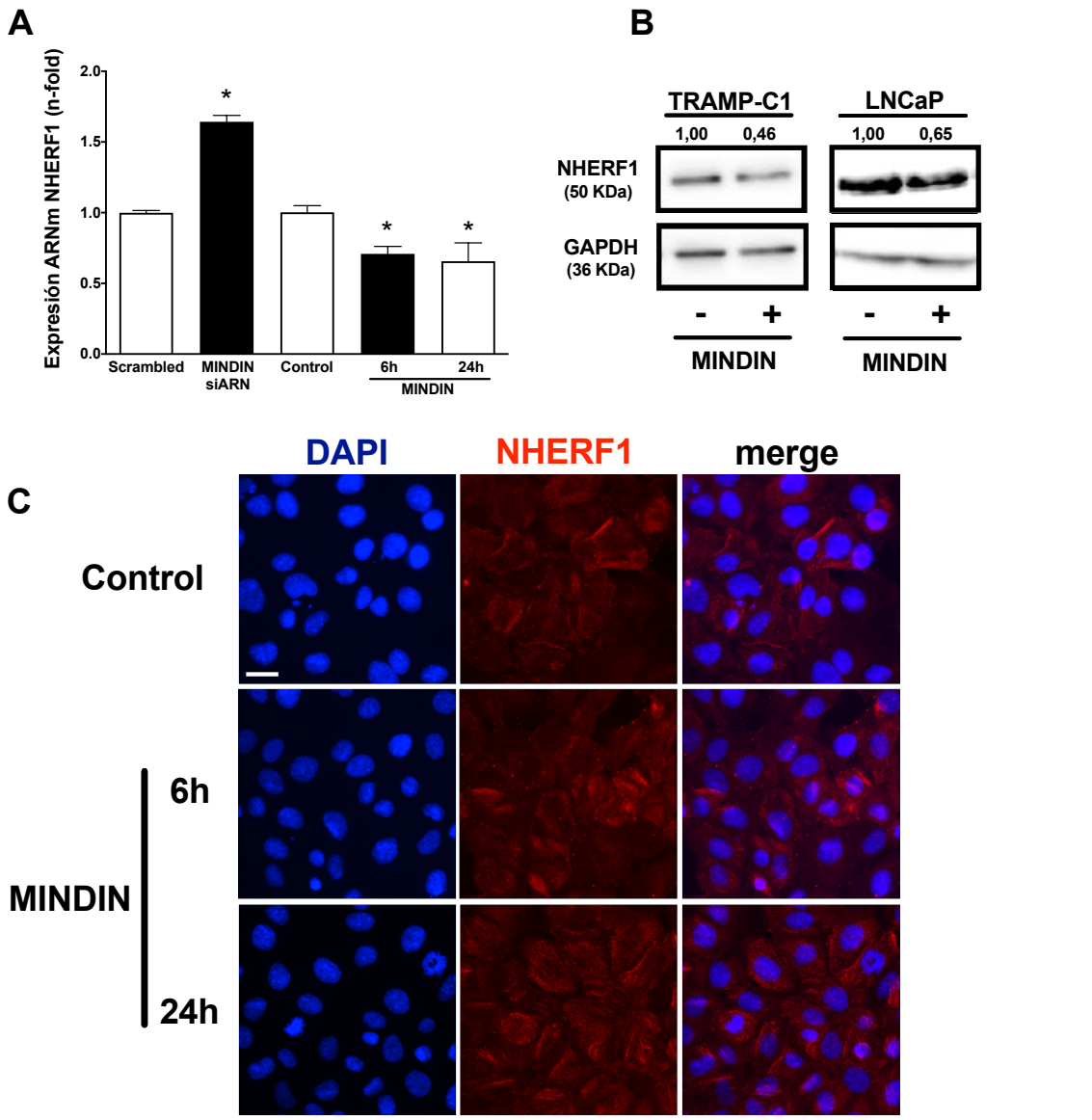

Figura 31. MINDIN reduce la expresión génica de NHERF1 y desencadena su movilización hacia el citoplasma en células TRAMP-C1. MINDIN se silenció usando siARNs específicos durante 48 horas. Las células TRAMP-C1 y LNCaP se estimularon con MINDIN (5 ng/ml) durante 6 o 24 horas. Se aisló el ARNm y la proteína de las células para evaluar la expresión de NHERF1 mediante PCR en tiempo real o Western Blot, respectivamente. (A) Expresión génica y (B) proteica de NHERF1. (C) Inmunofluorescencia de NHERF1 en células TRAMP-C1. Imágenes representativas que muestran la tinción DAPI y el inmunomarcaje de NHERF1 en células de cáncer de próstata TRAMP-C1 estimuladas o no (control) con 5 ng/ml de MINDIN durante 6 horas o 24 horas. La barra de escala denota 20 µm. Los resultados se representan como la media ± SEM de 3 experimentos independientes. *p<0,05 vs control.

Seguidamente, evaluamos los efectos de NHERF1 sobre la proliferación celular. Observamos que la estimulación con MINDIN incrementó el número de células TRAMP-C1 control en comparación con células sin estimular y que los efectos proliferativos de MINDIN se inhibieron por la sobreexpresión de NHERF1 (Figura 33 A-B). De manera similar las células TRAMP-C1 transfectadas con plásmido de NHERF1 y estimuladas con

MINDIN mostraron una reducción en su capacidad migratoria en comparación con células transfectadas con vector vacío PCDNA 3.1 y estimuladas con MINDIN (Figura 32C).

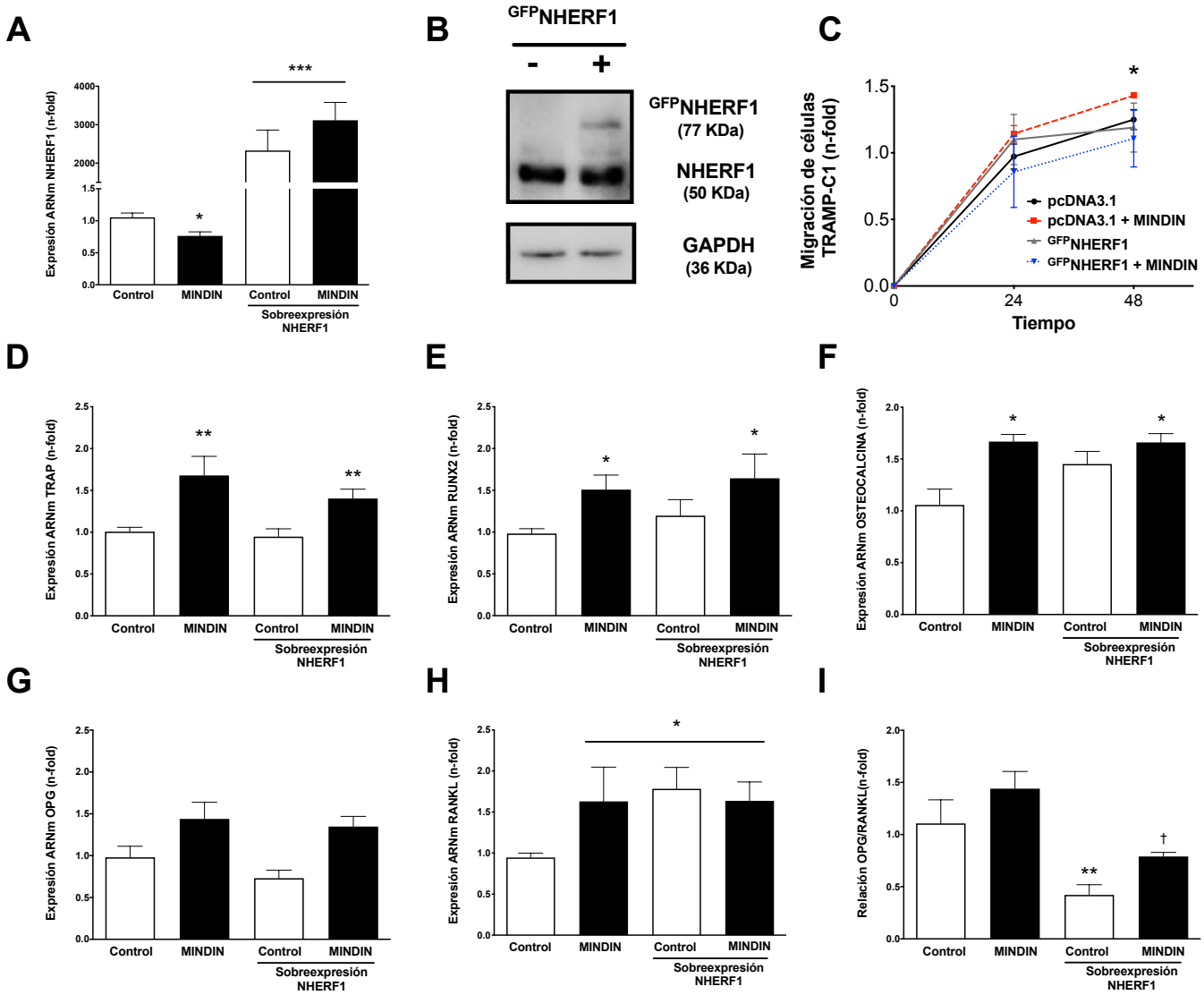

Figura 32. Sobreexpresión de NHERF1 en células TRAMP-C1. (A) Expresión génica y (B) proteica de NHERF1. Expresión de ARNm de células TRAMP-C1 evaluada mediante PCR en tiempo real de (D) TRAP, (E) RUNX2, (F) OSTEOCALCINA, (G) OPG, (H) RANKL y (I) relación OPG/RANKL. (C) Se evaluó la migración de las células TRAMP-C1 mediante un ensayo herida. Las células TRAMP-C1 se estimularon con MINDIN (5 ng/ml) durante 24 o 48 horas y/o se transfectaron con GFP-NHERF1 como se describe en materiales y métodos. Los resultados se representan como la media ± SEM de 3 experimentos independientes. *p<0,05 vs control; **p<0,01 vs control; ***p<0,001 vs control; †p <0,05 vs MINDIN.

Finalmente, en el ensayo de adhesión se observó que, aunque MINDIN indujo un aumento de la adherencia celular, la sobreexpresión de NHERF1 no fue capaz de inhibir la adhesión celular dependiente de MINDIN (Figura 33C).

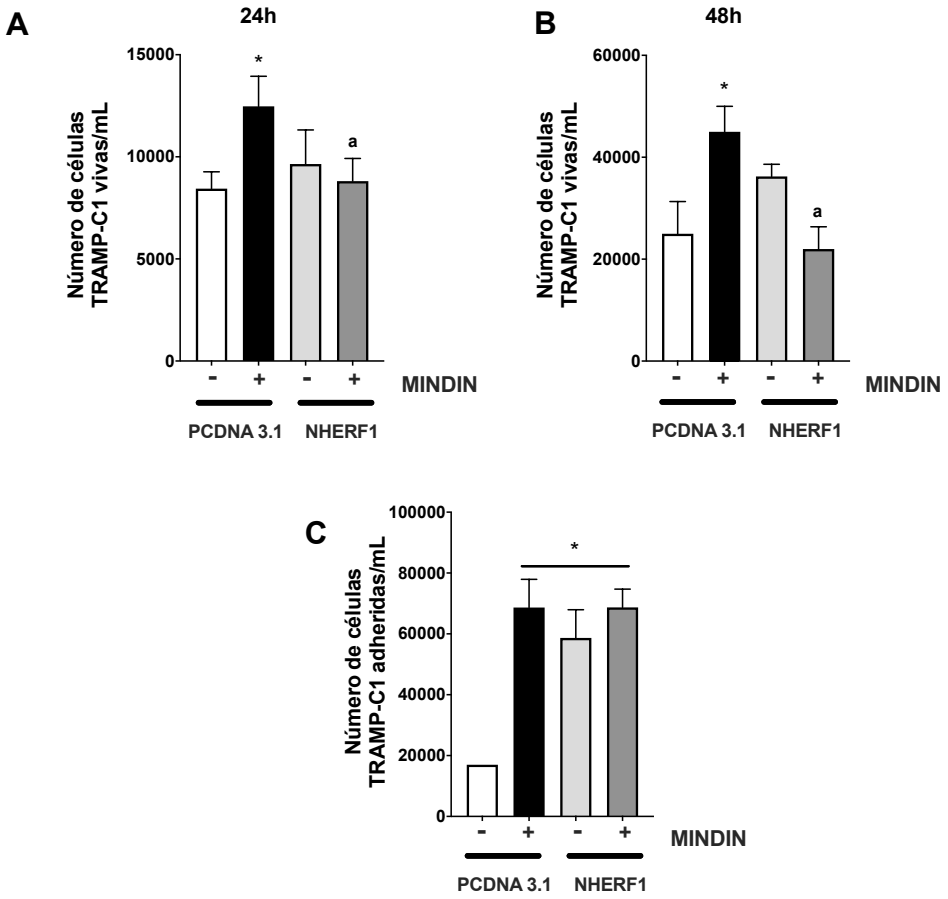

Figura 33. La sobreexpresión de NHERF1 disminuye la proliferación de células de adenocarcinoma de próstata. Se evaluó la proliferación mediante un ensayo de exclusión con azul tripan a las (A) 24 horas y (B) 48 horas. (C) Ensayo de adhesión sobre placas de colágeno. Las células TRAMP-C1 se estimularon con MINDIN (5 ng/ml) durante 24 horas y/o se transfectaron con PCDNA 3.1 o GFP-NHERF1 como se describe en los materiales y métodos. Los resultados se representan como la media ± SEM de 3 experimentos independientes. *p<0,05 vs PCDNA 3.1; [a]p<0,05 vs PCDNA 3.1+MINDIN.

Estos resultados sugieren que NHERF1 media algunos procesos celulares clave en la progresión tumoral inducidos por MINDIN como son la capacidad proliferativa y migratoria de las células tumorales.

6.5 Los efectos osteomiméticos, de adhesión y de migración inducidos por MINDIN son mediados por la vía de señalización de la quinasa ERK 1/2

A continuación, buscamos dilucidar el mecanismo molecular involucrado en las acciones de MINDIN sobre las células tumorales de próstata. Dado que estudios previos demuestran que la vía de señalización ERK 1/2 es activada por proteínas R-ESPONDINA durante la diferenciación osteoblástica de células madre mesenquimales derivadas de grasa (234), quisimos comprobar si esta MAP quinasa también media acciones dependientes de MINDIN en células tumorales de próstata. Apoyando esta hipótesis, observamos que MINDIN indujo la fosforilación de ERK 1/2 en células TRAMP-C1 (Figura 34A). Además, los cambios en la migración y la adhesión celular y en la expresión génica de RANKL y RUNX2 y la relación OPG/RANKL dependientes de MINDIN fueron inhibidos por U0126, un inhibidor de MAP quinasa ERK 1/2 (Figura 34 B-H).

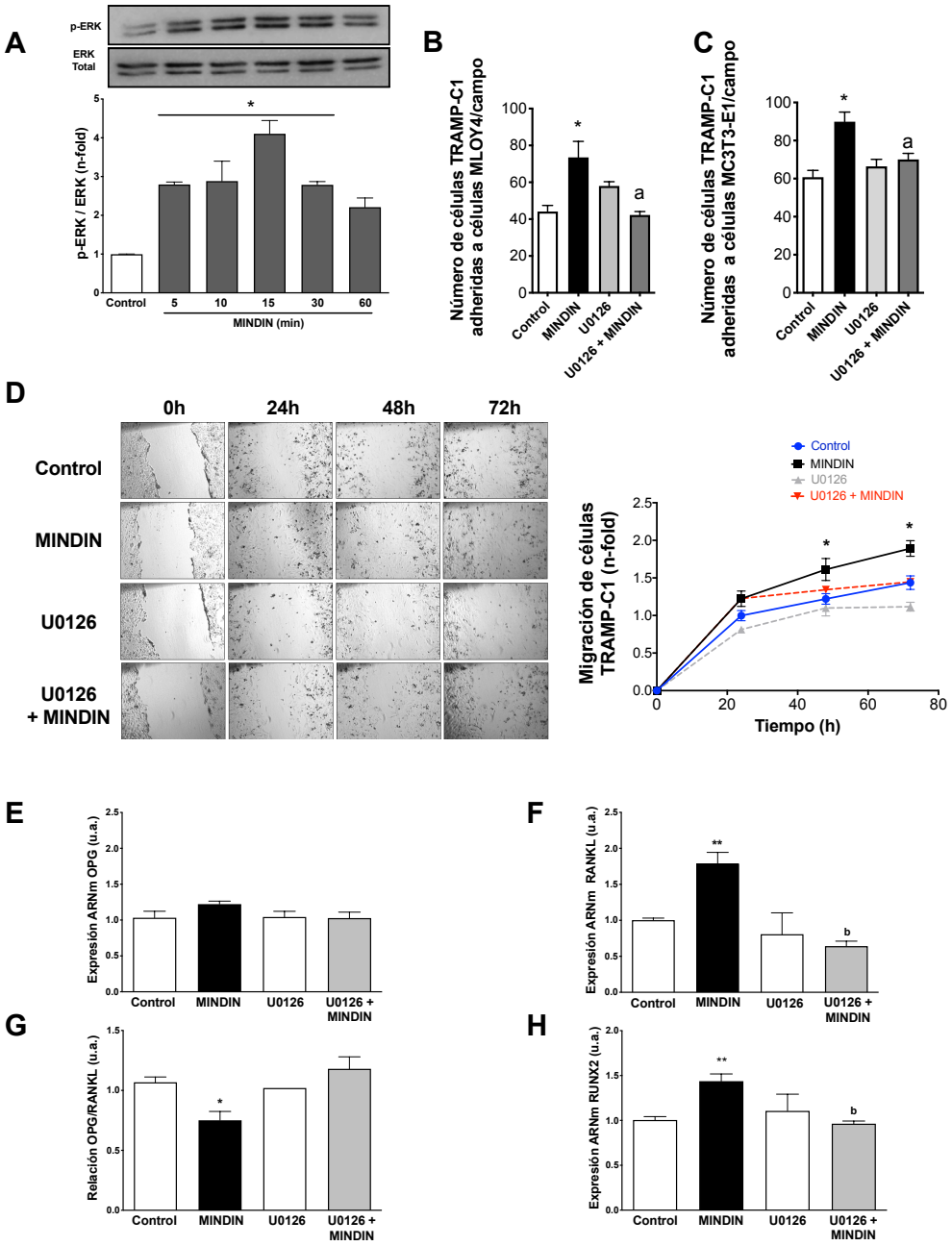

Figura 34. La adhesión, migración y los efectos osteomiméticos están mediados por ERK 1/2 en las células TRAMP-C1. (A) Se muestra la fosforilación de ERK dependiente de MINDIN, (B y C) la adhesión celular, (D) la migración celular y (E-H) los cambios en la expresión de genes osteomiméticos en las células TRAMP-C1. Las células TRAMP-C1 se estimularon con 5 ng/ml de MINDIN durante diferentes períodos de tiempo: (A) 5–60 minutos, (B – D) 24 horas o (E – H) 6 horas. Se muestra una imagen representativa de la fosforilación de ERK en el panel A. (B y C) Se muestra el número de células TRAMP-C1 marcadas con calceína adheridas a superficies cubiertas con células (B) MLO-Y4 y (C) MC3T3. (D) La migración se evaluó mediante un ensayo de herida (0-72 h) con células TRAMP-C1 estimuladas con MINDIN (5 ng/ml) y/o inhibidas con un inhibidor específico de ERK 1/2 (5 µM U0126) durante 1 h. El pretratamiento de células TRAMP-C1 con un inhibidor específico de ERK 1/2 (5 µM U0126) durante 1 hora anuló los efectos inducidos por MINDIN sobre la expresión génica de (E) OPG, (F) RANKL, (G) relación OPG/RANKL y (H) RUNX2. Los resultados se representan como la media ± SEM de tres experimentos independientes por triplicado. *p <0,05 vs control; **p <0.01 vs control; [a]p <0.05 vs MINDIN; [b]p <0.05 vs MINDIN.

6.6 MINDIN regula la comunicación e interacción entre el tumor primario de próstata y el hueso

Las células tumorales prostáticas pueden metastatizar a hueso e influir en el ambiente esquelético induciendo la liberación de varios factores que aumentan, a su vez, la proliferación y señalización de las células tumorales (235,236), estableciendo un "ciclo vicioso" de cooperación entre el tumor y el hueso (161). Para evaluar *in vitro* los posibles efectos de MINDIN sobre la cooperación tumor-hueso, evaluamos las acciones del secretoma (MC: medio condicionado) de células óseas MLO-Y4 (osteocitos) y MC3T3-E1 (osteoblastos) sobre las células tumorales de próstata TRAMP-C1.

El secretoma de las células MLO-Y4 pre-tratadas con MC de células TRAMP-C1 indujo la sobreexpresión de RANKL y disminuyó la relación OPG/RANKL en células TRAMP-C1 en comparación con los efectos que produjo el MC de células MLO-Y4 no tratadas o control (sin MC) (Figura 35 A–C). Además, el MC de células MC3T3-E1 pre-tratadas con MC de células TRAMP-C1 produjo un aumento de la expresión génica de RANKL, OPG, RUNX2, OSTEOCALCINA, OSTERIX, FOSFATASA ALCALINA y TRAP sin cambiar significativamente la relación OPG/RANKL en células TRAMP-C1 en comparación con el MC de células MC3T3-E1 no tratadas o control (sin MC) (Figura 35 A-H). De manera interesante, los efectos del secretoma de las células MLO-Y4 y MC3T3-E1 pre-tratadas sobre las células TRAMP-C1 se inhibieron, al menos en parte, al pre-tratar ambas células óseas con MC de células TRAMP-C1 silenciadas para MINDIN (Figura 36 A-H).

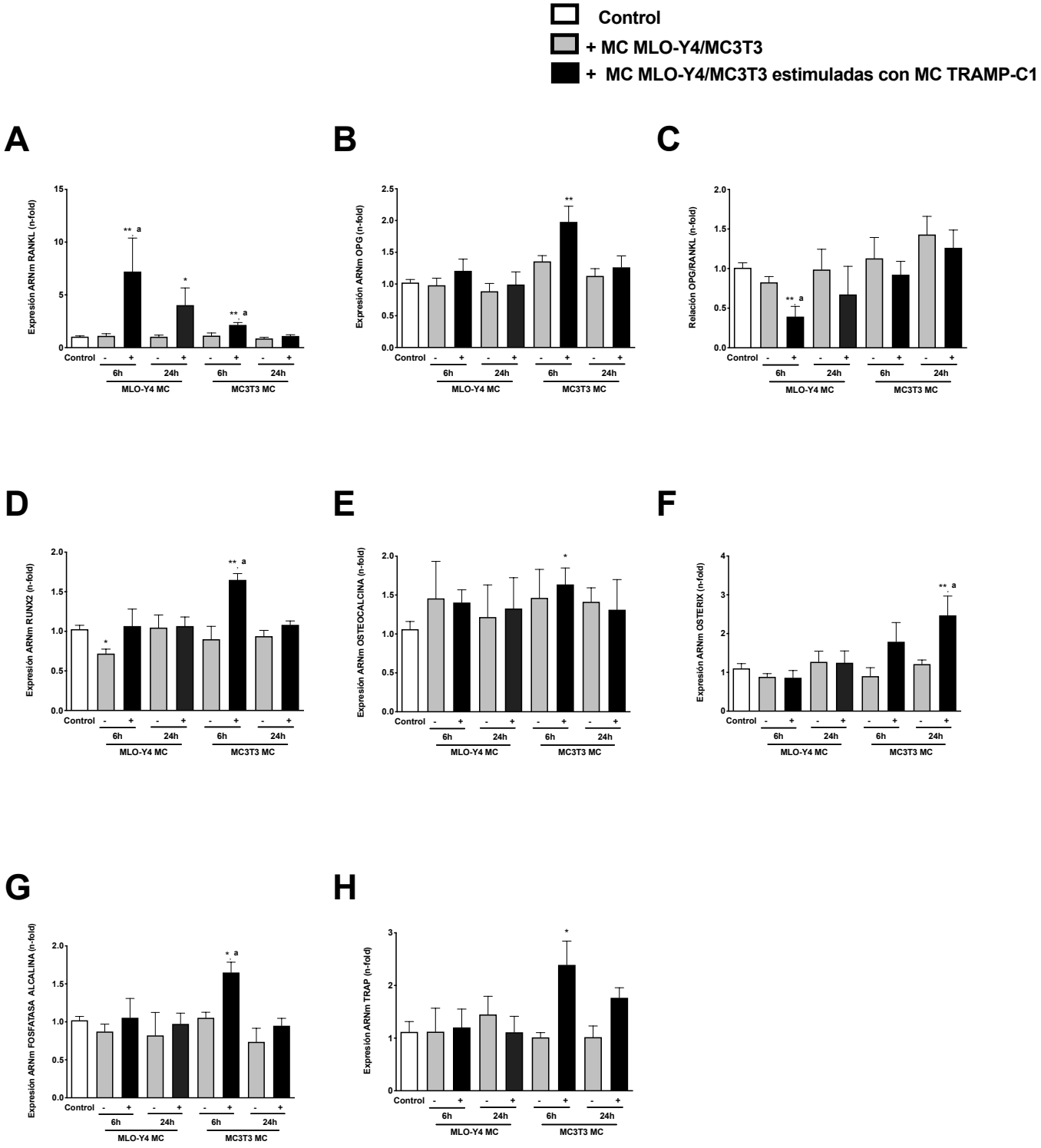

Figura 35. La comunicación entre células tumorales y células óseas induce cambios osteomiméticos en las células TRAMP-C1. Expresión de ARNm evaluada en células TRAMP-C1 en condiciones control, - (MC de células MLO-Y4 o MC3T3 no tratadas) y + (MC de células MLO-Y4 o MC3T3 pre-tratadas con MC TRAMP-C1) mediante PCR en tiempo real. (A) RANKL, (B) OPG, (C) relación OPG/RANKL, (D) RUNX2, (E) OSTEOCALCINA, (F) OSTERIX, (G) FOSFATASA ALCALINA y (H) TRAP. Los resultados se representan como la media ± SEM de tres experimentos independientes por triplicado. *p<0,05 vs control; **p<0,01 vs control; [a]p<0,05 vs la condición (-) correspondiente.

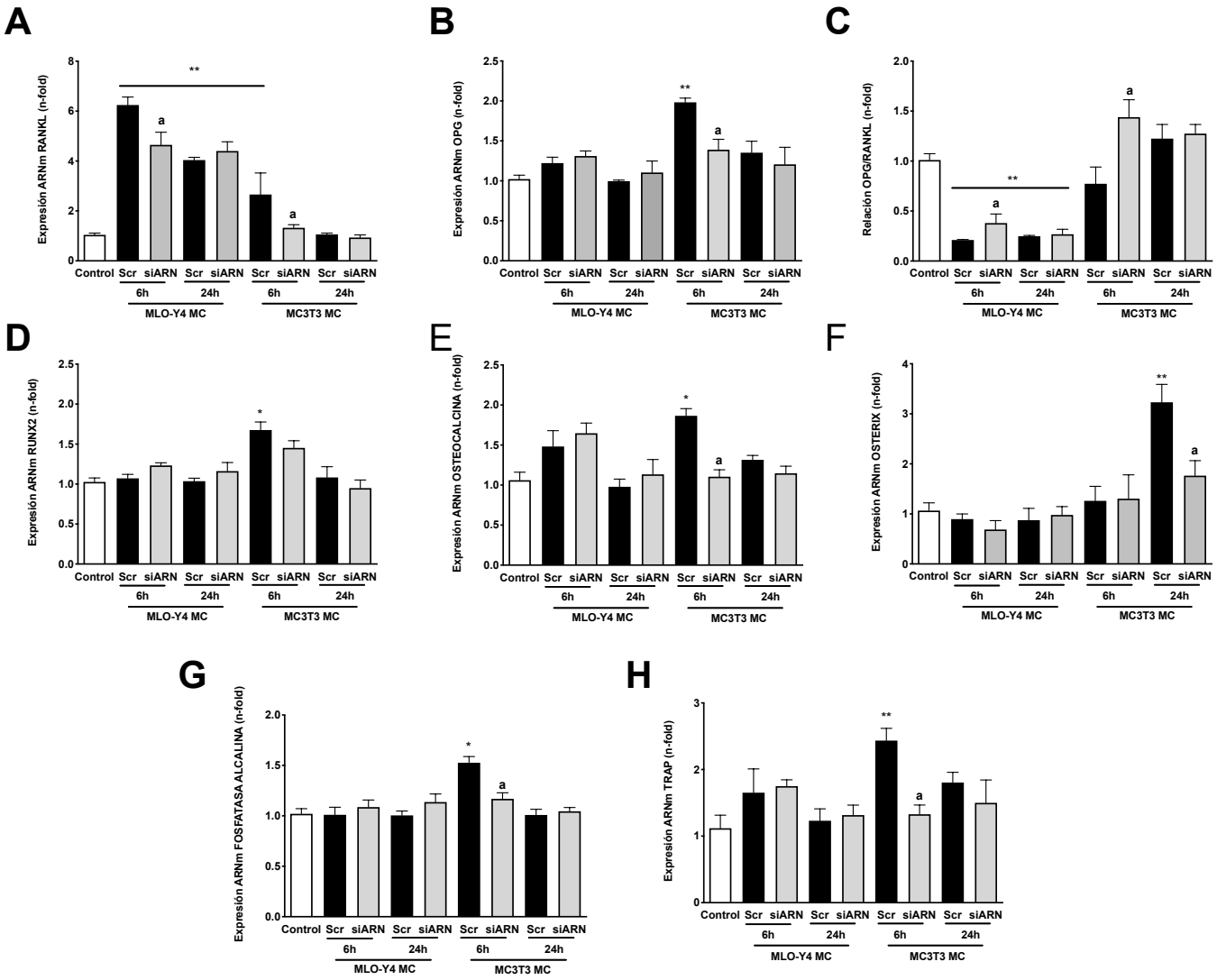

Figura 36. El osteomimetismo de las células TRAMP-C1 inducido por la comunicación entre células tumorales y óseas es inhibido cuando se silencia MINDIN. Expresión de ARNm evaluada mediante PCR en tiempo real en células TRAMP-C1 en condiciones control, "scrambled" (MC de células MLO-Y4 o MC3T3 previamente tratadas con MC de células TRAMP-C1 transfectadas con siARN "scrambled") y siARN (MC de células MLO-Y4 o MC3T3 previamente tratadas con MC de células TRAMP-C1 transfectadas con siARNs contra MINDIN). (A) RANKL, (B) OPG, (C) relación OPG/RANKL, (D) RUNX2, (E) OSTEOCALCINA, (F) OSTERIX, (G) FOSFATASA ALCALINA y (H) TRAP. Los resultados se representan como la media ± SEM de tres experimentos independientes por triplicado. *p<0.05 vs control; **p<0,01 vs control; [a]p<0,05 vs "scrambled" (Scr).

A continuación, evaluamos si MINDIN puede inducir cambios *in vivo* en el entorno óseo, los cuales podrían promover la metástasis de las células tumorales y el asentamiento de las mismas. Aunque el modelo tumoral de TRAMP-C1 potencialmente puede desarrollar metástasis óseas, el análisis de expresión de marcadores tumorales en fémures y tibias de nuestro modelo mostró niveles no significativos de PSCA y de MINDIN (Figura 37 A-

B). No obstante, las tibias de los ratones con tumor que expresa MINDIN mostraron sobreexpresión significativa de VEGFR2 (Figura 37 D). Además, la sobreexpresión de VEGFR2 se inhibió en las tibias de los ratones con tumor primario MINDIN silenciado (Figura 37D).

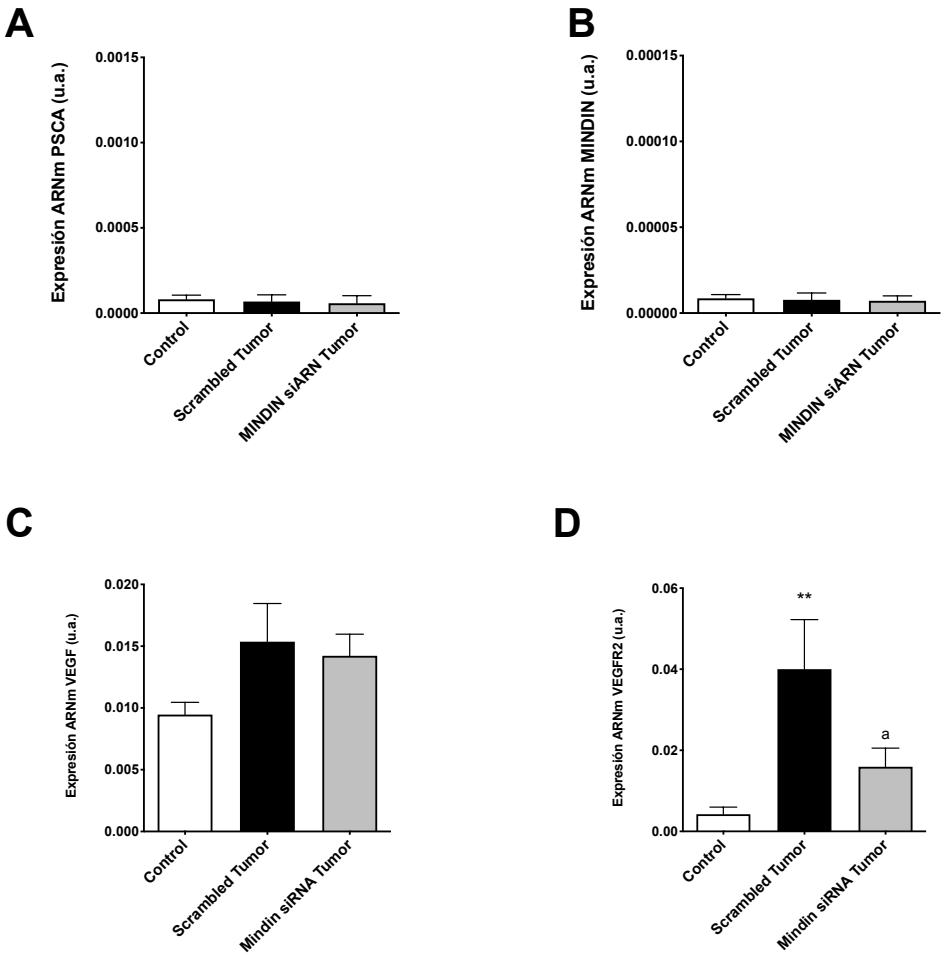

Figura 37: Ausencia de metástasis óseas en el modelo experimental de ratón con tumor prostático ortotópico inducido por TRAMP-C1. Expresión de ARNm evaluada mediante PCR en tiempo real de muestras de tibias de ratones. (A) PSCA, (B) MINDIN, (C) VEGF y (D) VEGFR2 en ratones control (inyección de PBS en la glándula prostática, sin tumor), ratones "scrambled" tumor (presencia de tumor causado por inyección de células TRAMP-C1 transfectadas con una secuencia "scrambled") y ratones MINDIN siARN tumor (presencia de tumor y sin expresión de MINDIN, causado por inyección de células TRAMP-C1 transfectadas con siARNS contra la secuencia codificante de MINDIN). Los datos se representan como la media ± SEM (n = 7-10 por grupo). **p<0,01 vs control; [a]p <0,05 vs "scrambled".

6.7 La expresión de MINDIN por parte del tumor primario de próstata induce cambios pre-metastásicos en la microarquitectura y la expresión génica ósea

Nuestro siguiente objetivo fue caracterizar en el modelo de ratón, antes del asentamiento y la propagación de la metástasis, los cambios estructurales y de

expresión génica que se producen en el microambiente óseo y que podrían favorecer la metástasis de las células tumorales de próstata. Como se ha mencionado anteriormente, MINDIN es capaz de actuar como mediador en algunas acciones de comunicación entre el hueso y el tumor primario de próstata, lo que sugiere el posible papel de MINDIN como inductor de cambios pre-metastásicos en el hueso.

La evaluación histomorfométrica de la microarquitectura ósea en el modelo de ratón mostró una disminución del volumen óseo, el grosor trabecular y el número de trabéculas (Figura 38 A-C) y un incremento de la separación trabecular y del número de osteoclastos y osteoblastos (Figura 38 D-F) en el fémur de ratones con tumor de próstata, en comparación con ratones control (sin tumor de próstata). Además, el análisis génico mostró una mayor expresión y actividad enzimática del marcador de resorción de osteoclastos en las tibias del grupo tumoral en comparación con los ratones control (Figura 39 H-I). Otros genes implicados en la formación (RUNX2, OSTERIX, OSTEOCALCINA) y resorción ósea (RANKL y RANK) y OPG no mostraron cambios significativos (Figura 39 C-G). Finalmente, observamos que el silenciamiento de MINDIN en los tumores originados por células TRAMP-C1 inyectadas en la próstata de ratón, revirtió los cambios histomorfométricos y de expresión génica observados en los fémures y tibias de nuestro modelo de ratón (Figuras 38 y 39). Estos resultados sugieren que los tumores de próstata que expresan MINDIN inducen alteraciones en el microambiente óseo antes de la metástasis.

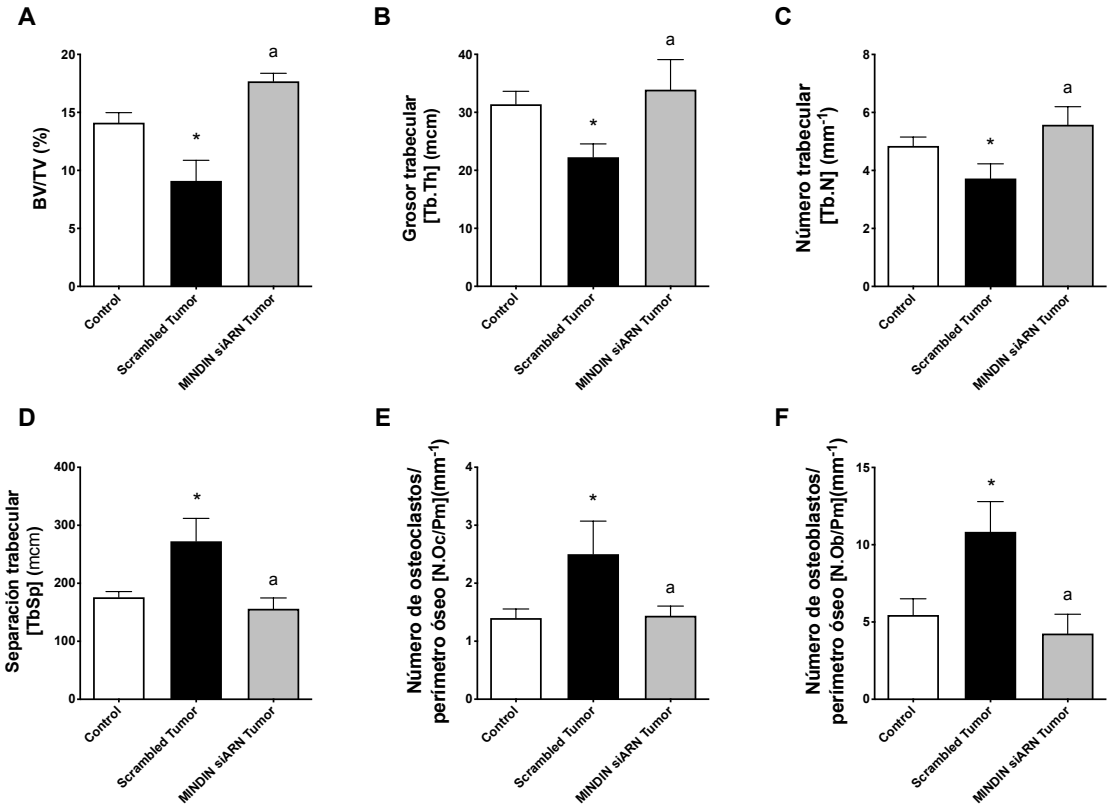

Figura 38. MINDIN induce cambios microestructurales en los fémures de ratones con tumor de próstata inducido por células TRAMP-C1. Los parámetros histomorfométricos óseos se evaluaron, como se describe en materiales y métodos, en los fémures de ratones control (inyección de PBS en la glándula prostática, sin tumor), ratones con tumor "scrambled" (presencia de tumor causado por la inyección, en la glándula prostática, de células TRAMP-C1 transfectadas con "scrambled") y ratones con tumor siARN (presencia de tumor causado por la inyección, en la glándula prostática, de células TRAMP-C1 transfectadas con siARNs contra MINDIN). (A) BV / TV: volumen óseo/volumen total; (B) Tb.Th: grosor trabecular; (C) Tb.N: número trabecular; (D) Tb.Sp: separación trabecular; (E) N.Oc/Pm: número de osteoclastos/perímetro óseo; (F) N.Ob/Pm: número de osteoblastos/perímetro óseo. Los datos se representan como la media ± SEM (n = 7-10 por grupo). *p <0.05 vs control; [a]p <0.05 vs "scrambled".

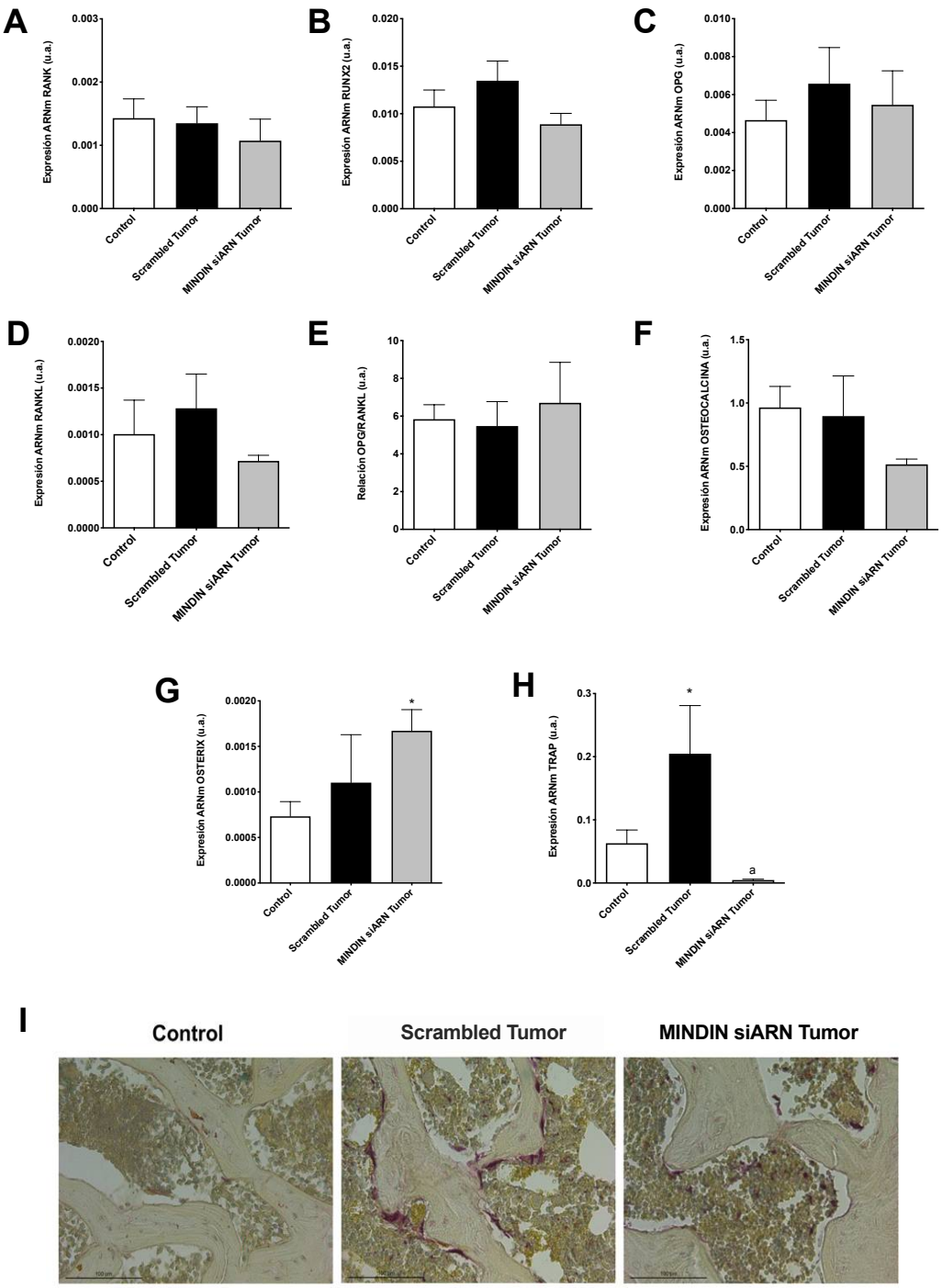

Figura 39: TRAP se sobreexpresa en tibias de ratones con tumores de próstata inducidos por TRAMP-C1. La expresión de ARNm se evaluó mediante PCR en tiempo real en tibias de las siguientes condiciones: control (inyección de PBS en la glándula prostática, sin tumor), ratones "scrambled" tumor (presencia de tumor causado por inyección de células TRAMP-C1 transfectadas con una secuencia "scrambled") y ratones MINDIN siARN tumor (presencia de tumor y sin expresión de MINDIN, causado por inyección de células TRAMP-C1 transfectadas con siARNs contra la secuencia codificante de MINDIN). (A) RANK, (B) RUNX2, (C) OPG, (D) RANKL, (E) OPG/RANKL, (F) OSTEOCALCINA, (G) OSTERIX y (H) Fosfatasa ácida resistente al tartrato (TRAP). (I) Se muestran imágenes representativas de la tinción de TRAP analizadas en secciones de hueso de fémures de los diferentes grupos. La barra de escala denota 100 µm. Los datos se representan como la media ± SEM (n = 7-10 por grupo). *p<0,05 vs control; [a]p<0,05 vs "scrambled".

6.8 MINDIN aumenta la adhesión de células de adenocarcinoma de próstata a tejido óseo

Estudios previos han demostrado que MINDIN aumenta la adhesión de diferentes tipos de células a la matriz extracelular, incluidos neutrófilos, macrófagos o linfocitos (212,213). Por lo tanto, nos preguntamos si la secreción de MINDIN por parte de los tumores de próstata podría aumentar la adhesión de las células de adenocarcinoma de próstata (TRAMP-C1) a las superficies óseas. Nuestros resultados mostraron una mayor capacidad adhesiva de las células TRAMP-C1 al hueso trabecular de los ratones del grupo tumoral en comparación con el grupo control (Figura 40A). No obstante, el silenciamiento de MINDIN en el tumor primario inhibió la adhesión de las células TRAMP-C1 al hueso trabecular (Figura 40A). Para dilucidar si la matriz extracelular o las células óseas eran necesarias para la adhesión de las células TRAMP-C1 al hueso, incubamos pre-osteoblastos MC3T3-E1, osteocitos MLO-Y4 y superficies recubiertas de colágeno tipo I con MINDIN. La presencia de MINDIN en las superficies recubiertas de colágeno aumentó ligeramente el número de células TRAMP-C1 unidas a la superficie de la placa en comparación con las superficies no recubiertas o recubiertas de colágeno sin MINDIN (Figura 40B). Además, el número de células tumorales TRAMP-C1 unidas a osteoblastos MC3T3-E1 u osteocitos MLO-Y4 estimuladas con MINDIN fue significativamente mayor en comparación con las superficies recubiertas de colágeno incubadas con MINDIN o con células no estimuladas (Figura 40B). La adhesión de células TRAMP-C1 a las células osteoblásticas MC3T3-E1 fue mayor que a las células osteocíticas MLO-Y4 (Figura 40B). Estos datos podrían señalar un papel de MINDIN en la adhesión de células tumorales al nicho endosteal.

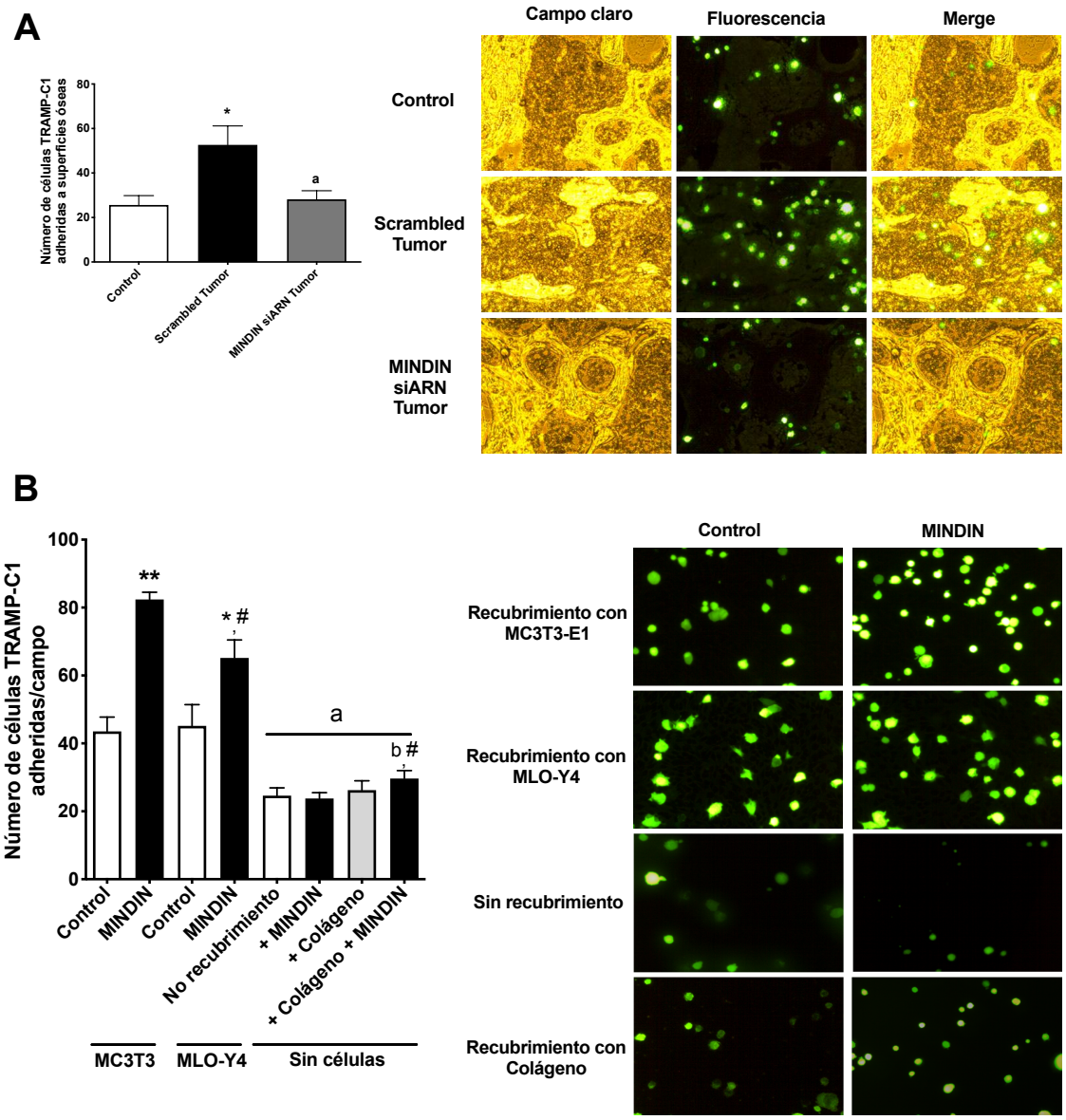

Figura 40: MINDIN aumenta la adhesión de células de adenocarcinoma TRAMP-C1 a las superficies óseas. Número de células TRAMP-C1 marcadas con calceína-AM y adheridas a las (A) superficies óseas de fémures de ratones control (inyección de PBS en la glándula prostática, sin tumor), ratones "scrambled" tumor (presencia de tumor causado por inyección de células TRAMP-C1 transfectadas con una secuencia "scrambled") y ratones MINDIN siARN tumor (presencia de tumor y sin expresión de MINDIN, causado por inyección de células TRAMP-C1 transfectadas con siARNS contra la secuencia codificante de MINDIN). (B) Superficies cubiertas por MC3T3-E1 o MLO-Y4 confluentes estimuladas o no con el péptido de MINDIN (5 ng/ml) durante 24 horas y placas recubiertas y no recubiertas de colágeno. Se muestran imágenes representativas de tres experimentos por triplicado. Los datos se muestran como la media ± SEM de tres experimentos por triplicado. *p<0,05 vs control, **p<0,01 vs control, $^{\#}$p<0,05 vs MC3T3 tratadas con MINDIN, ^{a}p<0,05 vs "scrambled" o superficies recubiertas con células y estimuladas con MINDIN, ^{b}p<0,05 vs condición correspondiente sin tratamiento con MINDIN.

6.9 MINDIN aumenta la expresión de genes implicados en la formación ósea, la mineralización de osteoblastos y la diferenciación osteoclástica

A continuación, comprobamos los efectos de MINDIN sobre las diferentes células óseas: células osteoblásticas MC3T3-E1, células osteocíticas MLO-Y4 y células monocíticas/pre-osteoclásticas RAW 264.7. La estimulación de las células MC3T3-E1 con MINDIN durante 6 y 24 horas produjo un aumento de la expresión génica de OPG y de marcadores de diferenciación osteoblástica, incluidos RUNX2, OSTEOCALCINA y OSTERIX, y una disminución de la expresión de RANKL (Figura 41 A-F).

Además, observamos un incremento de la expresión génica de OPG, RUNX2, OSTEOCALCINA y OSTERIX, así como una disminución de RANKL en células MC3T3-E1 estimuladas con el medio condicionado de células TRAMP-C1 durante 24 horas (Figura 41 G-L). Sin embargo, cuando se silenció MINDIN en células TRAMP-C1, los efectos producidos por el medio condicionado se revirtieron (Figura 41 G-L). La exposición prolongada de las células MC3T3-E1 a MINDIN (15 días) mantuvieron la sobreexpresión de Runx-2 y OSTEOCALCINA, pero sin embargo, no mostraron efecto sobre la expresión de OSTERIX, OPG o RANKL (Figura 42 A-E).

Cabe destacar que la estimulación con MINDIN durante 72 horas o 21 días indujo un aumento de la proliferación celular de las MC3T3-E1 y un incremento de la mineralización y deposición de mineral óseo (fosfato de calcio) por parte de las MC3T3-E1, respectivamente (Figura 43).

Por otra parte, la estimulación de las células MLO-Y4 con MINDIN durante 6 y 24 horas indujo un aumento de la expresión génica de OPG, OSTEOCALCINA y OSTERIX y una disminución de RUNX2 (Figura 44 A-F). La exposición prolongada a 15 días no mostró ningún cambio significativo en los marcadores óseos (Figura 42 F-I). La estimulación de las células MLO-Y4 con el medio condicionado de células tumorales TRAMP-C1 produjo un incremento de la expresión génica de OPG y OSTEOCALCINA (Figura 44 G-J). Estos cambios se revirtieron con el silenciamiento de MINDIN en las células TRAMP-C1 (Figura 44 G-J).

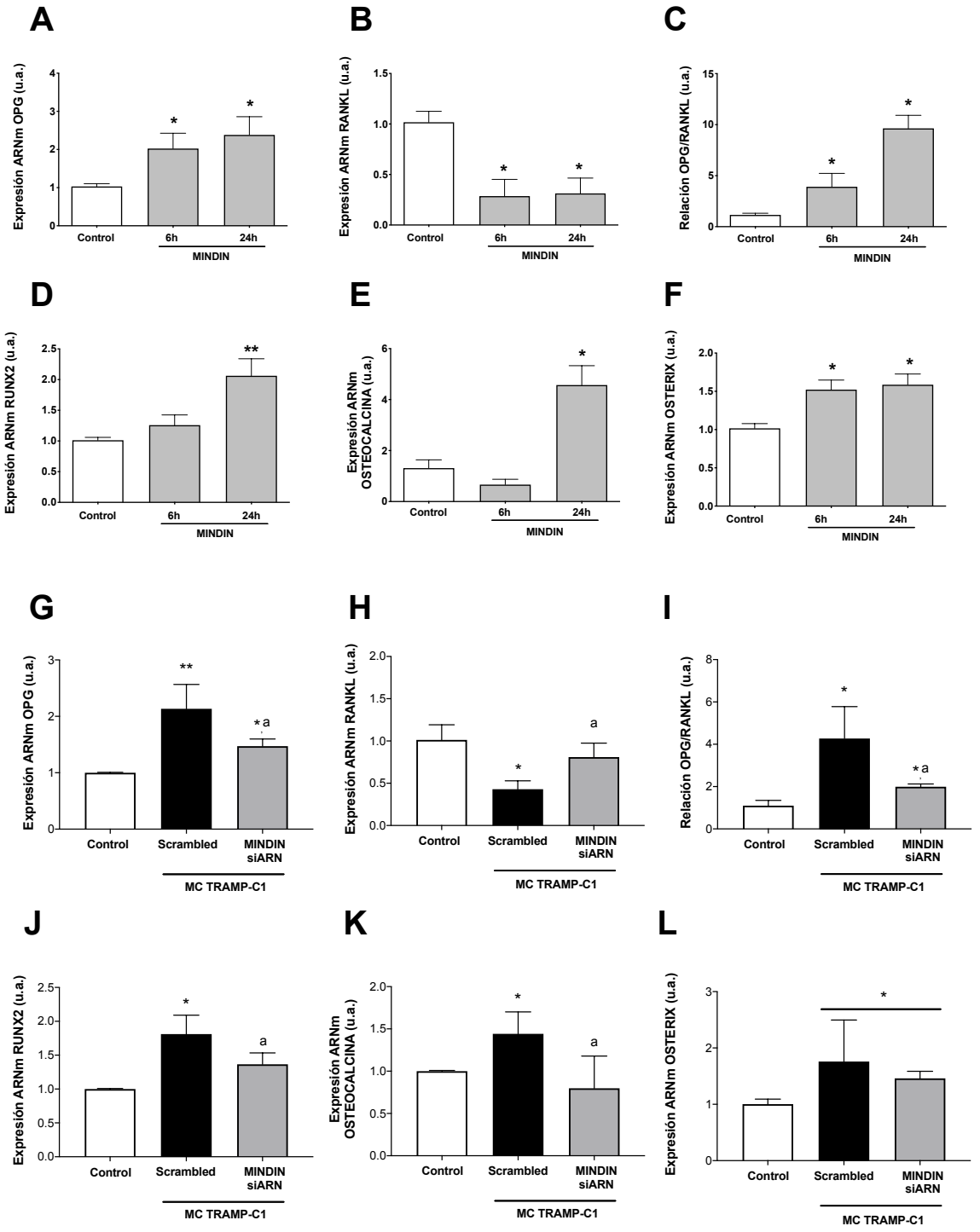

Figura 41. MINDIN y el medio condicionado de células TRAMP-C1 inducen cambios en los marcadores de remodelación ósea en MC3T3-E1. Las células MC3T3-E1 se estimularon con (A-F) MINDIN (5 ng / ml) durante 6 y 24 horas o (G-L) con medio condicionado de TRAMP-C1 (MC) durante 24 horas. Se evaluó la expresión de ARNm mediante PCR en tiempo real de (A y G) OPG, (B y H) RANKL, (C e I) relación OPG/RANKL, (D y J) RUNX2, (E y K) OSTEOCALCINA y (F y L) OSTERIX después de 6–24 horas de estimulación con MINDIN o con medio condicionado (MC) de células TRAMPC-1 silenciadas o no con siARNs específicos de MINDIN. Los valores experimentales son la media ± SEM de tres experimentos independientes. *p<0,05 vs control; **p<0,01 vs control; [a]p<0,05 vs MC "scrambled".

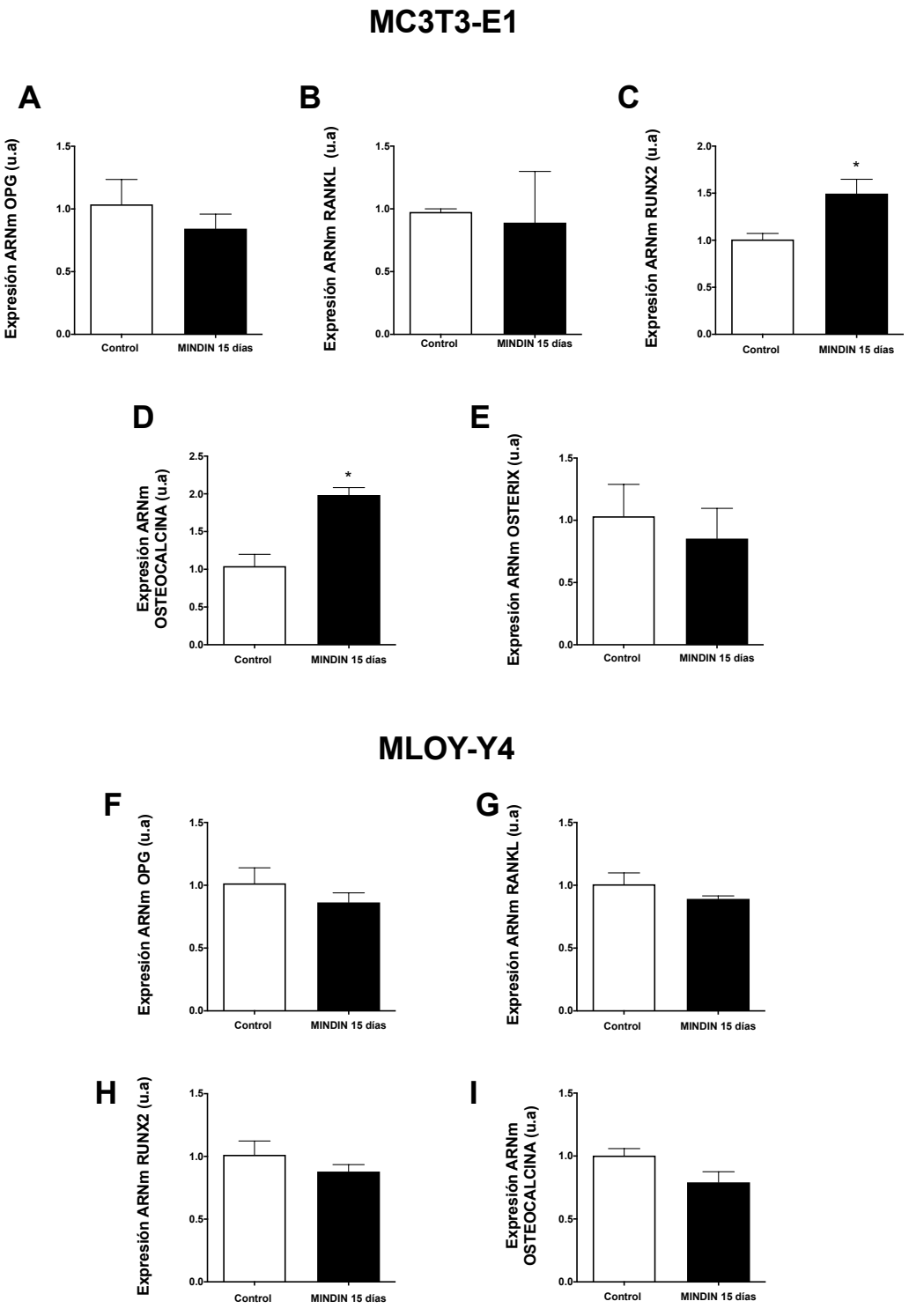

Figura 42. MINDIN induce a largo plazo (15 días) cambios en los marcadores de remodelación ósea en células osteoblásticas MC3T3-E1. Las células MC3T3-E1 y MLO-Y4 se estimularon con MINDIN (5 ng/ml) durante 15 días. Se evaluó la expresión de ARNm mediante PCR en tiempo real de (A y F) OPG, (B y G) RANKL, (C y H), RUNX2, (D e I) OSTEOCALCINA y (E) OSTERIX. Los valores experimentales son la media ± SEM de tres experimentos independientes. *p<0,05 vs control.

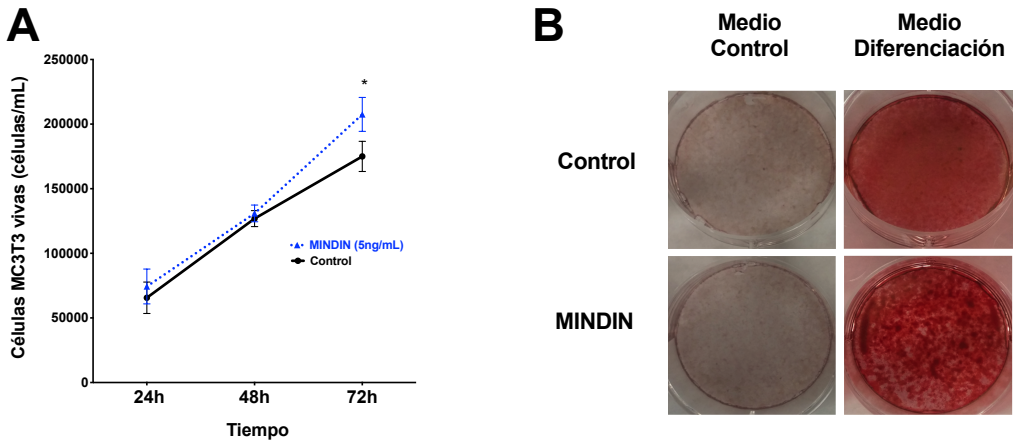

Figura 43. MINDIN induce la mineralización y la proliferación en MC3T3-E1. Las células MC3T3-E1 se estimularon con MINDIN (5 ng/ml) durante (A) 24, 48 y 72 horas o (B) 21 días. (A) La proliferación se evaluó mediante el método de exclusión con azul tripan. (B) La deposición de mineral óseo (fosfato de calcio) por las células osteoblásticas MC3T3-E1 se evaluó utilizando rojo de alizarina para teñir los depósitos de calcio. Se muestran imágenes representativas de tres experimentos independientes. Los valores experimentales son la media ± SEM de tres experimentos independientes. *p<0,05 vs control.

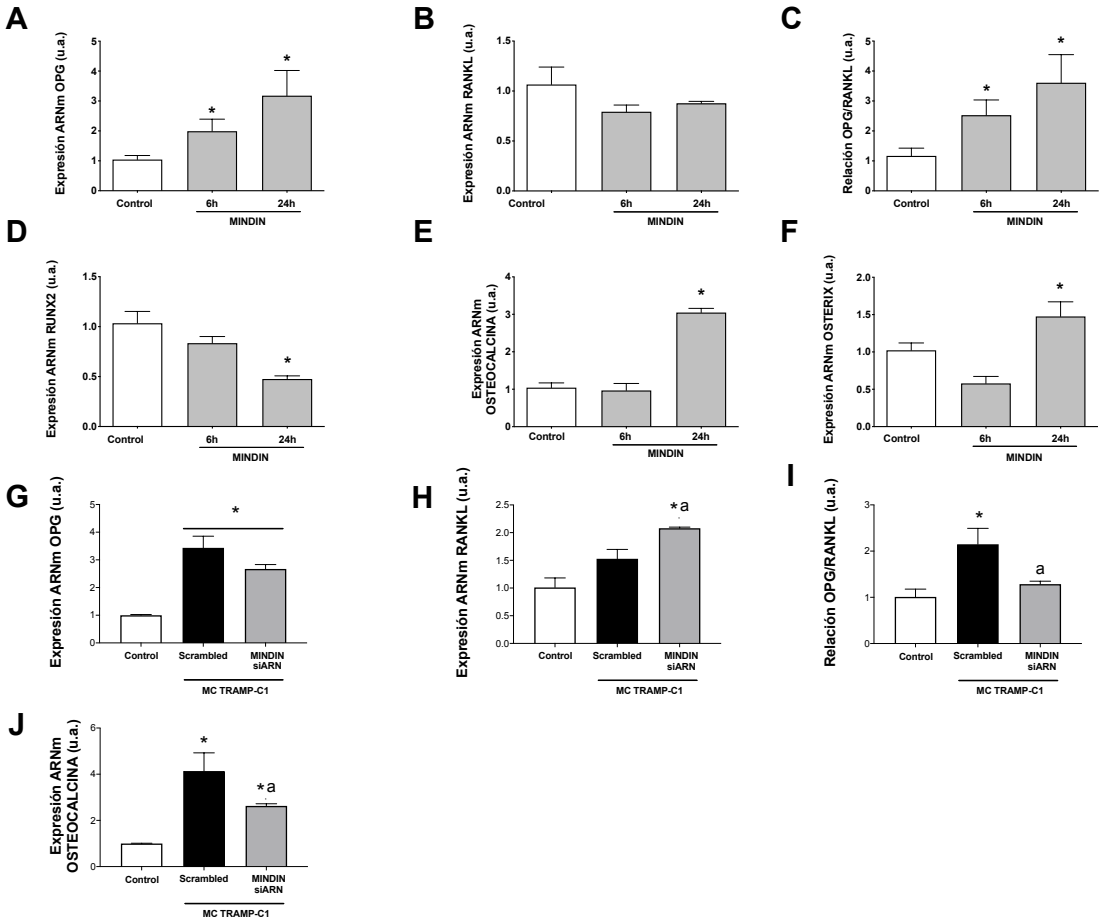

Figura 44. MINDIN y el medio condicionado de células TRAMP-C1 inducen cambios en los marcadores de remodelación ósea en MLO-Y4. Las células MLO-Y4 se estimularon (A-F) con MINDIN (5 ng/ml) durante 6 y 24 horas o (G-L) con medio condicionado de TRAMP-C1 (MC) durante 24 horas. Se evaluó la expresión de ARNm mediante PCR en tiempo real de (A y G) OPG, (B y H) RANKL, (C e I) relación OPG/RANKL, (D) RUNX2, (E y J) OSTEOCALCINA y (F) OSTERIX después de 6–24 horas de estimulación con MINDIN o con

medio condicionado (MC) de células TRAMPC-1 silenciadas o no con siARNs específicos de MINDIN. Los valores experimentales son la media ± SEM de tres experimentos independientes. *p<0,05 vs control; [a]p<0,05 vs MC "scrambled".

Por otro lado, los monocitos RAW 264.7 estimulados con MINDIN mostraron un aumento de los niveles del receptor RANK, un receptor fundamental en la inducción de diferenciación osteoclástica (Figura 45A). La diferenciación de monocitos RAW 264.7 a osteoclastos, mediante la incubación de estas células con RANKL durante 6 días, y la posterior estimulación con MINDIN, aumentó la expresión de TRAP, un marcador de osteoclastos, en comparación con la incubación con RANKL únicamente (Figura 45B).

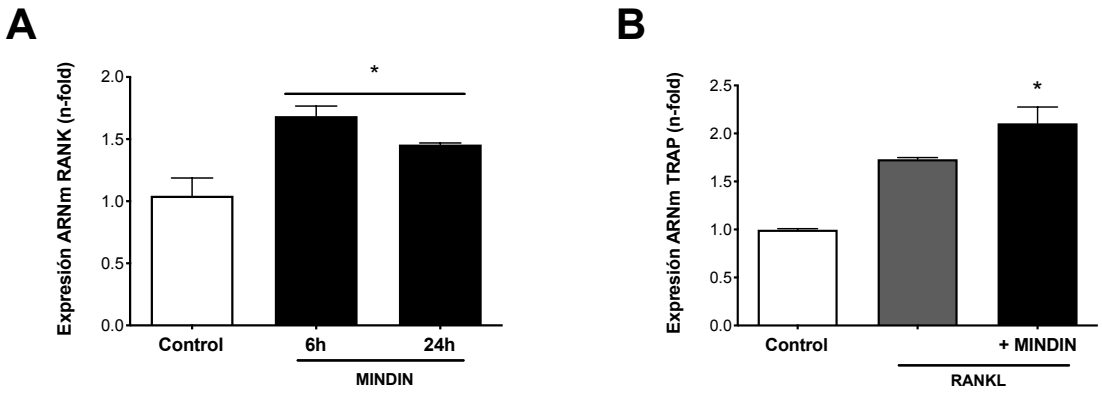

Figura 45. MINDIN desencadena la expresión de marcadores osteoclásticos en células monocíticas RAW 264.7. Las células RAW 264.7 se estimularon con MINDIN (5 ng/ml) durante (A) 6 y 24 horas o (B) 6 días. Los valores experimentales son la media ± SEM de tres experimentos independientes. *p<0,05 vs control.

En conjunto estos datos muestran que MINDIN favorece un perfil osteogénico en osteoblastos y osteocitos, y sugieren, además, que este factor puede promover la osteoclastogénesis.

6.10 MINDIN activa la vía de señalización de β-CATENINA en pre-osteoblastos

Otros miembros de la superfamilia de TROMBOESPONDINA que comparten algunos dominios estructurales con MINDIN, como son las R-ESPONDINAS (237), desencadenan cambios en el hueso al regular la vía de señalización de β-CATENINA (238). Dado que la señalización de β-CATENINA tiene un papel clave en la regulación ósea (239), nos preguntamos si los efectos de MINDIN en el hueso podrían ser causados por la activación de la vía de señalización de β-CATENINA.

La estimulación de células osteoblásticas MC3T3-E1 con MINDIN indujo la translocación de β-CATENINA al núcleo (Figura 46A) tras 3 horas de estimulación. Esta translocación también se observó a 6 y 24 horas después de la estimulación. Además, observamos incremento de los niveles nucleares de β-CATENINA (Figura 46B), disminución de la fosforilación de β-CATENINA y un aumento de los niveles de proteína total de β-CATENINA tras la estimulación con MINDIN en los osteoblastos MC3T3-E1 (Figura 46C).

Curiosamente, el silenciamiento de β-CATENINA inhibió la regulación negativa dependiente de MINDIN de los niveles de RANKL y el aumento de la relación OPG/RANKL en los osteoblastos (Figura 46 D-G). Sin embargo, el silenciamiento de β-CATENINA no inhibió el aumento dependiente de MINDIN en la adhesión de células de adenocarcinoma de próstata a los pre-osteoblastos (Figura 47A) o a la expresión inducida por MINDIN sobre RANK (Figura 47B) y TRAP (Figura 47C) en las células RAW 264.7, sugiriendo que existen vías alternativas a la β-CATENINA en estos procesos.

Datos previos mostraron que otro miembro de la familia de las ESPONDINAS, la ESPONDINA-1, se ha asociado con la migración e invasión de células de osteosarcoma a través de una vía de la quinasa de adhesión focal (FAK) y dependiente de la quinasa SRC (240). Por ello, estudiamos el papel de FAK y SRC en el aumento inducido por MINDIN en la adhesión de células de adenocarcinoma prostático a células óseas. Observamos que el tratamiento de las células MC3T3-E1 con el inhibidor Fak 14 y Saracatinib (inhibidor de la quinasa SRC), previo a la estimulación con MINDIN, disminuyó la adhesión de las células TRAMP-C1 a ambas células óseas (Figura 47D). Estos resultados sugieren que FAK y SRC juegan un papel importante en la adhesión promovida por MINDIN de células de cáncer de próstata a áreas con abundante presencia de células óseas.

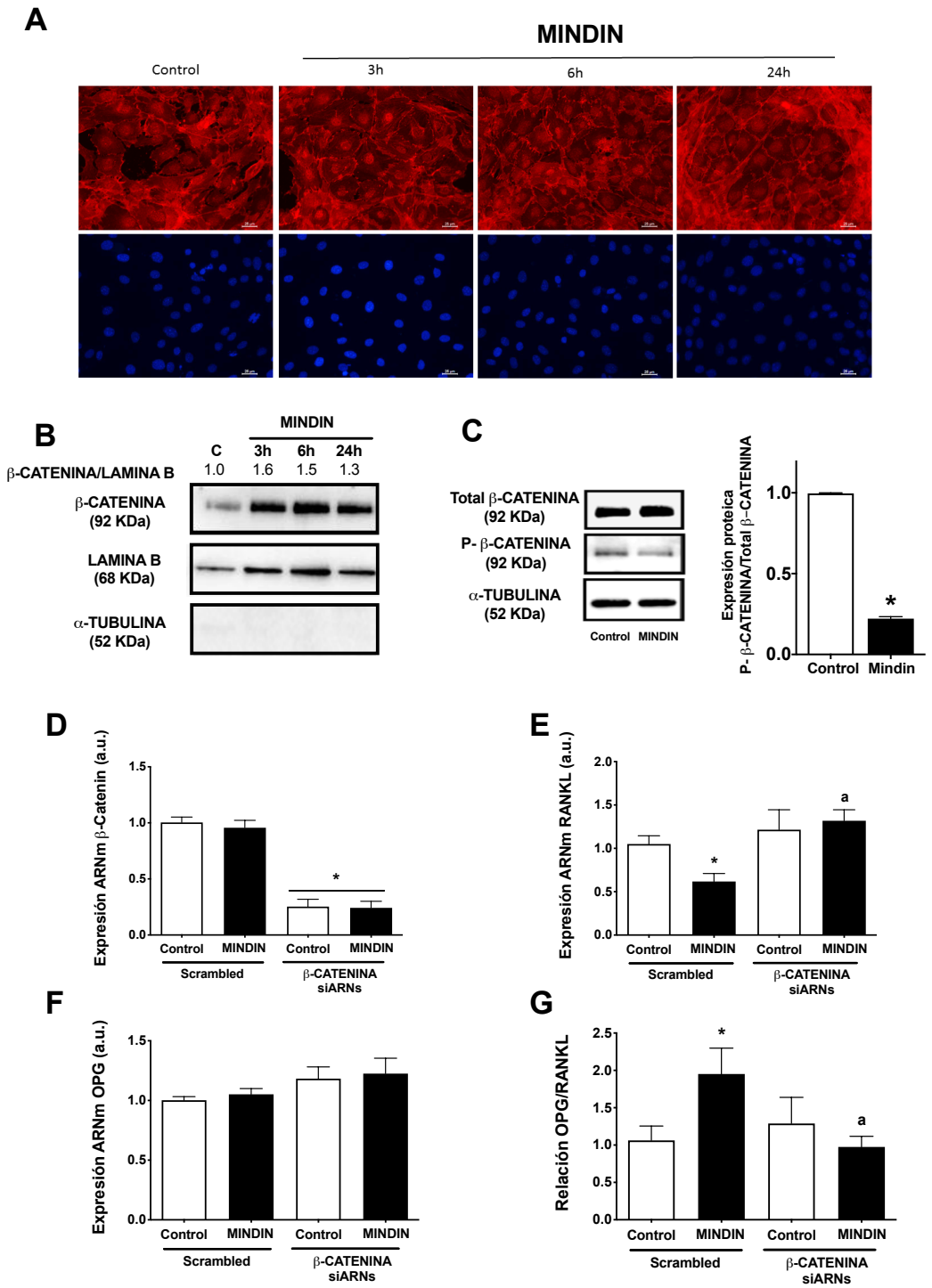

Figura 46. β-CATENINA actúa como mediador de los cambios inducidos por MINDIN en la expresión génica de las células osteoblásticas MC3T3-E1. Las células MC3T3-E1 se estimularon con MINDIN (5 ng/ml) durante diferentes períodos de tiempo (A: 3, 6 y 24 horas; B y C: 24 horas). β-CATENINA fue silenciada en algunos experimentos usando siARNs específicos como se describe en materiales y métodos. (A) La detección de β-CATENINA se realizó por inmunofluorescencia indirecta y microscopía de fluorescencia. Las imágenes representan los resultados de tres observaciones independientes. Se usó DAPI para teñir los núcleos. Las fracciones de proteína (B) nucleares o (C) totales se aislaron para evaluar la expresión de (B) CATENINA nuclear o (C) p-β-CATENINA y β-CATENINA total mediante Western Blot después de la estimulación con MINDIN durante 3-24 horas. Se muestran fotografías representativos. La α-TUBULINA se utilizó como control de carga. (D-G) Las células MC3T3-E1 se estimularon con MINDIN (5

ng/ml) durante 24 horas en presencia de "scrambled" o siARNs de β-CATENINA. El ARN total de células se aisló para evaluar mediante PCR en tiempo real los niveles de ARNm de (D) β-CATENINA, (E) RANKL, (F) OPG y (G) relación OPG/RANKL. Los valores experimentales son la media ± SEM de tres experimentos independientes. *p<0,05 vs control; [a]p<0,05 vs condición estimulada con MINDIN.

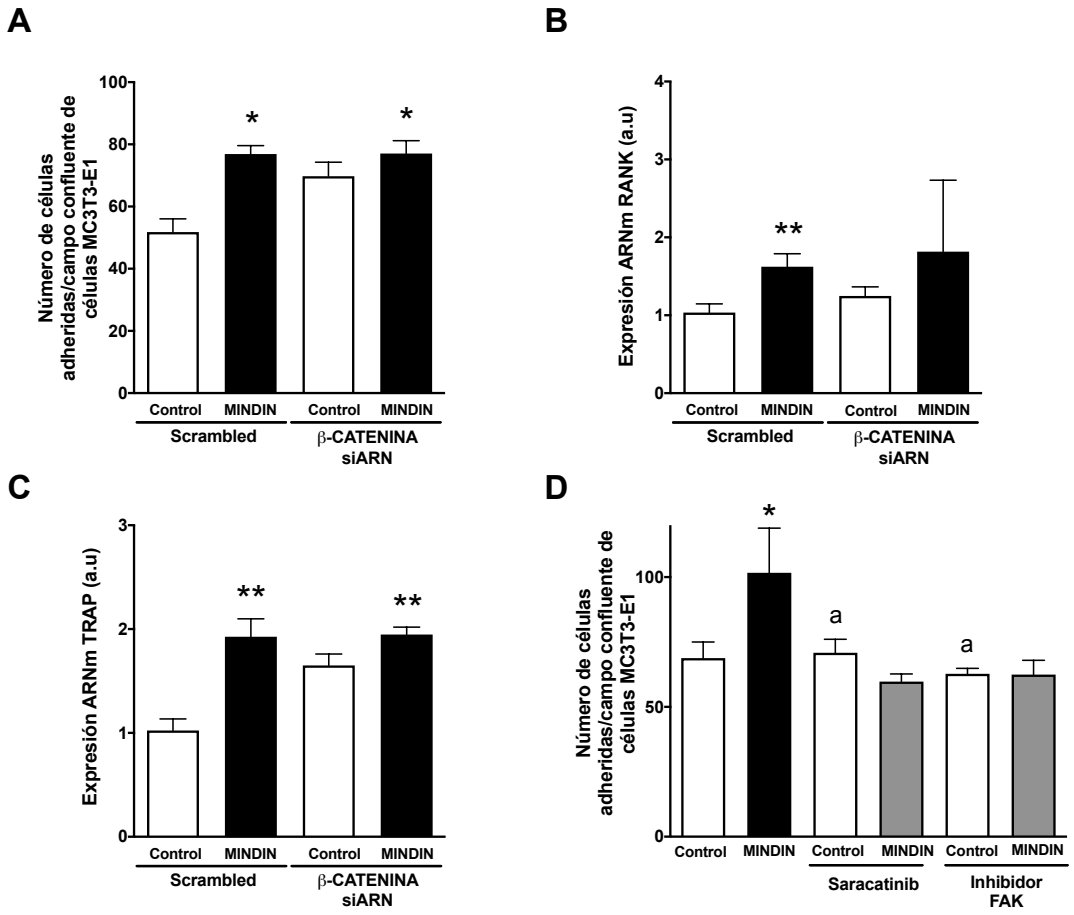

Figura 47. β-CATENINA no es un mediador de la adhesión de células de adenocarcinoma TRAMP-C1 inducida por MINDIN a las superficies cubiertas de osteoblastos o la diferenciación osteoclástica. Las células (A) MC3T3-E1 y (B y C) RAW 264.7 se transfectaron con siARNs específicos de β-CATENINA durante 24 horas y posteriormente se estimularon con MINDIN (5 ng/ml) durante 24 horas. (A) Se evaluó el número de células TRAMP-C1 marcadas con calceína-AM y adheridas a células MC3T3-E1. Se evaluó mediante PCR en tiempo real los niveles (B) RANK y (C) la expresión de TRAP en células RAW 264.7. (D) Se muestra el número de células TRAMP-C1 marcadas con calceína-AM y adheridas a superficies cubiertas de MC3T3-E1 confluentes. Las células MC3T3-E1 se trataron o no (control) con 1 µM del inhibidor Fak 14 o 1 µM de saracatinib (inhibidor de la quinasa SRC) durante 24 horas y se estimularon con MINDIN 5 ng/mL durante 24 horas. Los valores experimentales son la media ± SEM de tres experimentos independientes. *p<0,05 vs control; *p<0,01 vs control; [a]p <0,05 vs condición estimulada con MINDIN.

7. DISCUSIÓN

El cáncer de próstata es una de las principales causas de mortalidad y morbilidad por cáncer a nivel mundial (241). Las metástasis óseas derivadas de los tumores sólidos avanzados como el cáncer de próstata son dolorosas, difíciles de curar y con un mal pronóstico de supervivencia (169,242–244). Por lo tanto, la identificación de factores que regulan las interacciones tumor-hueso y el estudio de los mecanismos que regulan estas interacciones son necesarios para desarrollar nuevos enfoques terapéuticos. Se ha sugerido que el complejo proceso requerido para producir lesiones metastásicas óseas se basa en la plasticidad fenotípica de las células tumorales, lo que permite la adquisición de fenotipos pro-metastásicos como el osteomimetismo (es decir, la expresión de marcadores óseos, realizando comportamientos similares a las células óseas, para adaptarse y crecer en el hueso) (133,162,163,245). Esto implica que las células tumorales de próstata empiezan a expresar genes *de novo* involucrados en la fisiología ósea, lo que fomenta el potencial metastásico al aumentar la capacidad migratoria y de anclaje de las células tumorales al microambiente óseo (162–166). La adquisición de propiedades osteomimeticas del tumor de próstata y la modulación de las células tumorales por el entorno óseo se han propuesto como pasos importantes antes del establecimiento de la metástasis ósea del adenocarcinoma de próstata (246–250). Además, se ha descrito que los factores óseos liberados por las células tumorales contribuyen al "ciclo vicioso" de las metástasis óseas, permitiendo que las células tumorales prosperen en el hueso estableciendo una comunicación entre las células tumorales y óseas (251). Sin embargo, los mecanismos que rigen estos procesos aún no se conocen bien.

En nuestro estudio identificamos MINDIN como un factor secretado por los tumores de próstata que modula la expresión de genes óseos en las células tumorales, la proliferación, la migración y las propiedades adherentes de las células tumorales y su comunicación con las células óseas. Se ha descrito que la expresión de MINDIN es más alta en muestras de pacientes con cáncer de próstata más agresivo y peor pronóstico, y aún más alta en aquellos con metástasis óseas (219,252). La evaluación de la expresión de MINDIN mediante inmunotinción de tumores con diferentes puntuaciones Gleason también ha revelado en otros estudios que la tinción de MINDIN es más intensa en los grados Gleason 7–8 que en los tumores con grados Gleason 2–6 (219,252). Además, se

ha descrito que los niveles de MINDIN fueron más altos en individuos con cáncer de próstata con metástasis óseas, seguidos por individuos sin metástasis óseas, hiperplasia y controles (252). Sin embargo, no se ha descrito el papel de MINDIN en la progresión del cáncer, además de su posible papel como marcador metastásico. En este sentido, nuestros datos también muestran que la inmunotinción de MINDIN aumenta en muestras con puntuaciones altas de Gleason y valores altos de riesgo D'amico, lo que respalda el papel de MINDIN como un biomarcador del cáncer de próstata.

Con respecto a NHERF1 se ha descrito que esta proteína de andamiaje se encuentra involucrada tanto en la progresión como en la inhibición tumoral en diferentes tipos de cánceres (175,177,179,184–186,189–197). Nuestros resultados muestran una disminución del inmunomarcaje de NHERF1 en los tumores de próstata humanos en comparación con las muestras control. Apoyando estas observaciones, un estudio previo ha revelado que las intensidades de inmunotinción promedio de NHERF1 son más bajas en las muestras de cáncer de próstata y en aquellas con metástasis óseas en comparación con las muestras control (175). En particular, las muestras metastásicas mostraron una tinción significativamente menor que todas las demás condiciones, lo que indica que la pérdida de la expresión de NHERF1 puede desempeñar un papel fundamental en la metástasis del cáncer de próstata (175).

En el modelo animal y en las células de adenocarcinoma de próstata TRAMP-C1 observamos que MINDIN promueve la expresión de genes relacionados con osteoblastos y osteoclastos, los cuales han demostrado ser cruciales para el desarrollo de metástasis óseas (117,118,121,127–130,171–173). Curiosamente, diferentes niveles de expresión de MINDIN se asociaron con variaciones en los niveles de expresión de genes osteomiméticos tanto *in vitro* como *in vivo*. Aunque MINDIN se ha definido como una proteína de la matriz extracelular asociada con funciones de opsonización en macrófagos (207), los resultados obtenidos, así como estudios previos de otros grupos (219), muestran una intensa inmunotinción citoplasmática. Es probable que la distribución citoplasmática de MINDIN pueda tener un papel biológico diferente al de la proteína secretada pero aún desconocido.

La evaluación de la localización de NHERF1 revela que este factor se encuentra presente en la zona apical de la membrana celular y en el citoplasma en células control, mientras que las muestras tumorales presentan niveles disminuidos de NHERF1 y expresión citoplásmica. Estudios previos han mostrado que en condiciones fisiológicas NHERF1 suele localizar cerca de la membrana celular asociado al citoesqueleto de actina subcortical en los tejidos epiteliales (253–256). Además, se ha observado que la polaridad de las células epiteliales se pierde cuando NHERF1 no se expresa en la zona apical de la membrana plasmática (193), debido a que la localización apical de NHERF1 es necesaria para mantener la integridad epitelial (257). En este sentido, la pérdida de NHERF1 en la membrana celular en muestras tumorales podría estar asociada con la adquisición de características típicas del proceso de transición epitelio-mesénquima (TEM). Este proceso se caracteriza por la pérdida de características epiteliales como la polaridad o el contacto célula-célula y adquisición de características mesenquimales durante la progresión de varios tumores, incluido el cáncer de próstata (258). De hecho, estudios previos han asociado la relocalización de NHERF1 desde la zona apical al citoplasma con procesos de TEM y una mayor capacidad migratoria e invasiva celular en otros tipos de cáncer (193). Sin embargo, los mecanismos que desencadenan la desregulación de NHERF1 y la movilización desde la membrana plasmática al citoplasmas no se han descrito todavía en el cáncer de próstata. En este sentido, nuestras observaciones, *in vivo* e *in vitro,* muestran que la disminución en la expresión y la relocalización de NHERF1 es inducida por MINDIN en células tumorales de próstata.

Estudios previos han descrito el papel de RANKL como un inductor de la resorción ósea que media la activación de osteoclastos (164), pero también han demostrado que es un factor que podría desencadenar metástasis óseas y facilitaría la diseminación de varios tipos de células tumorales al tejido óseo, incluidas las células del CaP (121), a través de la activación de la señalización NF-kappa β (259). Cabe destacar que RANKL posee características proinflamatorias (116,260) y que los procesos inflamatorios se encuentran relacionados con el mecanismo de transformación y progresión tumoral (261). A pesar de que observamos un incremento de OPG (el receptor señuelo soluble de RANKL) en muestras tumorales de nuestro modelo, estos niveles de expresión fueron significativamente más bajos que los de RANKL, como demuestra la relación OPG/RANKL

disminuida en los tumores. Estos sugiere que la vía de señalización de RANKL es predominante en nuestro modelo tumoral. Es posible que la sobreexpresión de OPG por los tumores de próstata se deba a una vía compensatoria inducida para tratar de bloquear los niveles elevados de RANKL. En cualquier caso, nuestros datos muestran un aumento en la expresión de RANKL y en el marcador de osteoclastos TRAP, lo que sugiere que MINDIN desencadena señales tempranas pro-resorción en tumores de próstata.

Por otro lado, el factor transcripcional óseo RUNX2 ha demostrado ser un promotor fundamental en la osteogénesis y participar como factor de transcripción pro-metastásico en células tumorales de próstata (162). El potencial pro-metastásico de RUNX2 se ha asociado con la capacidad de este factor para sobreexpresar genes involucrados en la transición epitelio-mesénquima (SOX9, LCN2 y SNAI2), en la degradación de matriz extracelular (metaloproteasas de matriz 9 y 13) o en la angiogénesis (VEGF) (72,162,262–269). Además, como parte de su función reguladora, RUNX2 promueve la osteoblastogénesis y regula varios genes implicados en la formación ósea, como son los correspondiente a la OSTEOCALCINA y el factor de transcripción OSTERIX (78), dos proteínas cuya expresión también aumenta por la acción de MINDIN en nuestro modelo. *In vitro* también observamos que MINDIN aumentó la expresión de la FOSFATASA ALCALINA ósea, un marcador osteoblástico. No observamos este efecto *in vivo*, probablemente debido al patrón de expresión puntual y transitorio característico de la FOSFATASA ALCALINA durante la diferenciación temprana de osteoblastos (78). En conjunto, estas observaciones indican que MINDIN induce la adquisición de un fenotipo mixto osteoblástico y osteoclástico con propiedades pro-metastásicas en células tumorales de próstata. Aunque las metástasis óseas del cáncer de próstata se han caracterizado clásicamente como osteoblásticas, algunas pruebas sugieren que el desarrollo de metástasis óseas derivadas del cáncer de próstata requieren la actividad de los osteoclastos, además de la actividad osteoblástica, lo que inicialmente generaría osteólisis temprana seguida de la actividad osteoblástica posterior (262).

Como se ha comentado previamente, MINDIN promueve la expresión de genes osteoblásticos y osteoclásticos, lo cual se ha asociado con la progresión del tumor de próstata y el desarrollo de metástasis óseas (162,223,225). Sin embargo, la sobreexpresión de NHERF1 no causó ningún efecto en la mayoría de los genes relacionados con el hueso, lo cual sugiere que MINDIN induce osteomimetismo por mecanismos independientes de NHERF1. Curiosamente, la sobreexpresión de MINDIN y NHERF1 parece aumentar la expresión del factor pro-osteoclástico RANKL en las células de cáncer de próstata. Los resultados expuestos sugieren que MINDIN puede afectar a la expresión de RANKL por un mecanismo independiente de NHERF1, mientras que es posible que la sobreexpresión de NHERF1 más allá de cierto umbral también pueda desencadenar un aumento de RANKL. A este respecto, un estudio previo ha descrito la disminución de la función de los osteoclastos en ratones con deleción de NHERF1, por un mecanismo probablemente dependiente de la producción alterada de RANKL (270).

También observamos que MINDIN desencadena la proliferación de células tumorales, su migración y una mayor adhesión a las células óseas. En este sentido, estudios previos demostraron que MINDIN activa en monocitos RAW 264.7 y en células de cáncer de colon la señalización de NF-kappa β (271), una vía de señalización que promueve la proliferación de células de cáncer de próstata (259). La actividad de NHERF1 se ha asociado con la regulación de la activación de NF-kappa β en procesos de inflamación (272). Por lo tanto, podría ser posible que NHERF1 medie, al menos en parte, la acción dependiente de MINDIN sobre la proliferación de células tumorales de próstata.

También se ha propuesto un papel de MINDIN en la adhesión y crecimiento de las neuronas embrionarias del hipocampo (210). Además, se ha demostrado que MINDIN es un ligando para las integrinas, siendo las interacciones MINDIN-integrina críticas para el reclutamiento de neutrófilos y macrófagos en modelos inflamatorios *in vivo* (273). En estos estudios se ha propuesto que MINDIN actúa como un ligando de las integrinas, lo que mejora la adhesión y migración celular (212). A pesar de que MINDIN aumenta la adhesión de las células TRAMP-C1 a las superficies recubiertas de colágeno y a osteoblastos y osteocitos, el número de células TRAMP-C1 adheridas a las superficies cubiertas de osteoblastos (MC3T3) fue mayor en comparación con las de los osteocitos

(MLO-Y4) o las superficies cubiertas de colágeno. Esto sugiere que las células de adenocarcinoma de próstata se unen preferentemente a las células que recubren las cavidades de la médula ósea (superficies endosteales). Además, nuestros datos muestran que la sobreexpresión de NHERF1 inhibe las acciones dependientes de MINDIN sobre la migración de células de cáncer de próstata sin afectar la adhesión celular. De hecho, estudios previos han asociado la pérdida de NHERF1 con un aumento de la migración e invasión celular en otros tipos de tumores (42). Por lo tanto, aunque MINDIN podría unirse a integrinas en células de cáncer de próstata para promover la adhesión celular, es poco probable que NHERF1 actúe como mediador en la unión MINDIN-integrina o en su señalización, por lo tanto no afectaría a la adhesión celular inducida por MINDIN.

Con respecto a la modulación ósea de la progresión del cáncer de próstata, observaciones previas han demostrado que células similares a los osteoblastos (HOBIT) secretan factores que modifican la expresión génica de las células LNCaP, induciendo un fenotipo metastásico en esta línea celular de cáncer de próstata (273). En el caso de nuestros modelos celulares los factores secretados por las células osteoblásticas MC3T3-E1 o los osteocitos MLO-Y4 no indujeron cambios significativos en la expresión ectópica de genes óseos en las células TRAMP-C1. Sin embargo, los factores secretados por las MC3T3-E1 o MLO-Y4 pre-incubadas con medio condicionado de TRAMP-C1 desencadenaron un fenotipo osteomimético en las células de cáncer de próstata. Estos resultados sugieren que las células TRAMP-C1 secretan factores que afectan a los osteoblastos y los osteocitos y, a su vez, estas células óseas secretan factores que promueven la expresión de genes óseos en las células tumorales prostáticas. Además, dada la disminución de la expresión de genes óseos cuando se silenció MINDIN en las células TRAMP-C1, parece ser necesaria la secreción de esta proteína, al menos en parte, para inducir la comunicación entre las células de adenocarcinoma y los osteoblastos/osteocitos *in vitro*. Nuestros datos sugieren que la comunicación del cáncer de próstata con las células óseas parece seguir al menos dos vías diferentes: las moléculas secretadas por los osteocitos pre-estimulados inducen la activación del factor de remodelación ósea RANKL, mientras que los osteoblastos pre-estimulados promueven preferentemente la expresión de genes osteoblásticos (RUNX2 y OSTERIX)

en células tumorales de próstata. Por un lado, las interacciones con los osteocitos podrían desencadenar la liberación de señales pro-resorción por parte del tumor, probablemente causando osteolisis correspondiente a lesiones tempranas osteolíticas, además de participar en el "ciclo vicioso" de retroalimentación entre el tumor de próstata y las metástasis óseas. Por otro lado, la comunicación con los osteoblastos podría promover la expresión y secreción de factores de diferenciación ósea que causaría lesiones osteoblásticas en las metástasis óseas.

Además, se han encontrado niveles elevados de MINDIN en el suero de pacientes con cáncer de próstata (219), lo que sugiere que esta proteína podría ser secretada por el tumor primario a la sangre, actuar directamente sobre células óseas y desencadenar la liberación de factores inductores osteomiméticos por los osteoblastos y los osteocitos. Estos factores secretados por el tejido óseo podrían a su vez actuar sobre el tumor primario favoreciendo la adquisición de propiedades óseas pro-metastásicas en las células de cáncer de próstata y promoviendo un fenotipo agresivo y organotrópico óseo. A este respecto, hemos observado niveles incrementados de VEGFR2 en tibias de ratones con un tumor primario prostático con aparente ausencia de metástasis en el tejido óseo. VEGFR2 es un receptor pro-angiogénico expresado en osteoblastos que se ha propuesto como diana para tratar las metástasis óseas derivadas del cáncer de próstata (274,275). Hallazgos recientes muestran que la inhibición de VEGFR2 en los osteoblastos suprime la progresión del cáncer de próstata en las metástasis óseas y disminuye las acciones metastásicas inducidas por este tipo de tumor (274). Todos estos hallazgos y nuestras observaciones sugieren que los tumores inducidos por células TRAMP-C1 desencadenan cambios óseos en ratones que se parecen a los observados en las metástasis óseas humanas inducidas por los tumores prostáticos. Los tumores primarios crean nichos pre-metastásicos en órganos secundarios donde posteriormente se producirá la metástasis (276). En la fase inicial de la formación de nicho pre-metastásico, las células tumorales producen y secretan factores solubles para desencadenar la formación de un nicho pre-metastásico inmaduro (276). Por ello, el descubrimiento de factores específicos involucrados en la formación del nicho pre-metastásico ayudaría al desarrollo de futuras estrategias terapéuticas. Nuestros resultados muestran a este respecto que la secreción de la proteína de matriz

extracelular MINDIN, por las células tumorales prostáticas, induce cambios en el microambiente óseo que podrían promover las metástasis derivadas del cáncer de próstata.

Apoyando estos resultados, observamos que los tumores inducidos por las células TRAMP-C1 en ratones causan cambios en la microarquitectura ósea y en la expresión génica, sin presencia detectable de metástasis en el hueso. Los cambios observados en la microarquitectura ósea revelaron un patrón de resorción ósea, como se muestra por la disminución de BV/TV, número y grosor trabecular y aumento de la separación trabecular. Aunque las metástasis derivadas del cáncer de próstata se han definido clásicamente como osteoblásticas y asociadas con la formación de hueso, requieren una fase de reabsorción en sus etapas iniciales (277) y desarrollan lesiones mixtas (osteoblásticas y osteoclásticas) en etapas más avanzadas (277). En este sentido, observamos un mayor número de osteoclastos y una mayor expresión génica de TRAP y un incremento de la tinción de TRAP en los huesos de ratones con tumor de próstata. TRAP, una metaloenzima cuya expresión es característica en osteoclastos activados, también promueve propiedades metastásicas en células de cáncer de mama MDA-MB-231 (108) y se ha descrito que aumenta en metástasis óseas de cáncer de próstata avanzado (109).

Por otro lado, el aumento de la expresión del factor de transcripción osteogénico RUNX2 y el aumento del número de osteoblastos en los huesos de los ratones con tumores de próstata, sugieren que los tumores promueven la diferenciación y activación de los osteoblastos, a pesar de que exista actividad osteoclástica. En este sentido, un modelo de metástasis intra-tibial del cáncer de próstata mostró que los niveles de RUNX2 se asociaron con el desarrollo de tumores, aumento de la expresión de genes relacionados con metástasis (metaloproteinas de matriz 9 y 13, VEGF, osteopontina) y factores de resorción ósea (PTHrP, IL-8) (262). Estas observaciones sugieren que RUNX2 podría ser un factor fundamental que controla los procesos metastásicos osteoblásticos y osteoclásticos en el cáncer de próstata.

La unión de MINDIN a integrinas de osteoblastos y osteocitos podría desencadenar señales en estas células óseas que faciliten la adhesión de las células de cáncer de próstata. En este sentido, la interacción entre integrinas y quinasas FAK y SRC se ha relacionado con promoción de la adhesión celular (278). Nuestros resultados muestran las acciones inhibidoras de las quinasa FAK y SRC sobre la capacidad de las células óseas para promover la adhesión de células tumorales, sugieren una posible relación entre estas quinasas e integrinas en el proceso de colonización del hueso por las células tumorales. Además, los modelos tumorales prostáticos de ratón han demostrado que las células tumorales se localizan en áreas del nicho endosteal óseo, que presenta un gran número de osteoblastos. Se cree que la interacción del receptor 4 de quimiocina (CXCR4) con el ligando de quimiocina 12 (CXCL12) es un componente clave en la localización y adhesión de las células tumorales al nicho metastásico en el hueso (279). CXCL12 se expresa en las células endosteales y en capas de osteocitos cercanas al endosteo (280). Por lo tanto, MINDIN podría promover un aumento en la expresión de CXCL12 en las células del endosteo, en particular en los osteoblastos, para mejorar las interacciones CXCR4/CXCL12 entre el tumor y las células osteoblásticas. En este sentido, observamos que la adhesión de las células tumorales a las células osteoblásticas MC3T3-E1 estimuladas por MINDIN fue mayor en comparación con los osteocitos MLO-Y4, lo que sugiere que los osteoblastos, que son las células más expuestas en el nicho endosteal, median la unión de las células tumorales de próstata al hueso. Por lo tanto, los cambios dependientes de MINDIN en la microarquitectura ósea, la sobreexpresión de los factores óseos y la adhesión incrementada de las células tumorales a las superficies óseas, en conjunto, sugieren que la expresión de MINDIN en los tumores primarios de próstata induce un nicho favorable para las metástasis óseas.

Los efectos producidos por MINDIN en el hueso muestran, *in vitro,* las acciones de esta proteína en la proliferación y diferenciación de osteoblastos, así como la modulación de diferentes genes involucrados en la formación y remodelación ósea (RUNX2, osteocalcina, osterix, OPG, RANKL). La exposición prolongada a MINDIN mantuvo la sobreexpresión de los marcadores de diferenciación osteoblástica pero no afectó el eje OPG/RANKL, lo que sugiere que la estimulación continua con MINDIN promueve la diferenciación de osteoblastos pero no influye en la comunicación prolongada de

osteoblastos-osteoclastos. Estos resultados respaldan nuestros datos *in vivo* que muestran una mayor expresión de RUNX2. Aún así, no observamos cambios significativos en los niveles de OPG y RANKL en huesos de ratones con tumor de próstata. Además, los osteocitos, los principales reguladores de RANKL en el hueso (281), no sobreexpresaron OPG o RANKL después de una exposición prolongada a MINDIN. Curiosamente, MINDIN también desencadenó la diferenciación y activación de osteoclastos después de varios días de estimulación. Además, el fenotipo osteoclástico y de resorción ósea observado en nuestro modelo probablemente puede ser causado por la secreción de RANKL por parte del tumor primario, el cual podría llegar al microambiente óseo y participar como el principal regulador de la diferenciación osteoclástica.

No hay datos previos que describan las vías de señalización desencadenadas por MINDIN en las células óseas. Sin embargo, otros miembros de la familia MINDIN (familia de la ESPONDINA), con los que comparten un dominio de trombospondina, como la R-ESPONDINA, muestran la activación de la vía de la β-CATENINA durante la osteogénesis (238). La activación de β-CATENINA también se ha relacionado con la TEM previamente mencionada (proceso esencial por el cual las células pierden sus características epiteliales y adquieren características mesenquimales durante la progresión tumoral del cáncer de próstata) (258). Debido a la implicación de la vía β-CATENINA tanto en la osteogénesis como en procesos mediadores de progresión tumoral como la TEM, la activación dependiente de MINDIN de esta vía de señalización podría ser un mecanismo central en la progresión del tumor de próstata.

Curiosamente, la activación de WNT/β-CATENINA además de asociarse con TEM (178) también parece depender de NHERF1. Se ha demostrado que NHERF1 es necesario para mantener una fracción de β-CATENINA en la zona cortical en condiciones fisiológicas (192). Por el contrario, en células del carcinoma hepatocelular humano se produce acumulación de NHERF1 tanto en el citoplasma como en el núcleo , donde la localización de NHERF1 se correlaciona con la de la β-CATENINA nuclear, lo que sugiere una interacción funcional entre estas dos proteínas (177). La presencia de NHERF1 en el núcleo de las células tumorales se ha observado en varios tipos de cáncer (177,282–

284). En el núcleo, los ligandos de unión de NHERF1 identificados hasta ahora son β-CATENINA y TCF-1B, un factor de transcripción que se asocia con β-CATENINA y media su actividad transcripcional (177,283). Respecto a estos hallazgos, hemos observado que MINDIN induce la translocación de NHERF1 hacia los compartimentos citoplasmático y perinuclear, pero no hemos podido confirmar la localización de NHERF1 en el núcleo celular. Por lo tanto, estas observaciones sugieren que MINDIN podría promover la activación de la vía WNT/β-CATENINA en las células de cáncer de próstata al inducir una disminución en la expresión de NHERF1 en la membrana plasmática, liberando así la fracción de membrana de β-CATENINA. De este modo, esta fracción se encontraría disponible para translocarse al núcleo celular y promover las actividades transcripcionales dependientes de β-CATENINA. Sin embargo, sería necesario realizar más estudios para demostrar si NHERF1 se transloca al núcleo con β-CATENINA en cualquiera de las etapas de la progresión del cáncer de próstata.

8. CONCLUSIONES

Las conclusiones que se derivan del presente trabajo de investigación son las que se exponen a continuación:

1. El factor soluble tumoral MINDIN se expresa en células tumorales prostáticas humanas y de ratón.
2. Los tumores de próstata humanos presentan altos niveles de MINDIN y se asocian a la expresión de marcadores osteomiméticos y a la disminución de la expresión de NHERF1.
3. Los elevados niveles de MINDIN observados en los tumores de próstata de ratón se asocian a la sobreexpresión de marcadores osteomiméticos y se encuentran relacionados con la disminución de la expresión de NHERF1.
4. MINDIN regula el osteomimetismo, la proliferación, migración y adhesión de células de adenocarcinoma de próstata a través de la vía de señalización de la quinasa ERK 1/2. Además, MINDIN reduce la expresión de NHERF1 y promueve su movilización hacia el citoplasma en las células tumorales, lo que media en su capacidad proliferativa y migratoria.
5. MINDIN regula la comunicación e interacción entre el tumor primario de próstata y el hueso.
6. La expresión de MINDIN por parte del tumor primario de próstata induce cambios pre-metastásicos en la microarquitectura y la expresión génica ósea en ratones.
7. MINDIN promueve la activación de la β-CATENINA en osteoblastos y favorece la actividad de osteoblastos, osteocitos y la osteoclastogénesis.

Por todo ello, los datos presentados demuestran que MINDIN, secretada por el tumor primario de próstata, es un nuevo modulador de la progresión del cáncer de próstata y favorece la creación de un nicho pre-metastásico óseo.

9. BIBLIOGRAFÍA

1. Berman, D.M. *et al.* (2012) Development, Molecular Biology, and Physiology of the Prostate. In *Campbell-Walsh Urology*
2. Roy-Burman, P. *et al.* Genetically defined mouse models that mimic natural aspects of human prostate cancer development. , *Endocrine-Related Cancer*. (2004)
3. McNeal, J.E. *et al.* (1988) Zonal distribution of prostatic adenocarcinoma. Correlation with histologic pattern and direction of spread. *Am. J. Surg. Pathol.*, DOI: 10.1097/00000478-198812000-00001.
4. Day, T.F. *et al.* (2005) Wnt/β-catenin signaling in mesenchymal progenitors controls osteoblast and chondrocyte differentiation during vertebrate skeletogenesis. *Dev. Cell*, DOI: 10.1016/j.devcel.2005.03.016.
5. Cross (1999) Histology for Pathologists, 2nd edn. Edited by S Sternberg, Philadelphia, Lippincott-Raven; 1997, ISBN 0-397-51718-1, 1216 pages $195, int. $245. *Histopathology*, DOI: 10.1046/j.1365-2559.1999.00557.x.
6. Mcneal, J.E. (1981) The Zonal Anatomy of the. *Prostate*, DOI: 10.1055/s-2008-1075885.
7. McNeal, J.E. (1968) Regional morphology and pathology of the prostate. *Am. J. Clin. Pathol.*, DOI: 10.1093/ajcp/49.3.347.
8. McNeal, J.E. (1978) Origin and evolution of benign prostatic enlargement. *Invest. Urol.*,
9. De Marzo, A.M. *et al.* (1998) Stem cell features of benign and malignant prostate epithelial cells. *J. Urol.*, DOI: 10.1016/S0022-5347(01)62196-7.
10. Haffner, J. *et al.* (2009) Peripheral zone prostate cancers: Location and intraprostatic patterns of spread at histopathology. *Prostate*, DOI: 10.1002/pros.20881.
11. Shappell, S.B. *et al.* (2004) , Prostate Pathology of Genetically Engineered Mice: Definitions and Classification. The Consensus Report from the Bar Harbor Meeting of the Mouse Models of Human Cancer Consortium Prostate Pathology Committee. , in *Cancer Research*
12. Bosland, M.C. *et al.* (1990) Induction of Dorsolateral Prostate Adenocarcinomas

and Other Accessory Sex Gland Lesions in Male Wistar Rats by a Single Administration of N-Methyl-N-nitrosourea, 7,12-Dimethylbenz(a)anthracene, and 3,2-Dimethyl-4-aminobiphenyl after Sequential Treatment . *Cancer Res.*,

13. Hoover, D.M. *et al.* (1990) Experimental Induction of Neoplasia in the Accessory Sex Organs of Male Lobund-Wistar Rats. *Cancer Res.*,
14. Shirai, T. *et al.* (1991) Induction of Invasive Carcinomas in the Accessory Sex Organs Other Than the Ventral Prostate of Rats Given 3,2'-Dimethyl-4-aminobiphenyl and Testosterone Propionate. *Cancer Res.*,
15. Oliveira, D.S.M. *et al.* The mouse prostate: A basic anatomical and histological guideline. , *Bosnian Journal of Basic Medical Sciences*. (2016)
16. PRICE, D. COMPARATIVE ASPECTS OF DEVELOPMENT AND STRUCTURE IN THE PROSTATE. , *National Cancer Institute monograph*. (1963)
17. Berquin, I.M. *et al.* (2005) Expression signature of the mouse prostate. *J. Biol. Chem.*, DOI: 10.1074/jbc.M504945200.
18. Toivanen, R. *et al.* Prostate organogenesis: Tissue induction, hormonal regulation and cell type specification. , *Development (Cambridge)*. (2017)
19. Peng, Y.C. *et al.* (2015) Hedgehog signaling in prostate epithelial-mesenchymal growth regulation. *Dev. Biol.*, DOI: 10.1016/j.ydbio.2015.01.019.
20. Van Leenders, G.J.L.H. *et al.* (2003) , Epithelial cell differentiation in the human prostate epithelium: Implications for the pathogenesis and therapy of prostate cancer. , in *Critical Reviews in Oncology/Hematology*
21. Shen, M.M. *et al.* Molecular genetics of prostate cancer: New prospects for old challenges. , *Genes and Development*. (2010)
22. Barron, D.A. *et al.* The reactive stroma microenvironment and prostate cancer progression. , *Endocrine-Related Cancer*. (2012)
23. Valkenburg, K.C. *et al.* (2015) Drug discovery in prostate cancer mouse models. *Expert Opin. Drug Discov.*, **10**, 1011–1024.
24. Jemal, A. *et al.* (2003) Cancer Statistics, 2003. *CA. Cancer J. Clin.*, DOI: 10.3322/canjclin.53.1.5.
25. Pourmand, G. *et al.* (2007) The risk factors of prostate cancer: A multicentric case-control study in Iran. *Asian Pacific J. Cancer Prev.*,
26. Howlader N, Noone AM, Krapcho M, Miller D, Bishop K, Altekruse SF, Kosary CL,

Yu M, Ruhl J, Tatalovich Z, Mariotto A, Lewis DR, Chen HS, Feuer EJ, C.K. (eds). (2016) SEER Cancer Statistics Review 1975-2013 National Cancer Institute SEER Cancer Statistics Review 1975-2013 National Cancer Institute. *SEER Cancer Stat. Rev. 1975-2013, Natl. Cancer Institute. Bethesda, MD, http//seer.cancer.gov/csr/1975_2013/, based Novemb. 2015 SEER data submission, posted to SEER web site, April 2016.*,

27. Whittemore, A.S. *et al.* (1995) Prostate cancer in relation to diet, physical activity, and body size in blacks, whites, and Asians in the United States and Canada. *J. Natl. Cancer Inst.*, DOI: 10.1093/jnci/87.9.652.
28. Huncharek Michael MD, M.P.H. *et al.* (2010) Smoking as a Risk Factor for Prostate Cancer: A Meta-Analysis of 24 Prospective Cohort Studies. *Am. J. Public Health*,
29. Reissigl, A. *et al.* (1997) Frequency and clinical significance of transition zone cancer in prostate cancer screening. *Prostate*, DOI: 10.1002/(SICI)1097-0045(19970201)30:2<130::AID-PROS8>3.0.CO;2-S.
30. Noguchi, M. *et al.* (2000) An analysis of 148 consecutive transition zone cancers: Clinical and histological characteristics. *J. Urol.*, DOI: 10.1016/S0022-5347(05)67535-0.
31. Choi, N. *et al.* (2012) Adult Murine Prostate Basal and Luminal Cells Are Self-Sustained Lineages that Can Both Serve as Targets for Prostate Cancer Initiation. *Cancer Cell*, DOI: 10.1016/j.ccr.2012.01.005.
32. Grabowska, M.M. *et al.* Mouse models of prostate cancer: Picking the best model for the question. , *Cancer and Metastasis Reviews*. (2014)
33. De Marzo, A.M. *et al.* Inflammation in prostate carcinogenesis. , *Nature Reviews Cancer*. (2007)
34. Humphrey, P.A. Histological variants of prostatic carcinoma and their significance. , *Histopathology*. (2012)
35. Diamandis, E.P. *et al.* (2004) An update on human and mouse glandular kallikreins. *Clin. Biochem.*, DOI: 10.1016/j.clinbiochem.2003.12.013.
36. Fujimoto, N. *et al.* (2006) Identification of prostatic-secreted proteins in mice by mass spectrometric analysis and evaluation of lobe-specific and androgen-dependent mRNA expression. *J. Endocrinol.*, DOI: 10.1677/joe.1.06733.

37. Reiter, R.E. *et al.* (1998) Prostate stem cell antigen: A cell surface marker overexpressed in prostate cancer. *Proc. Natl. Acad. Sci. U. S. A.*, DOI: 10.1073/pnas.95.4.1735.

38. Lam, J.S. *et al.* (2005) Prostate stem cell antigen is overexpressed in prostate cancer metastases. *Clin. Cancer Res.*, DOI: 10.1158/1078-0432.CCR-04-1842.

39. Tang, S. *et al.* (2012) Positive and negative regulation of prostate Stem Cell Antigen expression by Yin Yang 1 in Prostate epithelial Cell lines. *PLoS One*, DOI: 10.1371/journal.pone.0035570.

40. Ono, H. *et al.* (2012) Prostate stem cell antigen, a presumable organ-dependent tumor suppressor gene, is down-regulated in gallbladder carcinogenesis. *Genes Chromosom. Cancer*, DOI: 10.1002/gcc.20928.

41. Elsamman, E. *et al.* (2006) Prostate stem cell antigen predicts tumour recurrence in superficial transitional cell carcinoma of the urinary bladder. *BJU Int.*, DOI: 10.1111/j.1464-410X.2006.06153.x.

42. Bahrenberg, G. *et al.* (2000) Reduced expression of PSCA, a member of the LY-6 family of cell surface antigens, in bladder, esophagus, and stomach tumors. *Biochem. Biophys. Res. Commun.*, DOI: 10.1006/bbrc.2000.3393.

43. Gu, Z. *et al.* (2000) Prostate stem cell antigen (PSCA) expression increases with high gleason score, advanced stage and bone metastasis in prostate cancer. *Oncogene*, DOI: 10.1038/sj.onc.1203426.

44. Uhlén, M. *et al.* (2015) Tissue-based map of the human proteome. *Science (80-.).*, DOI: 10.1126/science.1260419.

45. Hara, N. *et al.* (2002) Reverse transcription-polymerase chain reaction detection of prostate-specific antigen, prostate-specific membrane antigen, and prostate stem cell antigen in one milliliter of peripheral blood: Value for the staging of prostate cancer. *Clin. Cancer Res.*,

46. Zhigang, Z. *et al.* (2008) The association of prostate stem cell antigen (PSCA) mRNA expression and subsequent prostate cancer risk in men with benign prostatic hyperplasia following transurethral resection of the prostate. *Prostate*, DOI: 10.1002/pros.20701.

47. Raff, A.B. *et al.* Prostate stem cell antigen: A prospective therapeutic and diagnostic target. , *Cancer Letters*. (2009)

48. van der Toom, E.E. *et al.* Prostate-specific markers to identify rare prostate cancer cells in liquid biopsies. , *Nature Reviews Urology*. (2019)
49. Barve, A. *et al.* Prostate cancer relevant antigens and enzymes for targeted drug delivery. , *Journal of Controlled Release*. (2014)
50. Fawzy, M.S. *et al.* (2015) Prostate stem cell antigen (PSCA) mRNA expression in peripheral blood in patients with benign prostatic hyperplasia and/or prostate cancer. *Med. Oncol.*, DOI: 10.1007/s12032-015-0529-7.
51. Gamé, X. *et al.* (2003) Total and free serum prostate specific antigen levels during the first month of acute prostatitis. *Eur. Urol.*, DOI: 10.1016/S0302-2838(03)00158-1.
52. Roehrborn, C.G. *et al.* (2000) Serum prostate specific antigen is a strong predictor of future prostate growth in men with benign prostatic hyperplasia. *J. Urol.*, DOI: 10.1016/S0022-5347(05)67962-1.
53. Lilja, H. *et al.* (1987) Seminal vesicle-secreted proteins and their reactions during gelation and liquefaction of human semen. *J. Clin. Invest.*, DOI: 10.1172/JCI113070.
54. Humphrey, P.A. Gleason grading and prognostic factors in carcinoma of the prostate. , *Modern Pathology*. (2004)
55. Gleason, D.F. (1981) Histologic Grading and Staging of Prostatic Carcinoma. *Am. J. Surg. Pathol.*, DOI: 10.1097/00000478-198103000-00008.
56. A.V., D. *et al.* (1998) Biochemical outcome after radical prostatectomy, external beam radiation therapy, or interstitial radiation therapy for clinically localized prostate cancer. *J. Am. Med. Assoc.*,
57. D'Amico, A. V. *et al.* (2002) Determinants of prostate cancer-specific survival after radiation therapy for patients with clinically localized prostate cancer. *J. Clin. Oncol.*, DOI: 10.1200/JCO.2002.03.061.
58. Robling, A.G. *et al.* (2006) BIOMECHANICAL AND MOLECULAR REGULATION OF BONE REMODELING. *Annu. Rev. Biomed. Eng.*, DOI: 10.1146/annurev.bioeng.8.061505.095721.
59. Datta, H.K. *et al.* The cell biology of bone metabolism. , *Journal of Clinical Pathology*. (2008)
60. Boyce, B.F. *et al.* (2003) , Regulation of bone remodeling and emerging

breakthrough drugs for osteoporosis and osteolytic bone metastases. , in *Kidney International, Supplement*

61. Florencio-Silva, R. *et al.* Biology of Bone Tissue: Structure, Function, and Factors That Influence Bone Cells. , *BioMed Research International*. (2015)
62. Buckwalter, J.A. *et al.* Bone biology. I: Structure, blood supply, cells, matrix, and mineralization. , *Instructional course lectures*. (1996)
63. Downey, P.A. *et al.* Bone biology and the clinical implications for osteoporosis. , *Physical Therapy*. (2006)
64. Everts, V. *et al.* (2002) The bone lining cell: Its role in cleaning Howship's lacunae and initiating bone formation. *J. Bone Miner. Res.*, DOI: 10.1359/jbmr.2002.17.1.77.
65. Fakhry, M. (2013) Molecular mechanisms of mesenchymal stem cell differentiation towards osteoblasts. *World J. Stem Cells*, DOI: 10.4252/wjsc.v5.i4.136.
66. Damoulis, P.D. *et al.* (1997) Nitric oxide acts in conjunction with proinflammatory cytokines to promote cell death in osteoblasts. *J. Bone Miner. Res.*, DOI: 10.1359/jbmr.1997.12.3.412.
67. Karsenty, G. *et al.* Reaching a genetic and molecular understanding of skeletal development. , *Developmental Cell*. (2002)
68. Capulli, M. *et al.* Osteoblast and osteocyte: Games without frontiers. , *Archives of Biochemistry and Biophysics*. (2014)
69. Glimcher, M.J. (1998) The Nature of the Mineral Phase in Bone: Biological and Clinical Implications. In *Metabolic Bone Disease and Clinically Related Disorders*
70. Anderson, H.C. Matrix vesicles and calcification. , *Current rheumatology reports*. (2003)
71. Yoshiko, Y. *et al.* (2007) Osteoblast Autonomous Pi Regulation via Pit1 Plays a Role in Bone Mineralization. *Mol. Cell. Biol.*, DOI: 10.1128/mcb.00104-07.
72. Ducy, P. *et al.* (1997) Osf2/Cbfa1: A transcriptional activator of osteoblast differentiation. *Cell*, DOI: 10.1016/S0092-8674(00)80257-3.
73. Nakashima, K. *et al.* (2002) The novel zinc finger-containing transcription factor Osterix is required for osteoblast differentiation and bone formation. *Cell*, DOI: 10.1016/S0092-8674(01)00622-5.

74. Lian, J.B. *et al.* Regulatory Controls for Osteoblast Growth and Differentiation: Role of Runx/Cbfa/AML Factors. , *Critical Reviews in Eukaryotic Gene Expression*. (2004)

75. Liu, W. *et al.* (2001) Overexpression of Cbfa1 in osteoblasts inhibits osteoblast maturation and causes osteopenia with multiple fractures. *J. Cell Biol.*, DOI: 10.1083/jcb.200105052.

76. Liu, T.M. *et al.* Transcriptional regulatory cascades in Runx2-dependent bone development. , *Tissue Engineering - Part B: Reviews*. (2013)

77. Yagi, K. *et al.* (2003) Bone morphogenetic protein-2 enhances osterix gene expression in chondrocytes. *J. Cell. Biochem.*, DOI: 10.1002/jcb.10467.

78. Huang, W. *et al.* Signaling and transcriptional regulation in osteoblast commitment and differentiation. , *Frontiers in Bioscience*. (2007)

79. Westendorf, J.J. *et al.* Wnt signaling in osteoblasts and bone diseases. , *Gene*. (2004)

80. Rawadi, G. *et al.* Wnt signalling pathway: A new target for the treatment of osteoporosis. , *Expert Opinion on Therapeutic Targets*. (2005)

81. Bennett, C.N. *et al.* (2005) Regulation of osteoblastogenesis and bone mass by Wnt10b. *Proc. Natl. Acad. Sci. U. S. A.*, DOI: 10.1073/pnas.0408742102.

82. Hill, T.P. *et al.* (2005) Canonical Wnt/β-catenin signaling prevents osteoblasts from differentiating into chondrocytes. *Dev. Cell*, DOI: 10.1016/j.devcel.2005.02.013.

83. Behrens, J. *et al.* (1996) Functional interaction of β-catenin with the transcription factor LEF- 1. *Nature*, DOI: 10.1038/382638a0.

84. Jilka, R.L. *et al.* (1998) Osteoblast programmed cell death (apoptosis): Modulation by growth factors and cytokines. *J. Bone Miner. Res.*, DOI: 10.1359/jbmr.1998.13.5.793.

85. Miller, S.C. *et al.* Bone lining cells: Structure and function. , *Scanning Microscopy*. (1989)

86. Aarden, E.M. *et al.* (1994) Function of osteocytes in bone. *J. Cell. Biochem.*, DOI: 10.1002/jcb.240550304.

87. Andersen, T.L. *et al.* (2009) A physical mechanism for coupling bone resorption and formation in adult human bone. *Am. J. Pathol.*, DOI:

10.2353/ajpath.2009.080627.

88. Mosley, J.R. (2000) Osteoporosis and bone functional adaptation: Mechanobiological regulation of bone architecture in growing and adult bone, a review. *J. Rehabil. Res. Dev.*,
89. Franz-Odendaal, T.A. *et al.* Buried alive: How osteoblasts become osteocytes. , *Developmental Dynamics*. (2006)
90. Rochefort, G.Y. *et al.* Osteocyte: The unrecognized side of bone tissue. , *Osteoporosis International*. (2010)
91. Palumbo, C. *et al.* (1990) Osteocyte differentiation in the tibia of newborn rabbit: An ultrastructural study of the formation of cytoplasmic processes. *Acta Anat. (Basel).*,
92. Dallas, S.L. *et al.* The osteocyte: An endocrine cell . . . and more. , *Endocrine Reviews*. (2013)
93. Nefussi, J.R. *et al.* (1991) How osteoblasts become osteocytes: a decreasing matrix forming process. *J. Biol. Buccale*,
94. Bonewald, L.F. (2011) The amazing osteocyte. *J. Bone Miner. Res.*, DOI: 10.1002/jbmr.320.
95. Mikuni-Takagaki, Y. *et al.* (1995) Matrix mineralization and the differentiation of osteocyte-like cells in culture. *J. Bone Miner. Res.*, DOI: 10.1002/jbmr.5650100209.
96. Poole, K.E.S. *et al.* (2005) Sclerostin is a delayed secreted product of osteocytes that inhibits bone formation. *FASEB J.*, DOI: 10.1096/fj.05-4221fje.
97. Ubaidus, S. *et al.* (2009) FGF23 is mainly synthesized by osteocytes in the regularly distributed osteocytic lacunar canalicular system established after physiological bone remodeling. *J. Electron Microsc. (Tokyo).*, DOI: 10.1093/jmicro/dfp032.
98. Bonewald, L.F. (2007) , Osteocytes as dynamic multifunctional cells. , in *Annals of the New York Academy of Sciences*
99. Noble, B.S. *et al.* (1997) Identification of apoptotic changes in osteocytes in normal and pathological human bone. *Bone*, DOI: 10.1016/S8756-3282(96)00365-1.
100. Aguirre, J.I. *et al.* (2006) Osteocyte apoptosis is induced by weightlessness in

mice and precedes osteoclast recruitment and bone loss. *J. Bone Miner. Res.*, DOI: 10.1359/jbmr.060107.

101. Plotkin, L.I. Apoptotic osteocytes and the control of targeted bone resorption. , *Current Osteoporosis Reports*. (2014)
102. Boabaid, F. *et al.* (2001) Apoptotic bone cells may be engulfed by osteoclasts during alveolar bone resorption in young rats. *Tissue Cell*, DOI: 10.1054/tice.2001.0179.
103. Cerri, P.S. *et al.* (2003) Combined TUNEL and TRAP methods suggest that apoptotic bone cells are inside vacuoles of alveolar bone osteoclasts in young rats. *J. Periodontal Res.*, DOI: 10.1034/j.1600-0765.2003.02006.x.
104. Faloni, A.P.S. *et al.* (2007) Decrease in the number and apoptosis of alveolar bone osteoclasts in estrogen-treated rats. *J. Periodontal Res.*, DOI: 10.1111/j.1600-0765.2006.00932.x.
105. Soysa, N.S. *et al.* (2012) Osteoclast formation and differentiation: An overview. *J. Med. Dent. Sci.*,
106. Boyce, B.F. *et al.* Functions of RANKL/RANK/OPG in bone modeling and remodeling. , *Archives of Biochemistry and Biophysics*. (2008)
107. Hassan, M.Q. *et al.* (2006) BMP2 commitment to the osteogenic lineage involves activation of Runx2 by DLX3 and a homeodomain transcriptional network. *J. Biol. Chem.*, DOI: 10.1074/jbc.M604508200.
108. Reithmeier, A. *et al.* (2017) Tartrate-resistant acid phosphatase (TRAP/ACP5) promotes metastasis-related properties via TGFβ2/TβR and CD44 in MDA-MB-231 breast cancer cells. *BMC Cancer*, DOI: 10.1186/s12885-017-3616-7.
109. Nordstrand, A. *et al.* (2018) Bone cell activity in clinical prostate cancer bone metastasis and its inverse relation to tumor cell androgen receptor activity. *Int. J. Mol. Sci.*, DOI: 10.3390/ijms19041223.
110. Boyce, B.F. *et al.* Recent advances in bone biology provide insight into the pathogenesis of bone diseases. , *Laboratory Investigation*. (1999)
111. Yavropoulou, M.P. *et al.* Osteoclastogenesis - Current knowledge and future perspectives. , *Journal of Musculoskeletal Neuronal Interactions*. (2008)
112. Yoshida, H. *et al.* (1990) The murine mutation osteopetrosis is in the coding region of the macrophage colony stimulating factor gene. *Nature*, DOI:

10.1038/345442a0.

113. Crockett, J.C. *et al.* New knowledge on critical osteoclast formation and activation pathways from study of rare genetic diseases of osteoclasts: Focus on the RANK/RANKL axis. , *Osteoporosis International*. (2011)
114. Takayanagi, H. Osteoimmunology: Shared mechanisms and crosstalk between the immune and bone systems. , *Nature Reviews Immunology*. (2007)
115. Sodek, J. *et al.* (2000) Molecular and cellular biology of alveolar bone. *Periodontol. 2000*, DOI: 10.1034/j.1600-0757.2000.2240106.x.
116. Fata, J.E. *et al.* (2000) The osteoclast differentiation factor osteoprotegerin-ligand is essential for mammary gland development. *Cell*, DOI: 10.1016/S0092-8674(00)00103-3.
117. Kim, N.-S. *et al.* (2006) Receptor Activator of NF- B Ligand Regulates the Proliferation of Mammary Epithelial Cells via Id2. *Mol. Cell. Biol.*, DOI: 10.1128/mcb.26.3.1002-1013.2006.
118. Chen, G. *et al.* (2006) Expression of RANKL/RANK/OPG in primary and metastatic human prostate cancer as markers of disease stage and functional regulation. *Cancer*, DOI: 10.1002/cncr.21978.
119. Edwards, J.R. *et al.* Advances in osteoclast biology: Old findings and new insights from mouse models. , *Nature Reviews Rheumatology*. (2011)
120. Santini, D. *et al.* (2011) Receptor activator of NF-kB (rank) expression in primary tumors associates with bone metastasis occurrence in breast cancer patients. *PLoS One*, DOI: 10.1371/journal.pone.0019234.
121. Jones, D.H. *et al.* (2006) Regulation of cancer cell migration and bone metastasis by RANKL. *Nature*, DOI: 10.1038/nature04524.
122. Theoleyre, S. *et al.* The molecular triad OPG/RANK/RANKL: Involvement in the orchestration of pathophysiological bone remodeling. , *Cytokine and Growth Factor Reviews*. (2004)
123. Glass, D.A. *et al.* (2005) Canonical Wnt signaling in differentiated osteoblasts controls osteoclast differentiation. *Dev. Cell*, DOI: 10.1016/j.devcel.2005.02.017.
124. Kearns, A.E. *et al.* (2007) RANKL and OPG Regulation of Bone Remodeling in Health and Disease. *Endocr. Rev.*, DOI: er.2007-0014 [pii]10.1210/er.2007-0014.
125. Boyce, B.F. *et al.* (2015) NF-κB-mediated regulation of osteoclastogenesis.

Endocrinol. Metab., DOI: 10.3803/EnM.2015.30.1.35.

126. Walsh, M.C. *et al.* Biology of the RANKL-RANK-OPG system in immunity, bone, and beyond. , *Frontiers in Immunology*. (2014)
127. Garg, R. *et al.* (2012) Activation of nuclear factor κB (NF-κB) in prostate cancer is mediated by protein kinase C ∈ (PKC∈). *J. Biol. Chem.*, DOI: 10.1074/jbc.M112.398925.
128. Gutierrez-Uzquiza, A. *et al.* (2015) PKCε is an essential mediator of prostate cancer bone metastasis. *Mol. Cancer Res.*, DOI: 10.1158/1541-7786.MCR-15-0111.
129. Longoni, N. *et al.* (2013) ETS transcription factor ESE1/ELF3 orchestrates a positive feedback loop that constitutively activates NF-κB and drives prostate cancer progression. *Cancer Res.*, DOI: 10.1158/0008-5472.CAN-12-4537.
130. Chu, G.C.Y. *et al.* (2014) RANK-and c-Met-mediated signal network promotes prostate cancer metastatic colonization. *Endocr. Relat. Cancer*, DOI: 10.1530/ERC-13-0548.
131. Sisay, M. *et al.* (2017) The RANK/RANKL/OPG system in tumorigenesis and metastasis of cancer stem cell: Potential targets for anticancer therapy. *Onco. Targets. Ther.*, DOI: 10.2147/OTT.S135867.
132. Datta, K. *et al.* Mechanism of lymph node metastasis in prostate cancer. , *Future Oncology*. (2010)
133. Kan, C. *et al.* Cancer cell colonisation in the bone microenvironment. , *International Journal of Molecular Sciences*. (2016)
134. Weilbaecher, K.N. *et al.* Cancer to bone: A fatal attraction. , *Nature Reviews Cancer*. (2011)
135. Ell, B. *et al.* SnapShot: Bone metastasis. , *Cell*. (2012)
136. Small, E.J. *et al.* (2006) Placebo-controlled phase III trial of immunologic therapy with Sipuleucel-T (APC8015) in patients with metastatic, asymptomatic hormone refractory prostate cancer. *J. Clin. Oncol.*, DOI: 10.1200/JCO.2005.04.5252.
137. Chambers, A.F. *et al.* Dissemination and growth of cancer cells in metastatic sites. , *Nature Reviews Cancer*. (2002)
138. Fidler, I.J. The pathogenesis of cancer metastasis: The “seed and soil” hypothesis

revisited. , *Nature Reviews Cancer*. (2003)

139. Kang, Y. *et al.* Epithelial-mesenchymal transitions: Twist in development and metastasis. , *Cell*. (2004)
140. Alderton, G.K. Metastasis: Converging targets. , *Nature Reviews Cancer*. (2012)
141. Morrissey, C. *et al.* The role of tumor microenvironment in prostate cancer bone metastasis. , *Journal of Cellular Biochemistry*. (2007)
142. Wang, G. *et al.* Genetics and biology of prostate cancer. , *Genes and Development*. (2018)
143. Coleman, R.E. (2001) Metastatic bone disease: Clinical features, pathophysiology and treatment strategies. *Cancer Treat. Rev.*, DOI: 10.1053/ctrv.2000.0210.
144. URWIN, G.H. *et al.* (1985) Generalised Increase in Bone Resorption in Carcinoma of the Prostate. *Br. J. Urol.*, DOI: 10.1111/j.1464-410X.1985.tb07040.x.
145. Macedo, F. *et al.* (2017) Bone metastases: An overview. *Oncol. Rev.*, DOI: 10.4081/oncol.2017.321.
146. Yang, X. *et al.* Transcription factors in bone: Developmental and pathological aspects. , *Trends in Molecular Medicine*. (2002)
147. Lee, Y. *et al.* (2003) Differences in the cytokine profiles associated with prostate cancer cell induced osteoblastic and osteolytic lesions in bone. *J. Orthop. Res.*, DOI: 10.1016/S0736-0266(02)00095-5.
148. Selvaggi, G. *et al.* Management of bone metastases in cancer: A review. , *Critical Reviews in Oncology/Hematology*. (2005)
149. Taube, T. *et al.* (1994) Histomorphometric evidence for osteoclast-mediated bone resorption in metastatic breast cancer. *Bone*, DOI: 10.1016/8756-3282(94)90703-X.
150. Zhang, J. *et al.* (2001) Osteoprotegerin inhibits prostate cancer-induced osteoclastogenesis and prevents prostate tumor growth in the bone. *J. Clin. Invest.*, DOI: 10.1172/JCI11685.
151. Michigami, T. *et al.* (2001) Receptor activator of nuclear factor κB ligand (RANKL) is a key molecule of osteoclast formation for bone metastasis in a newly developed model of human neuroblastoma. *Cancer Res.*,
152. Coleman, R.E. (1997) Skeletal complications of malignancy. *Cancer*, DOI:

10.1002/(sici)1097-0142(19971015)80:8+<1588::aid-cncr9>3.3.co;2-z.

153. Liao, J. *et al.* (2008) Tumor expressed PTHrP facilitates prostate cancer-induced osteoblastic lesions. *Int. J. Cancer*, DOI: 10.1002/ijc.23602.
154. Kang, Y. *et al.* (2003) A multigenic program mediating breast cancer metastasis to bone. *Cancer Cell*, DOI: 10.1016/S1535-6108(03)00132-6.
155. Ursini-Siegel, J. *et al.* The influence of the pre-metastatic niche on breast cancer metastasis. , *Cancer Letters*. (2016)
156. Wang, N. *et al.* (2014) Prostate cancer cells preferentially home to osteoblast-rich areas in the early stages of bone metastasis: Evidence from in vivo models. *J. Bone Miner. Res.*, DOI: 10.1002/jbmr.2300.
157. Pedersen, E.A. *et al.* The prostate cancer bone marrow niche: More than just fertile soil. , *Asian Journal of Andrology*. (2012)
158. Ottewell, P.D. (2016) The role of osteoblasts in bone metastasis. *J. Bone Oncol.*, DOI: 10.1016/j.jbo.2016.03.007.
159. Sanders, J.L. *et al.* (2000) Extracellular calcium-sensing receptor expression and its potential role in regulating parathyroid hormone-related peptide secretion in human breast cancer cell lines. *Endocrinology*, DOI: 10.1210/endo.141.12.7849.
160. Kim, W. *et al.* (2016) Calcium-sensing receptor promotes breast cancer by stimulating intracrine actions of parathyroid hormone-related protein. *Cancer Res.*, DOI: 10.1158/0008-5472.CAN-15-2614.
161. Paget, S. (1889) THE DISTRIBUTION OF SECONDARY GROWTHS IN CANCER OF THE BREAST. *Lancet*, DOI: 10.1016/S0140-6736(00)49915-0.
162. Baniwal, S.K. *et al.* (2010) Runx2 transcriptome of prostate cancer cells: Insights into invasiveness and bone metastasis. *Mol. Cancer*, DOI: 10.1186/1476-4598-9-258.
163. Koeneman, K.S. *et al.* (1999) Osteomimetic properties of prostate cancer cells: A hypothesis supporting the predilection of prostate cancer metastasis and growth in the bone environment. *Prostate*, DOI: 10.1002/(SICI)1097-0045(19990601)39:4<246::AID-PROS5>3.0.CO;2-U.
164. Dougall, W.C. *et al.* (2014) Targeting RANKL in metastasis. *Bonekey Rep.*, DOI: 10.1038/bonekey.2014.14.
165. Pérez-Martínez, F.C. *et al.* (2008) Receptor activator of nuclear factor-κB ligand

(RANKL) as a novel prognostic marker in prostate carcinoma. *Histol. Histopathol.*,

166. Pérez-Martínez, F.C. *et al.* (2007) Immunohistochemical analysis of low-grade and high-grade prostate carcinoma: Relative chanqes or parathyroid hormone-related protein and its parathyroid hormone 1 receptor, osteoprotegerin and receptor activator of nuclear factor-kB ligand. *J. Clin. Pathol.*, DOI: 10.1136/jcp.2006.037853.
167. Thomas, R.J. *et al.* (1999) Breast cancer cells interact with osteoblasts to support osteoclast formation. *Endocrinology*, DOI: 10.1210/endo.140.10.7037.
168. Nannuru, K.C. *et al.* (2009) Enhanced expression and shedding of receptor activator of NF-κB ligand during tumor-bone interaction potentiates mammary tumor-induced osteolysis. *Clin. Exp. Metastasis*, DOI: 10.1007/s10585-009-9279-2.
169. Mundy, G.R. Metastasis to bone: Causes, consequences and therapeutic opportunities. , *Nature Reviews Cancer*. (2002)
170. Pearse, R.N. *et al.* (2001) Multiple myeloma disrupts the TRANCE/osteoprotegerin cytokine axis to trigger bone destruction and promote tumor progression. *Proc. Natl. Acad. Sci. U. S. A.*, DOI: 10.1073/pnas.201394498.
171. Zhau, H.E. *et al.* (2013) Interracial differences in prostate cancer progression among patients from the United States, China and Japan. *Asian J. Androl.*, DOI: 10.1038/aja.2013.86.
172. Hu, P. *et al.* (2013) Convergent RANK- and c-Met-Mediated Signaling Components Predict Survival of Patients with Prostate Cancer: An Interracial Comparative Study. *PLoS One*, DOI: 10.1371/journal.pone.0073081.
173. Huang, L. *et al.* Tumour cells produce receptor activator of NF-κB ligand (RANKL) in skeletal metastases [3]. , *Journal of Clinical Pathology*. (2002)
174. Ardura, J.A. *et al.* (2011) Regulation of G Protein-Coupled Receptor Function by Na+/H+ Exchange Regulatory Factors. *Pharmacol. Rev.*, DOI: 10.1124/pr.110.004176.
175. Bartholow, T.L. *et al.* (2011) Immunohistochemical analysis of ezrin-radixin-moesin-binding phosphoprotein 50 in prostatic adenocarcinoma. *BMC Urol.*, DOI: 10.1186/1471-2490-11-12.

176. Centonze, M. *et al.* NHERF1 Between Promises and Hopes: Overview on Cancer and Prospective Openings. , *Translational Oncology*. (2018)

177. Shibata, T. *et al.* (2003) EBP50, a β-catenin-associating protein, enhances Wnt signaling and is over-expressed in hepatocellular carcinoma. *Hepatology*, DOI: 10.1053/jhep.2003.50270.

178. Jiang, Y.-G. *et al.* (2007) Role of Wnt/β-catenin signaling pathway in epithelial-mesenchymal transition of human prostate cancer induced by hypoxia-inducible factor-1α. *Int. J. Urol.*, **14**, 1034–1039.

179. Stemmer-Rachamimov, A.O. *et al.* (2001) NHE-RF, a merlin-interacting protein, is primarily expressed in luminal epithelia, proliferative endometrium, and estrogen receptor-positive breast carcinomas. *Am. J. Pathol.*, DOI: 10.1016/S0002-9440(10)63944-2.

180. Weinman, E.J. *et al.* (1997) The Na-H exchanger regulatory factor. *Exp. Nephrol.*,

181. Wade, J.B. *et al.* (2017) Differential renal distribution of NHERF isoforms and their colocalization with NHE3, ezrin, and ROMK. *Am. J. Physiol. Physiol.*, DOI: 10.1152/ajpcell.2001.280.1.c192.

182. Shenolikar, S. *et al.* (2004) Regulation of Ion Transport by the NHERF Family of PDZ Proteins. *Physiology*, DOI: 10.1152/physiol.00020.2004.

183. Pan, Y. *et al.* (2006) Suppression of breast cancer cell growth by Na + /H + exchanger regulatory factor 1 (NHERF1). *Breast Cancer Res.*, DOI: 10.1186/bcr1616.

184. Molina, J.R. *et al.* (2012) PTEN, NHERF1 and PHLPP form a tumor suppressor network that is disabled in glioblastoma. *Oncogene*, DOI: 10.1038/onc.2011.324.

185. Zheng, J.F. *et al.* (2010) EBP50 exerts tumor suppressor activity by promoting cell apoptosis and retarding extracellular signal-regulated kinase activity. *Amino Acids*, DOI: 10.1007/s00726-009-0437-2.

186. Cardone, R.A. *et al.* (2007) The NHERF1 PDZ2 Domain Regulates PKA-RhoA-p38-mediated NHE1 Activation and Invasion in Breast Tumor Cells. *Mol. Biol. Cell*, DOI: 10.1091/mbc.e06-07-0617.

187. Kislin, K.L. *et al.* (2009) NHERF-1: modulator of glioblastoma cell migration and invasion. *Neoplasia*,

188. Liu, L. *et al.* (2012) Na+/H+ exchanger regulatory factor 1 (NHERF1) directly

regulates osteogenesis. *J. Biol. Chem.*, **287**, 43312–43321.

189. Molina, J.R. *et al.* (2010) Loss of PTEN binding adapter protein NHERF1 from plasma membrane in glioblastoma contributes to PTEN inactivation. *Cancer Res.*, DOI: 10.1158/0008-5472.CAN-10-1271.
190. Georgescu, M.-M. *et al.* (2008) Roles of NHERF1/EBP50 in Cancer. *Curr. Mol. Med.*, DOI: 10.2174/156652408785748031.
191. Morales, F.C. *et al.* (2004) Ezrin-radixin-moesin (ERM)-binding phosphoprotein 50 organizes ERM proteins at the apical membrane of polarized epithelia. *Proc. Natl. Acad. Sci.*, DOI: 10.1073/pnas.0407974101.
192. Kreimann, E.L. *et al.* (2007) Cortical stabilization of β-catenin contributes to NHERF1/EBP50 tumor suppressor function. *Oncogene*, DOI: 10.1038/sj.onc.1210336.
193. Hayashi, Y. *et al.* (2015) NHERF1/EBP50 Is a New Marker in Colorectal Cancer. *Neoplasia*, DOI: 10.1593/neo.10780.
194. Bellizzi, A. *et al.* NHERF1/EBP50 in breast cancer: Clinical perspectives. , *Breast Care*. (2010)
195. Tabrizi, A.D. *et al.* (2010) Primary ovarian mucinous carcinoma of intestinal type: Significance of pattern of invasion and immunohistochemical expression profile in a series of 31 cases. *Int. J. Gynecol. Pathol.*, DOI: 10.1097/PGP.0b013e3181bbbcc1.
196. Karn, T. *et al.* (2011) Gene expression profiling of luminal B breast cancers reveals NHERF1 as a new marker of endocrine resistance. *Breast Cancer Res. Treat.*, DOI: 10.1007/s10549-010-1333-x.
197. Ma, Q. *et al.* (2016) Targeting of NHERF1 through RNA interference inhibits the proliferation and migration of metastatic prostate cancer cells. *Oncol. Lett.*, DOI: 10.3892/ol.2015.4007.
198. Alowolodu, O. *et al.* (2016) Intrinsic disorder in spondins and some of their interacting partners. *Intrinsically Disord. Proteins*, DOI: 10.1080/21690707.2016.1255295.
199. Knight, M.N. *et al.* R-spondins: Novel matricellular regulators of the skeleton. , *Matrix Biology*. (2014)
200. Rodriguez-Leon, J. *et al.* (2013) Recent advances in the study of limb

development: The emergence and function of the apical ectodermal ridge. *J. Stem Cells*,

201. Mah, A.T. *et al.* Wnt pathway regulation of intestinal stem cells. , *Journal of Physiology*. (2016)
202. Fujii, M. *et al.* Culturing intestinal stem cells: Applications for colorectal cancer research. , *Frontiers in Genetics*. (2014)
203. Koo, B.K. *et al.* Stem cells marked by the r-spondin receptor LGR5. , *Gastroenterology*. (2014)
204. Meiniel, A. *et al.* (2003) The Thrombospondin Type 1 Repeat (TSR) and Neuronal Differentiation: Roles of SCO-Spondin Oligopeptides on Neuronal Cell Types and Cell Lines. *Int. Rev. Cytol.*, DOI: 10.1016/S0074-7696(03)30001-4.
205. Meiniel, A. (2001) SCO-spondin, a glycoprotein of the subcommissural organ/reissner's fiber complex: Evidence of a potent activity on neuronal development in primary cell cultures. *Microsc. Res. Tech.*, DOI: 10.1002/1097-0029(20010301)52:5<484::AID-JEMT1034>3.0.CO;2-0.
206. Li, Y. *et al.* (2009) Structure of the F-spondin domain of mindin, an integrin ligand and pattern recognition molecule. *EMBO J.*, DOI: 10.1038/emboj.2008.288.
207. He, Y.W. *et al.* (2004) The extracellular matrix protein mindin is a pattern-recognition molecule for microbial pathogens. *Nat. Immunol.*, DOI: 10.1038/ni1021.
208. Adams, J.C. *et al.* The thrombospondin type 1 repeat (TSR) superfamily: Diverse proteins with related roles in neuronal development. , *Developmental Dynamics*. (2000)
209. Higashijima, S. ichi *et al.* (1997) Mindin/F-spondin family: Novel ECM proteins expressed in the zebrafish embryonic axis. *Dev. Biol.*, DOI: 10.1006/dbio.1997.8760.
210. Feinstein, Y. *et al.* (1999) F-spondin and mindin: Two structurally and functionally related genes expressed in the hippocampus that promote outgrowth of embryonic hippocampal neurons. *Development*,
211. Jia, W. *et al.* (2008) Pattern Recognition Molecule Mindin Promotes Intranasal Clearance of Influenza Viruses. *J. Immunol.*, DOI: 10.4049/jimmunol.180.9.6255.

212. Jia, W. *et al.* (2005) The extracellular matrix protein mindin serves as an integrin ligand and is critical for inflammatory cell recruitment. *Blood*, DOI: 10.1182/blood-2005-04-1658.

213. Li, H. *et al.* (2006) Efficient dendritic cell priming of T lymphocytes depends on the extracellular matrix protein mindin. *EMBO J.*, DOI: 10.1038/sj.emboj.7601289.

214. Li, Z. *et al.* (2008) The extracellular matrix protein mindin regulates trafficking of murine eosinophils into the airspace. *J. Leukoc. Biol.*, DOI: 10.1189/jlb.0208135.

215. Murakoshi, M. *et al.* Role of mindin in diabetic nephropathy. , *Experimental Diabetes Research*. (2011)

216. Lucarelli, G. *et al.* (2013) Spondin-2, a secreted extracellular matrix protein, is a novel diagnostic biomarker for prostate cancer. *J. Urol.*, DOI: 10.1016/j.juro.2013.05.004.

217. Parry, R. *et al.* (2005) Identification of a novel prostate tumor target, mindin/RG-1, for antibody-based radiotherapy of prostate cancer. *Cancer Res.*, DOI: 10.1158/0008-5472.CAN-05-1203.

218. Romanuik, T.L. *et al.* (2009) Novel biomarkers for prostate cancer including noncoding transcripts. *Am. J. Pathol.*, DOI: 10.2353/ajpath.2009.080868.

219. Qian, X. *et al.* (2012) Spondin-2 (SPON2), a more prostate-cancer-specific diagnostic biomarker. *PLoS One*, DOI: 10.1371/journal.pone.0037225.

220. Gingrich, J.R. *et al.* (1996) Metastatic prostate cancer in a transgenic mouse. *Cancer Res.*,

221. Dempster, D.W. *et al.* Standardized nomenclature, symbols, and units for bone histomorphometry: A 2012 update of the report of the ASBMR Histomorphometry Nomenclature Committee. , *Journal of Bone and Mineral Research*. (2013)

222. Wang, B. *et al.* (2015) Chondrocytes-specific expression of osteoprotegerin modulates osteoclast formation in metaphyseal bone. *Sci. Rep.*, DOI: 10.1038/srep13667.

223. Ardura, J.A. *et al.* (2019) The secreted matrix protein mindin increases prostate tumor progression and tumor-bone crosstalk via ERK 1/2 regulation. *Carcinogenesis*, DOI: 10.1093/carcin/bgz105.

224. Liu, L. *et al.* (2012) Na^+/H^+exchanger regulatory factor 1 (NHERF1) directly regulates osteogenesis. *J. Biol. Chem.*, **287**,

225. Ardura, J.A. *et al.* (2020) Mindin secretion by prostate tumors induces premetastatic changes in bone via β-catenin. *Endocr. Relat. Cancer*, DOI: 10.1530/erc-20-0116.

226. Yang, D. *et al.* (2001) Murine six-transmembrane epithelial antigen of the prostate, prostate stem cell antigen, and prostate-specific membrane antigen: Prostate-specific cell-surface antigens highly expressed in prostate cancer of transgenic adenocarcinoma mouse prostate mice. *Cancer Res.*,

227. Jones, D.H. *et al.* (2006) Regulation of cancer cell migration and bone metastasis by RANKL. *Nature*, **440**, 692–696.

228. Bishop, K.A. *et al.* (2011) Mouse Rankl expression is regulated in T Cells by c-Fos through a cluster of distal regulatory enhancers designated the T cell control region. *J. Biol. Chem.*, DOI: 10.1074/jbc.M111.231548.

229. Schmittgen, T.D. *et al.* (2008) Analyzing real-time PCR data by the comparative C(T) method. *Nat. Protoc.*,

230. Alonso, R. *et al.* (2014) Fungal infection in patients with Alzheimer's disease. *J. Alzheimer's Dis.*, DOI: 10.3233/JAD-132681.

231. Strober, W. (2015) Trypan Blue Exclusion Test of Cell Viability. *Curr. Protoc. Immunol.*, DOI: 10.1002/0471142735.ima03bs111.

232. Friedman, M.S. *et al.* (2009) Wnt11 promotes osteoblast maturation and mineralization through R-spondin 2. *J. Biol. Chem.*, DOI: 10.1074/jbc.M808337200.

233. Michalaki, V. *et al.* (2004) Serum levels of IL-6 and TNF-α correlate with clinicopathological features and patient survival in patients with prostate cancer. *Br. J. Cancer*, DOI: 10.1038/sj.bjc.6601814.

234. Zhang, M. *et al.* (2017) RSPO3-LGR4 Regulates Osteogenic Differentiation of Human Adipose-Derived Stem Cells Via ERK/FGF Signalling. *Sci. Rep.*, DOI: 10.1038/srep42841.

235. Kingsley, L.A. *et al.* Molecular biology of bone metastasis. , *Molecular Cancer Therapeutics*. (2007)

236. Dougall, W.C. Molecular pathways: Osteoclast-dependent and osteoclast-

independent roles of the RANKL/RANK/OPG pathway in tumorigenesis and metastasis. , *Clinical Cancer Research*. (2012)

237. de Lau, W.B.M. *et al.* The R-spondin protein family. , *Genome Biology*. (2012)
238. Zhu, C. *et al.* (2016) LGR4 acts as a key receptor for R-spondin 2 to promote osteogenesis through Wnt signaling pathway. *Cell. Signal.*, DOI: 10.1016/j.cellsig.2016.04.010.
239. Baron, R. *et al.* Minireview: Targeting the Wnt/β-catenin pathway to regulate bone formation in the adult skeleton. , *Endocrinology*. (2007)
240. Chang, H. *et al.* (2015) Spondin 1 promotes metastatic progression through Fak and Src dependent pathway in human osteosarcoma. *Biochem. Biophys. Res. Commun.*, DOI: 10.1016/j.bbrc.2015.05.092.
241. Wong, M.C.S. *et al.* (2016) Global Incidence and Mortality for Prostate Cancer: Analysis of Temporal Patterns and Trends in 36 Countries. *Eur. Urol.*, DOI: 10.1016/j.eururo.2016.05.043.
242. Logothetis, C.J. *et al.* Osteoblasts in prostate cancer metastasis to bone. , *Nature Reviews Cancer*. (2005)
243. Salamanna, F. *et al.* (2016) An <i>in vitro</i> 3D bone metastasis model by using a human bone tissue culture and human sex-related cancer cells. *Oncotarget*, DOI: 10.18632/oncotarget.12763.
244. Coleman, R.E. *et al.* Metastasis and bone loss: Advancing treatment and prevention. , *Cancer Treatment Reviews*. (2010)
245. Croucher, P.I. *et al.* Bone metastasis: The importance of the neighbourhood. , *Nature Reviews Cancer*. (2016)
246. Ge, C. *et al.* (2016) Role of Runx2 phosphorylation in prostate cancer and association with metastatic disease. *Oncogene*, DOI: 10.1038/onc.2015.91.
247. Li, X. *et al.* (2014) Potential role of the OPG/RANK/RANKL axis in prostate cancer invasion and bone metastasis. *Oncol. Rep.*, DOI: 10.3892/or.2014.3511.
248. Gardner, T.A. *et al.* (2009) Differential expression of osteocalcin during the metastatic progression of prostate cancer. *Oncol. Rep.*, DOI: 10.3892/or_00000302.
249. Armstrong, A.P. *et al.* (2008) RANKL acts directly on RANK-expressing prostate tumor cells and mediates migration and expression of tumor metastasis genes.

Prostate, DOI: 10.1002/pros.20678.

250. Holen, I. *et al.* (2002) Osteoprotegerin (OPG) is a survival factor for human prostate cancer cells. *Cancer Res.*,
251. Gartrell, B.A. *et al.* Managing bone metastases and reducing skeletal related events in prostate cancer. , *Nature Reviews Clinical Oncology*. (2014)
252. Zhu, B.P. *et al.* (2017) Serum BSP, PSADT, and Spondin-2 levels in prostate cancer and the diagnostic significance of their ROC curves in bone metastasis. *Eur. Rev. Med. Pharmacol. Sci.*,
253. Reczek, D. *et al.* (1997) Identification of EPB50: A PDZ-containing phosphoprotein that associates with members of the ezrin-radixin-moesin family. *J. Cell Biol.*, DOI: 10.1083/jcb.139.1.169.
254. Sheng, R. *et al.* (2012) Cholesterol modulates cell signaling and protein networking by specifically interacting with PDZ domain-containing scaffold proteins. *Nat. Commun.*, DOI: 10.1038/ncomms2221.
255. Hanono, A. *et al.* (2006) EPI64 regulates microvillar subdomains and structure. *J. Cell Biol.*, DOI: 10.1083/jcb.200604046.
256. Chiba, H. *et al.* (2006) The nuclear receptor hepatocyte nuclear factor 4α acts as a morphogen to induce the formation of microvilli. *J. Cell Biol.*, DOI: 10.1083/jcb.200608012.
257. Vaquero, J. *et al.* Role of the PDZ-scaffold protein NHERF1/EBP50 in cancer biology: From signaling regulation to clinical relevance. , *Oncogene*. (2017)
258. Jiang, Y.G. *et al.* (2007) Role of Wnt/β-catenin signaling pathway in epithelial-mesenchymal transition of human prostate cancer induced by hypoxia-inducible factor-1α. *Int. J. Urol.*, DOI: 10.1111/j.1442-2042.2007.01866.x.
259. Jin, R. *et al.* (2013) Activation of NF-kappa B Signaling Promotes Growth of Prostate Cancer Cells in Bone. *PLoS One*, DOI: 10.1371/journal.pone.0060983.
260. Seshasayee, D. *et al.* (2004) A novel in vivo role for osteoprotegerin ligand in activation of monocyte effector function and inflammatory response. *J. Biol. Chem.*, DOI: 10.1074/jbc.M403968200.
261. Lucia, M.S. *et al.* (2004) Inflammation as a target for prostate cancer chemoprevention: Pathological and laboratory rationale. *J. Urol.*, DOI: 10.1097/01.ju.0000108142.53241.47.

262. Akech, J. *et al.* (2010) Runx2 association with progression of prostate cancer in patients: Mechanisms mediating bone osteolysis and osteoblastic metastatic lesions. *Oncogene*, DOI: 10.1038/onc.2009.389.

263. Barnes, G.L. *et al.* (2003) Osteoblast-related transcription factors Runx2 (Cbfa1/AML3) and MSX2 mediate the expression of bone sialoprotein in human metastatic breast cancer cells. *Cancer Res.*,

264. Shore, P. A role for Runx2 in normal mammary gland and breast cancer bone metastasis. , *Journal of Cellular Biochemistry*. (2005)

265. Khalid, O. *et al.* (2008) Modulation of Runx2 activity by estrogen receptor-α: Implications for osteoporosis and breast cancer. *Endocrinology*, DOI: 10.1210/en.2008-0680.

266. Javed, A. *et al.* (2005) Impaired intranuclear trafficking of Runx2 (AML3/CBFA1) transcription factors in breast cancer cells inhibits osteolysis in vivo. *Proc. Natl. Acad. Sci. U. S. A.*, DOI: 10.1073/pnas.0409121102.

267. Baniwal, S.K. *et al.* (2009) Repression of Runx2 by androgen receptor (AR) in osteoblasts and prostate cancer cells: AR binds Runx2 and abrogates its recruitment to DNA. *Mol. Endocrinol.*, DOI: 10.1210/me.2008-0470.

268. Komori, T. *et al.* (1997) Targeted disruption of Cbfa1 results in a complete lack of bone formation owing to maturational arrest of osteoblasts. *Cell*, DOI: 10.1016/S0092-8674(00)80258-5.

269. Otto, F., A.P. Thornell, T. Crompton, A. Denzel, K.C. Gilmour, I.R. Rosewell, G.W. Stamp, R.S. Beddington, S. Mundlos, B.R. Olsen, et al. 1997. *et al.* (1997) Cbfa1, a candidate gene for cleidocranial dysplasia syndrome, is essential for osteoblast differentiation and bone development. *Cell*,

270. Liu, L. *et al.* (2012) Na+/H+ exchanger regulatory factor 1 (NHERF1) directly regulates osteogenesis. *J. Biol. Chem.*, DOI: 10.1074/jbc.M112.422766.

271. Guleng, B. *et al.* (2010) Mindin is upregulated during colitis and may activate NF-κB in a TLR-9 mediated manner. *World J. Gastroenterol.*, DOI: 10.3748/wjg.v16.i9.1070.

272. Leslie, K.L. *et al.* (2013) Ezrin-Radixin-Moesin-binding phosphoprotein 50 (EBP50) and nuclear factor-κB (NF-κB). *J. Biol. Chem.*, **288**, 36426–36436.

273. Fu, Z. *et al.* (2002) Osteoblasts produce soluble factors that induce a gene

expression pattern in non-metastatic prostate cancer cells, similar to that found in bone metastatic prostate cancer cells. *Prostate*, DOI: 10.1002/pros.10056.

274. Lee, C. *et al.* (2018) Dual targeting c-met and VEGFR2 in osteoblasts suppresses growth and osteolysis of prostate cancer bone metastasis. *Cancer Lett.*, DOI: 10.1016/j.canlet.2017.11.016.
275. Smith, M. *et al.* (2016) , Phase III study of cabozantinib in previously treated metastatic castration-resistant prostate cancer: COMET-1. , in *Journal of Clinical Oncology*
276. Liu, Y. *et al.* Characteristics and Significance of the Pre-metastatic Niche. , *Cancer Cell*. (2016)
277. Jin, J.K. *et al.* (2011) Steps in prostate cancer progression that lead to bone metastasis. *Int. J. Cancer*, DOI: 10.1002/ijc.26024.
278. Huveneers, S. *et al.* Adhesion signaling - Crosstalk between integrins, Src and Rho. , *Journal of Cell Science*. (2009)
279. Wang, H. *et al.* (2015) The Osteogenic Niche Promotes Early-Stage Bone Colonization of Disseminated Breast Cancer Cells. *Cancer Cell*, DOI: 10.1016/j.ccell.2014.11.017.
280. Myers, T.J. *et al.* (2015) BMP2 Regulation of CXCL12 Cellular, Temporal, and Spatial Expression is Essential during Fracture Repair. *J. Bone Miner. Res.*, DOI: 10.1002/jbmr.2548.
281. Nakashima, T. *et al.* (2011) Evidence for osteocyte regulation of bone homeostasis through RANKL expression. *Nat. Med.*, DOI: 10.1038/nm.2452.
282. Wheeler, D.S. *et al.* (2011) Direct interaction between NHERF1 and Frizzled regulates B-catenin signaling. *Oncogene*, DOI: 10.1038/onc.2010.389.
283. Lin, Y.Y. *et al.* (2012) Aberrant nuclear localization of EBP50 promotes colorectal carcinogenesis in xenotransplanted mice by modulating TCF-1 and β-catenin interactions. *J. Clin. Invest.*, DOI: 10.1172/JCI45661.
284. Paradiso, A. *et al.* (2013) Nuclear NHERF1 expression as a prognostic marker in breast cancer. *Cell Death Dis.*, DOI: 10.1038/cddis.2013.439.

10. ANEXOS

Anexo I. Detalle de los pacientes diagnosticados de cáncer de próstata

Número de identificación	Edad	PSA ng/mL	Grado Gleason	Riesgo D'Amico	TNM	Invasión Perineural	Márgenes Quirúrgicos
S12-6445-A8	63	7.4	3+4	MEDIO	pT2c	0	Negativo
S12-6582-A14	60	14.0	3+3	MEDIO	pT2c	0	Negativo
S12-6655-A7	63	12.0	4+3	MEDIO	pT2c	1	Negativo
S12-6921-A13	69	8.6	3+3	BAJO	pT2c	0	Negativo
S12-7016-A1	67	5.9	4+3	BAJO	pT2c	0	Negativo
S12-7240-A1	62	8.8	3+3	BAJO	pT2c	0	Negativo
S12-7483-A1	53	9.0	3+3	BAJO	pT2a	0	Negativo
S12-8429-A1	67	6.5	3+3	BAJO	pT2c	0	Negativo
S12-8884-A19	65	12.6	3+4	MEDIO	pT3b	0	Negativo
S12-9815-A8	50	6.8	3+4	MEDIO	pT2a	0	Negativo
S12-10817-A4	71	8.8	4+5	ALTO	pT2b	0	Negativo
S13-00299-A11	63	5.7	3+3	BAJO	pT2c	0	Positivo
S13-00601-A8	65	4.6	3+3	BAJO	pT2a	0	Negativo
S13-00839-A25	60	6.3	4+3	ALTO	pT3a	0	Positivo
S13-01132-A80	60	ND	4+3	ALTO	pT3a	0	Positivo
S13-01126-A11	61	11.0	3+3	MEDIO	pT2c	0	Positivo
S13-03877-A11	52	7.0	3+3	MEDIO	pT2c	0	Positivo
S13-04240-A14	64	9.0	3+4	MEDIO	pT2c	0	Positivo
S13-04367-A22	41	4.4	3+3	BAJO	pT2c	0	Positivo
S13-05208-A14	62	10.0	3+4	MEDIO	pT3a	0	Negativo
S13-06056-A1	70	7.9	3+4	MEDIO	pT2c	1	Negativo
S13-07645-A14	55	4.7	3+4	MEDIO	pT2c	0	Negativo
S13-07881-A2	62	10.0	3+4	MEDIO	pT2c	1	Positivo

S13-05757-A22	64	7.0	3+3	BAJO	pT3a	0	Positivo
S14-00330-A46	54	5.0	3+3	BAJO	pT3a	1	Negativo
S14-00305-A10	58	12.5	3+4	MEDIO	pT2c	1	Negativo
S14-00608-A34	65	6.4	3+3	BAJO	pT2c	0	Negativo
S14-00898-A13	61	3.4	4+3	BAJO	pT3a	1	Negativo
S14-01471-A11	67	4.5	3+4	MEDIO	pT2c	0	Negativo
S14-02065-A8	66	7.0	3+4	BAJO	pT2c	0	Negativo
S14-03706 A23	72	23.4	4+3	ALTO	pT3a	0	Negativo
S14-04255 A20	62	4.7	3+3	BAJO	pT2c	0	Negativo
S14-04561 A11	52	5.8	3+3	MEDIO	pT2b	0	Negativo
S14-04586 A9	71	8.9	4+3	BAJO	pT2c	0	Negativo
S14-04742 A7	59	8.4	3+3	BAJO	pT2a	0	Negativo
S14-05759 A15	41	7.8	3+4	BAJO	pT2c	0	Positivo
S14-05813 A13	69	11.3	4+3	MEDIO	pT2c	0	Negativo
S14-06003 A16	65	6.9	3+3	BAJO	pT3a	0	Negativo
S14-06114 A37	70	10.0	4+3	MEDIO	pT3a	0	Negativo
S14-06637 A14	57	4.2	3+4	BAJO	pT2c	0	Negativo
S14-06642 A26	51	4.0	3+4	BAJO	pT3a	0	Negativo
S14-08126 A21	53	4.7	3+4	MEDIO	pT2c	0	Negativo
S14-08224 A2	71	6.8	3+3	BAJO	pT2c	0	Negativo
S14-08142 A16	56	11.0	3+4	MEDIO	pT2c	0	Negativo
S14-08281 A8	50	3.2	3+3	BAJO	pT2c	0	Negativo
S14-09146 A2	56	3.8	3+3	BAJO	pT2a	0	Negativo
S14-09420 A12	68	8.4	4+3	MEDIO	pT2c	0	Negativo
S14-09750 A13	65	16.5	3+4	MEDIO	pT3a	0	Negativo
S14-09948 A22	68	5.2	3+3	BAJO	pT2c	0	Negativo
S14-10232 A20	64	7.3	3+4	MEDIO	pT3a	1	Negativo
S14-10580 A11	63	5.0	3+3	BAJO	pT2c	0	Negativo

S14-10618 A1	60	6.9	4+3	MEDIO	pT2c	1	Negativo
S14-10929 A9	72	5.3	3+4	MEDIO	pT2a	1	Positivo
S14-11817 A12	47	7.4	3+4	MEDIO	pT2c	0	Negativo

Anexo II. Perfil proteico del secretoma de células de próstata no tumorales, células de adenocarcinoma de próstata LNCaP, PC-3 y TRAMP-C1, células osteoblásticas humanas y de ratón MC3T3-E1 y células osteocíticas de ratón MLO-Y4. El análisis del secretoma proteico mediante RP-LC-MS/MS reveló la secreción de mindin, también conocida como ESPONDINA-2 (aparece en subrayado amarillo), en células LNCaP y TRAMP-C1, pero no en el resto de líneas celulares.

A. Línea celular de próstata no tumoral

Accession	Description	MW [kDa]
P62258;P62261	14-3-3 protein epsilon OS=Homo sapiens GN=YWHAE PE=1 SV=1 - [1433E_HUMAN]	29,2
Q04917	14-3-3 protein eta OS=Homo sapiens GN=YWHAH PE=1 SV=4 - [1433F_HUMAN]	28,2
P61981;A7Z057	14-3-3 protein gamma OS=Homo sapiens GN=YWHAG PE=1 SV=2 - [1433G_HUMAN]	28,3
P27348;Q3SZI4	14-3-3 protein theta OS=Homo sapiens GN=YWHAQ PE=1 SV=1 - [1433T_HUMAN]	27,7
P63104;P63103	14-3-3 protein zeta/delta OS=Homo sapiens GN=YWHAZ PE=1 SV=1 - [1433Z_HUMAN]	27,7
P62263	40S ribosomal protein S14 OS=Homo sapiens GN=RPS14 PE=1 SV=3 - [RS14_HUMAN]	16,3
P62269;Q3T0R1	40S ribosomal protein S18 OS=Homo sapiens GN=RPS18 PE=1 SV=3 - [RS18_HUMAN]	17,7
H0YEN5	40S ribosomal protein S2 (Fragment) OS=Homo sapiens GN=RPS2 PE=1 SV=1 - [H0YEN5_HUMAN]	21,1
P23396;Q3T169	40S ribosomal protein S3 OS=Homo sapiens GN=RPS3 PE=1 SV=2 - [RS3_HUMAN]	26,7
P61247;Q56JV9	40S ribosomal protein S3a OS=Homo sapiens GN=RPS3A PE=1 SV=2 - [RS3A_HUMAN]	29,9
P62701;P79103	40S ribosomal protein S4, X isoform OS=Homo sapiens GN=RPS4X PE=1 SV=2 - [RS4X_HUMAN]	29,6
P62241;Q5E958	40S ribosomal protein S8 OS=Homo sapiens GN=RPS8 PE=1 SV=2 - [RS8_HUMAN]	24,2
P46781;A6QLG5	40S ribosomal protein S9 OS=Homo sapiens GN=RPS9 PE=1 SV=3 - [RS9_HUMAN]	22,6
C9J9K3	40S ribosomal protein SA (Fragment) OS=Homo sapiens GN=RPSA PE=1 SV=4 - [C9J9K3_HUMAN]	29,4
H0YFS2	4F2 cell-surface antigen heavy chain (Fragment) OS=Homo sapiens GN=SLC3A2 PE=1 SV=1 - [H0YFS2_HUMAN]	26,1
F1MUZ9	60 kDa heat shock protein, mitochondrial OS=Bos taurus GN=HSPD1 PE=1 SV=1 - [F1MUZ9_BOVIN]	60,9
G3V210	60S acidic ribosomal protein P0 OS=Homo sapiens GN=RPLP0 PE=1 SV=1 - [G3V210_HUMAN]	18,3
P62913;Q3T087	60S ribosomal protein L11 OS=Homo sapiens GN=RPL11 PE=1 SV=2 - [RL11_HUMAN]	20,2
Q02543;Q3T003	60S ribosomal protein L18a OS=Homo sapiens GN=RPL18A PE=1 SV=2 - [RL18A_HUMAN]	20,7
P08253	72 kDa type IV collagenase OS=Homo sapiens GN=MMP2 PE=1 SV=2 - [MMP2_HUMAN]	73,8
P11021	78 kDa glucose-regulated protein OS=Homo sapiens GN=HSPA5 PE=1 SV=2 - [GRP78_HUMAN]	72,3
P68032;Q3ZC07	Actin, alpha cardiac muscle 1 OS=Homo sapiens GN=ACTC1 PE=1 SV=1 - [ACTC_HUMAN]	42,0
P60709;P60712	Actin, cytoplasmic 1 OS=Homo sapiens GN=ACTB PE=1 SV=1 - [ACTB_HUMAN]	41,7
P23526	Adenosylhomocysteinase OS=Homo sapiens GN=AHCY PE=1 SV=4 - [SAHH_HUMAN]	47,7
Q3Y5Z3	Adiponectin OS=Bos taurus GN=ADIPOQ PE=1 SV=1 - [ADIPO_BOVIN]	26,1
C9JPM4	ADP-ribosylation factor 4 (Fragment) OS=Homo sapiens GN=ARF4 PE=1 SV=1 - [C9JPM4_HUMAN]	14,5
P84085;A4IFP7	ADP-ribosylation factor 5 OS=Homo sapiens GN=ARF5 PE=1 SV=2 - [ARF5_HUMAN]	20,5
P14550	Alcohol dehydrogenase [NADP(+)] OS=Homo sapiens GN=AKR1A1 PE=1 SV=3 - [AK1A1_HUMAN]	36,5
H0Y2X5	Aldehyde dehydrogenase 1 family, member A3, isoform CRA_b OS=Homo sapiens GN=ALDH1A3 PE=1 SV=1 - [H0Y2X5_HUMAN]	44,2
P15121	Aldose reductase OS=Homo sapiens GN=AKR1B1 PE=1 SV=3 - [ALDR_HUMAN]	35,8
Q3SZR3	Alpha-1-acid glycoprotein OS=Bos taurus GN=ORM1 PE=2 SV=1 - [A1AG_BOVIN]	23,2
G3V5I3	Alpha-1-antichymotrypsin (Fragment) OS=Homo sapiens GN=SERPINA3 PE=4 SV=2 - [G3V5I3_HUMAN]	4,7
P01011	Alpha-1-antichymotrypsin OS=Homo sapiens GN=SERPINA3 PE=1 SV=2 - [AACT_HUMAN]	47,6

P34955	Alpha-1-antiproteinase OS=Bos taurus GN=SERPINA1 PE=1 SV=1 - [A1AT_BOVIN]	46,1
Q2KJF1	Alpha-1B-glycoprotein OS=Bos taurus GN=A1BG PE=1 SV=1 - [A1BG_BOVIN]	53,5
P28800	Alpha-2-antiplasmin OS=Bos taurus GN=SERPINF2 PE=1 SV=2 - [A2AP_BOVIN]	54,7
P12763	Alpha-2-HS-glycoprotein OS=Bos taurus GN=AHSG PE=1 SV=2 - [FETUA_BOVIN]	38,4
C9JV77	Alpha-2-HS-glycoprotein OS=Homo sapiens GN=AHSG PE=1 SV=1 - [C9JV77_HUMAN]	39,4
Q7SIH1	Alpha-2-macroglobulin OS=Bos taurus GN=A2M PE=1 SV=2 - [A2MG_BOVIN]	167,5
O43707	Alpha-actinin-4 OS=Homo sapiens GN=ACTN4 PE=1 SV=2 - [ACTN4_HUMAN]	104,8
P06733	Alpha-enolase OS=Homo sapiens GN=ENO1 PE=1 SV=2 - [ENOA_HUMAN]	47,1
Q3SZ57	Alpha-fetoprotein OS=Bos taurus GN=AFP PE=2 SV=1 - [FETA_BOVIN]	68,5
P02771	Alpha-fetoprotein OS=Homo sapiens GN=AFP PE=1 SV=1 - [FETA_HUMAN]	68,6
H7C0V9	Amyloid beta A4 protein (Fragment) OS=Homo sapiens GN=APP PE=1 SV=1 - [H7C0V9_HUMAN]	55,1
Q3SZH5	Angiotensinogen OS=Bos taurus GN=AGT PE=2 SV=1 - [Q3SZH5_BOVIN]	45,4
P04083	Annexin A1 OS=Homo sapiens GN=ANXA1 PE=1 SV=2 - [ANXA1_HUMAN]	38,7
P07355	Annexin A2 OS=Homo sapiens GN=ANXA2 PE=1 SV=2 - [ANXA2_HUMAN]	38,6
D6RA82	Annexin A3 OS=Homo sapiens GN=ANXA3 PE=1 SV=1 - [D6RA82_HUMAN]	32,1
P81287	Annexin A5 OS=Bos taurus GN=ANXA5 PE=1 SV=3 - [ANXA5_BOVIN]	36,1
P08758	Annexin A5 OS=Homo sapiens GN=ANXA5 PE=1 SV=2 - [ANXA5_HUMAN]	35,9
P03973	Antileukoproteinase OS=Homo sapiens GN=SLPI PE=1 SV=2 - [SLPI_HUMAN]	14,3
F1MSZ6	Antithrombin-III OS=Bos taurus GN=SERPINC1 PE=1 SV=1 - [F1MSZ6_BOVIN]	52,4
P15497	Apolipoprotein A-I OS=Bos taurus GN=APOA1 PE=1 SV=3 - [APOA1_BOVIN]	30,3
F1MS32	Apolipoprotein D OS=Bos taurus GN=APOD PE=4 SV=2 - [F1MS32_BOVIN]	21,4
E9PEV4	Apolipoprotein E (Fragment) OS=Homo sapiens GN=APOE PE=1 SV=1 - [E9PEV4_HUMAN]	24,6
Q03247	Apolipoprotein E OS=Bos taurus GN=APOE PE=1 SV=1 - [APOE_BOVIN]	36,0
O43776	Asparagine--tRNA ligase, cytoplasmic OS=Homo sapiens GN=NARS PE=1 SV=1 - [SYNC_HUMAN]	62,9
P00505	Aspartate aminotransferase, mitochondrial OS=Homo sapiens GN=GOT2 PE=1 SV=3 - [AATM_HUMAN]	47,5
P06576	ATP synthase subunit beta, mitochondrial OS=Homo sapiens GN=ATP5B PE=1 SV=3 - [ATPB_HUMAN]	56,5
P98160	Basement membrane-specific heparan sulfate proteoglycan core protein OS=Homo sapiens GN=HSPG2 PE=1 SV=4 - [PGBM_HUMAN]	468,5
P17690	Beta-2-glycoprotein 1 OS=Bos taurus GN=APOH PE=1 SV=4 - [APOH_BOVIN]	38,2
H3BVI7	Cadherin-1 OS=Homo sapiens GN=CDH1 PE=1 SV=1 - [H3BVI7_HUMAN]	45,5
P27824	Calnexin OS=Homo sapiens GN=CANX PE=1 SV=2 - [CALX_HUMAN]	67,5
P17655	Calpain-2 catalytic subunit OS=Homo sapiens GN=CAPN2 PE=1 SV=6 - [CAN2_HUMAN]	79,9
P27797	Calreticulin OS=Homo sapiens GN=CALR PE=1 SV=1 - [CALR_HUMAN]	48,1
P07858	Cathepsin B OS=Homo sapiens GN=CTSB PE=1 SV=3 - [CATB_HUMAN]	37,8
P07339	Cathepsin D OS=Homo sapiens GN=CTSD PE=1 SV=1 - [CATD_HUMAN]	44,5
F5GXJ9	CD166 antigen OS=Homo sapiens GN=ALCAM PE=1 SV=1 - [F5GXJ9_HUMAN]	59,5
E9PNW4	CD59 glycoprotein OS=Homo sapiens GN=CD59 PE=1 SV=1 - [E9PNW4_HUMAN]	12,0
O00299	Chloride intracellular channel protein 1 OS=Homo sapiens GN=CLIC1 PE=1 SV=4 - [CLIC1_HUMAN]	26,9
Q9XSA7	Chloride intracellular channel protein 4 OS=Bos taurus GN=CLIC4 PE=2 SV=3 - [CLIC4_BOVIN]	28,7
H3BT58	Coactosin-like protein OS=Homo sapiens GN=COTL1 PE=1 SV=1 - [H3BT58_HUMAN]	8,2
G3V1A4	Cofilin 1 (Non-muscle), isoform CRA_a OS=Homo sapiens GN=CFL1 PE=1 SV=1 - [G3V1A4_HUMAN]	16,8
P02452	Collagen alpha-1(I) chain OS=Homo sapiens GN=COL1A1 PE=1 SV=5 - [CO1A1_HUMAN]	138,9
F1MXS8	Collagen alpha-1(III) chain OS=Bos taurus GN=COL3A1 PE=4 SV=2 - [F1MXS8_BOVIN]	138,8
P02461	Collagen alpha-1(III) chain OS=Homo sapiens GN=COL3A1 PE=1 SV=4 - [CO3A1_HUMAN]	138,5
A0A087WXW9	Collagen alpha-1(V) chain OS=Homo sapiens GN=COL5A1 PE=1 SV=1 - [A0A087WXW9_HUMAN]	183,5
A0A087X0S5	Collagen alpha-1(VI) chain OS=Homo sapiens GN=COL6A1 PE=1 SV=1 - [A0A087X0S5_HUMAN]	108,3
A0A087WTA8	Collagen alpha-2(I) chain OS=Homo sapiens GN=COL1A2 PE=1 SV=1 - [A0A087WTA8_HUMAN]	129,1
P08572	Collagen alpha-2(IV) chain OS=Homo sapiens GN=COL4A2 PE=1 SV=4 - [CO4A2_HUMAN]	167,4

A0A087WYX9	Collagen alpha-2(V) chain OS=Homo sapiens GN=COL5A2 PE=1 SV=1 - [A0A087WYX9_HUMAN]	106,9
P00736	Complement C1r subcomponent OS=Homo sapiens GN=C1R PE=1 SV=2 - [C1R_HUMAN]	80,1
F8WCZ6	Complement C1s subcomponent OS=Homo sapiens GN=C1S PE=1 SV=1 - [F8WCZ6_HUMAN]	57,5
Q2UVX4	Complement C3 OS=Bos taurus GN=C3 PE=1 SV=2 - [CO3_BOVIN]	187,1
P01024	Complement C3 OS=Homo sapiens GN=C3 PE=1 SV=2 - [CO3_HUMAN]	187,0
F1MY85	Complement C5a anaphylatoxin OS=Bos taurus GN=C5 PE=4 SV=2 - [F1MY85_BOVIN]	188,9
Q3MHN2	Complement component C9 OS=Bos taurus GN=C9 PE=2 SV=1 - [CO9_BOVIN]	62,0
P81187	Complement factor B OS=Bos taurus GN=CFB PE=1 SV=2 - [CFAB_BOVIN]	85,3
P00751	Complement factor B OS=Homo sapiens GN=CFB PE=1 SV=2 - [CFAB_HUMAN]	85,5
G3XAM2	Complement factor I OS=Homo sapiens GN=CFI PE=1 SV=1 - [G3XAM2_HUMAN]	65,0
Q15828	Cystatin-M OS=Homo sapiens GN=CST6 PE=1 SV=1 - [CYTM_HUMAN]	16,5
C9JFR7	Cytochrome c (Fragment) OS=Homo sapiens GN=CYCS PE=1 SV=1 - [C9JFR7_HUMAN]	11,3
Q5SZU1	D-3-phosphoglycerate dehydrogenase OS=Homo sapiens GN=PHGDH PE=1 SV=1 - [Q5SZU1_HUMAN]	53,1
Q14126	Desmoglein-2 OS=Homo sapiens GN=DSG2 PE=1 SV=2 - [DSG2_HUMAN]	122,2
O94907	Dickkopf-related protein 1 OS=Homo sapiens GN=DKK1 PE=1 SV=1 - [DKK1_HUMAN]	28,7
Q9H4M9	EH domain-containing protein 1 OS=Homo sapiens GN=EHD1 PE=1 SV=2 - [EHD1_HUMAN]	60,6
P68104;P68103	Elongation factor 1-alpha 1 OS=Homo sapiens GN=EEF1A1 PE=1 SV=1 - [EF1A1_HUMAN]	50,1
F1MG05	Elongation factor 1-gamma OS=Bos taurus GN=EEF1G PE=1 SV=1 - [F1MG05_BOVIN]	50,3
P26641	Elongation factor 1-gamma OS=Homo sapiens GN=EEF1G PE=1 SV=3 - [EF1G_HUMAN]	50,1
P13639	Elongation factor 2 OS=Homo sapiens GN=EEF2 PE=1 SV=4 - [EF2_HUMAN]	95,3
F8VY02	Endoplasmic reticulum resident protein 29 OS=Homo sapiens GN=ERP29 PE=1 SV=1 - [F8VY02_HUMAN]	18,1
P14625	Endoplasmin OS=Homo sapiens GN=HSP90B1 PE=1 SV=1 - [ENPL_HUMAN]	92,4
Q9H6S3	Epidermal growth factor receptor kinase substrate 8-like protein 2 OS=Homo sapiens GN=EPS8L2 PE=1 SV=2 - [ES8L2_HUMAN]	80,6
P60842;Q3SZ54	Eukaryotic initiation factor 4A-I OS=Homo sapiens GN=EIF4A1 PE=1 SV=1 - [IF4A1_HUMAN]	46,1
E7EQR4	Ezrin OS=Homo sapiens GN=EZR PE=1 SV=3 - [E7EQR4_HUMAN]	69,3
Q16658	Fascin OS=Homo sapiens GN=FSCN1 PE=1 SV=3 - [FSCN1_HUMAN]	54,5
I6L8B7	Fatty acid-binding protein, epidermal OS=Homo sapiens GN=FABP5 PE=1 SV=1 - [I6L8B7_HUMAN]	11,2
Q58D62	Fetuin-B OS=Bos taurus GN=FETUB PE=1 SV=1 - [FETUB_BOVIN]	42,6
P35555	Fibrillin-1 OS=Homo sapiens GN=FBN1 PE=1 SV=3 - [FBN1_HUMAN]	312,0
F1MYN5	Fibulin-1 OS=Bos taurus GN=FBLN1 PE=3 SV=2 - [F1MYN5_BOVIN]	77,4
Q5HY54	Filamin-A OS=Homo sapiens GN=FLNA PE=1 SV=1 - [Q5HY54_HUMAN]	276,4
P04075	Fructose-bisphosphate aldolase A OS=Homo sapiens GN=ALDOA PE=1 SV=2 - [ALDOA_HUMAN]	39,4
P09382	Galectin-1 OS=Homo sapiens GN=LGALS1 PE=1 SV=2 - [LEG1_HUMAN]	14,7
Q08380	Galectin-3-binding protein OS=Homo sapiens GN=LGALS3BP PE=1 SV=1 - [LG3BP_HUMAN]	65,3
Q92820	Gamma-glutamyl hydrolase OS=Homo sapiens GN=GGH PE=1 SV=2 - [GGH_HUMAN]	35,9
F1N1I6	Gelsolin OS=Bos taurus GN=GSN PE=1 SV=1 - [F1N1I6_BOVIN]	85,6
K7EQ48	Glucose-6-phosphate isomerase OS=Homo sapiens GN=GPI PE=1 SV=2 - [K7EQ48_HUMAN]	53,4
Q16769	Glutaminyl-peptide cyclotransferase OS=Homo sapiens GN=QPCT PE=1 SV=1 - [QPCT_HUMAN]	40,9
Q5TA02	Glutathione S-transferase omega-1 (Fragment) OS=Homo sapiens GN=GSTO1 PE=1 SV=1 - [Q5TA02_HUMAN]	23,3
A0A087X2E9	Glutathione S-transferase P (Fragment) OS=Homo sapiens GN=GSTP1 PE=1 SV=1 - [A0A087X2E9_HUMAN]	8,9
P04406	Glyceraldehyde-3-phosphate dehydrogenase OS=Homo sapiens GN=GAPDH PE=1 SV=3 - [G3P_HUMAN]	36,0
P41250	Glycine--tRNA ligase OS=Homo sapiens GN=GARS PE=1 SV=3 - [SYG_HUMAN]	83,1
P28799	Granulins OS=Homo sapiens GN=GRN PE=1 SV=2 - [GRN_HUMAN]	63,5
Q99988	Growth/differentiation factor 15 OS=Homo sapiens GN=GDF15 PE=1 SV=3 - [GDF15_HUMAN]	34,1
P62826;Q3T054	GTP-binding nuclear protein Ran OS=Homo sapiens GN=RAN PE=1 SV=3 - [RAN_HUMAN]	24,4
P62879;P11017	Guanine nucleotide-binding protein G(I)/G(S)/G(T) subunit beta-2 OS=Homo sapiens GN=GNB2 PE=1 SV=3 - [GBB2_HUMAN]	37,3

P63244;P63243	Guanine nucleotide-binding protein subunit beta-2-like 1 OS=Homo sapiens GN=GNB2L1 PE=1 SV=3 - [GBLP_HUMAN]	35,1
A0A0A0MTS5	HCG1811249, isoform CRA_f OS=Homo sapiens GN=LAMA3 PE=1 SV=1 - [A0A0A0MTS5_HUMAN]	183,9
P34931	Heat shock 70 kDa protein 1-like OS=Homo sapiens GN=HSPA1L PE=1 SV=2 - [HS71L_HUMAN]	70,3
P11142	Heat shock cognate 71 kDa protein OS=Homo sapiens GN=HSPA8 PE=1 SV=1 - [HSP7C_HUMAN]	70,9
P04792	Heat shock protein beta-1 OS=Homo sapiens GN=HSPB1 PE=1 SV=2 - [HSPB1_HUMAN]	22,8
P07900	Heat shock protein HSP 90-alpha OS=Homo sapiens GN=HSP90AA1 PE=1 SV=5 - [HS90A_HUMAN]	84,6
Q76LV1	Heat shock protein HSP 90-beta OS=Bos taurus GN=HSP90AB1 PE=2 SV=3 - [HS90B_BOVIN]	83,2
P02081	Hemoglobin fetal subunit beta OS=Bos taurus PE=1 SV=1 - [HBBF_BOVIN]	15,8
P01966	Hemoglobin subunit alpha OS=Bos taurus GN=HBA PE=1 SV=2 - [HBA_BOVIN]	15,2
P69905	Hemoglobin subunit alpha OS=Homo sapiens GN=HBA1 PE=1 SV=2 - [HBA_HUMAN]	15,2
P02070	Hemoglobin subunit beta OS=Bos taurus GN=HBB PE=1 SV=1 - [HBB_BOVIN]	15,9
Q3SZV7	Hemopexin OS=Bos taurus GN=HPX PE=2 SV=1 - [HEMO_BOVIN]	52,2
P08581	Hepatocyte growth factor receptor OS=Homo sapiens GN=MET PE=1 SV=4 - [MET_HUMAN]	155,4
D6R9P3	Heterogeneous nuclear ribonucleoprotein A/B OS=Homo sapiens GN=HNRNPAB PE=1 SV=1 - [D6R9P3_HUMAN]	30,3
D6RF44	Heterogeneous nuclear ribonucleoprotein D0 (Fragment) OS=Homo sapiens GN=HNRNPD PE=1 SV=4 - [D6RF44_HUMAN]	12,5
Q5E9J1	Heterogeneous nuclear ribonucleoprotein F OS=Bos taurus GN=HNRNPF PE=2 SV=3 - [HNRPF_BOVIN]	45,7
G3V4M8	Heterogeneous nuclear ribonucleoproteins C1/C2 (Fragment) OS=Homo sapiens GN=HNRNPC PE=1 SV=1 - [G3V4M8_HUMAN]	7,3
Q5T7C4	High mobility group protein B1 OS=Homo sapiens GN=HMGB1 PE=1 SV=1 - [Q5T7C4_HUMAN]	18,3
F1MLQ1	Histone H2A OS=Bos taurus GN=LOC524236 PE=3 SV=2 - [F1MLQ1_BOVIN]	14,2
P0C0S5;P0C0S4	Histone H2A.Z OS=Homo sapiens GN=H2AFZ PE=1 SV=2 - [H2AZ_HUMAN]	13,5
O60814;F2Z4F9	Histone H2B type 1-K OS=Homo sapiens GN=HIST1H2BK PE=1 SV=3 - [H2B1K_HUMAN]	13,9
Q32L48	Histone H2B type 1-N OS=Bos taurus GN=HIST1H2BN PE=1 SV=3 - [H2B1N_BOVIN]	13,9
P62805;P62803	Histone H4 OS=Homo sapiens GN=HIST1H4A PE=1 SV=2 - [H4_HUMAN]	11,4
Q5SRN7	HLA class I histocompatibility antigen, A-3 alpha chain OS=Homo sapiens GN=HLA-A PE=1 SV=2 - [Q5SRN7_HUMAN]	34,2
H7C3I1	Hsc70-interacting protein (Fragment) OS=Homo sapiens GN=ST13 PE=1 SV=1 - [H7C3I1_HUMAN]	16,3
H0YN67	Immunoglobulin superfamily-containing leucine-rich repeat protein (Fragment) OS=Homo sapiens GN=ISLR PE=1 SV=1 - [H0YN67_HUMAN]	16,2
P08476	Inhibin beta A chain OS=Homo sapiens GN=INHBA PE=1 SV=2 - [INHBA_HUMAN]	47,4
H0Y9D8	Inorganic pyrophosphatase 2, mitochondrial (Fragment) OS=Homo sapiens GN=PPA2 PE=1 SV=1 - [H0Y9D8_HUMAN]	25,6
A6XND1	Insulin-like growth factor binding protein 3 isoform b OS=Homo sapiens GN=IGFBP3 PE=1 SV=1 - [A6XND1_HUMAN]	29,0
F8VYK9	Insulin-like growth factor-binding protein 6 OS=Homo sapiens GN=IGFBP6 PE=1 SV=1 - [F8VYK9_HUMAN]	25,1
F1MMP5	Inter-alpha-trypsin inhibitor heavy chain H1 OS=Bos taurus GN=ITIH1 PE=4 SV=1 - [F1MMP5_BOVIN]	101,2
F1MNW4	Inter-alpha-trypsin inhibitor heavy chain H2 OS=Bos taurus GN=ITIH2 PE=4 SV=2 - [F1MNW4_BOVIN]	106,1
P56652	Inter-alpha-trypsin inhibitor heavy chain H3 OS=Bos taurus GN=ITIH3 PE=1 SV=2 - [ITIH3_BOVIN]	99,5
F1MMD7	Inter-alpha-trypsin inhibitor heavy chain H4 OS=Bos taurus GN=ITIH4 PE=1 SV=2 - [F1MMD7_BOVIN]	101,5
P05362	Intercellular adhesion molecule 1 OS=Homo sapiens GN=ICAM1 PE=1 SV=2 - [ICAM1_HUMAN]	57,8
Q12905;F2Z4E7	Interleukin enhancer-binding factor 2 OS=Homo sapiens GN=ILF2 PE=1 SV=2 - [ILF2_HUMAN]	43,0
B5MCZ3	Interleukin-6 OS=Homo sapiens GN=IL6 PE=1 SV=1 - [B5MCZ3_HUMAN]	21,5
P03956	Interstitial collagenase OS=Homo sapiens GN=MMP1 PE=1 SV=3 - [MMP1_HUMAN]	54,0
O75874	Isocitrate dehydrogenase [NADP] cytoplasmic OS=Homo sapiens GN=IDH1 PE=1 SV=2 - [IDHC_HUMAN]	46,6
P49788-2	Isoform 1 of Retinoic acid receptor responder protein 1 OS=Homo sapiens GN=RARRES1 - [TIG1_HUMAN]	25,8
P18206-2	Isoform 1 of Vinculin OS=Homo sapiens GN=VCL - [VINC_HUMAN]	116,6

P31947-2	Isoform 2 of 14-3-3 protein sigma OS=Homo sapiens GN=SFN - [1433S_HUMAN]	24,3
P21589-2	Isoform 2 of 5'-nucleotidase OS=Homo sapiens GN=NT5E - [5NTD_HUMAN]	57,9
Q07020-2	Isoform 2 of 60S ribosomal protein L18 OS=Homo sapiens GN=RPL18 - [RL18_HUMAN]	18,1
P52209-2	Isoform 2 of 6-phosphogluconate dehydrogenase, decarboxylating OS=Homo sapiens GN=PGD - [6PGD_HUMAN]	51,8
P01009-2	Isoform 2 of Alpha-1-antitrypsin OS=Homo sapiens GN=SERPINA1 - [A1AT_HUMAN]	40,2
P12814-2	Isoform 2 of Alpha-actinin-1 OS=Homo sapiens GN=ACTN1 - [ACTN1_HUMAN]	102,6
P08133-2	Isoform 2 of Annexin A6 OS=Homo sapiens GN=ANXA6 - [ANXA6_HUMAN]	72,4
P25705-2	Isoform 2 of ATP synthase subunit alpha, mitochondrial OS=Homo sapiens GN=ATP5A1 - [ATPA_HUMAN]	54,5
O94985-2	Isoform 2 of Calsyntenin-1 OS=Homo sapiens GN=CLSTN1 - [CSTN1_HUMAN]	108,6
Q9UI42-2	Isoform 2 of Carboxypeptidase A4 OS=Homo sapiens GN=CPA4 - [CBPA4_HUMAN]	43,5
P0C0L4-2	Isoform 2 of Complement C4-A OS=Homo sapiens GN=C4A - [CO4A_HUMAN]	187,6
P29279-2	Isoform 2 of Connective tissue growth factor OS=Homo sapiens GN=CTGF - [CTGF_HUMAN]	35,2
P09622-2	Isoform 2 of Dihydrolipoyl dehydrogenase, mitochondrial OS=Homo sapiens GN=DLD - [DLDH_HUMAN]	43,6
P53634-2	Isoform 2 of Dipeptidyl peptidase 1 OS=Homo sapiens GN=CTSC - [CATC_HUMAN]	15,2
Q12805-2	Isoform 2 of EGF-containing fibulin-like extracellular matrix protein 1 OS=Homo sapiens GN=EFEMP1 - [FBLN3_HUMAN]	53,7
P47756-2;P79136-2	Isoform 2 of F-actin-capping protein subunit beta OS=Homo sapiens GN=CAPZB - [CAPZB_HUMAN]	30,6
Q14315-2	Isoform 2 of Filamin-C OS=Homo sapiens GN=FLNC - [FLNC_HUMAN]	287,1
Q12841-2	Isoform 2 of Follistatin-related protein 1 OS=Homo sapiens GN=FSTL1 - [FSTL1_HUMAN]	31,2
P07093-2	Isoform 2 of Glia-derived nexin OS=Homo sapiens GN=SERPINE2 - [GDN_HUMAN]	44,0
Q16270-2	Isoform 2 of Insulin-like growth factor-binding protein 7 OS=Homo sapiens GN=IGFBP7 - [IBP7_HUMAN]	28,8
Q08431-2	Isoform 2 of Lactadherin OS=Homo sapiens GN=MFGE8 - [MFGM_HUMAN]	35,2
Q04760-2	Isoform 2 of Lactoylglutathione lyase OS=Homo sapiens GN=GLO1 - [LGUL_HUMAN]	19,0
P21741-2	Isoform 2 of Midkine OS=Homo sapiens GN=MDK - [MK_HUMAN]	9,5
P35579-2	Isoform 2 of Myosin-9 OS=Homo sapiens GN=MYH9 - [MYH9_HUMAN]	159,8
Q96TA1-2	Isoform 2 of Niban-like protein 1 OS=Homo sapiens GN=FAM129B - [NIBL1_HUMAN]	82,6
P00558-2	Isoform 2 of Phosphoglycerate kinase 1 OS=Homo sapiens GN=PGK1 - [PGK1_HUMAN]	41,4
P05155-2	Isoform 2 of Plasma protease C1 inhibitor OS=Homo sapiens GN=SERPING1 - [IC1_HUMAN]	49,7
P25788-2	Isoform 2 of Proteasome subunit alpha type-3 OS=Homo sapiens GN=PSMA3 - [PSA3_HUMAN]	27,6
O75326-2	Isoform 2 of Semaphorin-7A OS=Homo sapiens GN=SEMA7A - [SEM7A_HUMAN]	73,3
P52823-2	Isoform 2 of Stanniocalcin-1 OS=Homo sapiens GN=STC1 - [STC1_HUMAN]	20,5
O00391-2	Isoform 2 of Sulfhydryl oxidase 1 OS=Homo sapiens GN=QSOX1 - [QSOX1_HUMAN]	66,8
P50991-2	Isoform 2 of T-complex protein 1 subunit delta OS=Homo sapiens GN=CCT4 - [TCPD_HUMAN]	54,7
P40227-2	Isoform 2 of T-complex protein 1 subunit zeta OS=Homo sapiens GN=CCT6A - [TCPZ_HUMAN]	53,3
P10599-2	Isoform 2 of Thioredoxin OS=Homo sapiens GN=TXN - [THIO_HUMAN]	9,4
P60174-1	Isoform 2 of Triosephosphate isomerase OS=Homo sapiens GN=TPI1 - [TPIS_HUMAN]	26,7
P22314-2	Isoform 2 of Ubiquitin-like modifier-activating enzyme 1 OS=Homo sapiens GN=UBA1 - [UBA1_HUMAN]	113,7
Q02487-2	Isoform 2B of Desmocollin-2 OS=Homo sapiens GN=DSC2 - [DSC2_HUMAN]	93,7
P10909-3	Isoform 3 of Clusterin OS=Homo sapiens GN=CLU - [CLUS_HUMAN]	32,3
Q96CG8-3	Isoform 3 of Collagen triple helix repeat-containing protein 1 OS=Homo sapiens GN=CTHRC1 - [CTHR1_HUMAN]	24,8
Q15063-3	Isoform 3 of Periostin OS=Homo sapiens GN=POSTN - [POSTN_HUMAN]	87,2
P55058-3	Isoform 3 of Phospholipid transfer protein OS=Homo sapiens GN=PLTP - [PLTP_HUMAN]	44,1
P13797-3	Isoform 3 of Plastin-3 OS=Homo sapiens GN=PLS3 - [PLST_HUMAN]	65,6
Q15084-3	Isoform 3 of Protein disulfide-isomerase A6 OS=Homo sapiens GN=PDIA6 - [PDIA6_HUMAN]	47,8
Q14574-2	Isoform 3B of Desmocollin-3 OS=Homo sapiens GN=DSC3 - [DSC3_HUMAN]	93,4
Q9NY33-4	Isoform 4 of Dipeptidyl peptidase 3 OS=Homo sapiens GN=DPP3 - [DPP3_HUMAN]	79,3
Q15063-4	Isoform 4 of Periostin OS=Homo sapiens GN=POSTN - [POSTN_HUMAN]	83,8
O43852-5	Isoform 5 of Calumenin OS=Homo sapiens GN=CALU - [CALU_HUMAN]	26,9

O60506-5	Isoform 5 of Heterogeneous nuclear ribonucleoprotein Q OS=Homo sapiens GN=SYNCRIP - [HNRPQ_HUMAN]	46,3
O00468-6	Isoform 6 of Agrin OS=Homo sapiens GN=AGRN - [AGRIN_HUMAN]	214,7
P02751-6	Isoform 6 of Fibronectin OS=Homo sapiens GN=FN1 - [FINC_HUMAN]	240,4
P04899-6	Isoform 6 of Guanine nucleotide-binding protein G(i) subunit alpha-2 OS=Homo sapiens GN=GNAI2 - [GNAI2_HUMAN]	34,9
P09651-2;P09867	Isoform A1-A of Heterogeneous nuclear ribonucleoprotein A1 OS=Homo sapiens GN=HNRNPA1 - [ROA1_HUMAN]	34,2
P22626-2;Q2HJ60	Isoform A2 of Heterogeneous nuclear ribonucleoproteins A2/B1 OS=Homo sapiens GN=HNRNPA2B1 - [ROA2_HUMAN]	36,0
P13497-4	Isoform BMP1-5 of Bone morphogenetic protein 1 OS=Homo sapiens GN=BMP1 - [BMP1_HUMAN]	70,4
P23142-4	Isoform C of Fibulin-1 OS=Homo sapiens GN=FBLN1 - [FBLN1_HUMAN]	74,4
P07954-2	Isoform Cytoplasmic of Fumarate hydratase, mitochondrial OS=Homo sapiens GN=FH - [FUMH_HUMAN]	50,2
P31946-2	Isoform Short of 14-3-3 protein beta/alpha OS=Homo sapiens GN=YWHAB - [1433B_HUMAN]	27,8
P15291-2	Isoform Short of Beta-1,4-galactosyltransferase 1 OS=Homo sapiens GN=B4GALT1 - [B4GT1_HUMAN]	42,5
Q13753-2	Isoform Short of Laminin subunit gamma-2 OS=Homo sapiens GN=LAMC2 - [LAMC2_HUMAN]	121,5
P13611-4	Isoform V3 of Versican core protein OS=Homo sapiens GN=VCAN - [CSPG2_HUMAN]	74,2
M0R132	Kallikrein-10 (Fragment) OS=Homo sapiens GN=KLK10 PE=1 SV=1 - [M0R132_HUMAN]	15,7
Q9Y337	Kallikrein-5 OS=Homo sapiens GN=KLK5 PE=1 SV=2 - [KLK5_HUMAN]	32,0
Q92876	Kallikrein-6 OS=Homo sapiens GN=KLK6 PE=1 SV=1 - [KLK6_HUMAN]	26,8
P49862	Kallikrein-7 OS=Homo sapiens GN=KLK7 PE=1 SV=1 - [KLK7_HUMAN]	27,5
P13645	Keratin, type I cytoskeletal 10 OS=Homo sapiens GN=KRT10 PE=1 SV=6 - [K1C10_HUMAN]	58,8
K7ERE3	Keratin, type I cytoskeletal 13 OS=Homo sapiens GN=KRT13 PE=1 SV=1 - [K7ERE3_HUMAN]	45,2
P02533	Keratin, type I cytoskeletal 14 OS=Homo sapiens GN=KRT14 PE=1 SV=4 - [K1C14_HUMAN]	51,5
P08779	Keratin, type I cytoskeletal 16 OS=Homo sapiens GN=KRT16 PE=1 SV=4 - [K1C16_HUMAN]	51,2
Q04695	Keratin, type I cytoskeletal 17 OS=Homo sapiens GN=KRT17 PE=1 SV=2 - [K1C17_HUMAN]	48,1
F8VZY9	Keratin, type I cytoskeletal 18 OS=Homo sapiens GN=KRT18 PE=1 SV=1 - [F8VZY9_HUMAN]	43,7
P08727	Keratin, type I cytoskeletal 19 OS=Homo sapiens GN=KRT19 PE=1 SV=4 - [K1C19_HUMAN]	44,1
P35527	Keratin, type I cytoskeletal 9 OS=Homo sapiens GN=KRT9 PE=1 SV=3 - [K1C9_HUMAN]	62,0
P04264	Keratin, type II cytoskeletal 1 OS=Homo sapiens GN=KRT1 PE=1 SV=6 - [K2C1_HUMAN]	66,0
P35908	Keratin, type II cytoskeletal 2 epidermal OS=Homo sapiens GN=KRT2 PE=1 SV=2 - [K22E_HUMAN]	65,4
P13647	Keratin, type II cytoskeletal 5 OS=Homo sapiens GN=KRT5 PE=1 SV=3 - [K2C5_HUMAN]	62,3
P02538	Keratin, type II cytoskeletal 6A OS=Homo sapiens GN=KRT6A PE=1 SV=3 - [K2C6A_HUMAN]	60,0
P08729	Keratin, type II cytoskeletal 7 OS=Homo sapiens GN=KRT7 PE=1 SV=5 - [K2C7_HUMAN]	51,4
Q7RTS7	Keratin, type II cytoskeletal 74 OS=Homo sapiens GN=KRT74 PE=1 SV=2 - [K2C74_HUMAN]	57,8
P05787	Keratin, type II cytoskeletal 8 OS=Homo sapiens GN=KRT8 PE=1 SV=7 - [K2C8_HUMAN]	53,7
F1MNV5	Kininogen-1 OS=Bos taurus GN=KNG1 PE=1 SV=2 - [F1MNV5_BOVIN]	48,4
H3BVD9	Kunitz-type protease inhibitor 1 (Fragment) OS=Homo sapiens GN=SPINT1 PE=1 SV=1 - [H3BVD9_HUMAN]	52,3
Q13751	Laminin subunit beta-3 OS=Homo sapiens GN=LAMB3 PE=1 SV=1 - [LAMB3_HUMAN]	129,5
Q2KIF2	Leucine-rich alpha-2-glycoprotein 1 OS=Bos taurus GN=LRG1 PE=2 SV=1 - [Q2KIF2_BOVIN]	38,3
P15018	Leukemia inhibitory factor OS=Homo sapiens GN=LIF PE=1 SV=1 - [LIF_HUMAN]	22,0
P30740	Leukocyte elastase inhibitor OS=Homo sapiens GN=SERPINB1 PE=1 SV=1 - [ILEU_HUMAN]	42,7
P00338	L-lactate dehydrogenase A chain OS=Homo sapiens GN=LDHA PE=1 SV=2 - [LDHA_HUMAN]	36,7
Q5E9B1	L-lactate dehydrogenase B chain OS=Bos taurus GN=LDHB PE=2 SV=4 - [LDHB_BOVIN]	36,7
P07195	L-lactate dehydrogenase B chain OS=Homo sapiens GN=LDHB PE=1 SV=2 - [LDHB_HUMAN]	36,6
Q05443	Lumican OS=Bos taurus GN=LUM PE=1 SV=1 - [LUM_BOVIN]	38,7
P51884	Lumican OS=Homo sapiens GN=LUM PE=1 SV=2 - [LUM_HUMAN]	38,4
P10253	Lysosomal alpha-glucosidase OS=Homo sapiens GN=GAA PE=1 SV=4 - [LYAG_HUMAN]	105,3
Q9Y4K0	Lysyl oxidase homolog 2 OS=Homo sapiens GN=LOXL2 PE=1 SV=1 - [LOXL2_HUMAN]	86,7
P40925	Malate dehydrogenase, cytoplasmic OS=Homo sapiens GN=MDH1 PE=1 SV=4 - [MDHC_HUMAN]	36,4

P40926	Malate dehydrogenase, mitochondrial OS=Homo sapiens GN=MDH2 PE=1 SV=3 - [MDHM_HUMAN]	35,5
P09237	Matrilysin OS=Homo sapiens GN=MMP7 PE=1 SV=1 - [MMP7_HUMAN]	29,7
Q5H9A7	Metalloproteinase inhibitor 1 OS=Homo sapiens GN=TIMP1 PE=1 SV=1 - [Q5H9A7_HUMAN]	16,0
F1N430	Metalloproteinase inhibitor 2 OS=Bos taurus GN=TIMP2 PE=4 SV=1 - [F1N430_BOVIN]	24,4
P26038	Moesin OS=Homo sapiens GN=MSN PE=1 SV=3 - [MOES_HUMAN]	67,8
P60660;P60661	Myosin light polypeptide 6 OS=Homo sapiens GN=MYL6 PE=1 SV=2 - [MYL6_HUMAN]	16,9
F5H6X6	Neutral alpha-glucosidase AB OS=Homo sapiens GN=GANAB PE=1 SV=1 - [F5H6X6_HUMAN]	96,2
P80188	Neutrophil gelatinase-associated lipocalin OS=Homo sapiens GN=LCN2 PE=1 SV=2 - [NGAL_HUMAN]	22,6
Q02818	Nucleobindin-1 OS=Homo sapiens GN=NUCB1 PE=1 SV=4 - [NUCB1_HUMAN]	53,8
P19338	Nucleolin OS=Homo sapiens GN=NCL PE=1 SV=3 - [NUCL_HUMAN]	76,6
P15531	Nucleoside diphosphate kinase A OS=Homo sapiens GN=NME1 PE=1 SV=1 - [NDKA_HUMAN]	17,1
Q0VCP3	Olfactomedin-like protein 3 OS=Bos taurus GN=OLFML3 PE=2 SV=1 - [OLFL3_BOVIN]	45,9
Q58CQ9	Pantetheinase OS=Bos taurus GN=VNN1 PE=1 SV=1 - [VNN1_BOVIN]	56,9
P26022	Pentraxin-related protein PTX3 OS=Homo sapiens GN=PTX3 PE=1 SV=3 - [PTX3_HUMAN]	41,9
P62937	Peptidyl-prolyl cis-trans isomerase A OS=Homo sapiens GN=PPIA PE=1 SV=2 - [PPIA_HUMAN]	18,0
P23284	Peptidyl-prolyl cis-trans isomerase B OS=Homo sapiens GN=PPIB PE=1 SV=2 - [PPIB_HUMAN]	23,7
Q92626	Peroxidasin homolog OS=Homo sapiens GN=PXDN PE=1 SV=2 - [PXDN_HUMAN]	165,2
A0A0A0MSI0	Peroxiredoxin-1 (Fragment) OS=Homo sapiens GN=PRDX1 PE=1 SV=1 - [A0A0A0MSI0_HUMAN]	19,0
Q5E947	Peroxiredoxin-1 OS=Bos taurus GN=PRDX1 PE=2 SV=1 - [PRDX1_BOVIN]	22,2
P32119	Peroxiredoxin-2 OS=Homo sapiens GN=PRDX2 PE=1 SV=5 - [PRDX2_HUMAN]	21,9
O77834	Peroxiredoxin-6 OS=Bos taurus GN=PRDX6 PE=1 SV=3 - [PRDX6_BOVIN]	25,1
P30041	Peroxiredoxin-6 OS=Homo sapiens GN=PRDX6 PE=1 SV=3 - [PRDX6_HUMAN]	25,0
P13696	Phosphatidylethanolamine-binding protein 1 OS=Bos taurus GN=PEBP1 PE=1 SV=2 - [PEBP1_BOVIN]	21,0
P30086	Phosphatidylethanolamine-binding protein 1 OS=Homo sapiens GN=PEBP1 PE=1 SV=3 - [PEBP1_HUMAN]	21,0
P18669	Phosphoglycerate mutase 1 OS=Homo sapiens GN=PGAM1 PE=1 SV=2 - [PGAM1_HUMAN]	28,8
Q95121	Pigment epithelium-derived factor OS=Bos taurus GN=SERPINF1 PE=1 SV=1 - [PEDF_BOVIN]	46,2
P36955	Pigment epithelium-derived factor OS=Homo sapiens GN=SERPINF1 PE=1 SV=4 - [PEDF_HUMAN]	46,3
Q9N2I2	Plasma serine protease inhibitor OS=Bos taurus GN=SERPINA5 PE=1 SV=1 - [IPSP_BOVIN]	45,3
P13909	Plasminogen activator inhibitor 1 OS=Bos taurus GN=SERPINE1 PE=1 SV=1 - [PAI1_BOVIN]	45,3
P05121	Plasminogen activator inhibitor 1 OS=Homo sapiens GN=SERPINE1 PE=1 SV=1 - [PAI1_HUMAN]	45,0
E1B726	Plasminogen OS=Bos taurus GN=PLG PE=3 SV=2 - [E1B726_BOVIN]	91,2
A7E3Q8	Plastin-3 OS=Bos taurus GN=PLS3 PE=2 SV=1 - [PLST_BOVIN]	70,8
Q15365;Q5E9A3	Poly(rC)-binding protein 1 OS=Homo sapiens GN=PCBP1 PE=1 SV=2 - [PCBP1_HUMAN]	37,5
F8W0G4	Poly(rC)-binding protein 2 (Fragment) OS=Homo sapiens GN=PCBP2 PE=1 SV=1 - [F8W0G4_HUMAN]	16,6
Q6S8J3	POTE ankyrin domain family member E OS=Homo sapiens GN=POTEE PE=1 SV=3 - [POTEE_HUMAN]	121,3
A0A087X0D5	Pro-cathepsin H OS=Homo sapiens GN=CTSH PE=1 SV=1 - [A0A087X0D5_HUMAN]	36,2
Q15113	Procollagen C-endopeptidase enhancer 1 OS=Homo sapiens GN=PCOLCE PE=1 SV=2 - [PCOC1_HUMAN]	47,9
Q2HJB6	Procollagen C-endopeptidase enhancer OS=Bos taurus GN=PCOLCE PE=2 SV=1 - [Q2HJB6_BOVIN]	48,2
Q02809	Procollagen-lysine,2-oxoglutarate 5-dioxygenase 1 OS=Homo sapiens GN=PLOD1 PE=1 SV=2 - [PLOD1_HUMAN]	83,5
E7ETU9	Procollagen-lysine,2-oxoglutarate 5-dioxygenase 2 OS=Homo sapiens GN=PLOD2 PE=1 SV=1 - [E7ETU9_HUMAN]	81,1
E1BHJ0	Profilin OS=Bos taurus PE=3 SV=1 - [E1BHJ0_BOVIN]	15,0
P07737	Profilin-1 OS=Homo sapiens GN=PFN1 PE=1 SV=2 - [PROF1_HUMAN]	15,0
P35232;Q3T165	Prohibitin OS=Homo sapiens GN=PHB PE=1 SV=1 - [PHB_HUMAN]	29,8
F5GY37	Prohibitin-2 OS=Homo sapiens GN=PHB2 PE=1 SV=1 - [F5GY37_HUMAN]	29,7
P12273	Prolactin-inducible protein OS=Homo sapiens GN=PIP PE=1 SV=1 - [PIP_HUMAN]	16,6

Q3ZBH5	Proliferation-associated 2G4, 38kDa OS=Bos taurus GN=PA2G4 PE=1 SV=1 - [Q3ZBH5_BOVIN]	43,8
P07602	Prosaposin OS=Homo sapiens GN=PSAP PE=1 SV=2 - [SAP_HUMAN]	58,1
F5GX11	Proteasome subunit alpha type-1 OS=Homo sapiens GN=PSMA1 PE=1 SV=1 - [F5GX11_HUMAN]	26,5
P25789;Q3ZCK9	Proteasome subunit alpha type-4 OS=Homo sapiens GN=PSMA4 PE=1 SV=1 - [PSA4_HUMAN]	29,5
P28066;Q5E987	Proteasome subunit alpha type-5 OS=Homo sapiens GN=PSMA5 PE=1 SV=3 - [PSA5_HUMAN]	26,4
P60900;Q2YDE4	Proteasome subunit alpha type-6 OS=Homo sapiens GN=PSMA6 PE=1 SV=1 - [PSA6_HUMAN]	27,4
Q3ZBG0	Proteasome subunit alpha type-7 OS=Bos taurus GN=PSMA7 PE=1 SV=1 - [PSA7_BOVIN]	27,9
P49721	Proteasome subunit beta type-2 OS=Homo sapiens GN=PSMB2 PE=1 SV=1 - [PSB2_HUMAN]	22,8
P28074	Proteasome subunit beta type-5 OS=Homo sapiens GN=PSMB5 PE=1 SV=3 - [PSB5_HUMAN]	28,5
F1MMK9	Protein AMBP OS=Bos taurus GN=AMBP PE=4 SV=2 - [F1MMK9_BOVIN]	39,3
Q5E946	Protein deglycase DJ-1 OS=Bos taurus GN=PARK7 PE=2 SV=1 - [PARK7_BOVIN]	20,0
K7ELW0	Protein deglycase DJ-1 OS=Homo sapiens GN=PARK7 PE=1 SV=1 - [K7ELW0_HUMAN]	17,9
H7BZJ3	Protein disulfide-isomerase A3 (Fragment) OS=Homo sapiens GN=PDIA3 PE=1 SV=1 - [H7BZJ3_HUMAN]	13,5
P30101	Protein disulfide-isomerase A3 OS=Homo sapiens GN=PDIA3 PE=1 SV=4 - [PDIA3_HUMAN]	56,7
P13667	Protein disulfide-isomerase A4 OS=Homo sapiens GN=PDIA4 PE=1 SV=2 - [PDIA4_HUMAN]	72,9
H7BZ94	Protein disulfide-isomerase OS=Homo sapiens GN=P4HB PE=1 SV=2 - [H7BZ94_HUMAN]	52,5
Q92520	Protein FAM3C OS=Homo sapiens GN=FAM3C PE=1 SV=1 - [FAM3C_HUMAN]	24,7
E9PIT3	Prothrombin OS=Homo sapiens GN=F2 PE=1 SV=1 - [E9PIT3_HUMAN]	65,4
E9PLK3	Puromycin-sensitive aminopeptidase OS=Homo sapiens GN=NPEPPS PE=1 SV=1 - [E9PLK3_HUMAN]	102,9
B4DNK4	Pyruvate kinase PKM OS=Homo sapiens GN=PKM PE=1 SV=1 - [B4DNK4_HUMAN]	49,9
P50395	Rab GDP dissociation inhibitor beta OS=Homo sapiens GN=GDI2 PE=1 SV=2 - [GDIB_HUMAN]	50,6
F1MJJ8	Radixin (Fragment) OS=Bos taurus GN=RDX PE=4 SV=1 - [F1MJJ8_BOVIN]	68,5
P11233	Ras-related protein Ral-A OS=Homo sapiens GN=RALA PE=1 SV=1 - [RALA_HUMAN]	23,6
P61224;P61223	Ras-related protein Rap-1b OS=Homo sapiens GN=RAP1B PE=1 SV=1 - [RAP1B_HUMAN]	20,8
H0Y750	Renin receptor (Fragment) OS=Homo sapiens GN=ATP6AP2 PE=4 SV=1 - [H0Y750_HUMAN]	26,6
Q99969	Retinoic acid receptor responder protein 2 OS=Homo sapiens GN=RARRES2 PE=1 SV=1 - [RARR2_HUMAN]	18,6
P13489	Ribonuclease inhibitor OS=Homo sapiens GN=RNH1 PE=1 SV=2 - [RINI_HUMAN]	49,9
D6REQ6	Ribonuclease T2 OS=Homo sapiens GN=RNASET2 PE=1 SV=1 - [D6REQ6_HUMAN]	25,3
Q92743	Serine protease HTRA1 OS=Homo sapiens GN=HTRA1 PE=1 SV=1 - [HTRA1_HUMAN]	51,3
B3KQV6	Serine/threonine-protein phosphatase 2A 65 kDa regulatory subunit A alpha isoform OS=Homo sapiens GN=PPP2R1A PE=1 SV=1 - [B3KQV6_HUMAN]	45,6
G3X6N3	Serotransferrin OS=Bos taurus GN=TF PE=1 SV=1 - [G3X6N3_BOVIN]	77,6
P02787	Serotransferrin OS=Homo sapiens GN=TF PE=1 SV=3 - [TRFE_HUMAN]	77,0
A2I7M9	Serpin A3-2 OS=Bos taurus GN=SERPINA3-2 PE=3 SV=1 - [SPA32_BOVIN]	46,2
A2I7N1	Serpin A3-5 OS=Bos taurus GN=SERPINA3-5 PE=3 SV=1 - [SPA35_BOVIN]	46,4
A0A0A0MP92	Serpin A3-7 OS=Bos taurus GN=SERPINA3-7 PE=1 SV=1 - [A0A0A0MP92_BOVIN]	47,0
P35237	Serpin B6 OS=Homo sapiens GN=SERPINB6 PE=1 SV=3 - [SPB6_HUMAN]	42,6
P50454	Serpin H1 OS=Homo sapiens GN=SERPINH1 PE=1 SV=2 - [SERPH_HUMAN]	46,4
Q3SYR0	Serpin peptidase inhibitor, clade A (Alpha-1 antiproteinase, antitrypsin), member 7 OS=Bos taurus GN=SERPINA7 PE=2 SV=1 - [Q3SYR0_BOVIN]	46,0
A6QPP2	SERPIND1 protein OS=Bos taurus GN=SERPIND1 PE=2 SV=1 - [A6QPP2_BOVIN]	55,2
P02769	Serum albumin OS=Bos taurus GN=ALB PE=1 SV=4 - [ALBU_BOVIN]	69,2
P02768	Serum albumin OS=Homo sapiens GN=ALB PE=1 SV=2 - [ALBU_HUMAN]	69,3
A5PKC2	SHBG protein OS=Bos taurus GN=SHBG PE=2 SV=1 - [A5PKC2_BOVIN]	43,3
P01246	Somatotropin OS=Bos taurus GN=GH1 PE=1 SV=1 - [SOMA_BOVIN]	24,5
P09486	SPARC OS=Homo sapiens GN=SPARC PE=1 SV=1 - [SPRC_HUMAN]	34,6
H0YB13	Stanniocalcin-2 (Fragment) OS=Homo sapiens GN=STC2 PE=1 SV=1 - [H0YB13_HUMAN]	13,9
Q3ZCH0	Stress-70 protein, mitochondrial OS=Bos taurus GN=HSPA9 PE=2 SV=1 - [GRP75_BOVIN]	73,7
Q9Y490	Talin-1 OS=Homo sapiens GN=TLN1 PE=1 SV=3 - [TLN1_HUMAN]	269,6
B4DUR8	T-complex protein 1 subunit gamma OS=Homo sapiens GN=CCT3 PE=1 SV=1 - [B4DUR8_HUMAN]	55,6

Q2KIS7	Tetranectin OS=Bos taurus GN=CLEC3B PE=2 SV=1 - [TETN_BOVIN]	22,1
E9PIR7	Thioredoxin reductase 1, cytoplasmic OS=Homo sapiens GN=TXNRD1 PE=1 SV=1 - [E9PIR7_HUMAN]	53,1
P26639	Threonine--tRNA ligase, cytoplasmic OS=Homo sapiens GN=TARS PE=1 SV=3 - [SYTC_HUMAN]	83,4
P07996	Thrombospondin-1 OS=Homo sapiens GN=THBS1 PE=1 SV=2 - [TSP1_HUMAN]	129,3
P37837	Transaldolase OS=Homo sapiens GN=TALDO1 PE=1 SV=2 - [TALDO_HUMAN]	37,5
P21214	Transforming growth factor beta-2 OS=Bos taurus GN=TGFB2 PE=1 SV=3 - [TGFB2_BOVIN]	47,7
Q15582	Transforming growth factor-beta-induced protein ig-h3 OS=Homo sapiens GN=TGFBI PE=1 SV=1 - [BGH3_HUMAN]	74,6
P61586;P61585	Transforming protein RhoA OS=Homo sapiens GN=RHOA PE=1 SV=1 - [RHOA_HUMAN]	21,8
Q9TS87	Transgelin OS=Bos taurus GN=TAGLN PE=1 SV=4 - [TAGL_BOVIN]	22,6
X6RJP6	Transgelin-2 (Fragment) OS=Homo sapiens GN=TAGLN2 PE=1 SV=1 - [X6RJP6_HUMAN]	21,1
P55072	Transitional endoplasmic reticulum ATPase OS=Homo sapiens GN=VCP PE=1 SV=4 - [TERA_HUMAN]	89,3
P29401	Transketolase OS=Homo sapiens GN=TKT PE=1 SV=3 - [TKT_HUMAN]	67,8
Q5E956	Triosephosphate isomerase OS=Bos taurus GN=TPI1 PE=2 SV=3 - [TPIS_BOVIN]	26,7
Q71U36;F2Z4C1	Tubulin alpha-1A chain OS=Homo sapiens GN=TUBA1A PE=1 SV=1 - [TBA1A_HUMAN]	50,1
P68366;P81948	Tubulin alpha-4A chain OS=Homo sapiens GN=TUBA4A PE=1 SV=1 - [TBA4A_HUMAN]	49,9
P07437;Q2KJD0	Tubulin beta chain OS=Homo sapiens GN=TUBB PE=1 SV=2 - [TBB5_HUMAN]	49,6
Q13885;E1BJB1	Tubulin beta-2A chain OS=Homo sapiens GN=TUBB2A PE=1 SV=1 - [TBB2A_HUMAN]	49,9
P68371;Q3MHM5	Tubulin beta-4B chain OS=Homo sapiens GN=TUBB4B PE=1 SV=1 - [TBB4B_HUMAN]	49,8
Q9BUF5	Tubulin beta-6 chain OS=Homo sapiens GN=TUBB6 PE=1 SV=1 - [TBB6_HUMAN]	49,8
P62987;P63048	Ubiquitin-60S ribosomal protein L40 OS=Homo sapiens GN=UBA52 PE=1 SV=2 - [RL40_HUMAN]	14,7
G5E5T5	Uncharacterized protein (Fragment) OS=Bos taurus GN=IGHM PE=1 SV=1 - [G5E5T5_BOVIN]	42,4
F1MVK1	Uncharacterized protein (Fragment) OS=Bos taurus PE=4 SV=2 - [F1MVK1_BOVIN]	173,9
G3MYZ3	Uncharacterized protein OS=Bos taurus GN=AFM PE=4 SV=1 - [G3MYZ3_BOVIN]	69,5
E1BH06	Uncharacterized protein OS=Bos taurus GN=C4A PE=1 SV=2 - [E1BH06_BOVIN]	192,6
F1N4M7	Uncharacterized protein OS=Bos taurus GN=CFI PE=1 SV=2 - [F1N4M7_BOVIN]	68,9
F1MWU9	Uncharacterized protein OS=Bos taurus GN=HSPA6 PE=3 SV=2 - [F1MWU9_BOVIN]	70,9
F1MLW7	Uncharacterized protein OS=Bos taurus GN=IGLL1 PE=1 SV=2 - [F1MLW7_BOVIN]	24,4
E1BFV0	Uncharacterized protein OS=Bos taurus GN=KPNB1 PE=1 SV=2 - [E1BFV0_BOVIN]	97,2
F1MYG5	Uncharacterized protein OS=Bos taurus GN=LMNA PE=1 SV=1 - [F1MYG5_BOVIN]	74,1
G3N0S9	Uncharacterized protein OS=Bos taurus GN=LOC515150 PE=4 SV=1 - [G3N0S9_BOVIN]	22,3
E1BI82	Uncharacterized protein OS=Bos taurus GN=LOC525947 PE=4 SV=2 - [E1BI82_BOVIN]	69,1
A0A0A0MPA0	Uncharacterized protein OS=Bos taurus GN=LOC784932 PE=3 SV=1 - [A0A0A0MPA0_BOVIN]	46,9
E1BG25	Uncharacterized protein OS=Bos taurus GN=MFI2 PE=3 SV=1 - [E1BG25_BOVIN]	80,6
E1BMJ0	Uncharacterized protein OS=Bos taurus GN=SERPING1 PE=3 SV=2 - [E1BMJ0_BOVIN]	51,7
Q3ZBS7	Uncharacterized protein OS=Bos taurus GN=VTN PE=2 SV=1 - [Q3ZBS7_BOVIN]	53,5
F1MLW8	Uncharacterized protein OS=Bos taurus PE=4 SV=2 - [F1MLW8_BOVIN]	24,6
E7ET40	Urokinase-type plasminogen activator OS=Homo sapiens GN=PLAU PE=1 SV=1 - [E7ET40_HUMAN]	46,9
D6RIU4	Vesicular integral-membrane protein VIP36 (Fragment) OS=Homo sapiens GN=LMAN2 PE=1 SV=4 - [D6RIU4_HUMAN]	21,8
B0YJC4	Vimentin OS=Homo sapiens GN=VIM PE=1 SV=1 - [B0YJC4_HUMAN]	49,6
F1N5M2	Vitamin D-binding protein OS=Bos taurus GN=GC PE=1 SV=2 - [F1N5M2_BOVIN]	53,3
Q3MHN5	Vitamin D-binding protein OS=Bos taurus GN=GC PE=2 SV=1 - [VTDB_BOVIN]	53,3
P21796	Voltage-dependent anion-selective channel protein 1 OS=Homo sapiens GN=VDAC1 PE=1 SV=2 - [VDAC1_HUMAN]	30,8
Q15904	V-type proton ATPase subunit S1 OS=Homo sapiens GN=ATP6AP1 PE=1 SV=2 - [VAS1_HUMAN]	52,0
O75083	WD repeat-containing protein 1 OS=Homo sapiens GN=WDR1 PE=1 SV=4 - [WDR1_HUMAN]	66,2

B. LNCaP

Accession	Description	MW [kDa]
P62258;P62261	14-3-3 protein epsilon OS=Homo sapiens GN=YWHAE PE=1 SV=1 - [1433E_HUMAN]	29,2
P27348;Q3SZI4	14-3-3 protein theta OS=Homo sapiens GN=YWHAQ PE=1 SV=1 - [1433T_HUMAN]	27,7
P63104;P63103	14-3-3 protein zeta/delta OS=Homo sapiens GN=YWHAZ PE=1 SV=1 - [1433Z_HUMAN]	27,7
P62701;P79103	40S ribosomal protein S4, X isoform OS=Homo sapiens GN=RPS4X PE=1 SV=2 - [RS4X_HUMAN]	29,6
C9J9K3	40S ribosomal protein SA (Fragment) OS=Homo sapiens GN=RPSA PE=1 SV=4 - [C9J9K3_HUMAN]	29,4
P10809	60 kDa heat shock protein, mitochondrial OS=Homo sapiens GN=HSPD1 PE=1 SV=2 - [CH60_HUMAN]	61,0
P11021	78 kDa glucose-regulated protein OS=Homo sapiens GN=HSPA5 PE=1 SV=2 - [GRP78_HUMAN]	72,3
Q9UHI8	A disintegrin and metalloproteinase with thrombospondin motifs 1 OS=Homo sapiens GN=ADAMTS1 PE=1 SV=4 - [ATS1_HUMAN]	105,3
P68032;Q3ZC07	Actin, alpha cardiac muscle 1 OS=Homo sapiens GN=ACTC1 PE=1 SV=1 - [ACTC_HUMAN]	42,0
P60709;P60712	Actin, cytoplasmic 1 OS=Homo sapiens GN=ACTB PE=1 SV=1 - [ACTB_HUMAN]	41,7
C9JLK2	Acylamino-acid-releasing enzyme (Fragment) OS=Homo sapiens GN=APEH PE=1 SV=1 - [C9JLK2_HUMAN]	26,0
P23526	Adenosylhomocysteinase OS=Homo sapiens GN=AHCY PE=1 SV=4 - [SAHH_HUMAN]	47,7
P14550	Alcohol dehydrogenase [NADP(+)] OS=Homo sapiens GN=AKR1A1 PE=1 SV=3 - [AK1A1_HUMAN]	36,5
P01023	Alpha-2-macroglobulin OS=Homo sapiens GN=A2M PE=1 SV=3 - [A2MG_HUMAN]	163,2
P06733	Alpha-enolase OS=Homo sapiens GN=ENO1 PE=1 SV=2 - [ENOA_HUMAN]	47,1
P02771	Alpha-fetoprotein OS=Homo sapiens GN=AFP PE=1 SV=1 - [FETA_HUMAN]	68,6
P00505	Aspartate aminotransferase, mitochondrial OS=Homo sapiens GN=GOT2 PE=1 SV=3 - [AATM_HUMAN]	47,5
H3BVI7	Cadherin-1 OS=Homo sapiens GN=CDH1 PE=1 SV=1 - [H3BVI7_HUMAN]	45,5
P04040	Catalase OS=Homo sapiens GN=CAT PE=1 SV=3 - [CATA_HUMAN]	59,7
O00299	Chloride intracellular channel protein 1 OS=Homo sapiens GN=CLIC1 PE=1 SV=4 - [CLIC1_HUMAN]	26,9
G3V1A4	Cofilin 1 (Non-muscle), isoform CRA_a OS=Homo sapiens GN=CFL1 PE=1 SV=1 - [G3V1A4_HUMAN]	16,8
A0A087X0S5	Collagen alpha-1(VI) chain OS=Homo sapiens GN=COL6A1 PE=1 SV=1 - [A0A087X0S5_HUMAN]	108,3
F5GXS0	Complement C4-B OS=Homo sapiens GN=C4B PE=1 SV=1 - [F5GXS0_HUMAN]	187,6
P12277	Creatine kinase B-type OS=Homo sapiens GN=CKB PE=1 SV=1 - [KCRB_HUMAN]	42,6
P01034	Cystatin-C OS=Homo sapiens GN=CST3 PE=1 SV=1 - [CYTC_HUMAN]	15,8
E9PND2	Cysteine and glycine-rich protein 1 (Fragment) OS=Homo sapiens GN=CSRP1 PE=1 SV=1 - [E9PND2_HUMAN]	16,1
Q96KP4	Cytosolic non-specific dipeptidase OS=Homo sapiens GN=CNDP2 PE=1 SV=2 - [CNDP2_HUMAN]	52,8
P30046	D-dopachrome decarboxylase OS=Homo sapiens GN=DDT PE=1 SV=3 - [DOPD_HUMAN]	12,7
Q14126	Desmoglein-2 OS=Homo sapiens GN=DSG2 PE=1 SV=2 - [DSG2_HUMAN]	122,2
G3V3M6	DNA-(apurinic or apyrimidinic site) lyase (Fragment) OS=Homo sapiens GN=APEX1 PE=1 SV=1 - [G3V3M6_HUMAN]	29,2
P68104;P68103	Elongation factor 1-alpha 1 OS=Homo sapiens GN=EEF1A1 PE=1 SV=1 - [EF1A1_HUMAN]	50,1
P26641	Elongation factor 1-gamma OS=Homo sapiens GN=EEF1G PE=1 SV=3 - [EF1G_HUMAN]	50,1
P14625	Endoplasmin OS=Homo sapiens GN=HSP90B1 PE=1 SV=1 - [ENPL_HUMAN]	92,4
P60842;Q3SZ54	Eukaryotic initiation factor 4A-I OS=Homo sapiens GN=EIF4A1 PE=1 SV=1 - [IF4A1_HUMAN]	46,1
P04075	Fructose-bisphosphate aldolase A OS=Homo sapiens GN=ALDOA PE=1 SV=2 - [ALDOA_HUMAN]	39,4
K7EQ48	Glucose-6-phosphate isomerase OS=Homo sapiens GN=GPI PE=1 SV=2 - [K7EQ48_HUMAN]	53,4
P04406	Glyceraldehyde-3-phosphate dehydrogenase OS=Homo sapiens GN=GAPDH PE=1 SV=3 - [G3P_HUMAN]	36,0
P04792	Heat shock protein beta-1 OS=Homo sapiens GN=HSPB1 PE=1 SV=2 - [HSPB1_HUMAN]	22,8
P07900	Heat shock protein HSP 90-alpha OS=Homo sapiens GN=HSP90AA1 PE=1 SV=5 - [HS90A_HUMAN]	84,6
Q9Y5Z4	Heme-binding protein 2 OS=Homo sapiens GN=HEBP2 PE=1 SV=1 - [HEBP2_HUMAN]	22,9

D6R9P3	Heterogeneous nuclear ribonucleoprotein A/B OS=Homo sapiens GN=HNRNPAB PE=1 SV=1 - [D6R9P3_HUMAN]	30,3
D6RF44	Heterogeneous nuclear ribonucleoprotein D0 (Fragment) OS=Homo sapiens GN=HNRNPD PE=1 SV=4 - [D6RF44_HUMAN]	12,5
G3V5X6	Heterogeneous nuclear ribonucleoproteins C1/C2 (Fragment) OS=Homo sapiens GN=HNRNPC PE=1 SV=1 - [G3V5X6_HUMAN]	12,8
P16401	Histone H1.5 OS=Homo sapiens GN=HIST1H1B PE=1 SV=3 - [H15_HUMAN]	22,6
Q16777;A1A4R1	Histone H2A type 2-C OS=Homo sapiens GN=HIST2H2AC PE=1 SV=4 - [H2A2C_HUMAN]	14,0
O60814;F2Z4F9	Histone H2B type 1-K OS=Homo sapiens GN=HIST1H2BK PE=1 SV=3 - [H2B1K_HUMAN]	13,9
P62805;P62803	Histone H4 OS=Homo sapiens GN=HIST1H4A PE=1 SV=2 - [H4_HUMAN]	11,4
H0Y9D8	Inorganic pyrophosphatase 2, mitochondrial (Fragment) OS=Homo sapiens GN=PPA2 PE=1 SV=1 - [H0Y9D8_HUMAN]	25,6
C9JMY1	Insulin-like growth factor-binding protein 2 OS=Homo sapiens GN=IGFBP2 PE=1 SV=1 - [C9JMY1_HUMAN]	20,3
Q12905;F2Z4E7	Interleukin enhancer-binding factor 2 OS=Homo sapiens GN=ILF2 PE=1 SV=2 - [ILF2_HUMAN]	43,0
O75874	Isocitrate dehydrogenase [NADP] cytoplasmic OS=Homo sapiens GN=IDH1 PE=1 SV=2 - [IDHC_HUMAN]	46,6
P17174-2	Isoform 2 of Aspartate aminotransferase, cytoplasmic OS=Homo sapiens GN=GOT1 - [AATC_HUMAN]	44,1
O94985-2	Isoform 2 of Calsyntenin-1 OS=Homo sapiens GN=CLSTN1 - [CSTN1_HUMAN]	108,6
P16870-2	Isoform 2 of Carboxypeptidase E OS=Homo sapiens GN=CPE - [CBPE_HUMAN]	49,9
P62633-2;Q3T0Q6	Isoform 2 of Cellular nucleic acid-binding protein OS=Homo sapiens GN=CNBP - [CNBP_HUMAN]	18,7
Q04760-2	Isoform 2 of Lactoylglutathione lyase OS=Homo sapiens GN=GLO1 - [LGUL_HUMAN]	19,0
O94760-2	Isoform 2 of N(G),N(G)-dimethylarginine dimethylaminohydrolase 1 OS=Homo sapiens GN=DDAH1 - [DDAH1_HUMAN]	20,2
P00558-2	Isoform 2 of Phosphoglycerate kinase 1 OS=Homo sapiens GN=PGK1 - [PGK1_HUMAN]	41,4
P25788-2	Isoform 2 of Proteasome subunit alpha type-3 OS=Homo sapiens GN=PSMA3 - [PSA3_HUMAN]	27,6
O14818-2	Isoform 2 of Proteasome subunit alpha type-7 OS=Homo sapiens GN=PSMA7 - [PSA7_HUMAN]	20,2
Q8WVQ1-2	Isoform 2 of Soluble calcium-activated nucleotidase 1 OS=Homo sapiens GN=CANT1 - [CANT1_HUMAN]	27,7
O00391-2	Isoform 2 of Sulfhydryl oxidase 1 OS=Homo sapiens GN=QSOX1 - [QSOX1_HUMAN]	66,8
P60174-1	Isoform 2 of Triosephosphate isomerase OS=Homo sapiens GN=TPI1 - [TPIS_HUMAN]	26,7
Q02487-2	Isoform 2B of Desmocollin-2 OS=Homo sapiens GN=DSC2 - [DSC2_HUMAN]	93,7
P61978-3	Isoform 3 of Heterogeneous nuclear ribonucleoprotein K OS=Homo sapiens GN=HNRNPK - [HNRPK_HUMAN]	48,5
P00390-5	Isoform 4 of Glutathione reductase, mitochondrial OS=Homo sapiens GN=GSR - [GSHR_HUMAN]	47,2
P07288-5	Isoform 5 of Prostate-specific antigen OS=Homo sapiens GN=KLK3 - [KLK3_HUMAN]	25,1
P09651-2;P09867	Isoform A1-A of Heterogeneous nuclear ribonucleoprotein A1 OS=Homo sapiens GN=HNRNPA1 - [ROA1_HUMAN]	34,2
P22626-2;Q2HJ60	Isoform A2 of Heterogeneous nuclear ribonucleoproteins A2/B1 OS=Homo sapiens GN=HNRNPA2B1 - [ROA2_HUMAN]	36,0
P13645	Keratin, type I cytoskeletal 10 OS=Homo sapiens GN=KRT10 PE=1 SV=6 - [K1C10_HUMAN]	58,8
P02533	Keratin, type I cytoskeletal 14 OS=Homo sapiens GN=KRT14 PE=1 SV=4 - [K1C14_HUMAN]	51,5
F8VZY9	Keratin, type I cytoskeletal 18 OS=Homo sapiens GN=KRT18 PE=1 SV=1 - [F8VZY9_HUMAN]	43,7
P35527	Keratin, type I cytoskeletal 9 OS=Homo sapiens GN=KRT9 PE=1 SV=3 - [K1C9_HUMAN]	62,0
P04264	Keratin, type II cytoskeletal 1 OS=Homo sapiens GN=KRT1 PE=1 SV=6 - [K2C1_HUMAN]	66,0
P35908	Keratin, type II cytoskeletal 2 epidermal OS=Homo sapiens GN=KRT2 PE=1 SV=2 - [K22E_HUMAN]	65,4
Q7RTS7	Keratin, type II cytoskeletal 74 OS=Homo sapiens GN=KRT74 PE=1 SV=2 - [K2C74_HUMAN]	57,8
P05787	Keratin, type II cytoskeletal 8 OS=Homo sapiens GN=KRT8 PE=1 SV=7 - [K2C8_HUMAN]	53,7
P00338	L-lactate dehydrogenase A chain OS=Homo sapiens GN=LDHA PE=1 SV=2 - [LDHA_HUMAN]	36,7
P07195	L-lactate dehydrogenase B chain OS=Homo sapiens GN=LDHB PE=1 SV=2 - [LDHB_HUMAN]	36,6
P40925	Malate dehydrogenase, cytoplasmic OS=Homo sapiens GN=MDH1 PE=1 SV=4 - [MDHC_HUMAN]	36,4
P40926	Malate dehydrogenase, mitochondrial OS=Homo sapiens GN=MDH2 PE=1 SV=3 - [MDHM_HUMAN]	35,5
P26038	Moesin OS=Homo sapiens GN=MSN PE=1 SV=3 - [MOES_HUMAN]	67,8

P19338	Nucleolin OS=Homo sapiens GN=NCL PE=1 SV=3 - [NUCL_HUMAN]	76,6
P15531	Nucleoside diphosphate kinase A OS=Homo sapiens GN=NME1 PE=1 SV=1 - [NDKA_HUMAN]	17,1
P62937	Peptidyl-prolyl cis-trans isomerase A OS=Homo sapiens GN=PPIA PE=1 SV=2 - [PPIA_HUMAN]	18,0
P23284	Peptidyl-prolyl cis-trans isomerase B OS=Homo sapiens GN=PPIB PE=1 SV=2 - [PPIB_HUMAN]	23,7
Q02790	Peptidyl-prolyl cis-trans isomerase FKBP4 OS=Homo sapiens GN=FKBP4 PE=1 SV=3 - [FKBP4_HUMAN]	51,8
A0A0A0MSI0	Peroxiredoxin-1 (Fragment) OS=Homo sapiens GN=PRDX1 PE=1 SV=1 - [A0A0A0MSI0_HUMAN]	19,0
P32119	Peroxiredoxin-2 OS=Homo sapiens GN=PRDX2 PE=1 SV=5 - [PRDX2_HUMAN]	21,9
P30041	Peroxiredoxin-6 OS=Homo sapiens GN=PRDX6 PE=1 SV=3 - [PRDX6_HUMAN]	25,0
P30086	Phosphatidylethanolamine-binding protein 1 OS=Homo sapiens GN=PEBP1 PE=1 SV=3 - [PEBP1_HUMAN]	21,0
P18669	Phosphoglycerate mutase 1 OS=Homo sapiens GN=PGAM1 PE=1 SV=2 - [PGAM1_HUMAN]	28,8
Q9Y617	Phosphoserine aminotransferase OS=Homo sapiens GN=PSAT1 PE=1 SV=2 - [SERC_HUMAN]	40,4
P05121	Plasminogen activator inhibitor 1 OS=Homo sapiens GN=SERPINE1 PE=1 SV=1 - [PAI1_HUMAN]	45,0
Q15365;Q5E9A3	Poly(rC)-binding protein 1 OS=Homo sapiens GN=PCBP1 PE=1 SV=2 - [PCBP1_HUMAN]	37,5
Q6S8J3	POTE ankyrin domain family member E OS=Homo sapiens GN=POTEE PE=1 SV=3 - [POTEE_HUMAN]	121,3
P07737	Profilin-1 OS=Homo sapiens GN=PFN1 PE=1 SV=2 - [PROF1_HUMAN]	15,0
Q9UQ80	Proliferation-associated protein 2G4 OS=Homo sapiens GN=PA2G4 PE=1 SV=3 - [PA2G4_HUMAN]	43,8
P25789;Q3ZCK9	Proteasome subunit alpha type-4 OS=Homo sapiens GN=PSMA4 PE=1 SV=1 - [PSA4_HUMAN]	29,5
P28066;Q5E987	Proteasome subunit alpha type-5 OS=Homo sapiens GN=PSMA5 PE=1 SV=3 - [PSA5_HUMAN]	26,4
P60900;Q2YDE4	Proteasome subunit alpha type-6 OS=Homo sapiens GN=PSMA6 PE=1 SV=1 - [PSA6_HUMAN]	27,4
P49721	Proteasome subunit beta type-2 OS=Homo sapiens GN=PSMB2 PE=1 SV=1 - [PSB2_HUMAN]	22,8
P28074	Proteasome subunit beta type-5 OS=Homo sapiens GN=PSMB5 PE=1 SV=3 - [PSB5_HUMAN]	28,5
K7ELW0	Protein deglycase DJ-1 OS=Homo sapiens GN=PARK7 PE=1 SV=1 - [K7ELW0_HUMAN]	17,9
H0Y3Z3	Protein disulfide-isomerase (Fragment) OS=Homo sapiens GN=P4HB PE=1 SV=1 - [H0Y3Z3_HUMAN]	31,5
H7BZJ3	Protein disulfide-isomerase A3 (Fragment) OS=Homo sapiens GN=PDIA3 PE=1 SV=1 - [H7BZJ3_HUMAN]	13,5
P30101	Protein disulfide-isomerase A3 OS=Homo sapiens GN=PDIA3 PE=1 SV=4 - [PDIA3_HUMAN]	56,7
P00491	Purine nucleoside phosphorylase OS=Homo sapiens GN=PNP PE=1 SV=2 - [PNPH_HUMAN]	32,1
P14618	Pyruvate kinase PKM OS=Homo sapiens GN=PKM PE=1 SV=4 - [KPYM_HUMAN]	57,9
P50395	Rab GDP dissociation inhibitor beta OS=Homo sapiens GN=GDI2 PE=1 SV=2 - [GDIB_HUMAN]	50,6
H0Y6Z7	Receptor-type tyrosine-protein phosphatase F (Fragment) OS=Homo sapiens GN=PTPRF PE=1 SV=1 - [H0Y6Z7_HUMAN]	174,8
J3KRE2	Rho GDP-dissociation inhibitor 1 OS=Homo sapiens GN=ARHGDIA PE=1 SV=1 - [J3KRE2_HUMAN]	14,8
Q13228	Selenium-binding protein 1 OS=Homo sapiens GN=SELENBP1 PE=1 SV=2 - [SBP1_HUMAN]	52,4
A0A0C4DGB6	Serum albumin OS=Homo sapiens GN=ALB PE=4 SV=1 - [A0A0C4DGB6_HUMAN]	69,2
Q00796	Sorbitol dehydrogenase OS=Homo sapiens GN=SORD PE=1 SV=4 - [DHSO_HUMAN]	38,3
Q9BUD6	Spondin-2 OS=Homo sapiens GN=SPON2 PE=1 SV=3 - [SPON2_HUMAN]	35,8
A0A075B7D9	TATA-binding protein-associated factor 2N OS=Homo sapiens GN=TAF15 PE=1 SV=1 - [A0A075B7D9_HUMAN]	48,8
F2Z393	Transaldolase OS=Homo sapiens GN=TALDO1 PE=1 SV=1 - [F2Z393_HUMAN]	35,3
E9PFF2	Transketolase OS=Homo sapiens GN=TKT PE=1 SV=1 - [E9PFF2_HUMAN]	36,4
P68363;P81947	Tubulin alpha-1B chain OS=Homo sapiens GN=TUBA1B PE=1 SV=1 - [TBA1B_HUMAN]	50,1
P68366;P81948	Tubulin alpha-4A chain OS=Homo sapiens GN=TUBA4A PE=1 SV=1 - [TBA4A_HUMAN]	49,9
P07437;Q2KJD0	Tubulin beta chain OS=Homo sapiens GN=TUBB PE=1 SV=2 - [TBB5_HUMAN]	49,6
P68371;Q3MHM5	Tubulin beta-4B chain OS=Homo sapiens GN=TUBB4B PE=1 SV=1 - [TBB4B_HUMAN]	49,8

E5RIW3	Tubulin-specific chaperone A OS=Homo sapiens GN=TBCA PE=1 SV=1 - [E5RIW3_HUMAN]	10,1
M0R1V7	Ubiquitin-60S ribosomal protein L40 (Fragment) OS=Homo sapiens GN=UBA52 PE=1 SV=1 - [M0R1V7_HUMAN]	7,1
P61088;Q0P5K3	Ubiquitin-conjugating enzyme E2 N OS=Homo sapiens GN=UBE2N PE=1 SV=1 - [UBE2N_HUMAN]	17,1
Q6EMK4	Vasorin OS=Homo sapiens GN=VASN PE=1 SV=1 - [VASN_HUMAN]	71,7

C. PC-3

Accession	Description	MW [kDa]
P62258;P62261	14-3-3 protein epsilon OS=Homo sapiens GN=YWHAE PE=1 SV=1 - [1433E_HUMAN]	29,2
P61981;A7Z057	14-3-3 protein gamma OS=Homo sapiens GN=YWHAG PE=1 SV=2 - [1433G_HUMAN]	28,3
P27348;Q3SZI4	14-3-3 protein theta OS=Homo sapiens GN=YWHAQ PE=1 SV=1 - [1433T_HUMAN]	27,7
P63104;P63103	14-3-3 protein zeta/delta OS=Homo sapiens GN=YWHAZ PE=1 SV=1 - [1433Z_HUMAN]	27,7
P23396;Q3T169	40S ribosomal protein S3 OS=Homo sapiens GN=RPS3 PE=1 SV=2 - [RS3_HUMAN]	26,7
P11021	78 kDa glucose-regulated protein OS=Homo sapiens GN=HSPA5 PE=1 SV=2 - [GRP78_HUMAN]	72,3
P60709;P60712	Actin, cytoplasmic 1 OS=Homo sapiens GN=ACTB PE=1 SV=1 - [ACTB_HUMAN]	41,7
H7C3F9	Actin-related protein 2/3 complex subunit 2 (Fragment) OS=Homo sapiens GN=ARPC2 PE=1 SV=1 - [H7C3F9_HUMAN]	18,6
P23526	Adenosylhomocysteinase OS=Homo sapiens GN=AHCY PE=1 SV=4 - [SAHH_HUMAN]	47,7
P49588	Alanine--tRNA ligase, cytoplasmic OS=Homo sapiens GN=AARS PE=1 SV=2 - [SYAC_HUMAN]	106,7
H0Y2X5	Aldehyde dehydrogenase 1 family, member A3, isoform CRA_b OS=Homo sapiens GN=ALDH1A3 PE=1 SV=1 - [H0Y2X5_HUMAN]	44,2
O43707	Alpha-actinin-4 OS=Homo sapiens GN=ACTN4 PE=1 SV=2 - [ACTN4_HUMAN]	104,8
P06733	Alpha-enolase OS=Homo sapiens GN=ENO1 PE=1 SV=2 - [ENOA_HUMAN]	47,1
P07355	Annexin A2 OS=Homo sapiens GN=ANXA2 PE=1 SV=2 - [ANXA2_HUMAN]	38,6
D6RBE9	Annexin OS=Homo sapiens GN=ANXA5 PE=1 SV=1 - [D6RBE9_HUMAN]	24,7
E5RK69	Annexin OS=Homo sapiens GN=ANXA6 PE=1 SV=1 - [E5RK69_HUMAN]	51,7
P01008	Antithrombin-III OS=Homo sapiens GN=SERPINC1 PE=1 SV=1 - [ANT3_HUMAN]	52,6
P00505	Aspartate aminotransferase, mitochondrial OS=Homo sapiens GN=GOT2 PE=1 SV=3 - [AATM_HUMAN]	47,5
P53004	Biliverdin reductase A OS=Homo sapiens GN=BLVRA PE=1 SV=2 - [BIEA_HUMAN]	33,4
P27797	Calreticulin OS=Homo sapiens GN=CALR PE=1 SV=1 - [CALR_HUMAN]	48,1
P07858	Cathepsin B OS=Homo sapiens GN=CTSB PE=1 SV=3 - [CATB_HUMAN]	37,8
F8WD96	Cathepsin D OS=Homo sapiens GN=CTSD PE=1 SV=1 - [F8WD96_HUMAN]	30,0
F5GXJ9	CD166 antigen OS=Homo sapiens GN=ALCAM PE=1 SV=1 - [F5GXJ9_HUMAN]	59,5
E9PKC6	CD44 antigen OS=Homo sapiens GN=CD44 PE=1 SV=1 - [E9PKC6_HUMAN]	8,8
B4DJV2	Citrate synthase, mitochondrial OS=Homo sapiens GN=CS PE=1 SV=1 - [B4DJV2_HUMAN]	50,4
G3V1A4	Cofilin 1 (Non-muscle), isoform CRA_a OS=Homo sapiens GN=CFL1 PE=1 SV=1 - [G3V1A4_HUMAN]	16,8
A0A087X0S5	Collagen alpha-1(VI) chain OS=Homo sapiens GN=COL6A1 PE=1 SV=1 - [A0A087X0S5_HUMAN]	108,3
C9JFR7	Cytochrome c (Fragment) OS=Homo sapiens GN=CYCS PE=1 SV=1 - [C9JFR7_HUMAN]	11,3
Q96KP4	Cytosolic non-specific dipeptidase OS=Homo sapiens GN=CNDP2 PE=1 SV=2 - [CNDP2_HUMAN]	52,8
O94907	Dickkopf-related protein 1 OS=Homo sapiens GN=DKK1 PE=1 SV=1 - [DKK1_HUMAN]	28,7
P68104;P68103	Elongation factor 1-alpha 1 OS=Homo sapiens GN=EEF1A1 PE=1 SV=1 - [EF1A1_HUMAN]	50,1
P26641	Elongation factor 1-gamma OS=Homo sapiens GN=EEF1G PE=1 SV=3 - [EF1G_HUMAN]	50,1
P13639	Elongation factor 2 OS=Homo sapiens GN=EEF2 PE=1 SV=4 - [EF2_HUMAN]	95,3
P60842;Q3SZ54	Eukaryotic initiation factor 4A-I OS=Homo sapiens GN=EIF4A1 PE=1 SV=1 - [IF4A1_HUMAN]	46,1
Q14240;Q3SZ65	Eukaryotic initiation factor 4A-II OS=Homo sapiens GN=EIF4A2 PE=1 SV=2 - [IF4A2_HUMAN]	46,4

E7EQR4	Ezrin OS=Homo sapiens GN=EZR PE=1 SV=3 - [E7EQR4_HUMAN]	69,3
Q16658	Fascin OS=Homo sapiens GN=FSCN1 PE=1 SV=3 - [FSCN1_HUMAN]	54,5
Q01469	Fatty acid-binding protein, epidermal OS=Homo sapiens GN=FABP5 PE=1 SV=3 - [FABP5_HUMAN]	15,2
A0A087WWY3	Filamin-A OS=Homo sapiens GN=FLNA PE=1 SV=1 - [A0A087WWY3_HUMAN]	245,7
P04075	Fructose-bisphosphate aldolase A OS=Homo sapiens GN=ALDOA PE=1 SV=2 - [ALDOA_HUMAN]	39,4
P09382	Galectin-1 OS=Homo sapiens GN=LGALS1 PE=1 SV=2 - [LEG1_HUMAN]	14,7
Q08380	Galectin-3-binding protein OS=Homo sapiens GN=LGALS3BP PE=1 SV=1 - [LG3BP_HUMAN]	65,3
Q92820	Gamma-glutamyl hydrolase OS=Homo sapiens GN=GGH PE=1 SV=2 - [GGH_HUMAN]	35,9
H7C3P4	Glucosamine (N-acetyl)-6-sulfatase (Sanfilippo disease IIID), isoform CRA_b OS=Homo sapiens GN=GNS PE=1 SV=1 - [H7C3P4_HUMAN]	56,3
K7EQ48	Glucose-6-phosphate isomerase OS=Homo sapiens GN=GPI PE=1 SV=2 - [K7EQ48_HUMAN]	53,4
E7EUT5	Glyceraldehyde-3-phosphate dehydrogenase OS=Homo sapiens GN=GAPDH PE=1 SV=1 - [E7EUT5_HUMAN]	27,9
P11216	Glycogen phosphorylase, brain form OS=Homo sapiens GN=PYGB PE=1 SV=5 - [PYGB_HUMAN]	96,6
P28799	Granulins OS=Homo sapiens GN=GRN PE=1 SV=2 - [GRN_HUMAN]	63,5
P62826;Q3T054	GTP-binding nuclear protein Ran OS=Homo sapiens GN=RAN PE=1 SV=3 - [RAN_HUMAN]	24,4
P63244;P63243	Guanine nucleotide-binding protein subunit beta-2-like 1 OS=Homo sapiens GN=GNB2L1 PE=1 SV=3 - [GBLP_HUMAN]	35,1
P69905	Hemoglobin subunit alpha OS=Homo sapiens GN=HBA1 PE=1 SV=2 - [HBA_HUMAN]	15,2
D6R9P3	Heterogeneous nuclear ribonucleoprotein A/B OS=Homo sapiens GN=HNRNPAB PE=1 SV=1 - [D6R9P3_HUMAN]	30,3
D6RF44	Heterogeneous nuclear ribonucleoprotein D0 (Fragment) OS=Homo sapiens GN=HNRNPD PE=1 SV=4 - [D6RF44_HUMAN]	12,5
Q09028;Q3MHL3	Histone-binding protein RBBP4 OS=Homo sapiens GN=RBBP4 PE=1 SV=3 - [RBBP4_HUMAN]	47,6
Q5SRN7	HLA class I histocompatibility antigen, A-3 alpha chain OS=Homo sapiens GN=HLA-A PE=1 SV=2 - [Q5SRN7_HUMAN]	34,2
P08476	Inhibin beta A chain OS=Homo sapiens GN=INHBA PE=1 SV=2 - [INHBA_HUMAN]	47,4
A6XND1	Insulin-like growth factor binding protein 3 isoform b OS=Homo sapiens GN=IGFBP3 PE=1 SV=1 - [A6XND1_HUMAN]	29,0
F8VYK9	Insulin-like growth factor-binding protein 6 OS=Homo sapiens GN=IGFBP6 PE=1 SV=1 - [F8VYK9_HUMAN]	25,1
B5MCZ3	Interleukin-6 OS=Homo sapiens GN=IL6 PE=1 SV=1 - [B5MCZ3_HUMAN]	21,5
P18206-2	Isoform 1 of Vinculin OS=Homo sapiens GN=VCL - [VINC_HUMAN]	116,6
P02751-12	Isoform 12 of Fibronectin OS=Homo sapiens GN=FN1 - [FINC_HUMAN]	221,2
P31947-2	Isoform 2 of 14-3-3 protein sigma OS=Homo sapiens GN=SFN - [1433S_HUMAN]	24,3
P08195-2	Isoform 2 of 4F2 cell-surface antigen heavy chain OS=Homo sapiens GN=SLC3A2 - [4F2_HUMAN]	57,9
P52209-2	Isoform 2 of 6-phosphogluconate dehydrogenase, decarboxylating OS=Homo sapiens GN=PGD - [6PGD_HUMAN]	51,8
P08253-2	Isoform 2 of 72 kDa type IV collagenase OS=Homo sapiens GN=MMP2 - [MMP2_HUMAN]	65,7
P0C0L4-2	Isoform 2 of Complement C4-A OS=Homo sapiens GN=C4A - [CO4A_HUMAN]	187,6
P47756-2;P79136-2	Isoform 2 of F-actin-capping protein subunit beta OS=Homo sapiens GN=CAPZB - [CAPZB_HUMAN]	30,6
O75369-2	Isoform 2 of Filamin-B OS=Homo sapiens GN=FLNB - [FLNB_HUMAN]	275,5
Q14315-2	Isoform 2 of Filamin-C OS=Homo sapiens GN=FLNC - [FLNC_HUMAN]	287,1
P19883-2	Isoform 2 of Follistatin OS=Homo sapiens GN=FST - [FST_HUMAN]	34,8
Q12841-2	Isoform 2 of Follistatin-related protein 1 OS=Homo sapiens GN=FSTL1 - [FSTL1_HUMAN]	31,2
P09104-2	Isoform 2 of Gamma-enolase OS=Homo sapiens GN=ENO2 - [ENOG_HUMAN]	42,7
P14314-2	Isoform 2 of Glucosidase 2 subunit beta OS=Homo sapiens GN=PRKCSH - [GLU2B_HUMAN]	59,1
P08107-2	Isoform 2 of Heat shock 70 kDa protein 1A/1B OS=Homo sapiens GN=HSPA1A - [HSP71_HUMAN]	63,9
O00410-2	Isoform 2 of Importin-5 OS=Homo sapiens GN=IPO5 - [IPO5_HUMAN]	116,9
P22692-2	Isoform 2 of Insulin-like growth factor-binding protein 4 OS=Homo sapiens GN=IGFBP4 - [IBP4_HUMAN]	17,6
P10619-2	Isoform 2 of Lysosomal protective protein OS=Homo sapiens GN=CTSA - [PPGB_HUMAN]	52,5
P40121-2	Isoform 2 of Macrophage-capping protein OS=Homo sapiens GN=CAPG - [CAPG_HUMAN]	36,8

P00558-2	Isoform 2 of Phosphoglycerate kinase 1 OS=Homo sapiens GN=PGK1 - [PGK1_HUMAN]	41,4
Q9UQ80-2	Isoform 2 of Proliferation-associated protein 2G4 OS=Homo sapiens GN=PA2G4 - [PA2G4_HUMAN]	38,0
O14818-2	Isoform 2 of Proteasome subunit alpha type-7 OS=Homo sapiens GN=PSMA7 - [PSA7_HUMAN]	20,2
P55786-2	Isoform 2 of Puromycin-sensitive aminopeptidase OS=Homo sapiens GN=NPEPPS - [PSA_HUMAN]	94,5
O75326-2	Isoform 2 of Semaphorin-7A OS=Homo sapiens GN=SEMA7A - [SEM7A_HUMAN]	73,3
O75635-2	Isoform 2 of Serpin B7 OS=Homo sapiens GN=SERPINB7 - [SPB7_HUMAN]	41,1
P52823-2	Isoform 2 of Stanniocalcin-1 OS=Homo sapiens GN=STC1 - [STC1_HUMAN]	20,5
O00391-2	Isoform 2 of Sulfhydryl oxidase 1 OS=Homo sapiens GN=QSOX1 - [QSOX1_HUMAN]	66,8
P50991-2	Isoform 2 of T-complex protein 1 subunit delta OS=Homo sapiens GN=CCT4 - [TCPD_HUMAN]	54,7
P10599-2	Isoform 2 of Thioredoxin OS=Homo sapiens GN=TXN - [THIO_HUMAN]	9,4
P60174-1	Isoform 2 of Triosephosphate isomerase OS=Homo sapiens GN=TPI1 - [TPIS_HUMAN]	26,7
P06753-2;Q5KR47-2	Isoform 2 of Tropomyosin alpha-3 chain OS=Homo sapiens GN=TPM3 - [TPM3_HUMAN]	29,0
P23381-2	Isoform 2 of Tryptophan--tRNA ligase, cytoplasmic OS=Homo sapiens GN=WARS - [SYWC_HUMAN]	48,8
P22314-2	Isoform 2 of Ubiquitin-like modifier-activating enzyme 1 OS=Homo sapiens GN=UBA1 - [UBA1_HUMAN]	113,7
Q96CG8-3	Isoform 3 of Collagen triple helix repeat-containing protein 1 OS=Homo sapiens GN=CTHRC1 - [CTHR1_HUMAN]	24,8
P09622-3	Isoform 3 of Dihydrolipoyl dehydrogenase, mitochondrial OS=Homo sapiens GN=DLD - [DLDH_HUMAN]	49,3
P55060-3	Isoform 3 of Exportin-2 OS=Homo sapiens GN=CSE1L - [XPO2_HUMAN]	107,7
P55058-3	Isoform 3 of Phospholipid transfer protein OS=Homo sapiens GN=PLTP - [PLTP_HUMAN]	44,1
P13797-3	Isoform 3 of Plastin-3 OS=Homo sapiens GN=PLS3 - [PLST_HUMAN]	65,6
Q15084-3	Isoform 3 of Protein disulfide-isomerase A6 OS=Homo sapiens GN=PDIA6 - [PDIA6_HUMAN]	47,8
P31948-3	Isoform 3 of Stress-induced-phosphoprotein 1 OS=Homo sapiens GN=STIP1 - [STIP1_HUMAN]	59,7
Q15063-4	Isoform 4 of Periostin OS=Homo sapiens GN=POSTN - [POSTN_HUMAN]	83,8
Q15149-7	Isoform 7 of Plectin OS=Homo sapiens GN=PLEC - [PLEC_HUMAN]	512,3
P22626-2;Q2HJ60	Isoform A2 of Heterogeneous nuclear ribonucleoproteins A2/B1 OS=Homo sapiens GN=HNRNPA2B1 - [ROA2_HUMAN]	36,0
Q16222-2	Isoform AGX1 of UDP-N-acetylhexosamine pyrophosphorylase OS=Homo sapiens GN=UAP1 - [UAP1_HUMAN]	57,0
P07954-2	Isoform Cytoplasmic of Fumarate hydratase, mitochondrial OS=Homo sapiens GN=FH - [FUMH_HUMAN]	50,2
P02788-2	Isoform DeltaLf of Lactotransferrin OS=Homo sapiens GN=LTF - [TRFL_HUMAN]	73,1
P13645	Keratin, type I cytoskeletal 10 OS=Homo sapiens GN=KRT10 PE=1 SV=6 - [K1C10_HUMAN]	58,8
P02533	Keratin, type I cytoskeletal 14 OS=Homo sapiens GN=KRT14 PE=1 SV=4 - [K1C14_HUMAN]	51,5
P35527	Keratin, type I cytoskeletal 9 OS=Homo sapiens GN=KRT9 PE=1 SV=3 - [K1C9_HUMAN]	62,0
P04264	Keratin, type II cytoskeletal 1 OS=Homo sapiens GN=KRT1 PE=1 SV=6 - [K2C1_HUMAN]	66,0
P35908	Keratin, type II cytoskeletal 2 epidermal OS=Homo sapiens GN=KRT2 PE=1 SV=2 - [K22E_HUMAN]	65,4
P13647	Keratin, type II cytoskeletal 5 OS=Homo sapiens GN=KRT5 PE=1 SV=3 - [K2C5_HUMAN]	62,3
Q99538	Legumain OS=Homo sapiens GN=LGMN PE=1 SV=1 - [LGMN_HUMAN]	49,4
A8MW50	L-lactate dehydrogenase (Fragment) OS=Homo sapiens GN=LDHB PE=1 SV=1 - [A8MW50_HUMAN]	25,2
P00338	L-lactate dehydrogenase A chain OS=Homo sapiens GN=LDHA PE=1 SV=2 - [LDHA_HUMAN]	36,7
Q15046	Lysine--tRNA ligase OS=Homo sapiens GN=KARS PE=1 SV=3 - [SYK_HUMAN]	68,0
Q9Y4K0	Lysyl oxidase homolog 2 OS=Homo sapiens GN=LOXL2 PE=1 SV=1 - [LOXL2_HUMAN]	86,7
P40925	Malate dehydrogenase, cytoplasmic OS=Homo sapiens GN=MDH1 PE=1 SV=4 - [MDHC_HUMAN]	36,4
P40926	Malate dehydrogenase, mitochondrial OS=Homo sapiens GN=MDH2 PE=1 SV=3 - [MDHM_HUMAN]	35,5
P26038	Moesin OS=Homo sapiens GN=MSN PE=1 SV=3 - [MOES_HUMAN]	67,8
P35579	Myosin-9 OS=Homo sapiens GN=MYH9 PE=1 SV=4 - [MYH9_HUMAN]	226,4
F5H6X6	Neutral alpha-glucosidase AB OS=Homo sapiens GN=GANAB PE=1 SV=1 - [F5H6X6_HUMAN]	96,2
Q02818	Nucleobindin-1 OS=Homo sapiens GN=NUCB1 PE=1 SV=4 - [NUCB1_HUMAN]	53,8

P26022	Pentraxin-related protein PTX3 OS=Homo sapiens GN=PTX3 PE=1 SV=3 - [PTX3_HUMAN]	41,9
P62937	Peptidyl-prolyl cis-trans isomerase A OS=Homo sapiens GN=PPIA PE=1 SV=2 - [PPIA_HUMAN]	18,0
P23284	Peptidyl-prolyl cis-trans isomerase B OS=Homo sapiens GN=PPIB PE=1 SV=2 - [PPIB_HUMAN]	23,7
Q00688	Peptidyl-prolyl cis-trans isomerase FKBP3 OS=Homo sapiens GN=FKBP3 PE=1 SV=1 - [FKBP3_HUMAN]	25,2
A0A0A0MSI0	Peroxiredoxin-1 (Fragment) OS=Homo sapiens GN=PRDX1 PE=1 SV=1 - [A0A0A0MSI0_HUMAN]	19,0
P32119	Peroxiredoxin-2 OS=Homo sapiens GN=PRDX2 PE=1 SV=5 - [PRDX2_HUMAN]	21,9
P30041	Peroxiredoxin-6 OS=Homo sapiens GN=PRDX6 PE=1 SV=3 - [PRDX6_HUMAN]	25,0
P30086	Phosphatidylethanolamine-binding protein 1 OS=Homo sapiens GN=PEBP1 PE=1 SV=3 - [PEBP1_HUMAN]	21,0
P36871	Phosphoglucomutase-1 OS=Homo sapiens GN=PGM1 PE=1 SV=3 - [PGM1_HUMAN]	61,4
P18669	Phosphoglycerate mutase 1 OS=Homo sapiens GN=PGAM1 PE=1 SV=2 - [PGAM1_HUMAN]	28,8
P05121	Plasminogen activator inhibitor 1 OS=Homo sapiens GN=SERPINE1 PE=1 SV=1 - [PAI1_HUMAN]	45,0
P13796	Plastin-2 OS=Homo sapiens GN=LCP1 PE=1 SV=6 - [PLSL_HUMAN]	70,2
P09874	Poly [ADP-ribose] polymerase 1 OS=Homo sapiens GN=PARP1 PE=1 SV=4 - [PARP1_HUMAN]	113,0
Q6S8J3	POTE ankyrin domain family member E OS=Homo sapiens GN=POTEE PE=1 SV=3 - [POTEE_HUMAN]	121,3
Q15113	Procollagen C-endopeptidase enhancer 1 OS=Homo sapiens GN=PCOLCE PE=1 SV=2 - [PCOC1_HUMAN]	47,9
P07737	Profilin-1 OS=Homo sapiens GN=PFN1 PE=1 SV=2 - [PROF1_HUMAN]	15,0
P07602	Prosaposin OS=Homo sapiens GN=PSAP PE=1 SV=2 - [SAP_HUMAN]	58,1
H0YKK6	Proteasome activator complex subunit 1 OS=Homo sapiens GN=PSME1 PE=1 SV=1 - [H0YKK6_HUMAN]	10,6
P25789;Q3ZCK9	Proteasome subunit alpha type-4 OS=Homo sapiens GN=PSMA4 PE=1 SV=1 - [PSA4_HUMAN]	29,5
H7BZJ3	Protein disulfide-isomerase A3 (Fragment) OS=Homo sapiens GN=PDIA3 PE=1 SV=1 - [H7BZJ3_HUMAN]	13,5
P30101	Protein disulfide-isomerase A3 OS=Homo sapiens GN=PDIA3 PE=1 SV=4 - [PDIA3_HUMAN]	56,7
P13667	Protein disulfide-isomerase A4 OS=Homo sapiens GN=PDIA4 PE=1 SV=2 - [PDIA4_HUMAN]	72,9
H7BZ94	Protein disulfide-isomerase OS=Homo sapiens GN=P4HB PE=1 SV=2 - [H7BZ94_HUMAN]	52,5
P00491	Purine nucleoside phosphorylase OS=Homo sapiens GN=PNP PE=1 SV=2 - [PNPH_HUMAN]	32,1
P14618	Pyruvate kinase PKM OS=Homo sapiens GN=PKM PE=1 SV=4 - [KPYM_HUMAN]	57,9
P31150	Rab GDP dissociation inhibitor alpha OS=Homo sapiens GN=GDI1 PE=1 SV=2 - [GDIA_HUMAN]	50,6
P50395	Rab GDP dissociation inhibitor beta OS=Homo sapiens GN=GDI2 PE=1 SV=2 - [GDIB_HUMAN]	50,6
P46940	Ras GTPase-activating-like protein IQGAP1 OS=Homo sapiens GN=IQGAP1 PE=1 SV=1 - [IQGA1_HUMAN]	189,1
P61224;P61223	Ras-related protein Rap-1b OS=Homo sapiens GN=RAP1B PE=1 SV=1 - [RAP1B_HUMAN]	20,8
P13489	Ribonuclease inhibitor OS=Homo sapiens GN=RNH1 PE=1 SV=2 - [RINI_HUMAN]	49,9
B3KQV6	Serine/threonine-protein phosphatase 2A 65 kDa regulatory subunit A alpha isoform OS=Homo sapiens GN=PPP2R1A PE=1 SV=1 - [B3KQV6_HUMAN]	45,6
H0YA55	Serum albumin (Fragment) OS=Homo sapiens GN=ALB PE=1 SV=1 - [H0YA55_HUMAN]	51,5
H0YB13	Stanniocalcin-2 (Fragment) OS=Homo sapiens GN=STC2 PE=1 SV=1 - [H0YB13_HUMAN]	13,9
A0A0C4DG56	Superoxide dismutase [Mn], mitochondrial OS=Homo sapiens GN=SOD2 PE=4 SV=1 - [A0A0C4DG56_HUMAN]	18,3
Q9Y490	Talin-1 OS=Homo sapiens GN=TLN1 PE=1 SV=3 - [TLN1_HUMAN]	269,6
E9PKD3	Thioredoxin reductase 1, cytoplasmic (Fragment) OS=Homo sapiens GN=TXNRD1 PE=1 SV=1 - [E9PKD3_HUMAN]	19,4
P26639	Threonine--tRNA ligase, cytoplasmic OS=Homo sapiens GN=TARS PE=1 SV=3 - [SYTC_HUMAN]	83,4
P10646	Tissue factor pathway inhibitor OS=Homo sapiens GN=TFPI PE=1 SV=1 - [TFPI1_HUMAN]	35,0
P37837	Transaldolase OS=Homo sapiens GN=TALDO1 PE=1 SV=2 - [TALDO_HUMAN]	37,5
Q15582	Transforming growth factor-beta-induced protein ig-h3 OS=Homo sapiens GN=TGFBI PE=1 SV=1 - [BGH3_HUMAN]	74,6
Q01995	Transgelin OS=Homo sapiens GN=TAGLN PE=1 SV=4 - [TAGL_HUMAN]	22,6
X6RJP6	Transgelin-2 (Fragment) OS=Homo sapiens GN=TAGLN2 PE=1 SV=1 - [X6RJP6_HUMAN]	21,1
P29401	Transketolase OS=Homo sapiens GN=TKT PE=1 SV=3 - [TKT_HUMAN]	67,8
A0A0C4DGZ9	Tripeptidyl-peptidase 1 OS=Homo sapiens GN=TPP1 PE=4 SV=1 - [A0A0C4DGZ9_HUMAN]	60,4
Q71U36;F2Z4C1	Tubulin alpha-1A chain OS=Homo sapiens GN=TUBA1A PE=1 SV=1 - [TBA1A_HUMAN]	50,1

P68363;P81947	Tubulin alpha-1B chain OS=Homo sapiens GN=TUBA1B PE=1 SV=1 - [TBA1B_HUMAN]	50,1
P07437;Q2KJD0	Tubulin beta chain OS=Homo sapiens GN=TUBB PE=1 SV=2 - [TBB5_HUMAN]	49,6
Q13885;E1BJB1	Tubulin beta-2A chain OS=Homo sapiens GN=TUBB2A PE=1 SV=1 - [TBB2A_HUMAN]	49,9
Q13509;Q2T9S0	Tubulin beta-3 chain OS=Homo sapiens GN=TUBB3 PE=1 SV=2 - [TBB3_HUMAN]	50,4
P68371;Q3MHM5	Tubulin beta-4B chain OS=Homo sapiens GN=TUBB4B PE=1 SV=1 - [TBB4B_HUMAN]	49,8
D6RE83	Ubiquitin carboxyl-terminal hydrolase OS=Homo sapiens GN=UCHL1 PE=1 SV=1 - [D6RE83_HUMAN]	23,2
E7ET40	Urokinase-type plasminogen activator OS=Homo sapiens GN=PLAU PE=1 SV=1 - [E7ET40_HUMAN]	46,9
B0YJC4	Vimentin OS=Homo sapiens GN=VIM PE=1 SV=1 - [B0YJC4_HUMAN]	49,6
D6RD66	WD repeat-containing protein 1 (Fragment) OS=Homo sapiens GN=WDR1 PE=1 SV=1 - [D6RD66_HUMAN]	26,8

D. TRAMP-C1

Accession	Description	MW [kDa]
Q9CQV8	14-3-3 protein beta/alpha OS=Mus musculus GN=Ywhab PE=1 SV=3 - [1433B_MOUSE]	28,1
P62259;P62261	14-3-3 protein epsilon OS=Mus musculus GN=Ywhae PE=1 SV=1 - [1433E_MOUSE]	29,2
P68510;P68509	14-3-3 protein eta OS=Mus musculus GN=Ywhah PE=1 SV=2 - [1433F_MOUSE]	28,2
P61982;A7Z057	14-3-3 protein gamma OS=Mus musculus GN=Ywhag PE=1 SV=2 - [1433G_MOUSE]	28,3
Q8BG32	26S proteasome non-ATPase regulatory subunit 11 OS=Mus musculus GN=Psmd11 PE=1 SV=3 - [PSD11_MOUSE]	47,4
Q3TRH2	26S proteasome non-ATPase regulatory subunit 12 OS=Mus musculus GN=Psmd12 PE=1 SV=1 - [Q3TRH2_MOUSE]	48,3
P63325	40S ribosomal protein S10 OS=Mus musculus GN=Rps10 PE=1 SV=1 - [RS10_MOUSE]	18,9
P62264	40S ribosomal protein S14 OS=Mus musculus GN=Rps14 PE=1 SV=3 - [RS14_MOUSE]	16,3
D3YVC1	40S ribosomal protein S2 (Fragment) OS=Mus musculus GN=Rps2 PE=1 SV=1 - [D3YVC1_MOUSE]	28,6
P97351	40S ribosomal protein S3a OS=Mus musculus GN=Rps3a PE=1 SV=3 - [RS3A_MOUSE]	29,9
P62702;P79103	40S ribosomal protein S4, X isoform OS=Mus musculus GN=Rps4x PE=1 SV=2 - [RS4X_MOUSE]	29,6
Q6ZWN5;A6QLG5	40S ribosomal protein S9 OS=Mus musculus GN=Rps9 PE=1 SV=3 - [RS9_MOUSE]	22,6
P14206	40S ribosomal protein SA OS=Mus musculus GN=Rpsa PE=1 SV=4 - [RSSA_MOUSE]	32,8
Q61112	45 kDa calcium-binding protein OS=Mus musculus GN=Sdf4 PE=1 SV=1 - [CAB45_MOUSE]	42,0
P10852	4F2 cell-surface antigen heavy chain OS=Mus musculus GN=Slc3a2 PE=1 SV=1 - [4F2_MOUSE]	58,3
S4R1N1	60S acidic ribosomal protein P0 (Fragment) OS=Mus musculus GN=Rplp0 PE=1 SV=1 - [S4R1N1_MOUSE]	24,1
Q9DCD0	6-phosphogluconate dehydrogenase, decarboxylating OS=Mus musculus GN=Pgd PE=1 SV=3 - [6PGD_MOUSE]	53,2
P33434	72 kDa type IV collagenase OS=Mus musculus GN=Mmp2 PE=1 SV=1 - [MMP2_MOUSE]	74,1
P20029	78 kDa glucose-regulated protein OS=Mus musculus GN=Hspa5 PE=1 SV=3 - [GRP78_MOUSE]	72,4
Q9WV54	Acid ceramidase OS=Mus musculus GN=Asah1 PE=1 SV=1 - [ASAH1_MOUSE]	44,6
P68033;Q3ZC07	Actin, alpha cardiac muscle 1 OS=Mus musculus GN=Actc1 PE=1 SV=1 - [ACTC_MOUSE]	42,0
P60710;P60712	Actin, cytoplasmic 1 OS=Mus musculus GN=Actb PE=1 SV=1 - [ACTB_MOUSE]	41,7
P61161;A7MB62	Actin-related protein 2 OS=Mus musculus GN=Actr2 PE=1 SV=1 - [ARP2_MOUSE]	44,7
D3YXG6	Actin-related protein 2/3 complex subunit 2 OS=Mus musculus GN=Arpc2 PE=1 SV=1 - [D3YXG6_MOUSE]	32,5
P55264	Adenosine kinase OS=Mus musculus GN=Adk PE=1 SV=2 - [ADK_MOUSE]	40,1
P50247	Adenosylhomocysteinase OS=Mus musculus GN=Ahcy PE=1 SV=3 - [SAHH_MOUSE]	47,7
P40124	Adenylyl cyclase-associated protein 1 OS=Mus musculus GN=Cap1 PE=1 SV=4 - [CAP1_MOUSE]	51,5
P61205;Q5E9I6	ADP-ribosylation factor 3 OS=Mus musculus GN=Arf3 PE=2 SV=2 - [ARF3_MOUSE]	20,6

Q8BGQ7	Alanine--tRNA ligase, cytoplasmic OS=Mus musculus GN=Aars PE=1 SV=1 - [SYAC_MOUSE]	106,8
A1BN54	Alpha actinin 1a OS=Mus musculus GN=Actn1 PE=1 SV=1 - [A1BN54_MOUSE]	102,7
P57780	Alpha-actinin-4 OS=Mus musculus GN=Actn4 PE=1 SV=1 - [ACTN4_MOUSE]	104,9
G3UY72	Alpha-aminoadipic semialdehyde dehydrogenase (Fragment) OS=Mus musculus GN=Aldh7a1 PE=1 SV=1 - [G3UY72_MOUSE]	35,1
P17182	Alpha-enolase OS=Mus musculus GN=Eno1 PE=1 SV=3 - [ENOA_MOUSE]	47,1
P12023	Amyloid beta A4 protein OS=Mus musculus GN=App PE=1 SV=3 - [A4_MOUSE]	86,7
D3Z0S1	Annexin (Fragment) OS=Mus musculus GN=Anxa4 PE=1 SV=1 - [D3Z0S1_MOUSE]	28,5
P10107	Annexin A1 OS=Mus musculus GN=Anxa1 PE=1 SV=2 - [ANXA1_MOUSE]	38,7
P07356	Annexin A2 OS=Mus musculus GN=Anxa2 PE=1 SV=2 - [ANXA2_MOUSE]	38,7
P48036	Annexin A5 OS=Mus musculus GN=Anxa5 PE=1 SV=1 - [ANXA5_MOUSE]	35,7
F8WIT2	Annexin OS=Mus musculus GN=Anxa6 PE=1 SV=1 - [F8WIT2_MOUSE]	75,2
Q9D0I9	Arginine--tRNA ligase, cytoplasmic OS=Mus musculus GN=Rars PE=1 SV=2 - [SYRC_MOUSE]	75,6
Q61024	Asparagine synthetase [glutamine-hydrolyzing] OS=Mus musculus GN=Asns PE=1 SV=3 - [ASNS_MOUSE]	64,2
P05201	Aspartate aminotransferase, cytoplasmic OS=Mus musculus GN=Got1 PE=1 SV=3 - [AATC_MOUSE]	46,2
P05202	Aspartate aminotransferase, mitochondrial OS=Mus musculus GN=Got2 PE=1 SV=1 - [AATM_MOUSE]	47,4
B1B0C7	Basement membrane-specific heparan sulfate proteoglycan core protein OS=Mus musculus GN=Hspg2 PE=1 SV=1 - [B1B0C7_MOUSE]	468,7
K3W4Q8	Basigin OS=Mus musculus GN=Bsg PE=1 SV=1 - [K3W4Q8_MOUSE]	24,1
P15535	Beta-1,4-galactosyltransferase 1 OS=Mus musculus GN=B4galt1 PE=1 SV=1 - [B4GT1_MOUSE]	44,4
Q8BFZ3	Beta-actin-like protein 2 OS=Mus musculus GN=Actbl2 PE=1 SV=1 - [ACTBL_MOUSE]	42,0
Q8K2I4	Beta-mannosidase OS=Mus musculus GN=Manba PE=1 SV=1 - [MANBA_MOUSE]	100,8
Q9CWJ9	Bifunctional purine biosynthesis protein PURH OS=Mus musculus GN=Atic PE=1 SV=2 - [PUR9_MOUSE]	64,2
P98063	Bone morphogenetic protein 1 OS=Mus musculus GN=Bmp1 PE=1 SV=2 - [BMP1_MOUSE]	111,6
P55288	Cadherin-11 OS=Mus musculus GN=Cdh11 PE=1 SV=1 - [CAD11_MOUSE]	88,1
Q8VCQ8	Caldesmon 1 OS=Mus musculus GN=Cald1 PE=1 SV=1 - [Q8VCQ8_MOUSE]	60,4
P14211	Calreticulin OS=Mus musculus GN=Calr PE=1 SV=1 - [CALR_MOUSE]	48,0
Q9EPL2	Calsyntenin-1 OS=Mus musculus GN=Clstn1 PE=1 SV=1 - [CSTN1_MOUSE]	108,8
O35887	Calumenin OS=Mus musculus GN=Calu PE=1 SV=1 - [CALU_MOUSE]	37,0
Q6XLQ8	Calumenin OS=Mus musculus GN=Calu PE=1 SV=1 - [Q6XLQ8_MOUSE]	37,1
Q99LB4	Capping protein (Actin filament), gelsolin-like OS=Mus musculus GN=Capg PE=1 SV=1 - [Q99LB4_MOUSE]	38,7
Q00493	Carboxypeptidase E OS=Mus musculus GN=Cpe PE=1 SV=2 - [CBPE_MOUSE]	53,2
P10605	Cathepsin B OS=Mus musculus GN=Ctsb PE=1 SV=2 - [CATB_MOUSE]	37,3
P18242	Cathepsin D OS=Mus musculus GN=Ctsd PE=1 SV=1 - [CATD_MOUSE]	44,9
P06797	Cathepsin L1 OS=Mus musculus GN=Ctsl PE=1 SV=2 - [CATL1_MOUSE]	37,5
Q03366	C-C motif chemokine 7 OS=Mus musculus GN=Ccl7 PE=3 SV=1 - [CCL7_MOUSE]	11,0
P60766;Q2KJ93	Cell division control protein 42 homolog OS=Mus musculus GN=Cdc42 PE=1 SV=2 - [CDC42_MOUSE]	21,2
Q9QYB1	Chloride intracellular channel protein 4 OS=Mus musculus GN=Clic4 PE=1 SV=3 - [CLIC4_MOUSE]	28,7
D3Z1A9	Chromobox protein homolog 3 OS=Mus musculus GN=Cbx3 PE=1 SV=1 - [D3Z1A9_MOUSE]	8,1
Q06890	Clusterin OS=Mus musculus GN=Clu PE=1 SV=1 - [CLUS_MOUSE]	51,6
P18760	Cofilin-1 OS=Mus musculus GN=Cfl1 PE=1 SV=3 - [COF1_MOUSE]	18,5
Q8R2G6	Coiled-coil domain-containing protein 80 OS=Mus musculus GN=Ccdc80 PE=1 SV=2 - [CCD80_MOUSE]	107,5
P11087	Collagen alpha-1(I) chain OS=Mus musculus GN=Col1a1 PE=1 SV=4 - [CO1A1_MOUSE]	137,9
P08121	Collagen alpha-1(III) chain OS=Mus musculus GN=Col3a1 PE=1 SV=4 - [CO3A1_MOUSE]	138,9
Q04857	Collagen alpha-1(VI) chain OS=Mus musculus GN=Col6a1 PE=1 SV=1 - [CO6A1_MOUSE]	108,4
Q01149	Collagen alpha-2(I) chain OS=Mus musculus GN=Col1a2 PE=1 SV=2 - [CO1A2_MOUSE]	129,5
Q3U962	Collagen alpha-2(V) chain OS=Mus musculus GN=Col5a2 PE=1 SV=1 - [CO5A2_MOUSE]	144,9
D3Z7D5	Collagen alpha-2(VI) chain OS=Mus musculus GN=Col6a2 PE=1 SV=1 - [D3Z7D5_MOUSE]	98,9

P33435	Collagenase 3 OS=Mus musculus GN=Mmp13 PE=1 SV=1 - [MMP13_MOUSE]	54,1
Q8CG16	Complement C1r-A subcomponent OS=Mus musculus GN=C1ra PE=1 SV=1 - [C1RA_MOUSE]	80,0
Q8CG14	Complement C1s-A subcomponent OS=Mus musculus GN=C1sa PE=2 SV=2 - [CS1A_MOUSE]	76,8
P01027	Complement C3 OS=Mus musculus GN=C3 PE=1 SV=3 - [CO3_MOUSE]	186,4
Q9WUM3	Coronin-1B OS=Mus musculus GN=Coro1b PE=1 SV=1 - [COR1B_MOUSE]	53,9
P97792	Coxsackievirus and adenovirus receptor homolog OS=Mus musculus GN=Cxadr PE=1 SV=1 - [CXAR_MOUSE]	39,9
A2APX3	Cystatin-C (Fragment) OS=Mus musculus GN=Cst3 PE=1 SV=1 - [A2APX3_MOUSE]	11,1
P97315	Cysteine and glycine-rich protein 1 OS=Mus musculus GN=Csrp1 PE=1 SV=3 - [CSRP1_MOUSE]	20,6
Q9CPY7	Cytosol aminopeptidase OS=Mus musculus GN=Lap3 PE=1 SV=3 - [AMPL_MOUSE]	56,1
Q61753	D-3-phosphoglycerate dehydrogenase OS=Mus musculus GN=Phgdh PE=1 SV=3 - [SERA_MOUSE]	56,5
P28654	Decorin OS=Mus musculus GN=Dcn PE=1 SV=1 - [PGS2_MOUSE]	39,8
P10518	Delta-aminolevulinic acid dehydratase OS=Mus musculus GN=Alad PE=1 SV=1 - [HEM2_MOUSE]	36,0
Q9QZZ6	Dermatopontin OS=Mus musculus GN=Dpt PE=1 SV=1 - [DERM_MOUSE]	24,0
Q9R0P5	Destrin OS=Mus musculus GN=Dstn PE=1 SV=3 - [DEST_MOUSE]	18,5
Q99KK7	Dipeptidyl peptidase 3 OS=Mus musculus GN=Dpp3 PE=1 SV=2 - [DPP3_MOUSE]	82,8
Q9R1E6	Ectonucleotide pyrophosphatase/phosphodiesterase family member 2 OS=Mus musculus GN=Enpp2 PE=1 SV=3 - [ENPP2_MOUSE]	98,8
Q8BPB5	EGF-containing fibulin-like extracellular matrix protein 1 OS=Mus musculus GN=Efemp1 PE=1 SV=1 - [FBLN3_MOUSE]	54,9
E9Q3N9	EGF-containing fibulin-like extracellular matrix protein 2 OS=Mus musculus GN=Efemp2 PE=1 SV=1 - [E9Q3N9_MOUSE]	44,9
Q9D8N0	Elongation factor 1-gamma OS=Mus musculus GN=Eef1g PE=1 SV=3 - [EF1G_MOUSE]	50,0
P58252	Elongation factor 2 OS=Mus musculus GN=Eef2 PE=1 SV=2 - [EF2_MOUSE]	95,3
D9J2Z9	ENH isoform 1b OS=Mus musculus GN=Pdlim5 PE=1 SV=1 - [D9J2Z9_MOUSE]	52,4
Q9Z0J0	Epididymal secretory protein E1 OS=Mus musculus GN=Npc2 PE=1 SV=1 - [NPC2_MOUSE]	16,4
P60843;Q3SZ54	Eukaryotic initiation factor 4A-I OS=Mus musculus GN=Eif4a1 PE=1 SV=1 - [IF4A1_MOUSE]	46,1
P10630;Q3SZ65	Eukaryotic initiation factor 4A-II OS=Mus musculus GN=Eif4a2 PE=1 SV=2 - [IF4A2_MOUSE]	46,4
Q8BWY3;Q0VCX5	Eukaryotic peptide chain release factor subunit 1 OS=Mus musculus GN=Etf1 PE=1 SV=4 - [ERF1_MOUSE]	49,0
Q9Z0N1	Eukaryotic translation initiation factor 2 subunit 3, X-linked OS=Mus musculus GN=Eif2s3x PE=1 SV=2 - [IF2G_MOUSE]	51,0
Q8BGD9	Eukaryotic translation initiation factor 4B OS=Mus musculus GN=Eif4b PE=1 SV=1 - [IF4B_MOUSE]	68,8
P63242;Q6EWQ7	Eukaryotic translation initiation factor 5A-1 OS=Mus musculus GN=Eif5a PE=1 SV=2 - [IF5A1_MOUSE]	16,8
Q61508	Extracellular matrix protein 1 OS=Mus musculus GN=Ecm1 PE=1 SV=2 - [ECM1_MOUSE]	62,8
P26040	Ezrin OS=Mus musculus GN=Ezr PE=1 SV=3 - [EZRI_MOUSE]	69,4
P47754	F-actin-capping protein subunit alpha-2 OS=Mus musculus GN=Capza2 PE=1 SV=3 - [CAZA2_MOUSE]	32,9
F7CAZ6	F-actin-capping protein subunit beta (Fragment) OS=Mus musculus GN=Capzb PE=1 SV=1 - [F7CAZ6_MOUSE]	22,8
A0A0G2JDJ5	Farnesyl pyrophosphate synthase (Fragment) OS=Mus musculus GN=Fdps PE=3 SV=1 - [A0A0G2JDJ5_MOUSE]	13,9
Q61553	Fascin OS=Mus musculus GN=Fscn1 PE=1 SV=4 - [FSCN1_MOUSE]	54,5
Q05816	Fatty acid-binding protein, epidermal OS=Mus musculus GN=Fabp5 PE=1 SV=3 - [FABP5_MOUSE]	15,1
A0A087WS56	Fibronectin OS=Mus musculus GN=Fn1 PE=1 SV=1 - [A0A087WS56_MOUSE]	249,4
P37889	Fibulin-2 OS=Mus musculus GN=Fbln2 PE=1 SV=2 - [FBLN2_MOUSE]	131,7
Q9WVH9	Fibulin-5 OS=Mus musculus GN=Fbln5 PE=1 SV=1 - [FBLN5_MOUSE]	50,2
B7FAV1	Filamin, alpha (Fragment) OS=Mus musculus GN=Flna PE=1 SV=1 - [B7FAV1_MOUSE]	274,5
Q80X90	Filamin-B OS=Mus musculus GN=Flnb PE=1 SV=3 - [FLNB_MOUSE]	277,7
D3YW87	Filamin-C OS=Mus musculus GN=Flnc PE=1 SV=2 - [D3YW87_MOUSE]	287,2
Q62356	Follistatin-related protein 1 OS=Mus musculus GN=Fstl1 PE=1 SV=2 - [FSTL1_MOUSE]	34,5
P05064	Fructose-bisphosphate aldolase A OS=Mus musculus GN=Aldoa PE=1 SV=2 - [ALDOA_MOUSE]	39,3
P16045	Galectin-1 OS=Mus musculus GN=Lgals1 PE=1 SV=3 - [LEG1_MOUSE]	14,9

P16110	Galectin-3 OS=Mus musculus GN=Lgals3 PE=1 SV=3 - [LEG3_MOUSE]	27,5
Q07797	Galectin-3-binding protein OS=Mus musculus GN=Lgals3bp PE=1 SV=1 - [LG3BP_MOUSE]	64,4
Q9Z0L8	Gamma-glutamyl hydrolase OS=Mus musculus GN=Ggh PE=1 SV=2 - [GGH_MOUSE]	35,4
P13020	Gelsolin OS=Mus musculus GN=Gsn PE=1 SV=3 - [GELS_MOUSE]	85,9
P06745	Glucose-6-phosphate isomerase OS=Mus musculus GN=Gpi PE=1 SV=4 - [G6PI_MOUSE]	62,7
O08795	Glucosidase 2 subunit beta OS=Mus musculus GN=Prkcsh PE=1 SV=1 - [GLU2B_MOUSE]	58,8
Q9CQM9	Glutaredoxin-3 OS=Mus musculus GN=Glrx3 PE=1 SV=1 - [GLRX3_MOUSE]	37,8
A2AE89	Glutathione S-transferase Mu 1 (Fragment) OS=Mus musculus GN=Gstm1 PE=1 SV=1 - [A2AE89_MOUSE]	23,5
D3YX76	Glutathione S-transferase Mu 2 OS=Mus musculus GN=Gstm2 PE=1 SV=1 - [D3YX76_MOUSE]	21,7
E9PV63	Glutathione S-transferase Mu 5 OS=Mus musculus GN=Gstm5 PE=1 SV=1 - [E9PV63_MOUSE]	18,8
O09131	Glutathione S-transferase omega-1 OS=Mus musculus GN=Gsto1 PE=1 SV=2 - [GSTO1_MOUSE]	27,5
P16858	Glyceraldehyde-3-phosphate dehydrogenase OS=Mus musculus GN=Gapdh PE=1 SV=2 - [G3P_MOUSE]	35,8
Q9CZD3	Glycine--tRNA ligase OS=Mus musculus GN=Gars PE=1 SV=1 - [SYG_MOUSE]	81,8
E9Q197	Glyoxalase domain-containing protein 4 OS=Mus musculus GN=Glod4 PE=1 SV=1 - [E9Q197_MOUSE]	31,2
P28798	Granulins OS=Mus musculus GN=Grn PE=1 SV=2 - [GRN_MOUSE]	63,4
Q01721	Growth arrest-specific protein 1 OS=Mus musculus GN=Gas1 PE=2 SV=2 - [GAS1_MOUSE]	35,7
P62827;Q3T054	GTP-binding nuclear protein Ran OS=Mus musculus GN=Ran PE=1 SV=3 - [RAN_MOUSE]	24,4
P68040;P63243	Guanine nucleotide-binding protein subunit beta-2-like 1 OS=Mus musculus GN=Gnb2l1 PE=1 SV=3 - [GBLP_MOUSE]	35,1
P01897	H-2 class I histocompatibility antigen, L-D alpha chain OS=Mus musculus GN=H2-L PE=1 SV=2 - [HA1L_MOUSE]	40,7
Q61316	Heat shock 70 kDa protein 4 OS=Mus musculus GN=Hspa4 PE=1 SV=1 - [HSP74_MOUSE]	94,1
P07901	Heat shock protein HSP 90-alpha OS=Mus musculus GN=Hsp90aa1 PE=1 SV=4 - [HS90A_MOUSE]	84,7
P01942	Hemoglobin subunit alpha OS=Mus musculus GN=Hba PE=1 SV=2 - [HBA_MOUSE]	15,1
E0CXA0	Hepatoma-derived growth factor (Fragment) OS=Mus musculus GN=Hdgf PE=1 SV=1 - [E0CXA0_MOUSE]	22,1
P49312;P09867	Heterogeneous nuclear ribonucleoprotein A1 OS=Mus musculus GN=Hnrnpa1 PE=1 SV=2 - [ROA1_MOUSE]	34,2
E9Q5B6	Heterogeneous nuclear ribonucleoprotein D0 (Fragment) OS=Mus musculus GN=Hnrnpd PE=1 SV=1 - [E9Q5B6_MOUSE]	12,1
Q8BT23	Heterogeneous nuclear ribonucleoprotein K OS=Mus musculus GN=Hnrnpk PE=2 SV=1 - [Q8BT23_MOUSE]	10,8
G3UZI2	Heterogeneous nuclear ribonucleoprotein Q OS=Mus musculus GN=Syncrip PE=1 SV=1 - [G3UZI2_MOUSE]	58,7
A0A0J9YUD8	High mobility group protein B1 OS=Mus musculus GN=Hmgb1 PE=4 SV=1 - [A0A0J9YUD8_MOUSE]	19,8
Q61035	Histidine--tRNA ligase, cytoplasmic OS=Mus musculus GN=Hars PE=1 SV=2 - [SYHC_MOUSE]	57,4
Q64523;A1A4R1	Histone H2A type 2-C OS=Mus musculus GN=Hist2h2ac PE=1 SV=3 - [H2A2C_MOUSE]	14,0
P62806;P62803	Histone H4 OS=Mus musculus GN=Hist1h4a PE=1 SV=2 - [H4_MOUSE]	11,4
Q60972;Q3MHL3	Histone-binding protein RBBP4 OS=Mus musculus GN=Rbbp4 PE=1 SV=5 - [RBBP4_MOUSE]	47,6
A2AFI9	Histone-binding protein RBBP7 OS=Mus musculus GN=Rbbp7 PE=1 SV=1 - [A2AFI9_MOUSE]	43,6
P00493	Hypoxanthine-guanine phosphoribosyltransferase OS=Mus musculus GN=Hprt1 PE=1 SV=3 - [HPRT_MOUSE]	24,6
P70168	Importin subunit beta-1 OS=Mus musculus GN=Kpnb1 PE=1 SV=2 - [IMB1_MOUSE]	97,1
Q8BKC5	Importin-5 OS=Mus musculus GN=Ipo5 PE=1 SV=3 - [IPO5_MOUSE]	123,5
Q9D819	Inorganic pyrophosphatase OS=Mus musculus GN=Ppa1 PE=1 SV=1 - [IPYR_MOUSE]	32,6
O55023	Inositol monophosphatase 1 OS=Mus musculus GN=Impa1 PE=1 SV=1 - [IMPA1_MOUSE]	30,4
Q9JHU9	Inositol-3-phosphate synthase 1 OS=Mus musculus GN=Isyna1 PE=1 SV=1 - [INO1_MOUSE]	60,9
P47878	Insulin-like growth factor-binding protein 3 OS=Mus musculus GN=Igfbp3 PE=2 SV=2 - [IBP3_MOUSE]	31,7
P47880	Insulin-like growth factor-binding protein 6 OS=Mus musculus GN=Igfbp6 PE=2 SV=2 - [IBP6_MOUSE]	25,3
Q61581	Insulin-like growth factor-binding protein 7 OS=Mus musculus GN=Igfbp7 PE=1 SV=3 - [IBP7_MOUSE]	29,0

O88844	Isocitrate dehydrogenase [NADP] cytoplasmic OS=Mus musculus GN=Idh1 PE=1 SV=2 - [IDHC_MOUSE]	46,6
Q3TTY5	Keratin, type II cytoskeletal 2 epidermal OS=Mus musculus GN=Krt2 PE=1 SV=1 - [K22E_MOUSE]	70,9
P21956	Lactadherin OS=Mus musculus GN=Mfge8 PE=1 SV=3 - [MFGM_MOUSE]	51,2
Q61029	Lamina-associated polypeptide 2, isoforms beta/delta/epsilon/gamma OS=Mus musculus GN=Tmpo PE=1 SV=4 - [LAP2B_MOUSE]	50,3
P14733	Lamin-B1 OS=Mus musculus GN=Lmnb1 PE=1 SV=3 - [LMNB1_MOUSE]	66,7
O89017	Legumain OS=Mus musculus GN=Lgmn PE=1 SV=1 - [LGMN_MOUSE]	49,3
P59383	Leucine-rich repeat neuronal protein 4 OS=Mus musculus GN=Lrrn4 PE=1 SV=2 - [LRRN4_MOUSE]	80,4
A2A6G7	LIM and SH3 domain protein 1 (Fragment) OS=Mus musculus GN=Lasp1 PE=1 SV=6 - [A2A6G7_MOUSE]	11,6
Q61805	Lipopolysaccharide-binding protein OS=Mus musculus GN=Lbp PE=1 SV=2 - [LBP_MOUSE]	53,0
D3Z736	L-lactate dehydrogenase OS=Mus musculus GN=Ldha PE=1 SV=1 - [D3Z736_MOUSE]	26,0
Q99MN1	Lysine--tRNA ligase OS=Mus musculus GN=Kars PE=1 SV=1 - [SYK_MOUSE]	67,8
P16675	Lysosomal protective protein OS=Mus musculus GN=Ctsa PE=1 SV=1 - [PPGB_MOUSE]	53,8
P97873	Lysyl oxidase homolog 1 OS=Mus musculus GN=Loxl1 PE=2 SV=3 - [LOXL1_MOUSE]	66,5
P58022	Lysyl oxidase homolog 2 OS=Mus musculus GN=Loxl2 PE=1 SV=2 - [LOXL2_MOUSE]	86,9
D3Z090	Macrophage colony-stimulating factor 1 (Fragment) OS=Mus musculus GN=Csf1 PE=1 SV=1 - [D3Z090_MOUSE]	21,3
P14152	Malate dehydrogenase, cytoplasmic OS=Mus musculus GN=Mdh1 PE=1 SV=3 - [MDHC_MOUSE]	36,5
P08249	Malate dehydrogenase, mitochondrial OS=Mus musculus GN=Mdh2 PE=1 SV=3 - [MDHM_MOUSE]	35,6
Q99M71	Mammalian ependymin-related protein 1 OS=Mus musculus GN=Epdr1 PE=1 SV=1 - [EPDR1_MOUSE]	25,5
O08746	Matrilin-2 OS=Mus musculus GN=Matn2 PE=2 SV=2 - [MATN2_MOUSE]	106,7
G3X9V0	MCG22048, isoform CRA_a OS=Mus musculus GN=Psme2 PE=1 SV=1 - [G3X9V0_MOUSE]	26,1
F6USD5	Mesencephalic astrocyte-derived neurotrophic factor (Fragment) OS=Mus musculus GN=Manf PE=1 SV=1 - [F6USD5_MOUSE]	13,7
Q61468	Mesothelin OS=Mus musculus GN=Msln PE=1 SV=1 - [MSLN_MOUSE]	69,4
P12032	Metalloproteinase inhibitor 1 OS=Mus musculus GN=Timp1 PE=1 SV=2 - [TIMP1_MOUSE]	22,6
Q62000	Mimecan OS=Mus musculus GN=Ogn PE=1 SV=1 - [MIME_MOUSE]	34,0
P26041	Moesin OS=Mus musculus GN=Msn PE=1 SV=3 - [MOES_MOUSE]	67,7
P28665	Murinoglobulin-1 OS=Mus musculus GN=Mug1 PE=1 SV=3 - [MUG1_MOUSE]	165,2
Q60605;P60661	Myosin light polypeptide 6 OS=Mus musculus GN=Myl6 PE=1 SV=3 - [MYL6_MOUSE]	16,9
Q8VDD5	Myosin-9 OS=Mus musculus GN=Myh9 PE=1 SV=4 - [MYH9_MOUSE]	226,2
P26645	Myristoylated alanine-rich C-kinase substrate OS=Mus musculus GN=Marcks PE=1 SV=2 - [MARCS_MOUSE]	29,6
Q571E4	N-acetylgalactosamine-6-sulfatase OS=Mus musculus GN=Galns PE=1 SV=2 - [GALNS_MOUSE]	57,6
Q8BFR4	N-acetylglucosamine-6-sulfatase OS=Mus musculus GN=Gns PE=1 SV=1 - [GNS_MOUSE]	61,1
Q61477	Neuroblastoma suppressor of tumorigenicity 1 OS=Mus musculus GN=Nbl1 PE=1 SV=2 - [NBL1_MOUSE]	19,1
Q8BHN3	Neutral alpha-glucosidase AB OS=Mus musculus GN=Ganab PE=1 SV=1 - [GANAB_MOUSE]	106,8
P10493	Nidogen-1 OS=Mus musculus GN=Nid1 PE=1 SV=2 - [NID1_MOUSE]	136,5
O88322	Nidogen-2 OS=Mus musculus GN=Nid2 PE=1 SV=2 - [NID2_MOUSE]	153,8
Q02819	Nucleobindin-1 OS=Mus musculus GN=Nucb1 PE=1 SV=2 - [NUCB1_MOUSE]	53,4
P09405	Nucleolin OS=Mus musculus GN=Ncl PE=1 SV=2 - [NUCL_MOUSE]	76,7
E9PZF0	Nucleoside diphosphate kinase OS=Mus musculus GN=Gm20390 PE=3 SV=1 - [E9PZF0_MOUSE]	30,2
Q3V1G4	Olfactomedin-like protein 2B OS=Mus musculus GN=Olfml2b PE=1 SV=2 - [OLM2B_MOUSE]	83,5
Q8BK62	Olfactomedin-like protein 3 OS=Mus musculus GN=Olfml3 PE=2 SV=2 - [OLFL3_MOUSE]	45,7
P48759	Pentraxin-related protein PTX3 OS=Mus musculus GN=Ptx3 PE=1 SV=2 - [PTX3_MOUSE]	41,8
F7CAT1	Peptidyl-prolyl cis-trans isomerase (Fragment) OS=Mus musculus GN=Fkbp4 PE=1 SV=1 - [F7CAT1_MOUSE]	23,9
P17742	Peptidyl-prolyl cis-trans isomerase A OS=Mus musculus GN=Ppia PE=1 SV=2 - [PPIA_MOUSE]	18,0
P24369	Peptidyl-prolyl cis-trans isomerase B OS=Mus musculus GN=Ppib PE=1 SV=2 - [PPIB_MOUSE]	23,7

Q62009	Periostin OS=Mus musculus GN=Postn PE=1 SV=2 - [POSTN_MOUSE]	93,1
P35700	Peroxiredoxin-1 OS=Mus musculus GN=Prdx1 PE=1 SV=1 - [PRDX1_MOUSE]	22,2
D3Z4A4	Peroxiredoxin-2 (Fragment) OS=Mus musculus GN=Prdx2 PE=1 SV=6 - [D3Z4A4_MOUSE]	16,0
P99029	Peroxiredoxin-5, mitochondrial OS=Mus musculus GN=Prdx5 PE=1 SV=2 - [PRDX5_MOUSE]	21,9
D3Z0Y2	Peroxiredoxin-6 OS=Mus musculus GN=Prdx6 PE=1 SV=1 - [D3Z0Y2_MOUSE]	22,5
P53811	Phosphatidylinositol transfer protein beta isoform OS=Mus musculus GN=Pitpnb PE=1 SV=2 - [PIPNB_MOUSE]	31,5
Q9D0F9	Phosphoglucomutase-1 OS=Mus musculus GN=Pgm1 PE=1 SV=4 - [PGM1_MOUSE]	61,4
P09411	Phosphoglycerate kinase 1 OS=Mus musculus GN=Pgk1 PE=1 SV=4 - [PGK1_MOUSE]	44,5
Q9DBJ1	Phosphoglycerate mutase 1 OS=Mus musculus GN=Pgam1 PE=1 SV=3 - [PGAM1_MOUSE]	28,8
P55065	Phospholipid transfer protein OS=Mus musculus GN=Pltp PE=1 SV=1 - [PLTP_MOUSE]	54,4
Q99K85	Phosphoserine aminotransferase OS=Mus musculus GN=Psat1 PE=1 SV=1 - [SERC_MOUSE]	40,4
Q99LS3	Phosphoserine phosphatase OS=Mus musculus GN=Psph PE=1 SV=1 - [SERB_MOUSE]	25,1
P97298	Pigment epithelium-derived factor OS=Mus musculus GN=Serpinf1 PE=1 SV=2 - [PEDF_MOUSE]	46,2
G5E899	Plasminogen activator inhibitor 1 OS=Mus musculus GN=Serpine1 PE=1 SV=1 - [G5E899_MOUSE]	45,0
Q99K51	Plastin-3 OS=Mus musculus GN=Pls3 PE=1 SV=3 - [PLST_MOUSE]	70,7
P63005;A5D7P3	Platelet-activating factor acetylhydrolase IB subunit alpha OS=Mus musculus GN=Pafah1b1 PE=1 SV=2 - [LIS1_MOUSE]	46,6
E9Q3W4	Plectin OS=Mus musculus GN=Plec PE=1 SV=1 - [E9Q3W4_MOUSE]	498,8
Q61990	Poly(rC)-binding protein 2 OS=Mus musculus GN=Pcbp2 PE=1 SV=1 - [PCBP2_MOUSE]	38,2
Q6PB93	Polypeptide N-acetylgalactosaminyltransferase 2 OS=Mus musculus GN=Galnt2 PE=1 SV=1 - [GALT2_MOUSE]	64,5
P48678	Prelamin-A/C OS=Mus musculus GN=Lmna PE=1 SV=2 - [LMNA_MOUSE]	74,2
Q61398	Procollagen C-endopeptidase enhancer 1 OS=Mus musculus GN=Pcolce PE=1 SV=2 - [PCOC1_MOUSE]	50,1
F6WNR1	Procollagen-lysine,2-oxoglutarate 5-dioxygenase 1 (Fragment) OS=Mus musculus GN=Plod1 PE=1 SV=1 - [F6WNR1_MOUSE]	31,2
P62962	Profilin-1 OS=Mus musculus GN=Pfn1 PE=1 SV=2 - [PROF1_MOUSE]	14,9
P50580	Proliferation-associated protein 2G4 OS=Mus musculus GN=Pa2g4 PE=1 SV=3 - [PA2G4_MOUSE]	43,7
E9Q7B0	Prolyl 4-hydroxylase subunit alpha-1 OS=Mus musculus GN=P4ha1 PE=1 SV=1 - [E9Q7B0_MOUSE]	51,7
Q9QUR6	Prolyl endopeptidase OS=Mus musculus GN=Prep PE=1 SV=1 - [PPCE_MOUSE]	80,7
E9PZ00	Prosaposin OS=Mus musculus GN=Psap PE=1 SV=1 - [E9PZ00_MOUSE]	60,6
E9PW69	Proteasome subunit alpha type (Fragment) OS=Mus musculus GN=Psma4 PE=1 SV=1 - [E9PW69_MOUSE]	23,4
Q9R1P4	Proteasome subunit alpha type-1 OS=Mus musculus GN=Psma1 PE=1 SV=1 - [PSA1_MOUSE]	29,5
O70435	Proteasome subunit alpha type-3 OS=Mus musculus GN=Psma3 PE=1 SV=3 - [PSA3_MOUSE]	28,4
Q9Z2U0	Proteasome subunit alpha type-7 OS=Mus musculus GN=Psma7 PE=1 SV=1 - [PSA7_MOUSE]	27,8
Q9R1P3	Proteasome subunit beta type-2 OS=Mus musculus GN=Psmb2 PE=1 SV=1 - [PSB2_MOUSE]	22,9
O55234	Proteasome subunit beta type-5 OS=Mus musculus GN=Psmb5 PE=1 SV=3 - [PSB5_MOUSE]	28,5
Q60692	Proteasome subunit beta type-6 OS=Mus musculus GN=Psmb6 PE=1 SV=3 - [PSB6_MOUSE]	25,4
D3Z3N0	Protein arginine N-methyltransferase 1 OS=Mus musculus GN=Prmt1 PE=1 SV=1 - [D3Z3N0_MOUSE]	29,0
E9Q6C2	Protein C1s1 OS=Mus musculus GN=C1s1 PE=1 SV=1 - [E9Q6C2_MOUSE]	77,5
P27773	Protein disulfide-isomerase A3 OS=Mus musculus GN=Pdia3 PE=1 SV=2 - [PDIA3_MOUSE]	56,6
P08003	Protein disulfide-isomerase A4 OS=Mus musculus GN=Pdia4 PE=1 SV=3 - [PDIA4_MOUSE]	71,9
Q3TML0	Protein disulfide-isomerase A6 OS=Mus musculus GN=Pdia6 PE=1 SV=1 - [Q3TML0_MOUSE]	48,7
P09103	Protein disulfide-isomerase OS=Mus musculus GN=P4hb PE=1 SV=2 - [PDIA1_MOUSE]	57,0
Q64299	Protein NOV homolog OS=Mus musculus GN=Nov PE=1 SV=1 - [NOV_MOUSE]	38,9
F7B9A0	Protein Serpinb6b OS=Mus musculus GN=Serpinb6b PE=1 SV=1 - [F7B9A0_MOUSE]	23,1
O08797	Protein Serpinb9 OS=Mus musculus GN=Serpinb9 PE=1 SV=1 - [O08797_MOUSE]	42,2
B8JJG9	Protein Tfg (Fragment) OS=Mus musculus GN=Tfg PE=1 SV=1 - [B8JJG9_MOUSE]	10,2
E9Q1S3	Protein transport protein Sec23A OS=Mus musculus GN=Sec23a PE=1 SV=1 - [E9Q1S3_MOUSE]	82,9
P28301	Protein-lysine 6-oxidase OS=Mus musculus GN=Lox PE=1 SV=1 - [LYOX_MOUSE]	46,7

P23492	Purine nucleoside phosphorylase OS=Mus musculus GN=Pnp PE=1 SV=2 - [PNPH_MOUSE]	32,3
P52480	Pyruvate kinase PKM OS=Mus musculus GN=Pkm PE=1 SV=4 - [KPYM_MOUSE]	57,8
Q61598	Rab GDP dissociation inhibitor beta OS=Mus musculus GN=Gdi2 PE=1 SV=1 - [GDIB_MOUSE]	50,5
P97855	Ras GTPase-activating protein-binding protein 1 OS=Mus musculus GN=G3bp1 PE=1 SV=1 - [G3BP1_MOUSE]	51,8
P63001;P62998	Ras-related C3 botulinum toxin substrate 1 OS=Mus musculus GN=Rac1 PE=1 SV=1 - [RAC1_MOUSE]	21,4
P62492;F2Z4D5	Ras-related protein Rab-11A OS=Mus musculus GN=Rab11a PE=1 SV=3 - [RB11A_MOUSE]	24,4
Q05186	Reticulocalbin-1 OS=Mus musculus GN=Rcn1 PE=1 SV=1 - [RCN1_MOUSE]	38,1
P24549	Retinal dehydrogenase 1 OS=Mus musculus GN=Aldh1a1 PE=1 SV=5 - [AL1A1_MOUSE]	54,4
Q8C7E4	Ribonuclease 4 OS=Mus musculus GN=Rnase4 PE=1 SV=1 - [Q8C7E4_MOUSE]	17,0
Q91VI7	Ribonuclease inhibitor OS=Mus musculus GN=Rnh1 PE=1 SV=1 - [RINI_MOUSE]	49,8
Q5XJF6;Q5E9E6	Ribosomal protein OS=Mus musculus GN=Rpl10a PE=1 SV=1 - [Q5XJF6_MOUSE]	24,8
P97299	Secreted frizzled-related protein 2 OS=Mus musculus GN=Sfrp2 PE=2 SV=2 - [SFRP2_MOUSE]	33,4
Q8BH34	Semaphorin-3D OS=Mus musculus GN=Sema3d PE=1 SV=1 - [SEM3D_MOUSE]	89,5
A0A0J9YTY0	Septin-11 OS=Mus musculus GN=Sept11 PE=4 SV=1 - [A0A0J9YTY0_MOUSE]	48,9
Q9D6X6	Serine protease 23 OS=Mus musculus GN=Prss23 PE=2 SV=2 - [PRS23_MOUSE]	43,0
Q9R118	Serine protease HTRA1 OS=Mus musculus GN=Htra1 PE=1 SV=2 - [HTRA1_MOUSE]	51,2
Q6PDM2;Q0VCY7	Serine/arginine-rich splicing factor 1 OS=Mus musculus GN=Srsf1 PE=1 SV=3 - [SRSF1_MOUSE]	27,7
P63087;P61287	Serine/threonine-protein phosphatase PP1-gamma catalytic subunit OS=Mus musculus GN=Ppp1cc PE=1 SV=1 - [PP1G_MOUSE]	37,0
A2AFS1	Serine--tRNA ligase, cytoplasmic (Fragment) OS=Mus musculus GN=Sars PE=1 SV=6 - [A2AFS1_MOUSE]	21,2
Q921I1	Serotransferrin OS=Mus musculus GN=Tf PE=1 SV=1 - [TRFE_MOUSE]	76,7
Q60854	Serpin B6 OS=Mus musculus GN=Serpinb6 PE=1 SV=1 - [SPB6_MOUSE]	42,6
P19324	Serpin H1 OS=Mus musculus GN=Serpinh1 PE=1 SV=3 - [SERPH_MOUSE]	46,5
Q5NCU4	SPARC OS=Mus musculus GN=Sparc PE=1 SV=1 - [Q5NCU4_MOUSE]	34,3
Q8VIJ6	Splicing factor, proline- and glutamine-rich OS=Mus musculus GN=Sfpq PE=1 SV=1 - [SFPQ_MOUSE]	75,4
Q8BMS2	Spondin-2 OS=Mus musculus GN=Spon2 PE=2 SV=2 - [SPON2_MOUSE]	35,9
Q78PY7	Staphylococcal nuclease domain-containing protein 1 OS=Mus musculus GN=Snd1 PE=1 SV=1 - [SND1_MOUSE]	102,0
P38647	Stress-70 protein, mitochondrial OS=Mus musculus GN=Hspa9 PE=1 SV=3 - [GRP75_MOUSE]	73,4
Q60864	Stress-induced-phosphoprotein 1 OS=Mus musculus GN=Stip1 PE=1 SV=1 - [STIP1_MOUSE]	62,5
P28862	Stromelysin-1 OS=Mus musculus GN=Mmp3 PE=2 SV=2 - [MMP3_MOUSE]	53,8
Q8BND5	Sulfhydryl oxidase 1 OS=Mus musculus GN=Qsox1 PE=1 SV=1 - [QSOX1_MOUSE]	82,7
P08228	Superoxide dismutase [Cu-Zn] OS=Mus musculus GN=Sod1 PE=1 SV=2 - [SODC_MOUSE]	15,9
P09671	Superoxide dismutase [Mn], mitochondrial OS=Mus musculus GN=Sod2 PE=1 SV=3 - [SODM_MOUSE]	24,6
A2BE45	Sushi-repeat-containing protein SRPX OS=Mus musculus GN=Srpx PE=1 SV=1 - [A2BE45_MOUSE]	49,3
P26039	Talin-1 OS=Mus musculus GN=Tln1 PE=1 SV=2 - [TLN1_MOUSE]	269,7
P80314	T-complex protein 1 subunit beta OS=Mus musculus GN=Cct2 PE=1 SV=4 - [TCPB_MOUSE]	57,4
G5E839	T-complex protein 1 subunit delta OS=Mus musculus GN=Cct4 PE=1 SV=1 - [G5E839_MOUSE]	54,8
P80316	T-complex protein 1 subunit epsilon OS=Mus musculus GN=Cct5 PE=1 SV=1 - [TCPE_MOUSE]	59,6
H3BL49	T-complex protein 1 subunit theta OS=Mus musculus GN=Cct8 PE=1 SV=1 - [H3BL49_MOUSE]	53,0
P80317	T-complex protein 1 subunit zeta OS=Mus musculus GN=Cct6a PE=1 SV=3 - [TCPZ_MOUSE]	58,0
Q80YX0	Tenascin OS=Mus musculus GN=Tnc PE=1 SV=1 - [Q80YX0_MOUSE]	91,1
E9PXX7	Thioredoxin domain-containing protein 5 OS=Mus musculus GN=Txndc5 PE=1 SV=1 - [E9PXX7_MOUSE]	38,5
P10639	Thioredoxin OS=Mus musculus GN=Txn PE=1 SV=3 - [THIO_MOUSE]	11,7
Q9D0R2	Threonine--tRNA ligase, cytoplasmic OS=Mus musculus GN=Tars PE=1 SV=2 - [SYTC_MOUSE]	83,3
P82198	Transforming growth factor-beta-induced protein ig-h3 OS=Mus musculus GN=Tgfbi PE=1 SV=1 - [BGH3_MOUSE]	74,5
P37804	Transgelin OS=Mus musculus GN=Tagln PE=1 SV=3 - [TAGL_MOUSE]	22,6

Q9WVA4	Transgelin-2 OS=Mus musculus GN=Tagln2 PE=1 SV=4 - [TAGL2_MOUSE]	22,4
Q01853	Transitional endoplasmic reticulum ATPase OS=Mus musculus GN=Vcp PE=1 SV=4 - [TERA_MOUSE]	89,3
P40142	Transketolase OS=Mus musculus GN=Tkt PE=1 SV=1 - [TKT_MOUSE]	67,6
P63028	Translationally-controlled tumor protein OS=Mus musculus GN=Tpt1 PE=1 SV=1 - [TCTP_MOUSE]	19,4
P17751	Triosephosphate isomerase OS=Mus musculus GN=Tpi1 PE=1 SV=4 - [TPIS_MOUSE]	32,2
E9Q450	Tropomyosin alpha-1 chain OS=Mus musculus GN=Tpm1 PE=1 SV=1 - [E9Q450_MOUSE]	32,8
D3Z6I8	Tropomyosin alpha-3 chain OS=Mus musculus GN=Tpm3 PE=1 SV=1 - [D3Z6I8_MOUSE]	28,7
Q6IRU2	Tropomyosin alpha-4 chain OS=Mus musculus GN=Tpm4 PE=1 SV=3 - [TPM4_MOUSE]	28,5
A2AIM4	Tropomyosin beta chain OS=Mus musculus GN=Tpm2 PE=1 SV=1 - [A2AIM4_MOUSE]	33,0
P05213;P81947	Tubulin alpha-1B chain OS=Mus musculus GN=Tuba1b PE=1 SV=2 - [TBA1B_MOUSE]	50,1
Q9D6F9;Q3ZBU7	Tubulin beta-4A chain OS=Mus musculus GN=Tubb4a PE=1 SV=3 - [TBB4A_MOUSE]	49,6
P99024;Q2KJD0	Tubulin beta-5 chain OS=Mus musculus GN=Tubb5 PE=1 SV=1 - [TBB5_MOUSE]	49,6
Q91WQ3	Tyrosine--tRNA ligase, cytoplasmic OS=Mus musculus GN=Yars PE=1 SV=3 - [SYYC_MOUSE]	59,1
E9PYI8	Ubiquitin carboxyl-terminal hydrolase OS=Mus musculus GN=Usp14 PE=1 SV=1 - [E9PYI8_MOUSE]	52,3
Q3U4W8	Ubiquitin carboxyl-terminal hydrolase OS=Mus musculus GN=Usp5 PE=1 SV=1 - [Q3U4W8_MOUSE]	93,3
D3YWF6	Ubiquitin thioesterase OTUB1 OS=Mus musculus GN=Otub1 PE=1 SV=1 - [D3YWF6_MOUSE]	28,0
P61089;Q0P5K3	Ubiquitin-conjugating enzyme E2 N OS=Mus musculus GN=Ube2n PE=1 SV=1 - [UBE2N_MOUSE]	17,1
Q02053	Ubiquitin-like modifier-activating enzyme 1 OS=Mus musculus GN=Uba1 PE=1 SV=1 - [UBA1_MOUSE]	117,7
Q3TW96	UDP-N-acetylhexosamine pyrophosphorylase-like protein 1 OS=Mus musculus GN=Uap1l1 PE=1 SV=1 - [UAP1L_MOUSE]	56,6
Q9DBP5	UMP-CMP kinase OS=Mus musculus GN=Cmpk1 PE=1 SV=1 - [KCY_MOUSE]	22,2
Q91ZJ5	UTP--glucose-1-phosphate uridylyltransferase OS=Mus musculus GN=Ugp2 PE=1 SV=3 - [UGPA_MOUSE]	56,9
Q9EQH3	Vacuolar protein sorting-associated protein 35 OS=Mus musculus GN=Vps35 PE=1 SV=1 - [VPS35_MOUSE]	91,7
A0A0G2JFP9	Vascular cell adhesion protein 1 (Fragment) OS=Mus musculus GN=Vcam1 PE=1 SV=1 - [A0A0G2JFP9_MOUSE]	26,4
P20152	Vimentin OS=Mus musculus GN=Vim PE=1 SV=3 - [VIME_MOUSE]	53,7
Q64727	Vinculin OS=Mus musculus GN=Vcl PE=1 SV=4 - [VINC_MOUSE]	116,6
O88342	WD repeat-containing protein 1 OS=Mus musculus GN=Wdr1 PE=1 SV=3 - [WDR1_MOUSE]	66,4
Q62523	Zyxin OS=Mus musculus GN=Zyx PE=1 SV=2 - [ZYX_MOUSE]	60,5

E. Osteoblastos Humanos

Accession	Description	MW [kDa]
P62258;P62261	14-3-3 protein epsilon OS=Homo sapiens GN=YWHAE PE=1 SV=1 - [1433E_HUMAN]	29,2
Q04917	14-3-3 protein eta OS=Homo sapiens GN=YWHAH PE=1 SV=4 - [1433F_HUMAN]	28,2
P61981;A7Z057	14-3-3 protein gamma OS=Homo sapiens GN=YWHAG PE=1 SV=2 - [1433G_HUMAN]	28,3
P27348;Q3SZI4	14-3-3 protein theta OS=Homo sapiens GN=YWHAQ PE=1 SV=1 - [1433T_HUMAN]	27,7
P63104;P63103	14-3-3 protein zeta/delta OS=Homo sapiens GN=YWHAZ PE=1 SV=1 - [1433Z_HUMAN]	27,7
P62280;Q3T0V4	40S ribosomal protein S11 OS=Homo sapiens GN=RPS11 PE=1 SV=3 - [RS11_HUMAN]	18,4
P62263	40S ribosomal protein S14 OS=Homo sapiens GN=RPS14 PE=1 SV=3 - [RS14_HUMAN]	16,3
P62244;Q76I82	40S ribosomal protein S15a OS=Homo sapiens GN=RPS15A PE=1 SV=2 - [RS15A_HUMAN]	14,8
P62249;Q3T0X6	40S ribosomal protein S16 OS=Homo sapiens GN=RPS16 PE=1 SV=2 - [RS16_HUMAN]	16,4
P23396;Q3T169	40S ribosomal protein S3 OS=Homo sapiens GN=RPS3 PE=1 SV=2 - [RS3_HUMAN]	26,7
P61247;Q56JV9	40S ribosomal protein S3a OS=Homo sapiens GN=RPS3A PE=1 SV=2 - [RS3A_HUMAN]	29,9
P62701;P79103	40S ribosomal protein S4, X isoform OS=Homo sapiens GN=RPS4X PE=1 SV=2 - [RS4X_HUMAN]	29,6
P62241;Q5E958	40S ribosomal protein S8 OS=Homo sapiens GN=RPS8 PE=1 SV=2 - [RS8_HUMAN]	24,2
P46781;A6QLG5	40S ribosomal protein S9 OS=Homo sapiens GN=RPS9 PE=1 SV=3 - [RS9_HUMAN]	22,6

C9J9K3	40S ribosomal protein SA (Fragment) OS=Homo sapiens GN=RPSA PE=1 SV=4 - [C9J9K3_HUMAN]	29,4
P10809	60 kDa heat shock protein, mitochondrial OS=Homo sapiens GN=HSPD1 PE=1 SV=2 - [CH60_HUMAN]	61,0
G3V210	60S acidic ribosomal protein P0 OS=Homo sapiens GN=RPLP0 PE=1 SV=1 - [G3V210_HUMAN]	18,3
P30050;P61284	60S ribosomal protein L12 OS=Homo sapiens GN=RPL12 PE=1 SV=1 - [RL12_HUMAN]	17,8
E7EPB3	60S ribosomal protein L14 OS=Homo sapiens GN=RPL14 PE=1 SV=1 - [E7EPB3_HUMAN]	14,5
Q02543;Q3T003	60S ribosomal protein L18a OS=Homo sapiens GN=RPL18A PE=1 SV=2 - [RL18A_HUMAN]	20,7
P36578	60S ribosomal protein L4 OS=Homo sapiens GN=RPL4 PE=1 SV=5 - [RL4_HUMAN]	47,7
Q5T7N0	60S ribosomal protein L5 (Fragment) OS=Homo sapiens GN=RPL5 PE=1 SV=2 - [Q5T7N0_HUMAN]	14,1
M0R0U3	6-phosphogluconolactonase OS=Homo sapiens GN=PGLS PE=1 SV=1 - [M0R0U3_HUMAN]	18,9
H0YN26	Acidic leucine-rich nuclear phosphoprotein 32 family member A OS=Homo sapiens GN=ANP32A PE=1 SV=1 - [H0YN26_HUMAN]	20,0
P68032;Q3ZC07	Actin, alpha cardiac muscle 1 OS=Homo sapiens GN=ACTC1 PE=1 SV=1 - [ACTC_HUMAN]	42,0
P60709;P60712	Actin, cytoplasmic 1 OS=Homo sapiens GN=ACTB PE=1 SV=1 - [ACTB_HUMAN]	41,7
P61160;A7MB62	Actin-related protein 2 OS=Homo sapiens GN=ACTR2 PE=1 SV=1 - [ARP2_HUMAN]	44,7
P23526	Adenosylhomocysteinase OS=Homo sapiens GN=AHCY PE=1 SV=4 - [SAHH_HUMAN]	47,7
P00568	Adenylate kinase isoenzyme 1 OS=Homo sapiens GN=AK1 PE=1 SV=3 - [KAD1_HUMAN]	21,6
P61204;Q5E9I6	ADP-ribosylation factor 3 OS=Homo sapiens GN=ARF3 PE=1 SV=2 - [ARF3_HUMAN]	20,6
P14550	Alcohol dehydrogenase [NADP(+)] OS=Homo sapiens GN=AKR1A1 PE=1 SV=3 - [AK1A1_HUMAN]	36,5
P15121	Aldose reductase OS=Homo sapiens GN=AKR1B1 PE=1 SV=3 - [ALDR_HUMAN]	35,8
O43707	Alpha-actinin-4 OS=Homo sapiens GN=ACTN4 PE=1 SV=2 - [ACTN4_HUMAN]	104,8
P06733	Alpha-enolase OS=Homo sapiens GN=ENO1 PE=1 SV=2 - [ENOA_HUMAN]	47,1
P02771	Alpha-fetoprotein OS=Homo sapiens GN=AFP PE=1 SV=1 - [FETA_HUMAN]	68,6
P04083	Annexin A1 OS=Homo sapiens GN=ANXA1 PE=1 SV=2 - [ANXA1_HUMAN]	38,7
P07355	Annexin A2 OS=Homo sapiens GN=ANXA2 PE=1 SV=2 - [ANXA2_HUMAN]	38,6
P08758	Annexin A5 OS=Homo sapiens GN=ANXA5 PE=1 SV=2 - [ANXA5_HUMAN]	35,9
P00505	Aspartate aminotransferase, mitochondrial OS=Homo sapiens GN=GOT2 PE=1 SV=3 - [AATM_HUMAN]	47,5
F8W079	ATP synthase subunit beta, mitochondrial (Fragment) OS=Homo sapiens GN=ATP5B PE=1 SV=1 - [F8W079_HUMAN]	30,2
P98160	Basement membrane-specific heparan sulfate proteoglycan core protein OS=Homo sapiens GN=HSPG2 PE=1 SV=4 - [PGBM_HUMAN]	468,5
P07686	Beta-hexosaminidase subunit beta OS=Homo sapiens GN=HEXB PE=1 SV=3 - [HEXB_HUMAN]	63,1
P07814	Bifunctional glutamate/proline--tRNA ligase OS=Homo sapiens GN=EPRS PE=1 SV=5 - [SYEP_HUMAN]	170,5
P27797	Calreticulin OS=Homo sapiens GN=CALR PE=1 SV=1 - [CALR_HUMAN]	48,1
P07858	Cathepsin B OS=Homo sapiens GN=CTSB PE=1 SV=3 - [CATB_HUMAN]	37,8
F8WD96	Cathepsin D OS=Homo sapiens GN=CTSD PE=1 SV=1 - [F8WD96_HUMAN]	30,0
Q9UBR2	Cathepsin Z OS=Homo sapiens GN=CTSZ PE=1 SV=1 - [CATZ_HUMAN]	33,8
F5GXJ9	CD166 antigen OS=Homo sapiens GN=ALCAM PE=1 SV=1 - [F5GXJ9_HUMAN]	59,5
E9PKC6	CD44 antigen OS=Homo sapiens GN=CD44 PE=1 SV=1 - [E9PKC6_HUMAN]	8,8
P60953;Q2KJ93	Cell division control protein 42 homolog OS=Homo sapiens GN=CDC42 PE=1 SV=2 - [CDC42_HUMAN]	21,2
O00299	Chloride intracellular channel protein 1 OS=Homo sapiens GN=CLIC1 PE=1 SV=4 - [CLIC1_HUMAN]	26,9
Q13185	Chromobox protein homolog 3 OS=Homo sapiens GN=CBX3 PE=1 SV=4 - [CBX3_HUMAN]	20,8
P53621	Coatomer subunit alpha OS=Homo sapiens GN=COPA PE=1 SV=2 - [COPA_HUMAN]	138,3
P48444	Coatomer subunit delta OS=Homo sapiens GN=ARCN1 PE=1 SV=1 - [COPD_HUMAN]	57,2
Q9Y678	Coatomer subunit gamma-1 OS=Homo sapiens GN=COPG1 PE=1 SV=1 - [COPG1_HUMAN]	97,7
P02452	Collagen alpha-1(I) chain OS=Homo sapiens GN=COL1A1 PE=1 SV=5 - [CO1A1_HUMAN]	138,9
A0A087WXW9	Collagen alpha-1(V) chain OS=Homo sapiens GN=COL5A1 PE=1 SV=1 - [A0A087WXW9_HUMAN]	183,5
A0A087X0S5	Collagen alpha-1(VI) chain OS=Homo sapiens GN=COL6A1 PE=1 SV=1 - [A0A087X0S5_HUMAN]	108,3

A0A087WTA8	Collagen alpha-2(I) chain OS=Homo sapiens GN=COL1A2 PE=1 SV=1 - [A0A087WTA8_HUMAN]	129,1
P12110	Collagen alpha-2(VI) chain OS=Homo sapiens GN=COL6A2 PE=1 SV=4 - [CO6A2_HUMAN]	108,5
P00736	Complement C1r subcomponent OS=Homo sapiens GN=C1R PE=1 SV=2 - [C1R_HUMAN]	80,1
P01024	Complement C3 OS=Homo sapiens GN=C3 PE=1 SV=2 - [CO3_HUMAN]	187,0
Q07021	Complement component 1 Q subcomponent-binding protein, mitochondrial OS=Homo sapiens GN=C1QBP PE=1 SV=1 - [C1QBP_HUMAN]	31,3
Q9BR76	Coronin-1B OS=Homo sapiens GN=CORO1B PE=1 SV=1 - [COR1B_HUMAN]	54,2
E9PND2	Cysteine and glycine-rich protein 1 (Fragment) OS=Homo sapiens GN=CSRP1 PE=1 SV=1 - [E9PND2_HUMAN]	16,1
C9JFR7	Cytochrome c (Fragment) OS=Homo sapiens GN=CYCS PE=1 SV=1 - [C9JFR7_HUMAN]	11,3
Q5SZU1	D-3-phosphoglycerate dehydrogenase OS=Homo sapiens GN=PHGDH PE=1 SV=1 - [Q5SZU1_HUMAN]	53,1
P81605	Dermcidin OS=Homo sapiens GN=DCD PE=1 SV=2 - [DCD_HUMAN]	11,3
Q14126	Desmoglein-2 OS=Homo sapiens GN=DSG2 PE=1 SV=2 - [DSG2_HUMAN]	122,2
P60981;Q5E9D5	Destrin OS=Homo sapiens GN=DSTN PE=1 SV=3 - [DEST_HUMAN]	18,5
G3V5Q1	DNA-(apurinic or apyrimidinic site) lyase (Fragment) OS=Homo sapiens GN=APEX1 PE=1 SV=1 - [G3V5Q1_HUMAN]	27,1
A0A0C4DGL3	DUTP pyrophosphatase, isoform CRA_c OS=Homo sapiens GN=DUT PE=4 SV=1 - [A0A0C4DGL3_HUMAN]	15,4
E9PRU1	EGF-containing fibulin-like extracellular matrix protein 2 OS=Homo sapiens GN=EFEMP2 PE=1 SV=1 - [E9PRU1_HUMAN]	48,2
P68104;P68103	Elongation factor 1-alpha 1 OS=Homo sapiens GN=EEF1A1 PE=1 SV=1 - [EF1A1_HUMAN]	50,1
P26641	Elongation factor 1-gamma OS=Homo sapiens GN=EEF1G PE=1 SV=3 - [EF1G_HUMAN]	50,1
P14625	Endoplasmin OS=Homo sapiens GN=HSP90B1 PE=1 SV=1 - [ENPL_HUMAN]	92,4
P60842;Q3SZ54	Eukaryotic initiation factor 4A-I OS=Homo sapiens GN=EIF4A1 PE=1 SV=1 - [IF4A1_HUMAN]	46,1
Q14240;Q3SZ65	Eukaryotic initiation factor 4A-II OS=Homo sapiens GN=EIF4A2 PE=1 SV=2 - [IF4A2_HUMAN]	46,4
P62495;Q0VCX5	Eukaryotic peptide chain release factor subunit 1 OS=Homo sapiens GN=ETF1 PE=1 SV=3 - [ERF1_HUMAN]	49,0
P41091	Eukaryotic translation initiation factor 2 subunit 3 OS=Homo sapiens GN=EIF2S3 PE=1 SV=3 - [IF2G_HUMAN]	51,1
Q9GZV4;F1MN49	Eukaryotic translation initiation factor 5A-2 OS=Homo sapiens GN=EIF5A2 PE=1 SV=3 - [IF5A2_HUMAN]	16,8
Q16610	Extracellular matrix protein 1 OS=Homo sapiens GN=ECM1 PE=1 SV=2 - [ECM1_HUMAN]	60,6
E7EQR4	Ezrin OS=Homo sapiens GN=EZR PE=1 SV=3 - [E7EQR4_HUMAN]	69,3
Q16658	Fascin OS=Homo sapiens GN=FSCN1 PE=1 SV=3 - [FSCN1_HUMAN]	54,5
Q01469	Fatty acid-binding protein, epidermal OS=Homo sapiens GN=FABP5 PE=1 SV=3 - [FABP5_HUMAN]	15,2
Q9NQ88	Fructose-2,6-bisphosphatase TIGAR OS=Homo sapiens GN=TIGAR PE=1 SV=1 - [TIGAR_HUMAN]	30,0
P04075	Fructose-bisphosphate aldolase A OS=Homo sapiens GN=ALDOA PE=1 SV=2 - [ALDOA_HUMAN]	39,4
P09382	Galectin-1 OS=Homo sapiens GN=LGALS1 PE=1 SV=2 - [LEG1_HUMAN]	14,7
Q08380	Galectin-3-binding protein OS=Homo sapiens GN=LGALS3BP PE=1 SV=1 - [LG3BP_HUMAN]	65,3
Q92820	Gamma-glutamyl hydrolase OS=Homo sapiens GN=GGH PE=1 SV=2 - [GGH_HUMAN]	35,9
B8ZZK2	Gamma-glutamylcyclotransferase OS=Homo sapiens GN=GGCT PE=1 SV=1 - [B8ZZK2_HUMAN]	18,4
K7EQ48	Glucose-6-phosphate isomerase OS=Homo sapiens GN=GPI PE=1 SV=2 - [K7EQ48_HUMAN]	53,4
Q16769	Glutaminyl-peptide cyclotransferase OS=Homo sapiens GN=QPCT PE=1 SV=1 - [QPCT_HUMAN]	40,9
O76003	Glutaredoxin-3 OS=Homo sapiens GN=GLRX3 PE=1 SV=2 - [GLRX3_HUMAN]	37,4
Q5TA02	Glutathione S-transferase omega-1 (Fragment) OS=Homo sapiens GN=GSTO1 PE=1 SV=1 - [Q5TA02_HUMAN]	23,3
A0A087X2E9	Glutathione S-transferase P (Fragment) OS=Homo sapiens GN=GSTP1 PE=1 SV=1 - [A0A087X2E9_HUMAN]	8,9
P04406	Glyceraldehyde-3-phosphate dehydrogenase OS=Homo sapiens GN=GAPDH PE=1 SV=3 - [G3P_HUMAN]	36,0
P62826;Q3T054	GTP-binding nuclear protein Ran OS=Homo sapiens GN=RAN PE=1 SV=3 - [RAN_HUMAN]	24,4
P63244;P63243	Guanine nucleotide-binding protein subunit beta-2-like 1 OS=Homo sapiens GN=GNB2L1 PE=1 SV=3 - [GBLP_HUMAN]	35,1
G3V1N2	HCG1745306, isoform CRA_a OS=Homo sapiens GN=HBA2 PE=1 SV=1 - [G3V1N2_HUMAN]	11,9

P08107	Heat shock 70 kDa protein 1A/1B OS=Homo sapiens GN=HSPA1A PE=1 SV=5 - [HSP71_HUMAN]	70,0
Q9NRV9	Heme-binding protein 1 OS=Homo sapiens GN=HEBP1 PE=1 SV=1 - [HEBP1_HUMAN]	21,1
D6R9P3	Heterogeneous nuclear ribonucleoprotein A/B OS=Homo sapiens GN=HNRNPAB PE=1 SV=1 - [D6R9P3_HUMAN]	30,3
H0YA96	Heterogeneous nuclear ribonucleoprotein D0 (Fragment) OS=Homo sapiens GN=HNRNPD PE=1 SV=1 - [H0YA96_HUMAN]	23,9
Q5T6W2	Heterogeneous nuclear ribonucleoprotein K (Fragment) OS=Homo sapiens GN=HNRNPK PE=1 SV=1 - [Q5T6W2_HUMAN]	41,8
B4DT28	Heterogeneous nuclear ribonucleoprotein R OS=Homo sapiens GN=HNRNPR PE=1 SV=1 - [B4DT28_HUMAN]	55,7
G3V5X6	Heterogeneous nuclear ribonucleoproteins C1/C2 (Fragment) OS=Homo sapiens GN=HNRNPC PE=1 SV=1 - [G3V5X6_HUMAN]	12,8
Q5T7C4	High mobility group protein B1 OS=Homo sapiens GN=HMGB1 PE=1 SV=1 - [Q5T7C4_HUMAN]	18,3
P26583;P40673	High mobility group protein B2 OS=Homo sapiens GN=HMGB2 PE=1 SV=2 - [HMGB2_HUMAN]	24,0
B4E1C5	Histidine--tRNA ligase, cytoplasmic OS=Homo sapiens GN=HARS PE=1 SV=1 - [B4E1C5_HUMAN]	43,9
Q16777;A1A4R1	Histone H2A type 2-C OS=Homo sapiens GN=HIST2H2AC PE=1 SV=4 - [H2A2C_HUMAN]	14,0
O60814;F2Z4F9	Histone H2B type 1-K OS=Homo sapiens GN=HIST1H2BK PE=1 SV=3 - [H2B1K_HUMAN]	13,9
P62805;P62803	Histone H4 OS=Homo sapiens GN=HIST1H4A PE=1 SV=2 - [H4_HUMAN]	11,4
Q09028;Q3MHL3	Histone-binding protein RBBP4 OS=Homo sapiens GN=RBBP4 PE=1 SV=3 - [RBBP4_HUMAN]	47,6
E9PC52	Histone-binding protein RBBP7 OS=Homo sapiens GN=RBBP7 PE=1 SV=1 - [E9PC52_HUMAN]	46,9
P10316	HLA class I histocompatibility antigen, A-69 alpha chain OS=Homo sapiens GN=HLA-A PE=1 SV=2 - [1A69_HUMAN]	41,0
P30508	HLA class I histocompatibility antigen, Cw-12 alpha chain OS=Homo sapiens GN=HLA-C PE=1 SV=2 - [1C12_HUMAN]	40,9
Q95604	HLA class I histocompatibility antigen, Cw-17 alpha chain OS=Homo sapiens GN=HLA-C PE=1 SV=1 - [1C17_HUMAN]	41,2
A0A087WWL9	HLA class I histocompatibility antigen, Cw-6 alpha chain OS=Homo sapiens GN=HLA-C PE=1 SV=1 - [A0A087WWL9_HUMAN]	36,5
Q86YZ3	Hornerin OS=Homo sapiens GN=HRNR PE=1 SV=2 - [HORN_HUMAN]	282,2
H7C3I1	Hsc70-interacting protein (Fragment) OS=Homo sapiens GN=ST13 PE=1 SV=1 - [H7C3I1_HUMAN]	16,3
P08476	Inhibin beta A chain OS=Homo sapiens GN=INHBA PE=1 SV=2 - [INHBA_HUMAN]	47,4
H0Y9D8	Inorganic pyrophosphatase 2, mitochondrial (Fragment) OS=Homo sapiens GN=PPA2 PE=1 SV=1 - [H0Y9D8_HUMAN]	25,6
H0YBL1	Inositol monophosphatase 1 (Fragment) OS=Homo sapiens GN=IMPA1 PE=1 SV=1 - [H0YBL1_HUMAN]	28,6
F8W8T1	Interferon-induced GTP-binding protein Mx1 OS=Homo sapiens GN=MX1 PE=1 SV=1 - [F8W8T1_HUMAN]	73,3
P32455	Interferon-induced guanylate-binding protein 1 OS=Homo sapiens GN=GBP1 PE=1 SV=2 - [GBP1_HUMAN]	67,9
B5MCZ3	Interleukin-6 OS=Homo sapiens GN=IL6 PE=1 SV=1 - [B5MCZ3_HUMAN]	21,5
O75874	Isocitrate dehydrogenase [NADP] cytoplasmic OS=Homo sapiens GN=IDH1 PE=1 SV=2 - [IDHC_HUMAN]	46,6
P18206-2	Isoform 1 of Vinculin OS=Homo sapiens GN=VCL - [VINC_HUMAN]	116,6
P02751-12	Isoform 12 of Fibronectin OS=Homo sapiens GN=FN1 - [FINC_HUMAN]	221,2
P21589-2	Isoform 2 of 5'-nucleotidase OS=Homo sapiens GN=NT5E - [5NTD_HUMAN]	57,9
P52209-2	Isoform 2 of 6-phosphogluconate dehydrogenase, decarboxylating OS=Homo sapiens GN=PGD - [6PGD_HUMAN]	51,8
P08253-2	Isoform 2 of 72 kDa type IV collagenase OS=Homo sapiens GN=MMP2 - [MMP2_HUMAN]	65,7
Q01518-2	Isoform 2 of Adenylyl cyclase-associated protein 1 OS=Homo sapiens GN=CAP1 - [CAP1_HUMAN]	51,8
P08133-2	Isoform 2 of Annexin A6 OS=Homo sapiens GN=ANXA6 - [ANXA6_HUMAN]	72,4
P17174-2	Isoform 2 of Aspartate aminotransferase, cytoplasmic OS=Homo sapiens GN=GOT1 - [AATC_HUMAN]	44,1
Q7L1Q6-2	Isoform 2 of Basic leucine zipper and W2 domain-containing protein 1 OS=Homo sapiens GN=BZW1 - [BZW1_HUMAN]	40,5
P17655-2	Isoform 2 of Calpain-2 catalytic subunit OS=Homo sapiens GN=CAPN2 - [CAN2_HUMAN]	71,4
O94985-2	Isoform 2 of Calsyntenin-1 OS=Homo sapiens GN=CLSTN1 - [CSTN1_HUMAN]	108,6
Q9UI42-2	Isoform 2 of Carboxypeptidase A4 OS=Homo sapiens GN=CPA4 - [CBPA4_HUMAN]	43,5

P62633-2;Q3T0Q6	Isoform 2 of Cellular nucleic acid-binding protein OS=Homo sapiens GN=CNBP - [CNBP_HUMAN]	18,7
P0C0L4-2	Isoform 2 of Complement C4-A OS=Homo sapiens GN=C4A - [CO4A_HUMAN]	187,6
P28838-2	Isoform 2 of Cytosol aminopeptidase OS=Homo sapiens GN=LAP3 - [AMPL_HUMAN]	52,7
P09622-2	Isoform 2 of Dihydrolipoyl dehydrogenase, mitochondrial OS=Homo sapiens GN=DLD - [DLDH_HUMAN]	43,6
Q16555-2	Isoform 2 of Dihydropyrimidinase-related protein 2 OS=Homo sapiens GN=DPYSL2 - [DPYL2_HUMAN]	58,1
P47756-2;P79136-2	Isoform 2 of F-actin-capping protein subunit beta OS=Homo sapiens GN=CAPZB - [CAPZB_HUMAN]	30,6
Q14315-2	Isoform 2 of Filamin-C OS=Homo sapiens GN=FLNC - [FLNC_HUMAN]	287,1
Q12841-2	Isoform 2 of Follistatin-related protein 1 OS=Homo sapiens GN=FSTL1 - [FSTL1_HUMAN]	31,2
P09104-2	Isoform 2 of Gamma-enolase OS=Homo sapiens GN=ENO2 - [ENOG_HUMAN]	42,7
P07093-2	Isoform 2 of Glia-derived nexin OS=Homo sapiens GN=SERPINE2 - [GDN_HUMAN]	44,0
Q9HC38-2	Isoform 2 of Glyoxalase domain-containing protein 4 OS=Homo sapiens GN=GLOD4 - [GLOD4_HUMAN]	33,2
P22692-2	Isoform 2 of Insulin-like growth factor-binding protein 4 OS=Homo sapiens GN=IGFBP4 - [IBP4_HUMAN]	17,6
Q16270-2	Isoform 2 of Insulin-like growth factor-binding protein 7 OS=Homo sapiens GN=IGFBP7 - [IBP7_HUMAN]	28,8
Q08431-2	Isoform 2 of Lactadherin OS=Homo sapiens GN=MFGE8 - [MFGM_HUMAN]	35,2
Q04760-2	Isoform 2 of Lactoylglutathione lyase OS=Homo sapiens GN=GLO1 - [LGUL_HUMAN]	19,0
P40121-2	Isoform 2 of Macrophage-capping protein OS=Homo sapiens GN=CAPG - [CAPG_HUMAN]	36,8
P28482-2	Isoform 2 of Mitogen-activated protein kinase 1 OS=Homo sapiens GN=MAPK1 - [MK01_HUMAN]	36,4
O43684-2;Q1JQB2	Isoform 2 of Mitotic checkpoint protein BUB3 OS=Homo sapiens GN=BUB3 - [BUB3_HUMAN]	36,9
P00558-2	Isoform 2 of Phosphoglycerate kinase 1 OS=Homo sapiens GN=PGK1 - [PGK1_HUMAN]	41,4
P25788-2	Isoform 2 of Proteasome subunit alpha type-3 OS=Homo sapiens GN=PSMA3 - [PSA3_HUMAN]	27,6
O75326-2	Isoform 2 of Semaphorin-7A OS=Homo sapiens GN=SEMA7A - [SEM7A_HUMAN]	73,3
O95084-2	Isoform 2 of Serine protease 23 OS=Homo sapiens GN=PRSS23 - [PRS23_HUMAN]	39,6
O00391-2	Isoform 2 of Sulfhydryl oxidase 1 OS=Homo sapiens GN=QSOX1 - [QSOX1_HUMAN]	66,8
P50991-2	Isoform 2 of T-complex protein 1 subunit delta OS=Homo sapiens GN=CCT4 - [TCPD_HUMAN]	54,7
P48643-2	Isoform 2 of T-complex protein 1 subunit epsilon OS=Homo sapiens GN=CCT5 - [TCPE_HUMAN]	49,5
P50990-2	Isoform 2 of T-complex protein 1 subunit theta OS=Homo sapiens GN=CCT8 - [TCPQ_HUMAN]	57,6
P40227-2	Isoform 2 of T-complex protein 1 subunit zeta OS=Homo sapiens GN=CCT6A - [TCPZ_HUMAN]	53,3
Q8NBS9-2	Isoform 2 of Thioredoxin domain-containing protein 5 OS=Homo sapiens GN=TXNDC5 - [TXND5_HUMAN]	36,2
P10599-2	Isoform 2 of Thioredoxin OS=Homo sapiens GN=TXN - [THIO_HUMAN]	9,4
P30048-2	Isoform 2 of Thioredoxin-dependent peroxide reductase, mitochondrial OS=Homo sapiens GN=PRDX3 - [PRDX3_HUMAN]	25,8
P60174-1	Isoform 2 of Triosephosphate isomerase OS=Homo sapiens GN=TPI1 - [TPIS_HUMAN]	26,7
P06753-2;Q5KR47-2	Isoform 2 of Tropomyosin alpha-3 chain OS=Homo sapiens GN=TPM3 - [TPM3_HUMAN]	29,0
P23381-2	Isoform 2 of Tryptophan--tRNA ligase, cytoplasmic OS=Homo sapiens GN=WARS - [SYWC_HUMAN]	48,8
P22314-2	Isoform 2 of Ubiquitin-like modifier-activating enzyme 1 OS=Homo sapiens GN=UBA1 - [UBA1_HUMAN]	113,7
P63010-3	Isoform 3 of AP-2 complex subunit beta OS=Homo sapiens GN=AP2B1 - [AP2B1_HUMAN]	98,1
P55060-3	Isoform 3 of Exportin-2 OS=Homo sapiens GN=CSE1L - [XPO2_HUMAN]	107,7
O14979-3	Isoform 3 of Heterogeneous nuclear ribonucleoprotein D-like OS=Homo sapiens GN=HNRNPDL - [HNRDL_HUMAN]	27,2
P13797-3	Isoform 3 of Plastin-3 OS=Homo sapiens GN=PLS3 - [PLST_HUMAN]	65,6
Q99832-3	Isoform 3 of T-complex protein 1 subunit eta OS=Homo sapiens GN=CCT7 - [TCPH_HUMAN]	54,8
P00750-3	Isoform 3 of Tissue-type plasminogen activator OS=Homo sapiens GN=PLAT - [TPA_HUMAN]	57,3
P12955-3	Isoform 3 of Xaa-Pro dipeptidase OS=Homo sapiens GN=PEPD - [PEPD_HUMAN]	47,2
Q9NY33-4	Isoform 4 of Dipeptidyl peptidase 3 OS=Homo sapiens GN=DPP3 - [DPP3_HUMAN]	79,3

O60506-4	Isoform 4 of Heterogeneous nuclear ribonucleoprotein Q OS=Homo sapiens GN=SYNCRIP - [HNRPQ_HUMAN]	58,7
Q13492-4	Isoform 4 of Phosphatidylinositol-binding clathrin assembly protein OS=Homo sapiens GN=PICALM - [PICAL_HUMAN]	59,9
Q99873-4;Q5E949	Isoform 4 of Protein arginine N-methyltransferase 1 OS=Homo sapiens GN=PRMT1 - [ANM1_HUMAN]	40,5
O43852-5	Isoform 5 of Calumenin OS=Homo sapiens GN=CALU - [CALU_HUMAN]	26,9
Q12906-5	Isoform 5 of Interleukin enhancer-binding factor 3 OS=Homo sapiens GN=ILF3 - [ILF3_HUMAN]	74,6
O75369-6	Isoform 6 of Filamin-B OS=Homo sapiens GN=FLNB - [FLNB_HUMAN]	271,2
Q15149-7	Isoform 7 of Plectin OS=Homo sapiens GN=PLEC - [PLEC_HUMAN]	512,3
P09651-2;P09867	Isoform A1-A of Heterogeneous nuclear ribonucleoprotein A1 OS=Homo sapiens GN=HNRNPA1 - [ROA1_HUMAN]	34,2
P22626-2;Q2HJ60	Isoform A2 of Heterogeneous nuclear ribonucleoproteins A2/B1 OS=Homo sapiens GN=HNRNPA2B1 - [ROA2_HUMAN]	36,0
P23142-4	Isoform C of Fibulin-1 OS=Homo sapiens GN=FBLN1 - [FBLN1_HUMAN]	74,4
P02545-2	Isoform C of Prelamin-A/C OS=Homo sapiens GN=LMNA - [LMNA_HUMAN]	65,1
P30044-2	Isoform Cytoplasmic+peroxisomal of Peroxiredoxin-5, mitochondrial OS=Homo sapiens GN=PRDX5 - [PRDX5_HUMAN]	17,0
P13645	Keratin, type I cytoskeletal 10 OS=Homo sapiens GN=KRT10 PE=1 SV=6 - [K1C10_HUMAN]	58,8
P02533	Keratin, type I cytoskeletal 14 OS=Homo sapiens GN=KRT14 PE=1 SV=4 - [K1C14_HUMAN]	51,5
P08779	Keratin, type I cytoskeletal 16 OS=Homo sapiens GN=KRT16 PE=1 SV=4 - [K1C16_HUMAN]	51,2
P35527	Keratin, type I cytoskeletal 9 OS=Homo sapiens GN=KRT9 PE=1 SV=3 - [K1C9_HUMAN]	62,0
P04264	Keratin, type II cytoskeletal 1 OS=Homo sapiens GN=KRT1 PE=1 SV=6 - [K2C1_HUMAN]	66,0
P35908	Keratin, type II cytoskeletal 2 epidermal OS=Homo sapiens GN=KRT2 PE=1 SV=2 - [K22E_HUMAN]	65,4
P13647	Keratin, type II cytoskeletal 5 OS=Homo sapiens GN=KRT5 PE=1 SV=3 - [K2C5_HUMAN]	62,3
P04259	Keratin, type II cytoskeletal 6B OS=Homo sapiens GN=KRT6B PE=1 SV=5 - [K2C6B_HUMAN]	60,0
Q7RTS7	Keratin, type II cytoskeletal 74 OS=Homo sapiens GN=KRT74 PE=1 SV=2 - [K2C74_HUMAN]	57,8
P05787	Keratin, type II cytoskeletal 8 OS=Homo sapiens GN=KRT8 PE=1 SV=7 - [K2C8_HUMAN]	53,7
P20700	Lamin-B1 OS=Homo sapiens GN=LMNB1 PE=1 SV=2 - [LMNB1_HUMAN]	66,4
Q03252	Lamin-B2 OS=Homo sapiens GN=LMNB2 PE=1 SV=3 - [LMNB2_HUMAN]	67,6
C9J9W2	LIM and SH3 domain protein 1 (Fragment) OS=Homo sapiens GN=LASP1 PE=1 SV=1 - [C9J9W2_HUMAN]	19,0
P00338	L-lactate dehydrogenase A chain OS=Homo sapiens GN=LDHA PE=1 SV=2 - [LDHA_HUMAN]	36,7
P07195	L-lactate dehydrogenase B chain OS=Homo sapiens GN=LDHB PE=1 SV=2 - [LDHB_HUMAN]	36,6
Q9Y4K0	Lysyl oxidase homolog 2 OS=Homo sapiens GN=LOXL2 PE=1 SV=1 - [LOXL2_HUMAN]	86,7
P40925	Malate dehydrogenase, cytoplasmic OS=Homo sapiens GN=MDH1 PE=1 SV=4 - [MDHC_HUMAN]	36,4
P40926	Malate dehydrogenase, mitochondrial OS=Homo sapiens GN=MDH2 PE=1 SV=3 - [MDHM_HUMAN]	35,5
Q5H9A7	Metalloproteinase inhibitor 1 OS=Homo sapiens GN=TIMP1 PE=1 SV=1 - [Q5H9A7_HUMAN]	16,0
Q15691	Microtubule-associated protein RP/EB family member 1 OS=Homo sapiens GN=MAPRE1 PE=1 SV=3 - [MARE1_HUMAN]	30,0
P60660;P60661	Myosin light polypeptide 6 OS=Homo sapiens GN=MYL6 PE=1 SV=2 - [MYL6_HUMAN]	16,9
P35579	Myosin-9 OS=Homo sapiens GN=MYH9 PE=1 SV=4 - [MYH9_HUMAN]	226,4
H0YFA9	N-acetylglucosamine-6-sulfatase (Fragment) OS=Homo sapiens GN=GNS PE=1 SV=1 - [H0YFA9_HUMAN]	34,7
Q9Y266	Nuclear migration protein nudC OS=Homo sapiens GN=NUDC PE=1 SV=1 - [NUDC_HUMAN]	38,2
P67809;P67808	Nuclease-sensitive element-binding protein 1 OS=Homo sapiens GN=YBX1 PE=1 SV=3 - [YBOX1_HUMAN]	35,9
Q02818	Nucleobindin-1 OS=Homo sapiens GN=NUCB1 PE=1 SV=4 - [NUCB1_HUMAN]	53,8
P19338	Nucleolin OS=Homo sapiens GN=NCL PE=1 SV=3 - [NUCL_HUMAN]	76,6
P15531	Nucleoside diphosphate kinase A OS=Homo sapiens GN=NME1 PE=1 SV=1 - [NDKA_HUMAN]	17,1
P26022	Pentraxin-related protein PTX3 OS=Homo sapiens GN=PTX3 PE=1 SV=3 - [PTX3_HUMAN]	41,9
P62937	Peptidyl-prolyl cis-trans isomerase A OS=Homo sapiens GN=PPIA PE=1 SV=2 - [PPIA_HUMAN]	18,0
P23284	Peptidyl-prolyl cis-trans isomerase B OS=Homo sapiens GN=PPIB PE=1 SV=2 - [PPIB_HUMAN]	23,7
A0A0A0MSI0	Peroxiredoxin-1 (Fragment) OS=Homo sapiens GN=PRDX1 PE=1 SV=1 - [A0A0A0MSI0_HUMAN]	19,0

P32119	Peroxiredoxin-2 OS=Homo sapiens GN=PRDX2 PE=1 SV=5 - [PRDX2_HUMAN]	21,9
P30041	Peroxiredoxin-6 OS=Homo sapiens GN=PRDX6 PE=1 SV=3 - [PRDX6_HUMAN]	25,0
P30086	Phosphatidylethanolamine-binding protein 1 OS=Homo sapiens GN=PEBP1 PE=1 SV=3 - [PEBP1_HUMAN]	21,0
P36871	Phosphoglucomutase-1 OS=Homo sapiens GN=PGM1 PE=1 SV=3 - [PGM1_HUMAN]	61,4
Q96G03	Phosphoglucomutase-2 OS=Homo sapiens GN=PGM2 PE=1 SV=4 - [PGM2_HUMAN]	68,2
P18669	Phosphoglycerate mutase 1 OS=Homo sapiens GN=PGAM1 PE=1 SV=2 - [PGAM1_HUMAN]	28,8
Q8IV08	Phospholipase D3 OS=Homo sapiens GN=PLD3 PE=1 SV=1 - [PLD3_HUMAN]	54,7
P05121	Plasminogen activator inhibitor 1 OS=Homo sapiens GN=SERPINE1 PE=1 SV=1 - [PAI1_HUMAN]	45,0
P05120	Plasminogen activator inhibitor 2 OS=Homo sapiens GN=SERPINB2 PE=1 SV=2 - [PAI2_HUMAN]	46,6
Q15365;Q5E9A3	Poly(rC)-binding protein 1 OS=Homo sapiens GN=PCBP1 PE=1 SV=2 - [PCBP1_HUMAN]	37,5
P11940;P61286	Polyadenylate-binding protein 1 OS=Homo sapiens GN=PABPC1 PE=1 SV=2 - [PABP1_HUMAN]	70,6
Q6S8J3	POTE ankyrin domain family member E OS=Homo sapiens GN=POTEE PE=1 SV=3 - [POTEE_HUMAN]	121,3
Q15113	Procollagen C-endopeptidase enhancer 1 OS=Homo sapiens GN=PCOLCE PE=1 SV=2 - [PCOC1_HUMAN]	47,9
P07737	Profilin-1 OS=Homo sapiens GN=PFN1 PE=1 SV=2 - [PROF1_HUMAN]	15,0
P12004	Proliferating cell nuclear antigen OS=Homo sapiens GN=PCNA PE=1 SV=1 - [PCNA_HUMAN]	28,8
Q9UQ80	Proliferation-associated protein 2G4 OS=Homo sapiens GN=PA2G4 PE=1 SV=3 - [PA2G4_HUMAN]	43,8
Q06323	Proteasome activator complex subunit 1 OS=Homo sapiens GN=PSME1 PE=1 SV=1 - [PSME1_HUMAN]	28,7
F5GX11	Proteasome subunit alpha type-1 OS=Homo sapiens GN=PSMA1 PE=1 SV=1 - [F5GX11_HUMAN]	26,5
P25789;Q3ZCK9	Proteasome subunit alpha type-4 OS=Homo sapiens GN=PSMA4 PE=1 SV=1 - [PSA4_HUMAN]	29,5
P28066;Q5E987	Proteasome subunit alpha type-5 OS=Homo sapiens GN=PSMA5 PE=1 SV=3 - [PSA5_HUMAN]	26,4
P60900;Q2YDE4	Proteasome subunit alpha type-6 OS=Homo sapiens GN=PSMA6 PE=1 SV=1 - [PSA6_HUMAN]	27,4
P49721	Proteasome subunit beta type-2 OS=Homo sapiens GN=PSMB2 PE=1 SV=1 - [PSB2_HUMAN]	22,8
P28074	Proteasome subunit beta type-5 OS=Homo sapiens GN=PSMB5 PE=1 SV=3 - [PSB5_HUMAN]	28,5
P30101	Protein disulfide-isomerase A3 OS=Homo sapiens GN=PDIA3 PE=1 SV=4 - [PDIA3_HUMAN]	56,7
P13667	Protein disulfide-isomerase A4 OS=Homo sapiens GN=PDIA4 PE=1 SV=2 - [PDIA4_HUMAN]	72,9
H7BZ94	Protein disulfide-isomerase OS=Homo sapiens GN=P4HB PE=1 SV=2 - [H7BZ94_HUMAN]	52,5
P31949	Protein S100-A11 OS=Homo sapiens GN=S100A11 PE=1 SV=2 - [S10AB_HUMAN]	11,7
F5H365	Protein transport protein Sec23A OS=Homo sapiens GN=SEC23A PE=1 SV=1 - [F5H365_HUMAN]	82,9
E9PIT3	Prothrombin OS=Homo sapiens GN=F2 PE=1 SV=1 - [E9PIT3_HUMAN]	65,4
E7EVH9	Pseudouridine-5'-phosphatase (Fragment) OS=Homo sapiens GN=HDHD1 PE=1 SV=1 - [E7EVH9_HUMAN]	21,5
P00491	Purine nucleoside phosphorylase OS=Homo sapiens GN=PNP PE=1 SV=2 - [PNPH_HUMAN]	32,1
P14618	Pyruvate kinase PKM OS=Homo sapiens GN=PKM PE=1 SV=4 - [KPYM_HUMAN]	57,9
P31150	Rab GDP dissociation inhibitor alpha OS=Homo sapiens GN=GDI1 PE=1 SV=2 - [GDIA_HUMAN]	50,6
P50395	Rab GDP dissociation inhibitor beta OS=Homo sapiens GN=GDI2 PE=1 SV=2 - [GDIB_HUMAN]	50,6
Q13283	Ras GTPase-activating protein-binding protein 1 OS=Homo sapiens GN=G3BP1 PE=1 SV=1 - [G3BP1_HUMAN]	52,1
P46940	Ras GTPase-activating-like protein IQGAP1 OS=Homo sapiens GN=IQGAP1 PE=1 SV=1 - [IQGA1_HUMAN]	189,1
P63000;P62998	Ras-related C3 botulinum toxin substrate 1 OS=Homo sapiens GN=RAC1 PE=1 SV=1 - [RAC1_HUMAN]	21,4
P61026;A6QLS9	Ras-related protein Rab-10 OS=Homo sapiens GN=RAB10 PE=1 SV=1 - [RAB10_HUMAN]	22,5
P62491;F2Z4D5	Ras-related protein Rab-11A OS=Homo sapiens GN=RAB11A PE=1 SV=3 - [RB11A_HUMAN]	24,4
P62820;A1L528	Ras-related protein Rab-1A OS=Homo sapiens GN=RAB1A PE=1 SV=3 - [RAB1A_HUMAN]	22,7
P61224;P61223	Ras-related protein Rap-1b OS=Homo sapiens GN=RAP1B PE=1 SV=1 - [RAP1B_HUMAN]	20,8
J3KTF8	Rho GDP-dissociation inhibitor 1 (Fragment) OS=Homo sapiens GN=ARHGDIA PE=1 SV=4 - [J3KTF8_HUMAN]	21,5

P13489	Ribonuclease inhibitor OS=Homo sapiens GN=RNH1 PE=1 SV=2 - [RINI_HUMAN]	49,9
C9JXC1	Ribonucleoside-diphosphate reductase subunit M2 (Fragment) OS=Homo sapiens GN=RRM2 PE=1 SV=1 - [C9JXC1_HUMAN]	33,8
H0Y6E7	RNA-binding motif protein, X chromosome (Fragment) OS=Homo sapiens GN=RBMX PE=1 SV=2 - [H0Y6E7_HUMAN]	31,8
Q16181;Q6Q137	Septin-7 OS=Homo sapiens GN=SEPT7 PE=1 SV=2 - [SEPT7_HUMAN]	50,6
Q92743	Serine protease HTRA1 OS=Homo sapiens GN=HTRA1 PE=1 SV=1 - [HTRA1_HUMAN]	51,3
Q07955;Q0VCY7	Serine/arginine-rich splicing factor 1 OS=Homo sapiens GN=SRSF1 PE=1 SV=2 - [SRSF1_HUMAN]	27,7
P49591	Serine--tRNA ligase, cytoplasmic OS=Homo sapiens GN=SARS PE=1 SV=3 - [SYSC_HUMAN]	58,7
P35237	Serpin B6 OS=Homo sapiens GN=SERPINB6 PE=1 SV=3 - [SPB6_HUMAN]	42,6
P50453	Serpin B9 OS=Homo sapiens GN=SERPINB9 PE=1 SV=1 - [SPB9_HUMAN]	42,4
A0A0C4DGB6	Serum albumin OS=Homo sapiens GN=ALB PE=4 SV=1 - [A0A0C4DGB6_HUMAN]	69,2
O75368	SH3 domain-binding glutamic acid-rich-like protein OS=Homo sapiens GN=SH3BGRL PE=1 SV=1 - [SH3L1_HUMAN]	12,8
Q01082	Spectrin beta chain, non-erythrocytic 1 OS=Homo sapiens GN=SPTBN1 PE=1 SV=2 - [SPTB2_HUMAN]	274,4
K7ENG2	Splicing factor U2AF 65 kDa subunit OS=Homo sapiens GN=U2AF2 PE=1 SV=1 - [K7ENG2_HUMAN]	33,9
P52823	Stanniocalcin-1 OS=Homo sapiens GN=STC1 PE=1 SV=1 - [STC1_HUMAN]	27,6
H0YB13	Stanniocalcin-2 (Fragment) OS=Homo sapiens GN=STC2 PE=1 SV=1 - [H0YB13_HUMAN]	13,9
P38646	Stress-70 protein, mitochondrial OS=Homo sapiens GN=HSPA9 PE=1 SV=2 - [GRP75_HUMAN]	73,6
A0A0C4DG56	Superoxide dismutase [Mn], mitochondrial OS=Homo sapiens GN=SOD2 PE=4 SV=1 - [A0A0C4DG56_HUMAN]	18,3
Q99536	Synaptic vesicle membrane protein VAT-1 homolog OS=Homo sapiens GN=VAT1 PE=1 SV=2 - [VAT1_HUMAN]	41,9
Q9Y490	Talin-1 OS=Homo sapiens GN=TLN1 PE=1 SV=3 - [TLN1_HUMAN]	269,6
F8VQ14	T-complex protein 1 subunit beta OS=Homo sapiens GN=CCT2 PE=1 SV=1 - [F8VQ14_HUMAN]	44,8
B4DUR8	T-complex protein 1 subunit gamma OS=Homo sapiens GN=CCT3 PE=1 SV=1 - [B4DUR8_HUMAN]	55,6
E2QRB9	Thioredoxin reductase 1, cytoplasmic OS=Homo sapiens GN=TXNRD1 PE=1 SV=2 - [E2QRB9_HUMAN]	50,7
K7ER96	Thioredoxin-like protein 1 (Fragment) OS=Homo sapiens GN=TXNL1 PE=1 SV=1 - [K7ER96_HUMAN]	31,4
P26639	Threonine--tRNA ligase, cytoplasmic OS=Homo sapiens GN=TARS PE=1 SV=3 - [SYTC_HUMAN]	83,4
P37837	Transaldolase OS=Homo sapiens GN=TALDO1 PE=1 SV=2 - [TALDO_HUMAN]	37,5
Q15582	Transforming growth factor-beta-induced protein ig-h3 OS=Homo sapiens GN=TGFBI PE=1 SV=1 - [BGH3_HUMAN]	74,6
Q01995	Transgelin OS=Homo sapiens GN=TAGLN PE=1 SV=4 - [TAGL_HUMAN]	22,6
X6RJP6	Transgelin-2 (Fragment) OS=Homo sapiens GN=TAGLN2 PE=1 SV=1 - [X6RJP6_HUMAN]	21,1
P29401	Transketolase OS=Homo sapiens GN=TKT PE=1 SV=3 - [TKT_HUMAN]	67,8
P67936	Tropomyosin alpha-4 chain OS=Homo sapiens GN=TPM4 PE=1 SV=3 - [TPM4_HUMAN]	28,5
P68363;P81947	Tubulin alpha-1B chain OS=Homo sapiens GN=TUBA1B PE=1 SV=1 - [TBA1B_HUMAN]	50,1
P68366;P81948	Tubulin alpha-4A chain OS=Homo sapiens GN=TUBA4A PE=1 SV=1 - [TBA4A_HUMAN]	49,9
P07437;Q2KJD0	Tubulin beta chain OS=Homo sapiens GN=TUBB PE=1 SV=2 - [TBB5_HUMAN]	49,6
Q13885;E1BJB1	Tubulin beta-2A chain OS=Homo sapiens GN=TUBB2A PE=1 SV=1 - [TBB2A_HUMAN]	49,9
Q13509;Q2T9S0	Tubulin beta-3 chain OS=Homo sapiens GN=TUBB3 PE=1 SV=2 - [TBB3_HUMAN]	50,4
P68371;Q3MHM5	Tubulin beta-4B chain OS=Homo sapiens GN=TUBB4B PE=1 SV=1 - [TBB4B_HUMAN]	49,8
P09936	Ubiquitin carboxyl-terminal hydrolase isozyme L1 OS=Homo sapiens GN=UCHL1 PE=1 SV=2 - [UCHL1_HUMAN]	24,8
P62987;P63048	Ubiquitin-60S ribosomal protein L40 OS=Homo sapiens GN=UBA52 PE=1 SV=2 - [RL40_HUMAN]	14,7
P68036;Q3MHP1	Ubiquitin-conjugating enzyme E2 L3 OS=Homo sapiens GN=UBE2L3 PE=1 SV=1 - [UB2L3_HUMAN]	17,9
P61088;Q0P5K3	Ubiquitin-conjugating enzyme E2 N OS=Homo sapiens GN=UBE2N PE=1 SV=1 - [UBE2N_HUMAN]	17,1
A0A096LNZ9	Ubiquitin-like protein ISG15 (Fragment) OS=Homo sapiens GN=ISG15 PE=1 SV=2 - [A0A096LNZ9_HUMAN]	15,6

E7ET40	Urokinase-type plasminogen activator OS=Homo sapiens GN=PLAU PE=1 SV=1 - [E7ET40_HUMAN]	46,9
B0YJC4	Vimentin OS=Homo sapiens GN=VIM PE=1 SV=1 - [B0YJC4_HUMAN]	49,6
O75083	WD repeat-containing protein 1 OS=Homo sapiens GN=WDR1 PE=1 SV=4 - [WDR1_HUMAN]	66,2
B1AHC9	X-ray repair cross-complementing protein 6 OS=Homo sapiens GN=XRCC6 PE=1 SV=1 - [B1AHC9_HUMAN]	64,2
C9JJK5	Zyxin (Fragment) OS=Homo sapiens GN=ZYX PE=1 SV=1 - [C9JJK5_HUMAN]	19,1

F. MC3T3-E1

Accession	Description	MW [kDa]
P61982;A7Z057	14-3-3 protein gamma OS=Mus musculus GN=Ywhag PE=1 SV=2 - [1433G_MOUSE]	28,3
P14206	40S ribosomal protein SA OS=Mus musculus GN=Rpsa PE=1 SV=4 - [RSSA_MOUSE]	32,8
P68033;Q3ZC07	Actin, alpha cardiac muscle 1 OS=Mus musculus GN=Actc1 PE=1 SV=1 - [ACTC_MOUSE]	42,0
P60710;P60712	Actin, cytoplasmic 1 OS=Mus musculus GN=Actb PE=1 SV=1 - [ACTB_MOUSE]	41,7
P50247	Adenosylhomocysteinase OS=Mus musculus GN=Ahcy PE=1 SV=3 - [SAHH_MOUSE]	47,7
P17182	Alpha-enolase OS=Mus musculus GN=Eno1 PE=1 SV=3 - [ENOA_MOUSE]	47,1
B0V2N8	Annexin (Fragment) OS=Mus musculus GN=Anxa2 PE=1 SV=1 - [B0V2N8_MOUSE]	19,6
P10107	Annexin A1 OS=Mus musculus GN=Anxa1 PE=1 SV=2 - [ANXA1_MOUSE]	38,7
P48036	Annexin A5 OS=Mus musculus GN=Anxa5 PE=1 SV=1 - [ANXA5_MOUSE]	35,7
P05202	Aspartate aminotransferase, mitochondrial OS=Mus musculus GN=Got2 PE=1 SV=1 - [AATM_MOUSE]	47,4
Q8BFZ3	Beta-actin-like protein 2 OS=Mus musculus GN=Actbl2 PE=1 SV=1 - [ACTBL_MOUSE]	42,0
Q8VCQ8	Caldesmon 1 OS=Mus musculus GN=Cald1 PE=1 SV=1 - [Q8VCQ8_MOUSE]	60,4
Q00493	Carboxypeptidase E OS=Mus musculus GN=Cpe PE=1 SV=2 - [CBPE_MOUSE]	53,2
P10605	Cathepsin B OS=Mus musculus GN=Ctsb PE=1 SV=2 - [CATB_MOUSE]	37,3
P08121	Collagen alpha-1(III) chain OS=Mus musculus GN=Col3a1 PE=1 SV=4 - [CO3A1_MOUSE]	138,9
Q04857	Collagen alpha-1(VI) chain OS=Mus musculus GN=Col6a1 PE=1 SV=1 - [CO6A1_MOUSE]	108,4
Q01149	Collagen alpha-2(I) chain OS=Mus musculus GN=Col1a2 PE=1 SV=2 - [CO1A2_MOUSE]	129,5
Q8CG14	Complement C1s-A subcomponent OS=Mus musculus GN=C1sa PE=2 SV=2 - [CS1A_MOUSE]	76,8
P01027	Complement C3 OS=Mus musculus GN=C3 PE=1 SV=3 - [CO3_MOUSE]	186,4
Q61508	Extracellular matrix protein 1 OS=Mus musculus GN=Ecm1 PE=1 SV=2 - [ECM1_MOUSE]	62,8
P26040	Ezrin OS=Mus musculus GN=Ezr PE=1 SV=3 - [EZRI_MOUSE]	69,4
Q61553	Fascin OS=Mus musculus GN=Fscn1 PE=1 SV=4 - [FSCN1_MOUSE]	54,5
Q4KL80	Fibronectin OS=Mus musculus GN=Fn1 PE=1 SV=1 - [Q4KL80_MOUSE]	42,3
P47931	Follistatin OS=Mus musculus GN=Fst PE=2 SV=1 - [FST_MOUSE]	37,8
P47880	Insulin-like growth factor-binding protein 6 OS=Mus musculus GN=Igfbp6 PE=2 SV=2 - [IBP6_MOUSE]	25,3
A2A513	Keratin, type I cytoskeletal 10 OS=Mus musculus GN=Krt10 PE=1 SV=1 - [A2A513_MOUSE]	57,0
P06151	L-lactate dehydrogenase A chain OS=Mus musculus GN=Ldha PE=1 SV=3 - [LDHA_MOUSE]	36,5
Q02819	Nucleobindin-1 OS=Mus musculus GN=Nucb1 PE=1 SV=2 - [NUCB1_MOUSE]	53,4
G3UZJ4	Peroxiredoxin-5, mitochondrial OS=Mus musculus GN=Prdx5 PE=1 SV=1 - [G3UZJ4_MOUSE]	17,2
D3Z0Y2	Peroxiredoxin-6 OS=Mus musculus GN=Prdx6 PE=1 SV=1 - [D3Z0Y2_MOUSE]	22,5
P97298	Pigment epithelium-derived factor OS=Mus musculus GN=Serpinf1 PE=1 SV=2 - [PEDF_MOUSE]	46,2
P48678	Prelamin-A/C OS=Mus musculus GN=Lmna PE=1 SV=2 - [LMNA_MOUSE]	74,2
Q61398	Procollagen C-endopeptidase enhancer 1 OS=Mus musculus GN=Pcolce PE=1 SV=2 - [PCOC1_MOUSE]	50,1
Q9R1P4	Proteasome subunit alpha type-1 OS=Mus musculus GN=Psma1 PE=1 SV=1 - [PSA1_MOUSE]	29,5
P27773	Protein disulfide-isomerase A3 OS=Mus musculus GN=Pdia3 PE=1 SV=2 - [PDIA3_MOUSE]	56,6

P52480	Pyruvate kinase PKM OS=Mus musculus GN=Pkm PE=1 SV=4 - [KPYM_MOUSE]	57,8
Q921I1	Serotransferrin OS=Mus musculus GN=Tf PE=1 SV=1 - [TRFE_MOUSE]	76,7
Q60854	Serpin B6 OS=Mus musculus GN=Serpinb6 PE=1 SV=1 - [SPB6_MOUSE]	42,6
P28862	Stromelysin-1 OS=Mus musculus GN=Mmp3 PE=2 SV=2 - [MMP3_MOUSE]	53,8
Q8BND5	Sulfhydryl oxidase 1 OS=Mus musculus GN=Qsox1 PE=1 SV=1 - [QSOX1_MOUSE]	82,7
P40142	Transketolase OS=Mus musculus GN=Tkt PE=1 SV=1 - [TKT_MOUSE]	67,6
H7BXC3	Triosephosphate isomerase OS=Mus musculus GN=Tpi1 PE=1 SV=1 - [H7BXC3_MOUSE]	18,0

G. MLO-Y4

Accession	Description	MW [kDa]
P62259;P62261	14-3-3 protein epsilon OS=Mus musculus GN=Ywhae PE=1 SV=1 - [1433E_MOUSE]	29,2
Q9DCD0	6-phosphogluconate dehydrogenase, decarboxylating OS=Mus musculus GN=Pgd PE=1 SV=3 - [6PGD_MOUSE]	53,2
P20029	78 kDa glucose-regulated protein OS=Mus musculus GN=Hspa5 PE=1 SV=3 - [GRP78_MOUSE]	72,4
P68033;Q3ZC07	Actin, alpha cardiac muscle 1 OS=Mus musculus GN=Actc1 PE=1 SV=1 - [ACTC_MOUSE]	42,0
P60710;P60712	Actin, cytoplasmic 1 OS=Mus musculus GN=Actb PE=1 SV=1 - [ACTB_MOUSE]	41,7
P50247	Adenosylhomocysteinase OS=Mus musculus GN=Ahcy PE=1 SV=3 - [SAHH_MOUSE]	47,7
P45376	Aldose reductase OS=Mus musculus GN=Akr1b1 PE=1 SV=3 - [ALDR_MOUSE]	35,7
P17182	Alpha-enolase OS=Mus musculus GN=Eno1 PE=1 SV=3 - [ENOA_MOUSE]	47,1
B0V2N7	Annexin (Fragment) OS=Mus musculus GN=Anxa2 PE=1 SV=1 - [B0V2N7_MOUSE]	21,8
P10107	Annexin A1 OS=Mus musculus GN=Anxa1 PE=1 SV=2 - [ANXA1_MOUSE]	38,7
P48036	Annexin A5 OS=Mus musculus GN=Anxa5 PE=1 SV=1 - [ANXA5_MOUSE]	35,7
F7ALS6	Aspartate aminotransferase, cytoplasmic (Fragment) OS=Mus musculus GN=Got1 PE=1 SV=1 - [F7ALS6_MOUSE]	20,4
P05202	Aspartate aminotransferase, mitochondrial OS=Mus musculus GN=Got2 PE=1 SV=1 - [AATM_MOUSE]	47,4
P01887	Beta-2-microglobulin OS=Mus musculus GN=B2m PE=1 SV=2 - [B2MG_MOUSE]	13,8
P10605	Cathepsin B OS=Mus musculus GN=Ctsb PE=1 SV=2 - [CATB_MOUSE]	37,3
P06797	Cathepsin L1 OS=Mus musculus GN=Ctsl PE=1 SV=2 - [CATL1_MOUSE]	37,5
P18760	Cofilin-1 OS=Mus musculus GN=Cfl1 PE=1 SV=3 - [COF1_MOUSE]	18,5
P11087	Collagen alpha-1(I) chain OS=Mus musculus GN=Col1a1 PE=1 SV=4 - [CO1A1_MOUSE]	137,9
Q04857	Collagen alpha-1(VI) chain OS=Mus musculus GN=Col6a1 PE=1 SV=1 - [CO6A1_MOUSE]	108,4
Q8CG16	Complement C1r-A subcomponent OS=Mus musculus GN=C1ra PE=1 SV=1 - [C1RA_MOUSE]	80,0
P01027	Complement C3 OS=Mus musculus GN=C3 PE=1 SV=3 - [CO3_MOUSE]	186,4
O08553	Dihydropyrimidinase-related protein 2 OS=Mus musculus GN=Dpysl2 PE=1 SV=2 - [DPYL2_MOUSE]	62,2
P58252	Elongation factor 2 OS=Mus musculus GN=Eef2 PE=1 SV=2 - [EF2_MOUSE]	95,3
Q61508	Extracellular matrix protein 1 OS=Mus musculus GN=Ecm1 PE=1 SV=2 - [ECM1_MOUSE]	62,8
B7ZNJ1	Fibronectin OS=Mus musculus GN=Fn1 PE=1 SV=1 - [B7ZNJ1_MOUSE]	239,6
P05064	Fructose-bisphosphate aldolase A OS=Mus musculus GN=Aldoa PE=1 SV=2 - [ALDOA_MOUSE]	39,3
Q07797	Galectin-3-binding protein OS=Mus musculus GN=Lgals3bp PE=1 SV=1 - [LG3BP_MOUSE]	64,4
P13020	Gelsolin OS=Mus musculus GN=Gsn PE=1 SV=3 - [GELS_MOUSE]	85,9
P06745	Glucose-6-phosphate isomerase OS=Mus musculus GN=Gpi PE=1 SV=4 - [G6PI_MOUSE]	62,7
D3YX76	Glutathione S-transferase Mu 2 OS=Mus musculus GN=Gstm2 PE=1 SV=1 - [D3YX76_MOUSE]	21,7
Q9CZD3	Glycine--tRNA ligase OS=Mus musculus GN=Gars PE=1 SV=1 - [SYG_MOUSE]	81,8
P62827;Q3T054	GTP-binding nuclear protein Ran OS=Mus musculus GN=Ran PE=1 SV=3 - [RAN_MOUSE]	24,4

P49312;P09867	Heterogeneous nuclear ribonucleoprotein A1 OS=Mus musculus GN=Hnrnpa1 PE=1 SV=2 - [ROA1_MOUSE]	34,2
P30681	High mobility group protein B2 OS=Mus musculus GN=Hmgb2 PE=1 SV=3 - [HMGB2_MOUSE]	24,1
P70168	Importin subunit beta-1 OS=Mus musculus GN=Kpnb1 PE=1 SV=2 - [IMB1_MOUSE]	97,1
Q04998	Inhibin beta A chain OS=Mus musculus GN=Inhba PE=1 SV=1 - [INHBA_MOUSE]	47,4
P47879	Insulin-like growth factor-binding protein 4 OS=Mus musculus GN=Igfbp4 PE=1 SV=2 - [IBP4_MOUSE]	27,8
A2A513	Keratin, type I cytoskeletal 10 OS=Mus musculus GN=Krt10 PE=1 SV=1 - [A2A513_MOUSE]	57,0
Q61781	Keratin, type I cytoskeletal 14 OS=Mus musculus GN=Krt14 PE=1 SV=2 - [K1C14_MOUSE]	52,8
D3Z736	L-lactate dehydrogenase OS=Mus musculus GN=Ldha PE=1 SV=1 - [D3Z736_MOUSE]	26,0
O08746	Matrilin-2 OS=Mus musculus GN=Matn2 PE=2 SV=2 - [MATN2_MOUSE]	106,7
P26041	Moesin OS=Mus musculus GN=Msn PE=1 SV=3 - [MOES_MOUSE]	67,7
P11672	Neutrophil gelatinase-associated lipocalin OS=Mus musculus GN=Lcn2 PE=1 SV=1 - [NGAL_MOUSE]	22,9
Q02819	Nucleobindin-1 OS=Mus musculus GN=Nucb1 PE=1 SV=2 - [NUCB1_MOUSE]	53,4
P09405	Nucleolin OS=Mus musculus GN=Ncl PE=1 SV=2 - [NUCL_MOUSE]	76,7
P48759	Pentraxin-related protein PTX3 OS=Mus musculus GN=Ptx3 PE=1 SV=2 - [PTX3_MOUSE]	41,8
G3UZJ4	Peroxiredoxin-5, mitochondrial OS=Mus musculus GN=Prdx5 PE=1 SV=1 - [G3UZJ4_MOUSE]	17,2
D3Z0Y2	Peroxiredoxin-6 OS=Mus musculus GN=Prdx6 PE=1 SV=1 - [D3Z0Y2_MOUSE]	22,5
Q99K85	Phosphoserine aminotransferase OS=Mus musculus GN=Psat1 PE=1 SV=1 - [SERC_MOUSE]	40,4
P97298	Pigment epithelium-derived factor OS=Mus musculus GN=Serpinf1 PE=1 SV=2 - [PEDF_MOUSE]	46,2
P48678	Prelamin-A/C OS=Mus musculus GN=Lmna PE=1 SV=2 - [LMNA_MOUSE]	74,2
A0A0G2JE29	Procollagen C-endopeptidase enhancer 1 (Fragment) OS=Mus musculus GN=Pcolce PE=1 SV=1 - [A0A0G2JE29_MOUSE]	26,4
Q5SX49	Profilin OS=Mus musculus GN=Pfn1 PE=1 SV=1 - [Q5SX49_MOUSE]	11,8
E9PZ00	Prosaposin OS=Mus musculus GN=Psap PE=1 SV=1 - [E9PZ00_MOUSE]	60,6
Q91YR9	Prostaglandin reductase 1 OS=Mus musculus GN=Ptgr1 PE=1 SV=2 - [PTGR1_MOUSE]	35,5
P27773	Protein disulfide-isomerase A3 OS=Mus musculus GN=Pdia3 PE=1 SV=2 - [PDIA3_MOUSE]	56,6
P23492	Purine nucleoside phosphorylase OS=Mus musculus GN=Pnp PE=1 SV=2 - [PNPH_MOUSE]	32,3
P52480	Pyruvate kinase PKM OS=Mus musculus GN=Pkm PE=1 SV=4 - [KPYM_MOUSE]	57,8
Q921I1	Serotransferrin OS=Mus musculus GN=Tf PE=1 SV=1 - [TRFE_MOUSE]	76,7
E9PYY0	Serpin B6 (Fragment) OS=Mus musculus GN=Serpinb6a PE=1 SV=1 - [E9PYY0_MOUSE]	12,8
Q5NCU4	SPARC OS=Mus musculus GN=Sparc PE=1 SV=1 - [Q5NCU4_MOUSE]	34,3
P28862	Stromelysin-1 OS=Mus musculus GN=Mmp3 PE=2 SV=2 - [MMP3_MOUSE]	53,8
Q8BND5	Sulfhydryl oxidase 1 OS=Mus musculus GN=Qsox1 PE=1 SV=1 - [QSOX1_MOUSE]	82,7
P82198	Transforming growth factor-beta-induced protein ig-h3 OS=Mus musculus GN=Tgfbi PE=1 SV=1 - [BGH3_MOUSE]	74,5
P40142	Transketolase OS=Mus musculus GN=Tkt PE=1 SV=1 - [TKT_MOUSE]	67,6
P17751	Triosephosphate isomerase OS=Mus musculus GN=Tpi1 PE=1 SV=4 - [TPIS_MOUSE]	32,2
P99024;Q2KJD0	Tubulin beta-5 chain OS=Mus musculus GN=Tubb5 PE=1 SV=1 - [TBB5_MOUSE]	49,6
A0A0G2JFP9	Vascular cell adhesion protein 1 (Fragment) OS=Mus musculus GN=Vcam1 PE=1 SV=1 - [A0A0G2JFP9_MOUSE]	26,4
A0A0A6YWC8	Vimentin OS=Mus musculus GN=Vim PE=1 SV=1 - [A0A0A6YWC8_MOUSE]	49,2

11. PUBLICACIONES

Carcinogenesis, 2019, Vol. 40, No. 7, 828–839

doi:10.1093/carcin/bgz105
Advance Access Publication June 5, 2019
Original Article

ORIGINAL ARTICLE

The secreted matrix protein mindin increases prostate tumor progression and tumor-bone crosstalk via ERK 1/2 regulation

Juan A.Ardura[1,2], Irene Gutiérrez-Rojas[1], Luis Álvarez-Carrión[1], M. Rosario Rodríguez-Ramos[1,2], José M.Pozuelo[1,2] and Verónica Alonso[1,2,*]

[1]Bone Physiopathology laboratory, Applied Molecular Medicine Institute (IMMA) and [2]Departamento de Ciencias Médicas Básicas, Facultad de Medicina, Universidad San Pablo-CEU, CEU Universities, Campus Monteprincipe, 28925 Alcorcón, Madrid, Spain

*To whom correspondence should be addressed. Tel: +34 914566300 (ext 15058); Fax +34 913724000; Email: veronica.alonsorodriguez@ceu.es

Abstract

Advanced prostate cancer cells preferentially metastasize to bone by acquiring a bone phenotype that allows metastatic cells to thrive in the skeletal environment. Identification of factors that promote the expression of ectopic bone genes—process known as osteomimicry—leading to tumor progression is crucial to prevent and treat metastatic prostate cancer and prolong life expectancy for patients. Here, we identify the extracelular matrix protein mindin in the secretome of prostate adenocarcinoma cells and show that mindin overexpression in human and mouse TRAMP-C1-induced prostate tumors correlates with upregulated levels of bone-related genes in the tumorigenic prostate tissues. Moreover, mindin silencing decreased osteomimicry in adenocarcinoma cells and in the prostate tumor mice model, as well as reduced tumor cell proliferation, migration and adhesion to bone cells. Inhibition of the extracellular signal-regulated kinase 1/2 (ERK 1/2) phosphorylation decreased the proliferative, migratory and pro-adhesion actions of mindin on prostate tumor cells. In addition, conditioned media obtained by crosstalk stimulation of either osteocytes or osteoblasts with the secretome of TRAMP-C1 cells promoted osteomimicry in prostate tumor cells; an effect inhibited by mindin silencing of TRAMP-C1 cells. *In vivo*, tibiae of primary tumor-bearing mice overexpressed the pro-angiogenic and pro-metastattic factor vascular endothelial growth factor receptor 2 (VEGFR2) in a mindin-dependent manner. Our findings indicate that mindin is a novel regulator of osteomimicry in prostate tumors and potentially mediates tumor-bone cell crosstalk, suggesting its promising role as a target to inhibit bone metastases.

Introduction

Prostate cancer is one of the leading causes of cancer mortality and morbidity globally, especially in developed countries (1). Metastasis to bone is a frequent complication in advanced prostate cancer patients that has currently no cure (2,3). Preventing or slowing the spread of cancer to the bones is a major goal of treatment. Multiple steps are required for prostate adenocarcinoma cells to leave the primary tumor, migrate and 'home' to the bone microenvironment (4). A series of studies suggest that cancer cells that are prone to metastasize to bone acquire osteomimetic features, i.e. they express highly restricted markers of bone and take on behaviors of bone cells to adapt and grow in the skeletal environment (4–7). Thus, it is now recognized that prostate tumor cells express *de novo* genes involved in bone physiology, such as the bone formation transcription factor runt-related transcription factor 2 (Runx2) or the bone degradation inducer receptor activator of nuclear factor kappa-β-ligand (RANK-L), promoting bone tropism and colonization (6,8–10). Bone-related gene upregulation in prostate tumors has also been associated directly to increased metastasis-associated gene expression, *in vitro* migratory and invasive activity, increased cell survival

Received: October 30, 2018; **Revised:** May 3, 2019; **Accepted:** June 4, 2019

Abbreviations

CM	conditioned media
ERK 1/2	extracellular signal-regulated kinase 1/2
PBS	phosphate buffer saline
PSCA	prostate stem cell antigen
RANK-L	receptor activator of nuclear factor kappa-β-ligand
Runx2	runt-related transcription factor 2
TRAP	tartrate-resistant acid phosphatase
VEGF	vascular endothelial growth factor
VEGFR2	VEGF receptor 2

as well as to *in vivo* growth of tumor cell xenografts (11–15). Moreover, the expression of bone-related genes by cancer cells metastasizing to bone also influence the skeletal environment inducing, in turn, the release of several factors by osteoblasts (bone formation cells), osteoclasts (bone degradation or resorption cells) and osteocytes (bone monitoring cells) that increase metastasic cell proliferation and signaling (16,17). In this regard, the bone environment has proved to be a crucial regulator of malignant cell behavior in the metastasic niche. Tumor cells preferentially locate to osteoblast-rich regions where their proliferation, growth and phenotype were affected (18). Therefore, a 'vicious cycle' of prostate tumor and bone cooperation based on the secretion of bone factors is stablished (19). Even though prostate tumor osteomimicry and tumor cell modulation by the bone environment have been proposed as important steps prior to prostate tumor metastasis to bone (11–15), the mechanisms governing these processes are still not well understood.

Mindin, also known as spondin-2, a secreted extracellular matrix protein that belongs to the thrombospondin type 1 repeat-containing class of molecules, has recently been suggested as a specific diagnosis biomarker of prostate cancer (20,21) and a potential target for prostate cancer radiotherapy (22) revealing to be highly upregulated in prostate cancer patients with bone metastases (23). Although mindin is overexpressed and secreted by prostate tumors, its role in prostate cancer remains completely unknown. Other members of the type 1 repeat superfamily that share some structural domains with mindin, namely F-spondin and R-spondins (24,25) have shown to trigger changes in bone by regulating bone morphogenetic proteins or the Wnt signaling pathway (26,27). Considering the previously mentioned observations, we hypothesized that upregulation of mindin in prostate tumors triggers osteomimetic changes in prostate tumor cells thus enhancing tumor invasiveness.

In this study, we used a mouse model of prostatic tumorigenesis induced by orthotopic injection of TRAMP-C1 cells in order to evaluate the effects of mindin on the osteomimetic properties of the primary tumor. Tumor cell silencing of mindin showed to decrease the overexpression of bone-related proteins by the prostate tumor and the adenocarcinoma cells, as well as reduced tumor cell proliferation, migration and adhesion to osteocytes and osteoblasts.

Materials and methods

Ethics approval

Usage of clinical specimens was authorized by HM Group and Princesa Hospital Ethics and Clinical Research Committee. The human study was performed in accordance with the Declaration of Helsinki. The Animal Ethics Committee of San Pablo CEU University approved the animal experimental model. All animal experiments comply with the ARRIVE guidelines.

Human tissue specimens

Total 51 primary prostate cancer and 22 control prostate tissues without hyperplasia were collected from patients who had undergone radical prostatectomy at the HM Sanchinarro Universitary Hospital (Madrid, Spain) or from healthy deceased subjects following transplant multiorganic recovery at Princesa Universitary Hospital (Madrid, Spain), respectively. Usage of clinical specimens was authorized by HM Group and Princesa Hospital Ethics and Clinical Research Committee. Clinical data from human samples were compiled in an adenocarcinoma sample database following anatomopathological criteria, including the admission number, Prostatic Serum Antigen (PSA) levels, Gleason score, D'Amico risk, Tumor, Node and Metastasis (TNM) pathologic staining and perineural invasion (Supplementary Table I, available at *Carcinogenesis* Online).

Animal model

Three month old C57BL/6 male mice (Charles River, Wilmington, MA) were placed in cages under standard conditions (room temperature 20 ± 0.5°C, relative humidity 55 ± 5% and illumination with a 12 h/12 h light/dark photoperiod), without restriction of movement, and were maintained on a standard pellet diet (Teklad Global 18% Protein Rodent Diet, Envigo, Madison, WI) and tap water *ad libitum*. Surgical interventions were performed under aseptic conditions in anesthetized mice by isoflurane inhalation/ injection of xylazine (10 mg/Kg) and ketamine (25 mg/kg). Briefly, mice were injected in the right posterior prostatic lobe through a midline lower abdominal incision with vehicle (phosphate buffer saline [PBS]) or 5×10^5 TRAMP-C1 cells/50 µl, transfected with scrambled siRNAs or three mindin siRNAs (s97640;s97638;s87252) (Life Technologies, Paisley, UK), harvested after mild trypsinization and PBS washing, as previously described (28). A well-localized bleb within the injected prostatic lobe was considered a technically acceptable injection. The abdominal cavity, muscle and skin were closed with surgical staples. After 1 month, primary tumors and tibiae were extracted and stored in Trizol (Thermo Scientific) for real-time PCR analysis. Experimental protocols were approved by the Institutional Animal Care and Use Committee of San Pablo CEU University.

Cell culture

Mouse adenocarcinoma prostate TRAMP-C1 (ATCC: CRL-2730), human prostate carcinoma cells LNCaP (ATCC: CRL-1740) and PC-3 (ATCC: CRL1435), primary human prostate epithelial normal cells (ATCC: PCS-440-010) and mouse osteoblastic MC3T3-E1 (ATCC: CRL-2593) were purchased at ATCC in July 2014. The aforementioned cells and osteocyte MLO-Y4 cells (generously donated by Lynda Bonewald) were grown following ATCC recommendations.

Every 6 months, after its reception, we authenticate the cells by analyzing specific markers of each cell line. In this way, we study the mineralizing capacity of osteoblasts after differentiation with B glycerol phosphate and ascorbic acid. The gene expression of OPG and RANKL in osteocytes was analyzed by real-time PCR. In addition, the secretome of both osteoblastic and osteocytic cell lines was checked by secretome mass spectrometry analysis.

The expression of the tumor cell marker prostate stem cell antigen (PSCA) was analyzed by real-time PCR gene expression in the tumoral (expression) and normal prostatic (no expression) cell lines. In addition, the secretome of the normal prostate and prostate cancer cell lines were also verified.

As usual laboratory protocol, the presence of microplasma is checked in all cell cultures. Cells were incubated for 1 h with an inhibitor of extracellular signal-regulated kinase 1/2 (ERK 1/2) (U0126 [5 µM] Calbiochem) when appropriate. Conditioned media (CM) were obtained from serum depleted TRAMP-C1, MLO-Y4 or MC3T3-E1 cells cultured in α-MEM in the absence (-) or presence of CM of non-transfected TRAMP-C1 cells, scrambled siRNA or mindin siRNA-transfected TRAMP-C1 cells for 24 h.

Alternatively, TRAMP-C1 cells were incubated with 5 ng/ml mindin (R&D Systems, Minneapolis, MN) or with 1:4 MLO-Y4 or MC3T3-E1 CM for 6 or 24 h when appropriate.

Secretome mass spectrometry analysis

Secreted protein (50 µg) from TRAMP-C1, LNCAP and human prostate cells conditioned mediums were analyzed by liquid chromatography–mass

spectrometry followed by reverse phase-liquid chromatography–mass spectrometry in an Easy-nLC II system coupled to a LTQ-Orbitrap-Velos-Pro hybrid mass spectrometer (Thermo Scientific) as previously described (29). Processing of the MS data was carried out as previously described (29). Peptide identification from raw data was carried out using the SEQUEST algorithm (Proteome Discoverer 1.3, Thermo Scientific).

Cell silencing

TRAMP-C1 cells were silenced with a mixture of three siRNA (each at 20 nM) against different coding sequences of mouse mindin (s97640; s97638; s87252) (Life Technologies, Paisley, UK) using lipofectamine RNAiMax (Life Technologies) overnight at 37°C, following the manufacturer's instructions. A scrambled sequence (control siRNA-A, Santa Cruz Biotechnology, Dallas, TX) was used as a negative control for evaluating RNAi off-targeted effects, and in order to verify the accuracy of gene-specific siRNA-dependent changes in different parameters evaluated. Efficiency of mindin silencing, assessed by real-time PCR, represented 85% 48 h after transfection and 60% up to 15 days after transfection (Supplementary Figure 1, available at *Carcinogenesis* Online)

Cell proliferation assay

The number of viable TRAMP-C1 cells transfected with scrambled siRNA or mindin siRNA or stimulated with 5 ng/ml mindin peptide was evaluated by a trypan blue exclusion assay as previously described (30). Mitomycin C anti-proliferative actions in TRAMP-C1 cells were also tested using the trypan blue exclusion assay.

Adhesion assay

The adhesion of TRAMP-C1 adenocarcinoma cells to MLO-Y4 osteocytes or MC3T3 pre-osteoblasts *in vitro*, was assessed by seeding calcein-AM-labeled TRAMP-C1 cells in a 24-well plate pre-inoculated with MLO-Y4 or MC3T3-E1 cells at confluence. TRAMP-C1 cells were pre-incubated with 2 µM calcein-AM (Thermo Scientific) for 30 min, subsequently washed with PBS and seeded onto MLO-Y4 or MC3T3-E1 covered well surfaces. Non-adherent cells were removed after 30 min of incubation with complete medium followed by plate washing with PBS. Next, adherent cells were fixed with 4% paraformaldehyde and images were obtained with an epifluorescence microscope (Leica DM5500B). The number of fluorescence-labeled cells was counted in 10 different fields per condition.

Cell migration assay

TRAMP-C1 cell migration was assessed using an *in vitro* scratch assay in serum-free medium as previously described (31). Alternatively, migration was analyzed under anti-proliferative conditions in an *in vitro* scratch assay using TRAMP-C1 cells incubated with 5 µg/ml mitomycin C.

Real-time PCR

Total RNA was isolated by a standard procedure (Trizol, Life Technologies), and 2 µg of this RNA was retrotranscripted with cDNA high capacity retrotranscription kit (Applied Biosystems, Grand Island, NY) following manufacturer's instructions. Gene expression was analyzed by real-time PCR using an ABI PRISM 7500 system (Applied Biosystems). Real-time PCR was performed using Sybr premix ex Taq (Takara, Otsu, Japan) with mouse-specific primers for PSCA (32), RANK-L (33), OPG (34), osteocalcin (34), bone alkaline phosphatase (34), Runx2 (34), tartrate-resistant acid phosphatase (TRAP) (34) (Supplementary Table II, available at *Carcinogenesis* Online). Alternatively, real-time PCR was done using predeveloped fluorogenic mouse-specific TaqMan MGB probes for mindin (Mm00513596_m1), vascular endothelial growth factor [VEGF] (Mm00437306_m1) and VEGF receptor 2 [VEGFR2] (Mm01222421_m1) (Life Technologies). 18S or actin rRNA (housekeeping genes) were amplified in parallel with tested genes. The relative gene expression in cell assays was represented as previously described (35). Amplicon specificity was confirmed as the presence of a single peak in the melting curve for each qPCR reaction.

Western blot analysis

Total cell protein extracts were obtained with RIPA Buffer, supplemented with protease inhibitor cocktail (Sigma–Aldrich), and phosphatase inhibitor cocktail Set II (Calbiochem). Western blot was performed as previously described (26). We used the following rabbit polyclonal antibodies: Phosphorylated (p)-ERK1/2 (1:1000), ERK 1/2 (1:2000) (Cell Signaling Technology, Beverly, MA) and osterix (1:1000) (Abcam, UK) or mouse monoclonal antibodies against: Runx2 (1:1000) (Abcam). α-tubulin (Sigma–Aldrich) was used as a loading control.

Statistical analysis

All results are expressed as means ± SE. Differences among conditions were evaluated by nonparametric variance analysis (Kruskal-Wallis) followed by Dunn's test or Mann-Whitney test was performed to analyze the differences between vehicle control or scrambled siRNA samples and mindin-stimulated or mindin siRNA-transfected samples *in vitro*.

Correlation analysis was performed using the Spearman's nonparametric correlation test, obtaining a correlation coefficient (r) and an associated P value. $P < 0.05$ was considered significant.

Results

Mindin is expressed by human and mouse prostate cancer cells and regulates the osteomimetic expression of bone genes in prostate tumors

We first characterized the CM from two prostate cancer cell lines, TRAMP-C1 (mouse prostate adenocarcinoma) and LNCaP (human prostate lymph node metastasis) and a primary prostate epithelial cell line (human non-tumorigenic), to identify secreted proteins that could be used as novel targets to inhibit the osteomimetic phenotype of prostate tumors. After proteomic analysis, we identified 35 proteins that were only secreted by LNCaP but not by non-tumorigenic prostate epithelial cells (Supplementary Table III, available at *Carcinogenesis* Online). From the list of proteins identified, we sought those that potentially could modulate bone markers and had pro-tumorigenic features. Molecular function assessment of the selected proteins from the secretome identified mindin as a potential tumorigenic and osteomimetic-inducer candidate given that this protein forms part of a family with bone remodeling properties (36) and also displays connections to prostate tumor modulation, such as positive regulation of the prostate tumorigenic cytokines interleukine-6 (IL-6) and tumor necrosis factor-α (TNF-α) (37) (Figure 1A). Moreover, mindin secretion was observed in the secretome of both LNCaP and TRAMP-C1 cells compared to non-tumorigenic prostate epithelial or osteoblastic-like cells (Supplementary Table III, available at *Carcinogenesis* Online and data not shown).

Furthermore, we observed by immunohistochemistry analysis of human prostate samples increased mindin immunolabeling in primary prostate tumors compared to control non-tumorigenic specimens (Supplementary Figure 2, available at *Carcinogenesis* Online). Mindin immunolabeling revealed to be increased in tumors with high risk (4.82 ± 0.69), followed by medium (2.99 ± 0.47) and low (2.09 ± 0.27) risk of recurrence according to D'Amico risk classification for prostate cancer (Normalized mindin immunolabeling values ± SEM).

Previous reports suggest that prostate adenocarcinomas acquire osteomimetic properties that are positively associated with the invasiveness of the tumors (6). In this regard, we observed changes in bone markers associated with increased mindin immunolabeling in human prostate tumor samples (Supplementary Figure 2, available at *Carcinogenesis* Online). Similarly to mindin, osterix expression was higher in tumors with high risk (5.81 ± 2.58), followed by medium (4.32 ± 1.54) and low (2.96 ± 076) risk of recurrence according to D'Amico risk classification for prostate cancer (osterix gene expression values ± SEM).

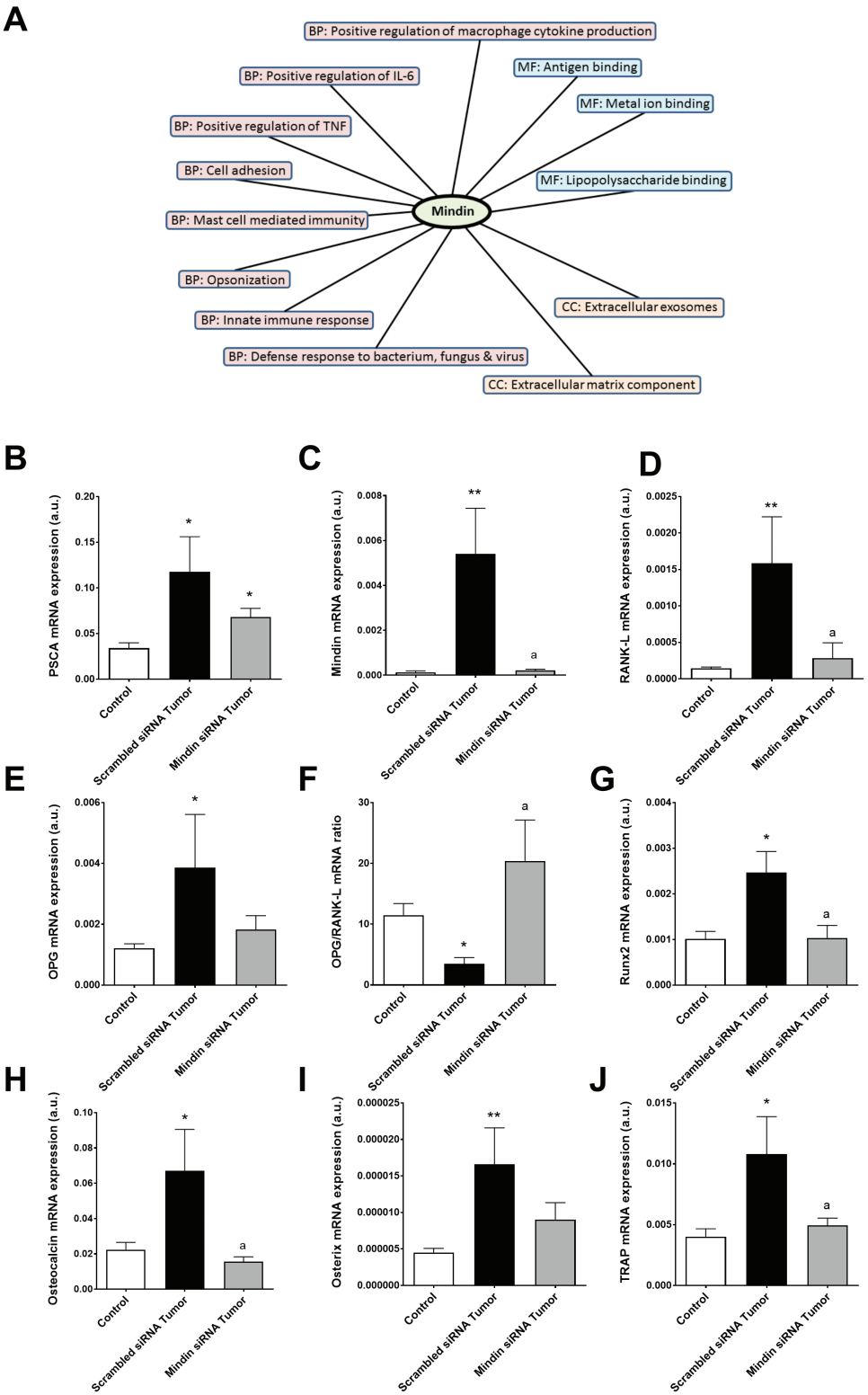

Figure 1. Mindin is overexpressed and increases the expression of osteomimetic genes in TRAMP-C1-induced prostate tumors. (A) Diagram depicting the biological processes (BP) related to diseases, molecular functions (MF) and cellular components (CC) that mindin is associated with. Diagram generated using information from Uniprot databases. (B) Prostate stem cell antigen (PSCA), (C) mindin, (D) RANK-L, (E) OPG, (G) Runx2, (H) Osteocalcin, (I) Osterix and (J) TRAP mRNA expression in control (vehicle: PBS injection), Scrambled siRNA Tumor (injection of TRAMP-C1 cells transfected with scrambled siRNA) and mindin siRNA Tumor (injection of TRAMP-C1 cells transfected with mindin siRNA) prostates from mice assessed by real-time PCR. OPG/RANK-L ratio is shown in F. The data are represented as the mean ± SEM (n = 7–10 per group). *P < 0.05 versus control; **P < 0.01 versus control; [a]P < 0.05 versus Scrambled siRNA Tumor.

To investigate whether mindin induces osteomimetic features in prostate tumors we orthotopically injected TRAMP-C1 cells, silenced by mindin siRNAs or not (scrambled siRNAs), in C57BL/6 male mice. The TRAMP model of prostate cancer induced in immunocompetent mice have detectable prostate tumors at 4 weeks after injection and can develop metastasis to different organs, including bone (38).

Prostate tumors induced by scrambled TRAMP-C1 cells overexpressed both the prostate tumor-specific marker PSCA (Figure 1B) (32) and mindin (Figure 1C) compared to vehicle-injected control mice. We next observed, using Spearman's rank correlation analysis, that mindin overexpression correlated to upregulated gene expression of several bone markers that have a key role in bone remodeling and metabolism, including significant positive correlation with RANK-L, OPG, Runx2, osteocalcin, osterix and TRAP expression and negative correlation with the OPG/RANK-L ratio (Supplementary Table IV, available at *Carcinogenesis* Online). Following, we evaluated the effects of silencing mindin in prostatic tumor induction and acquisition of an osteomimetic phenotype. PSCA gene expression levels remained high (Figure 1B) meanwhile decreased mindin (Figure 1C), RANK-L, Runx2, osteocalcin, osterix and TRAP expression and increased OPG/RANK-L ratio, were observed in tumors from TRAMP-C1 cells silenced with mindin siRNAs compared to scrambled siRNA TRAMP-C1-induced tumors (Figure 1D–J).

Mindin regulates bone osteomimetic gene expression and cell proliferation, migration and adhesion

Increased expression of mindin has been associated with higher grades of tumorigenicity in prostate tumors (21). To test whether different levels of mindin differentially affect the expression of osteomimetic genes, we stimulated cells with a mindin peptide or inhibited mindin expression using mindin siRNAs in TRAMP-C1 cells.

Upregulation of RANK-L, Runx2, osteocalcin, alkaline phosphatase and TRAP gene expression and downregulation of the OPG/RANK-L ratio in TRAMP-C1 cells stimulated for 6 h with mindin peptide was observed (Figure 2A). Similar effects were observed in LNCaP, PC-3 and primary human prostate epithelial normal cells (Supplementary Figure 3, available at *Carcinogenesis* Online). After 24 h of mindin stimulation TRAMP-C1 also showed osterix overexpression (Figure 2B). Runx2, osteocalcin, TRAP and mindin expression remained induced by mindin during all the period of study (Figure 2A and B). Furthermore, Runx2 and osterix protein expression were elevated 24 h and 48 h after mindin stimulation (Supplementary Figure 4, available at *Carcinogenesis* Online). In contrast, mindin silencing triggered OPG overexpression and increased the OPG/RANK-L ratio (Figure 2C). Gene expression of other markers was not significantly altered by mindin silencing.

In addition, we observed increased TRAMP-C1 cell proliferation (Figure 2D) and cell migration (Figure 3A and B) in mindin-stimulated cells compared to vehicle-stimulated cells. To confirm pro-migratory actions of mindin independent of proliferation, incubation of TRAMP-C1 cells with the anti-proliferative drug mitomycin C in a scratch assay was performed. Under these conditions, cell proliferation was inhibited and mindin induced significant changes in migration compared to cells incubated with mitomycin C alone (Figure 3C and Supplementary Figure 5, available at *Carcinogenesis* Online). Moreover, mindin silencing reduced TRAMP-C1 cell proliferation (Figure 2D), cell migration (Figure 3A and B) and cell adhesion to MLO-Y4 or MC3T3-E1 cell cultures (Figure 3D and E). Mindin silencing showed similar effects on TRAMP-C1 cell adhesion to collagen-coated surfaces (Scrambled siRNA: 26.3 ± 1.55 versus mindin siRNA: 17.5* ± 1.26 cells/400× field; *$P < 0.05$ versus scrambled siRNA). The number of TRAMP-C1 cells adhered to MC3T3-covered surfaces in scrambled siRNA control conditions (60.75 ± 5.9) was significantly higher than to MLO-Y4- (44.1 ± 2.82) or collagen-coated surfaces (26.3 ± 1.55).

Osteomimetic, adhesion and migration effects of mindin are mediated by ERK signaling

We next aimed to elucidate the mechanism involved in mindin actions on prostate tumor cells. Given that previous findings showed ERK 1/2 signaling pathway acting downstream of R-spondin 1–4 proteins regulating osteoblastic differentiation in adipose-derived mesenchymal stem cells (39), we tested whether this MAP Kinase was involved in mindin-dependent actions on prostate tumor cells. Supporting this concept, we observed that mindin induced time-dependent ERK 1/2 phosphorylation in TRAMP-C1 cells (Figure 4A). Moreover, mindin-dependent changes in migration, adhesion, RANK-L and Runx2 expression and OPG/RANK-L ratio were inhibited by an ERK 1/2 MAP kinase inhibitor (Figure 4B–H).

Prostate tumor-bone crosstalk regulates bone osteomimetic gene expression via mindin

Cancer cells metastasizing to bone influence the skeletal environment inducing the release of several factors that increase, in turn, tumor cell proliferation and signaling (16,17), establishing a 'vicious cycle' of prostate tumor and bone cooperation (19). To test *in vitro* the potential effects of secreted mindin on prostate tumor-bone cooperation, we assessed the actions of MLO-Y4 (osteocyte) and MC3T3 (osteoblast) secretome (CM) on TRAMP-C1 cells.

CM of MLO-Y4 cells pretreated with TRAMP-C1 CM stimulated RANK-L overexpression and decreased the OPG/RANK-L ratio in TRAMP-C1 cells compared to CM of untreated MLO-Y4 cells or controls (no CM) (Figure 5A–C). In addition, CM of MC3T3 cells pretreated with TRAMP-C1 CM stimulated RANK-L, OPG, Runx2, osteocalcin, osterix, alkaline phosphatase and TRAP expression without significantly changing the OPG/RANK-L ratio in TRAMP-C1 cells compared to CM of untreated MC3T3 cells or controls (no CM) (Figure 5A–H). Interestingly, the effects of adenocarcinoma-pretreated MLO-Y4 and MC3T3 secretome on TRAMP-C1 cells were inhibited at least in part, when pretreating both bone cells with CM of mindin-silenced TRAMP-C1 cells (Figure 6A–H).

We next assessed whether mindin induces *in vivo* changes in the bone environment that could promote tumor cell metastasis and 'homing'. We observed no significant expression of tumor cells markers (PSCA expression or cytokeratin immunolabeling) in tibiae of primary tumor-bearing mice in our model (data not shown). However, tibiae of mice with mindin-expressing tumors showed a slight increase of the pro-angiogenic factor VEGF and significant upregulation of VEGFR2 (Figure 6I and J). Additionally, VEGFR2 overexpression was inhibited in tibiae of mice with mindin-silenced tumors (Figure 6I and J). These results suggest that even though prostate adenocarcinoma cells do no not seem to metastasize to the bone in the current phase of our model, still mindin modifies the bone environment inducing changes that could promote tumor cell homing to the bone.

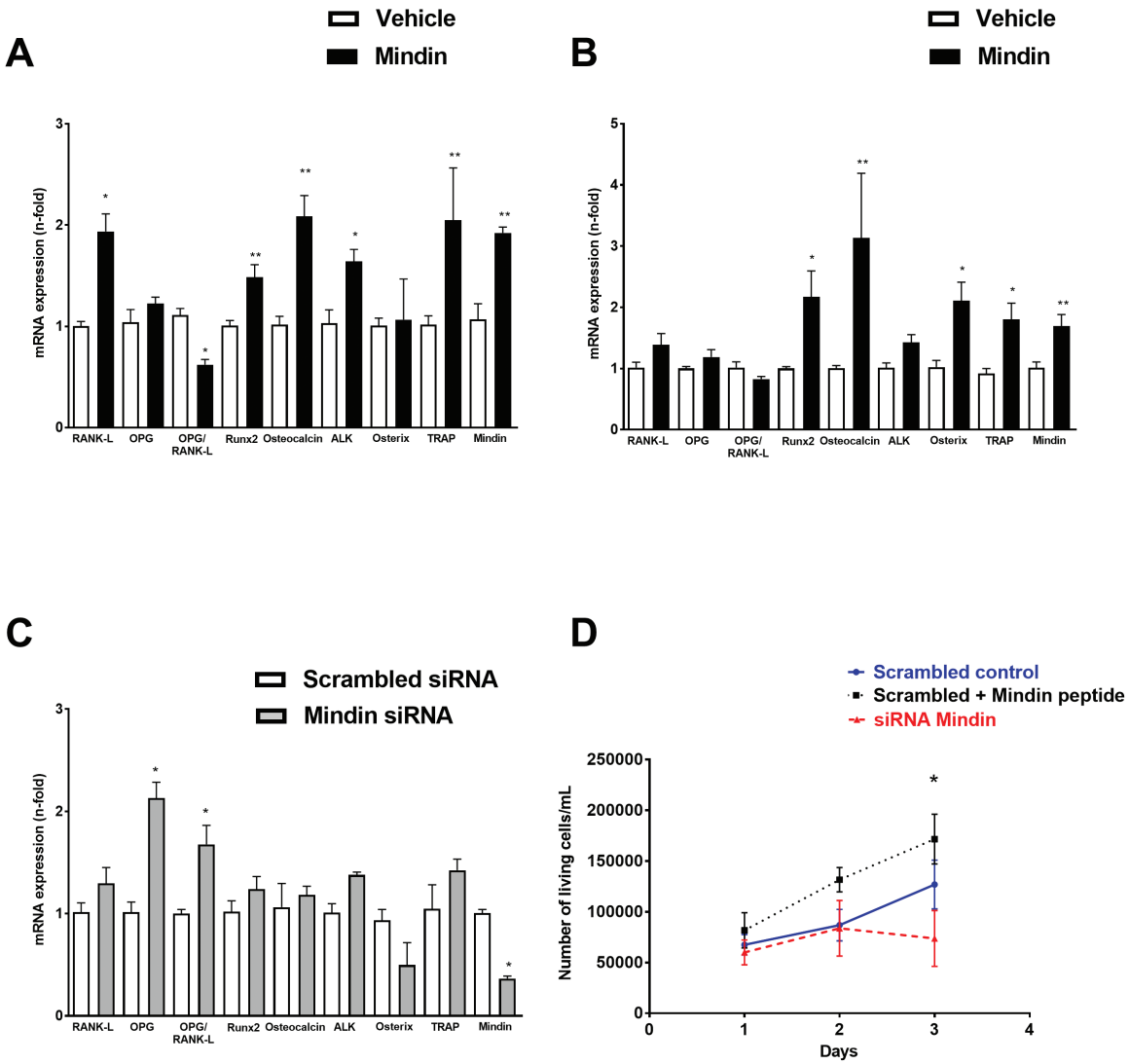

Figure 2. Mindin induces the expression of osteomimetic genes and proliferation in TRAMP-C1-cells. RANK-L, OPG, Runx2, osteocalcin, alkaline phosphatase, osterix, TRAP and mindin mRNA expression and OPG/RANK-L ratio were assessed by real-time PCR after stimulation with mindin (5 ng/ml) for 6 h (A) or 24 h (B) or transfected with three mindin siRNAs for 48 h (C) in TRAMP-C1 cells as previously described in materials and methods. Proliferation of TRAMP-C1 cells stimulated with mindin (5 ng/ml) or transfected with scrambled siRNAs or three mindin siRNAs for 48 h was assessed using a trypan blue proliferation assay (D). The data are represented as the mean ± SEM of three experiments in triplicate. *$P < 0.05$ versus corresponding control (vehicle or scrambled siRNA transfection), **$P < 0.01$ versus corresponding control (vehicle or scrambled siRNA transfection).

Discussion

Bone metastases are painful, difficult to cure and with a poor survival prognosis. Therefore, identifying factors that regulate tumor–bone interactions and improve our knowledge of the mechanisms that regulate these interactions are urgently needed to develop new therapeutic approaches. Acquisition of osteomimetic properties (i.e. ectopic expression of genes typically expressed in bone), has been suggested to increase the skeletal metastatic potential of prostate cancer cells by increasing the migration and homing of tumor cells to the bone microenvironment (6–10). Moreover, bone-related factors released by tumor cells contribute to the 'vicious cycle' of bone metastases, allowing cancer cells to thrive in bone by stablishing a crosstalk among cancer and bone cells (40). Herein, we identify mindin as a novel factor secreted by prostate tumors and prostate cancer cells that modulates adenocarcinoma cell expression of bone-related genes, tumor cell proliferation, migration, adhesive properties and communication with bone cells.

Mindin expression has been reported to be higher in specimens from patients with more aggressive prostate cancer and worse prognosis, and in those with bone metastases (21,23). Assessment of mindin by immunostaining of tumors with different gleason scores revealed that mindin staining was more intense in Gleason score sum 7–8 than in tumors with Gleason score sum 2–6 (21). Moreover, mindin levels were highest in prostate cancer individuals with bone metastasis, followed by individuals with no bone metastasis, hyperplasia and control (23). However, the role of mindin on cancer progression apart from being a possible metastatic marker, has not been described. In this regard, we observed in our animal model and in TRAMP-C1 cells that mindin promotes the expression of osteoclastic- and osteoblastic-related genes that have shown to be crucial for the development of bone metastases. Interestingly, different levels of mindin expression were associated with variations on the levels of osteomimetic gene expression both *in vitro* and *in vivo*. Previous studies described the role of RANK-L as an inducer of

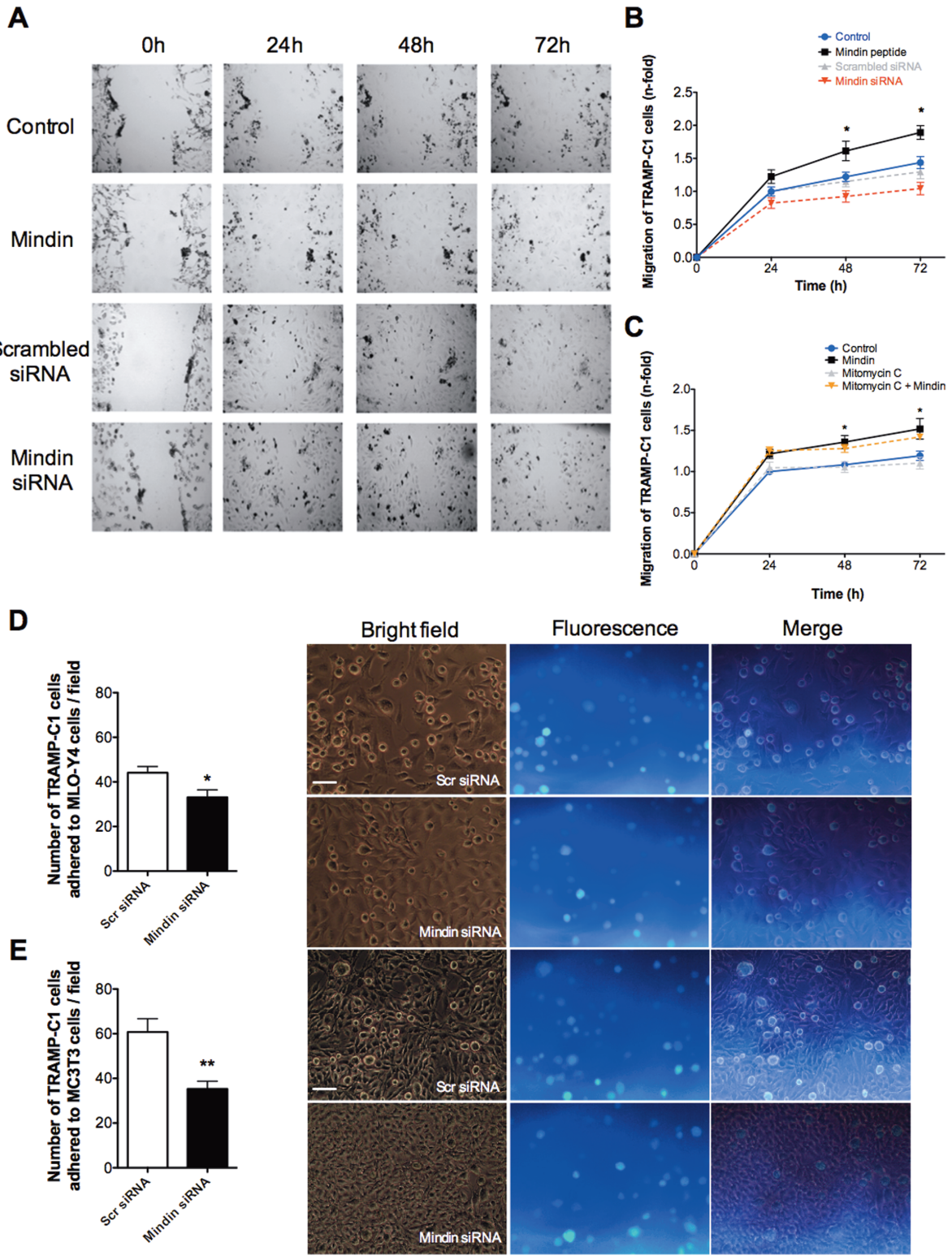

Figure 3. Mindin promotes TRAMP-C1 cell migration and adhesion. Migration of TRAMP-C1 cells stimulated with mindin peptide (5 ng/ml) or silenced with mindin siRNAs for 48 was assessed using a scratch assay in serum-depleted conditions (A and B) or cells incubated or not with mindin ± 5 μg/ml mitomycin C (C) (0–72 h). Number of adhered TRAMP-C1 cells labeled with calcein-AM per field to confluent MLO-Y4 (D) or MC3T3-E1(E)-covered surfaces is shown. Bar denotes 50 μm. Representing images from three experiments in triplicate are shown. The data are shown as the mean ± SEM of three experiments in triplicate. *$P < 0.05$ versus corresponding control (scrambled siRNA transfection).

bone resorption mediating osteoclast activation (8) but also as a factor that triggers bone-specific metastases of epithelial tumors and cancer cell migration (41) potentially through the activation of NF-kappa β signaling (42). Although we observed upregulated levels of OPG-the decoy soluble inhibitor of RANK-L in our model, these expression levels were significantly lower than

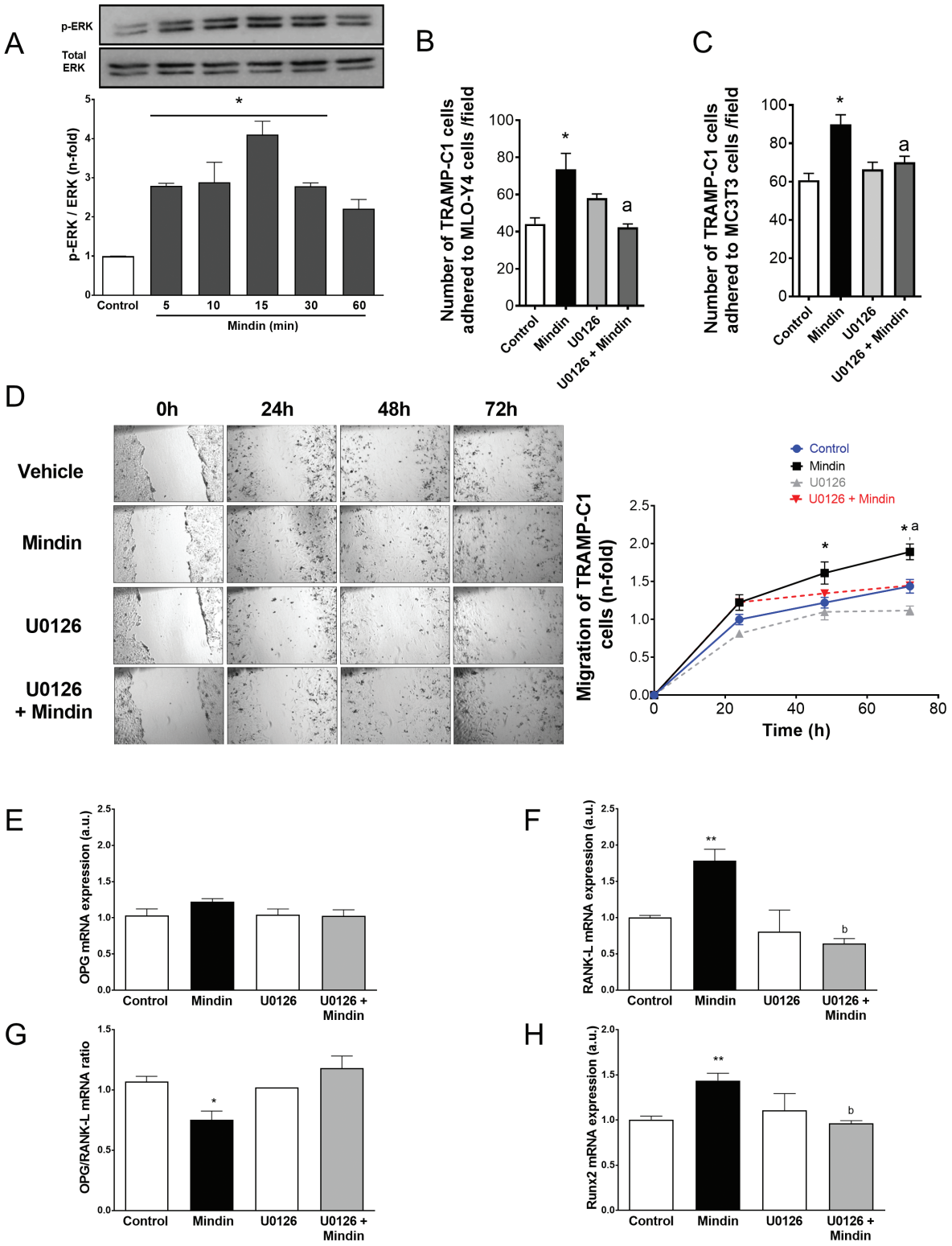

Figure 4. Mindin-induced adhesion, migration and osteomimicry effects are mediated by ERK 1/2 in TRAMP-C1 cells. Mindin-dependent ERK phosphorylation (A), cell adhesion (B and C), cell migration (D) and changes in osteomimetic gene expression (E–H) in TRAMP-C1 cells are shown. TRAMP-C1cells were stimulated with 5 ng/ml mindin for different periods of time: 5–60 min (A), 24 h (B–D) or 6 h (E–H). A representative autoradiogram is shown in A. (B and C) Number of calcein-labeled TRAMP-C1 cells attached to MLO-Y4 (B)- and MC3T3 (C)-covered surfaces per field is shown. (D) Migration of TRAMP-C1 cells stimulated with mindin peptide (5 ng/ml) and/or inhibited with an ERK 1/2 inhibitor (5 μM U0126) for 1 h was assessed using a scratch assay (0–72 h). (E–H) TRAMP-C1 cell pretreatment with an ERK 1/2 inhibitor (5 μM U0126) for 1-h abrogated mindin-induced effects on RANK-L (F) and Runx2 (H) mRNA expression and OPG/RANK-L ratio (G). Results represent mean ± SEM of three independent experiments. Representative autoradiograms are shown. *$P < 0.05$; **$P < 0.01$ versus control; $^{b}P < 0.05$ versus mindin.

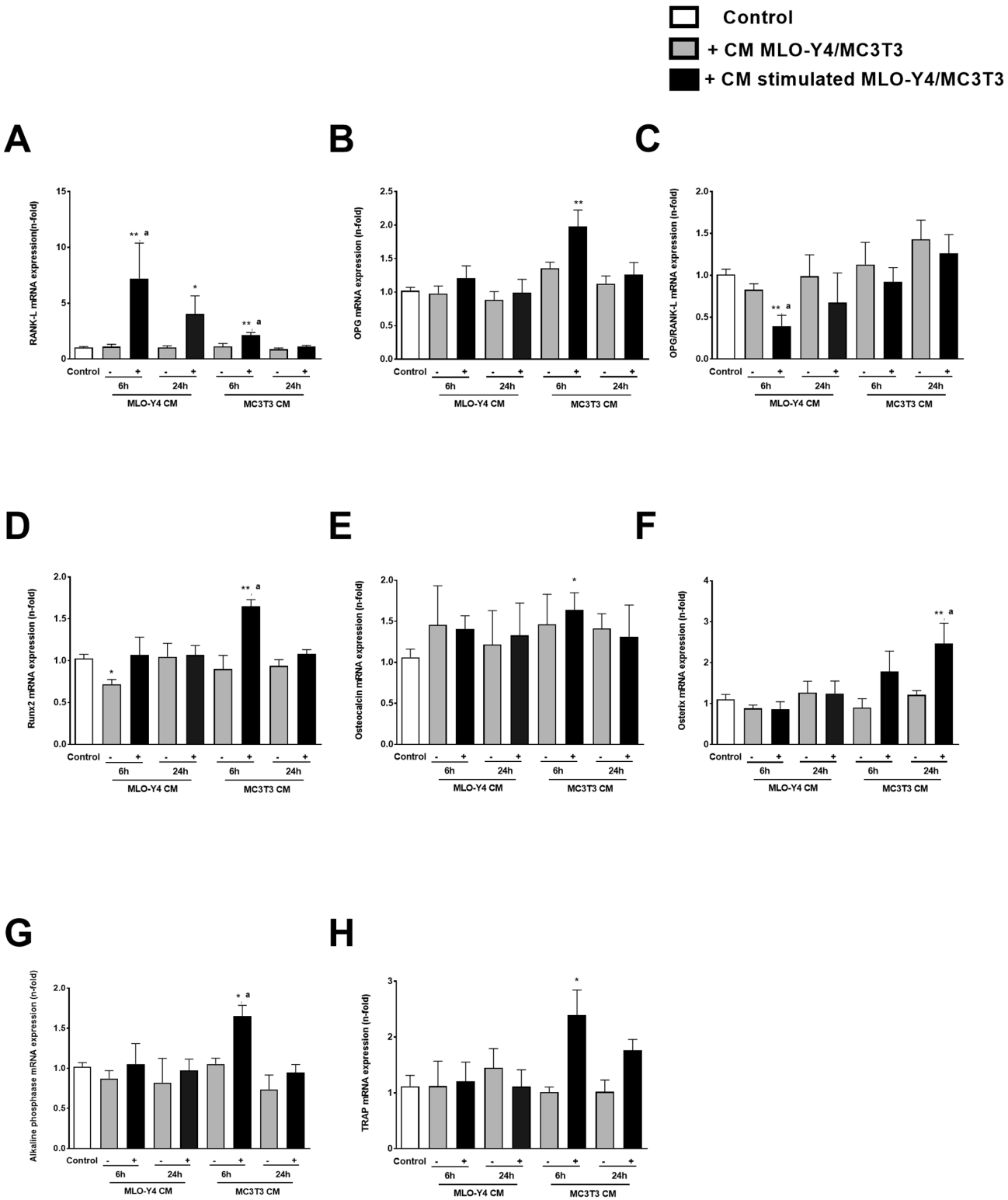

Figure 5. Crosstalk between tumor and bone cells induces changes in osteomimetic gene expression in TRAMP-C1 cells. RANK-L (A), OPG (B), Runx2 (D), Osteocalcin (E), Osterix (F), alkaline phosphatase (G) and TRAP (H) mRNA expression and OPG/RANK-L ratio (C) were assessed by real-time PCR in TRAMP-C1 cells under control, – (CM of untreated MLO-Y4 or MC3T3 cells) and + (CM of TRAMP-C1 CM-treated MLO-Y4 or MC3T3 cells) conditions. The data are represented as the mean ± SEM of three experiments in triplicate. *$P < 0.05$ versus control; **$P < 0.01$ versus control; $^{a}P < 0.05$ versus corresponding (–) condition.

those of RANK-L, as shown by a decreased OPG/RANK-L ratio, suggesting that the RANK-L signaling pathway is predominant in our prostate tumors model. It is possible though that OPG overexpression by prostate tumors might be due to a compensatory pathway induced to block the elevated levels of RANK-L. In any event, our data showing an increase in the expression

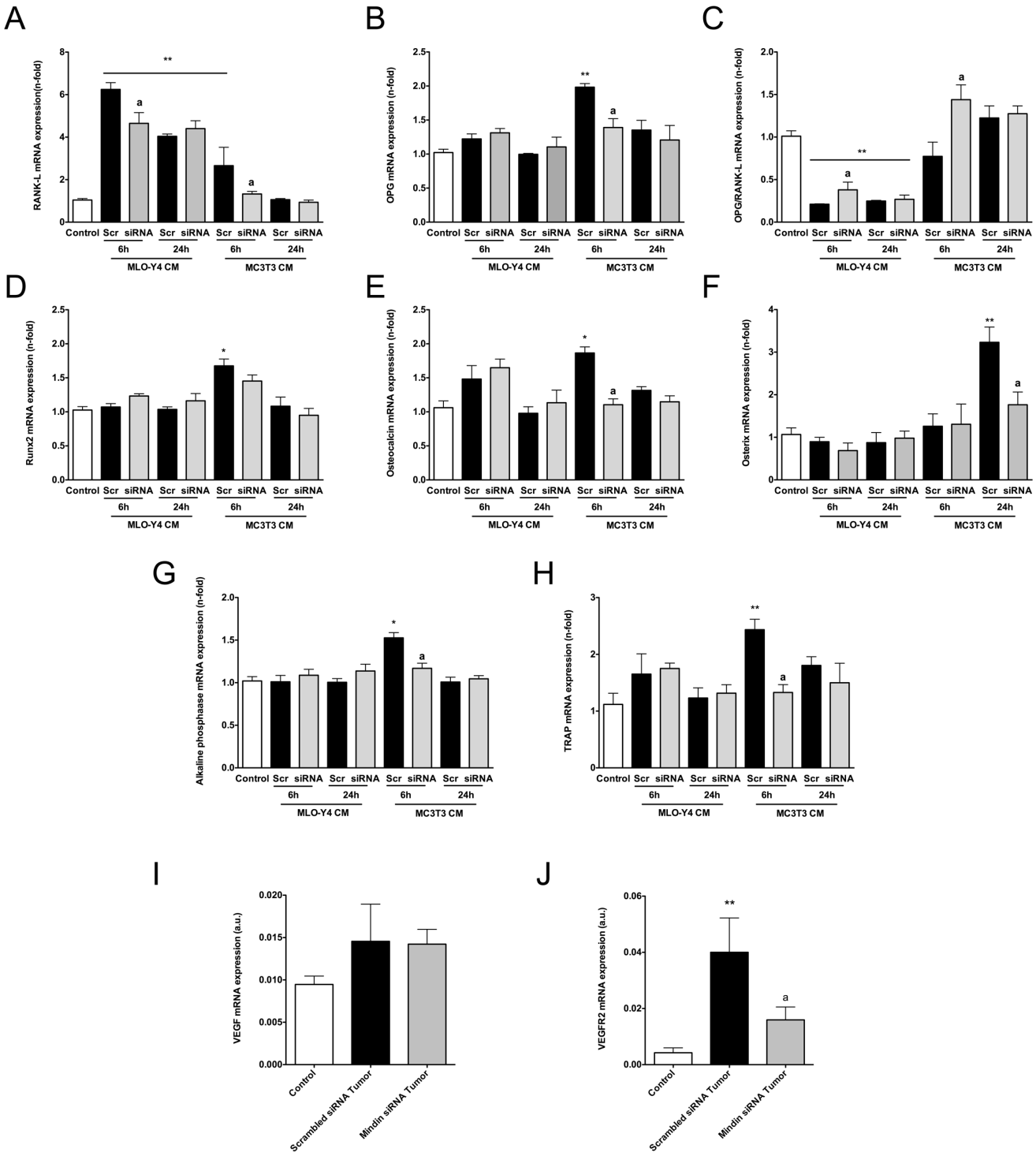

Figure 6. TRAMP-C1 cell osteomimicry induced by tumor and bone cell crosstalk is inhibited by mindin silencing. RANK-L (A), OPG (B), Runx2 (D), Osteocalcin (E), Osterix (F), alkaline phosphatase (G) and TRAP (H) mRNA expression and OPG/RANK-L ratio (C) were assessed by real-time PCR in TRAMP-C1 under control, Scr (CM of MLO-Y4 or MC3T3 cells previously treated with CM of scrambled siRNA-transfected TRAMP-C1 cells) and siRNA (CM of MLO-Y4 or MC3T3 cells previously treated with CM of mindin siRNA-transfected TRAMP-C1 cells) conditions. VEGF (I) and VEGFR2 (J) mRNA expression were assessed by real-time PCR in tibiae of control (vehicle: PBS injection), Scrambled siRNA Tumor (injection of TRAMP-C1 cells transfected with scrambled siRNA) and mindin siRNA Tumor (injection of TRAMP-C1 cells transfected with mindin siRNA) mice. *In vitro* data are represented as the mean ± SEM of three experiments in triplicate. *In vivo* data are represented as the mean ± SEM (n = 7–10 per group). *P < 0.05 versus control; **P < 0.01 versus control; ^{a}P < 0.05 versus corresponding Scrambled condition or Scrambled siRNA Tumor.

of RANK-L and in the osteoclast marker TRAP suggests that mindin triggers early pro-resorptive signals in prostate tumors. On the other hand, the transcription factor Runx2 has also been involved in the promotion of a metastatic phenotype in prostate tumor cells, inducing overexpression of genes involved in epithelial–mesenchymal transition (EMT) (SOX9, LCN2 and SNAI2), extracellular matrix degradation (matrix metalloproteinases 9 and 13) or angiogenesis (VEGF) (6). Furthermore, Runx2

promotes osteoblastogenesis and is a master regulator of bone formation genes, including osteocalcin and the transcription factor osterix (43), two genes that are increased by mindin in our model. We also observed that bone alkaline phosphatase, an osteoblastic marker, was increased by mindin *in vitro* although we did not observe upregulated levels *in vivo*, probably due to its characteristic transient pattern of expression during early osteoblast differentiation (43). Altogether, these observations indicate that mindin induces the acquisition of an osteoclast and osteoblast mixed phenotype with pro-metastatic properties in prostate tumor cells. Although prostate cancer bone metastases have been classically characterized as being osteoblastic, some evidence suggest that development of prostate cancer bone metastases requires osteoclastic in addition to osteoblastic activities, initially generating early mild osteolysis followed by later osteoblastic disease (44).

We also observed that mindin triggers tumor cell proliferation, migration and enhanced adhesion to bone cells. In this regard, previous studies reported that mindin activates NF-kappa β in RAW 264.7 cells (45), a signaling pathway that promotes growth of prostate cancer cells (42). A role of mindin in adhesion and outgrowth of hippocampal embryonic neurons has also been proposed (46). In addition, mindin has been shown to be a ligand for integrins, being mindin-integrin interactions critical for neutrophil and macrophage recruitment in *in vivo* inflammatory models (47). Whether one of these mechanisms mediates mindin-induced proliferation, migration or adhesion processes in prostate cancer cells would require further studies. Even though mindin increases adhesion of TRAMP-C1 cells to collagen and osteocyte cells, the number of TRAMP-C1 cells adhered to pre-osteoblast (MC3T3)-covered surfaces was higher compared to osteocyte (MLO-Y4)- or collagen-coated surfaces. These results suggest that prostate adenocarcinoma cells preferentially bind to cells that line the bone marrow cavities.

Concerning bone modulation of prostate cancer progression, previous observations have shown that osteoblast-like cells (HOBIT) secrete factors that modify LNCaP cell gene expression inducing a metastatic phenotype in this prostate cancer cell line (48). In our hands, secreted factors of MC3T3-E1 osteoblast-like cells or MLO-Y4 osteocytes did not induce significant changes in ectopic expression of bone-related genes in TRAMP-C1 cells. However, secreted factors of MC3T3-E1 or MLO-Y4 cells pre-incubated with TRAMP-C1 conditioned medium triggered an osteomimetic phenotype in prostate cancer cells. These results suggest that TRAMP-C1 cells secrete factors that affect osteoblasts and osteocytes, and in turn, these bone cells secrete factors that promote the expression of bone-related genes in prostate cancer cells. Furthermore, given the decreased expression of bone-related genes when mindin is silenced in TRAMP-C1 cells in the first term, secretion of mindin seems to be necessary, at least in part, to induce crosstalk among adenocarcinoma cells and osteoblasts/osteocytes *in vitro*. Our data suggests that communication of prostate cancer with bone cells seems to follow at least two different ways: secreted molecules from pre-stimulated osteocytes induce the activation of the bone remodeling factor RANK-L, whereas pre-stimulated osteoblasts preferentially promote the expression of osteoblastogenic genes (Runx2 and osterix) in prostate tumor cells. Thus, interactions with osteocytes might trigger the release of pro-resorptive signals by the tumor probably causing the previously mentioned early mild osteolysis and participating in the 'vicious cycle' of prostate tumor and bone cooperation in bone metastases. On the other hand, communication with osteoblasts might promote expression and secretion of bone differentiation factors that could lead to osteoblastic lesions in bone metastases.

Furthermore, elevated mindin levels have previously been found in the serum of prostate cancer patients (21), suggesting that this protein could be secreted by the primary tumor, target the bone and trigger the release of osteomimetic-inducing factors to the blood by osteoblasts and osteocytes. These bone-secreted factors may target back the primary tumor favoring the acquisition of pro-metastatic bone-related properties in prostate cancer cells and promoting an aggressive and bone organotropic phenotype. In this regard, we have observed upregulated levels of VEGFR2 in tibiae of primary tumor-bearing mice with apparent absence of tumor metastasis. VEGFR2, is a pro-angiogenic receptor expressed in osteoblasts that has been proposed as a target to ameliorate prostate cancer bone metastases (49,50). Recent findings show that inhibition of VEGFR2 in osteoblasts suppresses prostate cancer growth in bone metastases and decreases bone metastatic actions induced by prostate cancer (49). In addition, a VEGFR2 inhibitor, cabozantinib, showed improved symptomatic skeletal events, effects on circulating tumor cells and actions on bone biomarkers in a phase III study of metastatic castration-resistant prostate cancer (50). These findings and our observations suggest that even though TRAMP-C1 cells orthotopically injected in the prostate rarely metastasize to the bone, TRAMP-C1-induced tumors trigger some bone changes in mice that resemble those observed in prostate-induced human bone metastases.

The present data collectively shows that upregulation and secretion of mindin in the primary tumor potentiate ectopic expression of both osteoclastic and osteoblastic genes and favor proliferation, migration and bone adhesion properties of prostate tumor cells *via* ERK activation. In addition, *in vitro* prostate tumor-bone cell crosstalk based on mindin and induction of a pro-angiogenic marker in bone by mindin-expressing tumors are shown. Our results suggest that mindin is a novel modulator of prostate cancer progression and a possible new target to decrease prostate cancer-induced bone metastases and tumor malignancy.

Supplementary material

Supplementary data are available at *Carcinogenesis* online.

Funding

Instituto de Salud Carlos III (PI12/02390); CEU San Pablo-Santander (USP-BS-PPC 11/2012, USPB-BS-APP-2/2016 and MERMERG-2); Proyecto Emergente (MERMERG-2) to I.G.R.

Acknowledgements

We thank CBMSO PROTEIN CHEMISTRY FACILITY that belongs to ProteoRed, PRB2-ISCIII, supported by grant PT13/0001 for the proteomic analysis. We also thank the Animal and Experimental Surgery Service of San Pablo CEU University for the support.
Conflict of Interest Statement: None declared.

References

1. Wong, M.C. *et al.* (2016) Global incidence and mortality for prostate cancer: analysis of temporal patterns and trends in 36 countries. Eur. Urol., 70, 862–874.
2. Logothetis, C.J. *et al.* (2005) Osteoblasts in prostate cancer metastasis to bone. Nat. Rev. Cancer, 5, 21–28.

3. Eaton, C.L. *et al.* (2003) Pathophysiology of bone metastases from prostate cancer and the role of bisphosphonates in treatment. Cancer Treat. Rev., 29, 189–198.
4. Kan, C. *et al.* (2016) Cancer cell colonisation in the bone microenvironment. Int. J. Mol. Sci., 17, 1–16.
5. Croucher, P.I. *et al.* (2016) Bone metastasis: the importance of the neighbourhood. Nat. Rev. Cancer, 16, 373–386.
6. Baniwal, S.K. *et al.* (2010) Runx2 transcriptome of prostate cancer cells: insights into invasiveness and bone metastasis. Mol. Cancer, 9, 258.
7. Koeneman, K.S. *et al.* (1999) Osteomimetic properties of prostate cancer cells: a hypothesis supporting the predilection of prostate cancer metastasis and growth in the bone environment. Prostate, 39, 246–261.
8. Dougall, W.C. *et al.* (2014) Targeting RANKL in metastasis. Bonekey Rep., 3, 519.
9. Pérez-Martínez, F.C. *et al.* (2008) Receptor activator of nuclear factor-kappaB ligand (RANKL) as a novel prognostic marker in prostate carcinoma. Histol. Histopathol., 23, 709–715.
10. Pérez-Martínez, F.C. *et al.* (2007) Immunohistochemical analysis of low-grade and high-grade prostate carcinoma: relative changes of parathyroid hormone-related protein and its parathyroid hormone 1 receptor, osteoprotegerin and receptor activator of nuclear factor-kB ligand. J. Clin. Pathol., 60, 290–294.
11. Ge, C. *et al.* (2016) Role of Runx2 phosphorylation in prostate cancer and association with metastatic disease. Oncogene, 35, 366–376.
12. Li, X. *et al.* (2014) Potential role of the OPG/RANK/RANKL axis in prostate cancer invasion and bone metastasis. Oncol. Rep., 32, 2605–2611.
13. Gardner, T.A. *et al.* (2009) Differential expression of osteocalcin during the metastatic progression of prostate cancer. Oncol. Rep., 21, 903–908.
14. Armstrong, A.P. *et al.* (2008) RANKL acts directly on RANK-expressing prostate tumor cells and mediates migration and expression of tumor metastasis genes. Prostate, 68, 92–104.
15. Holen, I. *et al.* (2002) Osteoprotegerin (OPG) is a survival factor for human prostate cancer cells. Cancer Res., 62, 1619–1623.
16. Kingsley, L.A. *et al.* (2007) Molecular biology of bone metastasis. Mol. Cancer Ther., 6, 2609–2617.
17. Dougall, W.C. (2012) Molecular pathways: osteoclast-dependent and osteoclast-independent roles of the RANKL/RANK/OPG pathway in tumorigenesis and metastasis. Clin. Cancer Res., 18, 326–335.
18. Wang, N. *et al.* (2015) The frequency of osteolytic bone metastasis is determined by conditions of the soil, not the number of seeds; evidence from *in vivo* models of breast and prostate cancer. J. Exp. Clin. Cancer Res., 34, 124.
19. Paget, S. (1989) The distribution of secondary growths in cancer of the breast. 1889. Cancer Metastasis Rev., 8, 98–101.
20. Lucarelli, G. *et al.* (2013) Spondin-2, a secreted extracellular matrix protein, is a novel diagnostic biomarker for prostate cancer. J. Urol., 190, 2271–2277.
21. Qian, X. *et al.* (2012) Spondin-2 (SPON2), a more prostate-cancer-specific diagnostic biomarker. PLoS One, 7, e37225.
22. Parry, R. *et al.* (2005) Identification of a novel prostate tumor target, mindin/RG-1, for antibody-based radiotherapy of prostate cancer. Cancer Res., 65, 8397–8405.
23. Zhu, B.P. *et al.* (2017) Serum BSP, PSADT, and Spondin-2 levels in prostate cancer and the diagnostic significance of their ROC curves in bone metastasis. Eur. Rev. Med. Pharmacol. Sci., 21, 61–67.
24. Li, Y. *et al.* (2009) Structure of the F-spondin domain of mindin, an integrin ligand and pattern recognition molecule. EMBO J., 28, 286–297.
25. de Lau, W.B. *et al.* (2012) The R-spondin protein family. Genome Biol., 13, 242.
26. Palmer, G.D. *et al.* (2014) F-spondin deficient mice have a high bone mass phenotype. PLoS One, 9, e98388.
27. Zhu, C. *et al.* (2016) LGR4 acts as a key receptor for R-spondin 2 to promote osteogenesis through Wnt signaling pathway. Cell. Signal., 28, 989–1000.
28. Somers, K.D. *et al.* (2003) Orthotopic treatment model of prostate cancer and metastasis in the immunocompetent mouse: efficacy of flt3 ligand immunotherapy. Int. J. Cancer, 107, 773–780.
29. Alonso, R. *et al.* (2014) Fungal infection in patients with Alzheimer's disease. J. Alzheimers. Dis., 41, 301–311.
30. Strober, W. (2001) Trypan blue exclusion test of cell viability. Curr. Protoc. Immunol. Appendix 3: Appendix 3B. doi:10.1002/0471142735.ima03bs21
31. Liang, C.C. *et al.* (2007) *In vitro* scratch assay: a convenient and inexpensive method for analysis of cell migration *in vitro*. Nat. Protoc., 2, 329–333.
32. Yang, D. *et al.* (2001) Murine six-transmembrane epithelial antigen of the prostate, prostate stem cell antigen, and prostate-specific membrane antigen: prostate-specific cell-surface antigens highly expressed in prostate cancer of transgenic adenocarcinoma mouse prostate mice. Cancer Res., 61, 5857–5860.
33. Bishop, K.A. *et al.* (2011) Mouse Rankl expression is regulated in T cells by c-Fos through a cluster of distal regulatory enhancers designated the T cell control region. J. Biol. Chem., 286, 20880–20891.
34. Wang, B. *et al.* (2015) Chondrocytes-specific expression of osteoprotegerin modulates osteoclast formation in metaphyseal bone. Sci. Rep., 5, 1–12.
35. Schmittgen, T.D. *et al.* (2008) Analyzing real-time PCR data by the comparative C(T) method. Nat. Protoc., 3, 1101–1108.
36. Friedman, M.S. *et al.* (2009) Wnt11 promotes osteoblast maturation and mineralization through R-spondin 2. J. Biol. Chem., 284, 14117–14125.
37. Michalaki, V. *et al.* (2004) Serum levels of IL-6 and TNF-alpha correlate with clinicopathological features and patient survival in patients with prostate cancer. Br. J. Cancer, 90, 2312–2316.
38. Gingrich, J.R. *et al.* (1996) Metastatic prostate cancer in a transgenic mouse. Cancer Res., 56, 4096–4102.
39. Zhang, M. *et al.* (2017) RSPO3-LGR4 regulates osteogenic differentiation of human adipose-derived stem cells via ERK/FGF signalling. Sci. Rep., 7, 42841.
40. Gartrell, B.A. *et al.* (2014) Managing bone metastases and reducing skeletal related events in prostate cancer. Nat. Rev. Clin. Oncol., 11, 335–345.
41. Jones, D.H. *et al.* (2006) Regulation of cancer cell migration and bone metastasis by RANKL. Nature, 440, 692–696.
42. Jin, R. *et al.* (2013) Activation of NF-kappa B signaling promotes growth of prostate cancer cells in bone. PLoS One, 8, e60983.
43. Huang, W. *et al.* (2007) Signaling and transcriptional regulation in osteoblast commitment and differentiation. Front. Biosci., 12, 3068–3092.
44. Akech, J. *et al.* (2010) Runx2 association with progression of prostate cancer in patients: mechanisms mediating bone osteolysis and osteoblastic metastatic lesions. Oncogene, 29, 811–821.
45. Guleng, B. *et al.* (2010) Mindin is upregulated during colitis and may activate NF-kappaB in a TLR-9 mediated manner. World J. Gastroenterol., 16, 1070–1075.
46. Feinstein, Y. *et al.* (1999) F-spondin and mindin: two structurally and functionally related genes expressed in the hippocampus that promote outgrowth of embryonic hippocampal neurons. Development, 126, 3637–3648.
47. Jia, W. *et al.* (2005) The extracellular matrix protein mindin serves as an integrin ligand and is critical for inflammatory cell recruitment. Blood, 106, 3854–3859.
48. Fu, Z. *et al.* (2002) Osteoblasts produce soluble factors that induce a gene expression pattern in non-metastatic prostate cancer cells, similar to that found in bone metastatic prostate cancer cells. Prostate, 51, 10–20.
49. Lee, C. *et al.* (2018) Dual targeting c-met and VEGFR2 in osteoblasts suppresses growth and osteolysis of prostate cancer bone metastasis. Cancer Lett., 414, 205–213.
50. Smith, M. *et al.* (2016) Phase III study of cabozantinib in previously treated metastatic castration-resistant prostate cancer: COMET-1. J. Clin. Oncol., 34, 3005–3013.

RESEARCH

MINDIN secretion by prostate tumors induces premetastatic changes in bone via β-catenin

Juan A Ardura[1,2,*], Luis Álvarez-Carrión[1,*], Irene Gutiérrez-Rojas[1], Peter A Friedman[3], Arancha R Gortázar[1,2] and **Verónica Alonso[1,2]**

[1]Bone Physiopathology Laboratory, Applied Molecular Medicine Institute (IMMA), Universidad San Pablo-CEU, CEU Universities, Campus Monteprincipe, Madrid, Spain
[2]Departamento de Ciencias Médicas Básicas, Facultad de Medicina, Universidad San Pablo-CEU, CEU Universities, Campus Monteprincipe, Madrid, Spain
[3]Laboratory for G Protein-Coupled Receptor Biology, Department of Pharmacology & Chemical Biology, University of Pittsburgh School of Medicine, Pittsburgh, Pennsylvania, USA

Correspondence should be addressed to V Alonso: veronica.alonsorodriguez@ceu.es

*(J A Ardura and L Álvarez-Carrión contributed equally to this work)

Abstract

Bone metastases are common in advanced prostate cancer patients, but mechanisms by which specific pro-metastatic skeletal niches are formed before tumor cell homing are unclear. We aimed to analyze the effects of proteins secreted by primary prostate tumors on the bone microenvironment before the settlement and propagation of metastases. Here, using an *in vivo* pre-metastatic prostate cancer model based on the implantation of prostate adenocarcinoma TRAMP-C1 cells in immunocompetent C57BL/6 mice, we identify MINDIN as a prostate tumor secreted protein that induces bone microstructural and bone remodeling gene expression changes before tumor cell homing. Associated with these changes, increased tumor cell adhesion to the endosteum *ex vivo* and to osteoblasts *in vitro* was observed. Furthermore, MINDIN promoted osteoblast proliferation and mineralization and monocyte expression of osteoclast markers. β-catenin signaling pathway revealed to mediate MINDIN actions on osteoblast gene expression but failed to affect MINDIN-induced adhesion to prostate tumor cells or monocyte differentiation to osteoclasts. Our study evidences that MINDIN secretion by primary prostate tumors creates a favorable bone environment for tumor cell homing before metastatic spread.

Key Words

- MINDIN, bone
- prostate tumor
- pre-metastatic niche
- β-catenin

Endocrine-Related Cancer (2020) **27**, 441–456

Introduction

Advanced cancers that progress to tumor metastases are often considered incurable or difficult to treat (Weilbaecher *et al.* 2011, Logothetis *et al.* 2018). Bone is the third most frequent site for metastatic disease, with an incidence of 65–80% in patients suffering from common diagnosed tumors such as those of the prostate, breast, and lung (Mundy 2002, Salamanna *et al.* 2016). Preventing bone metastasis is a major goal of treatment, and elucidation of the crucial factors contributing to the development of skeletal metastasis is key to improve cancer survival. A series of studies suggest that bone metastatic organotropism, the ability of tumor cells to colonize specifically bone, is due to cancer cell acquisition of osteomimetic features,that is, they express highly restricted markers of bone and adopt behaviors of bone cells. Osteomimicry promotes productive interaction

https://erc.bioscientifica.com
https://doi.org/10.1530/ERC-20-0116

of cancer cells with the skeletal microenvironment, as well as survival advantages and cancer cell growth (Koeneman *et al.* 1999, Zayzafoon *et al.* 2004, Gupta & Massagué 2006, Kingsley *et al.* 2007, Baniwal *et al.* 2010, Croucher *et al.* 2016, Kan *et al.* 2016). In bone metastasis it is hypothesized that tumor cells home to specific niches such as the endosteal niche, the hematopoietic stem cell niche, and the vascular niche (Ottewell 2016). Primary tumor invasion of these niches in bone is associated with osteoclast and osteoblast activation by tumor cells, resulting in the liberation of growth factors from the bone matrix that can in turn enhance tumor growth. The resulting 'vicious cycle' of bone metastasis changes the normal bone physiology and triggers uncoupled bone remodeling (Roodman 2004, Guise *et al.* 2006, Akech *et al.* 2010). In this process, tumor cells produce cytokines and growth factors, which either directly stimulate osteoclast maturation or indirectly promote osteoclast differentiation (Ell & Kang 2012). Bone matrix resorption by activated osteoclasts releases TGF-β and insulin-like growth factor-1 (IGF-1) and promotes the survival and proliferation of cancer cells inducing osteolytic metastatic lesions (Quail & Joyce 2013). In contrast, other factors such as fibroblast growth factor (FGF), bone morphogenetic proteins (BMPs), and IGFs can also be secreted by tumor cells to stimulate osteoblast differentiation and subsequent uncontrolled bone formation, resulting in osteoblastic lesions (Suva *et al.* 2011). In the case of prostate cancer, it has been proposed that bone metastases are promoted by both osteolytic and osteoblastic activity (Keller & Brown 2004).

Although tumor-bone 'vicious cycle' mechanisms at metastatic sites have been described, the primary processes triggering formation of the metastatic niche and the colonization of a predetermined location by tumor cells are largely unknown. In this regard, bone marrow hematopoietic progenitor cells modify metastatic secondary sites, such as lung, before the establishment of the tumor cells (Kaplan *et al.* 2005). Tumors actively recruit various bone marrow-derived cell types to the tumor microenvironment, where these cells facilitate primary tumor development and metastasis (Polyak & Hu 2008). Other observations reveal a series of sequential events that imply formation of specific regions in the liver with respect to future metastases induced by pancreatic cancer (Costa-Silva *et al.* 2015). These studies propose pro-metastatic changes in organs where metastases later appear. Such changes involve the formation of pre-metastatic niches that can be defined as receptive tissue microenvironments undergoing molecular and cellular modifications to form the metastatic-designated sites, in preparation for metastatic tumor cell colonization, thus supporting tumor settlement in distant organs (Kaplan *et al.* 2005, Peinado *et al.* 2012, Cox *et al.* 2015, Liu & Cao 2016). Nevertheless, pre-metastatic niche formation in bone during primary prostate tumor progression has not been sufficiently studied.

Primary tumor-secreted soluble molecules play critical roles in preparing distant sites for *de novo* pre-metastatic niche formation, thereby promoting metastasis and even determining metastatic organotropism (Liu & Cao 2016). MINDIN, a secreted extracellular matrix protein, has been shown to be overexpressed in individuals with prostate tumors that present high risk to progress to metastatic disease compared with patients with low metastatic risk tumors, suggesting that this protein could be used as diagnostic biomarker of prostate cancer (Qian *et al.* 2012, Lucarelli *et al.* 2013, Zhu *et al.* 2017). Moreover, recently our group has described that overexpression of MINDIN in tumors and adenocarcinoma cells correlates with increased osteomimetic gene expression and with the potential of MINDIN-expressing cells to metastasize to bone (Ardura *et al.* 2019). This protein, also known as spondin-2, belongs to the thrombospondin type 1 repeat (TSR-1)-containing class of molecules (Li *et al.* 2009). Interestingly, other members of the TSR-1 superfamily that share some structural domains with MINDIN, namely F-spondin and R-spondins (de Lau *et al.* 2012), have been shown to trigger changes in bone by regulating bone morphogenetic proteins or the Wnt/β-catenin signaling pathway (Friedman *et al.* 2009, Palmer *et al.* 2014, Zhu *et al.* 2016). However, no previous reports describe the effects of MINDIN on bone or whether a crosstalk between MINDIN and Wnt/β-catenin signaling pathway exists.

Based on these observations, we hypothesized that MINDIN secreted by primary prostate tumors triggers changes in the bone microenviroment, thereby inducing the formation of a pre-metastatic bone niche.

Materials and methods

Cell culture

Mouse adenocarcinoma prostate TRAMP-C1 (ATCC: CRL-2730) cells were grown in DMEM supplemented with 5% FBS and 5% Nu-serum IV, 0.005 mg/mL bovine insulin and 10 nM dehydroisoandrosterone. Mouse osteoblastic MC3T3-E1 (ATCC: CRL-2593) and monocytic RAW 264.7 cells (ATCC: TIB-71) were grown in DMEM

https://erc.bioscientifica.com
https://doi.org/10.1530/ERC-20-0116

with 10% fetal bovine serum (FBS) and osteocyte MLO-Y4 cells (generously donated by Lynda Bonewald) were grown in α-MEM with 2.5% fetal calf serum (FCS) and 2.5% FBS in collagen-coated surface (collagen solution from calf skin (Sigma-Aldrich)), respectively as previously described (Ardura *et al.* 2018). All cells were cultured with penicillin (100 units/mL) and streptomycin (100 µg/mL) in a 5% CO_2 humidified incubator at 37°C. TRAMP-C1, MC3T3-E1, MLO-Y4 and RAW 264.7 cells were incubated with 5 ng/mL MINDIN (R&D Systems) for 6 h, 24 h or 15 days, when appropriate. To avoid effects of degradation during long exposures of the peptide we changed the cell culture medium every 48 h and included a fresh MINDIN dose every 2 days over the 15-day treatment. We confirm the suitability of these cells and markers to be used in the TRAMP-C1 mouse model. In this regard, MINDIN and the prostate-specific marker prostate stem cell antigen (PSCA) were specifically expressed in TRAMP-C1 cells but not in osteoblastic MC3T3-E1 or osteocytic MLO-Y4 cells (Supplementary Fig. 1A and B, see section on supplementary materials given at the end of this article). Similarly, MINDIN secretion has been described in TRAMP-C1 (Ardura *et al.* 2019) cells but not in MC3T3-E1 or MLO-Y4 cells (Supplementary Table 1).

Conditioned medium of TRAMP-C1 cells was obtained as follows: TRAMP-C1 cells were transfected with scrambled or MINDIN siRNAs for 24 h. Then, cells were washed with PBS and incubated with FBS-depleted DMEM for 24 h. Each conditioned medium was collected and added to bone cells at a 1/4 dilution in MC3T3-1 or MLO-Y4 corresponding culture medium.

Secretome mass spectrometry analysis

Initially, protein extracts (50 µg) from TRAMP-C1, MC3T3-E1 and MLO-Y4 cells conditioned mediums were separated by PAGE under reducing conditions according to Laemmli, with a 12.5% separating gel and a 5% stacking gel. Protein staining was carried out with GelCode Blue Stain Reagent (Thermo Scientific). Separation of proteins and gel excision were carried out essentially as previously described (Ardura *et al.* 2019). The peptide extracts were combined into three pools of discontinuous bands to reduce the analysis by liquid chromatography–mass spectrometry (LC-MS) to four runs per sample. Peptides were detected in survey scans from 400 to 1600 amu (1 µscan), followed by 20 data-dependent MS/MS scans (Top 20), using an isolation width of 2 µ (in mass-to-charge ratio units), normalized collision energy of 35%, and dynamic exclusion applied during 30-s periods.

Processing of the MS data was carried out as previously described (Ardura *et al.* 2019). Peptide identification from raw data was carried out using the SEQUEST algorithm (Proteome Discoverer 1.3, Thermo Scientific).

Cell silencing and inhibition

TRAMP-C1 and MC3T3-E1 cells were silenced with a mixture of three siRNA (each at 20 nM) against different coding sequences of mouse MINDIN (s97640; s97638; s87252; Life Technologies) or with two siRNAs against different coding sequences of mouse β-catenin (s63418; s63419; Life Technologies, each at 20 nM), respectively, using Lipofectamine RNAiMax (Life Technologies) overnight at 37°C, following the manufacturer's instructions. A scrambled sequence (control siRNA-A; Santa Cruz Biotechnology) was used as a negative control for evaluating RNAi off-targeted effects, and in order to verify the accuracy of gene-specific siRNA-dependent changes in different parameters evaluated. Efficiency of MINDIN or β-catenin silencing, assessed by real-time PCR, represented 85% 48 h after transfection and 60% up to 15 days after transfection (data not shown).

To inhibit focal adhesion kinase (Fak) and Src kinase addition of 1 µM Fak inhibitor 14 (Merck) and 1 µM saracatinib (Santa Cruz) for 24 h was performed when appropriate, respectively.

Animal model

Three-month-old C57BL/6 male mice (Charles River) were placed in cages under standard conditions (room temperature 20±0.5°C, relative humidity 55±5% and illumination with a 12 h/12 h light/dark photoperiod), without restriction of movement and were maintained on a standard pellet diet (Teklad Global 18% Protein Rodent Diet, Envigo Madison, WI, USA) and tap water *ad libitum*. Surgical interventions were performed under aseptic conditions in anaesthetized mice by isoflurane inhalation/injection of xylazine (10 mg/kg) and ketamine (25 mg/kg). Briefly, mice were injected in the right posterior prostatic lobe through a midline lower abdominal incision with vehicle (phosphate buffer saline (PBS)) or 5×10^5 TRAMP-C1 cells/50 µL, transfected with scrambled siRNAs or three MINDIN siRNAs (s97640; s97638; s87252) (Life Technologies), harvested after mild trypsinization and PBS washing, as previously described by our group (Ardura *et al.* 2019). A well-localized bleb within the injected prostatic lobe was considered a technically acceptable injection. The abdominal cavity, muscle and

https://erc.bioscientifica.com
https://doi.org/10.1530/ERC-20-0116

skin were closed with surgical staples. After 1 month, primary tumors were extracted and stored in TRIzol for real-time PCR analysis. We chose 1 month after orthotopic injection to ensure the presence of primary prostate tumors and avoid any early homing of TRAMP-C1 cells to the bone tissue. One month of tumor incubation is not sufficient to cause metastasis in the TRAMP-C1 model (a 18–30-week time period is required (Somers *et al.* 2003)). In this regard, no metastases were detected in any organ extracted. This model allows us to study the early effects of prostate tumors on bone tissue before cells metastasize. Next, we collected two different bones, namely femur and tibiae for bone histomorphometry and mRNA evaluation, respectively. Experimental protocols were approved by the Institutional Animal Care and Use Committee of San Pablo CEU University.

Bone histomorphometry

Bone histomorphometry was performed as previously described (Nuche-Berenguer *et al.* 2011). The femora specimens were dehydrated in graded ethanol and embedded in methylmethacrylate. Seven micron-thick sagittal longitudinal sections of the femora obtained with a rotation microtome for hard materials (Leica RM2255, Leica Microsystems) were stained with Goldner's trichrome. Histomorphometric measurements were performed using a light microscope with a reticule-mounted eyepiece grid, and the following parameters were calculated according to the American Society for Bone and Mineral Research recommendations. We used the standardized nomenclature, symbols, and units of the ASBMR Histomorphometry Nomenclature Committee for bone histomorphometry (Dempster *et al.* 2013): bone volume per total tissue volume ratio (BV/TV), trabecular thickness (Tb.Th), trabecular separation (Tb.Sp), trabecular number (Tb.N), osteoblast number/bone perimeter (N.Ob/Pm) and osteoclast number/bone perimeter (N.Oc/Pm).

Real-time PCR

Total RNA was isolated from mouse tibiae samples stored in RNAlater or from bone cells by a standard procedure (TRIzol, Life Technologies), and 2 µg of this RNA was retrotranscripted with cDNA high-capacity retrotranscription kit (Applied Biosystems) following manufacturer's instructions. Gene expression was analyzed by real-time PCR using an ABI PRISM 7500 system (Applied Biosystems). Real-time PCR was done using Sybr premix ex Taq (Takara) with the following mouse-specific primers for prostate stem cell antigen (PSCA): 5′-TTCTCCTGCTGGCCACCTAC-3′ (sense) and 5′-GCAGCTCATCCCTTCACAAT-3′ (antisense) (Ardura *et al.* 2019); RANK-L: 5′-TGTACTTTCGAGCGCAGATG-3′ (sense) and 5′-AGGCTTGTTTCATCCTCCTG-3′ (antisense) (Ardura *et al.* 2019); OPG: 5′-CAGAGCGAAACACAGTTTG-3′ (sense) and 5′-CACACAGGGTGACATCTATTC-3′ (antisense) (Ardura *et al.* 2019); osteocalcin: 5′-GCAATAAGGTAGTGAACAGACTCC-3′ (sense) and 5′-CCATAGATGCGTTTGTAGGCGG-3′ (antisense) (Ardura *et al.* 2019); bone alkaline phosphatase: 5′-CCAGAAAGACACCTTGACTGTGG-3′ (sense) and 5′-TCTTGTCCGTGTCGCTCACCAT-3′ (antisense) (Ardura *et al.* 2019); Runx2: 5′-CCTGAACTCTGCACCAAGTCCT-3′ (sense) and 5′-TCATCTGGCTCAGATAGGAGGG-3′ (antisense) (Ardura *et al.* 2019); TRAP: 5′-CACGAGAGTCCTGCTTGTC-3′ (sense) and 5′-AGTTGGTGTGGGCATACTTC-3′ (antisense) (Ardura *et al.* 2019); Wnt11: 5′-GCTGGCACTGTCCAAGACTC-3′ (sense) and 5′-CTCCCGTGTACCTCTCTCCA-3′ (antisense) (Touma *et al.* 2017). Alternatively, real-time PCR was done using predeveloped fluorogenic mouse-specific TaqMan MGB probes for MINDIN (Mm00513596_m1) (Life Technologies). The mRNA copy numbers were calculated for each sample by using the cycle threshold (Ct) value. 18S or actin rRNA (housekeeping genes) were amplified in parallel with tested genes. The number of amplification steps required to reach an arbitrary intensity Ct was computed. The relative gene expression in cell assays was defined as the relative expression, compared with control, calculated as $2^{-\Delta\Delta Ct}$, where $\Delta\Delta Ct = \Delta Ct$ treatment $- \Delta Ct$ control and $\Delta Ct = Ct$ target gene $- Ct$ 18S. Gene expression of animal samples was represented as individual data points by calculating the 2-ΔCt, as previously described (Schmittgen & Livak 2008). Amplicon specificity was confirmed as the presence of a single peak in the melting curve for each qPCR reaction.

Western blot analysis

Total cell protein extracts were obtained with 50 mM Tris–HCl, pH 7.4, 150 mM NaCl, 1 mM EDTA, 1% Triton X-100, 1% sodium deoxycholate, and 0.1% SDS, supplemented with protease inhibitor cocktail (Sigma-Aldrich), and phosphatase inhibitor cocktail Set II (Calbiochem). To isolate nuclear fractions a standardized nuclear fractioning protocol was followed (Abcam). Protein content in cell extracts was determined by the bicinchoninic acid (BCA) assay (Thermo Fisher Scientific), using BSA as standard.

https://erc.bioscientifica.com
https://doi.org/10.1530/ERC-20-0116

Cell proteins (30–60 µg/lane) were separated on 5–10% polyacrylamide–SDS gels under reducing conditions. After electrophoresis, samples were transferred onto nitrocellulose membranes (Bio-Rad), blocked with 5% defatted milk in 50 mmol/L Tris–HCl, pH 7.5, and 150 mmol/L NaCl with 0.05% Tween 20, and incubated overnight at 4°C with the following rabbit polyclonal antibodies (dilution): phosphorylated (p)-β-catenin (1:1000) and total β-catenin (1:2000) (Cell Signaling Technology). α-Tubulin (Sigma-Aldrich) was used as a loading control. After extensive washing, the membranes were incubated with peroxidase-conjugated goat anti-rabbit IgG and developed by ECL chemiluminiscence (GE Healthcare). Densitometric values of fluorogram bands were normalized to those of the corresponding α-tubulin band.

Immunofluorescence and immunohistochemistry

Cells grown on coverslips were stimulated with MINDIN, fixed in 4% paraformaldehyde and permeabilized with 0.1% Triton-X100 for 5 min. After blocking with 10% BSA for 1 h, they were incubated with a total β-catenin antibody (1:500) (Cell Signaling Technology) overnight at 4°C, followed by an Alexa 543 secondary antibody (1:500) for 1 h at room temperature. Absence of primary antibody was used as negative control. Samples were mounted in Fluorsave (Merck) and examined using a Leica DM-IRB epifluorescence microscope.

Deparaffinized and rehydrated tissue sections were treated for 30 min with hydrogen peroxide 0.3% in PBS to block endogenous peroxidase. Pretreatment of sections by heat (using microwave for two consecutive times of 10 min each at maximum and average power respectively) in citrate buffer, pH 6.0, was performed to enhance immunostaining. To detect cytokeratins, the samples were incubated overnight at 4°C with the anti-cytokeratin pan (Invitrogen) at 1:100 in PBS containing 2% donkey serum. Sections were first incubated for 10 min at room temperature with biotinylated anti-mouse IgG secondary antibody (IHC Kit ref. 95-9943B, Life Technologies) and then with streptavidin peroxidase (Histostatin-SP IHC Kit ref. 95-9943B, Life Technologies). Finally, immunostaining was visualized using diaminobenzidine (Liquid DAB Substrate Kit ref. 002014, Invitrogen). Nuclear contrast was obtained with Harris hematoxylin. Finally, sections were dehydrated in ethanol and mounted into a synthetic resin (Depex, Serva, Heidelberg, Germany). Pictures were obtained using a Leica DFC 425 camera connected to Leica 5500B microscope.

Adhesion assay

The adhesion of TRAMP-C1 adenocarcinoma cells to bone surfaces, MLO-Y4 osteocytes or MC3T3 pre-osteoblasts *in vitro*, was assessed by seeding calcein-AM-labeled TRAMP-C1 cells in deparaffined bone sections of control, scrambled siRNA tumor or MINDIN siRNA tumor groups or a 24-well plate pre-inoculated with collagen, MLO-Y4 or MC3T3-E1 cells at confluence tretated or not with MINDIN for 24 h. TRAMP-C1 cells were pre-incubated with 2 µM calcein-AM (Thermo Scientific) for 30 min, subsequently washed with PBS and seeded onto MLO-Y4 or MC3T3-E1 covered well surfaces. Non-adherent cells were removed after 30 min of incubation with complete medium followed by plate washing with PBS. Next, adherent cells were fixed with 4% paraformaldehyde and images were obtained with a fluorescence microscope (Leica DM5500B). The number of fluorescence-labeled cells was counted in ten different fields per condition.

Statistical analysis

All results are expressed as means ± S.E. Differences among conditions were evaluated by nonparametric variance analysis (Kruskal–Wallis) followed by Dunn's test. A Mann–Whitney test was performed to analyze the differences between vehicle control or scrambled siRNA samples and MINDIN-stimulated or MINDIN siRNA transfected samples *in vitro*.

Results

MINDIN expression by primary prostate tumors induces pre-metastatic modifications of bone microarchitecture and gene expression

Herein, we characterize for the first time, structural and gene expression patterns that could favor metastasis of prostate tumor cells in the bone microenvironment before the settlement and propagation of metastasis. We use a TRAMP-C1 mouse model that recapitulates progression of prostate cancer, from hyperplasia to prostatic intraepithelial neoplasia to potentially metastasize to lymphatic nodes, lungs and bone, as well as contains an intact immune system in which the initial phases of tumor progression and communication with bone are not compromised (Gingrich *et al.* 1996, Ardura *et al.* 2019).

The histomorphometric assessment of bone microarchitecture in this TRAMP-C1 mouse model showed decreased bone volume/total volume,

https://erc.bioscientifica.com
https://doi.org/10.1530/ERC-20-0116

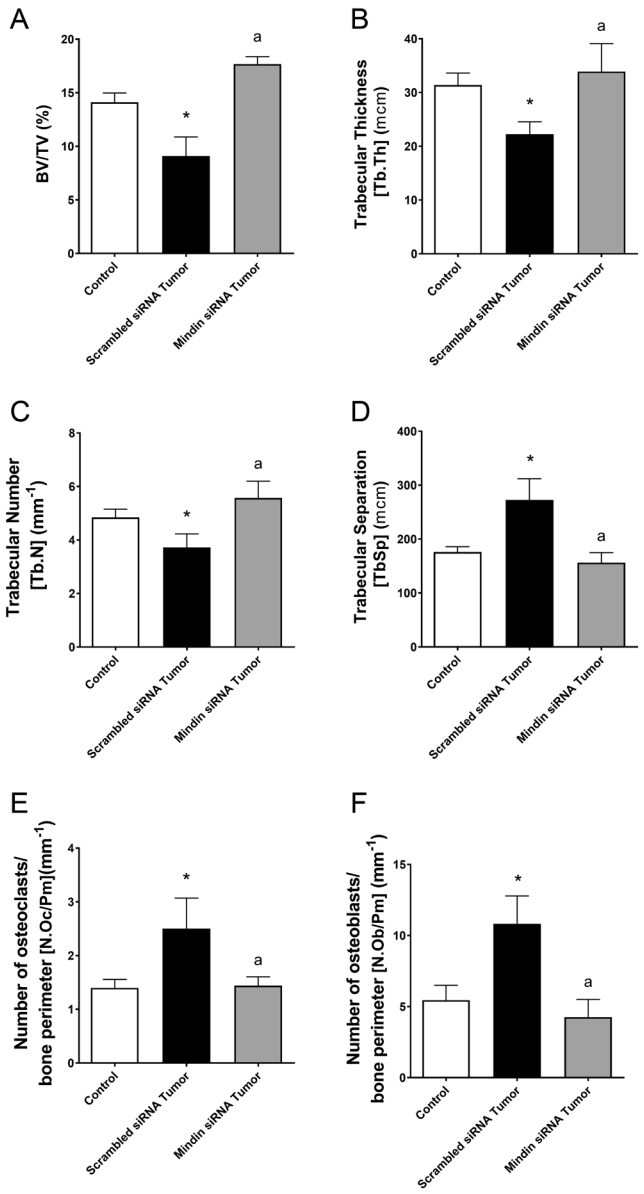

Figure 1
MINDIN induces microstructural changes in femora of mice with TRAMP-C1-generated prostate tumors. Bone histomorphometric parameters were evaluated in femora of control (PBS injection in the prostate gland, without tumor), scrambled siRNA tumor (presence of tumor caused by injection of TRAMP-C1 cells transfected with scrambled siRNA in the prostate gland) and MINDIN siRNA tumor (presence of tumor caused by injection of TRAMP-C1 cells transfected with MINDIN siRNA in the prostate gland) mice as described in materials and methods. BV/TV: Bone volume/total volume; Tb.Th: Trabecular thickness; Tb.N: trabecular number; Tb.Sp: Trabecular separation; N.Oc/Pm: Osteoclast number/ bone perimeter; N.Ob/Pm: Osteoblast number/bone perimeter. The data are represented as the mean ± S.E.M. (n = 7–10 per group). *P < 0.05 vs control; [a]P < 0.05 vs scrambled siRNA tumor.

trabecular thickness and trabecular number (Fig. 1A, B and C) and increased trabecular separation and number of osteoclasts and osteoblasts (Fig. 1D, E and F) in femora of mice with prostate tumors compared to control mice (without prostate tumors). Increased number of osteoclasts and osteoblasts in animals that harbor primary prostate tumors suggest altered skeletal remodeling processes that could lead to increased bone resorption. Altered bone remodeling could in turn be responsible for the aforementioned decreased levels of bone structure parameters as it has been previously described in other prostate animal models (Logothetis *et al.* 2018). Analysis of bone remodeling genes revealed increased expression and enzymatic activity of the osteoclast resorption marker TRAP in tibiae of the tumor group compared to control mice (Fig. 2A and I). Other genes involved in bone formation (Runx2, osterix, osteocalcin), resorption (RANK-L and RANK) or OPG, a decoy receptor for the RANKL-RANK interaction, showed no significant upregulation (Fig. 2C, D, E, F, G and H).

We hypothesized that factors secreted by prostate tumors induce the aforementioned microstructural and gene expression changes in bone before settlement of tumor cells in bone. We recently described overexpression of MINDIN, a member of the spondin family of bone regulatory proteins, in the secretome of prostate tumor TRAMP-C1 and LNCaP cells by proteomic analysis and in primary tumors of the TRAMP-C1-induced prostate cancer model (Ardura *et al.* 2019). Our observations revealed that this protein mediated some bone–tumor crosstalk actions (Ardura *et al.* 2019) and suggested the possible role of MINDIN as an inductor of pre-metastatic changes in bone. In this regard, MINDIN silencing of TRAMP-C1 cells injected in the prostate reversed the histomorphometric and gene expression changes observed in femora and tibiae of our mouse model (Figs 1A, B, C, D, E, F and 2A, B, C, D, E, F, G, H, I). We have confirmed in the TRAMP-C1-induced prostate cancer model that primary tumors overexpress MINDIN, RANK-L and the prostate tumor marker PSCA, whereas MINDIN-silenced tumors presented low levels of MINDIN and RANK-L expression but maintained high levels of PSCA (Ardura *et al.* 2019). MINDIN expression in prostate tumors was 35-fold higher compared to controls. In MINDIN-silenced tumors, expression of MINDIN was reduced to 1.4-fold compared to controls. MINDIN expression in primary prostate

https://erc.bioscientifica.com
https://doi.org/10.1530/ERC-20-0116

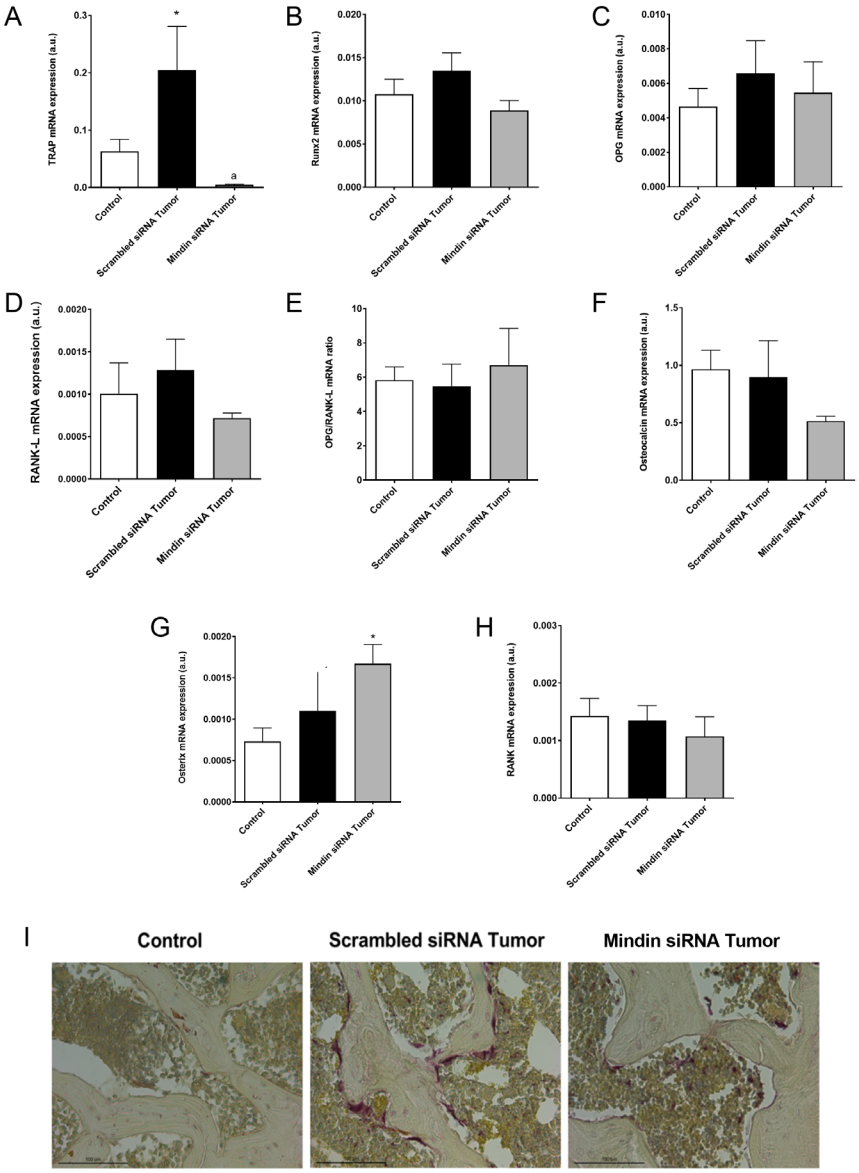

Figure 2
TRAP is overexpressed in tibiae of mice that harbor TRAMP-C1-induced prostate tumors via MINDIN. (A) Tartrate-resistant acid phosphatase (TRAP), (B) Runx2, (C) OPG, (D) RANK-L, (E) OPG/RANK-L, (F) Osteocalcin, (G) Osterix and (H) RANK mRNA expression was assessed by real-time PCR. mRNA expression was assessed in tibiae of the following conditions: control (PBS injection in the prostate gland, without primary tumor), scrambled siRNA tumor (presence of primary tumor caused by injection of TRAMP-C1 cells transfected with scrambled siRNA in the prostate gland) and MINDIN siRNA tumor (presence of tumor caused by injection of TRAMP-C1 cells transfected with MINDIN siRNA in the prostate gland). (I) Representative images of TRAP staining analyzed in femora bone sections of the different groups are shown. Scale bar denotes 100 µm. The data are represented as the mean ± S.E.M. (n = 7–10 per group). *P < 0.05 vs control; ^{a}P < 0.05 vs scrambled siRNA tumor. A full colour version of this figure is available at https://doi.org/10.1530/ERC-20-0116.

tumors in the different experimental conditions used was the following (mean ± S.E.M.); control: 0.00014 ± 0.00005, scrambled siRNA-tumor: 0:005 ± 0.002 and MINDIN siRNA-transfected tumors: 0.0002 ± 0.00005.

Even though the TRAMP model can potentially develop bone metastases after several weeks (Gingrich *et al.* 1996), analysis of the expression of prostate tumor cell markers in entire femora and tibiae of mice corresponding to our groups of study showed negligible levels of PSCA and MINDIN gene expression levels – similar to those observed in the non-tumoral group – (Fig. 3). In addition, there was no cytokeratin labeling in bones of the studied groups (data not shown) confirming the absence of bone metastases after 1 month of TRAMP-C1 orthotopic injection.

These results suggest that MINDIN-expressing prostate tumors induce alterations in the bone microenviroment in the absence of prostate cancer metastases.

MINDIN increases prostate adenocarcinoma cell adhesion to bone and Wnt11 expression

MINDIN has been reported to increase adhesion of different types of cells to the extracellular matrix, including neutrophils, macrophages or lymphocytes (Jia *et al.* 2005, Li *et al.* 2006). Thus, we wondered whether secretion of MINDIN by prostate tumors could increase adenocarcinoma cell adhesion to bone surfaces. TRAMP-C1 cells showed increased adhesion to trabecular

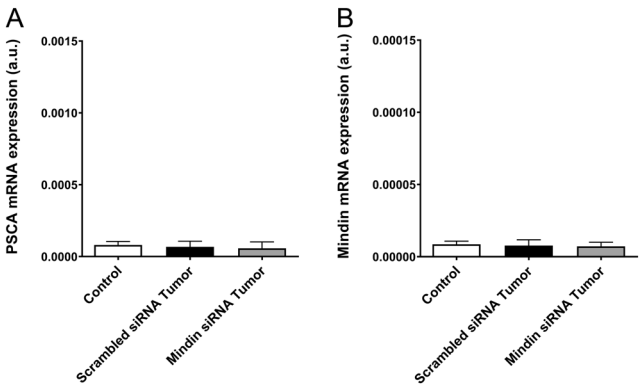

Figure 3
Absence of bone metastases in the experimental mouse model of prostatic tumor induced by TRAMPC-1. (A) Prostate stem cell antigen (PSCA) and (B) MINDIN mRNA expression in control (PBS injection in the prostate gland, without tumor), scrambled siRNA tumor (presence of tumor caused by injection of TRAMP-C1 cells transfected with scrambled siRNA in the prostate gland) and MINDIN siRNA tumor (presence of tumor caused by injection of TRAMP-C1 cells transfected with MINDIN siRNA in the prostate gland) entire tibiae from mice assessed by real-time PCR. The data are represented as the mean ± S.E.M. (n = 7–10 per group). *P < 0.05 vs control; [a]P < 0.05 vs scrambled siRNA tumor.

bone *ex vivo* in the prostate tumor group compared to the control group (Fig. 4A). Nonetheless, MINDIN silencing in the primary tumor inhibited TRAMP-C1 adhesion to trabecular bone (Fig. 4A). Even though Fig. 3 shows no TRAMP-C1 metastasis to the bone *in vivo* in our model, our *ex vivo* results suggest that MINDIN can potentially promote prostate cancer cell adhesion to pre-metastatic niches of the bone microenvironment. To elucidate whether extracellular matrix or bone cell surfaces were necessary for MINDIN-dependent adenocarcinoma cell adhesion to bone, we incubated MC3T3 osteoblast-like cells, osteocyte-like MLO-Y4 cells, and collagen I-coated surfaces with MINDIN. Incubation of collagen-coated surfaces with MINDIN slightly increased the number of TRAMP-C1 cells attached to the plate surface compared to uncoated or collagen-coated surfaces without peptide incubation (Fig. 4B). Moreover, the number of TRAMP-C1 cells attached to MINDIN-stimulated MC3T3 or MLO-Y4 cells was significantly higher compared to collagen-coated surfaces incubated with MINDIN or with non-stimulated cells (Fig. 4B). Furthermore, TRAMP-C1 adhesion to MC3T3 osteoblastic cells was higher than to osteocyte MLO-Y4 cells (Fig. 4B). These data could point out to a role of MINDIN on tumor cell-bone cell adhesion.

Given that osteogenic actions associated with Wnt11 and R-spondin 2 upregulation have been previously reported in osteoblasts (Friedman *et al.* 2009), we tested whether Wnt11 could be a mediator of MINDIN in prostate cancer cells. In this regard, we observed that MINDIN-silenced TRAMP-C1 cells expressed lower mRNA levels of Wnt11 compared to scrambled-silenced controls (Fig. 4C).

MINDIN increases the expression of bone formation genes and mineralization of osteoblasts and osteoclastic differentiation

We next tested the effects of MINDIN on different bone cells, namely osteoblastic MC3T3-E1, osteocyte-like MLO-Y4, and pre-osteoclast RAW 264.7 cells. Increased gene expression of the bone remodeling inhibitor osteoprotegerin (OPG) and osteoblastic differentiation markers including Runx2, osteocalcin, and osterix, and decreased RANK-L expression was observed in MC3T3 cells after MINDIN stimulation for 6 h and 24 h (Fig. 5A, B, C, D, E and F). Similar effects were observed in MC3T3-E1 cells treated with conditioned medium of scrambled siRNA-transfected TRAMP-C1 cells (Fig. 5G, H, I, J, K and L) and in MLO-Y4 cells stimulated with MINDIN (Fig. 6) or with conditioned medium of scrambled siRNA-transfected TRAMP-C1 cells (Fig. 6G, H, I and J). Interestingly, changes in bone markers induced by TRAMP-C1 conditioned medium in MC3T3-E1 (Fig. 5G, H, I, J, K and L) and MLO-Y4 (Fig. 6G, H, I and J) cells were inhibited when stimulating with conditioned medium of MINDIN-silenced TRAMP-C1 cells instead.

Prolonged exposure of MC3T3-E1 cells for 15 days to MINDIN sustained Runx-2 and osteocalcin overexpression but did not affect osterix, OPG, or RANK-L levels (Supplementary Fig. 1C, D, E, F and G). In contrast, prolonged exposure of MLO-Y4 cells for 15 days to MINDIN did not sustain overexpression of any bone marker (Supplementary Fig. 1H, I, J and K).

In addition, incubation with MINDIN for 72 h or 21 days induced an increase in MC3T3 cell proliferation and MC3T3-E1-dependent deposition of bone mineral (calcium phosphate), respectively (Fig. 7).

On the other hand, RAW 264.7 monocytes stimulated with MINDIN showed increased levels of the receptor for RANK-L, RANK (Fig. 7C). Differentiation of RAW 264.7 monocytes to osteoclasts by incubation of these cells with RANK-L for 6 days and subsequent stimulation with MINDIN further increased the expression of TRAP, a marker of osteoclasts, in RAW 264.7 cells compared to incubation with RANK-L alone (Fig. 7D).

https://erc.bioscientifica.com
https://doi.org/10.1530/ERC-20-0116

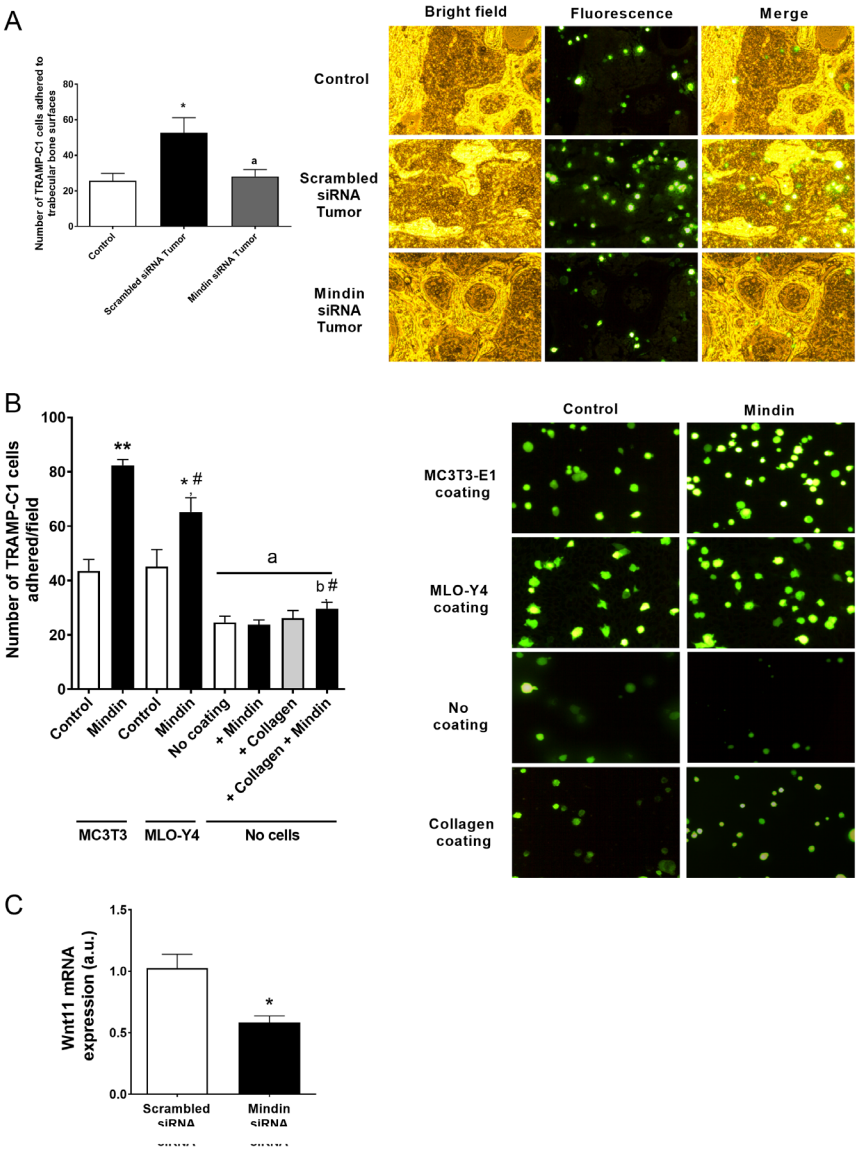

Figure 4
MINDIN increases adenocarcinoma TRAMP-C1 cell adhesion to osteoblastic-covered surfaces and Wnt11 expression. Number of TRAMP-C1 cells labeled with calcein-AM and adhered to bone surfaces in control (PBS injection in the prostate gland, without tumor), scrambled siRNA tumor (presence of tumor caused by injection of TRAMP-C1 cells transfected with scrambled siRNA in the prostate gland) and MINDIN siRNA tumor (presence of tumor caused by injection of TRAMP-C1 cells transfected with MINDIN siRNA in the prostate gland) mice (A), to confluent MC3T3-E1- or MLO-Y4-covered surfaces stimulated or not with MINDIN peptide (5 ng/mL) during 24 h or collagen-coated and non-coated plates is shown (B). Representing images from three experiments in triplicate are shown. (C) Wnt11 mRNA expression was assessed by real-time PCR in TRAMP-C1 cells after 24 h of scrambled or MINDIN siRNA transfection. The data are shown as the mean ± S.E.M. of three experiments in triplicate. $^{*}P < 0.05$ vs corresponding control or scrambled siRNA transfection, $^{**}P < 0.01$ vs corresponding control, $^{\#}P < 0.05$ vs MC3T3 MINDIN-treated condition, $^{a}P < 0.05$ vs scrambled siRNA tumor or cell-coated conditions, $^{b}p < 0.05$ vs corresponding condition without MINDIN treatment. A full colour version of this figure is available at https://doi.org/10.1530/ERC-20-0116.

MINDIN stimulates β-catenin signaling pathway in osteoblast-like cells

Other members of the TSR-1 superfamily that share some structural domains with MINDIN, namely R-spondins (de Lau *et al.* 2012), trigger changes in bone by regulating the β-catenin signaling pathway (Zhu *et al.* 2016). Given that β-catenin signaling has a key role in bone regulation (Baron & Rawadi 2007), we wondered whether MINDIN effects on bone in our model could be caused by activation of the β-catenin signaling pathway. Stimulation of MC3T3 pre-osteoblastic cells with MINDIN induced β-catenin translocation to the nucleus (Fig. 8A), increased nuclear β-catenin levels (Fig. 8B), decreased β-catenin phosphorylation and increased total protein levels of β-catenin (Fig. 8C). Interestingly, β-catenin silencing inhibited MINDIN-dependent downregulation of RANK-L levels and upregulation of the OPG/RANK-L ratio in osteoblasts (Fig. 8D, E, F and G). However, β-catenin silencing did not inhibit MINDIN-dependent increase of osteoblast-adenocarcinoma cell adhesion (Fig. 9A) or MINDIN-induced expression of RANK and TRAP markers in non-differentiated or differentiated RAW 264.7, respectively (Fig. 9B and C). Another member of the spondin family of proteins, spondin 1, has been associated with promotion of osteosarcoma cell migration and invasion through a focal adhesion kinase (Fak) and Src kinase-dependent pathway (Chang *et al.* 2015). Therefore, we tested the role of Fak and Src on MINDIN-induced increase of osteoblast-adenocarcinoma cell

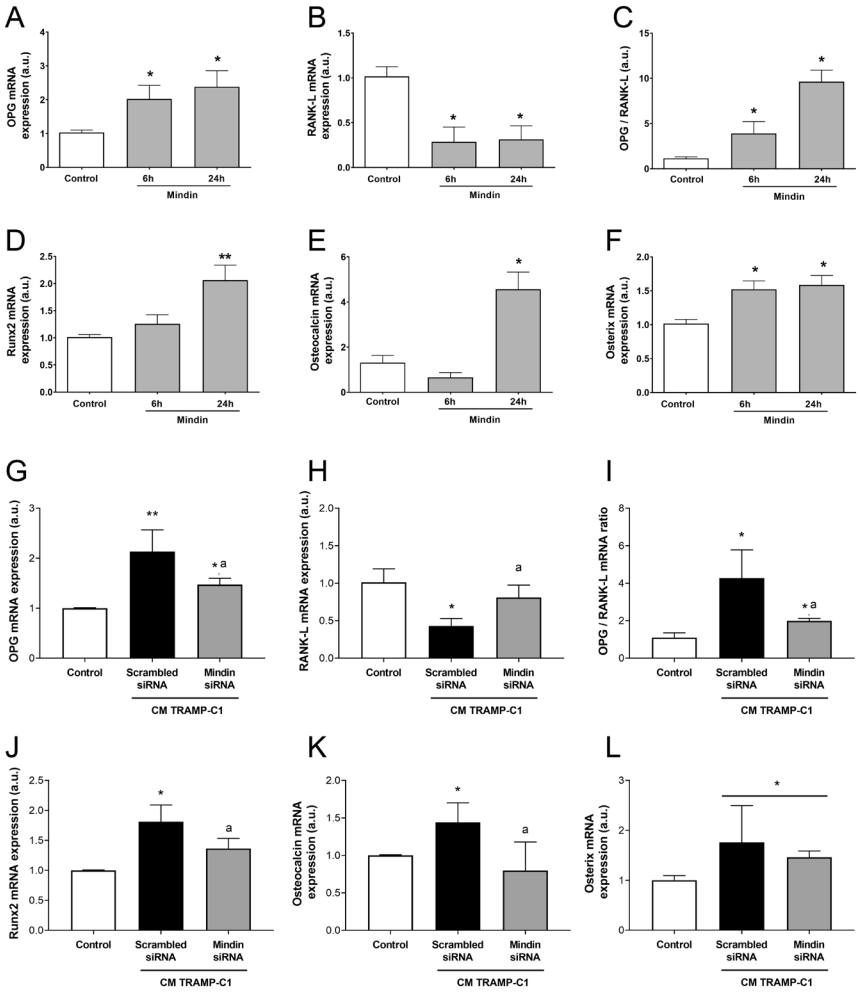

Figure 5
MINDIN and conditioned medium of TRAMP-C1 cells induce changes in bone remodeling markers in osteoblastic MC3T3-E1. MC3T3-E1 cells were stimulated with MINDIN (5 ng/mL) for 6 and 24 h (A, B, C, D, E and F) or with TRAMP-C1 conditioned medium (CM) for 24 h (G, H, I, J, K and L). Total cell RNA was isolated to assess mRNA levels of OPG (A and G), RANK-L (B and H), OPG/RANK-L ratio (C and I), Runx-2 (D and J), osteocalcin (E and K) osterix (F and L) after 6–24 h stimulation with MINDIN or with conditioned medium (CM) of scrambled siRNA- or MINDIN siRNA-transfected TRAMPC-1 cells. Evaluations were performed by real-time PCR. Experimental values are mean ± S.E.M. from three independent experiments. *$P < 0.05$ vs control; **$P < 0.01$ vs control; $^{a}P < 0.05$ vs CM of scrambled siRNA-transfected TRAMP-C1 cells.

adhesion. We observed that treatment of MC3T3-E1 and MLO-Y4 cells with Fak inhibitor 14 and Saracatinib (Src kinase inhibitor) prior to MINDIN stimulation decreased adhesion of TRAMP-C1 cells to both bone cells (Fig. 9D and data not shown). These results suggest that Fak and Src kinase play an important role in prostate cancer cell adhesion to areas rich in bone cells.

Discussion

Primary tumors create favorable pre-metastatic niches in secondary organs for subsequent metastases (Liu & Cao 2016). In the initial phase of pre-metastatic niche formation, primary tumor cells produce various soluble factors to trigger the formation of an immature pre-metastatic niche (Liu & Cao 2016). The discovery of specific factors involved in the formation of the pre-metastatic niche would help the development of future therapeutic strategies. In this regard, formation of a bone pre-metastatic niche by soluble factors is poorly defined in prostate cancer. Herein, we show that expression of the extracellular matrix protein MINDIN by prostate cancer cells induce changes in the bone microenvironment that could promote prostate cancer cell metastases.

We observed that TRAMP-C1-induced tumors in mice cause skeletal microarchitecture and gene expression changes with no detectable presence of metastatic adenocarcinoma cells in bone. MINDIN-dependent changes in osseous microarchitecture revealed a bone resorption pattern, as shown by decreased BV/TV, trabecular number and thickness and increased trabecular separation. Although prostate cancer metastases have been classically defined as mainly osteoblastic and associated with bone formation, they require a resorption phase in their initial steps (Jin *et al.* 2011), while developing mixed osteoblastic and osteoclastic lesions in more advanced stages (Jin *et al.* 2011). In this regard, we observed a higher number of osteoclasts and increased TRAP expression and staining in bones of prostate tumor mice.

https://erc.bioscientifica.com
https://doi.org/10.1530/ERC-20-0116

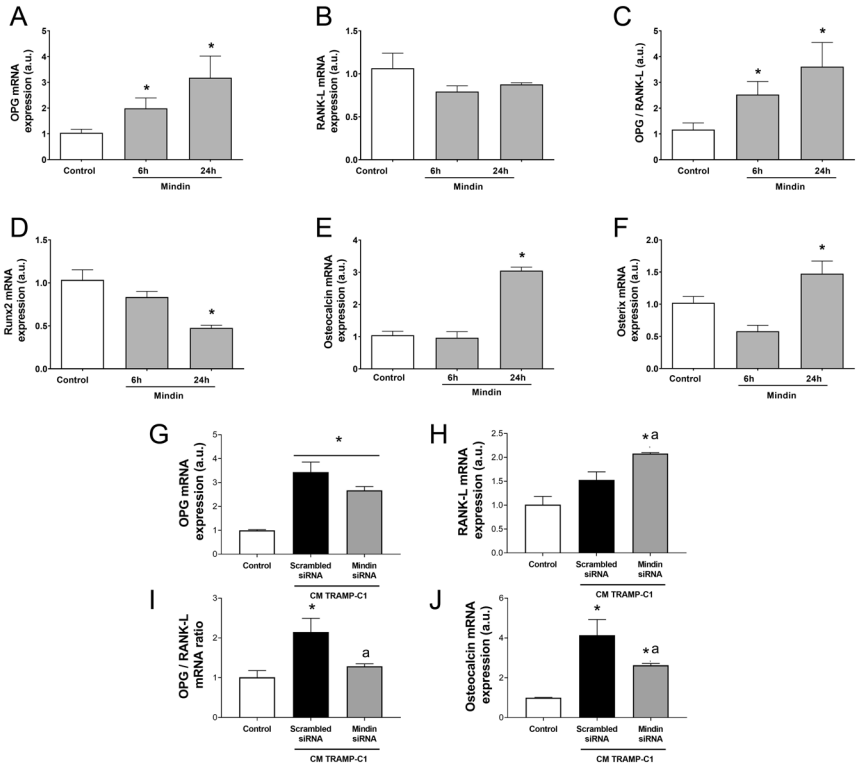

Figure 6
MINDIN and conditioned medium of TRAMP-C1 cells induce changes in bone remodeling markers in osteocytic MLO-Y4. MLO-Y4 cells were stimulated with MINDIN (5 ng/mL) for 6 and 24 h (A, B, C, D, E and F) or with TRAMP-C1 conditioned medium (CM) for 24 h (G, H, I and J). Total cell RNA was isolated to assess mRNA levels of OPG (A and G), RANK-L (B and H), OPG/RANK-L ratio (C and I), Runx-2 (D), osteocalcin (E and J) and osterix (F) after 6–24 h stimulation with MINDIN or with conditioned medium (CM) of scrambled siRNA- or MINDIN siRNA-transfected TRAMPC-1 cells. Evaluations were performed by real-time PCR. Experimental values are mean ± S.E.M. from three independent experiments. $^{*}P < 0.05$ vs control; $^{**}P < 0.01$ vs control; $^{a}P < 0.05$ vs CM of scrambled siRNA-transfected TRAMP-C1 cells.

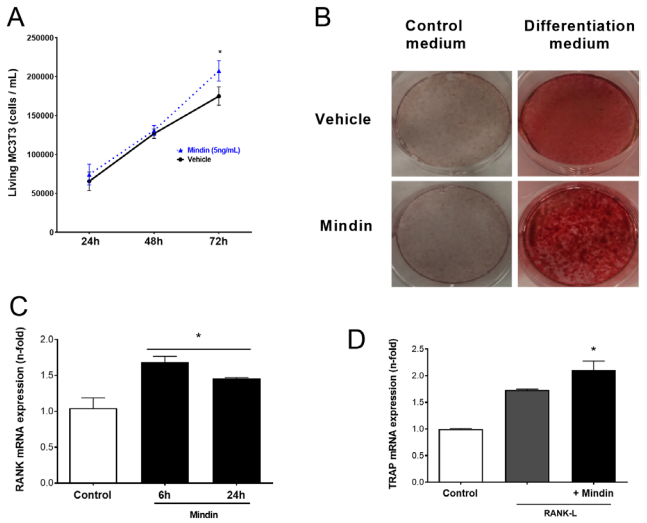

Figure 7
MINDIN induces cell mineralization and proliferation in osteoblastic MC3T3-E1 and triggers the expression of osteoclastic markers in RAW 264.7 macrophage-preosteoclastic cells. MC3T3-E1 cells were stimulated with MINDIN (5 ng/mL) for 24, 48 and 72 h (A) or 21 days (B). (A) Proliferation was assessed by trypan blue cell counting in a Neubauer chamber. (B) Deposition of bone mineral (calcium phosphate) by MC3T3-E1 osteoblastic cells was assessed using Alizarin red S to stain calcium deposits. Representative images of three independent experiments are shown. RAW 264.7 cells were stimulated with MINDIN (5 ng/mL) for 6 and 24 h (C) or 6 days (D). A full colour version of this figure is available at https://doi.org/10.1530/ERC-20-0116.

TRAP, a metalloenzyme that is characteristic for its expression in activated osteoclasts, also promotes metastasis-related cell properties in MDA-MB-231 breast cancer cells (Reithmeier *et al.* 2017) and has been described to be increased in bone metastases of advanced prostate cancer (Nordstrand *et al.* 2018).

On the other hand, increased osteoblast number in bones of prostate tumor-induced animals suggests that prostate tumors promote osteoblast differentiation and activation as evidenced here, even though osteoclastic activity and thus bone resorption is predominant in pre-metastatic bone. Although Runx2 was not substantially increased *in vivo*, our *in vitro* results show that Runx2 levels are upregulated by MINDIN in osteoblasts. In this regard, an intra-tibial metastasis model of prostate cancer showed that high Runx2 levels were associated with development of large tumors, increased expression of metastasis-related genes (Matrix metalloproteinase 9 and 13, VEGF, Osteopontin), and secreted bone resorbing factors (PTHrP, IL-8) promoting osteolytic disease (Akech *et al.* 2010). These observations suggest that Runx2 could be a pivotal factor controlling both osteoblastic and osteoclastic metastatic processes in prostate cancer.

Our data reveal that MINDIN could be a key factor that promotes increased prostate adenocarcinoma cell adhesion to bone surfaces. *In vitro* data suggest that MINDIN preferentially increases adhesion of prostate cancer cells to

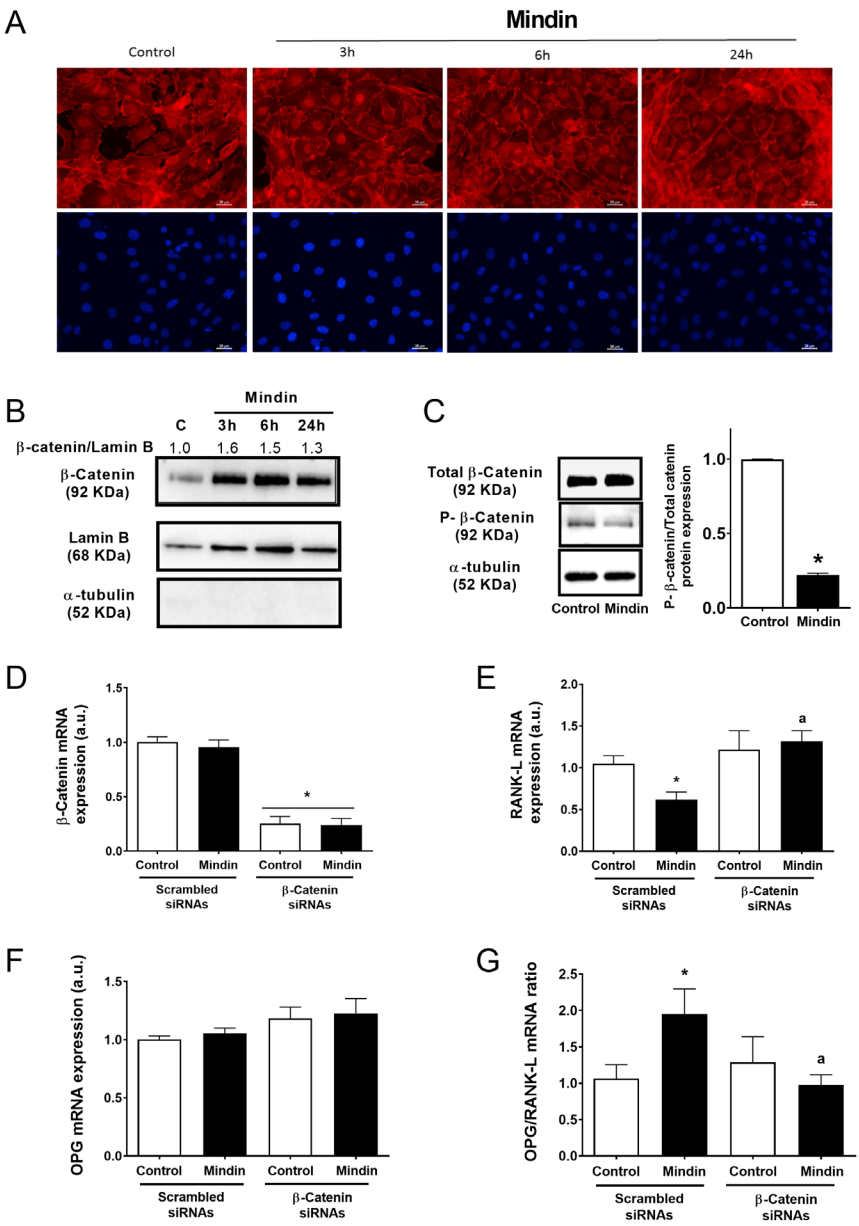

Figure 8
β-Catenin acts as a mediator of MINDIN-induced changes on gene expression of MC3T3-E1 osteoblastic cells. MC3T3-E1 cells were stimulated with MINDIN (5 ng/mL) for different time periods (A: 3 h, 6 h and 24 h; B and C: 24 h). β-Catenin was silenced in some experiments using specific siRNAs as described in materials and methods. (A) Detection of β-catenin was performed by indirect immunofluorescence and fluorescence microscopy. Images represent the results of three independent observations. DAPI was used to stain the nuclei. Nuclear (B) or total (C) cell protein fractions were isolated to evaluate nuclear catenin (B) or phospho-β-catenin and total β-catenin (C) protein expression by Western blot after MINDIN stimulation for 3–24 h. Representative autoradiograms are shown (top panels). α-tubulin was used as loading control. (D, E, F and G) MC3T3 cells were stimulated with MINDIN (5 ng/mL) during 24 h in the presence of scrambled or β-catenin siRNAs. Total cell RNA was isolated to assess mRNA levels of β-catenin (D), RANK-L (E), OPG (F) and OPG/RANK-L ratio (G) by real-time PCR. Experimental values are mean ± S.E.M. from three independent experiments. *$P < 0.05$ versus control; $^{a}P < 0.05$ vs MINDIN-stimulated condition. A full colour version of this figure is available at https://doi.org/10.1530/ERC-20-0116.

bone cell surfaces rather than to the extracellular matrix. Even though MINDIN significantly increased adhesion of prostate cancer cells to collagen, adhesion to osteoblastic or osteocytic cells was much higher. Previous studies showed that MINDIN serves as a ligand for integrins and that MINDIN-integrin interactions are critical for neutrophil, macrophage, and T lymphocyte recruitment *in vivo* (Jia *et al.* 2005, Li *et al.* 2006). It is thus possible that MINDIN binds to specific integrins in prostate cancer cells to enhance their adhesion to the bone extracellular matrix. Alternatively, binding of MINDIN to osteoblast and osteocyte integrins could trigger signals in these bone cells to facilitate adhesion of prostate cancer cells. In this regard, a crosstalk between integrins, Fak and Src kinases has been related with cell adhesion (Huveneers & Danen 2009). Our results showing inhibitory actions of Fak and Src kinase inhibitors on bone cell ability to promote TRAMP-C1 cell adhesion suggest an interplay between these kinases and integrins in prostate cancer cell homing to bone. Furthermore, mouse models of prostate cancer have shown that tumor cells home to areas in bone that have high numbers of osteoblasts in the endosteal niche (Shiozawa *et al.* 2011, Wang *et al.* 2014). The chemokine (C-X-C motif) receptor 4 (CXCR4)/chemokine ligand 12 (CXCL12) interaction is thought to be a key component in the homing and adhesion of tumor cells to

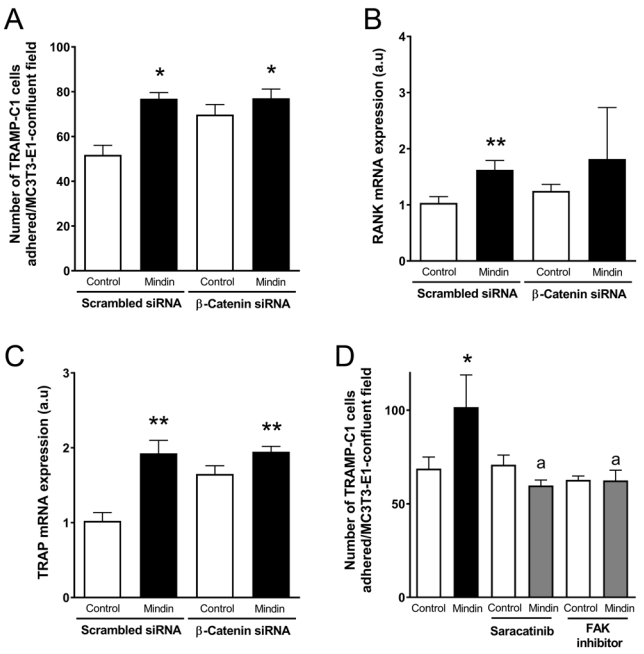

Figure 9

β-Catenin is not a mediator of MINDIN-induced adenocarcinoma TRAMP-C1 cell adhesion to osteoblastic-covered surfaces or osteoclastic differentiation. MC3T3-E1 (A) and RAW 264.7 (B and C) cells were transfected with scrambled control siRNA or β-catenin siRNA for 24 h and subsequently stimulated with PBS (control) or MINDIN peptide (5 ng/mL) for 24 h. (A) Number of TRAMP-C1 cells labeled with calcein-AM and adhered to MC3T3-E1 cells was assessed. (B) RANK and (C) TRAP gene expression in RAW 264.7 cells was evaluated by real-time PCR. (D) Number of TRAMP-C1 cells labeled with calcein-AM and adhered to confluent MC3T3-E1-covered surfaces is shown. MC3T3-E1 cells were treated or not (control) with 1 μM Fak inhibitor 14 or 1 μM saracatinib (Src kinase inhibitor) for 24 h and stimulated with 5 ng/mL MINDIN for 24 h. Experimental values are mean ± S.E.M. from three independent experiments. *$P < 0.05$; *$P < 0.01$ vs control; $^{a}P < 0.05$ vs MINDIN-stimulated condition.

the metastatic niche in bone (Wang *et al.* 2014). CXCL12 is expressed by endosteal cells and a few layers of osteocytes underneath the endosteum (Myers *et al.* 2015). Therefore, MINDIN could promote an increase in CXCL12 expression in cells of the endosteum, in particular osteoblasts, to enhance CXCR4/CXCL12 interactions between tumor and osteoblastic cells. In this regard, adhesion of tumor cells to MINDIN-stimulated MC3T3-E1 osteoblastic cells was higher compared to MLO-Y4 osteocytes in our *in vitro* assays, suggesting that osteoblasts, being the most exposed cells at the endosteal niche, preferentially mediate prostate tumor cell binding to bone. Thus, MINDIN-dependent changes in bone microarchitecture, overexpression of bone factors, and enhanced tumor cell adhesion to bone surfaces, altogether, suggest that expression of MINDIN by primary prostate tumors induce a favorable niche for prostate tumor metastases.

MINDIN effects on bone are further supported by our *in vitro* observations showing the actions of this protein on osteoblast proliferation and differentiation, as well as modulation of different genes involved in bone formation and remodeling (e.g., Runx2, osteocalcin, osterix, OPG, RANK-L). Our conditioned medium experiments also corroborate these findings. As reported in the conditioned medium assays, MINDIN seems to be an important factor secreted by prostate cancer cells that modulates the behavior of bone cells. Prolonged exposure to MINDIN sustained overexpression of osteoblastic differentiation markers in osteoblastic cells but did not affect the OPG/RANK-L axis, suggesting that continuous stimulation with MINDIN promotes osteoblast differentiation but fails to further influence prolonged osteoblast-osteoclast communication. These results support our *in vivo* data showing increased Runx2 expression but no significant changes in OPG and RANK-L levels in bones of prostate tumor-induced mice. Furthermore, osteocytes, the main regulators of RANK-L in bone (Nakashima *et al.* 2011), did not overexpress OPG or RANK-L after prolonged exposure to MINDIN, suggesting that osteogenic genes in osteoblastic cells are the main target of the bone formation actions of MINDIN. Interestingly, MINDIN also triggered osteoclast differentiation and activation after several days of stimulation. Stimulatory actions of MINDIN on both osteoblasts and osteoclasts in the absence of prolonged RANK-L and OPG overexpression could be responsible for uncoupled bone formation by osteoblasts and bone resorption by osteoclasts. In addition, the osteoclastic/resorptive phenotype observed in our model may probably be caused by primary tumor secretion of RANK-L – which could potentially reach the bone microenvironment and participate as the main regulator of osteoclastic differentiation – rather than bone-secreted RANK-L.

There are no previous observations describing the signaling pathways triggered by MINDIN in bone cells. However, other members of the MINDIN family (spondin family) that share a similar thrombospondin domain, namely R-spondin, exhibit activation of the Wnt/β-catenin pathway in association with osteogenesis (Friedman *et al.* 2009, Zhu *et al.* 2016). Wnt/β-catenin activation also has been related to epithelial-mesenchymal transition (EMT), an essential process by which cells lose their epithelial characteristics and acquire mesenchymal features during tumor progression of human prostate cancer (Jiang *et al.* 2007). Therefore, MINDIN-dependent activation of the Wnt/β-catenin pathway could be a central mechanism in prostate tumor progression and metastasis to bone. In this regard, our results showing Wnt11 downregulation

https://erc.bioscientifica.com
https://doi.org/10.1530/ERC-20-0116

in MINDIN-silenced prostate tumor cells suggest the putative role of Wnt signaling in prostate tumor EMT and in certain osteogenic actions of prostate cancer cells that express MINDIN.

The present data collectively show that overexpression of MINDIN in primary tumors promotes modifications of bone microarchitecture and gene expression in pre-metastatic areas in association with an increased adhesion potential to prostate tumor cells. In addition, pro-osteogenic effects were mediated by MINDIN-dependent actions on bone cells *via* a β-catenin signaling pathway. In conclusion, we propose that MINDIN favors the creation of pre-metastatic niches in bone by overexpressing bone remodeling factors and enhancing bone cell-dependent adhesion of prostate cancer cells.

Supplementary materials

This is linked to the online version of the paper at https://doi.org/10.1530/ERC-20-0116.

Declaration of interest

The authors declare that there is no conflict of interest that could be perceived as prejudicing the impartiality of the research reported.

Funding

This work was supported by grants from the Instituto de Salud Carlos III (PI12/02390) and CEU San Pablo-Santander (USP-BS-PPC11/2012, USPB-BS-APP-2/2016 and MERMERG-2 MCP19V10) and FEIOMM RESEARCH 2017 Scholarships.

Author contribution statement

Authors' roles: Study design: J A A and V A. Study conduct: V A. Data collection: I G R, L A C. Data analysis: J A A and V A. Data interpretation: J A A, A R G and V A. Drafting manuscript: J A A and V A. Revising manuscript content: J A A, P A F and V A. Approving final version of manuscript: J A A, I G R, L A C, A R G, P A F, and V A. V A takes responsibility for the integrity of the data analysis.

Acknowledgements

The authors thank CBMSO PROTEIN CHEMISTRY FACILITY that belongs to ProteoRed, PRB2-ISCIII, supported by grant PT13/0001" for the proteomic analysis. They also thank the Animal and Experimental Surgery Service of San Pablo CEU University for the support.

References

Akech J, Wixted JJ, Bedard K, Van Der Deen M, Hussain S, Guise TA, Van Wijnen AJ, Stein JL, Languino LR, Altieri DC, *et al.* 2010 Runx2 association with progression of prostate cancer in patients: mechanisms mediating bone osteolysis and osteoblastic metastatic lesions. *Oncogene* **29** 811–821. (https://doi.org/10.1038/onc.2009.389)

Ardura JA, Gutiérrez Rojas I, Álvarez Carrión L, Friedman PA & Alonso V 2018 Factors secreted by bone cells induce intracellular calcium accumulation and cyclic AMP and activation of ERK 1/2 in prostate cancer cells; evaluation by fluorescence techniques in living cells. *Revista de Osteoporosis y Metabolismo Mineral* **10** 131–138. (https://doi.org/10.4321/S1889-836X2018000400005)

Ardura JA, Gutiérrez-Rojas I, Álvarez-Carrión L, Rodríguez-Ramos MR, Pozuelo JM & Alonso V 2019 The secreted matrix protein mindin increases prostate tumor progression and tumor-bone crosstalk via ERK 1/2 regulation. *Carcinogenesis* **40** 828–839. (https://doi.org/10.1093/carcin/bgz105)

Baniwal SK, Khalid O, Gabet Y, Shah RR, Purcell DJ, Mav D, Kohn-Gabet AE, Shi Y, Coetzee GA & Frenkel B 2010 Runx2 transcriptome of prostate cancer cells: insights into invasiveness and bone metastasis. *Molecular Cancer* **9** 258. (https://doi.org/10.1186/1476-4598-9-258)

Baron R & Rawadi G 2007 Minireview: targeting the Wnt/β-catenin pathway to regulate bone formation in the adult skeleton. *Endocrinology* **148** 2635–2643. (https://doi.org/10.1210/en.2007-0270)

Chang H, Dong T, Ma X, Zhang T, Chen Z, Yang Z & Zhang Y 2015 Spondin 1 promotes metastatic progression through Fak and Src dependent pathway in human osteosarcoma. *Biochemical and Biophysical Research Communications* **464** 45–50. (https://doi.org/10.1016/j.bbrc.2015.05.092)

Costa-Silva B, Aiello NM, Ocean AJ, Singh S, Zhang H, Thakur BK, Becker A, Hoshino A, Mark MT, Molina H, *et al.* 2015 Pancreatic cancer exosomes initiate pre-metastatic niche formation in the liver. *Nature Cell Biology* **17** 816–826. (https://doi.org/10.1038/ncb3169)

Cox TR, Rumney RMH, Schoof EM, Perryman L, Høye AM, Agrawal A, Bird D, Latif NA, Forrest H, Evans HR, *et al.* 2015 The hypoxic cancer secretome induces pre-metastatic bone lesions through lysyl oxidase. *Nature* **522** 106–110. (https://doi.org/10.1038/nature14492)

Croucher PI, McDonald MM & Martin TJ 2016 Bone metastasis: the importance of the neighbourhood. *Nature Reviews: Cancer* **16** 373–386. (https://doi.org/10.1038/nrc.2016.44)

de Lau WBM, Snel B & Clevers HC 2012 The R-spondin protein family. *Genome Biology* **13** 242. (https://doi.org/10.1186/gb-2012-13-3-242)

Dempster DW, Compston JE, Drezner MK, Glorieux FH, Kanis JA, Malluche H, Meunier PJ, Ott SM, Recker RR & Parfitt AM 2013 Standardized nomenclature, symbols, and units for bone histomorphometry: a 2012 update of the report of the ASBMR Histomorphometry Nomenclature Committee. *Journal of Bone and Mineral Research* **28** 2–17. (https://doi.org/10.1002/jbmr.1805)

Ell B & Kang Y 2012 SnapShot: bone metastasis. *Cell* **151** 690.e1–690.e1. (https://doi.org/10.1016/j.cell.2012.10.005)

Friedman MS, Oyserman SM & Hankenson KD 2009 Wnt11 promotes osteoblast maturation and mineralization through R-spondin 2. *Journal of Biological Chemistry* **284** 14117–14125. (https://doi.org/10.1074/jbc.M808337200)

Gingrich JR, Barrios RJ, Morton RA, Boyce BF, DeMayo FJ, Finegold MJ, Angelopoulou R, Rosen JM & Greenberg NM 1996 Metastatic prostate cancer in a transgenic mouse. *Cancer Research* **56** 4096–4102. (https://doi.org/10.1073/PNAS.92.8.3439)

Guise TA, Mohammad KS, Clines G, Stebbins EG, Wong DH, Higgins LS, Vessella R, Corey E, Padalecki S, Suva L, *et al.* 2006 Basic mechanisms responsible for osteolytic and osteoblastic bone metastases. *Clinical Cancer Research* **12** 6213s–6216s. (https://doi.org/10.1158/1078-0432.CCR-06-1007)

Gupta GP & Massagué J 2006 Cancer metastasis: building a framework. *Cell* **127** 679–695. (https://doi.org/10.1016/j.cell.2006.11.001)

Huveneers S & Danen EHJ 2009 Adhesion signaling – crosstalk between integrins, Src and Rho. *Journal of Cell Science* **122** 1059–1069. (https://doi.org/10.1242/jcs.039446)

Jia W, Li H & He YW 2005 The extracellular matrix protein mindin serves as an integrin ligand and is critical for inflammatory cell recruitment. *Blood* **106** 3854–3859. (https://doi.org/10.1182/blood-2005-04-1658)

Jiang YG, Luo Y, He DL, Li X, Zhang LL, Peng T, Li MC & Lin YH 2007 Role of Wnt/β-catenin signaling pathway in epithelial-mesenchymal transition of human prostate cancer induced by hypoxia-inducible factor-1α. *International Journal of Urology* **14** 1034–1039. (https://doi.org/10.1111/j.1442-2042.2007.01866.x)

Jin JK, Dayyani F & Gallick GE 2011 Steps in prostate cancer progression that lead to bone metastasis. *International Journal of Cancer* **128** 2545–2561. (https://doi.org/10.1002/ijc.26024)

Kan C, Vargas G, Le Pape FL & Clézardin P 2016 Cancer cell colonisation in the bone microenvironment. *International Journal of Molecular Sciences* **17** 1674. (https://doi.org/10.3390/ijms17101674)

Kaplan RN, Riba RD, Zacharoulis S, Bramley AH, Vincent L, Costa C, MacDonald DD, Jin DK, Shido K, Kerns SA, *et al*. 2005 VEGFR1-positive haematopoietic bone marrow progenitors initiate the pre-metastatic niche. *Nature* **438** 820–827. (https://doi.org/10.1038/nature04186)

Keller ET & Brown J 2004 Prostate cancer bone metastases promote both osteolytic and osteoblastic activity. *Journal of Cellular Biochemistry* **91** 718–729. (https://doi.org/10.1002/jcb.10662)

Kingsley LA, Fournier PGJ, Chirgwin JM & Guise TA 2007 Molecular biology of bone metastasis. *Molecular Cancer Therapeutics* **6** 2609–2617. (https://doi.org/10.1158/1535-7163.MCT-07-0234)

Koeneman KS, Yeung F & Chung LW 1999 Osteomimetic properties of prostate cancer cells: a hypothesis supporting the predilection of prostate cancer metastasis and growth in the bone environment. *Prostate* **39** 246–261. (https://doi.org/10.1002/(sici)1097-0045(19990601)39:4<246::aid-pros5>3.0.co;2-u)

Li H, Oliver T, Jia W & He YW 2006 Efficient dendritic cell priming of T lymphocytes depends on the extracellular matrix protein mindin. *EMBO Journal* **25** 4097–4107. (https://doi.org/10.1038/sj.emboj.7601289)

Li Y, Cao C, Jia W, Yu L, Mo M, Wang Q, Huang Y, Lim JM, Ishihara M, Wells L, *et al*. 2009 Structure of the F-spondin domain of mindin, an integrin ligand and pattern recognition molecule. *EMBO Journal* **28** 286–297. (https://doi.org/10.1038/emboj.2008.288)

Liu Y & Cao X 2016 Characteristics and significance of the pre-metastatic niche. *Cancer Cell* **30** 668–681. (https://doi.org/10.1016/j.ccell.2016.09.011)

Logothetis C, Morris MJ, Den R & Coleman RE 2018 Current perspectives on bone metastases in castrate-resistant prostate cancer. *Cancer Metastasis Reviews* **37** 189–196. (https://doi.org/10.1007/s10555-017-9719-4)

Lucarelli G, Rutigliano M, Bettocchi C, Palazzo S, Vavallo A, Galleggiante V, Trabucco S, Di Clemente D, Selvaggi FP, Battaglia M, *et al*. 2013 Spondin-2, a secreted extracellular matrix protein, is a novel diagnostic biomarker for prostate cancer. *Journal of Urology* **190** 2271–2277. (https://doi.org/10.1016/J.JURO.2013.05.004)

Mundy GR 2002 Metastasis to bone: causes, consequences and therapeutic opportunities. *Nature Reviews: Cancer* **2** 584–593. (https://doi.org/10.1038/nrc867)

Myers TJ, Longobardi L, Willcockson H, Temple JD, Tagliafierro L, Ye P, Li T, Esposito A, Moats-Staats BM & Spagnoli A 2015 BMP2 regulation of CXCL12 cellular, temporal, and spatial expression is essential during fracture repair. *Journal of Bone and Mineral Research* **30** 2014–2027. (https://doi.org/10.1002/jbmr.2548)

Nakashima T, Hayashi M, Fukunaga T, Kurata K, Oh-hora M, Feng JQ, Bonewald LF, Kodama T, Wutz A, Wagner EF, *et al*. 2011 Evidence for osteocyte regulation of bone homeostasis through RANKL expression. *Nature Medicine* **17** 1231–1234. (https://doi.org/10.1038/nm.2452)

Nordstrand A, Ylitalo EB, Thysell E, Jernberg E, Crnalic S, Widmark A, Bergh A, Lerner UH & Wikström P 2018 Bone cell activity in clinical prostate cancer bone metastasis and its inverse relation to tumor cell androgen receptor activity. *International Journal of Molecular Sciences* **19** 1223. (https://doi.org/10.3390/ijms19041223)

Nuche-Berenguer B, Lozano D, Gutiérrez-Rojas I, Moreno P, Mariñoso ML, Esbrit P & Villanueva-Peñacarrillo ML 2011 GLP-1 and exendin-4 can reverse hyperlipidic-related osteopenia. *Journal of Endocrinology* **209** 203–210. (https://doi.org/10.1530/JOE-11-0015)

Ottewell PD 2016 The role of osteoblasts in bone metastasis. *Journal of Bone Oncology* **5** 124–127. (https://doi.org/10.1016/j.jbo.2016.03.007)

Palmer GD, Attur MG, Yang Q, Liu J, Moon P, Beier F & Abramson SB 2014 F-spondin deficient mice have a high bone mass phenotype. *PLoS ONE* **9** e98388. (https://doi.org/10.1371/journal.pone.0098388)

Peinado H, Alečković M, Lavotshkin S, Matei I, Costa-Silva B, Moreno-Bueno G, Hergueta-Redondo M, Williams C, García-Santos G, Ghajar CM, *et al*. 2012 Melanoma exosomes educate bone marrow progenitor cells toward a pro-metastatic phenotype through MET. *Nature Medicine* **18** 883–891. (https://doi.org/10.1038/nm.2753)

Polyak K & Hu M 2008 Molecular chacarterization of the tumor microenvironment in breast cancer. *European Journal of Cancer* **44** 2760–2765. (https://doi.org/10.1016/j.ejca.2008.09.038.Molecular)

Qian X, Li C, Pang B, Xue M, Wang J & Zhou J 2012 Spondin-2 (SPON2), a more prostate-cancer-specific diagnostic biomarker. *PLoS ONE* **7** e37225. (https://doi.org/10.1371/journal.pone.0037225)

Quail DF & Joyce JA 2013 Microenvironmental regulation of tumor progression and metastasis. *Nature Medicine* **19** 1423–1437. (https://doi.org/10.1038/nm.3394)

Reithmeier A, Panizza E, Krumpel M, Orre LM, Branca RMM, Lehtiö J, Ek-Rylander B & Andersson G 2017 Tartrate-resistant acid phosphatase (TRAP/ACP5) promotes metastasis-related properties via TGFβ2/TβR and CD44 in MDA-MB-231 breast cancer cells. *BMC Cancer* **17** 650. (https://doi.org/10.1186/s12885-017-3616-7)

Roodman GD 2004 Mechanisms of bone metastasis. *New England Journal of Medicine* **350** 1655–1664. (https://doi.org/10.1056/NEJMra030831)

Salamanna F, Borsari V, Brogini S, Giavaresi G, Parrilli A, Cepollaro S, Cadossi M, Martini L, Mazzotti A & Fini M 2016 An in vitro 3D bone metastasis model by using a human bone tissue culture and human sex-related cancer cells. *Oncotarget* **7** 76966–76983. (https://doi.org/10.18632/oncotarget.12763)

Schmittgen TD & Livak KJ 2008 Analyzing real-time PCR data by the comparative C(T) method. *Nature Protocols* **3** 1101–1108. (https://doi.org/10.1038/nprot.2008.73)

Shiozawa Y, Pedersen EA, Havens AM, Jung Y, Mishra A, Joseph J, Kim JK, Patel LR, Ying C, Ziegler AM, *et al*. 2011 Human prostate cancer metastases target the hematopoietic stem cell niche to establish footholds in mouse bone marrow. *Journal of Clinical Investigation* **121** 1298–1312. (https://doi.org/10.1172/JCI43414)

Somers KD, Brown RR, Holterman DA, Yousefieh N, Glass WF, Wright GL, Schellhammer PF, Qian J & Ciavarra RP 2003 Orthotopic treatment model of prostate cancer and metastasis in the immunocompetent mouse: efficacy of flt3 ligand immunotherapy. *International Journal of Cancer* **107** 773–780. (https://doi.org/10.1002/ijc.11464)

Suva LJ, Washam C, Nicholas RW & Griffin RJ 2011 Bone metastasis: mechanisms and therapeutic opportunities. *Nature Reviews: Endocrinology* **7** 208–218. (https://doi.org/10.1038/nrendo.2010.227)

Touma M, Kang X, Gao F, Zhao Y, Cass AA, Biniwale R, Xiao X, Eghbali M, Coppola G, Reemtsen B, *et al*. 2017 Wnt11 regulates cardiac chamber development and disease during perinatal maturation. *JCI Insight* **2** e94904. (https://doi.org/10.1172/jci.insight.94904)

Wang N, Docherty FE, Brown HK, Reeves KJ, Fowles AC, Ottewell PD, Dear TN, Holen I, Croucher PI & Eaton CL 2014 Prostate cancer cells preferentially home to osteoblast-rich areas in the early stages of bone metastasis: evidence from in vivo models. *Journal of Bone and Mineral Research* **29** 2688–2696. (https://doi.org/10.1002/jbmr.2300)

Weilbaecher KN, Guise TA & McCauley LK 2011 Cancer to bone: a fatal attraction. *Nature Reviews: Cancer* **11** 411–425. (https://doi.org/10.1038/nrc3055)

Zayzafoon M, Abdulkadir SA & McDonald JM 2004 Notch signaling and ERK activation are important for the osteomimetic properties of prostate cancer bone metastatic cell lines. *Journal of Biological Chemistry* **279** 3662–3670. (https://doi.org/10.1074/jbc.M308158200)

Zhu C, Zheng XF, Yang YH, Li B, Wang YR, Jiang SD & Jiang LS 2016 LGR4 acts as a key receptor for R-spondin 2 to promote osteogenesis through Wnt signaling pathway. *Cellular Signalling* **28** 989–1000. (https://doi.org/10.1016/J.CELLSIG.2016.04.010)

Zhu BP, Guo ZQ, Lin L & Liu Q 2017 Serum BSP, PSADT, and Spondin-2 levels in prostate cancer and the diagnostic significance of their ROC curves in bone metastasis. *European Review for Medical and Pharmacological Sciences* **21** 61–67.

Received in final form 3 April 2020
Accepted 29 April 2020
Accepted Manuscript published online 1 May 2020

https://erc.bioscientifica.com
https://doi.org/10.1530/ERC-20-0116

cancers

MDPI

Review

Role of Calcium Signaling in Prostate Cancer Progression: Effects on Cancer Hallmarks and Bone Metastatic Mechanisms

Juan A. Ardura [1,2], Luis Álvarez-Carrión [1], Irene Gutiérrez-Rojas [1] and Verónica Alonso [1,2,*]

[1] Bone Physiopathology laboratory, Applied Molecular Medicine Institute (IMMA), Universidad San Pablo-CEU, CEU Universities, Campus Monteprincipe, 28925 Alcorcón, Madrid, Spain; juanantonio.ardurarodriguez@ceu.es (J.A.A.); luis.alvarezcarrion@ceu.es (L.Á.-C.); irene.gutierrezrojas@ceu.es (I.G.-R.)

[2] Departamento de Ciencias Médicas Básicas, Facultad de Medicina, Universidad San Pablo-CEU, CEU Universities, Campus Monteprincipe, 28925 Alcorcón, Madrid, Spain

* Correspondence: veronica.alonsorodriguez@ceu.es

Received: 29 March 2020; Accepted: 23 April 2020; Published: 25 April 2020

Abstract: Advanced prostate cancers that progress to tumor metastases are often considered incurable or difficult to treat. The etiology of prostate cancers is multi-factorial. Among other factors, de-regulation of calcium signals in prostate tumor cells mediates several pathological dysfunctions associated with tumor progression. Calcium plays a relevant role on tumor cell death, proliferation, motility-invasion and tumor metastasis. Calcium controls molecular factors and signaling pathways involved in the development of prostate cancer and its progression. Such factors and pathways include calcium channels and calcium-binding proteins. Nevertheless, the involvement of calcium signaling on prostate cancer predisposition for bone tropism has been relatively unexplored. In this regard, a diversity of mechanisms triggers transient accumulation of intracellular calcium in prostate cancer cells, potentially favoring bone metastases development. New therapies for the treatment of prostate cancer include compounds characterized by potent and specific actions that target calcium channels/transporters or pumps. These novel drugs for prostate cancer treatment encompass calcium-ATPase inhibitors, voltage-gated calcium channel inhibitors, transient receptor potential (TRP) channel regulators or Orai inhibitors. This review details the latest results that have evaluated the relationship between calcium signaling and progression of prostate cancer, as well as potential therapies aiming to modulate calcium signaling in prostate tumor progression.

Keywords: Calcium; prostate cancer; cell signaling; therapies; cancer progression

1. Introduction to Prostate Cancer

Genetic and environmental factors contribute to alterations of prostate that may lead to uncontrolled cell growth and prostate tumorigenesis and cancer. Prostate cancer (PCa) is a heterogeneous and multifactorial disease [1]. Heterogeneity is reflected at different levels: (I) at the level of gene expression—not all the cells within a cancer mass express tumor markers to the same extent—(II) at the genetic level—with multiple loci susceptible to be affected [2]; and (III) in patient response to common therapies -tumors show diverse responses to standard chemotherapy treatments- [3].

PCa is asymptomatic in the early stages of the disease. However, in advanced stages PCa can block urine flow from the bladder, invade the adjacent seminal vesicles and metastasize mainly to bone, lung, liver, pleura and adrenals [4–6]. Patients with localized PCa can survive long periods of time and a large percent of patients develop skeletal metastases suggesting that bone provides a favorable microenvironment for its localization and progression [7]. Skeletal metastases cause a variety of

complications, such as bone pain, fractures, spinal cord compression, and bone marrow suppression severely compromising patients [8,9].

Androgens, male steroid hormones that act through the androgen receptor (AR), are required for prostate development and physiological prostate function [10]. Approximately 80–90% of PCas are dependent on androgens at initial stages. Although serum androgens alone do not promote prostate carcinogenesis, androgen actions and the functional status of AR are important mediators of PCa progression [11]. Therefore, androgen deprivation therapy is the first line treatment for PCa. Therapies based on chemical or surgical castration are directed towards the reduction of serum androgens and inhibition of AR activity [12–14]. Over 80% of patients show a positive response to androgen reduction. However, many patients with metastatic PCa will develop castrate resistant PCa after 2–3 years, leading to an increase in mortality [4]. The tumors of these patients are considered to be hormone refractory, in the sense that they progress despite a reduction in serum androgens [11]. Tumor cell growth is sustained in castrate resistant PCa by a diversity of mechanisms including intratumoral or adrenal production of androgens, overexpression of AR or mutated AR forms, ligand-independent activation of AR or stabilization of hyper-responsive AR by chaperones (reviewed in [15]). Neuroendocrine differentiation has also been associated with the progression of PCas to a castrate resistant phenotype and increased mortality [16,17].

PCa is a major cause of morbidity and mortality worldwide. It is the second most frequent cancer in men and the fifth leading cause of cancer death in men. It was estimated that 1.3 million new cases would be diagnosed causing 359,000 associated deaths worldwide in 2018 [18]. Due to the elevated incidence and mortality of PCa, there is an urgent need to determine the key mechanisms of disease development and response to treatments. Identification of biomarkers for disease progression and therapeutic targets is also considered of the utmost importance.

2. Role of Calcium Signaling in PCa Progression

Advanced PCa leading to bone metastases involves several phases regulated by mechanisms that are still not fully understood [19]. Calcium signaling has been described to contribute to the development of PCa characteristics and to participate in different phases of tumor progression [20–22]. Calcium signals that differ from those of normal cells in amplitude, subcellular localization or kinetics of the signal are characteristic of PCa cells. These differences on calcium signaling affect cell survival, proliferation, differentiation and other processes that contribute to PCa development [23].

Particular calcium-dependent modifications of prostate tumor cell processes rely on altered homeostasis of calcium and calcium-dependent pathways in these cells. Dysregulated calcium homeostasis in PCa depends on changes in the ratio of influx/efflux and storage of calcium compared with non-tumoral cells [23]. Alterations in plasma membrane and endoplasmic reticulum channels, as well as GAP junctions are mainly responsible for the abnormal calcium intracellular levels of PCa cells [24,25]. These alterations cause calcium influx into the cell and mobilization from internal stores by a variety of mechanisms including constitutive calcium entry [26] store-operated calcium entry (SOCE) [27] and store-independent calcium entry (SICE) [28] processes. On the other hand, increased concentrations of intracellular calcium ($[Ca2^{+}]_{i}$) due to dysregulated calcium homeostasis and tumorigenic overexpression of calcium-binding proteins result on altered calcium-dependent signaling pathways.

Evasion of apoptosis, self-sufficiency and limitless cell proliferation and promotion of angiogenesis are cancer hallmarks in PCa [29]. In addition, characteristics acquired by prostate tumors that are required for metastatic PCa include; epithelial to mesenchymal transition, pro-migration and invasion features and metastatic colonization of organs [19,29].

A large number of molecules and signaling pathways have been associated with calcium-dependent modulation of processes involved in PCa cancer hallmarks and PCa progression [21,23,30]. Several of them participate in various phases of PCa development. Herein, we briefly review the role of calcium signaling pathways directly involved in different acquired features and stages of PCa.

2.1. Evasion of Apoptosis

Calcium has a dual role in cells being able to induce cell survival or triggering apoptosis. For instance, oscillations in [Ca2+]i usually promote cell proliferation and survival whereas sustained cytosolic calcium induces cell apoptosis [31]. Calcium-dependent enhanced cell survival is based on a variety of molecular mechanisms in PCa (Figure 1).

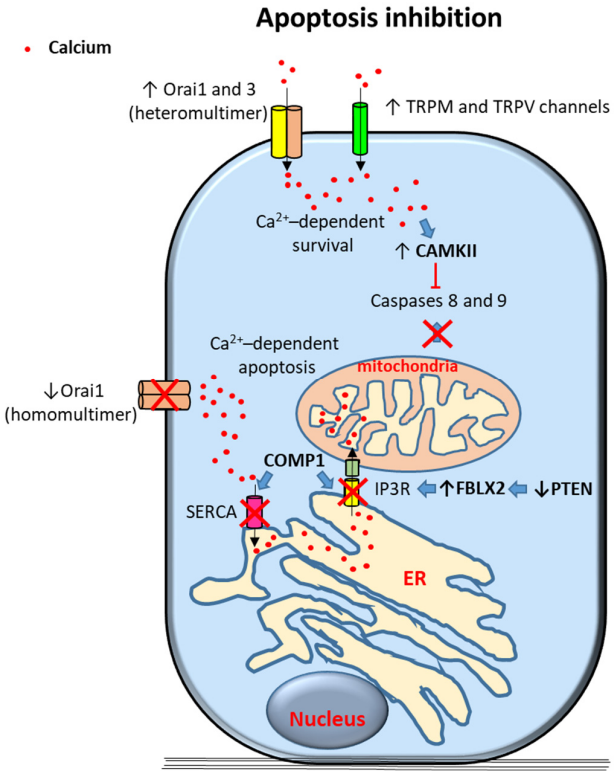

Figure 1. Proposed mechanisms of calcium-dependent apoptosis inhibition in prostate cancer (PCa) cells. Survival signals are induced by calcium entry through transient receptor potential (TRP) TRPM and TRPV channels and Orai 1 and 3 heteromultimers. Elevation of cytoplasmic calcium levels trigger different anti-apoptotic signals including caspase 8 and 9 inhibition by activation of Calcium/Calmodulin-Dependent Kinase II (CAMKII). Alternative mechanisms include inhibition of calcium-dependent mitochodrial apoptosis; excess of intracellular calcium is inhibited by downregulation of Orai homomultimers, of sarco/endoplasmic reticulum calcium ATPase (SERCA) (via cartilage oligomeric matrix protein (COMP) expression) and of IP3R (via COMP1 expression and PTEN (phosphatase and tensin homolog deleted on chromosome 10) channels in PCa cells. Arrows indicate upregulated expression or activity (↑) and downregulated expression or activity (↓). Crosses (X) and ⊢ symbol indicate inhibition. Blue filled arrows indicate stimulation. ER: Endoplasmic reticulum. F-box protein XL2: FBXL2.

2.1.1. Calcium Channels

A diversity of calcium channels have been involved in promotion of PCa cell survival.

PCa progression has been associated with enhanced Orai3 protein expression [24]. Orai proteins are calcium-channel subunits that form part of the calcium release-activated calcium channels (CRAC) in the SOCE pathway and of the arachidonic acid-regulated calcium (ARC) and leukotriene C4-regulated calcium (LRC) channels in the SICE pathway [24,27,28,32,33]. It has been described that increased levels of Orai3 proteins in PCa cells favors the formation of heteromultimeric channels with Orai1 leading to the formation of SICE channels that resemble ARC channels [24]. OraiI3-Orai1 heteromultimers were proposed to form to the detriment of Orai1 homomultimeric CRAC/SOCE channels [24]. OraiI3-Orai1 heteromultimer have shown to promote cytosolic calcium-dependent proliferation in PCa cells whereas

Orai1 homomultimeric channels potentially trigger ER calcium-dependent apoptosis. Given that Orai3-Orai1 heteromultimers could be formed at the expense of homomultimeric Orai1 channels, it has been proposed that Orai3-Orai1 channel predominance confers an oncogenic phenotype of apoptotic resistance and enhanced proliferation in PCa cells [24]. In contrast, another report has described Orai3 downregulation in tumorous versus non-tumorous tissues [34,35]. It was suggested that these contradictory results might be due to selection of different stages of cancer cell differentiation in these studies [36].

A role of members of the transient receptor potential (TRP) calcium ion channel family (reviewed in [37]) on promotion of PCa survival has also been proposed. In this regard, alterations in the expression of TRP Melastatin 2 (TRPM2), TRPM4, TRPM8, TRP Vanilloid 1 (TRPV1) and TRPV6 have been observed in PCa cells [38–44], some of them related to cancer cell survival. Increased TRPM2 expression in high grade PCa samples has been associated with alterations of autophagy leading to potential consequences on tumor cell survival [38]. Similarly, de novo expression of TRPV6 and translocation of the channel to the plasma membrane via an Orai1/SOCE-mediated mechanism has been shown in PCa cells. TRPV6 translocation would then constitutively increase cytosolic cellular calcium concentrations enhancing PCa cell survival [45]. Regarding TRPM8, experimental data have revealed that this channel modulates cell proliferation, survival, and invasion depending on the cancer cell type and AR requirements. TRPM8, a calcium permeable channel expressed in the endoplasmic reticulum and the plasma membrane that is experimentally activated in response to cooling and menthol has been described to be needed for the survival of AR-dependent LNCaP prostate cancer cells [46]. In contrast, PC-3 are AR-independent PCa cells that express low levels of TRPM8 [46]. In these cells, persistent cytosolic [Ca2+]i due to TRPM8 overexpression by permanent transfection has revealed increased susceptibility to cell apoptosis and decreased proliferation and migration capabilities [40]. Interestingly, TRPM8 has also been associated with inhibition of cell migration via a non-channel function in endothelial cells [47].

Calcium channels mainly located at the endoplasmic reticulum (ER) such as IP3 receptors (IP3Rs) have also been involved in PCa cell survival [48]. These receptors can mediate persistent transport of calcium through ER–mitochondria protein bridges allowing calcium transfer from the ER to mitochondria. This transport can lead to mitochondrial calcium overload and activate the mitochondria-dependent program of cell apoptosis [49]. It has been described that IP3R type3 (IP3R3)-induced apoptosis may be inhibited by F-box protein FBXL2 that targets IP3R3 to proteasome degradation [48]. In turn, activity of FBXL2 has been shown to be inhibited by PTEN (phosphatase and tensin homolog deleted on chromosome 10) tumor suppressor gene. Inactivation or mutation of PTEN tumor suppressor gene is common in PCa and is associated with poor prognosis and metastatic disease [50]. Therefore, it has been suggested that PTEN loss of activity in PCa cells leads to FBXL2 overactivation, IP3R3 proteasomal degradation and inhibition of persistent calcium-dependent mitochondrial apoptosis [48]. ER transfer of calcium to the mitochondria has also been involved in increased mitochondrial activity and subsequent enhanced proliferation and cell survival [51]. In this regard, calcium signals in the mitochondria can be interpreted differentially depending on its spatiotemporal features; intermittent and low calcium levels seem to stimulate metabolism and pro-survival signaling whereas mitochondrial calcium continuous overload results in apoptosis [52].

Several TRP channels are expressed and functional in the ER membrane [53]. Presence of TRP channels, such as TRPM8, has been described in the ER of androgen-sensitive LNCaP cells compared to preferential plasma membrane localization (although comparatively expressed at lower levels) in androgen-insensitive PC-3 cells [46]. TRPM8 localization at the ER membrane has been associated with release of calcium from intracellular stores to the cytoplasm leading to increased survival in AR-dependent LNCaP PCa cells [46].

Cartilage oligomeric matrix protein (COMP) has been shown to be expressed in PCa specimens related to increased growth and recurrence. In vitro, COMP has been associated with inhibition of calcium release from the ER in DU145 cells [54]. In this regard, it has been observed that

sarco/endoplasmic reticulum calcium ATPase (SERCA) is inhibited by COMP, thereby blocking ER calcium uptake [54]. Similarly, SOC entry into the ER was also decreased by COMP and thus ER calcium store refilling was diminished [54]. In addition, calcium release from the ER to the cytoplasm through IP3Rs as well as transport of calcium from the ER to mitochondria were hampered by COMP [54]. It has been proposed that these actions altogether result in COMP-dependent decrease of PCa cell apoptosis via inhibition of calcium overload of mitochondria [54].

2.1.2. Calcium-Dependent Proteins and Processes

Several calcium-binding proteins, when bound to calcium, interact with other protein targets to regulate a diversity of cellular functions. Therefore, increased levels of cytosolic calcium caused by overexpression of calcium channels might overactivate calcium-binding proteins—also often overexpressed in PCa—thus acting on processes involved in tumor cell progression.

Calcium/Calmodulin-Dependent Kinase II (CAMKII), among other proteins, seems to play an important role in PCa cell ability to escape apoptosis after androgen deprivation and facilitates the progression of PCa cells to an androgen-independent state. Promotion of PCa cell survival by this kinase is mediated by inhibiting pro-apoptotic triggers caspase-7 and caspase-8 [55].

2.2. Self-Sufficiency in Cell Proliferation and Insensitivity to Anti-Proliferatives and Cell Differentiation

Androgens play a key role in PCa progression [11] and calcium signaling has been involved in androgen receptor actions on PCa cell proliferation [16]. Furthermore, androgen-dependent increases of [Ca2+]i levels have previously been shown in LNCaP PCa cells [56]. Androgen-independent prostate tumor cell lines express multiple channels that are capable of elevating [Ca2+]i as well [57]. Mechanisms involved in calcium-dependent proliferation of prostate cancer cells are shown in Figure 2.

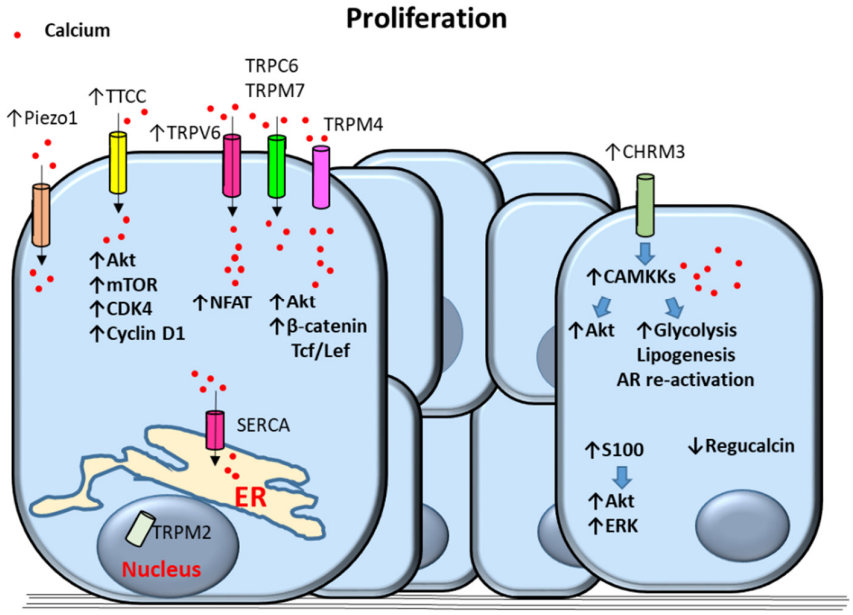

Figure 2. Proposed mechanisms of calcium-dependent proliferation in prostate cancer (PCa) cells. Upregulation of T-Type Calcium Channels (TTCC) increases the proliferative signals Akt kinase, mammalian target of rapamycin (mTOR), cyclin-dependent kinase 4 (CDK4) and cyclin D1. Transient receptor potential (TRP)V6 (TRPV6) increase proliferation via calcium-dependent activation of Nuclear factor of activated T-cells (NFAT). TRPM4 induces proliferation through activation of calcium-dependent Akt and catenin/Tcf/Lef signaling. Piezo1, TRPC6 and TRPM7 contribute to increased calcium cytosolic levels. Nuclear localization of TRPM2 as well as sarco/endoplasmic reticulum calcium ATPase (SERCA) also promote PCa cell proliferation. Upregulation of muscarinic acetylcholine receptor M3 (CHRM3) induces Akt, glycolysis, lipogenesis, and androgen receptor (AR) re-activation via activation of Calcium/Calmodulin-Dependent Kinase Kinase (CAMKK) causing cell proliferation. Proliferation is also triggered by overactivation of Akt and Extracellular-regulated (ERK) kinases by S100 proteins and by downregulation of regucalcin. Arrows indicate upregulated expression or activity (↑) and downregulated expression or activity (↓). Blue filled arrows indicate stimulation. ER: Endoplasmic reticulum.

2.2.1. Calcium Channels

Induction of cell proliferation by physiological stimuli, including epidermal growth factor, serum and androgens, has been described to be controlled by SERCA in LNCaP cells [58]. This study has revealed that the expression of SERCA correlates with PCa cell proliferation and ER intraluminal calcium levels [58].

Overexpression of voltage-operated calcium channel T-type calcium channels (TTCCs) has also been observed in PCa with androgen receptor mutations [59]. Moreover, it has been shown that pharmacological or silencing inhibition of TTCCs causes a decrease in PCa cell proliferation and survival [59]. Based on these observations, it has been proposed that TTCCs control the proliferation of androgen-receptor negative PCa cells [59]. It has also been suggested that an androgen refractory state in which androgen receptor signaling is disrupted causes overexpression of TTCCs and increased cytosolic calcium in PCa cells [16]. In this regard, TTCCs upregulation was associated with tumor progression and the acquisition of neuroendocrine morphological and biochemical changes by PCa cells [16,60].

It has been suggested that TRPV6 expression is upregulated by androgen receptors in a ligand-independent manner in LNCaP prostate tumor cells [61]. Overexpressed TRPV6 channels were described to be constitutively open and act as key mediators of calcium uptake and increased cytosolic calcium in this report. TRPV6-mediated calcium entry was associated with activation of NFAT transcription factor-mediated signaling pathways subsequently promoting cell proliferation [61]. TRP canonical 6 (TRPC6) channels have been proposed as mediators of hepatocyte growth factor

(HGF) effects on calcium entry in PCa cells [62]. TRPC6-mediated increase of cytosolic calcium triggered by HGF was shown to induce PCa cell proliferation [62]. In addition, overexpression of TRPM4 in PCa PC3 cells has been associated with increased cell proliferation via activation of β-catenin and phosphorylation of Akt signaling [63]. Both β-catenin and Akt signaling pathways have previously been related to PCa cell proliferation [64]. TRPM4 has been shown to regulate cytosolic calcium concentrations through changes in membrane potential and in calcium electrochemical driving force [65]. In PC3 cells TRPM4 levels positively correlated with enhanced proliferation, Akt activation, protein expression and nuclear localization of β-catenin and transcription of β-catenin target genes dependent on binding with Tcf/Lef transcription factors [63]. In this regard, it has been shown that TRPM4 promotes calcium influx associated with calcium/calmodulin-dependent activation of Akt kinase leading to PC-3 cell proliferation [63]. Similarly, TRPM2 has been associated with PC-3 and DU-145 cell proliferation [66]. Localization of TRPM2 into the cell nuclei has been described to induce cell proliferation in PC-3 and DU-145 cells by an unknown mechanism [66].

Piezo type mechanosensitive ion channel component 1 (Piezo1) is a nonselective cationic mechanosensitive channel able to induce calcium influx in cells [67] that has been described to be overexpressed in PCa cell lines and tissues [68]. Upregulation of Piezo1 has been associated with increased cytosolic [Ca2+]i, phosphorylation of Akt kinase and mammalian target of rapamycin (mTOR), activation of cyclin dependent kinase 4 (CDK4) and cyclin D1 and cell proliferation/survival in DU145 PCa cells [68].

Increased extracellular calcium ([Ca2+]o) levels have also been proposed as modulators of PCa cell proliferation via activation of calcium channels [69]. In particular, increased calcium/magnesium ratios overactivate TRPM7 channels leading to enhanced calcium entry and promotion of DU145 and PC3 PCa cell proliferation [69]. Moreover, increased serum ratios of calcium/magnesium have been observed in PCa patients compared with patients without any cancer [69]. These observations suggest a potential mechanism of PCa progression based on increased [Ca2+]o concentrations that boost cytosolic [Ca2+]i levels. Moreover, increased [Ca2+]o has been described to induce PC-3 proliferation by a mechanism associated with SOC entry and dependent on CasR and TRPC6 expression [70].

2.2.2. Calcium-Dependent Proteins and Processes

Increased cytosolic [Ca2+]i levels switch calcium/calmodulin-dependent kinases from a basal inactive state of auto-inhibition to an active state [71]. Moreover, it has also been described that the androgen receptor is recruited to the calcium/calmodulin-dependent protein kinase kinase 2 (CAMKK2) promoter in both androgen-dependent and castrate-resistant PCa cell lines [72]. Overexpression of the calcium-dependent CAMKK2 protein has previously been described in PCas and cell lines [72]. Therefore, androgen receptor signaling may promote CAMKK2 signaling by both increasing calcium intracellular levels and inducing CAMKK2 protein upregulation.

Previous reports have described that inhibition of CAMKK2 reduces glucose uptake and produces less lactate and citrate suggesting a reduction in aerobic glycolysis. Furthermore, CAMKK2 inhibition showed decreased anabolism from glucose to citrate, ribose and amino acids [72]. Other reports described androgen-dependent CAMKK2 promotion of the glucose transporter GLUT12 trafficking to the plasma membrane [73]. Altogether, these results support the role of CAMKK2 as a mediator of androgen receptor-fueling of PCa metabolism and biosynthesis [72]. In addition, CAMKK2 overexpression has been described to increase the lipogenic enzymes acetyl-CoA carboxylase and fatty acid synthase, thus promoting PCa cell growth by a mechanism dependent on de novo lipogenesis [74]. Furthermore, CAMKK2 upregulation and over-stimulation has been proposed as a mechanism that re-activates androgen receptor signaling in castrate-resistant PCa [75]. A feedback loop in which CAMKK2 is induced by the androgen receptor to maintain this receptor activity and trigger tumor cell proliferation has been proposed during PCa progression [76].

In addition, muscarinic acetylcholine receptor M3 (CHRM3) has been described to be highly upregulated in castration-resistant C4-2B and PC-3 cells and moderately upregulated in the

androgen-dependent cell line LNCaP [77]. Activation of CHRM3 revealed to cause castration-resistance growth in LNCaP cells through CAMKK–induced activation of Akt kinase [77].

Estrogens have been shown to induce calcium signaling in LNCaP cells [78] although whether these hormones trigger similar CAMPKK2 actions on PCa cells remains elusive.

Increased and persistent [Ca2+]i stimulates androgen receptor breakdown by the protease calpain that forms a complex with calmodulin in LNCaP cells [79]. The resulting androgen fragments have been associated with tumor cell growth arrest [79]. Moreover, persistent [Ca2+]i has been associated with downregulation of androgen receptor expression in LNCaP cells [80]. These results suggest that PCa cell proliferation could be decreased by constant [Ca2+]i via modulation of androgen receptor levels.

Regucalcin expression has been shown to be decreased in human PCas and downregulated in LNCaP PCa cells by an androgen-dependent pathway [81]. Regucalcin is a calcium-binding protein that regulates [Ca2+]i homeostasis by enhancing calcium pumping activity in the plasma membrane, ER and mitochondria of many cell types [82]. Regucalcin was shown to suppress cell proliferation, inhibit expression of oncogenes, and increase the expression of tumor suppressor genes [81].

Proteins of the calcium-binding S100 family have been described to be up-regulated in androgen-refractory and metastatic PCa [44]. One of the members of the S100 family of proteins, S100A16, has been involved in promotion of cell proliferation and metastasis via Akt and extracellular signal-regulated (ERK) kinases signaling pathways in human PCa [83].

2.3. *Angiogenesis*

During PCa progression formation of new blood vessels to supply tumor cell survival and proliferation is required [29]. Constant production of angiogenic factors such as vascular endothelial growth factor (VEGF) frequently occurs in prostate tumor progression (Figure 3).

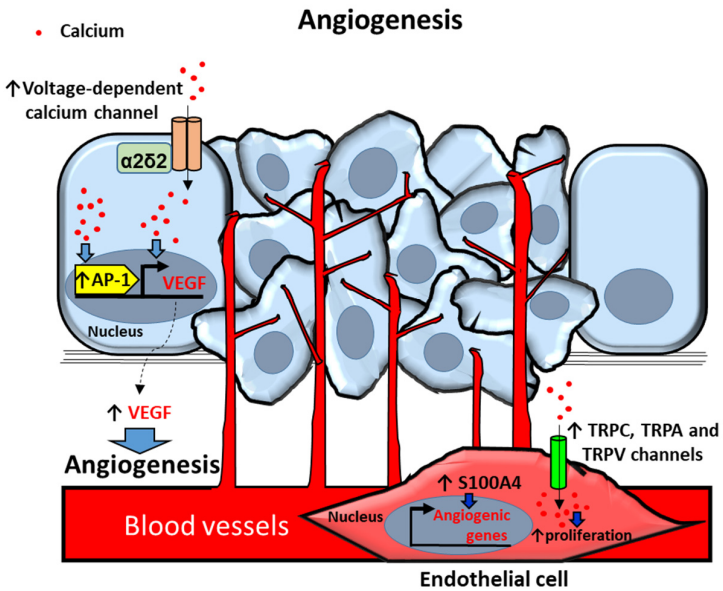

Figure 3. Proposed mechanisms of calcium-dependent angiogenesis in prostate cancer (PCa) and endothelial (EC) cells. PCa cells secrete the angiogenic factor VEGF (vascular endotelial growth factor) by increasing intracellular calcium [Ca2+]i via voltage-dependent calcium channel α2δ2 auxiliary subunit overexpression. [Ca2+]i upregulates VEGF through activation of transcription factor Activator protein 1 (AP-1). ECs in the primary prostate tumor induce angiogenic genes by overexpression of S100 proteins. [Ca2+]i upregulation by Transient receptor potential (TRP) TRPC, TRPA and TRPV channels induces proliferation of ECs in prostate primary tumors. Arrows indicate upregulated expression or activity (↑). Blue filled arrows indicate stimulation.

2.3.1. Calcium Channels

Voltage-dependent calcium channel α2δ2 auxiliary subunit has been reported to be more frequently expressed in PCa tissues compared with non-cancer tissues [84]. Overexpression of this protein has been described to trigger alterations of calcium homeostasis and stimulate angiogenesis via an increased secretion of VEGF in LNCaP nude mice xenografts. These actions have been associated with increased tumorigenesis of LNCaP cells in nude mice and with PCa cell proliferation and tumor development [84].

TRP channels have also been related to angiogenic responses and increased cytoplasmic calcium concentrations. Upregulation of TRPV2 levels has been associated with human prostate tumor-derived endothelial cell proliferation. Moreover, TRPC3 has been identified as an endothelial PCa cell attraction factor whereas TRP Ankyrin1 (TRPA1) has been described to act as a prostate tumor-derived endothelial cell angiogenic factor [85]. These actions were associated with constitutive calcium entry due to basal activation of the three overexpressed TRP channels in endothelial cells and experimentally corroborated with the TRPA1, TRPV2 and TRPC3 agonists Allyl isothiocyanate (AITC), L—Lysophosphatidylcholine(LPC) and 1-Oleoyl-2-acetyl-sn-glycerol (OAG), respectively [85].

2.3.2. Calcium-Dependent Proteins and Processes

It has been described that vasoactive intestinal peptide (VIP) triggers VEGF expression in LNCaP cells. These actions have been attributed to calcium-dependent activation of activator protein-1 (AP-1) response elements in the promoter region of the VEGF gene [86].

In addition, S100A4 calcium-binding protein has been shown to be a key player in development of prostate tumors [87]. It has been described that S100A4 induces capillary formation in endothelial cells in vitro whereas its silencing inhibits angiogenesis and tumor growth in human PCa xenografts of PC3 cells in mice [88]. These effects were associated with alterations in the expression of angiogenesis-related genes in S100A4 knockdown endothelial cells [downregulation of genes related with endothelial migration and microvessel formation; aquaporin-1, fibroblast growth factor 18, resistin, mitogen-activated protein kinase kinase kinase 5 (map3k5), thymus cell antigen, forkhead box O6 (foxo6), heparan sulfate 6-O-sulfotransferase 1 and matrix metalloproteinase 3 (mmp3), and upregulation of anti-angiogenesis genes; cyclin-dependent kinase inhibitor 1A (cdkn1a), thrombospondin 1, and sprouty homolog 4] [88].

2.4. Epithelial to Mesenchymal Transition (EMT), Migration and Invasion

EMT is a process whereby epithelial cells acquire a complete or partial mesenchymal phenotype [89]. EMT promotes a decrease of tumor cell adhesion to the basement membrane and migration of malignant cells from the primary tumor. These processes potentiate prostate tumor cell abilities to migrate to neighbor tissues and to entry into blood or lymphatic vessels [90,91]. EMT allows motility of tumorigenic cells but also contributes to different stages of cancer progression from initiation, primary tumor growth, invasion, dissemination and metastasis to colonization and resistance to therapy [92]. EMT transcriptional program is regulated by transcription factors mainly of the SNAIL, TWIST and Zinc finger E-box-binding homeobox (ZEB) families [92]. Recent findings have reported that calcium entry is required for the upregulation of Zeb1 expression in DU145 and PC-3 PCa cells [93] (Figure 4).

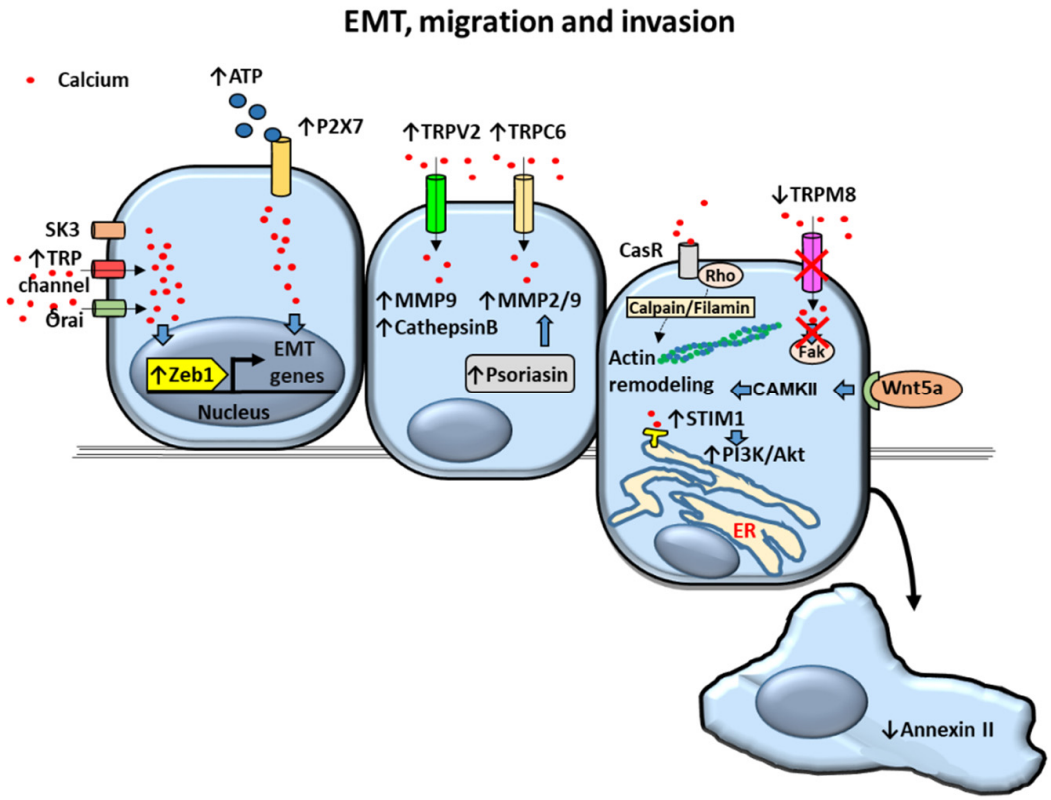

Figure 4. Proposed mechanisms of calcium-dependent Epithelial to Mesenchymal Transition (EMT), migration and invasion in prostate cancer (PCa) cells. Upregulation of intracellular calcium levels dependent on K+ channel (small conductance calcium-activated potassium channel 3) SK3, Transient receptor potential (TRP) and Orai channels overactivate transcription factor Zinc finger E-box-binding homeobox 1 (Zeb1) triggering the expression of *EMT* genes. EMT genes are also activated by ATP-stimulated P2X7 channel. Invasion of PCa cells is mediated by upregulation of metalloproteases (MMPs) and cathepsin B via TRPV2 and TRPC6-dependent increase of cytosolic calcium levels by a constitutive mechanism. MMPs are also increased by psoriasin. Prostate cell migration is promoted by actin remodeling via calcium receptor (CasR)/calpain/filamin and Wnt5a/Calcium/Calmodulin-Dependent Kinase (CAMK)II pathways. Decreased annexin II and increased Stromal-interacting molecule 1 (STIM1)/Akt kinase activation lead to enhanced cell migration as well. Decreased TRPM8 expression decrease in late stages of androgen-insensitive PCA and is associated with increased cell migration. Arrows indicate upregulated expression or activity (↑) and downregulated expression or activity (↓). Crosses (X) indicate inhibition. Blue filled arrows indicate stimulation. ER: Endoplasmic reticulum.

2.4.1. Calcium Channels

It has been shown that calcium-activated K+ channel (small conductance calcium-activated potassium channel 3) SK3 as well as Orai and TRP channels were required for promotion of calcium entry and subsequent Zeb1 expression in these cells [93]. In addition, TRPM7 channel overexpression in DU145 and PC3 was found to increase PCa cell migration mediated through EMT [94,95]. Although promotion of cell migration has been observed to be associated with overexpression of channels such as TRPM7, TRPM4 and TRPM2 [39,94–96] the role of calcium on TRPM-mediated cell motility is contradictory. TRPM2 channels induce cytosolic increase of not only calcium but also zinc [96]. Although TRPM2 itself does not directly contribute to calcium entry as a plasma membrane channel, it has been shown that activated TRPM2 induces calcium release from lysosomes contributing to increased cytosolic calcium concentrations in dendritic cells [97]. TRPM2-mediated increase of cytosolic [Ca2+]i has been described to regulate size and number of cell focal adhesions whereas

zinc promoted filopodia-cell protrusions required for cell migration- in PC-3 cells [96]. In this regard, migration and motility of PC-3 cells showed to be mediated by TRPM2 in a zinc-dependent rather that calcium-dependent manner [96]. Other reports suggest that promotion of PCa migration by channels is not exclusively due to ion transport. Formation of channel-dependent signaling complexes has been suggested to mediate migration in PCa cells [98]. For example, it has been proposed that the calcium-activated potassium channel BKCa, that is overexpressed in PCa cells, promotes PCa cell migration as well as proliferation [98]. BKCa would act by forming a complex with αvβ3 integrin subsequently increasing phosphorylation of focal adhesion kinase (FAK) in an ion-conducting independent fashion [98].

TRPV2 cationic channel levels are also overexpressed in metastatic PCa compared to primary tumors [99]. It has been shown that introducing TRPV2 into androgen-dependent LNCaP cells enhances cell migration along with expression of invasion markers matrix metalloproteinase (MMP) 9 and cathepsin B. Constitutive activity of TRPV2 showed to mediate the growth and invasive properties of PC3 prostate tumors suggesting that upregulation of this channel is a feature of castration-resistant PCa [99]. Similarly, overexpression of TRPC6 has been observed in PCa samples and different prostate carcinoma cell lines (PC3, DU145, LNCaP and 22Rv1) [100]. It has been described that upregulated levels of TRPC6 promote cell migration and overexpression of metalloproteases MMP2 and MMP9 [100]. Therefore, TRPV2 and TRPC6 role as promoters of proteolytic breakdown of tissue barriers by MMPs to increase PCa cell invasion potential has been proposed [99,100].

TRPM8 expression has been shown to decrease in late stages of androgen-insensitive PCa [101] and TRPM8 overexpression induced by transfection has been associated with reduced PCa cell migration [40,102]. Inhibitory actions of TRPM8 overexpression by transfection on cell migration have been proposed to act through inactivation of the cell migration regulator focal-adhesion kinase in the AR-deficient PC-3 cell line [40]. These actions were associated with persistent cytosolic [Ca2+]i concentrations. In addition, accumulation and activation of TRPM8 channels at the plasma membrane of TRPM8-transfected PC3 cells have been described to be induced by prostate-specific antigen (PSA) related with increased [Ca2+]i and decreased PCa cell migration [102].

2.4.2. Calcium Pumps and Cation Permeable Channels

Plasma membrane Ca^{2+}-ATPases (PMCAs) are calcium pumps that use ATP hydrolysis to push calcium from the cytosol into the extracellular milieu. PMCA1 has been identified as a protein that is regulated by the AR in PCa LNCaP cells [103]. Increased secretion of PMCA1 in extracellular vesicles has been associated with inhibition of the AR by the AR antagonist enzalutamide [103]. These results suggest that PMCA1 might have an important role in castrate-resistant PCa and invasion abilities.

Purinergic P2X7 are ligand-gated cation permeable channels activated by ATP that are highly expressed in PCa and PCa cell lines [104,105]. Moreover, extracellular ATP has been described as an important pro-migration and invasion molecule in prostate cancer cells [106]. P2X7 has been involved in ATP-induced enhanced migration and invasion of prostate cancer cells in association with ATP-dependent increase of cytoplasmic [Ca2+]I [105]. The expression of the EMT/invasion-related genes Snail, interleukin-8 (IL-8) and MMP-3 was described to increase whereas the expression of the non-tumor epithelial markers E-cadherin and Claudin-1 was reduced in PC-3M human prostate carcinoma 1E8 and 2B4 cell lines by ATP-activated P2X7 [105].

2.4.3. Calcium-Dependent Proteins and Processes

Stromal-interacting molecule 1 (STIM1), a calcium sensor located in the ER and a component required to induce SOCE, has been shown to be upregulated in PCa [107]. Overexpression of STIM1 has been described to mediate migration and invasion in LNCaP, PC-3 and DU-145 PCa cell lines via activation of the phosphatidylinositol 3-kinase (PI3K)/Akt signaling pathway [107].

Dysregulation of the annexin family of calcium-binding proteins has also been associated with PCa progression [108]. Decreased or absence of annexin II has been shown in Du145 and PC3 PCa cells,

respectively. Re-expression of annexin II in these cells inhibited PCa cell migration without affecting cell proliferation or apoptosis [109].

[Ca2+]o has been described to promote the migration of DU145 and PC-3 PCa cell lines (AR-deficient and metastatic) compared to LNCaP PCa cells (AR-positive and less metastatic) [110]. Regarding cell motility, cleavage of filamin A, an actin-binding protein overexpressed in PCa, was shown to be induced by [Ca2+]o [110]. Filamin A cleavage triggered by [Ca2+]o via a calcium-sensing receptor (CasR)-p115RhoGEF-calpain dependent pathway revealed to be essential for promotion of DU145 and PC-3 cell migration [110].

Calcium/calmodulin-dependent protein kinase kinase β (CaMKKβ) has shown to be upregulated in PCa too [111]. Expression and activity of CaMKKβ was described to be increased by androgens leading to phosphorylation of AMP-activated protein kinase (AMPK) [111]. The pathway CaMKKβ/phosphorylated AMPK was shown to induce androgen-mediated migration and invasion of LNCaP and VCaP cells [111].

Wnt5A is another protein that has been shown to be upregulated in PCas [112]. Stimulation of PCa cells with Wnt5A was described to cause [Ca2+]i waves and subsequent activation of CAMKII [112]. CAMKII calcium-dependent activation showed to be indispensable for actin cytoskeleton remodeling and increased motility in PC3 PCa cells [112].

Proteins of the S100 family have also been implicated in tumor cell invasion. The calcium-binding protein psoriasin (S100A7) has been shown to be expressed in PCa specimens and to increase PCa cell survival [113]. However, psoriasin main function was mainly related to increased cell invasiveness abilities through upregulation of matrix metalloproteases in PC-3 cells [113]. Other member of the S100 family of proteins, S100A4, has been reported to be overexpressed in PCa and increase the proliferative and invasive capabilities of PC-3 cells [114]. In this report, enhanced invasion was associated with S100A4-induced transcriptional activation and increased proteolytic activity of the metalloprotease MMP-9 [114].

2.5. Homing of PCa to Bone

Advanced PCa most frequently metastasize to bone, followed in frequency by lung, liver, pleura and adrenals [6,115]. Thus, bone metastasis is a common complication in advanced stages of patients with PCa [115]. It has been hypothesized that tumor cells establish in specific areas of bone such as the endosteal niche, the niche of hematopoietic stem cells and the vascular niche [116]. These niches are complex microenvironments in which bone cells secrete factors and stablish cell-cell interactions that promote cell proliferation and differentiation as well as bone turnover (bone resorption and formation). It has been shown that increasing the number of these niches experimentally also increases the number of primary tumor disseminated cells [117]. Therefore, the PCa high predilection for skeletal metastasis has been attributed to favorable reciprocal interactions between the bone microenvironment and cancer cells [118,119]. Such interactions may be different in nature, including actions of calcium channels, [Ca2+]o, bone soluble factors, bone-tumor cell-cell direct communication and bone matrix proteins (Figure 5).

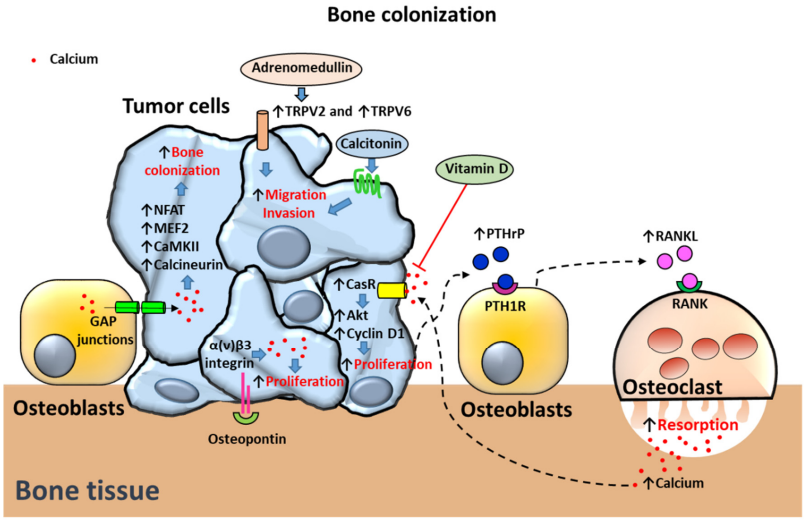

Figure 5. Proposed mechanisms of calcium-dependent bone colonization in prostate cancer (PCa) cells. Migration to bone and invasion mechanisms are induced by Transient receptor potential V2 TRPV2 and TRPV6-dependent upregulation of cytosolic calcium levels in PCa cells. Adrenomedullin translocates TRPV2 to the membrane triggering migration and invasion mechanisms. Calcitonin induces migration and invasion of PCa cells. Bone osteoblasts transfer calcium to tumor cells via GAP junctions. In turn, cytosolic calcium induces bone colonization by overactivation of NFAT and MEF2 transcription factors and calcium-binding proteins CaMKII and calcineurin. Proliferation of PCa cells in bone is triggered by osteopontin activation of α(v)β3 integrin-dependent upregulation of intracellular calcium levels. PCa cells also secrete the bone resorbing peptide parathyroid hormone-related protein (or PTHrP) inducing receptor activator of nuclear factor-κB (RANK) ligand (RANKL) secretion by osteoblasts. RANKL activates RANK receptor in osteoclasts promoting osteoclast-dependent bone resorption and release of calcium. [Ca2+]o activates the calcium receptor (CasR) in PCa cells triggering cell proliferation via Akt and cyclin D1 activation. Vitamin D antagonizes the effects of high extracellular calcium concentrations on CasR. Arrows indicate upregulated expression or activity (↑) and downregulated expression or activity (↓). Crosses (X) and ⊢ symbol indicate inhibition. Blue filled arrows indicate stimulation.

2.5.1. Calcium Channels

TRPV6 calcium channel overexpression has been associated with development of osteoblastic bone metastasis in addition to promotion of PCa cell survival [45]. PC-3 clones overexpressing TRPV6 have shown to generate osteoblastic lesions compared with control PC3 cells which generate osteolytic lesions when inoculated in the bone marrow of immunodeficient mice [45].

2.5.2. Calcium-Dependent Proteins and Processes

[Ca2+]o: During the process of bone turnover, calcium is the main inorganic component released to the extracellular medium. Normally, physiologic calcium levels are kept within a narrow range of 1.1 to 1.3 mmol/L [120]. However, in active bone resorptive lacunae, [Ca2+]o can reach levels as high as 8 to 40 mmol/L [121,122]. In this regard, [Ca2+]o has been involved in promotion of PCa cell metastasis to bone. [Ca2+]o acts mainly through activation of the heterotrimeric G-protein–coupled receptor CaSR [110]. Effects of [Ca2+]o have been associated with overexpression of calcium-sensing receptor (CasR) and activation of Akt kinase signaling pathway in PC-3 and C4-2B cell lines [7]. Stimulation of CasR and Akt pathways has also been shown to favor metastatic progression in vivo [7]. In vitro, cyclin D1-dependent proliferation and cell attachment of PC-3 cells was enhanced by activation of CasR and Akt, suggesting that [Ca2+]o mediates PCa bone metastasis [7]. Furthermore, the deleterious actions of [Ca2+]o on PCa progression have been associated not only with CasR upregulation but also with overexpression of TRPC6 [70]. Vitamin D has shown to antagonize the effects of high [Ca2+]o concentrations on PCa causing downregulation of both CasR and TRPC6 proteins [70].

It has been observed that elevated [Ca2+]o also stimulates PTHrP secretion in PCa cells [123,124]. PTHrP is a peptide that binds PTH receptor type 1 (PTH1R) in osteoblasts. PTH1R-stimulated osteoblasts secrete the pro-resorption factor RANKL that activates RANK in osteoclasts promoting bone resorption and calcium release [7]. Bone metastases have been associated with activation of the PTHrP-calcium-CaSR axis. It has been proposed that PCa cells cause PTHRP-dependent increase of calcium release from the bone microenvironment. In turn, increased [Ca2+]o levels activate CasR in PCa cells promoting tumor cell proliferation and supporting PCa cell homing to bone [7].

Bone soluble factors: Some reports have shown that bone cells can decrease [Ca2+]i levels while others have described an increase of [Ca2+]i levels in PCa cells [25,118]. This apparent contradiction might be explained due to the existence of dual mechanisms; some would promote high [Ca2+]i levels that sustain processes of prostate tumor bone colonization while others are activated to evade calcium-dependent apoptosis due to overload of mitochondrial calcium. In this regard, bone-metastatic PC3-ML PCa cells have shown downregulated levels of cytoplasmic [Ca2+]i levels upon agonist stimulation via decreased calcium entry when co-cultured with osteoblasts in vitro [118]. A role of the osteoblast microenvironment on reducing apoptosis of PCa cells caused by overload of cytoplasmic [Ca2+]i levels was suggested [118]. In contrast, other studies describe upregulated levels of [Ca2+]i upon stimulation with soluble factors. The role of TRPV2 has been described to mediate adrenomedullin promotion of PC-3 migration, adhesion and invasion abilities. Adrenomedullin, a peptide overexpressed in PCa, was shown to induce TRPV2 translocation to the plasma membrane via a PI3 kinase pathway [125]. In turn, TRPV2 translocation to the plasma membrane caused an increase of the resting cytosolic calcium levels of PC-3 cell line, which induced PCa cell migration, adhesion and invasion [125]. Some studies have linked adrenomedullin and other members of the calcitonin family of peptides including calcitonin itself and calcitonin gene-related peptide to the tropism of PCa to the bone (reviewed in [126]). Although calcitonin exerts hypocalcemic effects by inhibiting bone resorption, it has been described to be highly expressed in malignant prostate tumors and to promote PCa cell proliferation and invasion [126,127].

In addition, soluble factors from bone cells have been related to altered [Ca2+]i levels and increased proliferation in PCa cells [128]. Stimulation of PC-3 cells with conditioned media of pre-osteoblastic MC3T3-E1 and osteocytic MLO-Y4 cells induced an increase in PC-3 cell proliferation. Associated with these actions, osteoblastic and osteocytic conditioned media also caused transient increase in [Ca2+]i accumulation [128].

Bone-tumor cell-cell interactions: Bone colonization has revealed to be mediated through activation of the calcium transducers CaMKII and calcineurin in PCa cells [25]. Moreover, overexpression of transcription factors downstream of calcium and associated with promotion of EMT, migration, angiogenesis and invasion, such as NFAT and MEF2 [129,130] were also observed in PCa bone metastases [25]. It was suggested in these studies that bone colonization requires calcium flows from osteogenic cells to cancer cells via connexin 43-based gap junctions [118]. In this regard, it has been proposed that entry of calcium through calcium channels (Orai for example) mediate initial prostate tumorigenesis whereas bone-cancer cell to cell communication via gap junctions is responsible for bone metastasis after initial tumorigenesis [25].

Bone extracellular matrix proteins: Bone matrix protein fractions have been described to induce rapid fluctuations in cytosolic [Ca2+]i associated with PCa cell proliferation [131]. The non-collagenous matrix proteins osteonectin and osteopontin were able to trigger calcium signals in PCa cells derived from bone (PC-3), but not from lymph-nodes (LNCaP) or brain (DU-145) cells [131]. Effects of osteopontin on calcium signaling were described to be mediated by α(v)β3 integrin in PC-3 cells [131].

3. Targeted Calcium Signaling Therapies in PCa

The therapeutic field of PCa has broadened over the last years. These advances coincide with better understanding of the underlying molecular processes of PCa [132]. Aside from calcium-binding proteins, promising new therapies for treatment of PCa include compounds that mainly target various calcium channels and transporters [133]. Table 1 summarizes relevant clinical trials regarding prostate cancer treatment using calcium-targeted therapies.

Table 1. Clinical trials regarding prostate cancer treatment using calcium-targeted therapies.

Treatment	Results	Recruitment Status	Phase	Interventions	Conditions	Clinicaltrials.Gov Identifier	Study Title:
							Study: Suramin (antagonist of P2X purinergic receptors)
Patients receive low, intermediate or high-dose suramin IV over 1 hour on days 1, 2, 8, 9, 29, 30, 36, 37, 57, 58, 64, and 65 in the absence of disease progression or unacceptable toxicity. Patients with new progression after partial or complete response may receive additional courses, at the discretion of the study chairperson.	No Study Results Posted on ClinicalTrials.gov for this Study	Completed	Randomized phase III trial to compare the effectiveness of low, intermediate, and high dose suramin	Low (3.192g/square meter total dose given decreasing concentrations in 250 cc normal saline IV), Intermediate (5.320 g/square meter total dose given in decreasing concentrations in 250 cc normal saline via IV), or High (7.661 g/square meter toal dose given in decreasing concentrations in 250 cc normal saline IV) Dose Suramin	Stage IV prostate cancer that is refractory to hormone therapy	NCT00002723	Low, Intermediate, or High Dose Suramin in Treating Patients With Hormone-Refractory Prostate Cancer
Within 3 days after randomization, all patients receive daily flutamide. On day 4, patients undergo orchiectomy or begin monthly LHRH analogue therapy with leuprolide or goserelin. Patients randomized to receive suramin begin a 12-week course 8-25 days after orchiectomy/LHRH therapy. Hydrocortisone replacement therapy begins concomitantly with suramin and continues for at least 3 months after the completion of suramin treatment or until disease progression intervenes.	No Study Results Posted on ClinicalTrials.gov for this Study	Completed	Randomized phase III trial to evaluate the effectiveness of treatment with flutamide and suramin with or without hydrocortisone	ORCHIECTOMY/LHRH ANALOG + FLUTAMIDE + SURAMIN + HYDROCORTISONE VS ORCHIECTOMY/LHRH ANALOG + FLUTAMIDE	Metastatic or recurrent prostate cancer	NCT00002881	Flutamide, Suramin, and Hydrocortisone in Treating Patients With Prostate Cancer
	No Study Results Posted on ClinicalTrials.gov for this Study	Completed	Phase II Trial	Combine androgen blockage (Leuprolide and Flutamide) with suramin	Metastatic prostate cancer	NCT00001266	A Phase II Trial of Leuprolide + Flutamide + Suramin in Untreated Poor Prognosis Prostate Carcinoma
	No Study Results Posted on ClinicalTrials.gov for this Study	Completed	Phase I Trial	Suramin followed by doxorubicin in patients with advanced solid tumors.	Histologic or cytologic confirmation of malignant solid tumor including, but not limited to: Breast cancer Prostate cancer Colon cancer Adrenocortical tumors	NCT00003038	Combination Chemotherapy With Suramin Plus Doxorubicin in Treating Patients With Advanced Solid Tumors
							Study: Mipsagargin (G-202) [thapsigargin-based prodrug] Inhibitor of ER calcium ATPase (SERCA)
G-202 administered by intravenous infusion over one hour on Days 1, 2 and 3 of a 28-day treatment cycle. The G-202 dose will be 40 mg/m2 on Day 1 and 66.8 mg/m2 on Days 2 and 3.		Withdrawn	Phase 2 Study	G-202 dose will be 40 mg/m2 on Day 1 and 66.8 mg/m2 on Days 2 and 3.	Patients With Chemotherapy-Naïve Metastatic Castrate-Resistant Prostate Cancer	NCT01734681	Phase 2 Study of G-202 in Patients With Chemotherapy-Naïve Metastatic Castrate-Resistant Prostate Cancer

Table 1. *Cont.*

Treatment	Results	Recruitment Status	Phase	Interventions	Conditions	Clinicaltrials.Gov Identifier	Study Title:
G-202 administered by intravenous infusion on Days 1, 2 and 3 of each 28-day cycle for up to 3 cycles.	No Study Results Posted on ClinicalTrials.gov for this Study	Completed	Phase II clinical trial	G-202	Patients With Adenocarcinoma of the Prostate	NCT02381236	G-202 in the Neoadjuvant Setting Followed by Radical Prostatectomy in Patients With Prostate Cancer
G-202 administered by intravenous infusion over 1 hour on Days 1, 2 and 3 of each 28-day cycle.	No Study Results Posted on ClinicalTrials.gov for this Study	Completed	Dose-Escalation Phase 1 Study	G-202 on Days 1, 2 and 3 of each 28-day cycle.	Advanced Prostate Cancer	NCT01056029	Dose-Escalation Phase 1 Study of G-202 (Mipsagargin) in Patients With Advanced Solid Tumors
							Study: SOR-C13 (synthetic peptide inhibitor of TRPV6 developed from the C-terminal region of soricidin
Patients receive TRPV6 calcium channel inhibitor SOR-C13 IV over 2 hours on days 1, 2, 8, 9, 15, 16, 22, and 23. Cycles repeat every 28 days in the absence of disease progression or unacceptable toxicity.	No Study Results Posted on ClinicalTrials.gov for this Study	Recruiting	Phase I dose-escalation Study	SOR-C13 IV	Solid tumors that have spread to other places in the body (advanced) and does not respond to treatment. Stage III Prostate Cancer Stage IIIA Prostate Cancer Stage IIIB Prostate Cancer Stage IIIC Prostate Cancer Stage IV Prostate Cancer Stage IVA Prostate Cancer Stage IVB Prostate Cancer	NCT03784677	SOR-C13 in Treating Patients With Advanced Refractory Solid Tumors
Intravenous solution for infusion, potential dose range 1.375 mg/kg to 6.12 mg/kg, dosing frequency 2 cycles with a cycle consisting of infusions on days 1-3 and days 8-10 followed by a 11 day off period.	No Study Results Posted on ClinicalTrials.gov for this Study	Completed	Phase I, Open-label, Dose Escalation Study	SOR-C13 potential dose range 1.375 mg/kg to 6.12 mg/kg	Subjects with a histologic diagnosis of solid tumor cancers of epithelial origin	NCT01578564	Safety and Tolerability Study of SOR-C13 in Subjects With Advanced Cancers Commonly Known to Express the TRPV6 Channel

3.1. IP3R Receptor Targets

Unlike in other types of cancers altered IP3R activity has not been extensively described in PCa. However, an unexpected dependency on IP3R-mediated calcium transfer to mitochondria for viability of PCa cells has been found [51]. Treatment with xestospongin B (XeB), a specific IP3R inhibitor, has shown diminished formation of colonies by tumorigenic prostate PC3 cells. Furthermore, XeB-mediated killing and morphological changes including rounding up and shrinkage were observed in PC-3 and DU145 cells. Interestingly, little effect on viability and normal morphology on non-tumorigenic PNT2 prostate line were observed with XeB [51].

On the other hand, the BH4 domain of the anti-apoptotic protein Bcl-2 has been shown to inhibit calcium-mediated apoptosis by inhibiting IP3R-mediated calcium release [134,135]. Interestingly, increased levels of Bcl-2 are required for the progression of prostate cancer cells from an androgen-dependent to an androgen-independent growth stage [136]. Moreover, Bcl-2 upregulation is necessary for androgen-independent prostate cancer cell survival [136]. Therefore, targeting of Bcl-2/IP3R interactions could be a potential therapy in several cancer types including PCa [137]. In this regard, synthetic peptides such as Bcl-2 IP3R Disruptor-2 (BIRD2) are being developed [137]. BIRD2 disrupts Bcl-2-IP3R interplay by binding to the BH4 domain of Bcl-2 and inhibiting Bcl-2 control of IP3R leading to calcium-mediated apoptosis [137]. Whether this approach may be useful has been argued to be dependent on several factor including the levels of Bcl-2 in different stages of cancer cells and their reliance on Bcl-2 for survival [137].

3.2. Ca2+ -ATPase Inhibitors

3.2.1. SERCA Inhibitors

Thapsigargin (Tg), a potent inhibitor of ER calcium ATPase (i.e., *ATP2A2* or SERCA 2b) pumps [138] causes an increase in apoptotic death of metastatic castration-resistant PCa cells [139] and anti-proliferative effects after several days of treatment. Furthermore, it has been shown to inhibit the lysosomal degradative autophagy pathway in LNCaP cancer cells [140]. Thapsigargin also inhibits tumor angiogenesis, becoming an ideal agent to annihilate all the cell types present within the cancer microenvironment [141]. One benefit of using Tg compared with most common used chemotherapeutics is its ability to induce apoptosis on both proliferating but also non-proliferating cells. Use of Tg as an antineoplastic agent would require specific targeting towards cancer cells by chemical modification. Coupling to a peptide carrier to produce a water soluble prodrug that targets specifically metastatic accumulations of androgen independent prostate cells would be an option [142]. In this regard, prostate-specific membrane antigen-specific peptides coupled to analogs of thapsigargin (i.e., G202) have been tested. Some of these new analogues have shown a solid correlation between SERCA inhibition and cell death [143] whereas others behave as weak inducers of cell death and barely act as anti-proliferatives [144]. For example, G202 has been described to produce significant regression of a variety of human tumor xenografts in mice [145]. This approach is currently being tested as a clinical trial in patients with advanced solid tumors (ClinicalTrials.gov Identifier: NCT01056029).

3.2.2. PMCA Inhibitors

Recently, PMCA has been identified as putative chemotherapeutic target in advanced stages of PCa [133]. It has been described that resveratrol derivatives may increase [Ca2+]i by inhibiting PMCA and by activating calcium release from the ER. These actions have been associated with decreased PC-3 cell viability [146]. Moreover, compounds based on esterification of resveratrol at the 4′ hydroxyl with 4 carbon acids have shown to enhance [Ca2+]i levels and cause lower PCa cell survival compared to unmodified resveratrol [146].

3.3. Calcium Channels or Transporters-Targeted Therapies

The expression and/or activity of a large number of calcium channels or transporters are altered in PCas. Compounds or antibodies targeting some of the aforementioned cancer-involved calcium channels/transporters/pumps have been assessed in pre-clinical studies or even in clinical trials [133].

3.3.1. Inhibitors of Voltage-Gated Ca2+ Channels

Neuroendocrine PCa cells derived from LNCaP cells overexpress CaV3.2 T-type voltage-dependent calcium channels (TTCCs) [147]. These channels are also expressed by neuroendocrine cells in PCa tissues obtained from patients after surgery [148]. Recent reports have demonstrated that stimulation of LNCaP cells with bicalutamide—an antiandrogen compound—or hormone-depleted media evoke a significant increase in $Ca_v3.2$ protein expression and the appearance of functional T-type Ca^{2+} channels. These channels have been described to induce promotion of chemoresistance to docetaxel, a chemotherapy compound. Regarding these observations, inhibition of T-type calcium channels by sodium butyrate caused a significant reduction in LNCaP survival [149]. Other Cav3.2 channel blockers such as Ni^{2+} or NNC 55-0396 caused a significant reduction in the viability of LNCaP cells exposed to bicalutamide. However, co-treatment with docetaxel and T-type Ca^{2+} channel inhibitors had no further effect on cell viability [16].

Various research studies have found different effects of ghrelin as a treatment for PCa. It has been published that ghrelin inhibits proliferation of human prostate carcinoma cells through T-type calcium channel overexpression [150]. However, no effects of unacetylated ghrelin (UAG) administration on subcutaneous PC3 xenograft growth or metabolic parameters in a mouse model were found, suggesting that UAG is not likely to be an effective treatment for PCa [151]. Recent data has shown limited short-term effects on human PCa xenograft growth by the ghrelin receptor antagonist [D-Lys3]-GHRP-6 [152]. Therefore, further studies are required to elucidate the role of ghrelin and T-type voltage-dependent calcium channels in PCa therapy.

3.3.2. Transient Receptor Potential Channel Inhibitors

Targeting TRP channels has been suggested as a novel therapeutic strategy for PCa [133]. A TRPM8 channel truncated isoform (4TM-TRPM8) has been identified in PCa. Transcription of TRPM8 and 4TM-TRPM8 has been described to be regulated by short truncated TRPM8 isoforms, known as sM8. The suppression of sM8 isoforms by RNA silencers was shown to induce ER and mitochondrial oxidative stress, p21 induction and apoptosis in PCa cells [153].

TRPV6 has been described as an oncochannel and several TRPV6 inhibitors have been suggested as potential pharmacological therapies in PCa [133]. A peptidic inhibitor of TRPV6 (SOR-C13) has completed phase I in a clinical trial [154] and has been shown to reduce growth in cell and animal models of PCa [155–157].

3.4. STIM1 Inhibitors

ML-9, an inhibitor of Akt kinase and STIM1, is emerging as an interesting therapy for PCa. ML-9 induces cell death in PCa cells related to autophagy regulation and enhances the anticancer activity of docetaxel, suggesting its potential application as an adjuvant to existing anticancer chemotherapies [158]. This report suggests to use the chemical structure of ML-9 as a "template" for the synthesis of improved structurally related and more selective compounds to use in cancer treatment.

3.5. Purinergic Receptor

Suramin, is an antagonist of P2X purinergic receptors -ion channels permeable to calcium that open upon binding of ATP- [159]. Delays in disease progression for patients with hormone-refractory prostate (HPRC) cancer treated with the P2X antagonist support the potential role of suramin as an anti-neoplasic therapy in PCa [160]. Another study of lung metastases induced by PCa cells showed

reduction of tumor size, a decrease of non-apoptotic cells, and increased apoptotic cell number by suramin [161].

4. Conclusions

Dysregulation of calcium homeostasis plays an important role in PCa progression. Several mechanisms that increase or decrease $[Ca2^+]_i$ and a diversity of calcium-binding proteins regulate the various phases of PCa development. Different mechanisms allow PCa cells to mantain certain elevated levels of $[Ca2^+]_i$ that induce proliferation, angiogenesis, EMT, migration and bone colonization meanwhile other mechanisms guarantee evasion of $[Ca2^+]_i$ overload that could lead to mitochondria-dependent apoptosis. Future calcium-based therapies must specifically target prostate cancer cells either avoiding calcium entry or potentiating $[Ca2^+]_i$ overload that leads to apoptosis without affecting non-tumor cells.

Author Contributions: Conceptualization, J.A.A., V.A.; writing-original draft preparation, J.A.A., L.Á.-C., I.G.-R., V.A.; writing-reviewing and editing, J.A.A., V.A.; table/figure preparation, J.A.A., L.Á.-C.; supervision, V.A.; revised manuscript, J.A.A., V.A. All authors have read and agreed to the published version of the manuscript.

Funding: This work was supported by grants from the "Instituto de Salud Carlos III" (PI12/02390) and CEU San Pablo-Santander (MCP19V10, USP-BS-PPC11/2012, USPB-BS-APP-2/2016 and MERMERG-2)

Conflicts of Interest: The authors declare no conflict of interest.

References

1. Scott, E.; Munkley, J. Glycans as biomarkers in prostate cancer. *Int. J. Mol. Sci.* **2019**, *20*, 1389. [CrossRef] [PubMed]
2. Kote-Jarai, Z.; Olama, A.A.; Giles, G.G.; Severi, G.; Schleutker, J.; Weischer, M.; Campa, D.; Riboli, E.; Key, T.; Gronberg, H.; et al. Seven prostate cancer susceptibility loci identified by a multi-stage genome-wide association study. *Nat. Genet.* **2011**, *43*, 785–791. [CrossRef] [PubMed]
3. Frame, F.M.; Maitland, N.J. Epigenetic control of gene expression in the normal and malignant human prostate: A rapid response which promotes therapeutic resistance. *Int. J. Mol. Sci.* **2019**, *20*, 2437. [CrossRef] [PubMed]
4. Kohaar, I.; Petrovics, G.; Srivastava, S. A rich array of prostate cancer molecular biomarkers: Opportunities and challenges. *Int. J. Mol. Sci.* **2019**, *20*, 1831. [CrossRef] [PubMed]
5. Munkley, J.; Livermore, K.; Rajan, P.; Elliott, D.J. RNA splicing and splicing regulator changes in prostate cancer pathology. *Hum. Genet.* **2017**, *136*, 1143–1154. [CrossRef]
6. Bubendorf, L.; Schöpfer, A.; Wagner, U.; Sauter, G.; Moch, H.; Willi, N.; Gasser, T.C.; Mihatsch, M.J. Metastatic patterns of prostate cancer: An autopsy study of 1,589 patients. *Hum. Pathol.* **2000**, *31*, 578–583. [CrossRef]
7. Liao, J.; Schneider, A.; Datta, N.S.; McCauley, L.K. Extracellular calcium as a candidate mediator of prostate cancer skeletal metastasis. *Cancer Res.* **2006**, *66*, 9065–9073. [CrossRef]
8. Roodman, G.D. Mechanisms of Bone Metastasis. *N. Engl. J. Med.* **2004**, *350*, 1655–1664. [CrossRef]
9. Mundy, G.R. Metastasis to bone: Causes, consequences and therapeutic opportunities. *Nat. Rev. Cancer* **2002**, *2*, 584–593. [CrossRef]
10. Roy, A.K.; Lavrovsky, Y.; Song, C.S.; Chen, S.; Jung, M.H.; Velu, N.K.; Bi, B.Y.; Chatterjee, B. Regulation of Androgen Action. *Vitam. Horm.* **1998**, *55*, 309–352.
11. Heinlein, C.A.; Chang, C. Androgen receptor in prostate cancer. *Endocr. Rev.* **2004**, *25*, 276–308. [CrossRef]
12. Wang, G.; Zhao, D.; Spring, D.J.; Depinho, R.A. Genetics and biology of prostate cancer. *Genes Dev.* **2018**, *32*, 1105–1140. [CrossRef] [PubMed]
13. Wozney, J.L.; Antonarakis, E.S. Growth factor and signaling pathways and their relevance to prostate cancer therapeutics. *Cancer Metastasis Rev.* **2014**, *33*, 583–594. [CrossRef]
14. Denis, L.J.; Griffiths, K. Endocrine treatment in prostate cancer. *Semin. Surg. Oncol.* **2000**, *18*, 52–74. [CrossRef]
15. Leibowitz–Amit, R.; Joshua, A. Targeting the androgen receptor in the management of castrationresistant prostate cancer: Rationale, progress, and future directions. *Curr. Oncol.* **2012**, *19* (Suppl. 3). [CrossRef] [PubMed]

16. Hall, M.; Todd, B.; Allen, E.D.; Nguyen, N.; Kwon, Y.-J.; Nguyen, V.; Hearne, J.L.; Martin-Caraballo, M. Androgen receptor signaling regulates T-type Ca 2+ channel expression and neuroendocrine differentiation in prostate cancer cells. *Am. J. Cancer Res.* **2018**, *8*, 732–747. [PubMed]
17. Hirano, D.; Okada, Y.; Minei, S.; Takimoto, Y.; Nemoto, N. Neuroendocrine Differentiation in Hormone Refractory Prostate Cancer Following Androgen Deprivation Therapy. *Eur. Urol.* **2004**, *45*, 586–592. [CrossRef] [PubMed]
18. Bray, F.; Ferlay, J.; Soerjomataram, I.; Siegel, R.L.; Torre, L.A.; Jemal, A. Global cancer statistics 2018: GLOBOCAN estimates of incidence and mortality worldwide for 36 cancers in 185 countries. *CA. Cancer J. Clin.* **2018**, *68*, 394–424. [CrossRef] [PubMed]
19. Jin, J.-K.; Dayyani, F.; Gallick, G.E. Steps in Prostate Cancer Progression that lead to Bone Metastasis NIH Public Access. *Int. J. Cancer* **2011**, *128*, 2545–2561. [CrossRef]
20. Monteith, G.R.; Davis, F.M.; Roberts-Thomson, S.J. Calcium channels and pumps in cancer: Changes and consequences. *J. Biol. Chem.* **2012**, *287*, 31666–31673. [CrossRef]
21. Maly, I.V.; Hofmann, W.A. Calcium and nuclear signaling in prostate cancer. *Int. J. Mol. Sci.* **2018**, *19*, 1237. [CrossRef]
22. Wang, L.; Xu, M.M.; Li, Z.; Shi, M.; Zhou, X.; Jiang, X.; Bryant, J.; Balk, S.; Ma, J.; Isaacs, W.; et al. Calcium and CaSR/IP3R in prostate cancer development. *Cell Biosci.* **2018**, *8*, 16. [CrossRef]
23. Flourakis, M.; Prevarskaya, N. Insights into Ca2+ homeostasis of advanced prostate cancer cells. *Biochim. Biophys. Acta Mol. Cell Res.* **2009**, *1793*, 1105–1109. [CrossRef] [PubMed]
24. Dubois, C.; Vanden Abeele, F.; Lehen'kyi, V.; Gkika, D.; Guarmit, B.; Lepage, G.; Slomianny, C.; Borowiec, A.S.; Bidaux, G.; Benahmed, M.; et al. Remodeling of Channel-Forming ORAI Proteins Determines an Oncogenic Switch in Prostate Cancer. *Cancer Cell* **2014**, *26*, 19–32. [CrossRef] [PubMed]
25. Wang, H.; Tian, L.; Liu, J.; Goldstein, A.; Bado, I.; Zhang, W.; Arenkiel, B.R.; Li, Z.; Yang, M.; Du, S.; et al. The Osteogenic Niche Is a Calcium Reservoir of Bone Micrometastases and Confers Unexpected Therapeutic Vulnerability. *Cancer Cell* **2018**, *34*, 823–839. [CrossRef] [PubMed]
26. Mignen, O.; Constantin, B.; Potier-Cartereau, M.; Penna, A.; Gautier, M.; Guéguinou, M.; Renaudineau, Y.; Shoji, K.F.; Félix, R.; Bayet, E.; et al. Constitutive calcium entry and cancer: Updated views and insights. *Eur. Biophys. J.* **2017**, *46*, 395–413. [CrossRef] [PubMed]
27. Chen, Y.F.; Lin, P.C.; Yeh, Y.M.; Chen, L.H.; Shen, M.R. Store-Operated Ca2+ entry in tumor progression: From molecular mechanisms to clinical implications. *Cancers (Basel)* **2019**, *11*, 899. [CrossRef]
28. Cantonero, C.; Sanchez-Collado, J.; Gonzalez-Nuñez, M.A.; Salido, G.M.; Lopez, J.J.; Jardin, I.; Rosado, J.A. Store-independent Orai1-mediated Ca 2+ entry and cancer. *Cell Calcium* **2019**, *80*, 1–7. [CrossRef]
29. Hanahan, D.; Weinberg, R.A. The hallmarks of cancer. *Cell* **2000**, *100*, 57–70. [CrossRef]
30. Monteith, G.R. Prostate Cancer Cells Alter the Nature of Their Calcium Influx to Promote Growth and Acquire Apoptotic Resistance. *Cancer Cell* **2014**, *26*, 1–2. [CrossRef] [PubMed]
31. Prevarskaya, N.; Skryma, R.; Bidaux, G.; Flourakis, M.; Shuba, Y. Ion channels in death and differentiation of prostate cancer cells. *Cell Death Differ.* **2007**, *14*, 1295–1304. [CrossRef] [PubMed]
32. Mignen, O.; Thompson, J.L.; Shuttleworth, T.J. The molecular architecture of the arachidonate-regulated Ca2+ -selective ARC channel is a pentameric assembly of Orai1 and Orai3 subunits. *J. Physiol.* **2009**, *587*, 4181–4197. [CrossRef] [PubMed]
33. González-Cobos, J.C.; Zhang, X.; Zhang, W.; Ruhle, B.; Motiani, R.K.; Schindl, R.; Muik, M.; Spinelli, A.M.; Bisaillon, J.M.; Shinde, A.V.; et al. Store-independent Orai1/3 channels activated by intracrine leukotrienec4: Role in neointimal hyperplasia. *Circ. Res.* **2013**, *112*, 1013–1025. [CrossRef] [PubMed]
34. Holzmann, C.; Kilch, T.; Kappel, S.; Armbrüster, A.; Jung, V.; Stöckle, M.; Bogeski, I.; Schwarz, E.C.; Peinelt, C. ICRAC controls the rapid androgen response in human primary prostate epithelial cells and is altered in prostate cancer. *Oncotarget* **2013**, *4*, 2096–2107. [CrossRef] [PubMed]
35. Kilch, T.; Kappel, S.; Peinelt, C. Regulation of Ca2+ signaling in prostate cancer cells. *Channels* **2016**, *10*, 170–171. [CrossRef] [PubMed]
36. Kappel, S.; Marques, I.J.; Zoni, E.; Stokłosa, P.; Peinelt, C.; Mercader, N.; Kruithof-de Julio, M.; Borgström, A. Store-Operated Ca2+ Entry as a Prostate Cancer Biomarker—A Riddle with Perspectives. *Curr. Mol. Biol. Rep.* **2017**, *3*, 208–217. [CrossRef]
37. Samanta, A.; Hughes, T.E.T.; Moiseenkova-Bell, V.Y. Transient Receptor Ppotential (TRP) Channels. In *Membrane Protein Complexes: Structure and Function*; Springer: Singapore, 2018; Volume 87, pp. 141–165.

38. Tektemur, A.; Ozaydin, S.; Etem Onalan, E.; Kaya, N.; Kuloglu, T.; Ozercan, İ.H.; Tekin, S.; Elyas, H.M. TRPM2 mediates distruption of autophagy machinery and correlates with the grade level in prostate cancer. *J. Cancer Res. Clin. Oncol.* **2019**, *145*, 1297–1311. [CrossRef]
39. Holzmann, C.; Kappel, S.; Kilch, T.; Jochum, M.M.; Urban, S.K.; Jung, V.; Stöckle, M.; Rother, K.; Greiner, M.; Peinelt, C. Transient receptor potential melastatin 4 channel contributes to migration of androgen-insensitive prostate cancer cells. *Oncotarget* **2015**, *6*, 41783–41793. [CrossRef]
40. Yang, Z.H.; Wang, X.H.; Wang, H.P.; Hu, L.Q. Effects of TRPM8 on the proliferation and motility of prostate cancer PC-3 cells. *Asian J. Androl.* **2009**, *11*, 157–165. [CrossRef]
41. Bidaux, G.; Roudbaraki, M.; Merle, C.; Crépin, A.; Delcourt, P.; Slomianny, C.; Thebault, S.; Bonnal, J.L.; Benahmed, M.; Cabon, F.; et al. Evidence for specific TRPM8 expression in human prostate secretory epithelial cells: Functional androgen receptor requirement. *Endocr. Relat. Cancer* **2005**, *12*, 367–382. [CrossRef]
42. Sánchez, M.G.; Sánchez, A.M.; Collado, B.; Malagarie-Cazenave, S.; Olea, N.; Carmena, M.J.; Prieto, J.C.; Díaz-Laviada, I. Expression of the transient receptor potential vanilloid 1 (TRPV1) in LNCaP and PC-3 prostate cancer cells and in human prostate tissue. *Eur. J. Pharmacol.* **2005**, *515*, 20–27. [CrossRef] [PubMed]
43. Fixemer, T.; Wissenbach, U.; Flockerzi, V.; Bonkhoff, H. Expression of the Ca2+-selective cation channel TRPV6 in human prostate cancer: A novel prognostic marker for tumor progression. *Oncogene* **2003**, *22*, 7858–7861. [CrossRef] [PubMed]
44. Tsavaler, L.; Shapero, M.H.; Morkowski, S.; Laus, R. Trp-p8, a novel prostate-specific gene, is up-regulated in prostate cancer and other malignancies and shares high homology with transient receptor potential calcium channel proteins. *Cancer Res.* **2001**, *61*, 3760–3769. [PubMed]
45. Raphaël, M.; Lehen'kyi, V.; Vandenberghe, M.; Beck, B.; Khalimonchyk, S.; Abeele, F.V.; Farsetti, L.; Germain, E.; Bokhobza, A.; Mihalache, A.; et al. TRPV6 calcium channel translocates to the plasma membrane via Orai1-mediated mechanism and controls cancer cell survival. *Proc. Natl. Acad. Sci. USA* **2014**, *111*, E3870–E3879. [CrossRef]
46. Zhang, L.; Barritt, G.J. Evidence that TRPM8 is an androgen-dependent Ca2+ channel required for the survival of prostate cancer cells. *Cancer Res.* **2004**, *64*, 8365–8373. [CrossRef]
47. Genova, T.; Grolez, G.P.; Camillo, C.; Bernardini, M.; Bokhobza, A.; Richard, E.; Scianna, M.; Lemonnier, L.; Valdembri, D.; Munaron, L.; et al. TRPM8 inhibits endothelial cell migration via a nonchannel function by trapping the small GTPase Rap1. *J. Cell Biol.* **2017**, *216*, 2107–2130. [CrossRef] [PubMed]
48. Kuchay, S.; Giorgi, C.; Simoneschi, D.; Pagan, J.; Missiroli, S.; Saraf, A.; Florens, L.; Washburn, M.P.; Collazo-Lorduy, A.; Castillo-Martin, M.; et al. PTEN counteracts FBXL2 to promote IP3R3- and Ca 2+ -mediated apoptosis limiting tumour growth. *Nature* **2017**, *546*, 554–558. [CrossRef]
49. Orrenius, S.; Zhivotovsky, B.; Nicotera, P. Regulation of cell death: The calcium-apoptosis link. *Nat. Rev. Mol. Cell Biol.* **2003**, *4*, 552–565. [CrossRef]
50. Jamaspishvili, T.; Berman, D.M.; Ross, A.E.; Scher, H.I.; De Marzo, A.M.; Squire, J.A.; Lotan, T.L. Clinical implications of PTEN loss in prostate cancer. *Nat. Rev. Urol.* **2018**, *15*, 222–234. [CrossRef]
51. Cárdenas, C.; Müller, M.; McNeal, A.; Lovy, A.; Jaňa, F.; Bustos, G.; Urra, F.; Smith, N.; Molgó, J.; Diehl, J.A.; et al. Selective Vulnerability of Cancer Cells by Inhibition of Ca2+ Transfer from Endoplasmic Reticulum to Mitochondria. *Cell Rep.* **2016**, *14*, 2313–2324. [CrossRef]
52. Kerkhofs, M.; Bittremieux, M.; Morciano, G.; Giorgi, C.; Pinton, P.; Parys, J.B.; Bultynck, G. Emerging molecular mechanisms in chemotherapy: Ca2+ signaling at the mitochondria-associated endoplasmic reticulum membranes. *Cell Death Dis.* **2018**, *9*, 1–15. [CrossRef] [PubMed]
53. Dong, X.P.; Wang, X.; Xu, H. TRP channels of intracellular membranes. *J. Neurochem.* **2010**, *113*, 313–328. [CrossRef] [PubMed]
54. Englund, E.; Canesin, G.; Papadakos, K.S.; Vishnu, N.; Persson, E.; Reitsma, B.; Anand, A.; Jacobsson, L.; Helczynski, L.; Mulder, H.; et al. Cartilage oligomeric matrix protein promotes prostate cancer progression by enhancing invasion and disrupting intracellular calcium homeostasis. *Oncotarget* **2017**, *8*, 98298–98311. [CrossRef] [PubMed]
55. Rokhlin, O.W.; Taghiyev, A.F.; Bayer, K.U.; Bumcrot, D.; Koteliansk, V.E.; Glover, R.A.; Cohen, M.B. Calcium/calmodulin-dependent kinase II plays an important role in prostate cancer cell survival. *Cancer Biol. Ther.* **2007**, *6*, 732–742. [CrossRef] [PubMed]
56. Sun, Y.H.; Gao, X.; Tang, Y.J.; Xu, C.L.; Wang, L.H. Androgens induce increases in intracellular calcium via a G protein-coupled receptor in LNCaP prostate cancer cells. *J. Androl.* **2006**, *27*, 671–678. [CrossRef]

57. Wasilenko, W.J.; Cooper, J.; Palad, A.J.; Somers, K.D.; Blackmore, P.F.; Rhim, J.S.; Wright, G.L.; Schellhammer, P.F. Calcium signaling in prostate cancer cells: Evidence for multiple receptors and enhanced sensitivity to bombesin/GRP. *Prostate* **1997**, *30*, 167–173. [CrossRef]
58. Legrand, G.; Humez, S.; Slomianny, C.; Dewailly, E.; Abeele, F.V.; Mariot, P.; Wuytack, F.; Prevarskaya, N. Ca2+ pools and cell growth: Evidence for sarcoendoplasmic Ca2+-ATPases 2B involvement in human prostate cancer cell growth control. *J. Biol. Chem.* **2001**, *276*, 47608–47614. [CrossRef]
59. Silvestri, R.; Pucci, P.; Venalainen, E.; Matheou, C.; Mather, R.; Chandler, S.; Aceto, R.; Rigas, S.H.; Wang, Y.; Rietdorf, K.; et al. T-type calcium channels drive the proliferation of androgen-receptor negative prostate cancer cells. *Prostate* **2019**, *79*, 1580–1586. [CrossRef]
60. Weaver, E.M.; Zamora, F.J.; Hearne, J.L.; Martin-Caraballo, M. Posttranscriptional regulation of T-type Ca2+ channel expression by interleukin-6 in prostate cancer cells. *Cytokine* **2015**, *76*, 309–320. [CrossRef]
61. Lehen'kyi, V.; Flourakis, M.; Skryma, R.; Prevarskaya, N. TRPV6 channel controls prostate cancer cell proliferation via Ca 2+/NFAT-dependent pathways. *Oncogene* **2007**, *26*, 7380–7385. [CrossRef]
62. Wang, Y.; Yue, D.; Li, K.; Liu, Y.L.; Ren, C.S.; Wang, P. The role of TRPC6 in HGF-induced cell proliferation of human prostate cancer DU145 and PC3 cells. *Asian J. Androl.* **2010**, *12*, 841–852. [CrossRef] [PubMed]
63. Sagredo, A.I.; Sagredo, E.A.; Cappelli, C.; Báez, P.; Andaur, R.E.; Blanco, C.; Tapia, J.C.; Echeverría, C.; Cerda, O.; Stutzin, A.; et al. TRPM4 regulates Akt/GSK3-β activity and enhances β-catenin signaling and cell proliferation in prostate cancer cells. *Mol. Oncol.* **2018**, *12*, 151–165. [PubMed]
64. Benelli, R.; Monteghirfo, S.; Venè, R.; Tosetti, F.; Ferrari, N. The chemopreventive retinoid 4HPR impairs prostate cancer cell migration and invasion by interfering with FAK/AKT/GSK3β pathway and β-catenin stability. *Mol. Cancer* **2010**, *9*, 142. [CrossRef]
65. Launay, P.; Fleig, A.; Perraud, A.L.; Scharenberg, A.M.; Penner, R.; Kinet, J.P. TRPM4 is a Ca2+-activated nonselective cation channel mediating cell membrane depolarization. *Cell* **2002**, *109*, 397–407. [CrossRef]
66. Zeng, X.; Sikka, S.C.; Huang, L.; Sun, C.; Xu, C.; Jia, D.; Abdel-Mageed, A.B.; Pottle, J.E.; Taylor, J.T.; Li, M. Novel role for the transient receptor potential channel TRPM2 in prostate cancer cell proliferation. *Prostate Cancer Prostatic Dis.* **2010**, *13*, 195–201. [CrossRef] [PubMed]
67. Gudipaty, S.A.; Lindblom, J.; Loftus, P.D.; Redd, M.J.; Edes, K.; Davey, C.F.; Krishnegowda, V.; Rosenblatt, J. Mechanical stretch triggers rapid epithelial cell division through Piezo1. *Nature* **2017**, *543*, 118–121. [CrossRef] [PubMed]
68. Han, Y.; Liu, C.; Zhang, D.; Men, H.; Huo, L.; Geng, Q.; Wang, S.; Gao, Y.; Zhang, W.; Zhang, Y.; et al. Mechanosensitive ion channel piezo1 promotes prostate cancer development through the activation of the akt/mtorpathway and acceleration of cell cycle. *Int. J. Oncol.* **2019**, *55*, 629–644. [PubMed]
69. Sun, Y.; Selvaraj, S.; Varma, A.; Derry, S.; Sahmoun, A.E.; Singh, B.B. Increase in serum Ca2+/Mg2+ ratio promotes proliferation of prostate cancer cells by activating TRPM7 channels. *J. Biol. Chem.* **2013**, *288*, 255–263. [CrossRef] [PubMed]
70. Bernichtein, S.; Pigat, N.; Delongchamps, N.B.; Boutillon, F.; Verkarre, V.; Camparo, P.; Reyes-Gomez, E.; Méjean, A.; Oudard, S.M.; Lepicard, E.M.; et al. Vitamin D3 prevents calcium-induced progression of early-stage prostate tumors by counteracting TRPC6 and calcium sensing receptor upregulation. *Cancer Res.* **2017**, *77*, 355–365. [CrossRef] [PubMed]
71. Soderling, T.R. Ca2+-calmodulin-dependent protein kinase cascade. *Trends Biochem. Sci.* **1999**, *24*, 232–236. [CrossRef]
72. Massie, C.E.; Lynch, A.; Ramos-Montoya, A.; Boren, J.; Stark, R.; Fazli, L.; Warren, A.; Scott, H.; Madhu, B.; Sharma, N.; et al. The androgen receptor fuels prostate cancer by regulating central metabolism and biosynthesis. *EMBO J.* **2011**, *30*, 2719–2733. [CrossRef]
73. White, M.A.; Tsouko, E.; Lin, C.; Rajapakshe, K.; Spencer, J.M.; Wilkenfeld, S.R.; Vakili, S.S.; Pulliam, T.L.; Awad, D.; Nikolos, F.; et al. GLUT12 promotes prostate cancer cell growth and is regulated by androgens and CaMKK2 signaling. *Endocr. Relat. Cancer* **2018**, *25*, 453–469. [CrossRef] [PubMed]
74. Penfold, L.; Woods, A.; Muckett, P.; Nikitin, A.Y.; Kent, T.R.; Zhang, S.; Graham, R.; Pollard, A.; Carling, D. CaMKK2 promotes prostate cancer independently of AMPK via increased lipogenesis. *Cancer Res.* **2018**, *78*, 6747–6761. [CrossRef] [PubMed]
75. Karacosta, L.G.; Kuroski, L.A.; Hofmann, W.A.; Azabdaftari, G.; Mastri, M.; Gocher, A.M.; Dai, S.; Hoste, A.J.; Edelman, A.M. Nucleoporin 62 and Ca2+/calmodulin dependent kinase kinase 2 regulate androgen receptor activity in castrate resistant prostate cancer cells. *Prostate* **2016**, *76*, 294–306. [CrossRef] [PubMed]

76. Karacosta, L.G.; Foster, B.A.; Azabdaftari, G.; Feliciano, D.M.; Edelman, A.M. A regulatory feedback loop between Ca2+/calmodulin-dependent protein kinase kinase 2 (CaMKK2) and the androgen receptor in prostate cancer progression. *J. Biol. Chem.* **2012**, *287*, 24832–24843. [CrossRef] [PubMed]
77. Wang, N.; Yao, M.; Xu, J.; Quan, Y.; Zhang, K.; Yang, R.; Gao, W.Q. Autocrine activation of CHRM3 promotes prostate cancer growth and castration resistance via CaM/CaMKK-mediated phosphorylation of Akt. *Clin. Cancer Res.* **2015**, *21*, 4676–4685. [CrossRef] [PubMed]
78. Audy, M.C.; Vacher, P.; Dufy, B. 17β-Estradiol stimulates a rapid Ca2+ influx in LNCaP human prostate cancer cells. *Eur. J. Endocrinol.* **1996**, *135*, 367–373. [CrossRef]
79. Pelley, R.P.; Chinnakannu, K.; Murthy, S.; Strickland, F.M.; Menon, M.; Dou, Q.P.; Barrack, E.R.; Reddy, G.P.V. Calmodulin-androgen receptor (AR) interaction: Calcium-dependent, calpain-mediated breakdown of AR in LNCaP prostate cancer cells. *Cancer Res.* **2006**, *66*, 11754–11762. [CrossRef] [PubMed]
80. Gong, Y.; Blok, L.J.; Perry, J.E.; Lindzey, J.K.; Tindall, D.J. Calcium regulation of androgen receptor expression in the human prostate cancer cell line LNCaP. *Endocrinology* **1995**, *136*, 2172–2178. [CrossRef]
81. Maia, C.; Santos, C.; Schmitt, F.; Socorro, S. Regucalcin is under-expressed in human breast and prostate cancers: Effect of sex steroid hormones. *J. Cell. Biochem.* **2009**, *107*, 667–676. [CrossRef]
82. Yamaguchi, M. Role of regucalcin in maintaining cell homeostasis and function (review). *Int. J. Mol. Med.* **2005**, *15*, 371–389. [CrossRef]
83. Zhu, W.; Xue, Y.; Liang, C.; Zhang, R.; Zhang, Z.; Li, H.; Su, D.; Liang, X.; Zhang, Y.; Huang, Q.; et al. S100A16 promotes cell proliferation and metastasis via AKT and ERK cell signaling pathways in human prostate cancer. *Tumor Biol.* **2016**, *37*, 12241–12250. [CrossRef]
84. Warnier, M.; Roudbaraki, M.; Derouiche, S.; Delcourt, P.; Bokhobza, A.; Prevarskaya, N.; Mariot, P. CACNA2D2 promotes tumorigenesis by stimulating cell proliferation and angiogenesis. *Oncogene* **2015**, *34*, 5383–5394. [CrossRef]
85. Bernardini, M.; Brossa, A.; Chinigo, G.; Grolez, G.P.; Trimaglio, G.; Allart, L.; Hulot, A.; Marot, G.; Genova, T.; Joshi, A.; et al. Transient receptor potential channel expression signatures in tumor-derived endothelial cells: Functional roles in prostate cancer angiogenesis. *Cancers (Basel)* **2019**, *11*, 956. [CrossRef]
86. Collado, B.; Sánchez, M.G.; Díaz-Laviada, I.; Prieto, J.C.; Carmena, M.J. Vasoactive intestinal peptide (VIP) induces c-fos expression in LNCaP prostate cancer cells through a mechanism that involves Ca2+ signalling. Implications in angiogenesis and neuroendocrine differentiation. *Biochim. Biophys. Acta Mol. Cell Res.* **2005**, *1744*, 224–233. [CrossRef]
87. Mishra, S.K.; Siddique, H.R.; Saleem, M. S100A4 calcium-binding protein is key player in tumor progression and metastasis: Preclinical and clinical evidence. *Cancer Metastasis Rev.* **2012**, *31*, 163–172. [CrossRef]
88. Ochiya, T.; Takenaga, K.; Endo, H. Silencing of S100A4, a metastasis-associated protein, in endothelial cells inhibits tumor angiogenesis and growth. *Angiogenesis* **2014**, *17*, 17–26. [CrossRef]
89. Nieto, M.A.; Huang, R.Y.Y.J.; Jackson, R.A.A.; Thiery, J.P.P. EMT: 2016. *Cell* **2016**, *166*, 21–45. [CrossRef]
90. He, H.; Yang, X.; Davidson, A.J.; Wu, D.; Marshall, F.F.; Chung, L.W.K.; Zhau, H.E.; Wang, R. Progressive epithelial to mesenchymal transitions in ARCaPE prostate cancer cells during xenograft tumor formation and metastasis. *Prostate* **2010**, *70*, 518–528. [CrossRef]
91. Tsuji, T.; Ibaragi, S.; Hu, G.F. Epithelial-mesenchymal transition and cell cooperativity in metastasis. *Cancer Res.* **2009**, *69*, 7135–7139. [CrossRef]
92. Brabletz, T.; Kalluri, R.; Nieto, M.A.; Weinberg, R.A. EMT in cancer. *Nat. Rev. Cancer* **2018**, *18*, 128–134. [CrossRef] [PubMed]
93. Figiel, S.; Bery, F.; Chantôme, A.; Fontaine, D.; Pasqualin, C.; Maupoil, V.; Domingo, I.; Guibon, R.; Bruyère, F.; Potier-Cartereau, M.; et al. A novel calcium-mediated EMT pathway controlled by lipids: An opportunity for prostate cancer adjuvant therapy. *Cancers (Basel)* **2019**, *11*, 1814. [CrossRef] [PubMed]
94. Sun, Y.; Schaar, A.; Sukumaran, P.; Dhasarathy, A.; Singh, B.B. TGFβ-induced epithelial-to-mesenchymal transition in prostate cancer cells is mediated via TRPM7 expression. *Mol. Carcinog.* **2018**, *57*, 752–761. [CrossRef]
95. Chen, L.; Cao, R.; Wang, G.; Yuan, L.; Qian, G.; Guo, Z.; Wu, C.L.; Wang, X.; Xiao, Y. Downregulation of TRPM7 suppressed migration and invasion by regulating epithelial–mesenchymal transition in prostate cancer cells. *Med. Oncol.* **2017**, *34*, 127. [CrossRef] [PubMed]
96. Li, F.; Abuarab, N.; Sivaprasadarao, A. Reciprocal regulation of actin cytoskeleton remodelling and cell migration by Ca2+ and Zn2+: Role of TRPM2 channels. *J. Cell Sci.* **2016**, *129*, 2016–2029. [CrossRef]

97. Sumoza-Toledo, A.; Lange, I.; Cortado, H.; Bhagat, H.; Mori, Y.; Fleig, A.; Penner, R.; Partida-Sánchez, S. Dendritic cell maturation and chemotaxis is regulated by TRPM2-mediated lysosomal Ca 2+ release. *FASEB J.* **2011**, *25*, 3529–3542. [CrossRef]
98. Du, C.; Zheng, Z.; Li, D.; Chen, L.; Li, N.; Yi, X.; Yang, Y.; Guo, F.; Liu, W.; Xie, X.; et al. BKCa promotes growth and metastasis of prostate cancer through facilitating the coupling between αvβ3 integrin and FAK. *Oncotarget* **2016**, *7*, 40174–40188. [CrossRef]
99. Monet, M.; Lehen'kyi, V.; Gackiere, F.; Firlej, V.; Vandenberghe, M.; Roudbaraki, M.; Gkika, D.; Pourtier, A.; Bidaux, G.; Slomianny, C.; et al. Role of cationic channel TRPV2 in promoting prostate cancer migration and progression to androgen resistance. *Cancer Res.* **2010**, *70*, 1225–1235. [CrossRef]
100. Wang, D.; Li, X.; Liu, J.; Li, J.; Li, L.J.; Qiu, M.X. Effects of TRPC6 on invasibility of low-differentiated prostate cancer cells. *Asian Pac. J. Trop. Med.* **2014**, *7*, 44–47. [CrossRef]
101. Henshall, S.M.; Afar, D.E.H.; Hiller, J.; Horvath, L.G.; Quinn, D.I.; Rasiah, K.K.; Gish, K.; Willhite, D.; Kench, J.G.; Gardiner-Garden, M.; et al. Survival analysis of genome-wide gene expression profiles of prostate cancers identifies new prognostic targets of disease relapse. *Cancer Res.* **2003**, *63*, 4196–4203.
102. Gkika, D.; Flourakis, M.; Lemonnier, L.; Prevarskaya, N. PSA reduces prostate cancer cell motility by stimulating TRPM8 activity and plasma membrane expression. *Oncogene* **2010**, *29*, 4611–4616. [CrossRef] [PubMed]
103. Soekmadji, C.; Rockstroh, A.; Ramm, G.A.; Nelson, C.C.; Russell, P.J. Extracellular Vesicles in the Adaptive Process of Prostate Cancer during Inhibition of Androgen Receptor Signaling by Enzalutamide. *Proteomics* **2017**, *17*, 1600427. [CrossRef]
104. Slater, M.; Danieletto, S.; Gidley-Baird, A.; Teh, L.C.; Barden, J.A. Early prostate cancer detected using expression of non-functional cytolytic P2X7 receptors. *Histopathology* **2004**, *44*, 206–215. [CrossRef] [PubMed]
105. Qiu, Y.; Li, W.H.; Zhang, H.Q.; Liu, Y.; Tian, X.X.; Fang, W.G. P2X7 mediates ATP-driven invasiveness in prostate cancer cells. *PLoS ONE* **2014**, *9*, e114371. [CrossRef] [PubMed]
106. Li, W.H.; Qiu, Y.; Zhang, H.Q.; Liu, Y.; You, J.F.; Tian, X.X.; Fang, W.G. P2Y2 receptor promotes cell invasion and metastasis in prostate cancer cells. *Br. J. Cancer* **2013**, *109*, 1666–1675. [CrossRef]
107. Zhou, Y.; Gu, P.; Li, J.; Li, F.; Zhu, J.; Gao, P.; Zang, Y.; Wang, Y.; Shan, Y.; Yang, D. Suppression of STIM1 inhibits the migration and invasion of human prostate cancer cells and is associated with PI3K/Akt signaling inactivation. *Oncol. Rep.* **2017**, *38*, 2629–2636. [CrossRef]
108. Xin, W.; Rhodes, D.R.; Ingold, C.; Chinnaiyan, A.M.; Rubin, M.A. Dysregulation of the annexin family protein family is associated with prostate cancer progression. *Am. J. Pathol.* **2003**, *162*, 255–261. [CrossRef]
109. Liu, J.W.; Shen, J.J.; Tanzillo-Swarts, A.; Bhatia, B.; Maldonado, C.M.; Person, M.D.; Lau, S.S.; Tang, D.G. Annexin II expression is reduced or lost in prostate cancer cells and its re-expression inhibits prostate cancer cell migration. *Oncogene* **2003**, *22*, 1475–1485. [CrossRef]
110. Huang, C.; Miller, R.T.; Freter, C.E. Signaling regulation and role of filamin A cleavage in Ca2+-stimulated migration of androgen receptor-deficient prostate cancer cells. *Oncotarget* **2017**, *8*, 3840–3853.
111. Frigo, D.E.; Howe, M.K.; Wittmann, B.M.; Brunner, A.M.; Cushman, I.; Wang, Q.; Brown, M.; Means, A.R.; McDonnell, D.P. CaM kinase kinase β-mediated activation of the growth regulatory kinase AMPK is required for androgen-dependent migration of prostate cancer cells. *Cancer Res.* **2011**, *71*, 528–537. [CrossRef]
112. Wang, Q.; Symes, A.J.; Kane, C.A.; Freeman, A.; Nariculam, J.; Munson, P.; Thrasivoulou, C.; Masters, J.R.W.; Ahmed, A. A novel role for Wnt/Ca2+ signaling in actin cytoskeleton remodeling and cell motility in prostate cancer. *PLoS ONE* **2010**, *5*, e10456. [CrossRef] [PubMed]
113. Ye, L.; Sun, P.H.; Martin, T.A.; Sanders, A.J.; Mason, M.D.; Jiang, W.G. Psoriasin (S100A7) is a positive regulator of survival and invasion of prostate cancer cells. *Urol. Oncol. Semin. Orig. Investig.* **2013**, *31*, 1576–1583. [CrossRef] [PubMed]
114. Saleem, M.; Kweon, M.H.; Johnson, J.J.; Adhami, V.M.; Elcheva, I.; Khan, N.; Hafeez, B.B.; Bhat, K.M.R.; Sarfaraz, S.; Reagan-Shaw, S.; et al. S100A4 accelerates tumorigenesis and invasion of human prostate cancer through the transcriptional regulation of matrix metalloproteinase 9. *Proc. Natl. Acad. Sci. USA* **2006**, *103*, 14825–14830. [CrossRef]
115. Wong, M.C.S.; Goggins, W.B.; Wang, H.H.X.; Fung, F.D.H.; Leung, C.; Wong, S.Y.S.; Ng, C.F.; Sung, J.J.Y. Global Incidence and Mortality for Prostate Cancer: Analysis of Temporal Patterns and Trends in 36 Countries. *Eur. Urol.* **2016**, *70*, 862–874.
116. Ottewell, P.D. The role of osteoblasts in bone metastasis. *J. Bone Oncol.* **2016**, *5*, 124–127. [CrossRef]

117. Shiozawa, Y.; Pedersen, E.A.; Havens, A.M.; Jung, Y.; Mishra, A.; Joseph, J.; Kim, J.K.; Patel, L.R.; Ying, C.; Ziegler, A.M.; et al. Human prostate cancer metastases target the hematopoietic stem cell niche to establish footholds in mouse bone marrow. *J. Clin. Invest.* **2011**, *121*, 1298–1312. [CrossRef]
118. D'Ambrosio, J.; Fatatis, A. Osteoblasts modulate Ca2+ signaling in bone-metastatic prostate and breast cancer cells. *Clin. Exp. Metastasis* **2009**, *26*, 955–964. [CrossRef]
119. Álvarez Carrión, L.; Gutiérrez Rojas, I.; Ardura, J.; Alonso, V. Osteogenic cells affected by soluble tumor factors contribute to bone pre-metastatic niche formation. *Rev. Osteoporos. y Metab. Miner.* **2019**, *11*, 64–71. [CrossRef]
120. Dvorak, M.M.; Siddiqua, A.; Ward, D.T.; Carter, D.H.; Dallas, S.L.; Nemeth, E.F.; Riccardi, D. Physiological changes in extracellular calcium concentration directly control osteoblast function in the absence of calciotropic hormones. *Proc. Natl. Acad. Sci. USA* **2004**, *101*, 5140–5145. [CrossRef]
121. Berger, C.E.M.; Rathod, H.; Gillespie, J.I.; Horrocks, B.R.; Datta, H.K. Scanning electrochemical microscopy at the surface of bone-resorbing osteoclasts: Evidence for steady-state disposal and intracellular functional compartmentalization of calcium. *J. Bone Miner. Res.* **2001**, *16*, 2092–2102. [CrossRef]
122. Silver, I.A.; Murrills, R.J.; Etherington, D.J. Microelectrode studies on the acid microenvironment beneath adherent macrophages and osteoclasts. *Exp. Cell Res.* **1988**, *175*, 266–276. [CrossRef]
123. Sanders, J.L.; Chattopadhyay, N.; Kifor, O.; Yamaguchi, T.; Brown, E.M. Ca2+-sensing receptor expression and PTHrP secretion in PC-3 human prostate cancer cells. *Am. J. Physiol.* **2001**, *281*, E1267–E1274. [CrossRef]
124. Yano, S.; Macleod, R.J.; Chattopadhyay, N.; Tfelt-Hansen, J.; Kifor, O.; Butters, R.R.; Brown, E.M. Calcium-sensing receptor activation stimulates parathyroid hormone-related protein secretion in prostate cancer cells: Role of epidermal growth factor receptor transactivation. *Bone* **2004**, *35*, 664–672. [CrossRef]
125. Oulidi, A.; Bokhobza, A.; Gkika, D.; Vanden Abeele, F.; Lehen'kyi, V.; Ouafik, L.; Mauroy, B.; Prevarskaya, N. TRPV2 Mediates Adrenomedullin Stimulation of Prostate and Urothelial Cancer Cell Adhesion, Migration and Invasion. *PLoS ONE* **2013**, *8*, e64885. [CrossRef]
126. Warrington, J.I.; Richards, G.O.; Wang, N. The Role of the Calcitonin Peptide Family in Prostate Cancer and Bone Metastasis. *Curr. Mol. Biol. Reports* **2017**, *3*, 197–203. [CrossRef]
127. Sabbisetti, V.S.; Chirugupati, S.; Thomas, S.; Vaidya, K.S.; Reardon, D.; Chiriva-Internati, M.; Iczkowski, K.A.; Shah, G.V. Calcitonin increases invasiveness of prostate cancer cells: Role for cyclic AMP-dependent protein kinase A in calcitonin action. *Int. J. Cancer* **2005**, *117*, 551–560. [CrossRef] [PubMed]
128. Ardura, J.A.; Gutiérrez Rojas, I.; Alvarez Carrion, L.; Friedman, P.A.; Alonso, V. Factors secreted by bone cells induce intracellular calcium accumulation and cyclic AMP and activation of ERK 1/2 in prostate cancer cells; evaluation by fluorescence techniques in living cells. *Rev. Osteoporos. y Metab. Miner.* **2018**, *10*, 131–137.
129. Mancini, M.; Toker, A. NFAT proteins: Emerging roles in cancer progression. *Nat. Rev. Cancer* **2009**, *9*, 810–820. [CrossRef]
130. Di Giorgio, E.; Hancock, W.W.; Brancolini, C. MEF2 and the tumorigenic process, hic sunt leones. *Biochim. Biophys. Acta Rev. Cancer* **2018**, *1870*, 261–273. [CrossRef]
131. Lecrone, V.; Li, W.; Devoll, R.E.; Logothetis, C.; Farach-Carson, M.C. Calcium signals in prostate cancer cells: Specific activation by bone matrix proteins. *Cell Calcium* **2000**, *27*, 35–42. [CrossRef]
132. Teo, M.Y.; Rathkopf, D.E.; Kantoff, P. Treatment of Advanced Prostate Cancer. *Annu. Rev. Med.* **2019**, *70*, 479–499. [CrossRef]
133. Cui, C.; Merritt, R.; Fu, L.; Pan, Z. Targeting calcium signaling in cancer therapy. *Acta Pharm. Sin. B* **2017**, *7*, 3–17. [CrossRef] [PubMed]
134. Ivanova, H.; Luyten, T.; Decrock, E.; Vervliet, T.; Leybaert, L.; Parys, J.B.; Bultynck, G. The BH4 domain of Bcl-2 orthologues from different classes of vertebrates can act as an evolutionary conserved inhibitor of IP3 receptor channels. *Cell Calcium* **2017**, *62*, 41–46. [CrossRef] [PubMed]
135. Eckenrode, E.F.; Yang, J.; Velmurugan, G.V.; Kevin Foskett, J.; White, C. Apoptosis protection by Mcl-1 and Bcl-2 modulation of inositol 1,4,5-trisphosphate receptor-dependent Ca2+ signaling. *J. Biol. Chem.* **2010**, *285*, 13678–13684. [CrossRef]
136. Lin, Y.; Fukuchi, J.; Hiipakka, R.A.; Kokontis, J.M.; Xiang, J. Up-regulation of Bcl-2 is required for the progression of prostate cancer cells from an androgen-dependent to an androgen-independent growth stage. *Cell Res.* **2007**, *17*, 531–536. [CrossRef]

137. Distelhorst, C.W. Targeting Bcl-2-IP 3 receptor interaction to treat cancer: A novel approach inspired by nearly a century treating cancer with adrenal corticosteroid hormones. *Biochim. Biophys. Acta Mol. Cell Res.* **2018**, *1865*, 1795–1804. [CrossRef]
138. Thastrup, O.; Cullen, P.J.; Drobak, B.K.; Hanley, M.R.; Dawson, A.P. Thapsigargin, a tumor promoter, discharges intracellular Ca2+ stores by specific inhibition of the endoplasmic reticulum Ca2+-ATPase. *Proc. Natl. Acad. Sci. USA* **1990**, *87*, 2466–2470. [CrossRef]
139. Short, A.D.; Gill, D.L.; Isaacs, J.T. The Role of Calcium, pH, and Cell Proliferation in the Programmed (Apoptotic) Death of Androgen-independent Prostatic Cancer Cells Induced by Thapsigargin. *Cancer Res.* **1994**, *54*, 6167–6175.
140. Engedal, N.; Torgersen, M.L.; Guldvik, I.J.; Barfeld, S.J.; Bakula, D.; Sætre, F.; Hagen, L.K.; Patterson, J.B.; Proikas-Cezanne, T.; Seglen, P.O.; et al. Modulation of intracellular calcium homeostasis blocks autophagosome formation. *Autophagy* **2013**, *9*, 1475–1490. [CrossRef]
141. Akinboye, E.S.; Brennen, W.N.; Denmeade, S.R.; Isaacs, J.T. Albumin-linked prostate-specific antigen-activated thapsigargin- and niclosamide-based molecular grenades targeting the microenvironment in metastatic castration-resistant prostate cancer. *Asian J. Urol.* **2019**, *6*, 99–108. [CrossRef]
142. Denmeade, S.R.; Isaacs, J.T. The SERCA Pump as a Therapeutic Target. *Cancer Biol. Ther.* **2005**, *4*, 14–22. [CrossRef]
143. Dubois, C.; Vanden Abeele, F.; Sehgal, P.; Lesen, C.; Junker, S.; Christensen, S.B.; Prevarskaya, N.; Møller, J.V. Differential effects of thapsigargin analogues on apoptosis of prostate cancer cells: Complex regulation by intracellular calcium. *FEBS J.* **2013**, *280*, 5430–5440. [CrossRef] [PubMed]
144. Sehgal, P.; Szalai, P.; Olesen, C.; Praetorius, H.A.; Nissen, P.; Christensen, S.B.; Engedal, N.; Møller, J.V. Inhibition of the sarco/endoplasmic reticulum (ER) Ca 2-ATPase by thapsigargin analogs induces cell death via ER Ca 2 depletion and the unfolded protein response. *J. Biol. Chem.* **2017**, *292*, 19656–19673. [CrossRef] [PubMed]
145. Denmeade, S.R.; Mhaka, A.M.; Rosen, D.M.; Brennen, W.N.; Dalrymple, S.; Dach, I.; Olesen, C.; Gurel, B.; Demarzo, A.M.; Wilding, G.; et al. Engineering a prostate-specific membrane antigen-activated tumor endothelial cell prodrug for cancer therapy. *Sci. Transl. Med.* **2012**, *4*, 140ra86. [CrossRef] [PubMed]
146. Peterson, J.A.; Crowther, C.M.; Andrus, M.B.; Kenealey, J.D. Resveratrol derivatives increase cytosolic calcium by inhibiting plasma membrane ATPase and inducing calcium release from the endoplasmic reticulum in prostate cancer cells. *Biochem. Biophys. Reports* **2019**, *19*, 100667. [CrossRef]
147. Mariot, P.; Vanoverberghe, K.; Lalevee, N.; Rossier, M.F.; Prevarskaya, N. Overexpression of an alpha 1H (Cav3.2) T-type calcium channel during neuroendocrine differentiation of human prostate cancer cells. *J. Biol. Chem.* **2002**, *277*, 10824–10833. [CrossRef] [PubMed]
148. Gackière, F.; Bidaux, G.; Delcourt, P.; Van Coppenolle, F.; Katsogiannou, M.; Dewailly, E.; Bavencoffe, A.; Van Chuoï-Mariot, M.T.; Mauroy, B.; Prevarskaya, N.; et al. CaV3.2 T-type calcium channels are involved in calcium-dependent secretion of neuroendocrine prostate cancer cells. *J. Biol. Chem.* **2008**, *283*, 10162–10173. [CrossRef] [PubMed]
149. Weaver, E.M.; Zamora, F.J.; Puplampu-Dove, Y.A.; Kiessu, E.; Hearne, J.L.; Martin-Caraballo, M. Regulation of T-type calcium channel expression by sodium butyrate in prostate cancer cells. *Eur. J. Pharmacol.* **2015**, *749*, 20–31. [CrossRef]
150. Díaz-Lezama, N.; Hernández-Elvira, M.; Sandoval, A.; Monroy, A.; Felix, R.; Monjaraz, E. Ghrelin inhibits proliferation and increases T-type Ca2+ channel expression in PC-3 human prostate carcinoma cells. *Biochem. Biophys. Res. Commun.* **2010**, *403*, 24–29. [CrossRef] [PubMed]
151. Maugham, M.L.; Seim, I.; Thomas, P.B.; Crisp, G.J.; Shah, E.T.; Herington, A.C.; Brown, K.A.; Gregory, L.S.; Nelson, C.C.; Jeffery, P.L.; et al. No effect of unacylated ghrelin administration on subcutaneous PC3 xenograft growth or metabolic parameters in a Rag1-/- mouse model of metabolic dysfunction. *PLoS ONE* **2018**, *13*, e0198495. [CrossRef]
152. Maugham, M.L.; Seim, I.; Thomas, P.B.; Crisp, G.J.; Shah, E.T.; Herington, A.C.; Gregory, L.S.; Nelson, C.C.; Jeffery, P.L.; Chopin, L.K. Limited short-term effects on human prostate cancer xenograft growth and epidermal growth factor receptor gene expression by the ghrelin receptor antagonist [D-Lys3]-GHRP-6. *Endocrine* **2019**, *64*, 393–405. [CrossRef] [PubMed]

153. Bidaux, G.; Borowiec, A.S.; Dubois, C.; Delcourt, P.; Schulz, C.; Abeele, F.V.; Lepage, G.; Desruelles, E.; Bokhobza, A.; Dewailly, E.; et al. Targeting of short TRPM8 isoforms induces 4TM-TRPM8-dependent apoptosis in prostate cancer cells. *Oncotarget* **2016**, *7*, 29063–29080. [CrossRef]
154. Fu, S.; Hirte, H.; Welch, S.; Ilenchuk, T.T.; Lutes, T.; Rice, C.; Fields, N.; Nemet, A.; Dugourd, D.; Piha-Paul, S.; et al. First-in-human phase I study of SOR-C13, a TRPV6 calcium channel inhibitor, in patients with advanced solid tumors. *Investig. New Drugs* **2017**, *35*, 1–10.
155. Xue, H.; Wang, Y.; MacCormack, T.J.; Lutes, T.; Rice, C.; Davey, M.; Dugourd, D.; Ilenchuk, T.T.; Stewart, J.M. Inhibition of Transient Receptor Potential Vanilloid 6 channel, elevated in human ovarian cancers, reduces tumour growth in a xenograft model. *J. Cancer* **2018**, *9*, 3196–3207. [CrossRef] [PubMed]
156. Bowen, C.V.; DeBay, D.; Ewart, H.S.; Gallant, P.; Gormley, S.; Ilenchuk, T.T.; Iqbal, U.; Lutes, T.; Martina, M.; Mealing, G.; et al. In vivo detection of human TRPV6-rich tumors with anti-cancer peptides derived from soricidin. *PLoS ONE* **2013**, *8*, e58866. [CrossRef]
157. Stewart, J.M. TRPV6 as A Target for Cancer Therapy. *J. Cancer* **2020**, *11*, 374–387. [CrossRef] [PubMed]
158. Kondratskyi, A.; Yassine, M.; Slomianny, C.; Kondratska, K.; Gordienko, D.; Dewailly, E.; Lehen'kyi, V.; Skryma, R.; Prevarskaya, N. Identification of ML-9 as a lysosomotropic agent targeting autophagy and cell death. *Cell Death Dis.* **2014**, *5*, e1193. [CrossRef] [PubMed]
159. Sauer, H.; Hescheler, J.; Wartenberg, M. Mechanical strain-induced Ca(2+) waves are propagated via ATP release and purinergic receptor activation. *Am. J. Physiol. Cell Physiol.* **2000**, *279*, C295–C307. [CrossRef] [PubMed]
160. Small, E.J.; Meyer, M.; Marshall, M.E.; Reyno, L.M.; Meyers, F.J.; Natale, R.B.; Lenehan, P.F.; Chen, L.; Slichenmyer, W.J.; Eisenberger, M. Suramin therapy for patients with symptomatic hormone-refractory prostate cancer: Results of a randomized phase III trial comparing suramin plus hydrocortisone to placebo plus hydrocortisone. *J. Clin. Oncol.* **2000**, *18*, 1440–1450. [CrossRef]
161. Song, S.; Wientjes, M.G.; Walsh, C.; Au, J.L. Nontoxic doses of suramin enhance activity of paclitaxel against lung metastases. *Cancer Res.* **2001**, *61*, 6145–6150.

Ardura JA[1,2], Gutiérrez Rojas I[1], Álvarez Carrión L[1], Friedman PA[3], Alonso V[1,2]

1 Laboratorio de Fisiopatología Ósea - Instituto de Medicina Molecular Aplicada (IMMA) - Universidad San Pablo-CEU - Madrid (España)

2 Departamento de Ciencias Médicas Básicas - Facultad de Medicina - Universidad San Pablo-CEU - Madrid (España)

3 Departamento de Farmacología y Biología Química - Universidad de Pittsburgh - Pensilvania (Estados Unidos)

Factors secreted by bone cells induce intracellular calcium accumulation and cyclic AMP and activation of ERK 1/2 in prostate cancer cells; evaluation by fluorescence techniques in living cells

DOI: http://dx.doi.org/10.4321/S1889-836X2018000400005

Correspondence: Verónica Alonso Rodríguez - Instituto de Medicina Molecular Aplicada (IMMA) - Facultad de Medicina - Universidad San Pablo-CEU - 28925 Alcorcón - Madrid (Spain)
e-mail: veronica.alonsorodriguez@ceu.es

Date of receipt: 05/07/2018
Date of acceptance: 18/11/2018

Scholarship work to attend the 39th Congress of the ASBMR (Denver, 2017).

Summary

Objectives: To analyze in prostate tumor cells the effects caused by the secretome of bone cells on proliferation and on intracellular signaling pathways related to the progression of prostate cancer.

Materials and methods: The effects of secreted factors present in conditioned media of pre-osteoblasts MC3T3-E1 and osteocytes MLO-Y4 on the proliferation of metastatic prostate adenocarcinoma cells PC-3 were characterized using trypan blue staining. The effects of media conditioned by MC3T3-E1 and MLO-Y4 cells on intracellular signaling molecules involved in the tumor progression of prostate adenocarcinoma cells PC-3 were observed by fluorescence techniques in living cells. The accumulation of intracellular calcium was studied using the fluorescent calcium indicator Fluo-4AM and the generation of cyclic AMP, and ERK 1/2 activation by Fluorescent Resonance Energy Transfer (FRET) using the EPAC and ERK-NES biosensors, respectively.

Results: The stimulation of PC-3 cells with conditioned media of pre-osteoblasts MC3T3-E1 and osteocytes MLO-Y4 induced an increase in PC-3 adenocarcinoma cell proliferation. Media conditioned by bone cells also caused a transient increase in intracellular calcium accumulation and generation of cyclic AMP and increased ERK 1/2 activation.

Conclusions: Bone cells secrete proliferation-activating factors and signaling pathways that favor the tumor progression of prostate cancer cells, suggesting that cross-communication between these cell types may favor the development of metastatic niches of prostate cancer in the bone.

Key words: *prostate cancer, secreted bone factors, intracellular signaling, fluorescence in living cells, calcium, cyclic AMP, ERK 1/2.*

Introduction

Bone metastasis is a frequent complication in advanced stages of patients with prostate cancer, one of the cancers with greater mortality and morbidity in developed countries[1]. Avoiding the different stages necessary for the tumor cell to abandon the primary tumor, migrate and establish itself in the bone microenvironment is one of the main strategies to prevent bone metastases[2]. The invasion of primary tumor cells into skeletal niches is associated with the activation of bone cells that release growth factors and cytokines, which in turn promote tumor growth in metastases. As a result, the so-called "vicious cycle" of bone metastases is generated, which varies the physiology of bone and alters bone remodeling[3,4]. In the case of bone metastases caused by prostate cancer, osteolytic and osteoblastic lesions are produced as a result of the activation of osteoclasts and osteoblasts respectively[5]. In bone metastasis processes, it has been observed that tumor cells are able to secrete factors such as tumor necrosis factor alpha (TNF-α), interleukin 11 (IL-11), matrix metalloprotease 1 (MMP1), Jagged1 and protein related to parathormone (PTHrP), which directly or indirectly activate osteoclasts, giving rise to osteoclast metastases[6]. Matrix degradation by osteoclasts releases transforming growth factor β (TGF-β) and insulin-like growth factor (IGF-1) that promote the survival of tumor cells[7]. In contrast, the secretion by tumor cells of other factors such as fibroblast growth factor (FGF) and bone morphogenetic proteins (BMPs) can stimulate osteoblast differentiation resulting in osteoblastic lesions[8].

On the other hand, some studies have described the importance of second messengers and intracellular signaling pathways in the modulation of proliferation, malignancy and metastatic capacity of tumor cells. In this way molecules such as calcium, cyclic adenosine monophosphate (cyclic AMP) or kinases regulated by extracellular signals 1/2 (ERK 1/2), have been proposed as mediators and possible therapeutic targets in tumor progression and bone metastasis[9-11].

Despite the existence of various observations analyzing the factors secreted by tumor cells that affect bone cells, there is little information on the factors secreted by osteoblasts and osteocytes that act on tumorigenic prostate cells. In particular, the effect of factors secreted by bone cells on signaling pathways and second relevant messengers in the mediation of processes of tumor progression and metastasis to bone in tumor cells of prostate is little known.

In this study we have used fluorescence techniques in living cells to analyze whether factors secreted by bone cells can modify signaling pathways and second messengers in prostate adenocarcinoma cells. Our observations show that factors secreted by osteoblasts and osteocytes can induce proliferation of prostate tumor cells associated with accumulation of intracellular cyclic AMP and calcium and activation of the ERK kinase. These results suggest the key role of bone factors in intracellular mechanisms relevant to tumor progression and bone metastasis.

Material and methods

Cell cultures

Human prostatic carcinoma cells derived from bone metastases (PC-3, ATCC: CRL-1435) were cultured in RPMI 1640, supplemented with 10% fetal bovine serum (FBS). The murine pre-osteoblastic cell line MC3T3-E1 (ATCC: CRL-2593) and murine osteocytic MLO-Y4 (generously donated by Lynda Bonewald) were cultured in DMEM with 10% FBS or α-MEM with 2.5% fetal serum from Ram (SCF) and 2.5% SFB, respectively. All cells were cultured in media containing penicillin (100 units/mL) and streptomycin (100 µg/mL) in a humidified incubator at 37°C and 5% atmospheric CO_2. Conditioned media were obtained from PC-3, MLO-Y4 or MC3T3-E1 cells cultured in α-MEM in the absence of serum for 24 h.

Transfections

For transient transfections, PC-3 cells were cultured on glass coverslips of 25 mm diameter for 12 h prior to transfection with FuGENE 6 (Roche Applied Science), which was performed in complete culture medium. After 24 h the cover slips were transferred in an Attofluor chamber (Invitrogen, Carlsbad, CA) with HEPES/bovine serum albumin solution (BSA) (pH=7.4) (HEPES 0.1% (w/v) ASB solution) for real-time fluorescence experiments.

Cell proliferation assay

The number of viable PC-3 cells stimulated with conditioned media of cells MC3T3-E1, MLO-Y4 or of the PC-3 itself was evaluated by the trypan blue exclusion test as previously described[12].

Measurement of intracellular calcium

The accumulation of intracellular calcium was quantified with the calcium sensitive sensor Fluo-4/AM (Invitrogen, Carlsbard, CA) following the manufacturer's protocol as previously described[13]. Briefly, PC-3 cells were cultured on MatTek culture plates with 2 µM Fluo-4/AM in Hanks' balanced salt solution (Invitrogen) at 22°C for 45 min. The cells were washed three times in the Hanks' solution and incubated at 22°C for 30 min. The intracellular calcium quantifications were performed with the inverted fluorescence microscope Nikon A1s. The fluorescence levels were measured at intervals of 1 s to 20 min. At least 30-40 cells were evaluated under each condition. The reagents ionomycin (increases the entrance of calcium ions in the cells) 10 µM and EGTA (calcium chelator) 10 mM were used to obtain the maximum and minimum stimulation in each cell analyzed.

Fluorescent Resonance Energy Transfer (FRET): assessment of intracellular

PC-3 cells were transiently transfected with EPAC cyclical AMP biosensor[14] or with the ERK phosphorylation biosensor, ERK-NES[15]. The generation of cyclic AMP and the activation by phosphorylation of ERK were evaluated by Energy Transfer by Fluorescent Resonance (FRET) as previously des-

cribed[16]. The cells were cultured in Ibidi culture plates of 35 mm diameter and kept in FRET buffer solution (137 mM NaCl, 5 mM KCl, 1 mM CaCl 2, 1 mM MgCl 2, 20 mM HEPES, 0.1% bovine serum albumin, pH 7.4) where they were transiently transfected with constructs consisting of the fusion proteins: fluorescent protein cyan (CFP)-EPAC-yellow fluorescent protein (YFP) or by CFP-ERK-NES-YFP and which is activated by direct binding of cyclic AMP or by phosphorylation, respectively, undergoing conformational changes that result in variations in FRET responses. Quantifications were carried out on a Leica microscope equipped with a 40x objective of immersion oil, sequential records of the CFP and YFP fluorescence channels being made. The intensities of the fluorescence emission were determined at 535/15 nm (YFP) and 480/20 nm (CFP) with a long dichroic passage (DCLP) of 505 nm. The FRET signal was monitored as the emission index of YFP (FYFP) and CFP (FCFP). The results are shown as the normalized mean (nFRET) ± standard error.

Statistical analyses

The data were expressed as mean ± standard error. The differences between the experimental conditions and the controls were made using the U Mann Whitney statistical test, in which values of $p<0.05$ were considered significant.

Results

Soluble factors of MC3T3-E1 and MLOY-4 induce increased proliferation in human prostate adenocarcinoma cells PC-3

Previous studies suggest that the bone environment favors the stimulation of prostate cancer cells promoting the establishment of skeletal metastases[17]. To evaluate the effects of factors secreted by bone cells on prostate carcinoma cells, we first analyzed the actions of conditioned media of osteoblasts MC3T3-E1 and osteocytes MLO-Y4 on the proliferation of PC-3 prostate cancer cells. Both the conditioned means of osteoblasts MC3T3-E1 and those of MLO-Y4 were found to induce an increase in the proliferation of PC-3 cells after 3 days of stimulation compared to control conditioned media (of the PC-3 cells themselves) (Figure 1).

Osteoblastic and osteoblastic bone soluble factors induce the formation of cyclic AMP and intracellular calcium release in human prostate adenocarcinoma cells PC-3

Next, the effects of conditioned media of bone cells in the activation of second messengers and signaling pathways related to tumor progression, metastasis and the activation of osteogenic responses[9-11,18] were studied by means of fluorescence techniques in living cells. The conditioned media of osteoblasts MC3T3-E1 and osteocytes MLO-Y4 caused a rapid and transient increase in intracellular calcium concentration in prostate cancer cells PC-3 compared to stimulation with medium conditioned by the PC-3 cells themselves (Figure 2A-C). Similarly, the generation of cyclic AMP detected by FRET was stimulated by conditioned means of osteoblasts and osteocytes (Figure 3A-C). The levels of cyclic AMC did not vary when stimulating the PC-3 cells with conditioned media of PC-3 (data not shown).

Activation of the ERK 1/2 signaling pathway in human prostate adenocarcinoma cells PC-3 after stimulation of soluble bone factors

Phosphorylation of ERK 1/2 kinase, a protein directly involved in the proliferation of prostate tumor cells[19], was also induced by conditioned media of osteoblasts MC3T3-E1 and osteocytes MLO-Y4 (Figure 4A and B). The conditioned medium of PC-3 cells, on the other hand, did not cause changes in the phosphorylation of ERK 1/2 of PC-3 cells (Figure 4B).

These results as a whole show that the factors secreted by bone cells modulate key signaling molecules in cellular processes such as the proliferation of prostate tumor cells.

Discussion

Our results show that metastatic prostatic adenocarcinoma cells increase their proliferation with factors secreted by both osteoblastic and osteocytic cells. In the case of bone metastases, it has been hypothesized that tumor cells are established in specific areas of bone such as the endosteal niche, the niche of hematopoietic stem cells and the vascular niche[20]. These niches are complex microenvironments in which factors that promote the physiological functions of the cells that compose them are secreted. It has been shown that increasing the number of these niches experimentally also increases the number of disseminated tumor cells of primary tumors[21]. These observations suggest that the same factors that maintain the correct functioning of the cells of the bone niches are able in turn to promote the establishment and growth of tumor cells in bone metastases. From this point of view, osteoblasts and osteocytes located near the surface would form part of the endosteal niche and may generate factors that promote the growth of prostate tumor cells in this niche.

There are several mechanisms that regulate the mitotic cycle of metastatic cells in bone, including regulatory processes of the immune system, angiogenesis, extracellular matrix, various factors and hormones, and intracellular processes[22]. Among these mechanisms, it was observed that the balance in the activation between 2 protein kinases activated by mitogens (MAP kinases), p38 and ERK 1/2 affects in a key way the mitosis of metastatic tumor cells[23]. When ERK 1/2 is activated in comparison with p38, cell proliferation is favored, and on the contrary the activation of p38 against ERK 1/2 induces a cellular quiescent state[23]. We have observed that pre-osteoblasts and osteocytes can send soluble factors that activate the ERK 1/2 kinase in PC-3 cells thus promoting the proliferation of tumor cells.

Figure 1. Factors secreted by osteoblasts MC3T3-E1 and osteocytes MLO-Y4 increase the proliferation of PC-3 prostate carcinoma cells. The PC-3 cells were incubated for 1-3 days with conditioned media (MC) obtained from MC3T3-E1 or MLO-Y4 and the number of cells was evaluated by trypan blue assay. The data shown are means ± standard error of 3 independent experiments *p<0.05; **p <0.01 vs. Conditioned medium (MC) Control

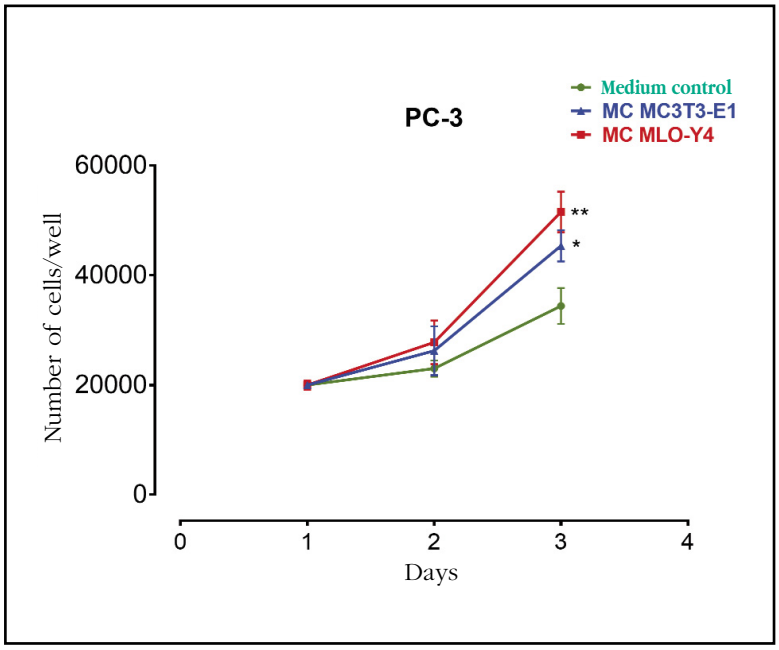

In addition, we have observed that factors secreted into the environment conditioned by pre-osteoblasts and osteocytes also caused a transient increase in intracellular calcium concentration and in the generation of cyclic AMP. Both second messengers can regulate processes of proliferation and tumor metastasis and have been proposed as possible therapeutic targets in several cancers[9,10,24]. Cyclic AMP can have positive or negative effects on the growth and survival of tumor cells depending on the cell type[10]. In tumors of epithelial origin such as prostate cancer, cyclic AMP seems to play a role in promoting oncogenesis by activating protein kinase A and other proteins activated below (for example, EPAC and CREB)[25,26].

On the other hand, it has been shown that the increase in intracellular calcium concentration of extracellular origin is a factor that induces the proliferation of prostate cell lines of bone metastases (PC-3 and C4-2B), but does not affect the proliferation of non-metastatic prostatic cell lines such as LNCaP[9] cells. The increase in the concentration of calcium of extracellular origin causes PC-3 an increase in the expression of cyclin D1 (a regulatory protein of the cell cycle necessary in the proliferation), in the activation of Akt (protein required for the proliferation and tumor progression)[27,28], and increases the binding capacity of tumor cells to substrate[9]. In addition, alterations in the gene expression of various calcium ion channels, such as TRP and Orai, have been associated with increases in calcium entry in prostate tumor cells that facilitate proliferation and resistance to apoptosis of those cells[29,30].

Overall, these studies show the relevant function of the activation of the kinase ERK 1/2, calcium and cyclic AMP in the progression of prostate cancer. Although the modulation of these signaling pathways by factors secreted by bone cells has not been previously described, some studies have demonstrated the ability of resident bone cells to modulate the activity of tumor cells in metastatic niches. It has been observed that osteocytes mechanically stimulated by increased pressure caused by metastatic tumors induce growth and invasiveness of prostate tumors through the secretion of chemokine (C-C) ligand 5 (CCL5)[31]. Interestingly, the stimulation of cells of different types of cancer by CCL5 is able to increase the invasive and migratory capacity of tumor cells through mechanisms dependent on the intracellular mobilization of calcium[32] or activation of the ERK kinase[33,34]. These observations suggest that CCL5 or other similar factors of the secret of bone cells could be responsible for the changes in signaling pathways of tumor cells that we have observed in the present study. On the other hand, previous publications have also demonstrated the key role of bone cells in promoting the activation of tumor cells and favoring metastatic processes based on direct bone cell-tumor cell contact through the activation of the Notch-Jagged signaling pathway[35]. Factors secreted by bone cells may mediate initial metastatic tumor recruitment and growth processes, where there is no direct contact between the tumor and the bone cells, while signaling pathways such as Notch-Jagged may regulate the interactions of the tumor. tumor in more advanced metastatic phases (in which the tumor does come into direct contact with bone cells).

Based on these investigations and our results, we propose that osteoblastic and osteocytic cells regulate the proliferation and activation of molecular mediators of tumor progression in metastatic prostate cancer cells by the secretion of soluble factors. We also suggest that the modulation of calcium intracellular mediators, cyclic AMP and ERK 1/2 by factors secreted by bone cells could be key in the establishment of bone metastases by prostate tumor cells.

Conflict of interest: The authors declare no conflict of interest.

Funding support: This work was carried out thanks to projects of the Health Institute Carlos III (PI12 / 02390) and CEU San Pablo-Santander (USP-BS-PPC 11/2012, USPB-BS-APP-2/2016 and MERMERG-2).

Bibliography

1. Wong MC, Goggins WB, Wang HH, Fung FD, Leung C, Wong SY, et al. Global incidence and mortality for prostate cancer: analysis of temporal patterns and trends in 36 countries. Eur Urol. 2016;70(5):862-74.
2. Kan C, Vargas G, Pape FL, Clézardin P. Cancer cell colonisation in the bone microenvironment. Int J Mol Sci. 2016;17(10):1-16.
3. Roodman GD. Mechanisms of bone metastasis. N Engl J Med. 2004; 350(16):1655-64.
4. Guise TA, Mohammad KS, Clines G, Stebbins EG, Wong DH, Higgins LS, et al. Basic mechanisms responsible for osteolytic and osteoblastic bone metastases. Clin Cancer Res. 2006;12(20 Pt 2):6213-7.
5. Keller ET, Brown J. Prostate cancer bone metastases promote both osteolytic and osteoblastic activity. J Cell Biochem. 2004;91(4):718-29.
6. Ell B, Kang Y. SnapShot: bone metastasis. Cell. 2012;151(3):690-690.e1.
7. Quail DF, Joyce JA. Microenvironmental regulation of tumor progression and metastasis. Nat Rev Cancer. 2013;19(11):1423-37.
8. Suva LJ, Washam C, Nicholas RW, Griffin RJ. Bone metastasis: mechanisms and therapeutic opportunities. Nat Rev Endocrinol. 2011; 7(4):208-18.
9. Liao J, Schneider A, Datta NS, McCauley LK. Extracellular calcium as a candidate mediator of prostate cancer skeletal metastasis. Cancer Res. 2006;66(18):9065-73.
10. Fajardo AM, Piazza GA, Tinsley HN. The role of cyclic nucleotide signaling pathways in cancer: targets for prevention and treatment. Cancers (Basel). 2014;6(1):436-58.
11. McCubrey JA, Steelman LS, Chappell WH, Abrams SL, Wong EW, Chang F, et al. Roles of the Raf/MEK/ERK pathway in cell growth, malignant transformation and drug resistance. Biochim Biophys Acta. 2007; 1773(8):1263-84.
12. Strober W. Trypan blue exclusion test of cell viability. Curr Protoc Immunol. 2001; Appendix 3: Appendix 3B.
13. Wang B, Ardura JA, Romero G, Yang Y, Hall RA, Friedman PA. Na/H exchanger regulatory factors control parathyroid hormone receptor signaling by facilitating differential activation of G(alpha) protein subunits. J Biol Chem. 2010;285(35):26976-86.
14. Nikolaev VO, Bunemann M, Hein L, Hannawacker A, Lohse MJ. Novel single chain cAMP sensors for receptor-induced signal propagation. J Biol Chem. 2004;279(36): 37215-8.
15. Komatsu N, Aoki K, Yamada M, Yukinaga H, Fujita Y, Kamioka Y, et al. Development of an optimized back bone of FRET biosensors for kinases and GTPases, Mol Biol Cell. 2011;22(23):4647-56.

Figure 2. Factors secreted by MC3T3-E1 and MLO-Y4 increase the intracellular calcium signaling of PC-3. We analyzed the effects of conditioned secreted factors obtained during 24 hours of MC3T3-E1 (A), MLO-Y4 (B) or PC-3 (C) in the intracellular calcium release of PC-3. The evaluation of intracellular calcium levels was performed by confocal fluorescence in living cells with the Fluo-4AM indicator as described in the text. The arrows indicate the moment of stimulation with conditioned means. The data shown are means ± standard error of 3 independent experiments

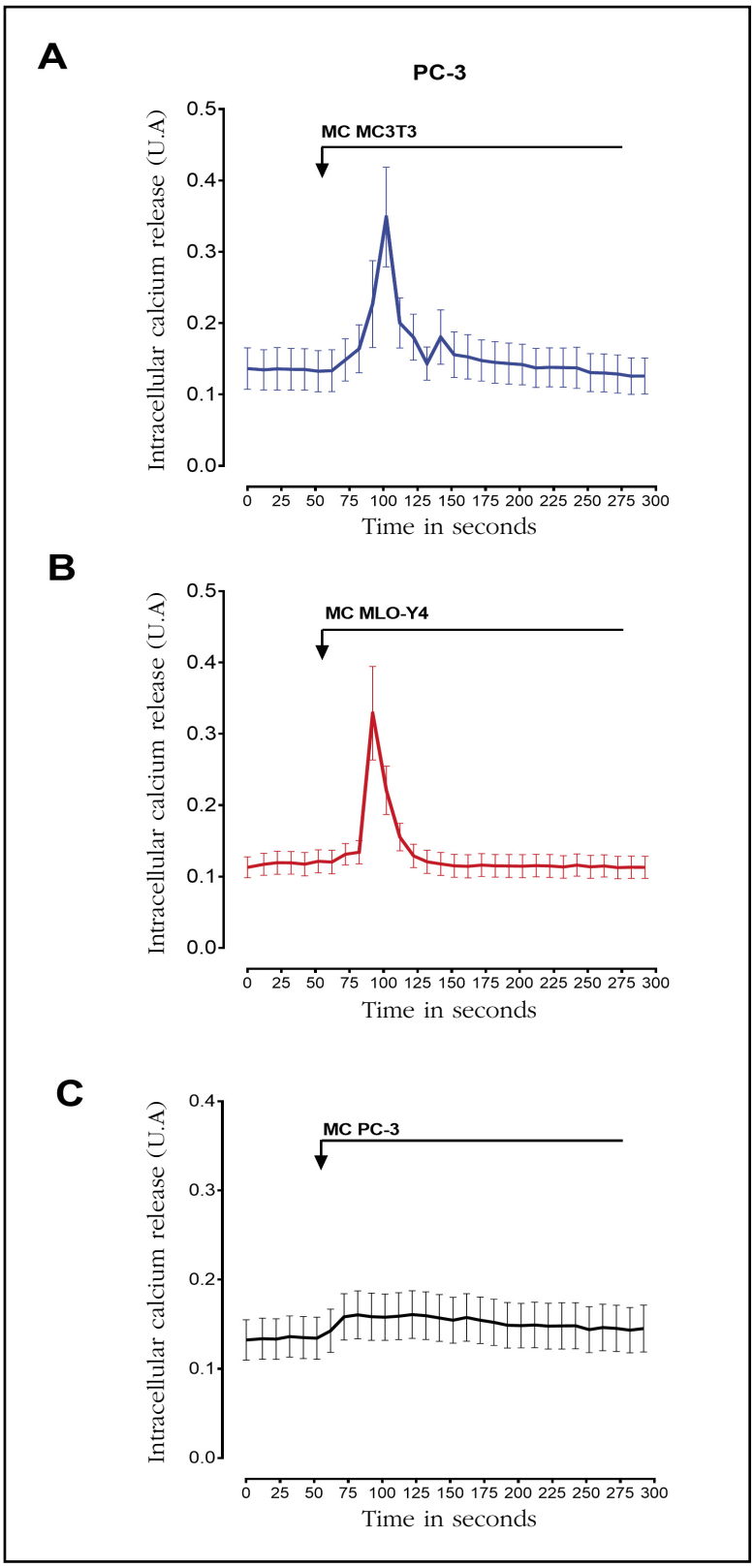

Figure 3. Factors secreted by MC3T3-E1 and MLO-Y4 increase the cyclic AMP signaling of PC-3. (A) We analyzed the effects of conditioned secreted factors obtained during 24 hours of MC3T3-E1 and MLO-Y4 in the activation of PC-3 cyclic AMP. The evaluation of cyclic AMP was performed by confocal fluorescence in living cells with the CFPE-PACYFP sensor as described in the text. The arrows indicate the moment of stimulation with conditioned means. Forskolin was used to obtain maximum stimulation of cyclic AMP. The data shown are means ± standard error of 3 independent experiments. (B and C) Representative images of the fluorescence changes of the CFP and YFP fluorescent proteins of the EPAC cyclic AMP sensor in PC-3 cells after stimulation with conditioned medium of MC3T3-E1 or MLO-Y4 cells

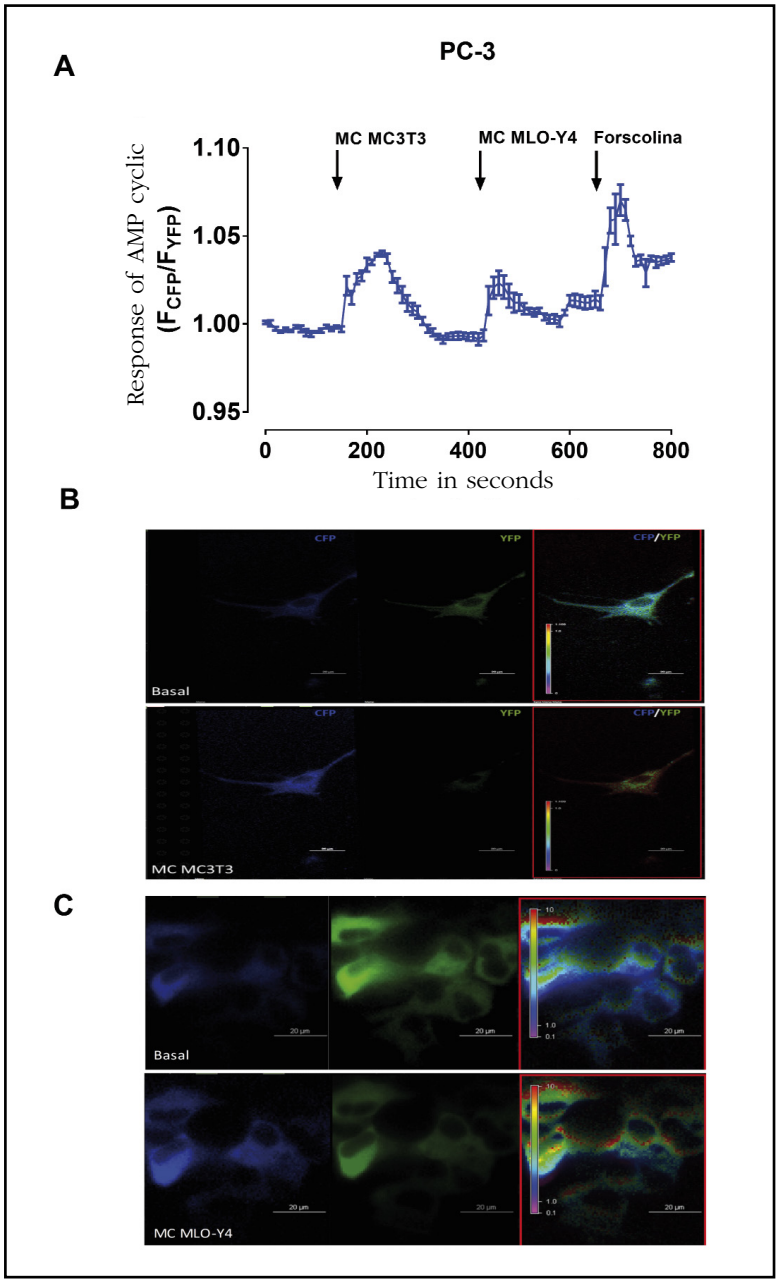

16. Alonso V, Ardura JA, Wang B, Sneddon WB, Friedman PA. A naturally occurring isoform inhibits parathyroid hormone receptor trafficking and signaling. J Bone Miner Res. 2011;26(1):143-55.
17. Karlsson T, Sundar R, Widmark A, Landström M, Persson E. Osteoblast-derived factors promote metastatic potential in human prostate cancer cells, in part via non-canonical transforming growth factor β (TGFβ) signaling. Prostate. 2018;78(6):446-56.
18. Thompson WR, Rubin CT, Rubin J. Mechanical regulation of signaling pathways in bone. Gene. 2012;503(2): 179-93.
19. Rodríguez-Berriguete G, Fraile B, Martínez-Onsurbe P, Olmedilla G, Paniagua R, Royuela M. MAP kinases and prostate cancer. J Signal Transduct. 2012;2012:169170.
20. Ottewell PD. The role of osteoblasts in bone metastasis. J Bone Oncol. 2016;5(3):124-7.
21. Shiozawa Y, Pedersen EA, Havens AM, Jung Y, Mishra A, Joseph J, et al. Human prostate cancer metastases target the hematopoietic stem cell niche to establish footholds in mouse bone marrow. J Clin Invest. 2011; 121(4):1298-312.
22. Shaked Y, McAllister S, Fainaru O, Almog N. Tumor dormancy and the angiogenic switch: possible implications of bone marrow-derived cells. Curr Pharm Des. 2014;20(30):4920-33.
23. Aguirre-Ghiso JA, Ossowski L, Rosenbaum SK. Green fluorescent protein tagging of extracellular signal-regulated kinase and p38 pathways reveals novel dynamics of pathway activation during primary and metastatic growth. Cancer Res. 2004;64(20):7336-45.
24. Cui C, Merritt R, Fu L, Pan Z. Targeting calcium signaling in cancer therapy. Acta Pharm Sin B. 2017;7(1):3-17.
25. Caretta A., Mucignat-Caretta C. Protein kinase A in cancer. Cancers. 2011;3(1):913-26.
26. Borland G, Smith BO, Yarwood SJ. EPAC proteins transduce diverse cellular actions of cAMP. Br J Pharmacol. 2009;158(1):70-86.
27. Graff JR, Konicek BW, McNulty AM, Wang Z, Houck K, Allen S, et al. Increased AKT activity contributes to prostate cancer progression by dramatically accelerating prostate tumor growth and diminishing p27Kip1 expression. J Biol Chem. 2000;275(32):24500-5.
28. Chen H, Zhou L, Wu X, Li R, Wen J, Sha J, et al. The PI3K/AKT pathway in the pathogenesis of prostate cancer. Front Biosci. 2016;21:1084-91.
29. Monet M, Lehen'kyi V, Gackiere F, Firlej V, Vandenberghe M, Roudbaraki M, et al. Role of cationic channel TRPV2 in promoting prostate cancer migration and progression to androgen resistance. Cancer Res. 2010;70(3):1225-35.
30. Dubois C, Vanden Abeele F, Lehen'kyi V, Gkika D, Guarmit B, Lepage G, et al. Remodeling of channel-forming ORAI proteins determines an oncogenic switch in prostate cancer. Cancer Cel. 2014;26(1):19-32.
31. Sottnik JL, Dai J, Zhang H, Campbell B, Keller ET. Tumor-induced pressure in the bone microenvironment causes osteocytes to promote the growth of prostate cancer bone metastases. Cancer Res. 2015;75(11):2151-8.
32. Singh SK, Mishra MK, Eltoum IA, Bae S, Lillard JW Jr, Singh R. CCR5/CCL5 axis interaction promotes migratory and invasiveness of pancreatic cancer cells. Sci Rep. 2018;8(1):1323.
33. Huang CY, Fong YC, Lee CY, Chen MY, Tsai HC, Hsu HC,

et al. CCL5 increases lung cancer migration via PI3K, Akt and NF-kappaB pathways. Biochem Pharmacol. 2009;77(5):794-803.
34. Kato T, Fujita Y, Nakane K, Mizutani K, Terazawa R, Ehara H, et al. CCR1/CCL5 interaction promotes invasion of taxane-resistant PC3 prostate cancer cells by increasing secretion of MMPs 2/9 and by activating ERK and Rac signaling. Cytokine. 2013;64(1):251-7.
35. Sethi N, Dai X, Winter CG, Kang Y. Tumor-derived JAGGED1 promotes osteolytic bone metastasis of breast cancer by engaging notch signaling in bone cells. Cancer Cell. 2011;19(2):192-205.

Figure 4. Factors secreted by MC3T3-E1 and MLO-Y4 increase the phosphorylation of the ERK 1/2 kinase of PC-3. We analyzed the effects of conditioned secreted factors obtained during 24 hours of MC3T3-E1 (A) or MLOY-4 (B) on phosphorylation of the ERK 1/2 kinase in PC-3. As a control, PC-3 cells were stimulated with conditioned medium of PC-3 cells. The evaluation of cyclic AMP was performed by confocal fluorescence in living cells with the CFPERK-NESYFP sensor as described in the text. The arrows indicate the moment of stimulation with conditioned means. The data shown are means ± standard error of 3 independent experiments

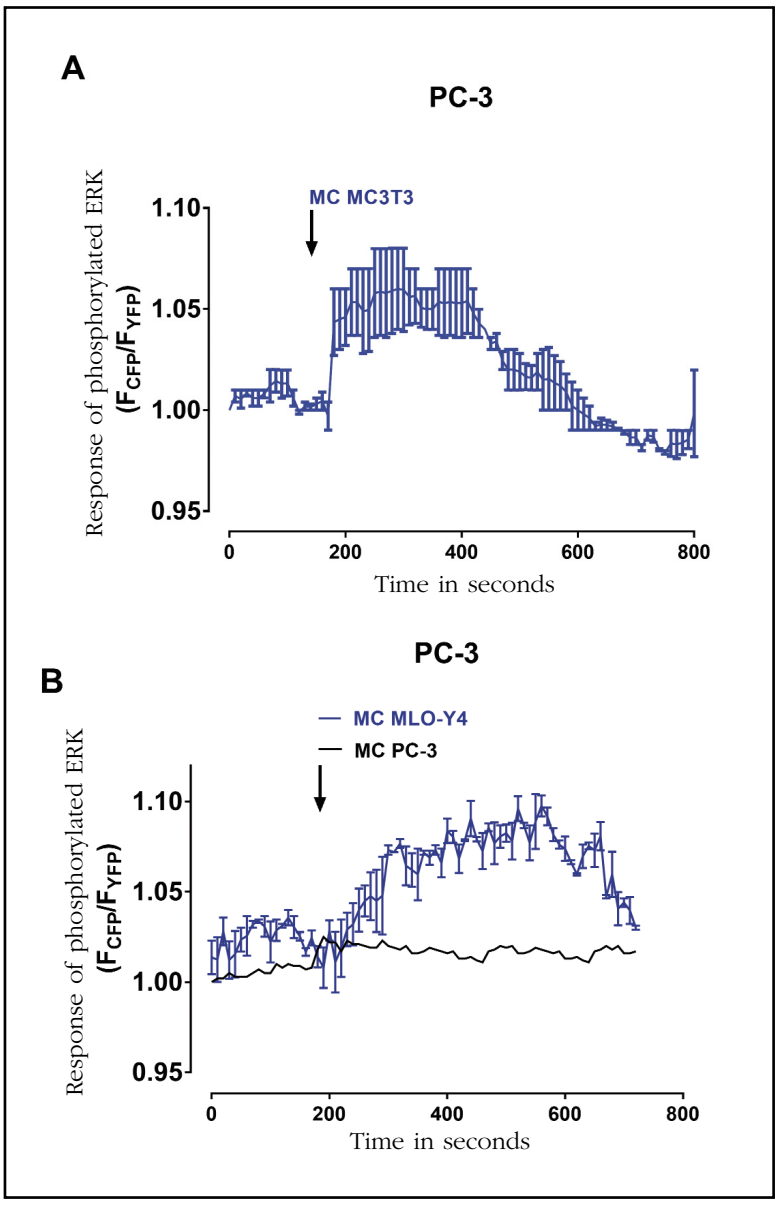

Rev Osteoporos Metab Miner. 2019;11(2):64-71

Osteogenic cells affected by soluble tumor factors contribute to bone pre-metastatic niche formation

DOI: http://dx.doi.org/10.4321/S1889-836X2019000300005

Álvarez Carrión L[1], Gutiérrez Rojas I[1], Ardura JA[1,2], Alonso V[1,2]
1 Bone Pathophysiology Laboratory - Institute of Applied Molecular Medicine (IMMA) - University San Pablo-CEU - Alcorcón - Madrid (Spain)
2 Department of Basic Medical Sciences - Faculty of Medicine - University San Pablo-CEU - Alcorcón - Madrid (Spain)

Date of receipt: 12/07/2019 - Date of acceptance: 07/10/2019

Study awarded a FEIOMM Scholarship for Basic Research 2017

Summary

Objective: To analyze the effect of the secrets of solid organotropic tumors towards bone in osteogenic, osteoblastic and osteocytic lineage cells, in the expression of genes related to bone metabolism.
Material and method: We characterize the changes in gene expression by quantitative real-time PCR of the OPG/RANKL axis, as well as other genes related to osteoblastic differentiation such as Runx2 and osteocalcin, induced by the conditioned means of prostate tumor cells, breast and melanoma in pre MC3T3-E1 osteoblasts and murine MLO-Y4 osteocytes or in human osteoblasts, as appropriate by species.
Results: Stimulation of osteocitic cells with conditioned means of melanoma or prostate adenocarcinoma cells induced an increase in OPG and RANKL gene expression, with the OPG/RANKL ratio being increased. Only the secretome of prostate adenocarcinoma cells altered the expression of Runx2 in osteocytes. Conditioned media of breast cancer cells only modified the expression of RANKL in osteoblast cells, with a decrease in OPG/RANKL ratio.
Conclusion: Soluble tumor factors have osteocitic cells as their cellular target, favoring the induction of a pre-metastatic bone niche by modifying the OPG/RANKL ratio in the bone environment, and, thus, the progression of bone organotropic tumors such as melanoma and prostatic adenocarcinomas.

Key words: bone organotropic tumors, soluble tumor factors, pre-metastatic bone niche, bone metastases, osteocytes and osteoblasts.

Introduction

The appearance of metastatic disease seriously threatens the survival rate of patients who develop a tumor. Certain types of tumors have been found to present a high tendency to colonize specific organs. From the hypothesis formulated by Paget ("seed-and-soil")[1], few studies have deciphered the regulatory mechanisms of metastatic organotropism. Initial studies focused on the function of the intrinsic properties of the tumor cell, such as gene expression and colonization regulation pathways, in the direction of organotropism[2-4].

Bone is an organ frequently infiltrated by the metastatic spread of solid tumors[5,6]. The appearance of metastatic disease is a serious threat in the survival rate of patients who develop a tumor. From 65-80% of subjects with prostate cancer or metastatic breast present skeletal complications[5]. The study of bone metastases has mainly focused on the interaction of the tumor cell with the bone, once the metastasis has been established, ignoring the subclinical stages of the process that occurs previously. The establishment of tumor cells in the bone microenvironment alters the balance of the bone remodeling process between bone formation, induced by osteoblasts, and osteoclast-mediated resorption. Consequently, the survival and proliferation pathways of tumor cells are favored, inducing the formation of "a vicious cycle of bone metastases"[7].

Though not exclusive, tumors cause two different types of skeletal lesions. The most common form, represented by breast cancer is the osteolytic lesion associated with an alteration of bone remodeling with an increase in osteoclastic activity and subsequent osteolysis[8-11].

A second type of so-called osteoblastic lesions is characterized by high bone remodeling with an increase in osteoblast activity with an increase in osteoid and mineralization rate. These areas of de novo-formed bone in areas of metastasis are called osteoesclerotic lesions, which are usually weak and unstable, with a tendency to break. This type of lesions is characteristic of prostate cancer. However, the existence of a osteoclast mediated component is currently recognized as a previous step for the establishment of osteoblastic lesions[12,13].

Correspondence: Verónica Alonso Rodríguez (veronica.alonsorodriguez@ceu.es)

Rev Osteoporos Metab Miner. 2019;11(2):64-71

Recent studies have described pro-metastatic changes in organs where metastases will later appear. Such changes induce the formation of pre-metastatic niches that favor the implantation of tumor cells in target organs[14,15].

The cellular complexity of the bone (osteocytes, osteoblasts, osteoclasts, bone covering cells, endothelial cells and hematopoietic tissue), as well as the functions they carry out in regulating the metabolism and bone remodeling, raises the possibility that the formation of the pre niche-metastatic bone is the result of a complex network of combined and sequential modifications and alterations of all these cells[16].

Despite the existence of some observations analyzing the effect of the factors secreted by tumor cells that affect the viability of bone cells[17], the existence of common mechanisms or changes in bone cells induced by solid tumors with high organotropism is unknown. He made the bone as a metastatic target organ.

In this study, we have analyzed the changes in the transcriptional profile of cytokines related to bone metabolism in osteoblastic and osteocitic cells, induced by soluble tumor factors of breast, prostate and melanoma tumor cells. Our observations show that these factors significantly modify the transcriptional profile of osteocytes. These results suggest a relevant role of osteocytes as the initial inducing cell in the formation of the pre-metastatic bone niche.

Material and method

Cell cultures

The MC3T3-E1 murine pre-osteoblastic cell lines (ATCC: CRL-2593) and MLO-Y4 murine osteocitic cells (donated by Lynda Bonewald) were cultured in DMEM with 10% bovine fetal serum (SFB) or α-MEM with 2.5% fetal sheep serum (SCF) and 2.5% SFB, respectively. All cells were cultured in media containing penicillin (100 units/mL) and streptomycin (100 µg/mL) in the humidified incubator at 37°C and 5% atmospheric CO_2.

The hFOB 1.19 human osteoblastic continuous line (ATCC® CRL-11372TM) was grown in a 1:1 mixture of Ham's F12 and DMEM with 2.5 mM L-glutamine, 0.3 mg/mL G418 and 10% SFB in the humidified incubator at 34°C and 5% atmospheric CO_2.

We use the TRAMPC-1 mouse prostate adenocarcinoma (ATCC® CRL-2730TM), murine melanoma B16 (ATCC® CRL-6323) and human breast cancer (ATCC® MDA-MB-231 HTB-26) lines to obtain of tumor secretoma. These cells were cultured in DMEM culture medium supplemented with penicillin (100 U/ml), streptomycin (100 µg/ml), 1% glutamine and 10% SFB. When the culture reached confluence, they were washed with a phosphate solution (PBS). Next, tumor secrets and bone conditioned media used for stimulation of previously activated tumor cells with soluble bone factors were obtained..

To obtain the conditioned media of both tumor cells and bone cells, the cell lines were grown to confluence with α-MEM culture medium supplemented with penicillin and 0% streptomycin of SFB, after 24 hours of incubation, the media were collected and cell debris and dead cells were removed by centrifugation (5,000 rpm, 10 minutes).

To avoid any type of cross-biological reactivity of cytokines of one species in cells of another species[18] and reproduce as faithfully as possible the communication of tumor cells with bone cells, our *in vitro* experimental models were designed according mainly to the criteria of species. In this way, the effects of the tumor secretoma of the human breast cancer line on the human osteoblastic line were evaluated. There is currently no well characterized osteocitic continuous line. The effects of the secrets of prostate and mouse melanoma tumor lines were studied on bone murine lines (osteoblastic, MC3T3, and osteocitic, MLOY4). Figure 1 shows the protocol used to obtain conditioned media and its stimulation in the different 25% cell lines.

Cell viability assay

The number of viable bone cells MC3T3, MLOY4 and hFOBs stimulated or not with 25% tumor secretoma was evaluated by the trypan blue exclusion test as previously described[19].

Gene expression studies by real-time PCR

Total RNA was extracted from cell cultures by the Trizol method. CDNA synthesis was performed using the reverse transcriptase of the avian myeloblastosis virus (Promega) and random hexamer primers. Real-time PCR was carried out in the ABI PRISM 7500 system (Applied Biosystems) using Sybr premix ex Taq (Takara, Otsu, Japan) and specific primers of each gene (Table 1). All results were expressed in number of mRNA copies calculated for each sample using the cycle threshold value (Ct). The relative gene expression is represented as: 2-ΔΔCt, where ΔΔCt = ΔCtgen target - ΔCt18S/GAPDH. The change in the number of times with respect to treatment is defined as the expression compared to the control, calculated as 2-ΔΔCt, where ΔΔCt = ΔCreating - ΔCcontrol. The specificity of the amplicon was confirmed as the presence of a single amplification after melting curve analysis. The results shown correspond to the average of at least 3 independent experiments in triplicate.

Statistical analysis

Data were expressed as mean ± standard error. The differences between experimental conditions and controls were analyzed using the Mann Whitney U test where the values of $p<0.05$ were considered significant.

Results

Communication by soluble factors between tumorigenic melanocytes and bone cells regulates the expression of bone remodeling genes in osteocytes

In order to study the communication between tumor cells and bone cells in the formation of pre-metastatic bone niches, mouse or human bone cells were stimulated with the secrets of different tumor cells with organotropism to bone tissue, which had previously been stimulated or not with osteomas or osteoblast secrets (Figure 1).

First, we corroborate that the conditioned tumor media of the TRAMPC-1 or B16, that is to say tumor secretoma, does not affect the viability of the osteoblast cells, MC3T3, and osteocitic, MLOY4 after 24 h of stimulation (Figure 2). However, stimulation of MLO-Y4 osteocytes with secrets obtained from conditioned media of B16 melanoma cells induced overexpression of the OPG gene with a net increase in the OPG/RANK-L ratio, without significantly affecting the gene expression of RANK-L, nor to the transcription factor Runx2 (Figure 3A-D). In contrast, the secrets of B16 melanoma cells, which had previously

Figure 1. Graphical representation of the work protocol used to obtain pre-treated or not conditioned means (MC). Untreated MLO-Y4, MC3T3-E1, human osteoblasts, B16, TRAMP-C1 or MDA-231 MCs were obtained after 24 h of culture in 0% SFB α-MEM and were used to stimulate the different cell lines The pre-treated MCs were obtained after 24 h cultivation of the B16 or MDA-231 with MC of MLO-Y4, MC3T3-E1 or human osteoblasts followed by a wash with PBS and 24 h of culture with 0% SFB α-MEM. Finally, a cell lysate was obtained which was analyzed by PCR

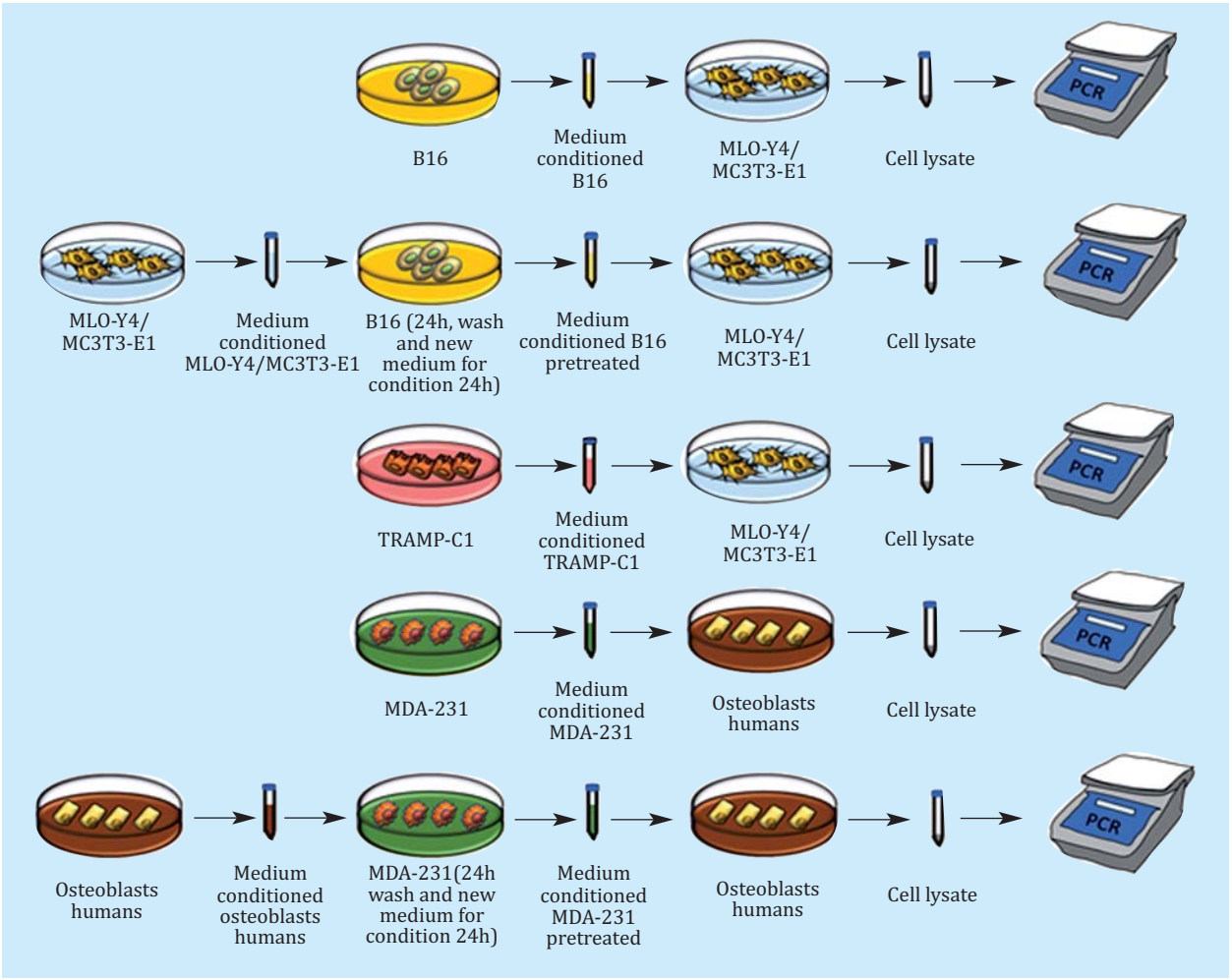

been exposed to conditioned media of MLO-Y4 cells, caused an increase in the expression of RANK-L and a decrease in the OPG/RANK-L ratio. No changes were observed in the expression of OPG or Runx2 with respect to conditioned media without pre-stimulation (Figure 3A-D). These data suggest that melanoma tumor cells, which have been exposed to osteocyte secretoma, secrete soluble factors that cause a bone remodeling gene augmentation response, particularly increasing the expression of the osteoclastogenic factor RANK-L in osteocytes.

Interestingly, these effects did not reproduce in MC3T3-E1 osteoblastic cells, in which the conditioned media of B16 cells did not cause gene overstimulations (Figure 3E-H).

Communication by soluble factors between tumor cells of the breast and bone cells regulates the expression of remodeling genes in osteblasts

We then analyze the effects of cells of another type of tumor that metastasize to bone, such as breast cancer[5], on the gene expression of bone cells. In this case, we examine the effects of the secretome of the human tumor line of breast cancer MDA-MB-231 on human osteoblasts (Figure 1). The conditioned media of MDA-MB-231 cells was found to cause an increase in the expression of RANK-L and a decrease in the OPG/RANK-L ratio, without affecting the expression of OPG or Runx2 in human osteoblasts (Figure 3A -D). The effects on gene expression of osteoblasts were similar using the secretomes of MDA-MB-231, both pre-treated and not pre-treated with conditioned media of human osteoblasts (Figure 4A-C).

Communication through soluble factors between tumorous prostate cells and bone cells regulates the expression of remodeling and osteogenic genes in osteocytes

We then attempted to check if prostate tumor cells, potentially capable of metastasizing to bone[20,21], also established communication with bone cells through soluble factors (Figure 1). In this case, we observe that the secrets of TRAMP-C1 mouse prostate adenocarcinoma cells induced overexpression of the OPG and RANK-L genes, causing an increase in the OPG/RANK-L ratio, in addition to overexpressing the osteogenic transcription factor Runx2 in osteocytes MLO-Y4 (Figure 5A-D). Given

Rev Osteoporos Metab Miner. 2019;11(2):64-71

Table 1. Primers used in real-time PCR analysis

Gene	Sense (5´-3´)	Antisense (5´-3´)
RANK-L	TGTACTTTCGAGCGCAGATG	AGGCTTGTTTCATCCTCCTG
OPG	CAGAGCGAAACACAGTTTG	CACACAGGGTGACATCTATTC
Osteocalcin	GCAATAAGGTAGTGAACAGACTCC	CCATAGATGCGTTTGTAGGCGG
Runx2	CCTGAACTCTGCACCAAGTCCT	TCATCTGGCTCAGATAGGAGGG

Figure 2. Soluble factors secreted by mouse tumorigenic melanocytes (B16) or mouse prostate tumor cells (TRAMPC-1) do not affect the viability of pre-osteoblastic murine bone cells (MC3T3-E1) or osteocitic (MLO-Y4) data. Represented as the mean ± SEM of 2 experiments in triplicate

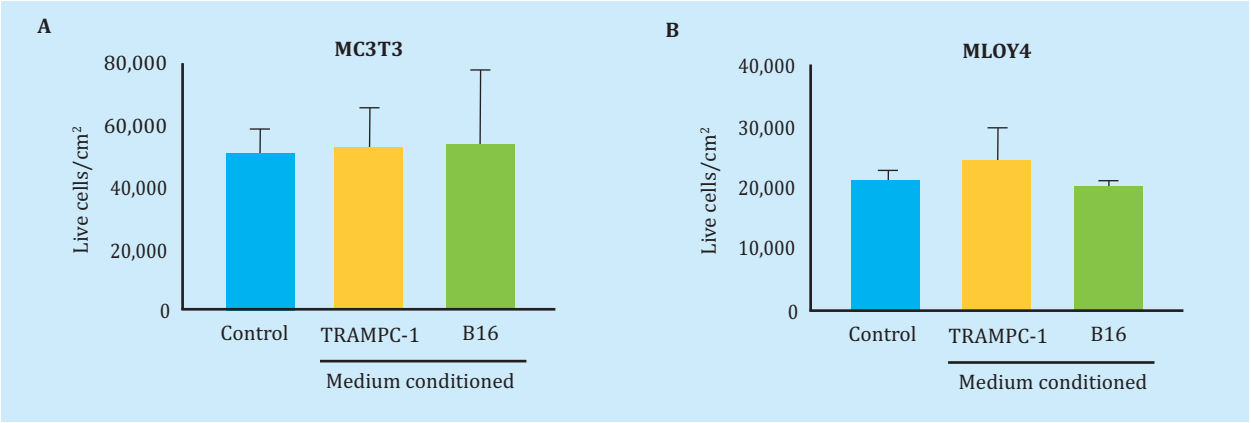

the gene overexpression of Runx2 in these cells, we wanted to check if the osteocalcin protein, a protein associated with bone formation and regulated by Runx2[22], also underwent changes in these conditions. Similar to Runx2, the expression of osteocalcin increased after stimulation with the secretion of TRAMP-C1 cells in MLO-Y4 osteocytes (Figure 5E).

Similar to the data observed with the secretomas of B16 melanoma cells, the conditioned media of TRAMP-C1 cells did not affect the gene expression of the markers previously mentioned in MC3T3-E1 osteoblasts (Figure 5F-J).

Discussion

The formation of a microenvironment that favors the implantation of circulating tumor cells was described by Kapplan. Their results demonstrated the formation of a pre-metastatic niche, in which a series of molecular and cellular changes were observed in the lung prior to the establishment of metastatic melanoma[15,23]. Other researchers subsequently described a series of sequential events that could involve the formation of a pre-metastatic niche in the liver, suggesting the involvement of exosomes derived from malignant pancreatic lesions as triggers of the process[14]. In this sense, little has been described about the formation of the pre-metastatic bone niche and the responses of the different bone subpopulations to the stimulation by secretomes of different tumors with high metastatic frequency to bone are unknown. In this article, we show for the first time how the secretome of solid tumors, with high organotropic potential in the formation of bone metastases, modifies the gene expression of genes related to bone metabolism in osteogenic lineage cells, and can be the triggering process in the induction of a favorable microenvironment for the settlement of tumor cells.

It has recently been suggested that primary tumor cells produce soluble tumor factors that trigger immature pre-metastatic niche formation[24]. Our results confirm that the secretomes of primary tumor cells (such as melanoma and prostate), or breast tumor cells derived from non-bone metastatic processes, mainly modify the balance between OPG and RANKL expression levels. This imbalance would decouple the relationship between osteoblastic bone formation and osteoclastic bone resorption, generating the release of growth factors and cytokines and thus initiating a "previous vicious cycle" of feedback that encourages the formation of future metastatic areas in bone[10]. In this sense, our results suggest the osteocyte as the cell most susceptible to soluble tumor factors. In our *in vitro* experimental model, in which we treat both osteocitic cells and mouse osteoblastic cells with conditioned media of murine cells of primary melanoma and prostate tumor, we observe significant changes in the gene expression of the osteocitic line without observing significant changes in the osteoblast line.

Given these observations, we conclude that, although both types of tumors will generate different types of metastases in the future, those derived from melanoma with a more osteolytic character[25] and those of preferably osteoblastic prostatic adenocarcinoma, the initial stages, in which alterations occur in bone cell physiology, are common. These observations suggest that the modifications that originate in the pre-metastatic niche do not predispose the specific type of skeletal lesions that will develop in metastatic disease.

Figure 3. Soluble factors secreted by tumorgenic melanocytes (B16) modify gene expression of bone remodeling in osteocytes (MLO-Y4) but not in pre-osteoblasts (MC3T3-E1). The expression of OPG (A, E), RANK-L (B, F), OPG/RANK-L ratio (C, G) and Runx2 (D, H) was evaluated by real-time PCR after stimulating 24 h MLO-Y4 and MC3T3-E1 with conditioned medium of B16 pre-treated or not. Data are represented as the mean ± SEM of three independent experiments in triplicate. *p<0.05 vs control, **p<0.01 vs control

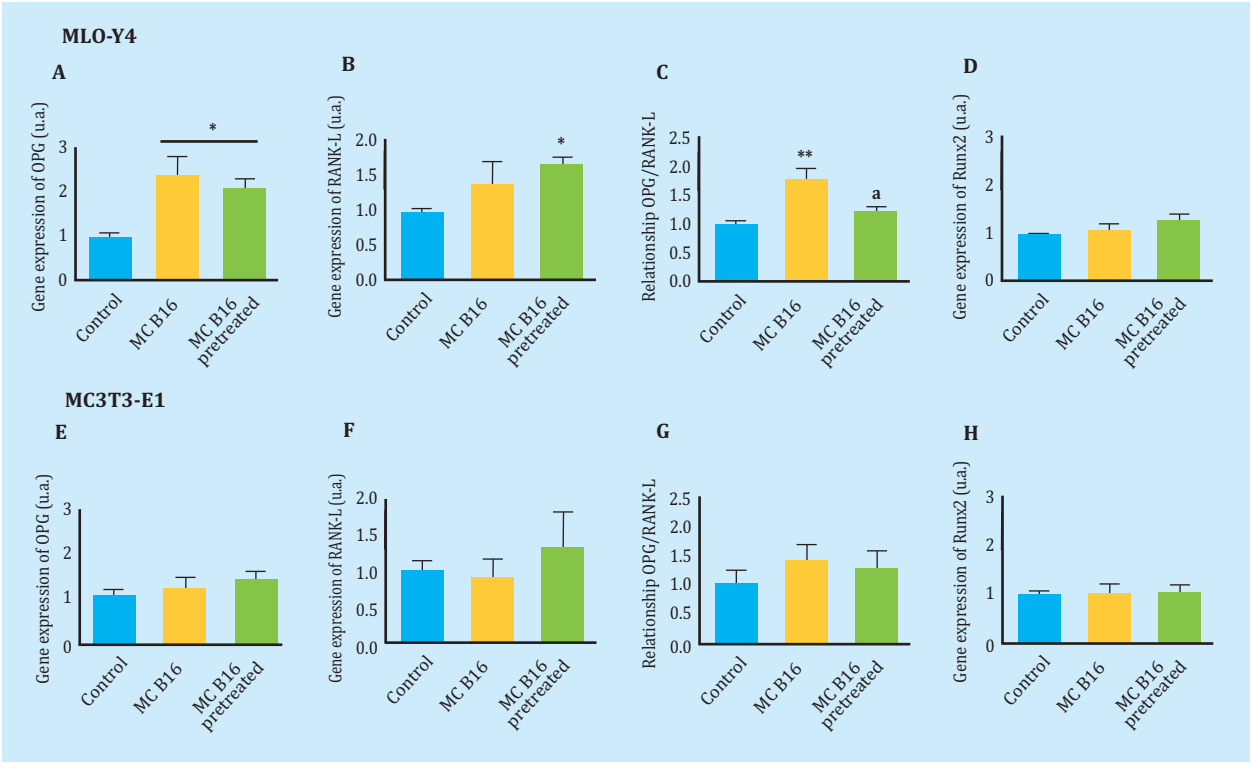

Figure 4. Soluble factors secreted by breast cancer tumor cells (MDA-MB-231) modify bone remodeling gene expression in human osteoblasts (hFOB 1.19). The expression of OPG (A), RANK-L (B), OPG/RANK-L (C) and Runx2 (D) ratio was evaluated by real-time PCR after 24 h stimulation of human osteoblasts with conditioned medium of pre-MDA treated or not. Data are represented as the mean ± SEM of three independent experiments in triplicate. *p<0.05 vs control

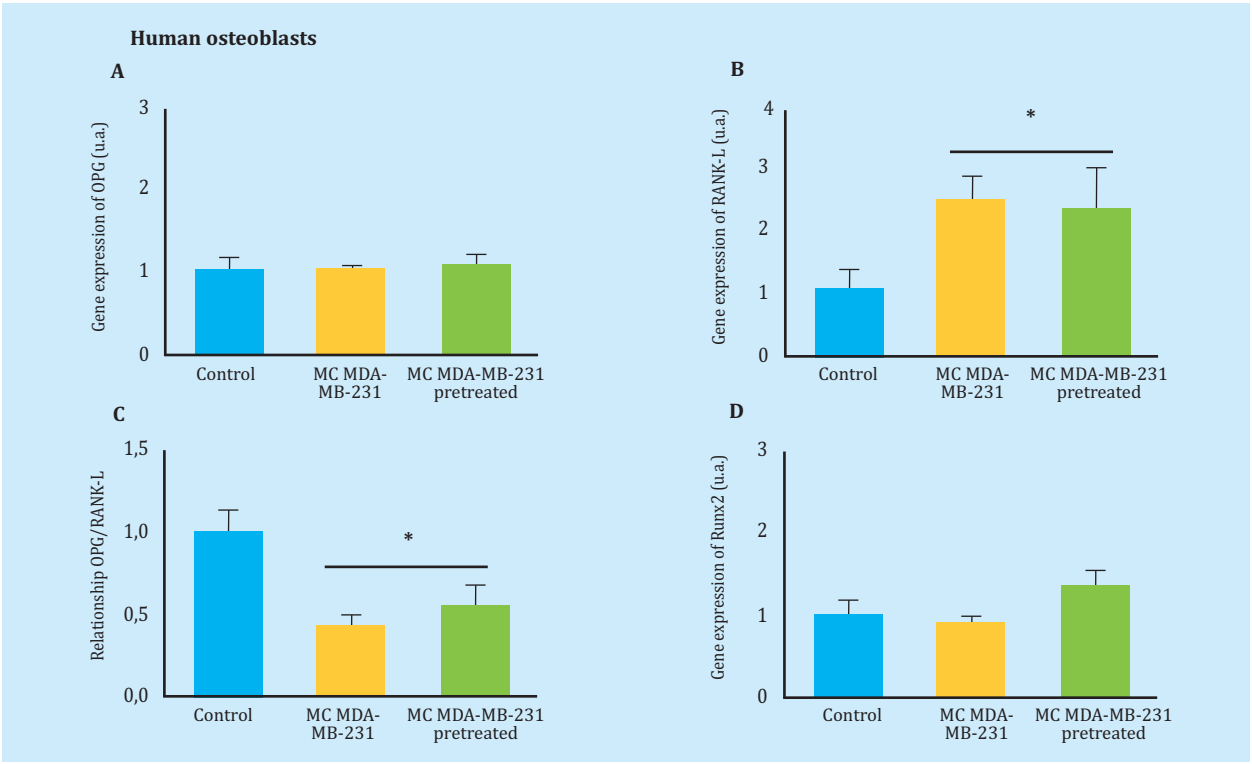

Rev Osteoporos Metab Miner. 2019;11(2):64-71

Figure 5. Soluble factors secreted by prostate tumor cells (TRAMP-C1) modify the expression of bone remodeling genes in osteocytes (MLO-Y4) but not in pre-osteoblasts (MC3T3-E1). The expression of OPG (A, F), RANK-L (B, G), OPG/RANK-L ratio (C, H), Runx2 (D, I) and osteocalcin (E, J) was evaluated by time PCR after stimulating 24 hours MLO-Y4 and MC3T3-E1 with conditioned medium of TRAMP-C1. Data are represented as the mean ± SEM of three independent experiments in triplicate. *p<0.05 vs control

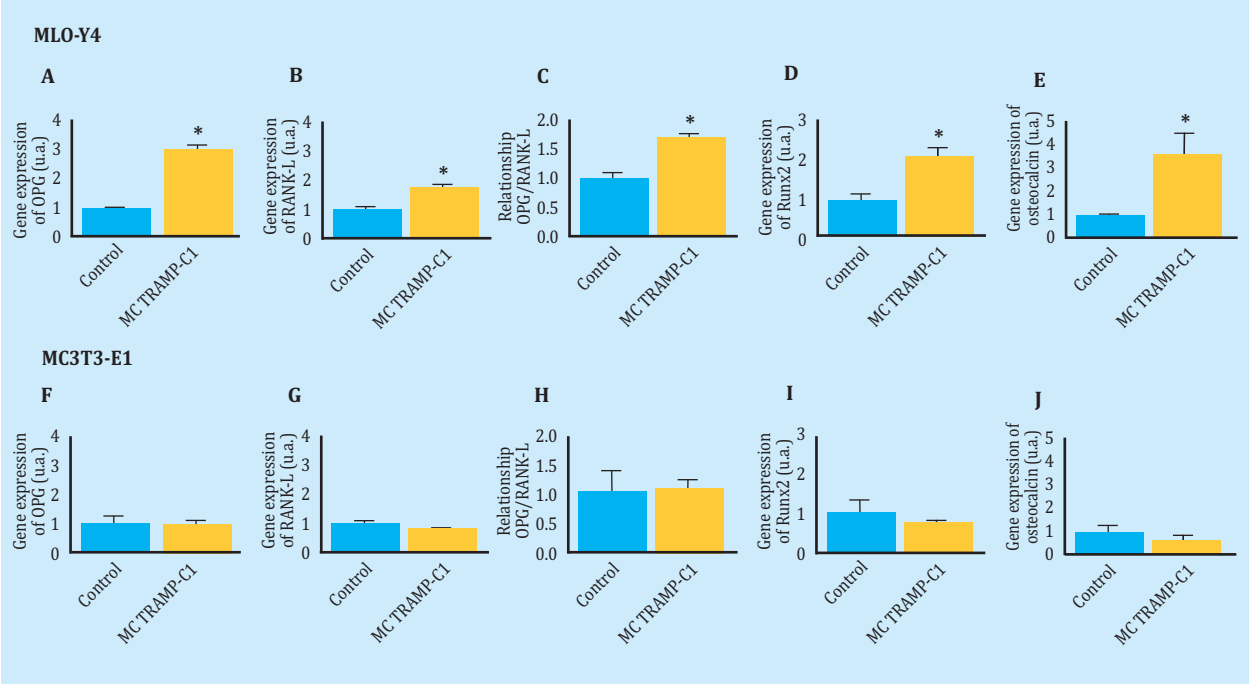

Notably, we suggest osteocyte as the main target cell of soluble tumor factors. Since there is no human osteocitic cell model of continuous lineage, we could not corroborate the results obtained by the melanoma and prostate cancer secretomes compared to the breast cancer secretomes in these cells.

The study of the changes induced by the secretome of breast cancer cells on bone cells was limited to the effects on the human osteoblastic continuous line hFOBs. The results obtained suggest that breast cancer cells are capable of affecting osteoblasts by soluble factors and that they mainly modulate the gene expression of RANK-L without the need to maintain cross-communication with these cells, confirming the alteration of the OPG/RANKL axis, as well as the changes induced by the other tumor secretomes studied. Given that osteocytes are the majority cells in bone, with a half-life of 25 years, with a multifunctional character and role of director-coordinator of the bone environment[26,27], their modulation, either pharmacological or as a therapeutic target, could be key to avoid pre-metastatic niche formation and bone metastasis. It has been proposed that osteocytes, and not the rest of the cells of the osteogenic lineage, are the main source that the osteoclasts require for their formation and activation in the remodeling of the trabecular bone[28,29], and may also be the only ones responsible for initiating the vicious cycle of the bone metastatic process. Few studies have established a clear role of the osteocyte and its relationship with cancer. In this sense, Delgado-Calle et al. showed that the osteocytes could be regulators of the proliferation of myeloma-like cancer cells by direct interaction with them through their cytoplasmic prolongations, which are capable of reaching the periodic and endocortical surfaces, as well as the bone marrow surface[30]. This direct interaction would lead to activation of the Notch signaling pathway in myeloma cells. This pathway mediates cell-to-cell communication, and participates in the control and activation of cell proliferation and death programs. Its pharmacological inhibition, using an inhibitor of said pathway, prevented the proliferation of myeloma induced by osteocytes[30]. In addition to regulating and coordinating the rest of cell lines in the bone environment, the osteocytes could secrete factors that reach distant cells, such as, for example, primary tumor cells, and modify them. This communication has been suggested in the case of prostate adenocarcinoma, where osteocitic and osteoblastic cells regulated their osteomimetic properties[21]. In addition, this communication could modulate key signaling pathways in prostate tumor cells, such as calcium intracellular mediators, cyclic AMP and ERK ½[31], and may enhance tumor progression of prostate cancer to bone. All these results, together with our results shown in this paper, suggest that in the cross-communication between the primary tumor and bone cells, the composition of the factors involved in the secretome may vary. During the evolution of the tumor, soluble tumor factors could reach the bone environment and induce changes in their cells. These cells could also send soluble factors to the primary tumor, which will generate changes in the tumor cells inducing them a greater osteomimetic phenotype.

The secretome of these osteomimetic tumor cells (in the figures presented as pre-treated conditioned media), upon reaching the bone environment again, could affect in the same direction or induce different variations of the changing microenvironment towards the formation of the niche. In this sense, in the proteomic analysis of the secretome of two continuous prostate tumor lines with different origin, DU145 (from brain metastases) and PC-3 (from bone metastases) 211 differentially expressed

Figure 6. Tumor secretomes modify the bone environment, the osteocytes being the most sensitive cells to these changes. The soluble factors secreted by prostate and melanoma tumors are those that mainly affect the osteocyte, increasing the gene expression of different factors related to bone remodeling. In turn, the osteocytes secrete factors that modify and induce a greater osteomimetic phenotype in the tumor cells themselves

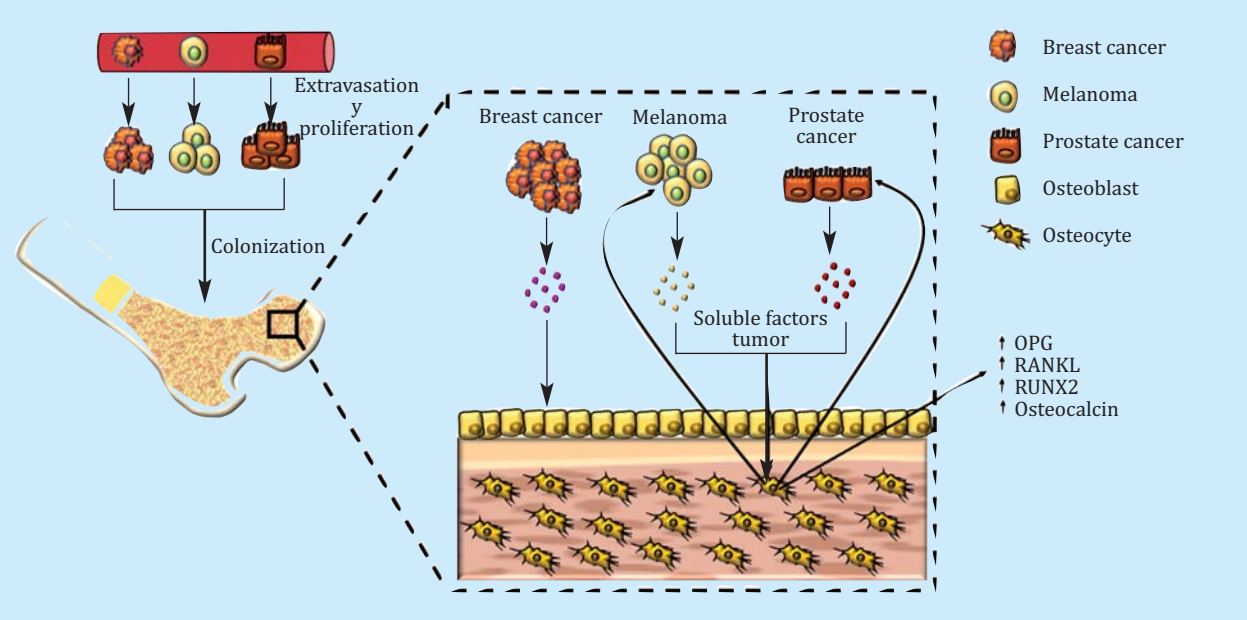

secretion proteins were found, which meant a 37.6% of the total proteins analyzed, indicating that the secretion proteins were considerably different between both cell lines[32]. Based on these investigations and our results, we propose that tumor secretomes modify the bone environment, the osteocytic line being more sensitive (Figure 6). The results shown open a wide field of study in the knowledge of the communication between the primary tumor cells and the cells of the future metastatic organ, in this case, the bone microenvironment. However, they should deepen their knowledge, due to the limitations of the present study. As previously mentioned, nonspecific effects have been avoided as a result of using cell cultures of different species, and an *in vitro* cell model based on widely used cell lines has been used as a reference for the study of bone metabolism and physiology, in the case of the MC3T3, MLOY-4 and hFOBs; as well as in the study of cancer, in the case of prostate tumor cells, melanoma or breast. With respect to the breast tumor line (MDA-MB-231 HTB-26), one of the limitations of its use in *in vitro* models is its metastatic origin[33], its behavior can be seen as a primary tumor and with it metastatic organotrophic communication .

Thus, the other two tumor lines with bone metastatic organotropism whose origin comes from primary tumors have been studied. However, it would be advisable to confirm the results obtained in this work in an *in vivo* experimentation model where you can study and confirm the changes in the bone microenvironment prior to the establishment of the metastasis, quantifying in the serum/plasma the altered bone cytokines and determining the temporality of bone and primary tumor communication as well as the level of change in bone tissue. The more detailed knowledge of the molecular changes that involve the formation of the pre-metastatic bone niche, as well as the secretory factors that induce it, could provide new therapeutic targets or action protocols, thus improving its prognosis. These actions would reduce the metastatic skeletal events developed by patients with solid tumors such as prostate or breast tumors, thus increasing their quality of life.

Funding: This research study was funded by CEU San Pablo-Santander projects (USP-BS-PPC 11/2012, USPB-BS-APP-2/2016 and MERMERG-2), and a 2017 FEIOMM Basic Research Grant.

Conflict of interests: The authors declare no conflict of interest.

Bibliography

1. Paget S. The distribution of secondary growths in cancer of the breast. Cancer Metastasis Rev. 1989;8:98-101.
2 Müller A. Homey B, Soto H, Ge N, Catron D, Buchanan ME, et al. Involvement of chemokine receptors in breast cancer metastasis. Nature. 2001;410:50-6.
3 Zhou, W, Fong MY, Min Y, Somlo G, Liu L, Palomares MR, et al. Cancer-secreted miR-105 destroys vascular endothelial barriers to promote metastasis. Cancer Cell. 2014; 25:501-15.
4 Lu X, Kang Y. Organotropism of breast cancer metastasis. J Mammary Gland Biol Neoplasia. 2007;12:153-62.
5 Weilbaecher KN, Guise TA, McCauley LK. Cancer to bone: A fatal attraction. Nat Rev Cancer. 2011;11:411-25.
6 Ell B, Kang Y. SnapShot: bone metastasis. Cell. 2012;151:690-690.e1
7 Guise TA. The vicious cycle of bone metastases. J Musculoskelet Neuronal Interact. 2002;2;570-2.
8 Bagi CM. Targeting of therapeutic agents to bone to treat metastatic cancer. Adv Drug Deliv Rev. 2005;57:995-1010.
9 Guise TA. Molecular mechanisms of osteolytic bone metastases. Cancer. 2000;88:2892-8.
10 Kingsley LA, Fournier PG, Chirgwin JM, Guise TA. Molecular biology of bone metastasis. Mol Cancer Ther. 2007;6:2609-17.
11 Käkönen SM, Mundy GR. Mechanisms of osteolytic bone metastases in breast carcinoma. Cancer. 2003;97:834-9.
12 Yoneda T. Cellular and molecular mechanisms of breast and prostate cancer metastasis to bone. Eur J Cancer. 1998;34:240-5.
13 Urwin GH, Percival RC, Harris S, Beneton MN, Williams JL, Kanis JA. Generalised increase in bone resorption in carcinoma of the prostate. Br J Urol. 1985;57:721-3.
14 Costa-Silva B, Aiello NM, Ocean AJ, Singh S, Zhang H, Thakur BK, et al. Pancreatic cancer exosomes initiate pre-metastatic niche formation in the liver. Nat Cell Biol. 2015;17:816-26.
15 Kaplan R, Riba RD, Zacharoulis S, Bramley AH, Vincent L, Costa C, et al. VEGFR-1 positive haematopoietic bone marrow progenitors initiate the pre-metastatic niche. Nature. 2005; 438:820-7.
16 Kan C, Vargas G, Pape FL, Clézardin P. Cancer cell colonisation in the bone microenvironment. Int J Mol Sci. 2016;17(10):E1674.
17 Yu KJ, Li JK, Lee YC, Yu G, Lin SC, Pan T, et al. Cabozantinib-induced osteoblast secretome promotes survival and migration of metastatic prostate cancer cells in bone. Oncotarget. 2017;8(43): 74987-5006.
18 Scheerlinck JP. Functional and structural comparison of cytokines in different species. Vet Immunol Immunopathol. 1999;72:39-44.
19 Strober W. Trypan blue exclusion test of cell viability. Curr Protoc Immunol. 2001 May; Appendix 3: Appendix 3B.
20 Gingrich JR, Barrios RJ, Morton RA, Boyce BF, DeMayo FJ, Finegold MJ, et al. Metastatic prostate cancer in a transgenic mouse. Cancer Res. 1996; 56:4096-102.
21 Ardura JA, Gutiérrez-Rojas I, Álvarez-Carrión L, Rodríguez-Ramos MR, Pozuelo JM, Alonso V. The secreted matrix protein mindin increases prostate tumor progression and tumor-bone crosstalk via ERK 1/2 regulation. Carcinogenesis. 2019;40(7):828-39.
22 Alonso V, de Gortázar AR, Ardura JA, Andrade-Zapata I, Alvarez-Arroyo MV, Esbrit P. Parathyroid hormone-related protein (107-139) increases human osteoblastic cell survival by activation of vascular endothelial growth factor receptor-2. J Cell Physiol. 2008;217:717-27.
23 Kaplan RN, Psaila B, Lyden D. Bone marrow cells in the 'pre-metastatic niche': within bone and beyond. Cancer Metastasis Rev. 2007;25:521-9.
24 Liu Y, Cao X. Characteristics and significance of the pre-metastatic niche. Cancer Cell, 2016;30(5):668-81.
25 Mohammad KS, Javelaud D, Fournier PG, Niewolna M, McKenna CR, Peng XH, et al. TGF-β-RI kinase Inhibitor SD-208 reduces the development and progression of melanoma bone metastases. Cancer Res. 2011;71(1):175-84.
26 Atkinson EG, Delgado-Calle J. The emerging role of osteocytes in cancer in bone. JBMR Plus. 2019;3(3):e10186.
27 Bonewald LF. The amazing osteocyte. J Bone Miner Res. 2011;26(2):229-38.
28 Xiong J, Piemontese M, Onal M, Campbell J, Goellner JJ, Dusevich V, et al. Osteocytes, not osteoblasts or lining cells, are the main source of the RANKL required for osteoclast formation in remodeling bone. PLoS One. 2015;10(9):e0138189.
29 Compto, JT, Lee FY. A review of osteocyte function and the emerging importance of sclerostin. J Bone Joint Surg Am. 2014;96(19):1659-68.
30 Delgado-Calle J, Anderson J, Cregor MD, Hiasa M, Chirgwin JM, Carlesso N, et al. Bidirectional Notch signaling and osteocyte-derived factors in the bone marrow microenvironment promote tumor cell proliferation and bone destruction in multiple myeloma. Cancer Res. 2016;76:1089-100.
31 Ardura JA, Gutiérrez Rojas I, Álvarez Carrión L, Friedman PA, Alonso V. Factors secreted by bone cells induce intracellular calcium accumulation and cyclic AMP and activation of ERK 1/2 in prostate cancer cells; evaluation by fluorescence techniques in living cells. Rev Osteoporos Metab Miner. 2018;10 (4):131-8.
32 Kwon OK, Jeon JM, Sung E, Na AY, Kim SJ, Lee S. Comparative secretome profiling and mutant protein identification in metastatic prostate cancer cells by quantitative mass spectrometry-based proteomics. Cancer Genomics Proteomics. 2018;15(4):279-90.
33 Ali R, Samman N, Al Zahrani H, Nehdi A, Rahman S, Khan AL, et al. Isolation and characterization of a new naturally immortalized human breast carcinoma cell line, KAIMRC1. BMC Cancer. 2017; 17(1):803.